REFERENCE HANDBOOK ON POWER, CONTROL & COMMUNICATION SYSTEMS : RECENT HEADWAYS

Dr. Vikas Mittal, Dr. Lillie Dewan,
Dr. Monika Mittal, Dr. Shelly Vadhera
& Dr. Rajender Kumar

ISBN 978-81-933897-2-0
9 788193 389720

Elixir PUBLICATIONS

Editors:

Dr. Vikas Mittal (Head of Department)
Department of Electronics & Communication Engineering
National Institute of Technology, Kurukshetra, Haryana, India

Dr. Lillie Dewan
Department of Electrical Engineering
National Institute of Technology, Kurukshetra, Haryana, India

Dr. Monika Mittal
Department of Electrical Engineering
National Institute of Technology, Kurukshetra, Haryana, India

Dr. Shelly Vadhera
Department of Electrical Engineering
National Institute of Technology, Kurukshetra, Haryana, India

Dr. Rajender Kumar
Department of Electronics & Communication Engineering
National Institute of Technology, Kurukshetra, Haryana, India

Type set by Elixir Publications, A unit of Athal Services Private Limited.

Cover Design by Mr. Jugaad Sobti.

ISBN 978-81-933897-2-0

Preface

Interdisciplinary research efforts are more required nowadays to address various challenges faced by the world such as secure communication, alternate and efficient energy resources, sustainable and healthy development etc. Indeed, boundaries between different disciplines are getting blurred these days. This is evident more by the prevalence of information and communication technologies (ICT) in different walks of life, which along with hardware is playing an increasingly important role in almost all of the modern systems; be it modern day power systems, automobiles, defense applications, communication systems etc. Modern day tools like machine learning, artificial intelligence and signal processing are abundantly used to provide an intelligent, efficient and self-sufficient automated systems these days.

This book titled "**Reference Handbook on Power, Control and Communication Systems: Recent Headways**" is an effort to showcase such developments. The title of the book reflects the importance of the three in a system – a system needs power to be able to deliver, needs communication to convey/adapt and needs control to be sensible. In this book, the reader will find a collection of Chapters edited by a number of experts from different disciplines, covering recent happenings in the fields of signal processing, renewable energy, power-, control- and communication systems along with their applications. This book intends to provide highlights of the current research and applications related to the above fields. A book of this kind is the need of the hour to be a concise and comprehensive reference for the researchers working in the relevant fields and for those who wish to initiate in any of the areas. Therefore, this book has been edited with the objective of creating chapters from some papers so as to propel the research further.

The book has been organized into several chapters – six to be precise. The book begins with the chapter on **Recent headways in Applications of Signal Processing.** The chapter discusses the importance of signal processing in various applications such as system analysis, biomedical field, linguistic and navigation systems etc. In system analysis applications, the difficulty in analyzing complex systems is shown to be overcome using Haar wavelet. Analysis of LTV system using non-recursive Haar wavelet integral operational matrix has been taken as a case study. The computational advantages have been illustrated with the help of a MATLAB profiler. In the second part of this chapter, EMG signal processing and feature extraction techniques are reviewed. Various time and frequency domain features have been enlisted. Second application from the biomedical field has been included which is related to recognition of isolated words in Hindi language using neural networks. Third part of this chapter deals with estimation of an object by reducing errors in GPS measurements through Kalman filter.

The second chapter is **Recent headways in Applications of Control Systems.** This chapter delves on mathematical modeling and its importance in designing and implementing various controllers in the beginning. Statistical method on measure system data from the domain of system identification has been presented. Modeling of different types of systems such as linear, non-linear, parametric etc. is discussed. Wiener system identification using iterative instrumental variable method has been included as a case study. The wiener model form is formulated based assuming coefficients of first basis function resulting in a bilinear parameterized form. Second part of this chapter discusses issues of implementation of controllers by considering its various characteristics that ensure stability of a system. As an illustration, controllers are implemented on servo systems (DC and Induction motor), benchmark problem (Rotary Inverted Pendulum), and highly nonlinear under actuated system (Robotic manipulator), biomedical systems outlining the procedure of achieving automation.

Third to fifth chapters highlight recent headways on **FACTS devices, Renewable energy and power systems** respectively. The three components of an electrical power system i.e., generation, transmission and distribution system have to work in utmost co-ordination to meet with the basic necessity of an individual and the economy of a nation on a broader aspect. The increasing load demand pressurizes all the components to perform all round the clock and with maximum efficiency to maintain reliability and sustainability of power in the system. The bulk power generated and transmitted to fulfill the rising demand makes the system face technical anomalies which may lead to voltage instability, low power factor, and hence reduced power quality, power loss and blackout at extremities.

With global awareness and initiatives taken to uplift environment friendly methods, power production through renewable energy is the best aid to the power system. It may help reduce the carbon footprint by reducing dependency over conventional means and move closer towards efficient and mindful utilization of clean green energy resources. Renewable energy sources though abundantly available in nature, are backed up by several issues related to power system. The intermittent nature of the sources, large power integration, conversion systems used exposes the existing power system to various technical issues including voltage variability, inclusion of harmonics, lower power factor, and a threat to destabilize the existing system.

Research and development initiatives have paved path for innovations in the field of renewable source based applications, solutions to power system problems as well as use of integrated power electronic devices. Integration of FACTS devices, implementation of distributed generation using standalone renewable energy sources, switching over to smart grids, use of artificial intelligence in various domains of power systems for better and optimized results are all

the means adopted to meet the goal of stable, reliable and economic electrical power generation, transmission and distribution..

Sixth chapter in this book presents **Recent Headways in Communication Engineering Paradigm**. This chapter deals with various paradigm advancements in communication engineering fields like IoT, Fog Computing and optical wireless communication.

Contents

Chapter 1

Recent headways in Applications of Signal Processing

Signal Processing has evolved as a most powerful technology that will have a deep impact on various engineering systems. Revolutionary developments and advances have taken place in broad range of applications such as system analysis, biomedical, linguistic and navigation systems, to name just a few.

Signal processing uses a unique type of data known as signals unlike other data types used in computer engineering. These signals provide information and interface between the real and machine world. Signal processing in nutshell can be recognized as techniques to manipulate these signals usually with the help of computers with a wide variety of goals such as information extraction, understanding system behavior, intelligent and sophisticated biomedical applications etc.

Signal processing has witnessed a journey from a technology belonging to national endeavours involving national security, generating resources like oil and gas exploration, space ventures and medical from sixties and seventies to common people usage technology such as mobiles and multimedia applications etc. and many more during current times.

An overview of some recent applications of signal processing in various domains will help the readers to make a better understanding and further headways towards realizing its several new applications. Therefore, in this chapter, some novel applications have been included to provide a glimpse of the potential of signal processing.

Application in System Analysis:

System analysis is a very important domain from the viewpoint of understanding the design and applications of a system. The task of analyzing a system analytically becomes more difficult and sometimes intractable when the system is complex, non-linear or time varying. Numerical methods come to rescue in such situations. But they are having their own pitfalls and shortcomings such as computational complexity, non-convergent solutions and need for extensive programming for implementation etc.

One of the promising alternatives is orthogonal functions, such as Walsh, block, Fourier, Legendre, Laguerre, Hartley, discrete cosine etc., based numerical methods. Use of orthogonal functions as basis helps in overcoming the twin issues – non-convergence and need for extensive programming for implementations – by using an operational approach. This approach converts the involved integro-differential system equations into equivalent matrix algebraic equations with the

help of operator matrices approximating various mathematical operations. However, time support of an orthogonal function has an impact on the computational complexity and approximation errors in the developed system analysis algorithms. Therefore, orthogonal functions such as Haar, Block and Walsh functions with compact time support are preferred over others in the operational approach for reducing the computational complexity and solution approximation errors.

Haar functions came out to be winner out of the orthogonal functions with compact support due to its additional properties of sparsity and multiresolution. Sparsity in Haar operator matrices result in reduced computational complexity and multi-resolution captures the sharp transitions in system response effectively thereby reducing the errors in approximate solutions further. Even though Haar functions based operational approach is five to six decades old, but hitherto only recursive implementation of Haar operator matrices and algorithms have been reported. This continued till the beginning of 21^{st} century and beyond, until, non-recursive formulation of Haar integral operator matrix has been proposed. This non-recursive formulation helps in further reducing the computational complexity with additional benefits like fewer calls during processing and low memory requirements of the computing platform.

One such paper has been included in this section where an alternative implementation of ***Haar wavelet based approach for state analysis of linear time variant systems*** has been presented. Piecewise constant solutions of a LTV system has been obtained by using non-recursive formulation of Haar integral operator matrix. It has been demonstrated with the help of MATLAB profiler that the proposed methodology accomplishes the task with fewer function calls than those made in the existing benchmark algorithm in the literature.

An Alternate Implementation of Haar Wavelet Based Approach for State Analysis of Linear Time-variant Systems

Sheetal[1] and Monika Mittal[2]

***Abstract*–In the proposed paper an efficient alternative implementation for state analysis of linear time varying systems (LTV) via Haar wavelets for the computational saving is presented. The problem of time varying systems has been solved based on few useful characteristics of the Haar functions. The properties include operational matrix of integration, a special product matrix and a related coefficient matrix. Despite the use of the conventional Hsiao method an alternative approach is used for the computational saving. MATLAB PROFILER is used for the demonstration of the effectiveness of the proposed method for different resolutions.**

***Keyword*–connection coefficients, linear time varying system, operational matrices, Haar wavelet**

I. INTRODUCTION

Solution of most of the problems related to Linear Time Varying systems analysis has been already presented using various numerical methods. It is cumbersome to analyze the linear time varying system using the numerical and analytical methods. Now the system analysis becomes more simple and the computational time for complex problems if greatly reduced by the use of orthogonal functions. For the optimization and identification of non-linear and linear systems and getting the differential equation as piece wise constant solutions for different problems [1-3].Some of the orthogonal functions has been greatly used. Those functions include: Walsh functions, block pulse functions, Laguerre functions, Legendre functions, Fourier functions and Haar functions [4]. This algorithm is utilized for converting the simple differential equation into algebraic equation without necessity of first finding the general equation and then calculating the arbitrary constants. It itself takes care of initial conditions required for calculating the arbitrary constants and hence the identification and optimization techniques are either much diminished or greatly simplified accordingly. When the relevant conventional methodology fails then piecewise constant solutions give the only way to obtain the solution. They are computationally more efficient. Haar wavelets have been applied tremendously in communications for signal processing and indicated to be a useful and computationally more efficient mathematical tool than others.

This paper adopted Haar wavelets properties like multiplicative property and local basis property [5] to solve LTV problems.

Chen and Hsiao have first derived tear operational matrix for the integrals of the Haar function vector [3] and have done the pioneer work for analyzing different systems using the concept other wavelets. Haar product matrix and a coefficient matrix were first presented by Hsiao [1, 5] and used them for solving the problems having lumped and distributed – parameter via Haar wavelet. But all these operational matrices are based on recursive formulation. For performing analysis and optimal control of linear time invariant systems number of studies are proposed but comparatively there are very limited studies for Linear Time Varying systems. Haar operational matrix of integration was also given by Lin Wu [2, 6] but it is based on non-recursive formulation. This paper presents an alternative Haar wavelet based approach for state analysis of LTV system which is based on non-recursive operational matrix of integration and coefficient matrix given by Hsiao [11].

The paper is structured as follows: In II section definition of Haar wavelet is explained. In section III Properties of Haar wavelets including various operation matrices are described. Alternative method of state analysis of LTV system is given in section IV. Section V includes an example illustrating the method and verification of result is presented. Both the methods are compared in section VI.

II. HAAR WAVELETS

The Haar wavelet is a sequence of rescaled "square-shaped" functions and these sequences combine together forming a wavelet family.

A group of square waves form the orthogonal set of Haar functions $h_i(t)$with magnitude ±1 in some intervals and zero elsewhere.

In general,

$$h_n(t) = h_1(2^i t - b/2^i), \quad (1)$$

$$n = 2^i + b, i \geq 0, 0 \leq b < 2^i, n, i, b \in Z$$

[1]Sheetal is with Department of Electrical and Electronics Engineering, KIET group of Institutions, India

[2]M. Mittal is with the Department of Electrical Engineering, National Institute of Technology, Kurukshetra, India

(e-mail: sheetal.sheetal02@gmail.com, monika_mittalkkr@rediff.com).

Fig.1 (a) showing the scaling function h_0 (t) =1 during the whole interval $0 \leq t \leq 1$. The h_1 (t) is considered as the mother wavelet and implementing two operations: dilation and translation other subsequent curves can be obtained from it.

Fig. 1(a) First Haar Fig. 1(b) Integral of 1(a)

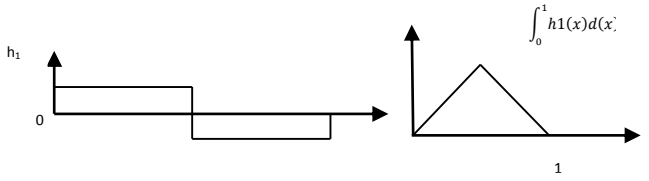

Fig. 2(a) Second Haar Function Fig. 2(b) Integral of 2(a)

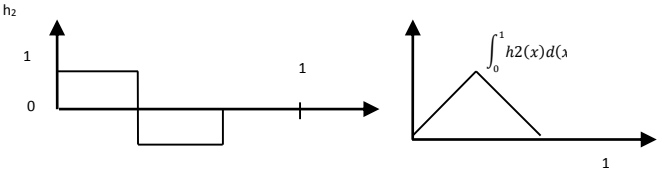

Fig. 3(a) Third Haar Function Fig. 3(b) Integral of 3(a)

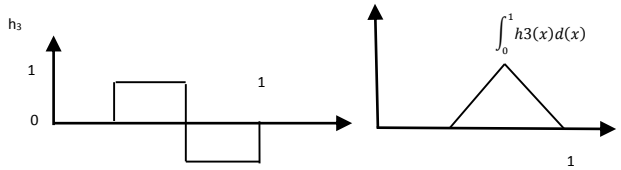

Fig. 4(a) Fourth Haar Fig. 4(b) Integral of

Assuming (t) to be a function which is square integrable in the interval [0, 1) then it can be expanded in a Haar series:

$$y(t) = c_0 h_0(t) + c_1 h_1(t) + c_2 h_2(t) \ldots\ldots\ldots\ldots = c_m^T H_m(t), \quad (2)$$

$$m = 2^i, \; i \geq 0$$

$$c_j = 2^i \int_0^1 y(t) h_j(t) dt \quad (3)$$

For m=4, $H_m(t)$ is calculatedcombining the first four Haar functions samples as follows:

$H_4(t) = [h_0(t) \quad h_1(t) \quad h_2(t) \quad h_3(t)]^T$

$$H_4(t) \triangleq \begin{bmatrix} h_0(t) \\ h_1(t) \\ h_2(t) \\ h_3(t) \end{bmatrix} = \begin{bmatrix} 1 & 1 & 1 & 1 \\ 1 & 1 & -1 & -1 \\ 1 & -1 & 0 & 0 \\ 0 & 0 & 1 & -1 \end{bmatrix} \quad (4)$$

The Haar coefficient $c_j$can be obtained by (3); but it can be evaluated by matrix inversion which is more convenient method as

$$c^T = y(t) H_m^{-1} \quad , \quad (5)$$

Eq. (5) converts the time function $y(t)$ into the coefficient vector $c^T$and is called the *forward transform* and eq. (2) recovers $y(t)$ from $c^T$is called the *inverse transform*. Because of containing many zeros in H and H^{-1}, the Haar transform takes less time for computation than the Fourier transform and even Walsh transform is slower than it [1].

III. SOME IMPORTANT PROPERTIES OF HAAR WAVELETS

In wavelet analysis of a dynamic system, it is required to transform all functions into Haar series. The integration of Haar wavelets [1] is preferred as Haar wavelet is not continuous in nature, and therefore not differentiable. Using this operational approach, a differential equation is transformed into an algebraic equation and its complexity has been reduced.

It is notified that all the Haar wavelet have orthogonal property to each other:

$$\int_0^1 h_j(t) h_l(t) dt = 2^{-i} \delta_{jl} = \begin{cases} 2^i \; j = l = 2^i + k \\ 0 \; j \neq l \end{cases} \quad (6)$$

For the analysis of LTV problems three matrices are used a) operational matrix of integration b) product matrix and c) connection matrix.

A. Operational matrix of integration

The integration of Haar wavelets should be converted into Haar series using Haar coefficient matrix P_m as [3]

$$\int_0^t H_m(\mathrm{t}) dt \approx P_m H_m(t), \quad t \in [0,1) \quad (7)$$

Where the m-square matrix P_m is called the *operational matrix* of integration**.** Integrals of first four Haar functions from fig.1 (b), 2(b), 3(b) and 4(b) by taking samples can be expressed as:

$$\int_0^t H_4(t) dt = \frac{1}{8} \begin{bmatrix} 1 & 3 & 5 & 7 \\ 1 & 3 & 3 & 1 \\ 1 & 1 & 0 & 0 \\ 0 & 0 & 1 & 1 \end{bmatrix} \quad (8)$$

Haar transform coefficient matrix of the integrals is represented by the operational matrix P_m and is defined in (8):

$$P_m = \left[\int_0^t H_m(\tau)\, \mathrm{d}\tau\right] H_m^{-1} \quad (9)$$

For m = 4, $P_4 = \frac{1}{16} \begin{bmatrix} 8 & -4 & -2 & -2 \\ 4 & 0 & -2 & 2 \\ 1 & 1 & 0 & 0 \\ 1 & -1 & 0 & 0 \end{bmatrix}$

To calculate P_m recursive methodgiven by Hsiao [3, 9] and non-recursive method given by Lin Wu [2] can be used.

1) Recursive formulation of Haar operational matrix of integration

In general for resolution m, the P_m is given as

$$P_m = \frac{1}{2m}\begin{bmatrix} 2mP_m & -H_m \\ H_m^{-1} & 0_m \end{bmatrix}, \quad P_1 = \frac{1}{2} \tag{10}$$

2) Non-recursive formulation of operational matrix of integration P

Lin Wu et al. [2] presented the integrated method for calculating the integration matrix for different orthogonal functions in terms of the generic orthogonal function $\Phi_m(t)$i.e.:

$$Q_\Phi(t) = \Phi \,.Q_{B_m}.\Phi^{-1} \tag{11}$$

Where Φ is sampled version of $\Phi_m(t)$.

For obtaining Non-recursive formulation of the operational matrix of integration of Haar wavelet which is denoted as $P_m$at resolution *m*, the corresponding basis function from(4) are substituted in (11)in place of generic orthogonal basis function, results in

$$P_m = H_m \,.\, Q_{B_m}.\, H_m{}^{-1} \tag{12}$$

Where Q_{B_m} is the operational matrix of integration for resolution *m* for block pulse function.

Over [0, 1], the Block pulse function is defined as [10]:

$$b_j(t) = \begin{cases} 1, & t \in \left[\frac{j}{N}, \frac{j+1}{N}\right], \; j = 0,1,2,\ldots, \text{N-1} \\ 0, & \textit{elsewhere} \end{cases} \tag{13}$$

And its operator matrix of integration [8] for resolution *m* is given as:

$$\mathrm{Q}_{B_m} = \frac{1}{m}\begin{bmatrix} \frac{1}{2} & 1 & \ldots & 1 \\ 0 & \ldots & \ldots & \vdots \\ \vdots & 0 & \frac{1}{2} & 1 \\ 0 & \ldots & 0 & \frac{1}{2} \end{bmatrix} \tag{14}$$

Non-recursive formulation in (12) and recursive formulation in (10) gave the same result or P_m. but computational time taken by (12) is less when compared to (10).

B. Haar Product Matrix

The condition of Haar product matrix arises when the product of two Haar wavelet basis, i.e. $H_m(t)H_m^T(t)$is faced.The *Haar product matrix M* represents the product $H_m(t)H_m^T(t)$ *as*

$$M_m(t) \triangleq H_m(t)H_m^T(t)$$

$$M_m(t) \triangleq \begin{bmatrix} M_{m/2}(t) & H_{m/2}diag[h_b] \\ diag[h_b]H_{m/2}^T & diag[H_{m/2}^{-1}\, h_a] \end{bmatrix}, M_1(t) = h_0(t) \tag{15}$$

Where $h_a \triangleq [h_0 h_1 \ldots h_{m/2-1}]^T = h_{m/2}$

$$h_b \triangleq [h_{m/2} h_{m/2+1} \ldots h_{m-1}]^T$$

C. Haar Connection Coefficients

When the condition of multiplication of two functions in Haar domain arises and the result is to be represented as single Haar series expansion then the Haar connection coefficients matrix is used[4,5].

In general, product matrix satisfies

$$H_m(t)H_m^T(t)c_m = M_m(t)c_m = C_m\, H_m(t), \tag{16}$$

Where C_m is Haar connection coefficient matrix having dimension *mxm*, in correspondence to Haar expansion coefficients c_m.

The recursive formulation of connection coefficient matrix C_m[11]is defined as follows:

$$C_m \triangleq \begin{bmatrix} C_{m/2} & H_{m/2}diag[c_b] \\ diag[c_b]H_{m/2}^{-1} & diag[c_a^T H_{m/2}] \end{bmatrix}, C_1 = c_0 \tag{17}$$

Where $c_a \triangleq [c_0\, c_1 \ldots c_{m/2-1}]^T = c_{m/2}$ (18)

$$c_b \triangleq [c_{m/2} c_{m/2+1} \cdots \; c_{m-1}]^T \tag{19}$$

Proof of (15) and (17) can be found in [11]
An alternative approach of [5] is explained in next section.

IV. An Alternative Approach for State Analysis of Linear Time Varying System via Haar Wavelets

Consider a general LTV system given as:

$$y(t) = A(t)y(t) + B(t)u(t), y(0)=y_0 \tag{20}$$

where $y(t) \in R^n$ is the state, $u(t) \in R^r$, and $A(t) \in R^{n\times r}$ and $B(t) \in R^{n\times r}$. The response $y(t)$, $0 \le t < t_f$, is required to be found. Since the Haar function if defined for [0,1), the time scale should be normalized by defining $t = t_f.\tau$, then (20) becomes

$$\dot{y}(\tau) \triangleq \frac{dy(\tau)}{d\tau} = t_f[A(\tau)y(\tau) + B(\tau)u(\tau)], \quad y(0) = y_0 \tag{21}$$

Where $\tau \in [0,1)$. Let $t_f A(\tau)$ and $t_f B(\tau)u(\tau)$ be decomposed into the form :

$$t_f.A(\tau) = A_1\alpha_1(\tau) + A_2\alpha_2(\tau) + \ldots\ldots + A_p\alpha_p(\tau) = \sum_{j=1}^{q} A_j\, \alpha_j(\tau), \quad (p \le n^2) \tag{22}$$

where each $A_j$is a $n \times n$ constant matrix, and $\alpha_j(\tau)$ is a scalar time function; and

$$t_f.B(\tau)\, u(\tau) = b_1\beta_1(\tau) + b_2\beta_2(\tau) + \ldots\ldots\ldots + b_q\beta_q(\tau) = B_i\beta_i(\tau), (q \le n) \tag{23}$$

Where each b_j is a constant n-vector, and $\beta_i(\tau)$ is a scalar time function. Thus (21) becomes

$$\dot{y}(\tau) = \sum_{j=1}^{p} A_j\, \alpha_j(\tau)y(\tau) + \sum_{i=1}^{q} b_i\, i(\tau), \quad y(0) = y_0 \tag{24}$$

where $\alpha_j(\tau) = d_j^T h_m(\tau)$ (25)

$\beta_j(\tau) = e_j^T h_m(\tau)$ (26)

$y(\tau)$ can be expanded into Haar series as

$$y(\tau) = \begin{bmatrix} f_1^T \\ f_2^T \\ \vdots \\ f_n^T \end{bmatrix} h_m(\tau) \triangleq F h_m(\tau) \qquad (27)$$

where F is an $n \times m$ matrix. For $0 \leq \tau < 1$ Integration of (24) yields

$$y(\tau) - x_0 = \sum_{i=1}^{p} \int_0^\tau A_i \, \alpha_i(\tau) x(\tau) d\tau + \sum_{j=1}^{q} \int_0^\tau b_j \, \beta_j(\tau) d\tau, \qquad (30)$$

Applying (25)-(26), state equation (30) becomes

$$F h_m(\tau) - [y_0 \underbrace{0 \ldots\ldots 0}_{\text{(m-1) columns}}] h_m(\tau)$$

$$= \sum_{i=1}^{p} A_i \int_0^\tau [d_i^T \, h_m(\tau) F h_m(\tau) d(\tau) + \sum_{j=1}^{q} b_j \int_0^\tau e_j^T \, h_m(\tau) d\tau$$

$$= \sum_{i=1}^{p} A_i \, F \int_0^\tau h_m(\tau) h_m^T(\tau) d_i d\tau + \sum_{j=1}^{q} b_j \int_0^\tau e_j^T \, h_m(\tau) d\tau \qquad (31)$$

Using non-recursive integral operational matrix given by Lin Wu [2] from (12) and connection matrix by Hsiao [11] from (17), (31) becomes

$$F h_m(\tau) - [x_0 0 \ldots 0] h_m(\tau) = \sum_{i=1}^{p} A_i \cdot F \cdot D_i \int_0^\tau h_m(\tau) d\tau + \sum_{j=1}^{q} b_j \, e_j^T \int_0^\tau h_m(\tau) d\tau \qquad (32)$$

Where $D_i \, h_m(\tau) = M_{(m \times m)}(\tau) d_i = h_m(\tau) h_m^T(\tau) d_i$ is a copy of (16). The integral of (32) can be obtained by multiplying the *operational matrix* of integration as follows:

$$F h_m(\tau) - [y_0 \, 0 \ldots 0] h_m(\tau) = \sum_{i=1}^{p} A_i \cdot F \cdot D_i \cdot P_m h_m(\tau) + \sum_{j=1}^{q} b_j \, e_j^T P_m h_m(\tau) \qquad (33)$$

Therefore,

$$F - [y_0 \, 0 \ldots 0] = \sum_{i=1}^{p} A_i \cdot F \cdot D_i \cdot P + \sum_{j=1}^{q} b_j \, e_j^T P \qquad (34)$$

Let $G \triangleq [y_0 \; 0 \ldots\ldots 0] + \sum_{j=1}^{q} b_j \, e_j^T P \qquad (35)$

and

$$G = \begin{bmatrix} g_{10} & g_{11} & \cdots & g_{1(m-1)} \\ g_{20} & g_{21} & \cdots & g_{2(m-1)} \\ \vdots & \vdots & \vdots & \vdots \\ g_{n0} & g_{n1} & \cdots & g_{n(m-1)} \end{bmatrix} \triangleq \begin{bmatrix} g_1^T \\ g_2^T \\ \vdots \\ g_n^T \end{bmatrix}, \qquad (36)$$

$g_j = [g_{j0} g_{j1} \cdots g_{j(m-1)}]^T$

Equation (34) is rewritten as

$$F = \sum_{i=1}^{p} A_i \, . \, F \, . \, D_i \, . \, P + G \qquad (37)$$

or

$$F - \sum_{i=1}^{p} A_i \, . \, F \, . \, D_i \, . \, P = G \qquad (38)$$

$$\begin{bmatrix} f_1 \\ f_2 \\ \cdot \\ \cdot \\ f_n \end{bmatrix} = \left\{ I - \sum_{j=1}^{p} A_j \otimes (D_j \cdot P)^T \right\}^{-1} \begin{bmatrix} g_1 \\ g_2 \\ \cdot \\ \cdot \\ g_n \end{bmatrix} \qquad (39)$$

Where $\otimes$ is Kronecker product and (38) can be solved with Kronecker product which results in (39).

Once f_j ,j= 1,2,...,n, are known, the state variable y(τ) in the Haar series expansion can be calculated from (27).

In the next section the LTV problem analysis using alternative method is done. State response of a LTV system is also presented.

V. EXAMPLE AND RESULTS

In order to verify above analysis, a linear time varying system is considered which is described by the state equation [8]

$$\dot{y}(t) = \begin{bmatrix} 0 & 0 \\ t & 0 \end{bmatrix} y(t), \quad y(0) = (1 \; 1)^T \qquad (40)$$

analytical solution [8] of (40) is

$y_1(t) = 1,$

$y_2(t) = \frac{t^2}{2} + 1$

Using alternative method presented above, system is solved for resolution m=8.It is shown by Fig.5 that the alternative method is verifying with the analytical solution.

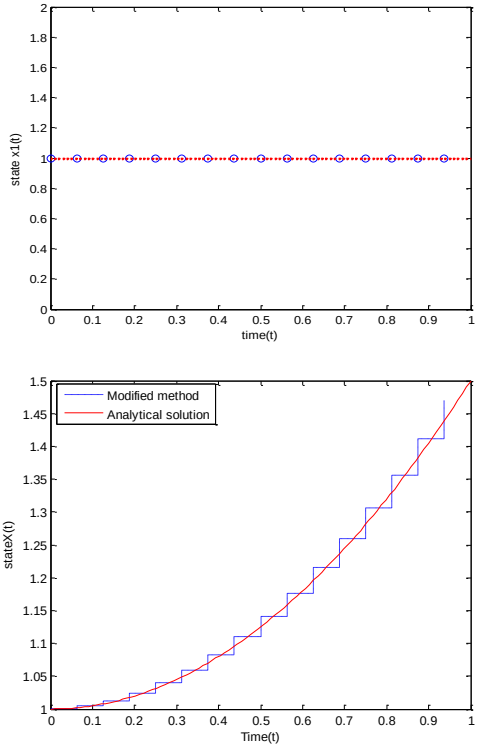

Fig. 5. State response of linear time varying

A mutual comparison of the achieved computational savings using existing method with modified method which uses non-recursive operational matrix of

integration and recursive connection coefficient formulation is displayed using MATLAB PROFILER in Table1

A transparent representation for the computational time of the distinct resolutions using the two methods is shown Fig. 6. It is evident from the results there is saving of time with increase in the resolution.

TABLE I COMPUTATIONAL EFFICIENCY FOR ALTERNATIVE METHOD & EXISTING RECURSIVE APPROACH

	Modified Hsiao method	Hsiao Method
m= 16	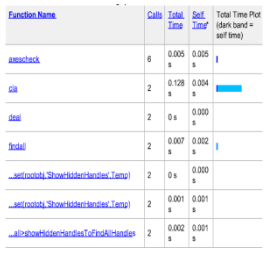	
m= 128		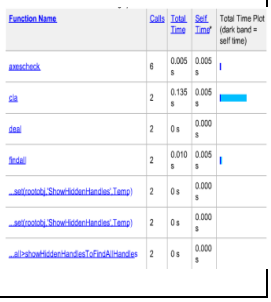

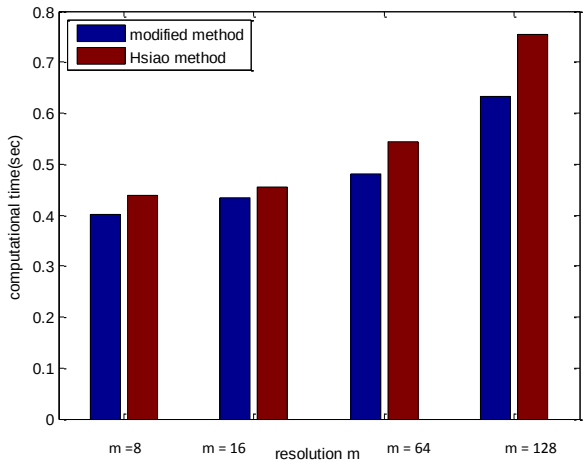

Fig. 6 Bargraph showing computational saving

VI. CONCLUSION

In the proposed paper the analytical solution is used to verify the system solution using Haar wavelet method. MATLAB PROFILER is used to demonstrate the effectiveness of the method called non-recursive formulation with respect to the existing method proposed by Hsiao for the analysis of linear time variant system for the computational saving. As the Haar wavelet basis includes the property of time frequency localization, the time information and frequency both are included in the solution of the system. Hence by using the proposed method it is evident that for many practical applications vast computer memory and large computational time is not required and we can achieve the control and competition with high level of precision.

REFERENCES

[1] Hsiao, C.H., Wang, W.J."Short communications in state analysis and optimal control of linear timevarying systems via Haar wavelets," J. Optim. Control Appl. Math.19, 423–433 (1998)

[2] Wu J.L., Chen C.H., Chen C.F., A unified derivation of operational matrices of integration for integration in system analysis, IEEE Proc. Int. Conf. on Information Technology: Coding and Computing, 2000, p. 436-442.

[3] Chen, C.F., Hsiao, C.H.: Haar wavelet method for solving lumped and distributed-parameter systems.IEEE Proc., Control Theory Appl.144(1), 87–94 (1997)

[4] M. Garg, L. Dewan,"An integrated approach for non-recursive formulation of connection-coefficients of orthogonal functions,"Leonardo Journal of Sciences, vol. 20, pp. 1-14,January-June 2012.

[5] Wang .W.J, Hsiao .C.H, "state analysis and optimal control of linear time varying systems via haar wavelets", Optimal control applications and methods, Vol.19, 1998,pp-423-433

[6] Wu J.L.,Chen C.H.,Chen C.F.,"Numerical inversion of laplace transform using Haar wavelet operational matrices,"IEEE Trans. On Circuits and Systems-Part I: Fundamental Theory and Applications,2001,48(1), pp. 120-122.

[7] Chen, S.L., Lai, H.C., Ho, K.C., "Identification of linear time varying systems by Haar wavelet," Int. J.Syst. Sci.37(9), 619–628 (2006)

[8] Hsu, N., Cheng, ''Analysis and optimal control of time-varying linear systems via block pulse functions. Int. J. Control33(6)," 1107–1122 (1981)

[9] Hsiao, C.H., Wang, W.J., "Optimal control of linear time-varying systems via haar wavelets," J. Optim. Theory Appl.103, 641–655 (1999)

[10] K. Maleknejad, M. Shahrezaee, H. Khatami,''Numerical solution of integral equations system of the second kind by Block–Pulse functions," Applied Mathematics and Computation 166 (2005) 15–24.

[11] C.H. Hsiao, C.H. Hsiao, W.J. Wang, "States analysis and parameters estimation of bilinear systems via Haar wavelets," IEEE Trans. Circuits and Systems-I: Fundamental Theory and Applications (1996), submitted for publication.

Application in Biomedical Engineering:

Signal processing use in biomedical engineering increased with the increased use of advanced electronic instruments in this domain. Various new instruments have been invented that can detect signals due to different biological organisms and analyze them for diagnostic purpose. There has been distinct literature on signal processing use for the analysis of biomedical signals, termed specifically, as Biomedical Signal Processing (BMP). It has revolutionized the medical field to a large extent. It has made life easier and increased life expectancy of the people by decades.

Biomedical signals can observe various physiological activities of organisms, ranging from gene and protein sequences, to neural and cardiac rhythms, to tissue and organ images. In nutshell, BMP encompasses clinical study of the internal body metabolisms, diagnosis of ailments, and detection of diseases using the electronic instrumentation. It aims at extracting significant information from biomedical signals which can help biologists in discovering new biology and physicians in monitoring distinct illnesses. Various biomedical engineering techniques such as medical resonance imaging (MRI), X-Ray, electrocardiography (ECG), computer tomography (CT) scan, Ultra Sound, electroencephalogram (EEG) and electromyography (EMG) etc. are commonplace nowadays.

Some of the most important applications in this domain are deoxyribonucleic acid (DNA) analysis and comparison, ribonucleic acid (RNA) fingerprinting, ECG, EEG & EMG signal analysis and speech processing etc. In general, DNA analysis and comparison can be categorized as genomic signal processing (GSP). The most important challenge of GSP is to minimize processing time and detection error of the protein coding region in a specified DNA. Processing of genomic sequence is done after transforming it to numerical sequences consisting of numbers, represented mathematically, by character strings of alphabets A, T, G and C, denoting each one of nucleotide bases. For proteins, the string size consists of 20 alphabets for possible amino acids.

Characterization of fingerprint, iris, retina, signature, face etc. finds application in biometric systems. Out of these, fingerprint recognition and verification systems are more efficient as compared to other biometric systems. RNA fingerprinting is a powerful tool which can isolate differentially expressed genes. It has to be standardized by identifying a number of efficient and selective primers. The issue of ensuring efficiency of RNA fingerprinting due to abundance of RNA is very important.

ECG, EEG and EMG represent electrical signals generated from the activity of heart, brain and skeletal muscles, respectively. Electrocardiogram (ECG) represents electrical activity of human heart. ECG is a composite signal consisting of 5 waves - P, Q, R, S and T. Accurate detection of

any one of these waves or combination thereof can be useful for detecting various heart conditions such as auricular and ventricular hypertrophy, myocardial infarction aka heart attack, arrhythmias, pericarditis, generalized suffering affecting heart and blood pressure, cardiac medicine effects and electrolytic transformations etc. Noise during ECG data acquisition and its non-linearity are of prime concern for effective automated early detection of heart conditions for successful treatment. EEG, on the other hand, is the recording of electrical signals emanated from human brain collected from the scalp. The parameters of this signal and various patterns in it indicate brain health. Signal processing techniques can be utilized to analyze EEG signals for proper diagnosis of the affected person. Automated functionality can reduce the inspection time taken by a doctor for analysis of complex EEG signals. This can also find applications in evolving systems involving human-computer interaction (HCI) interfaces and cybernetics etc.

Electromyography (EMG) signals are becoming increasingly important in many applications involving clinical, prosthesis or rehabilitation devices and more. Noisy EMG signals are a major hurdle in achieving improved performance in different applications. Standardization of various neurophysiological, rehabitational and assistive technologies require detection, processing and classification of EMG signals in which signal processing techniques and algorithms can help immensely.

Another very important application of signal processing is in speech recognition. A typical speech recognition system usually uses a collection of algorithms from various domains such as statistical pattern recognition, communication theory, signal processing, combinational mathematics, and linguistics, among others. Although, each one of the above domains relies on different recognition systems, but perhaps the common denominator of all systems is signal processing, at-least at the front end. The signal is converted to some parametric representation and then recognized at the back-end using different recognizers. Speech is the most common way through which human interacts amongst themselves and also it is desired that the machines should also understand and interpret the speech to act accordingly. Therefore, numerous applications such as speech emotion recognition in intelligent household robots, speaker verification, speech identification on the basis of mood, interactive voice response systems, train reservation systems, automation of operator services, voice dialing, voice navigation of a desktop, call center automation and many more are prevalent around us.

In general, various analytical signal processing methods that are to be evaluated in all the above applications can be summarized as; Spectral Estimation, Periodogram, Maximum Entropy Method, AR Method, Moving Average Methods, ARMA Method, Maximum Likelihood method etc.

Two such papers have been included in this section titled ***Techniques for EMG signal processing and feature extraction: a review*** and ***Automatic isolated Hindi words recognition using neural networks.*** In the first paper related to EMG signal processing, different algorithms and methodologies to analyze EMG signals are presented. Also a comprehensive list of various time- and frequency-domain features of EMG signals has been presented to aware the researchers of various research dimensions in this domain.

In the second paper, related to the application from speech recognition domain, the need of native language recognition has been emphasized. Methodology to recognize isolated Hindi words using neural networks has been presented in this chapter. Suitable comparisons have been included to demonstrate that the proposed methodology indeed improves recognition of isolated words in our mother tongue.

Techniques for EMG Signal processing and feature extraction: A Review

Monika[1], L. M. Saini[2], and Saravjeet Singh[3]

***Abstract* - Electromyography (EMG) signal is a measure of electrical activity of muscles and can be used for numerous clinical and biomedical applications. Advanced techniques are required to detect, process and classify the EMG signal so that it could be better understood and evaluated in various applications. The aim of this paper is to present different algorithms and methodologies to analyze the EMG signal. Moreover, most complete time domain and frequency domain features are also given in this study. This study provides researchers a better understanding about EMG signal and its analysis.**

Index Terms – Electromyography, muscle, signal, feature.

I. INTRODUCTION

A. EMG signal generation

The Electromyography (EMG) signal is a biomedical signal that measures electrical potentials generated in muscle cells during its contraction. EMG represents neuromuscular activity where the nerves controls the muscular activity like contraction and relaxation. So, EMG signal is a complex signal dependent on the anatomical and physiological activity of muscles and is controlled by the nervous system [1]. Motor Units (MUs) are the basic functional blocks of the neuromuscular activity and is defined as one motor neuron and all the muscle fibers that are innervated by it. When a motor unit fires, an impulse is travelled down the neuron through the neuromuscular junction to the muscle fibers. After this an action potential is induced in all the muscle fibers that are innervated by that particular motor unit and their sum is called as Motor Unit Action Potential. The evaluation of MUs properties tends to the understanding of motor control strategies, neuromuscular disorders, myoelectric manifestations of fatigue, neuromuscular disorders, and a variety of open issues in ergonomics, geriatrics, sport, and rehabilitation medicine.

B. Processing steps for EMG signals

In figure-1 given below, a typical system to quantify the EMG signal is depicted. First, the row EMG signal is picked from the muscle of interest by using either surface or needle EMG sensors. The data acquisition device records the row EMG signal into digital form. As the row EMG signal consists of several noise and artifacts like electrical interferences, ECG artifacts, baseline drift, and motion artifacts, signal filtering is performed to remove such effects in the processing of EMG signal. Then the Time-Domain (TD) and Frequency-Domain (FD) features are extracted for better interpretation of EMG signal. The success of an EMG classification system depends on the quality of the feature selected and extracted.

[1]Monika is with Department of Biomedical Engineering, National Institute of Technology, Kurukshetra, India
[2]L. M. Saini is with Department of Biomedical Engineering, National Institute of Technology, Kurukshetra, India
[3]Saravjeet Singh is with Department of Biomedical Engineering, DCRUST, Murthal, Sonipat, India
(e-mail: monikanitadhiman@gmail.com, dsanitk@gmail.com, saravjeetsingh01@gmail.com).

II. EMG SIGNAL PRE-PROCESSING METHODOLOGIES

Row EMG signal consists of valuable information with some useless data. In clinical and biomedical fields, the quantification of the row EMG signal by analysing and processing it with some advanced methods is becoming necessary for healthcare providers. These methods will extract accurate and actual EMG signal from row EMG signal.

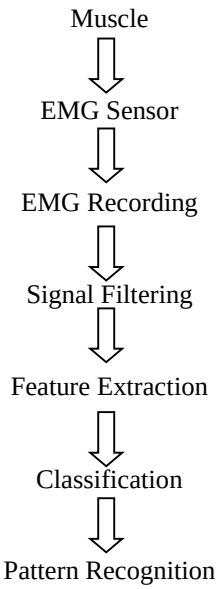

Fig. 1. An EMG quantification system.

This section reviews various EMG signal processing methods:

A. Wavelet Transform (WT)

Wavelet Transform is the mathematical function that provides the time-frequency representation of the signal. This time-frequency representation of the signal enables us to analyse the frequency components of the signal as well as the time at which they occur. In WT, the signal is passed through various high pass and low pass filters and

is decomposed to the pre-defined certain level. This will results into cluster of signals that represents the same signal but all corresponding to different frequency bands. Lower frequencies are better resolve in frequency whereas higher frequencies are better resolved in time.

WT is of two types: Continuous WT (CWT) and Discrete WT (DWT). The CWT is defined as:

$$W(m,n)= \int_{-\infty}^{+\infty} x(t) \frac{1}{\sqrt{m}} \varphi\left(\frac{t-n}{m}\right) dt \quad (1)$$

The above equation represents the convolution of the wavelet function $\varphi(t)$ with the signal $x(t)$. This results into transformed signal of two variables m and n, where m is the scale parameter and n is the translation parameter. φ is the mother wavelet and is the transforming function.

On the other hand, DWT requires lesser computational time as compared to CWT and provides requisite information for both the analysis and synthesis of the original signal. DWT decomposes the signal into a coarse approximation and detailed information and then analyses it at different frequency band with different resolutions. In DWT, the time domain signal is decomposed into various frequency bands by passing the signal through high pass filter (wavelet function) and low pass filter (scaling function). The mathematical representation of DWT is given as:

$$x(t) = \sum_{k=-\infty}^{+\infty} \sum_{l=-\infty}^{+\infty} d(k,l)\, 2^{k/2}\, \varphi(2^{-k}t - 1) \quad (2)$$

Here a = $2k$ and b = $2kl$. $d(k,l)$ is sampling of w(a,b) at discrete level k and l.

B. Wigner-Ville Distribution (WVD)

Wigner- Ville Distribution (WVD) is a time-frequency method which was introduced to overcome the problems of the spectrogram. WVD is one of the most studied and best understood of the many time–frequency methods and used extensively to quantify EMG signals [2]. This distribution was actually developed by Wigner in 1932 for use in quantum mechanics, but later applied to signal processing and spectral analysis by Ville, hence the dual name. The WVD represents the signal x(t) as a function of time with analytic associate s(t) is given as :

$$WVDx(t,\omega) = \int_{-\infty}^{+\infty} s\left(t+\frac{\tau}{2}\right) s^*\left(t-\frac{\tau}{2}\right) e^{-j\omega t}\, d\tau \quad (3)$$

Here τ is the shift of the signal with respect to itself and s^* is complex conjugate of the signal s(t) where s(t) is complex signal of x(t) given as :

$$s(t) = x(t) + iH[x(t)] \quad (4)$$

$H[x(t)]$ is the Hilbert Transform of signal x(t).

C. Higher Order Statistics (HOS)

Based on probabilistic theory, HOS is a technique to analyze and interpret the attributes of random process [3]. As the EMG signal is non-linear, other significant statistics tools like first and second order statistics are unable to extract the useful information from the EMG signal. Hence HOS are developed and introduced in the processing of EMG signals. Moments and Cumulants are the terms to define HOS of the signal. Deterministic signals are analysed by using moments and moment spectra whereas stochastic signals are analysed by using cumulant and cumulant spectra [4]. The moments and cumulants of the third order and above, are known as Polyspectra or higher order spectra in the spectral representation of Higher Order Statistics (HOS). HOS is a function of two or more frequencies and can be complex valued having phase and magnitude.

HOS is important in the diagnosis of neuromuscular function to obtain information on innervation pulse trains and Motor-Unit Action Potentials (MUAPs) characteristics.

D. Independent Component Analysis (ICA)

Also known as Blind Source Separation (BSS), ICA technique was first proposed by Comon in 1994 but Makeig et al. first applied this approach to biomedical time series analysis. The ICA algorithm has become one of the most prominent signal processing technique used for pattern recognition [5]. ICA is used to distinguish a source(s), from mixtures(x) and assumes that the activity of each source is statistically independent of the other sources i.e. the mutual information between any two sources is zero. The mixing model can be represented as:

$$x = As \quad (5)$$

In this ICA model, X is an i vector of linear mixtures given as X = $[x_1, x_2, .., x_i]^T$, S is an n-dimensional random vector of independent source signals shown as S = $[s_1, s_2, .., s_n]^T$ and A is full-rank i × j scalar linearly mixing matrix (j x i).

ICA is most popular method for source separation and EMG signal decomposition and used widely to separate and remove noise sources from EMG signal. This technique decompose EMG signals into a maximum number of independent components (IC).

E. Autoregressive Model

AR model estimates the power spectrum of the signal by using linear processes. The parameters of the AR model are adjusted to obtain the best match between interested waveform and the model output. The best estimate of the waveform's spectrum is given by frequency characteristics of the model, once the best match is obtained. In a non- stationary context, the mathematical expression for a classical AR complex process is given as:

$$X(n)= -\sum_{i=1}^{m} a(i)x(n-i) + u(n) \quad (6)$$

Here x(n) represents the model output , a(i) are complex parameters, m is the order of the AR model, u(n) is the input or noise and n is the sample time. Burg's algorithm is the most popular method to estimate the AR parameter. Selection of the model order is one of the most important aspect for the model based method.

III. EMG SIGNAL FEATURE EXTRACTION

Feature extraction stage is very critical in the EMG signal processing. By transforming the row EMG signal into a feature vector, this stage will help the classifier for better motion pattern recognition. Broadly, in the analysis of EMG signal, the features can be divided into three main groups namely Time-Domain (TD)

features, Frequency-Domain (FD) features, and Time-Frequency Domain (TFD) or Time-Scale features.

The TD features are evaluated based on EMG signal amplitude that varies with time, where the signal amplitude depends upon the muscle type and condition during observation. TD features are generally quick and easily implementable and do not require any transformation. These features have been widely used in medical and engineering applications such as for onset detection, muscle contraction, and muscle activity detection. Various TD features with their mathematical formula is given in the table as:

TABLE 1: TIME-DOMAIN FEATURES

Features	Abbreviation	Mathematical Expression	References
Integrated EMG	IEMG	$\sum_{m=1}^{M} \lvert x_m \rvert$	[6],[7]
Mean Absolute Value	MAV	$\frac{1}{M}\sum_{m=1}^{M} \lvert x_m \rvert$	[6],[8], [9],[10]
Modified Mean Absolute Value	MMAV1	$\frac{1}{M}\sum_{m=1}^{M} w_m \lvert x_m \rvert$ and $w_m = \begin{cases} 1, if\ 0.25M \le m \le 0.75M \\ 0.5, \quad otherwise \end{cases}$	[6],[10]
Modified Mean Absolute Value Type-2	MMAV2	$\frac{1}{M} \sum_{m=1}^{M} w_m \lvert x_m \rvert$ and $w_m = \begin{cases} 1, if\ 0.25M \le m \le 0.75M \\ 4m/M, \ elseif\ m < 0.25M \\ 4(m-M)/M, \quad otherwise \end{cases}$	[6],[11]
Mena Absolute Value Slope Value	MAVS	$MAVS_m = MAV_{m+1} - MAV_m$	[6],[10]
Differential Absolute Mean	DAMV	$\overline{\Delta x_m} = \frac{1}{M-1}\sum_{m=1}^{M-1} \lvert x_{m+1} - x_m \rvert$	[7],[6]
Simple Square Integral	SSI	$\sum_{m=1}^{M} {x_m}^2$	[10],[6]
Variance of EMG	VAR	$\frac{1}{M-1}\sum_{m=1}^{M} {x_m}^2$	[8],[6], [10]
Standard Deviation	SD	$\sqrt{\frac{1}{M-1}\sum_{m=1}^{M}(y_m - \bar{y})^2}$	[12],[13],[9]
Absolute Value of the 3^{rd}, 4^{th}, and Temporal Moment	TM3, TM4, and TM5	TM3 = $\left\lvert \frac{1}{M}\sum_{m=1}^{M} {x_m}^3 \right\rvert$; TM4 = $\left\lvert \frac{1}{M}\sum_{m=1}^{M} {x_m}^4 \right\rvert$; TM5 = $\left\lvert \frac{1}{M}\sum_{m=1}^{M} {x_m}^5 \right\rvert$	[12]
Root Mean Square	RMS	$\sqrt{\frac{1}{M}\sum_{m=1}^{M} {x_m}^2}$	[8],[13],[9],[6],[12]
v-order	V	$\left(\frac{1}{M}\sum_{m=1}^{M} {x_m}^V\right)^{\frac{1}{V}}$	[12]
Log Detector	LOG	$e^{\frac{1}{M}\sum_{m=1}^{M} log\lvert x_m \rvert}$	[6]
Waveform Length	WL	$\sum_{m=1}^{M-1} \lvert x_{m+1} - x_m \rvert$	[10],[8],[6]
Average Amplitude Change	AAC	$\frac{1}{M}\sum_{m=1}^{M-1} \lvert x_{m+1} - x_m \rvert$	[6]
Difference Absolute Standard Deviation Value	DASDV	$\sqrt{\frac{1}{M-1}\sum_{m=1}^{M-1}(x_{m+1} - x_m)^2}$	[8],[6]
Amplitude of The First Burst	AFB		[6]
Zero Crossing	ZC	$\sum_{m=1}^{M-1} [sgn(x_m \times x_{m+1}) \cap \lvert x_m - x_{m+1} \rvert \ge$	[10],[9]

		; and Sgn(x) = $\begin{cases}1, & if\ x \geq t\square res\square old\\ 0, & ot\square erwise\end{cases}$	
Myopulse Percentage Rate	MYOP	$\frac{1}{M}\sum_{m=1}^{M-1}[f(x_m)]$ and $f(x) = \begin{cases}1, & if\ x \geq t\square res\square old\\ 0, & ot\square erwise\end{cases}$	[6]
Willison Amplitude	WAMP	$\sum_{m=1}^{M-1}[f(\lvert x_m - x_{m+1}\rvert)]$ and $f(x) = \begin{cases}1, & if\ x \geq t\square res\square old\\ 0, & ot\square erwise\end{cases}$	[10],[14],[6]
Slope Sign Change	SSC	$\sum_{m=2}^{M-1}[f[(x_m - x_{m-1}) \times (x_m - x_{m+1})]]$ And $f(x) = \begin{cases}1, & if\ x \geq t\square res\square old\\ 0, & ot\square erwise\end{cases}$	[10],[6],[9]
Mean Absolute Value Slope	MAVSLP	$MAVSLP_k = MAV_{k+1} - MAV_k$	[6]
Multiple Hamming Windows	MHW	$MHW_k = \sum_{m=0}^{M-1}(x_m w_{m-m_k})^2$	[15],[6]
Multiple Trapezoidal Windows	MTW	$MTW_k = \sum_{m=0}^{M-1}(x_m^2 w_{m-m_k})$	[6]
Histogram of EMG Signal	HIST		[6],[16]
Auto-regressive Coefficients	AR	$x_m = \sum_{p=1}^{P} a_p x_{m-p} + w_m$	[10],[6]
Cepstral	CC	$c_p = -a_p - \sum_{m=1}^{p-1}\left(1 - \frac{m}{p}\right)a_p a_{p-m}$	[7], [6]
Coefficients			

The Frequency-Domain (FD) features are generally used for the analysis of muscle fatigue and MU recruitment. By using PSD of the signal, in FD analysis, various statistical properties were applied to PSD. It can be calculated by using either Parametric methods or Periodogram. Various TD features with their mathematical formula is given in the table as:

TABLE 2: FREQUENCY-DOMAIN FEATURES

Features	Abbreviation	Mathematical Expression	References
Mean Frequency	MNF	$\sum_{m=1}^{M}(f_m P_m) \Big/ \sum_{m=1}^{M}(P_m)$	[9],[10]
Median Frequency	MDF	$\sum_{m=1}^{MDF} P_m = \sum_{m=MDF}^{M} P_m = \frac{1}{2}\sum_{m=1}^{M} P_m$	[10]
Features	Abbreviation	Mathematical Expression	References
speak Frequency	PKF	max(P_m)	[6]
Manpower	MNP	$\sum_{m=1}^{M} P_m \Big/ M$	[6]
Total Power	TTP	$\sum_{m=1}^{M} P_m$= SM0	[12[6]
The $1^{st}, 2^{nd},$ Spectral Moments	SM1, SM2, and SM3	SM1 = $\sum_{m=1}^{M} P_m f_m$; SM2 = $\sum_{m=1}^{M} P_m {f_m}^2$; and SM2 = $\sum_{m=1}^{M} P_m {f_m}^3$	[6]
Frequency Ratio	FR	$\sum_{m=LLC}^{ULC} P_m \Big/ \sum_{m=LHC}^{UHC} P_m$	[6]
Power Spectrum Ratio	PSR	$\frac{P_0}{P} = \sum_{m=f_0-n}^{f_0+n} P_m \Big/ \sum_{m=-\infty}^{+\infty} P_m$	[6]
Variance of Central Frequency	VCF	$\frac{1}{SM0}\sum_{m=1}^{M} P_m(f_m - f_c)^2 = \frac{SM2}{SM0} - \left(\frac{SM1}{SM0}\right)^2$	[6]
Hjorth Activity	Hjorth-1	${\sigma_x}^2 = \frac{1}{M}\sum_{m=1}^{M}(x_m - \bar{x})^2$	[8]
Hjorth Mobility	Hjorth-2	$\frac{\sigma_{x'}}{\sigma_x}$	[8]

Hjorth Complexity	Hjorth-3	$\frac{\sigma_{x'''}/\sigma_{x'}}{\sigma_{x''}/\sigma_{x}}$	[8]

IV CONCLUSION

As the EMG signals presents useful information so their analysis with the advanced and powerful technique has become an essential requirement for the healthcare providers in various clinical and medical field. This paper provides information about the EMG signal and the methodologies for analyzing it in order to extract the useful information from the EMG signals. This study emphasizes different techniques that are used for EMG signal processing. Moreover, most complete Time-Domain and Frequency-Domain features available for EMG signal also are presented in this paper. It will benefit the researchers in selecting the best technique for EMG signal analysis in wide areas of biomedical and clinical end user applications.

REFERENCES

[1] M. B. I. Reaz, M. S. Hussain, and F. Mohd-Yasin, "Techniques of EMG signal analysis: Detection, processing, classification and applications," Biol. Proced. Online, vol. 8, no. 1, pp. 11–35, 2006.

[2] A. Subasi and M. K. Kiymik, "Muscle fatigue detection in EMG using time-frequency methods, ICA and neural networks," J. Med. Syst., vol. 34, no. 4, pp. 777–785, 2010.

[3] K. C. Chua, V. Chandran, U. R. Acharya, and C. M. Lim, "Application of higher order statistics/spectra in biomedical signals-A review," Med. Eng. Phys., vol. 32, no. 7, pp. 679–689, 2010.

[4] M. Sanaullah, "A Review of Higher Order Statistics and Spectra in Communication Systems A Review of Higher Order Statistics and Spectra in Communication Systems A Review of Higher Order Statistics and Spectra in Communication Systems," Glob. J. Sci. Front. Res. Phys. Sp. Sci., vol. 13, no. 4, 2013.

[5] R. Chowdhury, M. Reaz, M. Ali, A. Bakar, K. Chellappan, and T. Chang, "Surface Electromyography Signal Processing and Classification Techniques," Sensors, vol. 13, no. 9, pp. 12431–12466, 2013.

[6] A. Phinyomark, P. Phukpattaranont, and C. Limsakul, "Feature reduction and selection for EMG signal classification," Expert Syst. Appl., vol. 39, no. 8, pp. 7420–7431, 2012.

[7] S. H. Park and S. P. Lee, "EMG pattern recognition based on artificial intelligence techniques.," IEEE Trans. Rehabil. Eng., vol. 6, no. 4, pp. 400–405, 1998.

[8] W. Caesarendra and D. Pamungkas, "EMG based Classification of Hand Gestures using PCA and ANFIS," pp. 18–23, 2017.

[9] M. Jahan, M. Manas, B. B. Sharma, and B. B. Gogoi, "Feature extraction and pattern recognition of EMG-based signal for hand movements," 2015 Int. Symp. Adv. Comput. Commun. ISACC 2015, pp. 49–52, 2016.

[10] A. Phinyomark, S. Hirunviriya, C. Limsakul, and P. Phukpattaranont, "Evaluation of EMG feature extraction for hand movement recognition based on Euclidean distance and standard deviation," Electr. Eng. Comput. Telecommun. Inf. Technol. (ECTI-CON), 2010 Int. Conf., pp. 856–860, 2010.

[11] S. Negi, Y. Kumar, and V. . Mishra, "Feature Extraction and Classification for EMG Signals Using Linear Discriminant Analysis," Adv. Comput. Commun. Autom. (Fall), Int. Conf., pp. 1–6, 2016.

[12] K. Mahaphonchaikul, D. Sueaseenak, C. Pintavirooj, M. Sangworasil, and S. Tungjitkusolmun, "EMG signal feature extraction based on wavelet transform," Electr. Eng. Comput. Telecommun. Inf. Technol. (ECTI-CON), 2010 Int. Conf., no. 1, pp. 327–331, 2010.

[13] W. M. B. W. Daud, A. B. Yahya, C. S. Horng, M. F. Sulaima, and R. Sudirman, "Features Extraction of Electromyography Signals in Time Domain on Biceps Brachii Muscle," Int. J. Model. Optim., vol. 3, no. 6, pp. 515–519, 2013.

[14] F. Tenore, A. Ramos, A. Fahmy, S. Acharya, R. Etienne-Cummings, and N. V. Thakor, "Towards the control of individual fingers of a prosthetic hand using surface EMG signals," Annu. Int. Conf. IEEE Eng. Med. Biol. - Proc., pp. 6145–6148, 2007.

[15] Sijiang Du and M. Vuskovic, "Temporal vs. spectral approach to feature extraction from prehensile EMG signals," Proc. 2004 IEEE Int. Conf. Inf. Reuse Integr. 2004. IRI 2004., pp. 344–350.

[16] A. Phinyomark, C. Limsakul, and P. Phukpattaranont, "A Novel Feature Extraction for Robust EMG Pattern Recognition A Novel Feature Extraction for Robust EMG Pattern Recognition," vol. 1, no. January 2016, pp. 71–80, 2009.

Automatic Isolated Hindi Words Recognition Using Neural Networks

Ashok Kumar[1] and Vikas Mittal[2]

***Abstract*- Speech is basic form of communication between human beings. Speech recognition is a process to convert speech sound to corresponding text. Speech recognition technology has been developed to a large extend in last few years. But speech recognition in native languages is still in developing stage. MATLAB's neural network toolbox is a complete package for analysis of different characteristics in various domains. The objective of this paper is to recognize isolated words in Hindi Language using MATLAB neural network tool box and analyze it for improved speech recognition characteristics.**

Keywords—Feature extraction, MATLAB, Modeling, Speech processing, Speech recognition, Training & Testing.

I. INTRODUCTION

Speech recognition, also known as Automatic Speech Recognition (ASR) is the process of converting speech signal to a sequence of words by means of an algorithm implemented as a computer program. Speech processing is one of the major fields of signal processing. Speech recognition area aims at to develop techniques for speech input to machine [1]. The early computer systems were limited in scope and power. But the revolution in computer technology has evolved the field of automatic speech recognition. Now-a-days it's easy to store huge database for speech recognition due to advancement in computer technology. Language is basic medium for communication so it's better to expect human computer interfaces in native languages [2]. Recognition of speech by machine involves matching of different generated sequence of words. Speech recognition includes various applications like travel information and reservation, natural language understanding and translators etc [3], [4].The research in multilingual speech recognition is gaining much importance in different fields. MATLAB's neural network tool box is a complete software package for performing research in different domains. Here, MATLAB R2012b, neural network tool box is used for analyzing different parameter of speech in native language Hindi.

II. SPEECH RECOGNITION SYSTEM

The speech sound is captured using microphone to convert it into electrical signal. The purpose of sound card inside the computer is to change analog signal into digital signal. Sound card has capabilities to store and play this speech signal. There are following building blocks for general speech recognition system [5].

- Signal preprocessing
- Feature extraction
- Language modeling
- Decoder

A. Signal preprocessing

Speech signal captured by microphone, telephone are analog in nature so required to be digitized as per Nyquist theorem. This theorem states signal is to be sampled more than twice the rate of highest frequency present in the speech signal. Generally sampling frequencies for speech signal are 8 KHz and 20 KHz. [6].

B. Feature extraction

Feature extraction is used to find a set of properties that are stable and acoustically correlated to each other. So it is a type of parameterization of speech signal. Such parameters can form the observation vectors. Linear predictive cepstral coefficients (LPCC), Mel Frequency Cepstral Coefficients (MFCC) and PLP are some of important features extraction technique out of them [7].

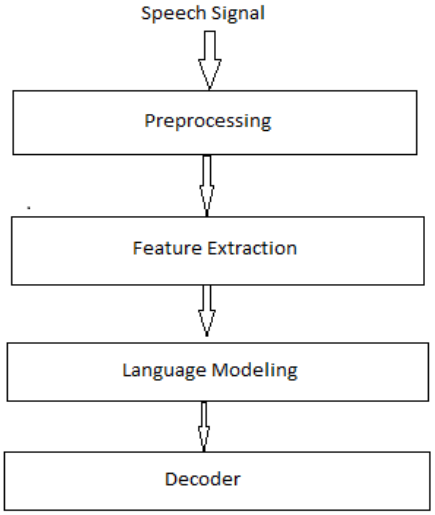

Fig.1. Basic working of Speech recognition system

C. Language modeling

Language modeling is used to find correct word sequence by predicting nth words using (n-1) preceding words. Language modeling is of various types.

[1]Ashok Kumar is with Department of Electronics and Communication Engineering, National Institute of Technology, Kurukshetra, India
[2]Vikas Mittal is with Department of Electronics and Communication Engineering, National Institute of Technology, Kurukshetra, India
(e-mail: ashokgiri010@gmail.com, vikasmittalkkr@gmail.com).

- Uniform model: where occurrence of each word is equally probable.
- Stochastic model: probability of present word depends on probability of word preceding it.
- Finite state languages: language use finite state network to define allowed word sequence.
- Context free grammar: It is used to encode allowed sequence [8].

D. Decoder

This stage is involved to find out most likely word sequence for the given observation sequence. Generally dynamic programming algorithms are used to solve this problem. The purpose of these algorithms is to search single path through the network to have best match for the given sequence, Viterbi algorithm is mostly used for this purpose. In case of large vocabulary, a beam search method is useful for Viterbi iteration [9].

III. TYPES OF SPEECH RECOGNITION

Speech recognition systems can be of various types depending on types of utterances to recognize. These various types are classified as follows:

A. Isolated Words

Isolated word recognizers generally obtain each utterance to have quiet on both sides of sample window. These systems usually have two states Listen/Not- Listen states, where speaker has to wait between two utterances. The pauses between utterances are used for processing speech signals.

B. Connected Words

Connected words are similar to isolated words with only difference of minimal pause between them.

C. Continuous Words

Continuous speech recognition involves almost natural way of speaking. It is difficult to design continuous speech recognizers because it considers special methods to determine utterance boundaries [10].

D. Spontaneous Words

Spontaneous speech covers the mispronounced, unrehearsed non-words with false statements which are difficult to read [11]. An ASR system under this category is to handle a variety of features such as words being run together such as "ums" and "ahs" [12].

IV. EXPERIMENTATION, ANALYSIS & RESULTS

A. Recording of Voice

```
>> Voice_Rec_Pre(1500)
Enter the File Name: 1
Press y To Record:
```

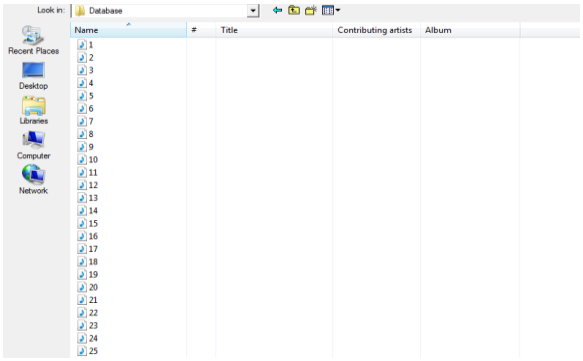

Fig. 2. Total 25 voice samples are recorded

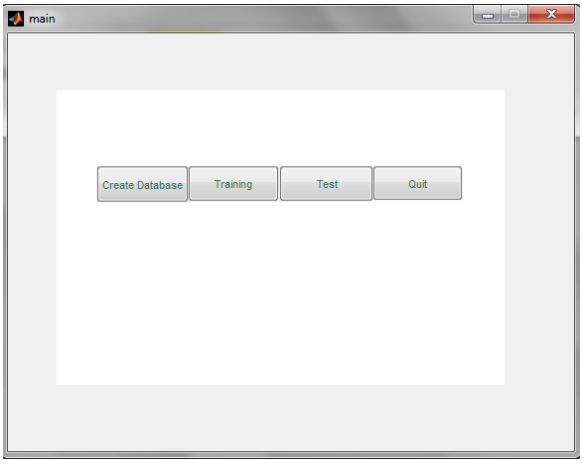

Fig.3 GUI for creating database, Training & Testing

B. Database Creation

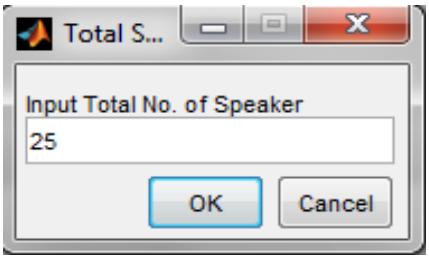

Fig. 4. Total No. of Speakers

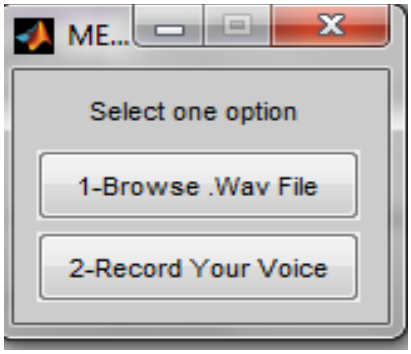

Fig. 5. Selecting Option

For database creation Total No. of Speakers is set to 25. Two options are provided either to select recorded voice file or real time voice.

C. *Preprocessing and Feature Extraction*

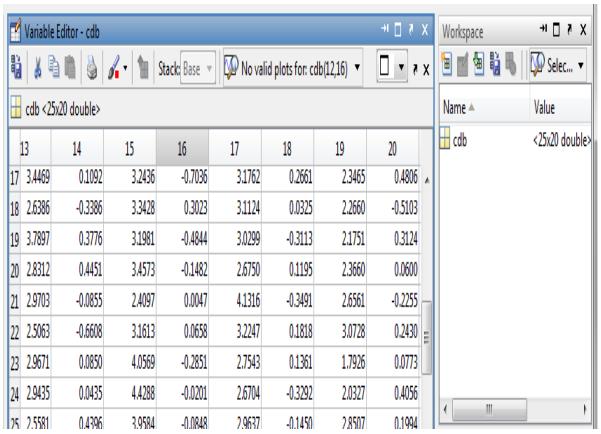

Fig. 6. Workspace Values

Speech pre-processing includes several steps as: (1) Noise detection and elimination, (2) Pre-emphasis, (3) Framing (4) Windowing etc. In pre-emphasis step speech signal is filtered with a first order FIR filter with pre-emphasis parameter value. After that framing and windowing is done.

Size of Feature matrix is 25*20. Here 25 is no. of samples and 20 are the extracted features. First 10 are MFCC and next 10 are PLP.

D. *Training*

A multi-layer perceptron with many hidden layers is used for training.

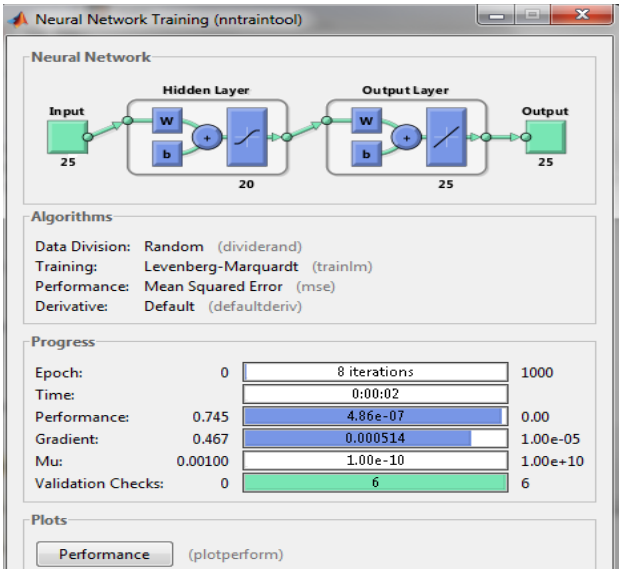

Fig.7. Neural Network Training

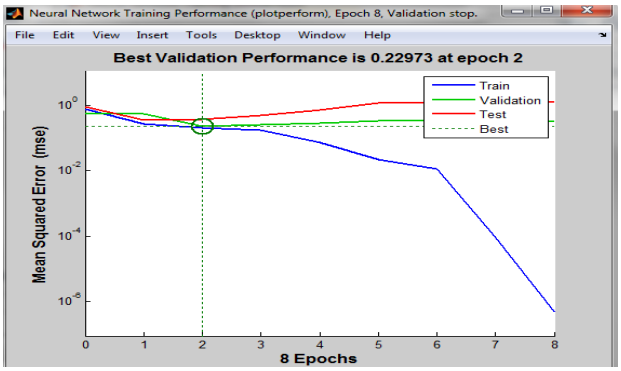

Fig.8. Neural Network Training Performance

The above figure shows neural network training performance.

E. *Testing*

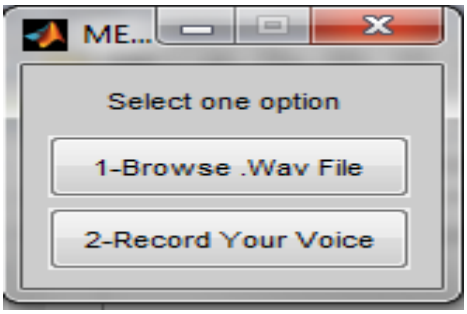

Fig.9. Select one option

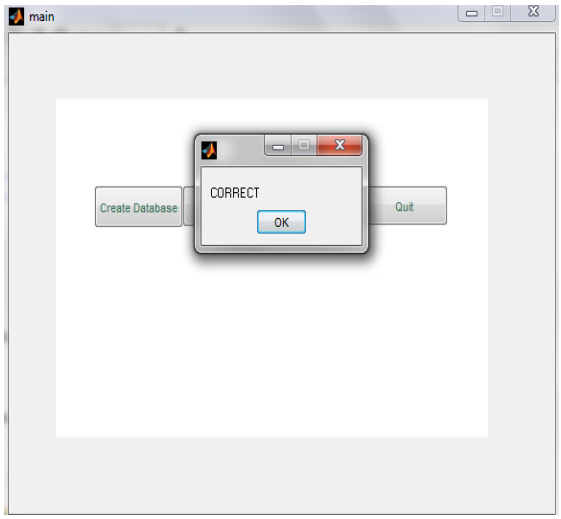

Fig.10. Testing

For testing any recorded file from database or real time voice can be tested.

V. CONCLUSION

Speech recognition can be of many types depending upon its utterances like isolated, connected & continuous etc. Isolated word recognition is based on recognition of separated words. But situation becomes complex when this recognition is done for continuous words due to complex boundaries and pauses. So extended work can

associate with hybrid feature extraction techniques along with DNN for recognizing continuous word.

REFERENCES

[1]S. K. Gaikward et.al, "A review on speech recognition technique", International journal of Computer Applications, vol. 10, no. 3, pp. 16-24, November 2010.

[2] K. Samudravijaya, "Speech and Speaker recognition tutorial" TIFR Mumbai 4000005.

[3] W. M. Campbell, D. E. Sturim et.al, "The MIT- LL/IBM speaker recognition system using high performance reduced complexity recognition" MIT Lincoln Laboratory IBM 2006.

[4] K. Brady, M. Brandstein et.al, "An evaluation of audio-visual person recognition on the XM2VTS corpus using the Lausanne protocol", MIT Lincoln Laboratory, 244 Wood St., Lexington MA.

[5] D. Shweta, M. Rajni, "Speech Recognition Techniques: A Review", International journal of advanced research in computer science and software engineering, vol. 4, issue 8, August 2014.

[6] K. Kuldeep, Aggarwal, R. K., "A Hindi speech recognition system for connected words using HTK", Int. J. Computational systems Engineering, vol. 1, No. 1. , Haryana, India, 2012.

[7] D. Mayank, Aggarwal, R. K., "Implementing a speech recognition system interface for Indian languages", proc.of the IJCNLP-08 workshop on NLP", pp. 105-112, Hyderabad, India, January 2008.

[8] S. Preeti, K. Parneet, "Automatic Speech Recognition: A Review", International journal of engineering trends and technology, vol. 41, Issue 2, Haryana India, 2013.

[9] S. Karpagavalli and E. Chandra, "A review on automatic speech recognition architecture and approaches", International journal of signal processing, image processing and pattern recognition", Vol. 9, No. 4, pp. 393-204, Coimbatore, India, 2016.

[10] Sanjivani S. Bhabad, Ganjana K. Kharate, "An overview of technical progress in speech recognition",

[11] S. Shaikh Naziya, R. R Deshmukh, "Speech recognition system – A review", IOSR journal of Computer engineering (IOSR-JCE), vol.18, Issue 4, pp. 1-9, Aurangabad, India, (Jul.-Aug. 2016).

[12] A. Megha, T. Raikhwar, "Speech recognition using signal processing techniques", International journal of engineering and innovative technology (IJEIT), vol. 5, Issue 8, February 2016.

Application in Navigation:

Navigational aids are being used by one and all in day-to-day life. For example, Google Map is one such application which is ubiquitous these days. Other applications include surveillance and security of the country. Navigation technology is emerging as state-of-the-art as supported by launch of numerous satellites.

Signal processing in navigational systems introduces us to the generalized approach leading later to its theory and applications. Ultimate goal is to enhance noise immunity of the systems leading to better detection performances. Classically, and even in modern times, noise immunity has been enhanced based on statistic of mean of the likelihood function alone or joint statistic of its mean and variance. Signal Processing is common platform to serve these kinds of high-end applications.

Nowadays, global positioning system (GPS) is mainstay for all kinds of navigational needs. It is used for military purpose, farming technologies, civil, transportation and many more uses. GPS is a satellite navigation system using which location and time information can be provided to the user irrespective of the climatic or weather conditions. It is a unified platform providing continuous real time, 3-dimensional positioning, navigation and timing services to the whole world. It consists of three segments; Space segment, control system and user segment.

There are many sources of possible errors in the location and tracking applications provided by GPS receiver such as atmospheric effects, noise, distortion, information about satellite orbits, variations in the on-board atomic clocks, multipath effects etc. Some the desired characteristics of a typical GPS based system are; better positioning accuracy, enhanced availability and reliability, fine tuned trajectories, greater data security and integrity requirements etc.

Many applications which need high accuracy position estimates malfunction due to errors in GPS estimates. Accuracy in position estimates is a reflection on the system's capability of providing quality performance which in turn depends on, among other factors, measurement noise and used algorithm. Out of numerous existing algorithm, Kalman filter has emerged a winner due to its exceptional performances in a wide range of real time applications. It has faster convergence rate and high accuracy. One such application is to estimate the position of a vehicle using GPS. Greater accuracy is achieved in vehicle position estimation using Kalman filter based on its initial state. It has also been applied in fusing the data from dynamic systems aimed at controlling the influence of system model uncertainties. Other applications include development of performance-enhanced GPS receivers that are more flexible and easier to develop than their FPGA or ASIC based counterparts.

One such paper titled ***A review: Position estimation of an object using Kalman filter algorithm based on GPS system*** has been included in this section where an exhaustive review has been presented on obtaining estimates of an object position using a GPS based system. It has been demonstrated that how various errors in GPS devices measurements are reduced by using Kalman filtering algorithm in real applications. Iterative least square method is also used to improve the estimates.

A Review: Position Estimation of an Object using Kalman Filter Algorithm Based on GPS System

Akash Deep[1], Monika Mittal[2], Vikas Mittal[3]

***Abstract*— Over the past few years Kalman filter has gained attraction and its significance among the researchers, as this filtering technique can be applied to variety of application. One of its application which is studied in this paper is GPS based system application. The GPS devices used for position determination are not very accurate. They include are many sources of error. Signals received by the GPS devices often suffer from atmospheric effect, multipath effect, clock errors, interference from radio signal. This paper presents a review on how GPS signal accuracy can be improved with the help of Kalman filter and iterative least square method.**

Keywords—Kalman filter;Extended Kalman filter (EKF) ; GPS; Standard Position Services(SPS); Precise Position Services(PPS); Geometric dilution of precision(GDOP);Total electron content(TEC);Earth-Centered Earth-Fixed (ECEF).

I. INTRODUCTION

The Global Positioning System (GPS) was first introduced by US department of defense in 1973. Its space based radio navigation system owned by United States government [2]. It is a satellite navigation system used for providing geolocation and time information to a GPS receiver present anywhere on earth where there is direct path between GPS receiver and the satellite. GPS services are of two types 1) Standard Position Services (SPS). 2) Precise Position Services (PPS). The former is for civilians and the latter is for military purposes. The SPS freely available to unlimited users all around the world. It has an accuracy of 100m in horizontal plane and 156m in vertical plane. The PPS is primarily intended for military and other government agency. It has an accuracy of at least 22m in horizontal and 27m in vertical [2].

Devices with GPS-enabled are growing rapidly nowadays. A large sector of this growth is due to the emergence of smartphone. Some simple location-based application require, rough position estimate while other application such as navigation is directly connected with accuracy of GPS positioning. The standard positioning service of GPS technology is available 24 hours per day. The accuracy of this service is thus not consistent, varying on no. of satellite time of the day and place. Buildings can block or reflect the signals, atmosphere delays it, satellite clock and an orbit error introduces some difference in time. Many times we run into application where high accuracy of GPS positioning is needed, there this simple SPS services would not provide fruitful results. Thus some different methodology should be adopted as a means of improving GPS positioning.

[1]Akash Deep is with Department of Electrical Engineering, National Institute of Technology, Kurukshetra, India
[2]M. Mittal is with Department of Electrical Engineering, National Institute of Technology, Kurukshetra, India
[3]Vikas Mittal is with Department of Electronics and Communication Engineering, National Institute of Technology, Kurukshetra, India
(e-mail: mail2deep.akash@gmail.com, monika_mittalkkr@rediff.com, vikas_mittal@nitkkr.ac.in)

II. ERROR IN GPS SIGNALS

The GPS satellite signal is subjected with various disturbances before reaching the receiver. These disturbances degrade the signal, decreasing the pseudo range accuracies and thus the overall obtained position estimate. Some of the errors in GPS signals are listed below.

1. Geometric dilution of precision

The geometry of how the satellite arranged in their orbits with respect to the receiver has an effect on position estimation. The perfect situation is when, one satellite on top and the remaining satellite dispersed evenly around the receiver near the surface. Satellite grouped together would yield nearly equal pseudo range estimates and will not provide sufficient information. The effect of how the satellites are placed in the orbit is called geometric dilution of precision (GDOP) [4, 12].

2. *Emphemeris errors*

The positions of satellite are effected by the solar radiation and the gravitational pull of the sun and the moon, thus disturbing their orbital position. These changes can be observed by the control segment from the monitor station placed at known location. The predicted error on the satellite orbit position is of the range 1-6m. The average pseudo range error due to ephemeris prediction error is about 0.8 m [4].

3. Satellite clock errors

The atomic clocks placed on the satellite are very accurate and precise, but small bias do occur over time. This changes leads to huge effect on the location estimate error margin if not eliminated. For example an error of 10ns in atomic clock results in 3m range error at the receiver. This deviation in atomic clock is closely monitored by observation facilities in the control segment. It is difficult to synchronize the time across all the satellite, thus a clock correction data is generated and sent along the GPS message so that the receiver can correct for the clock bias [4].

4. Atmospheric errors

Signal from satellite passes through different layers of the atmosphere that affects its speed. Factors such as refractive index of the medium through which the signal propagated, and the distance of air mass the signal must pass through before it reaches the receiver. Satellite present nearer to the horizon relative to receiver experience large amount of air mass compared to the satellite at larger angles. Given the rough position estimate and some metrological parameters this error can be modeled and largely compensated for [4].

5. *Ionospheric errors*

The ionosphere, ranging from 85km of the earth's surface up to 1000km, consisting of ionized gases by solar radiation. These ionized gases disperse the GPS signal. The error in the signal is proportional to amount of ionization suffer due to dispersion, or the total electron content (TEC). The TEC varies depending on latitude and the amount of solar radiation. The Ionospheric error mainly decreases transmission speed of the signal, causing a delay. By comparing the different times of arrival of the L_1 and L_2 frequency, the ionospheric delay error can be estimated and compensated for higher accuracy [4].

6. *Multipath effects*

Multipath error is caused when the GPS signal received by the receiver is not only directly from the satellite, but also from reflected and diffracted from the local objects. These multipath error disturbs the pseudo range measurement, since the multipath signal take longer time to reach than the direct path, thus affecting the positioning accuracy. The amount of error not only depends on the time delay also on the power of multipath signal received compared to the direct signal. In order to reduce multipath error, an antenna that only records the incoming signal from where the signal is expected to arrive should be used [4, 13].

III. LITERATURE REVIEW

Peter H. Dana (1997) in his work illustrated the Global Positioning System (GPS) operation and basic features of GPS and also emphasized on the GPS errors as they are faced by user [2]. An overview of receiver types, principal and receiver tasks gives the support to understanding the time transfer techniques of GPS. The modern receiver improvement and needs of GPS frequency and time receivers are described. The accuracies served by different time transfer techniques are analysis. The global standard for GPS to trace throughout the world by the user applications is described. GPS time propagation failure modes that cause failure of space craft, receivers and other control problems are outlined [12].

Mohinder S. Grewal and Angus P. Andrews (2001) in their book introduced the necessary background on linear systems, modeling and stochastic processes [3]. Detailed examples of application in linear optimal filters and predictors probability where given. Also, represented the Kalman filter historical background and the many more practical ways of implementation included: aspects of solving the problem in a mathematical model, oversee the estimator performance as it is concerned with model parameters, how to implement the mechanization equations in numerically stable algorithms, analyzed its appliance requirements, test the results validity, and monitored the filter performance in operation [1].

Dan Simon (2001) presented the basic concepts that needed to be known in the design and implementation of a Kalman filter. Introduced Kalman filter algorithm and the use of this filter to solve a vehicle navigation problem. Kalman filtering worked as a tool to obtain the reliable estimated position of the moving vehicle. Kalman is not only theoretical but also practical attractive tool, because it minimizes the variance in estimated error among all other filters. He gave description of Kalman filter equations and algorithm, further more explains the historical perspective of Kalman filter, showed vehicle position and velocity errors with the help of graphs [11].

Greg Welch and Gary Bishop (2001) introduced and gave the description about discrete Kalman filter. Kalman filter algorithm containing time and measurement update equations was also described in details. In their work, they presented the process model, filter equations and tuning of Kalman filter parameters. It was shown that the selection of parameters P, Q and effects it has on changing the value of R on the measurements. For nonlinear process, the basic operation of an extended Kalman filter was also presented [14].

Maria Isabel Ribeiro (2004) derived the Kalman filter and the Extended Kalman filter dynamics. It was shown that the Kalman filter is a discrete time linear, optimal, time-varying system that calculates the estimated states and minimizes the mean-square error. The Kalman filter dynamics followed the consecutive cycles of prediction and filtering. Derived steady state filter and the steady state gain at which Kalman filter dynamics converges under additional conditions on the system dynamics. Introduce the process that contained the novel information associated with the filter transmitted using last system measurement to estimate the state [9].

Kosanam, Srikiran, and Daniel J. Simon (2004) described the robustness of Kalman filter against measurement and process noise. An alternate robust Kalman filter was proposed which dealt with uncertainties better than the standard Kalman filter. Earlier researchers have worked only on the statistics rather than assuming any bounds on the uncertainties in covariance's. Some preceding results were shown for aircraft gas turbine engine, where efficiencies of fan, compressor, high and low pressure of turbine airflow and enthalpy changes were calculated when the covariance was changed zero, it was observed that, the standard Kalman filter performs better than the robust Kalman filter. However, with more changes in the covariance, the robust filter gains more and more performance in comparison to the standard Kalman filter [8].

Matthew Lashley (2006) introduced the several new tracking algorithms based on Kalman filter for software

GPS receivers in alternative to traditional Delay Lock Loops (DLL) and Costas loops used to track Pseudo-Random Noise (PRN) signals and carrier signals of navigation messages broadcast by GPS satellites respectively. The Extended Kalman Filter (EKF) is used to track the PRN sequence and to estimate position of the user in the Earth-Centered Earth-Fixed (ECEF) coordinate frame. The researcher used a Spirent GPS simulator to collect the data and the collected data was used to show outperform of traditional tracking methods by the new algorithms based on Kalman filter [7].

Cesar Barrios and Yuichi Motai (2011) used Kalman filter to estimate the future position of the vehicle. Many small models of Kalman filters were used to cover all possible position in which an automobile can be found 3s ahead. Inaccuracies in different possible states such as constant locations, velocity, acceleration, and constant jerks dealt with comprehensive Kalman filters (KFs). The Kalman filter can be used as the part of interacting-multiple-model (IMM) system which provides the future prediction of location of automobile [10].

Srinivasaiah B, Tiwari R, Dhinagar S (2014) focused on getting accuracy within few meters for position solution, using kinematic based position estimation algorithm. Raw GPS data acquired by tracing a trajectory and further processed using estimation algorithm. Recursive least square approach resulted in a poor accuracy and error of about 10m-15m. Subsequently, Kalman filter algorithm improved the overall accuracy of the kinematic system. Hence Kalman filter algorithm was found to be smoother with error within 5m in situation of occasional GPS outages [6, 3].

Jakkaraju P Kumar, Namit R, Uma Maheswari (2015) in their work found that when the GPS signal are weak, the receivers can no longer process the navigation data unless the code and the carrier comes in lock again. Thus the receiver fails to estimate the user's position until the signal becomes strong. Kalman filter with its recursive property provides greater estimation of phase/frequency of the incoming received signal with the initial state of the system, and the process and measurement noise errors. Thus it is shown that the tracking channel with Kalman filter provide better estimate for tracking [5].

IV. METHODOLOGY

The prime motivation behind this work is to develop an algorithm that minimizes the errors and provide the most accurate position determination solution. The proposed algorithm is such, as to provide better navigation solution than the simple GPS navigation solution.

1. LEAST SQUARES

One of the popular way to estimate user's position and clock bias is to used recursive least square approach. This approach requires a predetermined or supposed estimate of user's position and clock bias [6, 7]. The pseudo range formulas are in general non-linear. Thus linearizing them about the supposed values and solving the resulting linear system of equation produces improvement in the user's position and clock bias. These improvements are added to the initial estimate. The corrected estimates are then used to linearize the pseudo range equation as the previous initial estimate. Corrections are again solved for to produce a further refined estimate of the user's position and clock bias. This recursive process goes on till the estimated user's position and clock bias approach a constant value.

The pseudo range measured from the n^{th} satellite is expressed as shown

$$p_i=\sqrt{(x_n - x_m)^2 + (y_n - y_m)^2 + (z_n - z_m)^2} + ct_u \quad (1)$$

$$p_i = f(x_m,y_m,z_m,t_m) \quad (2)$$

$$f(x_m,y_m,z_m,t_m) = f(\hat{x}_m + \delta x_m, \hat{y}_m + \delta y_m, \hat{z}_m + \delta z_m, \hat{t}_m + \delta t_m) \quad (3)$$

The pseudo range of a specific satellite is a nonlinear function of the user's position and clock bias[7]. This function, of the user's position and clock bias, can be rewritten as a function of a nominal trajectory $(\hat{x}_m, \hat{y}_m, \hat{z}_m, \hat{t}_m)$ and the error term $(\delta x_u, \delta y_m, \delta z_m, \delta t_m)$ about the nominal trajectory.

The pseudo ranges can then be approximated by a first order Taylor series about the nominal trajectory. Truncating the Taylor series at the first order produces a linear system of equation, shown below in the equation.

$$p_n \approx \hat{p}_n - \frac{x_n-\hat{x}_m}{\hat{r}_n}\delta x_m - \frac{y_n-\hat{y}_m}{\hat{r}_n}\delta y_m - \frac{z_n-\hat{z}_m}{\hat{r}_n}\delta z_m + c\delta t_m \quad (4)$$

where,

$$\hat{p}_n = \sqrt{(\hat{x}_n - x_m)^2 + (\hat{y}_n - y_m)^2 + (\hat{z}_n - z_m)^2} + c\hat{t}_m \quad (5)$$

$$\hat{r}_u = \hat{p}_u - c\hat{t}_u \quad (6)$$

The linearized pseudo range equation for each satellite can be rearranged into a cosine matrix formulation, presented below $p_n - \hat{p}_n \approx \frac{x_n-\hat{x}_m}{\hat{r}_n}\delta x_m - \frac{y_n-\hat{y}_m}{\hat{r}_n}\delta y_m - \frac{z_n-\hat{z}_m}{\hat{r}_n}\delta z_m - c\delta t_m$ (7)

$$p_n \approx \alpha_{x,n}\delta x_m + \alpha_{y.n}\delta y_m + \alpha_{z,n}\delta z_m - ct_m \quad (8)$$

$$\begin{bmatrix}\delta p_1 \\ \vdots \\ \delta p_n\end{bmatrix} \approx \begin{bmatrix}\alpha_{x,1} & \alpha_{y,1} & \alpha_{z,1} \\ \vdots & \vdots & \vdots \\ \alpha_{x,n} & \alpha_{y,n} & \alpha_{z,n}\end{bmatrix} \begin{bmatrix}\delta x_m \\ \delta y_m \\ \delta z_m \\ \delta t_m\end{bmatrix} \quad (9)$$

$$\Delta p = H\Delta x \quad (10)$$

Using the matrix interpretation of the linearized pseudo range measurements, the vector of correction terms Δx can be solved. In the case of four pseudo range measurement, this is achieved by inverting the H matrix when more than four pseudo range measurements are used, the system of equation is solved using the Moore-Penrose pseudo range, as shown below in equation.

$$\Delta x = H^{-1}\Delta p \text{ when } i = 4 \quad (11)$$

$\Delta x = (H^T H)^{-1} H^T \Delta p$ when i > 4 (12)

i = no of satellite

The vector of correction is then added to the initial nominal trajectory to produce a second, refined estimate of the user's position and clock bias. These new estimate can then be used to produce more accurate of position by repeating the process. The least squares approach frequently used and can also produce an estimate of the accuracy of the position solution.

2. KALMAN FILTER

A Kalman filter is an ideal estimator which infers parameters of interest from indirect, inaccurate and uncertain observation. It is a recursive data processing algorithm which takes a series of data observed over time, which is perturbed by noise and other inaccuracies for the estimation of unknown variables of interest with more accuracy. It was proposed by R.E Kalman in 1960[1]. Practically it is one of the greatest discoveries in the history of estimation theory. It's most important application is control of complex dynamic systems such as manufacturing process, aircraft, spacecraft or ships. To control such complex system one must infers what it is doing. For such systems it's not always possible to determine every state variable you want to control, and the Kalman filter provides the means for getting the unknown data from the noisy measurements.

This method revolves between two steps, prediction stage and the measurement update stage [9]. In the prediction stage the system states is predicted forward in time using a model based prediction, given the present system state as input. In the measurement update stage the forecasted stage is corrected using a weighted average of noisy sensory input based on the noise and estimated confidence for each sensor.

Let a nonlinear system represented by following state space equations

$$x_{t+1} = A_t x_t + B_t u_t + v_t \quad (13)$$

$$z_t = H_t x_t + w_t \quad (14)$$

where the random variable $v_t and\ w_t$ are process and measurement noise, respectively. Both the process noise and measurement noise are assumed to be white, Gaussian and independent [3, 9]. The normal probability distribution of these noises is known to be

$P(v) \sim N(0,Q)$ (15)

$P(w) \sim N(0,R)$ (16)

The n*n system matrix A in equation (13) relates the earlier state at instant t-1to the present state t, in the absence of either input function or process noise. The n*1 matrix B relates the control input to the predicted state x. The H matrix in the measurement equation gives the relation between states and the corresponding measurement z_t.

Kalman filter equation given as

Table: 1

Prediction Step	Measurement update/Correction step
State vector is given by $\hat{x}_{t(-)} = \emptyset \hat{x}_{t-1(+)}$	Kalman gain is given by, $K_t = P_{t(-)} H_t^T (H_t P_{t(-)} H_t^T + R_t)^1$
Covariance matrix is given by $P_{t(-)} = \emptyset_t P_{t-1(+)} \emptyset_t^T + Q_{t-1}$	State estimation is given by, $\hat{x}_{t(+)} = \hat{x}_{t(-)} + K_t(z_t - H_t \hat{x}_{t(-)}$ Corrected covariance matrix is given by, $P_{t(+)} = P_{t(-)} - K_t H_t P_{t(-)}$

$P_{t(-)}$ and $\hat{x}_{t(-)}$ are the estimated/initial estimate of covariance matrix and state vector, where t represents the time index. H_t represents the measurement sensitivity matrix and K_t is the Kalman gain, $\emptyset_t$ is the state transition matrix, Q_{t-1} represents the covariance of noise uncertainties and R_t is the measurement uncertainties, $P_{t(+)}$ and $\hat{x}_{t(+)}$ are the corrected estimate of covariance and state vector.

V. CONCLUSION

This paper provides a small glimpse into the area of GPS receiver's based system and Kalman filter. It also provide brief literature survey on the existing and potential application in Kalman filtering with a recent investigation in control engineering. This paper gives an overview about the sources of error in GPS signal, and how some of the error can be reduced with Kalman filter and least square method. Few other works like replacement of tracking channel with Kalman filter have also been discussed. The overview shows that still a lot of improvement in smoothing of GPS signal can be done. Therefore for future work modeling of each and every error source can be done.

REFERENCES

1. R.E Kalman , "A new approach to linear filtering and prediction problems," 1960 Tranction of the ASME, Ser.D, Journal of Basic Engineering, vol.82, pp. 35-45.
2. Elliot D. Kaplan, "Understanding GPS – Principle and Application", 1996 Artech House England.
3. MohinderS. Grewal, Angus P.Andrews,"Kalman filtering-Theory and practice using Matlab", 2001 John Wiley & Sons, Second Edition, U.S.A.
4. E.Mattias," A Kalman filter approach to reduce position error for predestrain application in ares of bad gps reception", 2014 phd thesis.
5. Jakkaruju.B Kumar, Namita R, M.Uma" Design and implementation of kalman filter for GPS receiver", 2015 Indian Journal of Science And Technology, Vol 8(25).
6. Srinivasaiah B, Tiwari R, Dhinagar S," Kalman filter based estimation algorithm to improve the accuracy of automobile GPS navigation solution", In SAE 2014 World Congress & Exhibition., Detroit , Michigan, U.S.A.
7. Mathew, Lashley, " Kalman filter based tracking algorithm for software GPS recievers", 2006 Phd thesis.
8. Kosanam, Srikiran, and Daniel J. Simon," Kalman filtering with uncertain noise covariances", Proceedingsof the IASTED International Conference on Intelligent System and control. 2004.

9. Ribeiro, M.Isabel," Kalman and Extented Kalman filters: Concept , Derivation and Properties", Institute for System and Robotics, vol. 43.2004.
10. C. Barrios and Y.Motai," Improving Estimation of Vehicle's Trajectory Using the Latest Global Positioning Syatem With Kalman Filtering," in IEEE transaction on Instrumentaion and Measurement, vol. 60, no. 12, pp. 3747-3755, Dec. 2011.
11. D. Simon," Kalman Filtering Embedded System programming", Embedded.com article, June 2001.
12. Yunlong Teng, Jinling Wang, Qi Huang," Minimum of Geometric Dilution of Precesion (GDOP) for five satellite with dual-GNSS constellation", Advances in Space Research, vol. 56, issue 2, pp 229-236, 2015.
13. L.Cheng,J.Chen and M.G. Gan,"Multipath error analysis of carrier Tracknig loop in GPS receiver," Proceedings of the 29th Chinese Control Conference, Beijing ,pp. 4137-4141, 2010.
14. G. Welch and G.Bishop," An Introduction to Kalman Filter",University of North Carolina, chapel hill, US, 2006.

Conclusion:

This chapter showcases capabilities of signal processing techniques in general and in important applications of system analysis, biomedical engineering and navigation in particular. Present state-of-the-art, future challenges and issues have been summarized to acquaint the readers with overall scenario of signal processing applications.

The chapter has been organized to include various subsections one each for each of the included application domain. And in each of the subsection, some important papers deliberating that particular application have been included for quick reference. For instance, the application of system analysis has been dealt with in a novel manner using Haar wavelet based operational approach. An alternative more computationally efficient method based on non-recursive formulation of integral operator matrix for the analysis of linear time varying system has been presented. Computational advantage is established by including profilers generated using MATLAB. Both less memory requirement and less solution error have been cited as other advantages due to this non-recursive formulation.

For second application domain of biomedical engineering, two papers have been included. The first paper delves on the utility of the analysis of EMG signals for healthcare providers in various clinical and medical fields. Useful information from EMG signals is extracted using signal processing techniques. Lastly, a comprehensive list of both time and frequency domains is presented for the benefit of readers. The second paper highlights the application of recognition of isolated local dialects' words using neural networks. It has also been mentioned that the situation becomes complex when recognition of continuous words is attempted which requires further extension of the present work.

The third application domain of navigation includes only one paper. This paper provides a glimpse of GPS based system that uses Kalman filter. Various sources of errors in GPS system have been outlined and shown to be overcome effectively using Kalman filter for object position estimates.

The next chapter will concentrate on recent headways in the field of control systems covering all aspects related to mathematical modeling, design and implementation of various controllers on different types of systems.

Chapter -2

Recent headways in Applications of Control Systems

Control engineering has an essential role in a wide range of control systems, from simple household washing machines to high-performance missiles. It seeks to understand physical systems, using mathematical modelling, in terms of inputs, outputs and various components with different behaviors; use control systems design tools to develop controllers for those systems; and implement controllers in physical systems. A system can be mechanical, electrical, fluid, chemical, financial or biological, and the mathematical modelling, analysis and controller design uses control theory in one or many of the time, frequency and complex-s domains, depending on the nature of the design problem.

A comprehensive treatment of certain pertinent mathematic with good examples of its applications to a specific systems followed by some consolidation of latest advancements is considered in this chapter.

Mathematical Modelling

A dynamical mathematical model in this context is a mathematical description of the dynamic behavior of a system or process in either the time or frequency domain. To build mathematical models of dynamical systems with measured data using statistical method is the field of system identification.

System identification tries to estimate a black or grey box model based on observing the input-output data from experimental analysis. It is an approximation problem as it is impossible for a mathematical model to reproduce exact behavior of a physical system. The identification procedure depends on certain assumptions given a priori, which arises either from the theoretical analysis or from the observations of past experiments. The popular approach to estimate the discrete-time linear dynamic models is the ordinary least squares (OLS).There are number of models that can be classified as linear, nonlinear, and parametric and semi parametric models etc. Identification of nonlinear systems has importance, since a large class of nonlinear processes exhibit nonlinearities that cannot be linearized. The presence of non-linearity in physical systems makes the modeling inaccurate using the linear modeling. Therefore, non-linear modeling is crucial to capture the nonlinear response of the nonlinear process.

The research on system identification in last two decades has led to the development of modeling and identification of non-linear systems that can be represented by the block oriented models among these models, two of the common model structures are Hammerstein (nonlinear-linear) and Wiener

(linear-nonlinear). In the identification perspective, this might seem look like a restricted class, however, these models have been successfully used in the modeling of several industrial applications. The Hammerstein model is composed of a static nonlinearity followed by a linear dynamic system, and Wiener model is composed of a linear dynamic system followed by static nonlinearity. So the identification problem has been decoupled into two distinct steps; identification of the linear dynamic subsystems and characterization of the static nonlinearity.

Paper ***Iterative Instrumental Variable Method for Wiener System Identification*** deals with the iterative identification method for Wiener model with invertible nonlinearity and rational linear part. The wiener model form is formulated using the assumption on the coefficient of first basis function involved in the expansion of static nonlinearity resulting a bilinear parameterized form. The Wiener model in the presence of output correlated noise is estimated using the instrumental variable method to address the inconsistency involved in the LS procedure. Based on the filtering of the observed and auxiliary variables, an extended dimension IV method is derived using the iterative updates of the estimate. It is shown that the instrumental variables are independent of the noise and IV method provides consistent estimates with better statistical properties.

Iterative Instrumental Variable Method for Wiener System Identification

Vikram Saini[1], Lillie Dewan[2]

***Abstract*— This paper presents an iterative instrumental variable method for Wiener system identification by using bilinear parameterized formulation. This method is based on the decomposition of model form and assumes the invertibility of the non-linearity involved in the modeling of wiener model. In addition, the output of the linear block is corrupted with noise signal resulting in a model with correlated noise disturbance. The consistent estimates are obtained by combining Instrumental Variable method wherein the instruments are constructed by means of data filtering of observed and auxiliary variables. To support the speculation, the paper presents performance analysis using simulation results.**

Keywords-Instrumental Variable; Parameter estimation; least square; Wiener models; Data filtering

I. INTRODUCTION

Many physical systems even with nonlinear behavior can be approximated using the linear model. However, if the nonlinear distortions are too large and a model is required to capture the nonlinear behavior in a much large operating region, it is reasonable to characterize the behavior using nonlinear models which is useful to improve the identification performance. One way is to describe the behavior using the block-oriented models. Wiener model is one of the simplest block-oriented model with linear dynamic block and static output nonlinearity block. Identification of wiener systems has been an active research topic as its structure effectively reflects the practical dynamical systems. Wiener models have been successfully used for the modeling and control of many industrial applications such as control of distillation columns, linear dynamical systems combined with nonlinear sensors and nonlinear biological systems [1-4]

In the context of estimation methods employed for the Wiener models, the identification approaches can be classified into four groups [5]. Iterative methods using the linear and nonlinear optimization cover the vast literature on the identification of wiener models [6-8]. This particular formulation transforms the problem in pseudo linear regression and provides estimate using the iterative nonlinear least square method [6, 8]. On the other hand, Wiener model derived with invertible non-linearity has attractive applications in the control system design and was considered for the compensation of non-linear distortions [9]. In the case of invertible nonlinearity, the Wiener model can be transformed into the linear in parameters regression form and provides a solution using existing linear estimation techniques, for example, using the least square method.

This paper deals with the iterative identification method for Wiener model with invertible nonlinearity and rational linear part. The wiener model form is formulated using the assumption on the coefficient of first basis function involved in the expansion of static nonlinearity resulting a bilinear parameterized form. The Wiener model in the presence of output correlated noise is estimated using the instrumental variable method to address the inconsistency involved in the LS procedure. Based on the filtering of the observed and auxiliary variables, an extended dimension IV method is derived using the iterative updates of the estimate. It is shown that the instrumental variables are independent of the noise and IV method provides consistent estimates with better statistical properties.

This paper is organized as follows. Section II describes the Wiener model description and the identification problem formulation. The iterative instrumental variable method based on the data filtering of predicted outputs is presented in section III along with the consistency conditions to obtain the unbiased estimates. Section IV presents results and analysis based on simulation example through Monte-Carlo simulation study. Finally, section V presents some conclusions.

II. WIENER MODEL DESCRIPTION

The Wiener model is composed of a linear dynamic block
In series with a static non-linearity block. The linear system is parameterized using rational function representation using the numerator and denominator coefficients. Then, the rational transfer function can be described as an ARMAX model

$$x(k) = \sum_{i=1}^{n_a} a_i x(k-i) + \sum_{j=1}^{n_b} b_j u(k-j) + e(k) \qquad (1)$$

where

[1]Vikram Saini is with Department of Electrical Engineering, GEC Jhalawar, India
[2]Lillie Dewan is with the Department of Electrical Engineering, National Institute of Technology, Kurukshetra, India
(e-mail: sheetal.sheetal02@gm, l_dewan@nitkkr.ac.in).

$$e(k) = C(q^{-1})\epsilon(k) = \epsilon(k) + \sum_{i=1}^{n_c} c_i \epsilon(k-i) \quad (2)$$

and $x(k)$ represents the output of linear system. Denote the nonlinear block as a function f.Let Ωbe a compact subset of $\mathbb{R}$. The static non-linearity is defined by non-linear mapping, $f : \Omega \rightarrow \mathbb{R}$and the output can be expressed using $y(k) = f(x(k))$.

$$y(k) = f\big(x(k)\big) = \sum_{i=1}^{n_p} p_i x^i(k) \quad (3)$$

It is assumed that f is continuous, one-one on Ω, and inverse of f namely $g(\cdot) : f(\Omega) \rightarrow \Omega$ is either polynomial or can be expressed as linear combination of polynomials. Therefore, $x(k)$ can be written as

$$x(k) = g\big(y(k)\big) = \sum_{i=1}^{n_q} q_i y^i(k) \quad (4)$$

Without loss of generality and to make the unique parameterization, the first parameter of nonlinear basis function is assumed as 1 i.e. $q_1 = 1$. In order to identifying the Wiener model, assumption on nonlinearity to be invertible leads to the linear regression form. For this, rewrite the equation (4) as

$$x(k) = g\big(y(k)\big) = y(k) + \sum_{i=2}^{n_q} q_i y^i(k) \quad (5)$$

Let $g_i\big(y(k)\big) = y^i(k)$ for $i = 1,2,\dots,n_q$. From equations (1) and (5), it follows that

$$y(k) = -\sum_{m=2}^{n_q} q_m g_m\big(y(k)\big) - \sum_{i=1}^{n_a} a_i \sum_{m=1}^{n_q} q_m g_m\big(y(k-i)\big) + \sum_{j=1}^{n_b} b_j u(k-j) + e(k) \quad (6)$$

with $q_1 = 1$. The Wiener model can be written in the linear regression form

$$y(k) = \boldsymbol{\psi}(k)\boldsymbol{\theta} + e(k) \quad (7)$$

Define $\beta = \begin{bmatrix} 1 & q_2 & \cdots & q_{n_q} \end{bmatrix}$, then the parameter vector $\boldsymbol{\theta} \in \mathbb{R}^{n_q + n_a n_q + n_b - 1}$is defined as

$$\boldsymbol{\theta} = \begin{bmatrix} q_2 & q_3 & \cdots & q_{n_q} & a_1\boldsymbol{\beta}^T & a_2\boldsymbol{\beta}^T & \cdots & a_{n_a}\boldsymbol{\beta}^T & b_1 & b_2 & \cdots & b_{n_b} \end{bmatrix} \quad (8)$$

and the information vector $\boldsymbol{\psi}(k)$ is defined as

$$\boldsymbol{\psi}(k) = \begin{bmatrix} -g_2(y(k)) & -g_3(y(k)) & \cdots & g_{n_q}(y(k)) \\ -g_1(y(k-1)) & -g_2(y(k-1)) & \cdots & -g_{n_q}(y(k-1)) \\ -g_1(y(k-2)) & -g_2(y(k-2)) & \cdots & -g_{n_q}(y(k-2)) & \dots\dots \\ -g_1(y(k-n_a)) & -g_2(y(k-n_a)) & \cdots & -g_{n_q}(y(k-n_a)) \\ u(k-1) & u(k-2) & \cdots & u(k-n_b) \end{bmatrix} \quad (9)$$

Then, the unconstrained Least Square estimates can be obtained by

$$\hat{\boldsymbol{\theta}} = \min_{\boldsymbol{\theta}} \|\boldsymbol{Y} - \boldsymbol{\psi}\boldsymbol{\theta}\|_2^2. \quad (10)$$

Given Nmeasurements of input-output data pairs$(u(k), y(k))$, the objective of the identification is to determine the consistent estimates of the Wiener model. In order to identify the model, an iterative algorithm based on the instrumental variable approach is presented.

III. IDENTIFICATION OF WIENER MODEL

This section presents the iterative extended IV method for the consistent estimation of the over-parameterized Wiener model with invertible nonlinearity.

B. Extended Instrumental Variable Method

The consistency and asymptotic efficiency of the IV method depends on the instrumental variables. Therefore, the choice of instrumental variables is an important design problem. The only requirement for the instruments is that they must be observable or at least can be constructed using observed $u(k)$ and $y(k)$. The best possible way is to use the auxiliary model outputs and filtering of the elements of the regressor matrix$\boldsymbol{\psi}(k)$, resulting filtered instrumental variables. The instrumental vector can be obtained as

$$\boldsymbol{\xi}^T(k) = \begin{bmatrix} -\hat{g}_2(y(k)) & -\hat{g}_3(y(k)) & \cdots & \hat{g}_{n_{q'}}(y(k)) \\ -\hat{g}_1(\hat{y}(k-1)) & -\hat{g}_2(\hat{y}(k-1)) & \cdots & -\hat{g}_{n_{q'}}(\hat{y}(k-1)) \\ -\hat{g}_1(\hat{y}(k-2)) & -\hat{g}_2(\hat{y}(k-2)) & \cdots & -\hat{g}_{n_{q'}}(\hat{y}(k-2)) & \dots\dots \\ -\hat{g}_1(\hat{y}(k-n_a)) & -\hat{g}_2(\hat{y}(k-n_a)) & \cdots & -\hat{g}_{n_{q'}}(\hat{y}(k-n_{a'})) \\ u(k-1) & u(k-2) & \cdots & u(k-n_b) \end{bmatrix} \quad (11)$$

where $n_a \leq n_{a'}$, $n_b \leq n_{b'}$ and $n_q \leq n_{q'}$. In equation (6), the model output $y(k)$ depends on the functions of present value $y(k)$. The predicted output $\hat{x}(k)$ of linear system given by

$$\hat{x}(k) = -\sum_{i=1}^{n_a} \hat{a}_i x(k-i) + \sum_{j=1}^{n_b} \hat{b}_j u(k-j) \quad (12)$$

Then for the $|q_i - \hat{q}_i|, i = 1,2,\dots,n_q$ with $q_1 = \hat{q}_1 = 1$, small enough the estimated signal $\hat{y}(k)$ is computed using the model output defined as

$$\hat{y}(k) = -\sum_{i=2}^{n_q} \hat{q}_i g_i\big(y(k)\big) - \sum_{m=1}^{n_a} \hat{a}_m \hat{x}(k-m) + \sum_{j=1}^{n_b} \hat{b}_j u(k-j) \quad (13)$$

where

$$\hat{g}_l\big(\hat{y}(k-j)\big) = \frac{1}{\hat{C}(q^{-1})} g_l\big(\hat{y}(k-j)\big), \quad j = 1,2,\dots,n_{a'} \text{ and } l = 1,2,\dots,n_{q'} \quad (14)$$

$$\hat{g}_i\big(y(k)\big) = \frac{1}{\hat{C}(q^{-1})} g_i\big(y(k)\big), \quad i = 1,2,\dots,n_{q'} \quad (15)$$

Here $\hat{C}(q^{-1})$ is the estimate of $C(q^{-1})$ and can be determined from a preliminary estimating stage using the least square method. Define the following

$$\hat{\boldsymbol{R}}_{\xi\psi}(N) = \frac{1}{N}\sum_{k=1}^{N} \boldsymbol{\xi}(k)\boldsymbol{\psi}^T(k) \quad (16)$$

$$\hat{\boldsymbol{r}}_{\xi y}(N) = \frac{1}{N}\sum_{k=1}^{N} \boldsymbol{\xi}(k) y(k) \quad (17)$$

Now if for a square matrix $\boldsymbol{W} \succ 0$ and consistency conditions are satisfied (discussed in the next subsection) with

$$rank(\hat{\boldsymbol{R}}_{\xi\psi}^T \boldsymbol{W} \hat{\boldsymbol{R}}_{\xi\psi}) = \mathbb{R}^{n_q + n_a n_q + n_b - 1} \quad (18)$$

then, an extended IV estimator of $\boldsymbol{\theta}$ is given by

$$\hat{\boldsymbol{\theta}}^{IV} = \big(\hat{\boldsymbol{R}}_{\xi\psi}^T \boldsymbol{W} \hat{\boldsymbol{R}}_{\xi\psi}\big)^{-1} \hat{\boldsymbol{R}}_{\xi\psi}^T \boldsymbol{W} \hat{\boldsymbol{r}}_{\xi\psi} \quad (19)$$

Here $\hat{\boldsymbol{\theta}}^{IV}$ represents the IV estimate. To ensure the consistency of instruments, the following assumptions are made

A_1 The signals $u(k)$ and $\epsilon(k)$ are stationary, ergodic and have zero mean so that ensemble average may be replaced by time average over one sample function.

A_2 The signals $u(k)$ and $\epsilon(k)$ are statistically independent with each other.

C. Consistency of the Estimates

The consistency of the estimates can be shown by the following conditions [10]

$$\mathbb{E}[\boldsymbol{\xi}(k)e(k)] = 0 \quad (20)$$

$$rank(\hat{\boldsymbol{R}}_{\xi\psi}^T \boldsymbol{W} \hat{\boldsymbol{R}}_{\xi\psi}) = \mathbb{R}^{n_q + n_a n_q + n_b - 1} \quad (21)$$

The vector of instrumental variables satisfies the consistency conditions given by equations. Let the basis functions satisfy

$$\big|y^i(k)\big| \le \mu_{max}, i = 1,2,\dots,n_q \text{ for some } \mu_{max} > 0 \quad (22)$$

This condition implies that the basis functions are bounded in the given experimental range of $y(k)$ with the assumption that the output is bounded. The independence assumption A_1 of $u(k)$ and $\epsilon(k)$ implies that $u(k)$ and $\epsilon(k)$ are independent and therefore, their functions namely $\varphi(u(k))$ and $\phi\big(e(k)\big)$ are also independent (page 49 [11]). In particular, if ϕ is the identity function, then, $\varphi(u(k))$ and $e(k)$ are independent, and the instrumental variables vector in equation (11) and $e(k)$ is independent.

The consistency of estimates depends on the choice of matrix $\boldsymbol{W}$ which is assumed to be positive definite. The common choice to ensure that the matrix $\boldsymbol{W}$ is positive definite is to choose it as an identity matrix. But, this choice provides poor asymptotic efficiency of the estimates. In the presented IV method, in addition to this choice the weight matrix is taken as $\boldsymbol{W} = \hat{\boldsymbol{R}}_{\xi\xi}$ which improves the asymptotic efficiency of estimates and also ensures the consistency of estimates.

The steps of the EIV method are as follows:

Step 1: Obtain LS estimates $\hat{\boldsymbol{\theta}}^{LS}$ and compute the residuals.

Step 2: Estimate $C(q^{-1})$ using the computed residual vector. Compute the predicted outputs $x(k)$ and $y(k)$ using equations (12) and (13) respectively.

Step 3: Make an instrumental variables vector using equation (11) and compute the IV estimates using equation (19). Compute the residuals using the IV estimate $\hat{\boldsymbol{\theta}}^{IV}$.

Step 4: Repeat the steps 2 and 3 until some criterion is fulfilled.

IV. SIMULATION STUDY

This section presents numerical example to compare the performance of the EIV method presented in the previous section with the LS method and the data filtering-based LS method (briefly written as DFLS method for natation purpose). The stochastic properties are investigated using 300 Monte-Carlo simulation study in MATLAB environment. A number of measurements

have been generated to form the observed data. In each example, two different cases have been investigated with different noise levels. The accuracy and convergence analysis described by bias and standard deviation are evaluated based on the performance criterion i.e. statistically estimation error (SEE) and average coefficient of variation (ACV). The SEE is defined as

$$\text{SEE} = \sqrt{\frac{\|m(\widehat{\boldsymbol{\theta}}_s) - \boldsymbol{\theta}_s^{\circ}\|_2}{\|\boldsymbol{\theta}_s^{\circ}\|_2}}$$

where $m(\widehat{\boldsymbol{\theta}}_s)$ represents the sample mean of estimator for 300 simulation runs. And, the ACV is computed as ($\widehat{\boldsymbol{\theta}}_s(i)$ represents the ith component)

$$\text{ACV} = \frac{1}{n_s}\sum_{i=1}^{n_s}\frac{\sigma\left(\widehat{\boldsymbol{\theta}}_s(i)\right)}{\left|m\left(\widehat{\boldsymbol{\theta}}_s(i)\right)\right|}$$

where $n_s = n_a + n_b + n_p - 1$and $\sigma\left(\widehat{\boldsymbol{\theta}}_s(i)\right)$ represents the standard deviation of estimates.

MONTE-CARLO SIMULATION RESULTS FOR EXAMPLE WITH SNR = 13.36 dB.

Parameters			a_1	a_2	b_1	b_2	p_2	p_3	SEE	ACV
LS		mean	-0.2171	0.4293	0.4125	-1.0810	-0.1999	0.0130	0.2097	0.0145
		Std	0.0053	0.0060	0.0064	0.0069	0.0020	0.0002		
DFLS		mean	-0.2558	0.4417	0.4180	-1.1076	-0.2003	0.0132	0.1203	0.0110
		Std	0.0052	0.0045	0.0042	0.0055	0.0015	0.0002		
EIV $n_{a'}=3$ $n_{b'}=2$	$\boldsymbol{W}=\boldsymbol{I}$	mean	-0.2488	0.4436	0.4208	-1.1122	-0.2037	0.0136	0.1002	0.0452
		std	0.0302	0.0144	0.0082	0.0166	0.0062	0.0007		
	$\boldsymbol{W}=\widehat{\boldsymbol{R}}_{\xi\xi}$	mean	-0.2512	0.4453	0.4191	-1.1111	-0.2023	0.0135	0.1017	0.0257
		std	0.0118	0.0080	0.0044	0.0066	0.0054	0.0006		
EIV $n_{a'}=5$ $n_{b'}=2$	$\boldsymbol{W}=\boldsymbol{I}$	mean	-0.2432	0.4441	0.4214	-1.1149	-0.2041	0.0137	0.0987	0.1380
		Std	0.0642	0.0415	0.0428	0.0502	0.0244	0.0028		
	$\boldsymbol{W}=\widehat{\boldsymbol{R}}_{\xi\xi}$	mean	-0.2516	0.4451	0.4190	-1.1106	-0.2024	0.0135	0.1037	0.0250
		Std	0.0115	0.0075	0.0044	0.0065	0.0052	0.0006		
EIV $n_{a'}=5$ $n_{b'}=5$	$\boldsymbol{W}=\boldsymbol{I}$	mean	-0.2424	0.4436	0.4210	-1.1147	-0.2043	0.0137	0.1019	0.1402
		Std	0.0661	0.0419	0.0413	0.0490	0.0250	0.0029		
	$\boldsymbol{W}=\widehat{\boldsymbol{R}}_{\xi\xi}$	mean	-0.2569	0.4470	0.4183	-1.1080	-0.2024	0.0135	0.1152	0.0240
		Std	0.0104	0.0069	0.0044	0.0061	0.0053	0.0006		
True value			-1.60	1.3	0.80	-0.60	1.50	0.4		

The data filtering-based LS method is implemented using the steps described [12-13]. The EIV method is implemented using the instrumental variable vector defined in equation (11)

Example: In this example, the linear part of Wiener system with invertible nonlinearity is given by

$$x(k) = \frac{0.4238q^{-1} - 1.1227q^{-2}}{1 - 0.25q^{-1} + 0.45q^{-2}}u(k) + \frac{1 - 1.0q^{-1} - 0.20q^{-2}}{1 - 0.25q^{-1} + 0.45q^{-2}}\epsilon(k)$$

The nonlinearity is given by

$$y(k) = f\big(x(k)\big) = \left(5\sqrt[3]{0.6\,x(k) - 1} + 5\right)$$

and the inverse of the nonlinearity is expressed using basis functions as

$$x(k) = g\big(y(k)\big) = y(k) - 0.2y^2(k) + 0.0133y^3(k)$$

Two different noise levels corresponding SNR=13.91 dB and 05.84 dB respectively are considered. The order of numerator polynomial of noise model is taken as $n_c = 2$ for DFLS method. In this example, EIV method is implemented using the ARMAX model structure with MA noise model (i.e. $n_c = 2$). The choice of $n_{a'}, n_{b'}$ and $n_{q'}$ (number of instruments) effects the consistency and efficiency of the estimates. Therefore, the simulation study is carried out using different combinations of $n_{a'}$ and $n_{b'}$ ranges between 2 (order n_a and n_b) to 5 (arbitrary chosen). The order for the basis functions of the invertible nonlinearity in the instrumental variable vector is taken as 3 i.e. $n_{q'}$ = 3. The estimates obtained using three combinations are shown which are selected among different combinations based on the best performance criterion i.e. with minimum SEE. Two different weight matrices $\boldsymbol{W} = \boldsymbol{I}$ and $\boldsymbol{W} = \widehat{\boldsymbol{R}}_{\xi\xi}$ are considered for the EIV method. The SEE, ACV and estimates for SNR = 13.36 dB and 05.41 dB are shown in Table I and Table II respectively. Form Table I and Table II, following are the clear observations

The DFLs method provides consistent estimates with lower SEE and ACV as compared to estimates obtained using the LS method which are heavily biased,

The proposed EIV method provide estimates with lower SEE than the DFLS method for both SNR cases. However, the ACV is higher than obtained using the DFLS method. This suggests that bias-variance trade-off problem exists in the estimation procedure.

The effect of choice of weight matrix is also visible on the obtained ACV i.e. with $\boldsymbol{W} = \widehat{\boldsymbol{R}}_{\xi\xi}$, asymptotic efficiency improves as compared to $\boldsymbol{W} = \boldsymbol{I}$.

V. CONCLUSION

In this paper, iterative method using the introduction of instrumental variables is presented for the identification of Wiener system with invertible nonlinearity. An IV method using the extended instrumental variable vector consists of the filtered instruments is suggested. As a result, the estimates with lower SEE and better bias-variance trade-off have been obtained as compared to the DFLS method which is validated using a simulation example with two different cases of noise level through Monte-Carlo simulation study.

MONTE-CARLO SIMULATION RESULTS FOR EXAMPLE WITH SNR = 05.41 dB.

Parameters			a_1	a_2	b_1	b_2	p_2	p_3	SEE	ACV
LS		mean	-0.1018	0.3536	0.3683	-0.9226	-0.1950	0.0115	0.4544	0.0454
		Std	0.0128	0.0133	0.0147	0.0167	0.0035	0.0004		
DFLS		mean	-0.2871	0.4043	0.3916	-1.0387	-0.1997	0.0125	0.2853	0.0241
		Std	0.0117	0.0105	0.0108	0.0129	0.0028	0.0003		
EIV $n_{a'} = 3$ $n_{b'} = 2$	$\boldsymbol{W} = \boldsymbol{I}$	mean	-0.2645	0.4216	0.4001	-1.0547	-0.2095	0.0137	0.2451	0.1032
		std	0.0733	0.0399	0.0198	0.0397	0.0121	0.0014		
	$\boldsymbol{W} = \widehat{\boldsymbol{R}}_{\xi\xi}$	mean	-0.2660	0.4222	0.3956	-1.0502	-0.2073	0.0134	0.2529	0.0537
		std	0.0291	0.0197	0.0110	0.0162	0.0092	0.0011		
EIV $n_{a'} = 5$ $n_{b'} = 2$	$\boldsymbol{W} = \boldsymbol{I}$	mean	-0.2369	0.4123	0.3719	-1.0436	-0.2126	0.0140	0.2798	0.4466
		Std	0.1323	0.0874	0.4488	0.2143	0.0384	0.0044		
	$\boldsymbol{W} = \widehat{\boldsymbol{R}}_{\xi\xi}$	mean	-0.2692	0.4209	0.3949	-1.0476	-0.2072	0.0134	0.2581	0.0502
		Std	0.0264	0.0180	0.0110	0.0160	0.0088	0.0010		
EIV $n_{a'} = 5$ $n_{b'} = 5$	$\boldsymbol{W} = \boldsymbol{I}$	mean	-0.2344	0.4140	0.4062	-1.0601	-0.2128	0.0141	0.2415	0.3242
		Std	0.1450	0.0879	0.1636	0.1871	0.0414	0.0048		
	$\boldsymbol{W} = \widehat{\boldsymbol{R}}_{\xi\xi}$	mean	-0.2870	0.4301	0.3937	-1.0424	-0.2100	0.0137	0.2697	0.0571
		Std	0.0286	0.0189	0.0115	0.0177	0.0116	0.0013		
True value			-1.60	1.3	0.80	-0.60	1.50	0.4		

REFERENCES

[1] M. Schetzen, "Nonlinear System modeling based on the Wiener theory," Proceedings ofIEEE, vol. 69, no.12, pp. 1557-1573, 1981.

[2] A.D. Kalafatis, L. Wang, W.R. Cluett, "Identification of Wiener-type non-linear systems in a noisy environment," Int. J. Control, vol. 66, pp. 923–941, 1997.

[3] A.D. Kalafatis, L. Wang, W.R. Cluett, "Identification of time-varying pH processes using sinusoidal signals," Automatica, vol. 41, pp. 685–691, 2005.

[4] I.W. Hunter, M.J. Korenberg, **"**The identification of nonlinear biological systems: Wiener and Hammerstein cascade models," Biological Cybernetics, vol. 55, no. 2–3, pp. 135–144, 1986.

[5] Janczak, "Identification of nonlinear systems using Neural networks and polynomial models", ser. Lecture notes in control and information scineces. Berlin, Germany: Springer, 2005, vol. 310.

[6] J. Bruls, C. Chou, B. Haverkamp, and M. Verhaegen, "Linear and non-linear system idnetification using seperable least-squares," European Jouranl of Control, vol. 5, no. 1, pp. 116-128, 1999.

[7] P. Celka, N. J. Bershad, and J. M. Vesin, " Stochastic gradient identification of polynomial Wiener systems: Analysis and apllications," IEEE Transactions on signal processing, vol. 49, no. 2, pp. 301-313, 2001.

[8] J. Voros, "Modeling and identification of Wiener systems with two-segment nonlinearities," IEEE Transaction on Control Systems Technology, vol. 11, no. 2, pp. 253-257, 2003.

[9] H. W. Kang, Y. S. Cho, and D. H. Youn, "Adaptive precompensation of Wiener systems," IEEE Transactions on Signal Processing, vol. 46, no. 10, pp. 2825-2829, 1998.

[10] P. Stoica and T. Soderstrom, " Optimal instrumental varaible estimation and approximate implemetations," IEEE Transactions on Automatic Control, vol. 28, no. 7, pp. 757-772, 1983.

[11] Grimmett G, Stirzaker D. Probability and Random Processes. Oxford University 18 Press, 2001.

[12] Wang, and F. Ding, " Parameter estimation algorithms for multivaraible Hammerstein CARMA systems," Information sciences, vol. 355-356, no. 356, pp. 237-248, 2016.

[13] Y. Wang, and F. Ding, "Iterative estimation for a nonlinear IIR filter with moving average noise by means of the data filtering technique," IMA Journal of Mathematical Control and Information, 2015.

Implementation of Controller

Once the mathematical model of the system is available, next objective is to develop a control model for controlling such systems using a control action in an optimum manner without delay or overshoot and ensuring stability. To do this, a controller with the requisite corrective behavior is required. In the next subsections Controllers are implemented on servo systems (DC and Induction motor), benchmark problem (Rotary Inverted Pendulum), and highly nonlinear under actuated system (Robotic manipulator), biomedical systems and how the automation can be achieved.

Control of Variable Speed Motors

Most of the industrial applications use variable speed motors, e.g. vary flow rate, pumping pressure, rolling mills to name a few. Most versatile is a variable speed DC motor because of good speed regulations, adjustable speed, and frequent starting, braking and reversing.

Most commonly used controller for controlling the speed is PID controller. Tuning of parameters of PID controller has led to another area of research. Different optimization techniques are used may be mathematical or nature inspired. Paper ***Speed Control of DC Motor Using Seeker Optimization Based PID Controller*** is one such paper, in which nature inspired seeker algorithm has been utilized to tune the PID controller for the control the speed of the DC drive. The major drawback of dc motors is the presence of commutators and brushes, which require frequent maintenance and make the motor unsuitable for explosive and dirty environments.

To overcome these drawbacks there is a search for the substitute of dc motors in variable speed drives. Induction motors, particularly squirrel-cage induction motors are having many advantages when compared to dc motors. Some of the main advantages of induction motors are simple and rugged design, low cost and low maintenance. Many researchers have proposed different techniques for efficient use of induction motors invariable speed drive. One of the control scheme of indirect vector control and speed estimation process using stator current MRAS based speed estimation method with and without speed sensor under various condition has been proposed in paper ***Vector Control of Induction Motor with and without Speed Sensor.***

An overview on various control techniques of rolling mill system is presented in paper ***A Survey on Rolling mill system with various Control technique***s and a thorough study of different features in previous research papers related to the control techniques in rolling mills have been carried out. Mainly those control techniques have been used for reduction of plate thickness, strip tension, roll eccentricity, loop position and strip breakage in them. Some of these control techniques has been discussed with their results.

Speed control of DC motor using Seeker optimization based PID controller

Swarup Kumar Saha[1] and Krishanu Nath[2]

***Abstract*—DC motor drives are leading in the world of industrial applications which require good speed regulations, adjustable speed, and frequent starting, braking and reversing. Industries have been using PID (proportional-integral-derivative) controller for various control applications with tremendous success. This paper presents tuning of PID controller using a novel heuristic search algorithm for speed control of DC motor. A comparative analysis of the performance of the speed control system with various nature-inspired optimization techniques for tuning of PID controllers for speed control of DC motor. A comparative investigation of the performance of the speed control system is achieved.**

Keywords—DC motor; PID controller; Particle swarm optimization; Genetic algorithm; Seeker optimization

Nomenclature

v_a=armature voltage of the motor.
v_f=voltage across field winding.
R_f= field winding resistance
i_f= current through the field winding.
L_f= field windinginductance
R_a= armature winding resistance
L_a= armature winding inductance
e_b= induced armature voltage
$\emptyset$= per pole flux (Wb)
k= constant of motor back emf and torque ($\mathrm{NmA^{-1}}$)
ω_m=speed of motor (rad/s)
J= moment of inertia of motor shaft ($\mathrm{Nm^2}$)
B = co-efficient of viscous friction (Nm-s)
T_M= motoring torque (Nm)
T_L= load torque (Nm)

I. INTRODUCTION

DC machine is one of the greatest inventions in the field of electrical engineering. It can convert electrical energy into mechanical energy or vice versa. Although, it was predicted by many researchers that AC drives are superior to DC drives and would replace DC drives, but even today the applications which required precise speed control are dominated by DC drives.High starting torque, wide-range speed control and a high degree of flexibility etc. are the advantages of the DC drives. Speed control of DC motor came into the picture in 1981 by Ward Leonard. Since then various methods have been suggested by researchers for performing the goal.

PID controllers have been dominating the world of control from the 19th century. With the application of feedback, it is just the matter of obtaining the parameters of the controller to obtain the desired response. These parameters can be obtained from various methods manual tuning, empirical tuning or from various optimization methods.

In 1942, two researchers Ziegler and Nichols presented a very good tuning technique of PID controller which is based on time response and experiences of the system. Although this method has some disadvantages like excessive overshoot in time response and it lack in the selection parameters but still opens the way of tuning parameters [1]. Now let's come to the point of optimization techniques; the optimal solution to a problem or optimum for some objective function can be finding out by these techniques. The word optimum has come from the Latin word 'optimus', meaning best [2]. Use of these optimization techniques to tune the parameters of PID controller become very much popular as it takes us to the destination of faster tuning and a more precise PID controller.

Particle Swarm Optimization, Genetic Algorithm and other population based techniques are the most popular among the various optimization techniques. GA has been used by D. K.Meena et al. and N. Thomas et al. for tuning the PID controller for DC drive's speed control [3] and position control [4]. Swarm intelligence is also another form of nature's unique characteristics that have excited the researchers for their smart social interaction for the accomplishment of the goal which has been successfully used by Lailis Syafaah et al. to optimize the PID controller vales [5].Many other researchers also tried to optimally choose these PID parameters by using various optimization techniques such as teacher-learning based optimization [6], bacterial foraging optimization [7], and differential evolution and simulated annealing [8].

In this paper a novel stochastic method i.e.seeker algorithm has been utilized to tune the PID controller for the control the speed of the DC drive. The performance of this optimization technique is justified in terms of maximum overshoot and the settling time of the response. It is also compared with GA and PSO techniques to prove the supremacy of seeker optimization technique which gives an efficient tuning of the PID controller parameters.

II. DC MOTOR

The DC motor is the plant under consideration. Construction wise it has basically two parts i.e. stator and

[1]Swarup Kumar Saha is with School of Renewable Energy and Efficiency, National Institute of Technology, Kurukshetra, India
[2]Krishanu Nath is with the Department of Electrical Engineering, National Institute of Technology, Kurukshetra, India
(e-mail: swarup.saha6@gmail.com, krishanunathee2015@gmail.com).

rotor. The armature winding of the dc motor is placed on the rotor whereas the stator consists of the field winding. The equivalent circuit diagram; based on laws of physics for the separately excited dc motor is shown in Fig 1.

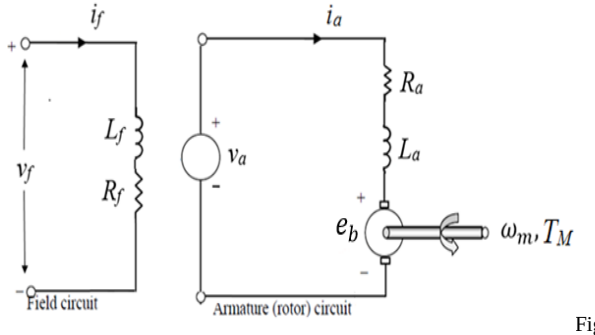

Fig. 1: Equivalent circuit of separately excited DC motor

The governing equations of DC motor are:

$$v_a = e_b + i_a R_a + L_a \frac{di_a}{dt} \quad (1)$$

$$v_f = R_f i_f + L_f \frac{di_f}{dt} \quad (2)$$

$$T_M = K\emptyset i_a \quad (3)$$

$$T_M - T_L = J\frac{d\omega_m}{dt} + B\omega_m \quad (4)$$

$$e_b = k\emptyset\omega_m \quad (5)$$

A. Speed control of DC motor

Using equation (5) and (1) the back emf can be expressed as:

$$e_b = K\emptyset\omega_m = v_a - i_a R_a - L_a \frac{di_a}{dt} \quad (6)$$

Rearranging the terms,

$$\omega_m = (v_a - i_a R_a - L_a \frac{di_a}{dt})/K\emptyset \quad (7)$$

From (7) it can be observed that speed can be controlled by varying applied voltage, V_a(Voltage Control), flux/pole, $\emptyset$ (Flux Control), resistance,R_a of armature (Rheostat Control)

In this paper armature voltage control is employed to achieve the required speed control.

B. Modelling of DC motor

The mathematical model of the dc motor can be attained by using the Laplace transform form of (1) and (4) and repositioning the terms as below.

$$\frac{I_a(s)}{V_a(s)-E(s)} = \frac{1}{sL_a + R_a} \quad (8)$$

$$\frac{\omega_m(s)}{T_M(s)-T_L(s)} = \frac{1}{Js+B} \quad (9)$$

Using (3), (5), (8) and (9), the block diagram model is obtained as in Fig. 2.

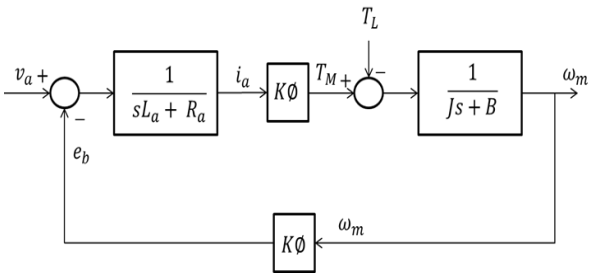

Fig. 2: Block diagram model of separately excited DC motor

The model of dc motor used is a 5 HP, 240V machine with a rated speed of 1750 rpm. The other parameters of the DC motor are given in table I.

DC MOTOR PARAMETERS

Sl. no.	Parameters	Value
1	Torque constant	1.976NmA^{-1}
2	Armature inductance	0.5 H
3	Armature resistance	2 Ω
4	Damping factor	0.2 Nm-s
5.	Moment of inertia	0.02Nm^2
6.	Field inductance	1.4 H
7.	Field resistance	120 Ω

III. PID CONTROLLER

In the world of the controller, PID controllers are widely used for the ease of their implementation. The control structure of PID controller is very simple. This controller has three separate parameters, and that is why it is also called as a three-term control [9]. The control action of a PID controller is given by

$$u(t) = K_P e(t) + K_I \int_0^t e(\tau)\, d\tau + K_d \frac{de(t)}{dt} \quad (10)$$

where

$u(t)$ is the control signal generated

$e(t)$ is the error signal (di the fference between reference signal and plant output)

K_P is the proportional gain

K_I is the integral gain

K_d is the differential gain

As the name suggests in the P-controller the actuating signal is proportional to the error signal, whereas the actuating signal of D and I controller is proportional to the derivative and the integral of the error signal respectively. The P-controller reduces the steady state error but at the same time, it increases the maximum overshoot of the plant output. In case of I-controller though it reduces the error as the order of the close-loop transfer function increases the system becomes sluggish. Whereas the limitation of the D-controller is that it can only improve the transient state characteristics but it can't eliminate the steady state error properly [10]. Therefore it is very much essential to find the optimum

value of these parameters to get the satisfactory result from the system.

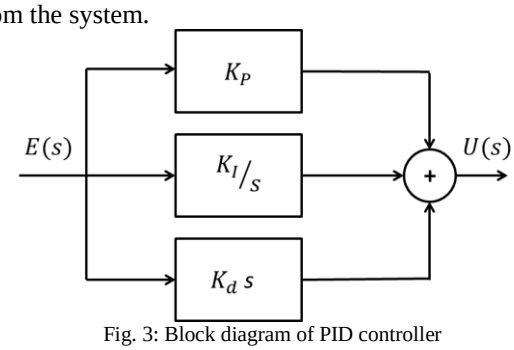

Fig. 3: Block diagram of PID controller

There are various techniques for the tuning of PID controller and among them, Zeigler-Nichols method is one of the earliest and a very popular method to tune the PID controller. This is basically an empirical method in which the values of K_P, K_I and K_d are a function of gain, delay time and time constant of the given system [11]. Various new other methods such as Chien-Hrones-Reswick PID tuning algorithm [12], Cohen Coon tuning [13], Refined Ziegler Nichlos tuning [14] and Wang-Juang-Chan tuning [15] are also available. Further the future trend has to optimally tune the gains of PID controller using various optimization techniques.

IV. OPTIMIZATION TECHNIQUES

The stochastic optimization techniques are gradient free and are inspired fromvarious natural phenomenon. These techniques have been over powering the classical optimization techniques when the objective function is nonlinear.

A. Seeker Optimization Algorithm

Seeker optimization algorithm is a population based optimization technique which is influenced by the search techniques of a human group. This algorithm explores the interactive behavior of the individuals when a group of people randomly searches any particular thing [16]. Rather than other population based techniques this algorithm continuously searches around the present position within a search radius of the partials until it converges to optima. In this way this algorithm reduces the chances of a particle to get lost. The particles of the algorithm are known as seeker [17]. The parameters of this algorithm are start point vector, search direction, search radius and trust degree and they are related with each other by the equation as described below.

$$\vec{c} = \vec{x}(t) + \emptyset_1\big(\vec{p}(t) - \vec{x}(t)\big) + \emptyset_2\big(\vec{g}(t) - \vec{x}(t)\big) \quad (11)$$

Where$\emptyset_1$ and $\emptyset_2$ are random numbers chosen in the interval of 0 to 1

The search direction is governed by four significant directions called global spatial direction$\vec{d}_{gs}$, global temporal direction$\vec{d}_{gt}$, local temporal direction $\vec{d}_{lt}$ and local spatial direction $\vec{d}_{ls}$ which are expressed by

$$\vec{d}_{lt} = \begin{cases} sign\big(\vec{x}(t) - \vec{x}(t-1)\big) \;\; if\; fit(\vec{x}(t)) \geq fit(\vec{x}(t-1)) \\ sign\big(\vec{x}(t-1) - \vec{x}(t)\big) \;\; if\; fit(\vec{x}(t)) < fit(\vec{x}(t-1)) \end{cases} \quad (12)$$

$$\vec{d}_{ls} = sign\left(\vec{l}(t) - \vec{x}(t)\right) \quad (13)$$

$$\vec{d}_{gt} = sign\big(\vec{p}(t) - \vec{x}(t)\big) \quad (14)$$

$$\vec{d}_{gs} = sign\big(\vec{g}(t) - \vec{x}(t)\big) \quad (15)$$

Another definition of search direction as per literature [17] is directly obtained by

$$\vec{d} = sign\Big(\omega\Big(sign\Big(fit\big(\vec{x}(t)\big) - fit\big(\vec{x}(t-1)\big)\Big)\Big)\big(\vec{x}(t) - \vec{x}(t-1)\big) + \emptyset_3(\vec{p}(t) - \vec{x}(t)) + \emptyset_4(\vec{g}(t) - \vec{x}(t))\Big) \quad (16)$$

Where$\emptyset_3$ and $\emptyset_4$ are random numbers chosen in the interval of 0 to 1 ω is an inertia weight given by

$$\omega = (T_{max} - t)/T_{max} \quad (17)$$

Another crucial parameter to SOA is the search radius, which has different methods in the literature [17]; the one used for computation here is given by (38). To compute the same it is required to compute the following

$$E_n = \vec{x}_{max} - \vec{x}_{min} \quad (18)$$

$$H_e = E_n/c_2 \quad (19)$$

$$\vec{r}' = randn(E_n, H_e) \quad (20)$$

$$\vec{r} = randn(0, \vec{r}') \quad (21)$$

Where $\vec{x}_{max}$ and $\vec{x}_{min}$ are the positions with maximum and minimum fitness within its fellow neighbors.

The parameter μ is a quality evaluation of different positions dependent on the fitness of $\vec{x}(t)$. The global best has $\mu = 1$ and for the rest seeker is calculated by

$$\mu = \mu_{max} - \frac{S - I_i}{S-1}(\mu_{max} - \mu_{min}) \quad (22)$$

Where S is the neighbor search group size and I_i is the index of $\vec{x}_i(t)$ after sorting on the basis of fitness.

Finally, the position update of each seeker is given by

$$\vec{x}(t+1) = \vec{c} + \vec{d} * \vec{r} * \sqrt{-\log(\mu)} \quad (23)$$

B. Genetic algorithm

Genetic algorithm is an optimization technique by which we can find out the optimum value of any constrained or unconstrained problem. This method is basically based on the concept of biological evolution process of nature. Like evolution, this algorithm also evolved its population towards the best. It has basically three operators: - selection, crossover, and mutation [4].

Now before the genetic operators come into the picture, first of all we have to define the population on which the operators will work. A population is basically a subset of the set of all possible solutions for the given problem. Typically a population is selected randomly.

Selection is the process where we select the parent chromosome based on their fitness value. The fittest parent will allow for the process of producing offsprings.

Crossover is the genetic operator, which produces the offspring from the parent chromosomes and in the offspring both the qualities of the parent will be present. In other words we can say that this crossover is the process of exchanging information between the parents and producing one or more offsprings.

Mutation is the genetic operator that changes one or more gene values i.e. binary bits of the chromosome to avoid local minima.

C. Particle swarm optimization

PSO is also one of the best optimization techniques which are based on the concept of social behavior of birds. As a group of birds explores any 3-d space for searching of foods, similarly in PSO we initialize some particles which explore the N-dimensional objective space for the search of the optimum value of the function [5]. There are basically four steps in PSO such as:-

4.1 First of all we randomly initialize a population of particles and also initialize their velocities.

4.1 2nd step: - We find out the personal best for each particle.

4.1 3rd step: - we find out the global best among all particles.

4.1 And in the final step depending upon the logic as described in the equations, we update the new velocity and position of the particles.

V. SIMULATION

This section a discussion of the simulation work done is explained.

A. Problem Formulation

To formulate the cost function lets define some of the time domain parameters of our interest.

Maximum overshoot (M_p): If we eliminate the peak value of the response curve from the desired output of the system then we get the maximum overshoot.

Settling time (t_s): The time required for response to reach 98% of the final value is known as settling time.

Steady state error (e_{ss}): It is defined as the difference between the input and the output of a system in the limit as time goes to infinity

The cost function is taken to be a linear combination of four specifications

$$J = w_1 t_s + w_2 M_p + w_3 e_{ss} (24)$$

B. Simulink implementation

The Simulink block for modeled DC motor is given in Fig. 4. The implementation of the PID controller along with the DC motor with unity feedback is shown in Fig. 5. The values of PID controller parameters obtained through minimization of the formulated cost function are tabulated in table II. The responses using these values of controller gains are given in fig. 6, 7 and 8.

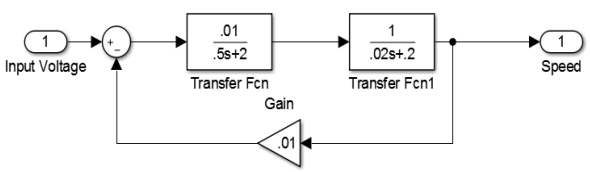

Fig. 4: Simulink model of DC motor

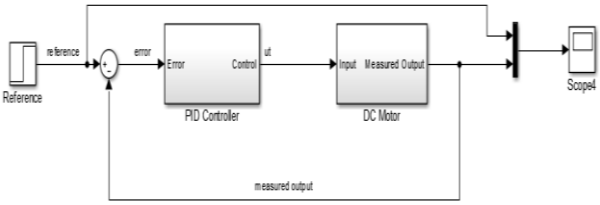

Fig. 5: Simulink model of the PID control of DC motor

PID CONTROLLER GAINS

Methods	K_P	K_I	K_d
SOA	351.5	647.2	23.7
PSO	89.87	551.4	146.2
GA	366.7	74.2	127.4

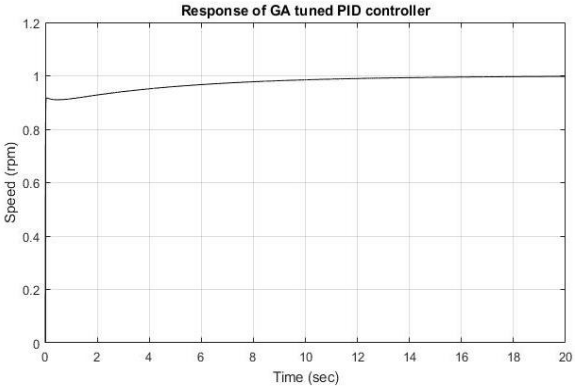

Fig. 6: Block diagram of PID controller

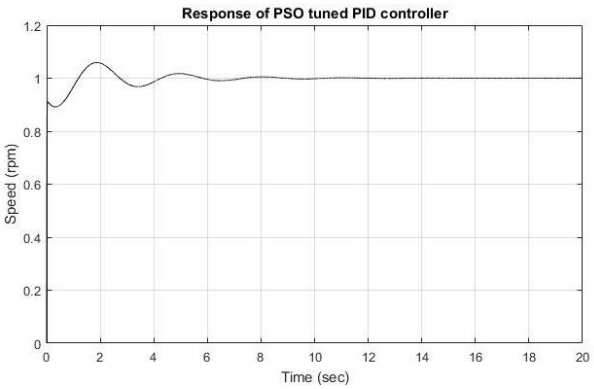

Fig. 7: Block diagram of PID controller

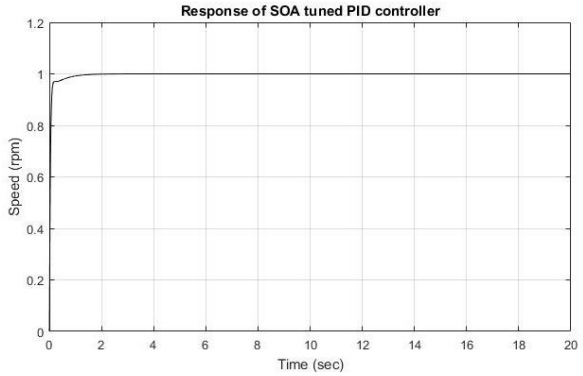

Fig. 8: Block diagram of PID controller

VI. RESULTS

On applying the optimized gains of the PID controller the responses are obtained to be satisfactory in terms of the steady state error. Better performance is found in terms of the cost function from SOA. The settling time, maximum overshoot and steady state error for all the three optimization based PID controller are tabulated in table no III. PSO has a smaller settling time than GA but it exhibits some over shoot in the response whereas GA provides an Over damped response. SOA on the other hand provides least settling time with no overshoot in the response. Finally it can be concluded that SOA based PID controller has satisfied the required objective with minimal settling time and steady state error and overshoot.

PARAMETERS OF DC MOTOR

Methods	M_p	t_s**(sec)**	e_{ss}
SOA	-	0.56	0
PSO	5.9%	0.9	0
GA	-	3.85	0

REFERENCES

[1] K. Manoj, P. Ashish, "PID controller tuning using Ziegler-Nichols method for speed control of DC motor". IJSETR, Vol.03,Issue.13 June-2014

[2] E. Goldberg, "Genetic Algorithms in Search, Optimization, and Machine Learning". Asia: Pearson Education, 2001

[3] D.K.Meena and Mrs. S.Chahar, "Speed Control of DC Servo Motor Using Genetic Algorithm". IEEE, 2017.

[4] N. Thomas, Dr. P. Poongodi, "Position control of DC motor using genetic algorithm based PID controller", Proceedings of the World Congress on Engineering 2009 Vol II WCE 2009.

[5] L.Syafaah, Widianto, I. Pakaya, D.Suhardi and M. Irfan, "PID Designs using DE and PSO Algorithms for damping oscillations in a DC Motor speed", IEEE, EECSI 2017.

[6] S. Shrivastava1, V. P. Singh, R. K. Dohare, S. P. Singh and D. P. S. Chauhan, " PID tuning for position control of DC servo-motor using TLBO", International Journal of Advanced Technology and Engineering Exploration, Vol 4(27)

[7] D.R. Chowdhury, J.Dey, R.Mondal, "Optimal parameter selection of fractional order PI controller for speed control of DC Motor", IEEE, 2017

[8] L.Y. Kok, I. Elamvazuthi and K. Ramani, "Development of a Nature Inspired Algorithm based controller for DC Servo Motor", 2017 IEEE 3rd International Symposium in Robotics and Manufacturing Automation.

[9] Roy, S. Srivastava, "Design of optimal PID controller for speed control of DC motor using constrained particle swarm optimization," IEEE Trans on Circuit, Power and Computing Technologies, 2016

[10] K. Ogata, Modern control engineering, Pearson Education India; 5 edition.

[11] J.G. Ziegler and N.B. Nichols. "Optimum settings for automatic controllers". Trans. ASME, Vol. 64, 1942.

[12] N.Hambali, A. Masngut, A. A. Ishak, Z. Janin, "Process Controllability for Flow Control System Using Ziegler-Nichols (ZN), Cohen-Coon (CC) and Chien-Hrones-Reswick (CHR) Tuning Methods ", IEEE International Conference on Smart Instrumentation, Measurement and Applications, 2014.

[13] G.C. Goodwin, S.F.Graebe and M.E. Salgado, Control sysem design, Pearson, 2000.

[14] P. M. Meshram and R. G. Kanojiya, "Tuning of PID controller using Ziegler-Nichols method for speed control of DC Motor", IEEE- International Conference On Advances In Engineering, Science And Management,2012

[15] Xue, Y. Q. Chen, and D. P. Atherton, "Linear feedback control analysis and Design with MATLAB," SIAM, Advances in Design and Control 2007

[16] Dai W. Chen and Y. Zhu, "Seeker Optimization Algorithm", IEEE,2006.

[17] Chaohua Dai, Weirong Chen, Zhanli Cheng, Qi Li, Zhiling Jiang, and Junbo Jia, "Seeker optimization algorithm for global optimization: A case study on optimal modelling of proton exchange membrane fuel cell (PEMFC)", Electrical Power and Energy Systems Vol 33 (2011) 369–376.

Vector Control of Induction Motor with and without Speed Sensor

G. Murali Krishna, Sourav Bose

***Abstract*—In this paper, vector control of induction motor (IM) with and without speed sensors has been anlysed using MATLAB/Simulink environment. Stator current model reference adaptive system (MRAS) based speed estimation method is used for rotor speed estimation in sensor less condition. The performance of a 5kW machine is analysed using this control schemes during various speed and load conditions.**

Keywords—Model reference adaptive system(MRAS), Induction motor(IM), vector control

I. INTRODUCTION

Variable speed drives (VSD) are having a wide range of applications such as fans, air conditioning systems, combustion air for boiler system, water pumping systems [1]. In the past, mostly dc motors are used in variable speed drives. Because torque and speed are controlled independently in them comfortably and efficiently. The major drawback of dc motors is the presence of commutators and brushes, which require frequent maintenance and make the motor unsuitable for explosive and dirty environments[2].

To overcome this drawbacks there is a search for the substitute of dc motors in variable speed drives. Induction motors, particularly squirrel-cage induction motors are having many advantages when compared to dc motors. Some of the main advantages of induction motors are simple and rugged design, low cost and low maintenance. However, until now, they have been mainly used in constant speed applications because conventional methods for speed control of induction motor are either expensive or sloppy. Many researchers have proposed different techniques for efficient use of induction motorsinVSD.Themostpopularspeedcontrolmethod,vector control has been proposed by Hasse and Blaschke as given in [3].

In vector control, the induction motor is operated as a dc motor to achieve independent control of speed and torque. This is done by modeling the three axes (abc) quantities of the motor into two axes (dq) quantities as given in [4]. The speed of induction motor is controlled along d-axis current and torque is controlled along q-axis current. As d-axis and q-axis are perpendicular to each other independent control of speed and torque is feasible.

The control schemes of the indirect vector control is given in [2] [5]. These control schemes requires speed information of of induction motor exactly. For this purpose ,usually a speed sensor is cling to the shaft of the motor. But the usage of the speed sensor increase the cost and a connection between the control system and motor is required. Some times speed control may also be required in the operating environment, where the usage of speed sensor is impossible. To over come these issues, several estimation methods for sensor less AC drives have been proposed in the literature over the past few years, such as signal injection based methods [6]- [7], observer based methods [8]- [10], and model reference adaptive system (MRAS) based methods [11]- [21]. Model reference adaptive system (MRAS) based speed estimation methods are widely used because of their simplicity and efficiency. In this paper stator current MRAS based method of speed estimation is described and implemented in MATLAB/Simulink environment.

Structure of the paper is organised as following. Section II presents the control scheme of indirect vector control and speed estimation process using stator current MRASbased speed estimation method. Section III includes the simulation results of indirect vector controlled IM with and with out speed sensor under various condition. Section IV contains the conclusion of the workdone.

TABLE I: Terminology used in this paper

i_{abc}, i^*_{abc}	Stator phase currents
v_{abc}	Stator phase voltages
i_{ds}, i_{qs}, $\hat{i}_{ds}, i_{qs}$	Stationary reference frame d-axis and q-axis stator currents
v_{ds} , v_{qs}	Stationary reference frame d-axis and q-axis stator voltages
$i^I_{ds}, i^I_{qs} i^*_{ds}$, i^*_{qs}	Synchronous reference frame d-axis and q-axis stator currents
λ_{ds} , λ_{qs}	Stationary reference frame d-axis and q-axis stator fluxes
λ_{dr}, λ_{qr}	Stationary reference frame d-axis and q-axis rotor fluxes
λ_r , λ_{ref}	Estimated and reference rotor fluxes
ω_r, ω_{ref}	Estimated and reference rotor speeds
T_{em}, T^*_e	Electromagnetic torque
T_L	Load torque

[1]G Murli Krishna is with Department of Electrical Engineering, National Institute of Technology Uttarakhand, India

[2]Sourav Bose is with the Department of Electrical Engineering, National Institute of Technology, Uttarakhand, India.

(e-mail: muralikrishnagowra@gmail.com, souravbose@nituk.ac.in)

II. SENSORLESS INDIRECT VECTORCONTROL

The block diagram of sensorless vector controlled squirrel cage IM is shown in the Fig. 1.

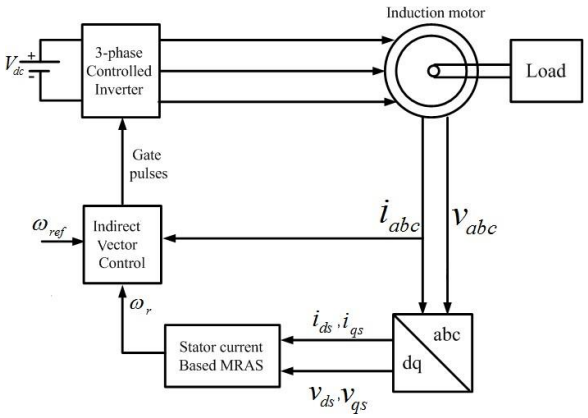

Fig. 1: Block Diagram of Indirect Vector Control

The sensor less vector control scheme is divided into two major parts. One part used for estimation of rotor speed and the other implementing the control logics using this estimated speed. Here, the speed estimation is done using stator current MRAS based speed estimation technique and the working of the same is shown in section II-A. Indirect vector control scheme is used for controlling the IM and the working of this control scheme is explained in section II-B.

A. Stator current MRAS based speed estimation

The basic block diagram of MRAS based speed estimator is shown in Fig.2.

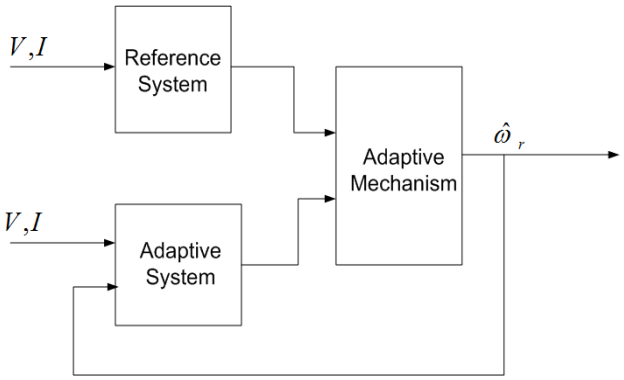

Fig. 2: Control block of MRAS based speed estimator

As shown in the figure the control scheme of MRAS technique is differentiable into three subsystems called reference system, adaptive system, an adaptive mechanism. Reference system uses measured voltages and currents for estimating the desired quantities. Whereas adaptive system also uses estimated speed along with measured voltages and/or currents for estimating the respective output quantities. The mechanism consists a PI controller, which gives the rotor speed by taking the error between reference system quantities and adaptive system quantities as input. Fig. 3 isshowing the control scheme of stator current MRAS based speed estimation.

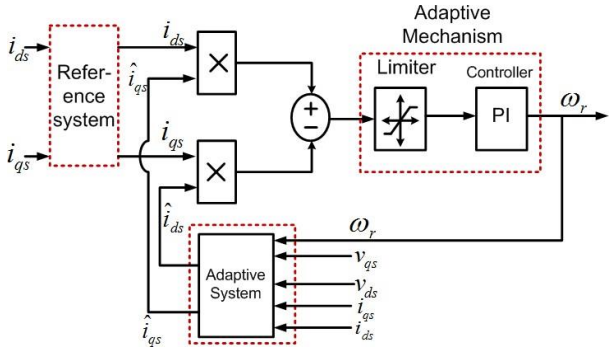

Fig. 3: Block Diagram of Stator Current MRAS based speed estimator

In this control scheme the desired output quantities from the reference system and adaptive system are stationary dq reference frame stator currents. i_{ds}, $i_{qs}$are the inputs as well as outputs of the reference system. The inputs of the adaptive system are i_{ds}, i_{qs}, v_{ds}, v_{qs}, and ω_r. From the available inputs, the outputs of the adaptive system$\hat{}$ids,$\hat{}$iqs are computed as given in the Eq. (1) - Eq. (6).

$$\lambda_{ds} = (V_{ds} - r_s i_{ds})/dt \quad (1)$$

$$\lambda_{qs} = (V_{qs} - r_s i_{qs})/dt \quad (2)$$

$$\lambda_{dr} = \frac{Lm}{Lr}(\lambda_{ds} - \sigma L_s i_{ds}) \quad (3)$$

$$\lambda_{qr} = \frac{Lm}{r}(\lambda_{qs} - \sigma L_s i_{qs}) \quad (4)$$

$$\hat{i}_{ds} = \left(\frac{\lambda}{L_m}_{dr} + \frac{1}{T_r} P\lambda_{dr} + \frac{1}{T_r} \omega\lambda_{r\,qr}\right) \quad (5)$$

$$\hat{i}_{qs} = \left(\frac{1}{L_m}\lambda_{qr} + \frac{1}{T_r} P\lambda_{qr} - \frac{1}{T_r} \omega\lambda_{r\,dr}\right) \quad (6)$$

adaptive. The input to the adaptive mechanism block is the error signal E calculated from the output quantities of reference system and adaptive system as given in Eq. (7).

$$E = i_{ds}\hat{i}_{qs} - i_{qs}\hat{i}_{ds} \quad (7)$$

The rotor speed is obtained after passing this error signal through PI controller as given in Eq. (8).

$$\omega_r = E\left(K_p + \frac{K_i}{s}\right) \quad (8)$$

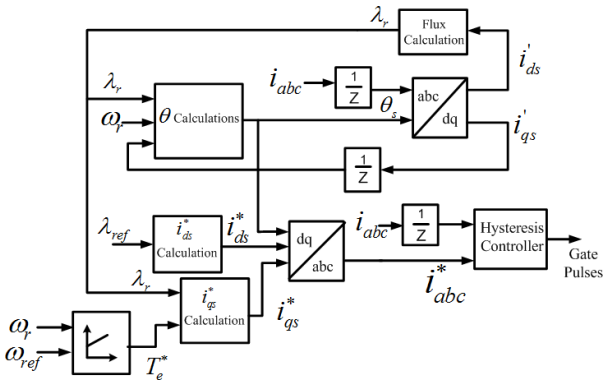

Fig. 4: Block Diagram of Indirect Vector Control

B. Indirect Vector Control

From Fig.1 it can be observed that the inputs to the indirect Vector Control block are i_{abc}, ω_r, $\omega_{ref}$and the output is the gate pulses for the inverter. The block diagram of indirect vector control scheme is shown in the Fig.4. The computations in the indirect vector control are done in synchronous dq reference frame and by considering $\lambda^t_{dr}= \lambda_r$, $\lambda^t_{qr}= 0$.

Stator currents i^t_{ds}, $i^t_{qs}$are computed by the Park's transformation of phase currents i_{abc}into synchronous dq reference frame. This conversion requires θ_s, which is calculated using the Eq. (9)

$$\theta_s = \int \omega_s dt \qquad (9)$$

Where $\omega_s$is calculated using Eq. (10)

$$\omega_s = \omega_r + \omega_{sl} \qquad (10)$$

$\omega_r$is the estimated rotor speed, which is input of vector control block. $\omega_{sl}$is the slip speed calculated as given in Eq. (11)

$$\omega_{sl} = \frac{L_m i^t_{qs}}{T_r \lambda_r} \qquad (11)$$

Rotor flux $\lambda_r$is calculated as given in Eq. (12)

$$\lambda_r = \frac{L_m i^t_{ds}}{(1+T_r p)} \qquad (12)$$

The reference stator currents i∗qs, i∗ds are calculated as given in Eq. (13) and Eq. (14)

$$i^*_{qs} = \frac{T^*_e}{K_T \lambda_r} \qquad (13)$$

$$i^*_{ds} = \frac{\lambda_{ref}}{L_m} \qquad (14)$$

Where $K_T = \frac{3PL_m}{22L_r}$, $T_r = \frac{L_r}{R_r}$

Reference stator phase currents i_{*abc} are obtained after the inverse Plark's transformation of i_{*qs}, i_{*ds}. The currents i_{abc} and i_{*abc} are fed to Hysterisis controller, which in turn produces the gate pulses for the inverter.

III. RESULTS

This section presents the performance of squirrelcage IM under various conditions controlled using above mentioned method. The machine ratings and parameters are shown in the Table II.

TABLE II: Machine Parameters

Machine Parameter	Value
Voltage (V_{LL})	440V
Power	5kW
Number of pole pairs(P)	2
Stator resistance (R_S)	1.21Ω
Rotorresistance(R_r)	1.4Ω
Stator Inductance (L_S)	0.17 H
RotorInductance(L_r)	0.17 H
Mutual Inductance (L_m)	0.165 H
Inertia (J)	0.12 Kg. m^2

Case:1 Constant load and Variable speed

In this case $T_L$is maintained constant at 10 N-m. The input reference speed is varied from 140 rad/sec to 70 rad/sec , from 70 rad/sec to 110 rad/sec at time 3sec and 6sec respectively.

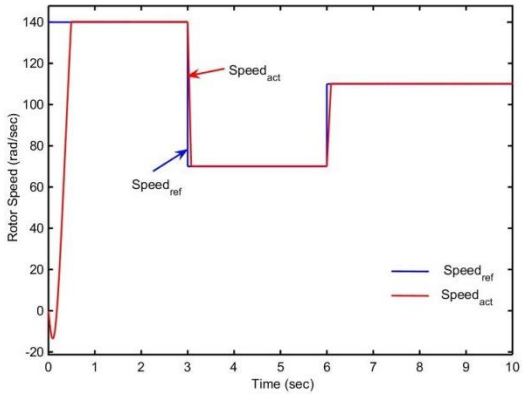

(a) Rotor mechanicalspeeds

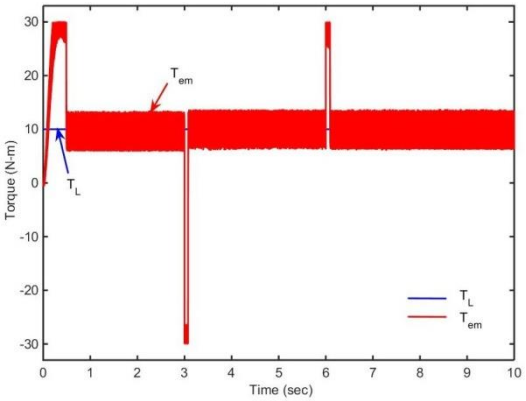

Fig. 5: Speed and Torque waveforms of IM with speed sensor under constant load condition

Fig. 5a is showing the waveforms of reference speed and actual speed of the IM when speed sensor is not used (i.e. measured speed used as input to the vector control block). Fig. 5b is showing the waveforms of load torque and electromagnetic torque in this case.

Fig. 6a is showing the waveforms of reference speed, estimated speed and actual speed of the IM during sensor less operation. Fig. 6b is showing the waveforms of load torque and electromagnetic torque.

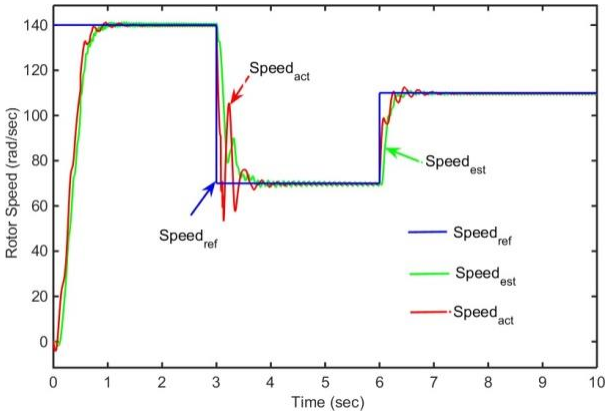

(a) Rotor mechanicalspeeds

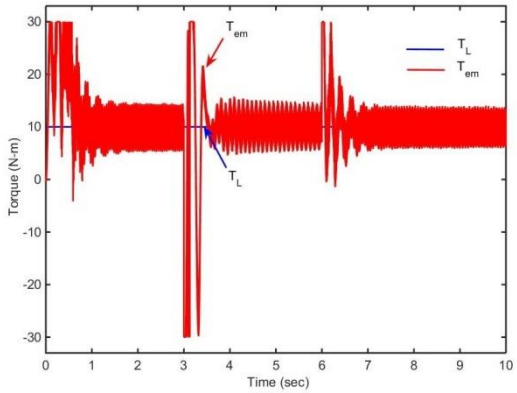

(b) Torque

Fig. 6: Speed and Torque waveforms of IM without speed sensor under constant load condition

The waveforms of actual and estimated rotor positions of IM in sensorless control operation are shown in Fig. 7.
Fig.8 is showing the reference current i_{*qs} and i_{*ds}. When there is change in speed the torque controlling current i_{*qs} is undergoing some transient state and settling in less time.
As observed from the Fig.6 and Fig.8 the i_{*qs} is constant irrespective of changes in speed and so the torque is constant.
The reference flux of IM is constant when the machine operates below rated speed. Therefore the i_{*ds}, responsible for flux controlisalsoconstantasshowninFig.8.

The d-axix stator currents for speed estimation using stator current MRAS based speed estimation i_{ds} & $\hat{i}_{ds}$ are shown in Fig. 9.

Case:2 No load and variable speed In this case the IM is operated at no load. The input reference speed is varied from

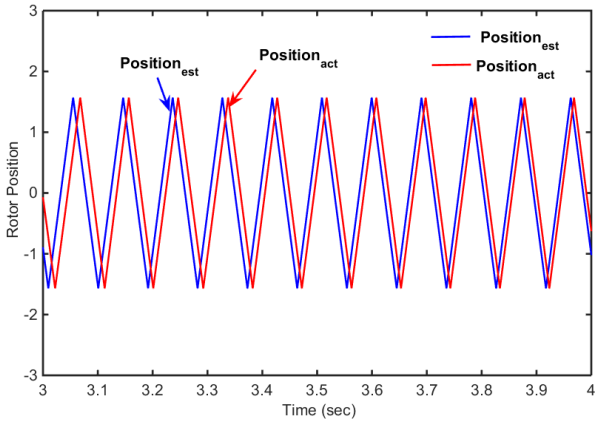

Fig. 7: Actual and Estimated Rotor positions under constant load condition

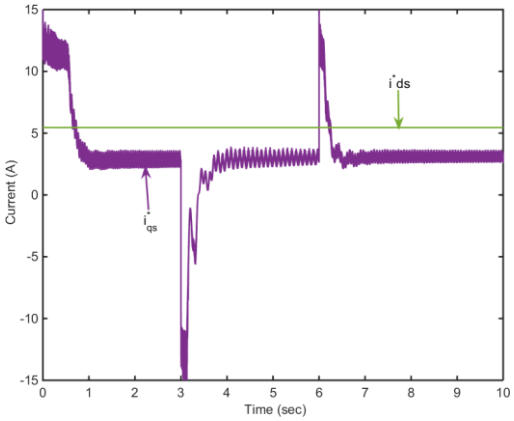

Fig.8: i_{ds}^{*} & i_{qs}^{*}

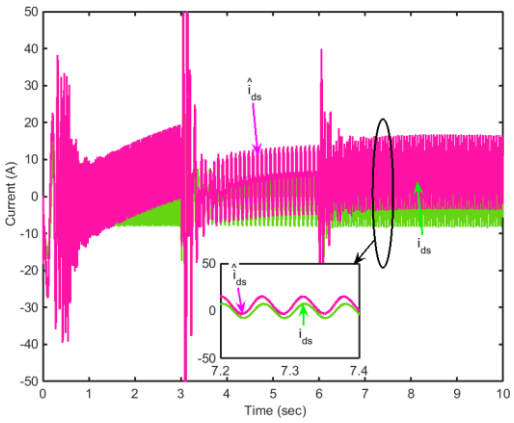

Fig.9: i_{ds} & $\hat{i}_{ds}$

140 rad/sec to 100 rad/sec, from 100 rad/sec to 120 rad/sec at time 3sec and 6sec respectively.

Fig. 10a is showing the waveforms of reference speed and actual speed of the IM when speed sensor is not used. Fig. 10b is showing the waveforms of load torque and electromagnetic torque in this case.

Fig. 11a is showing the waveforms of reference speed ,

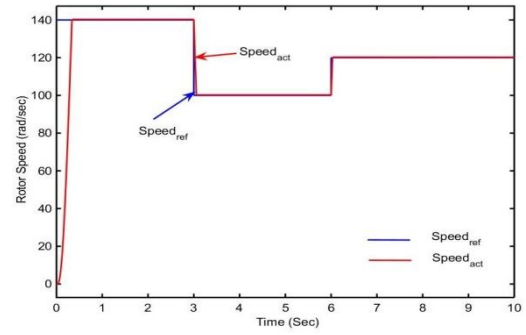

(a) Rotor mechanicalspeeds

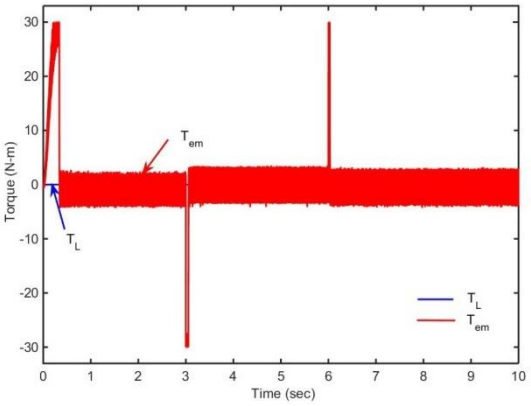

(b) Torque

Fig. 10: Speed and Torque waveforms of IM with speed sensor under no load condition

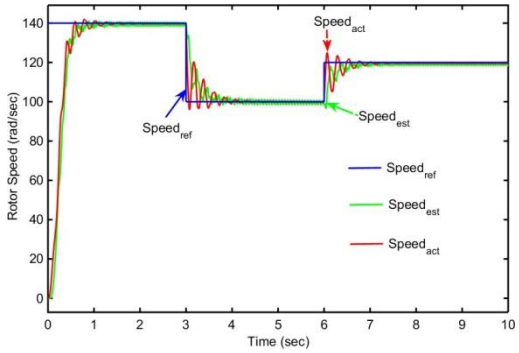

(a) Rotor mechanicalspeeds

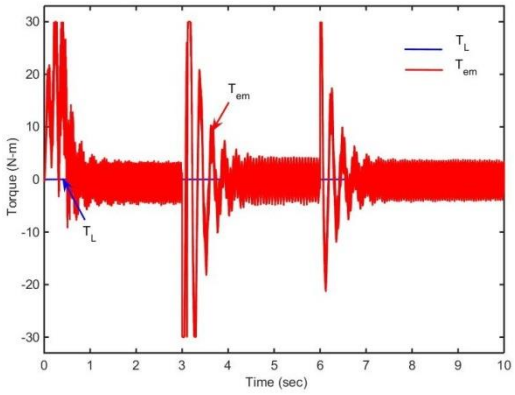

(b) Torque

Fig. 11: Speed and Torque waveforms of IM without speed sensor under no load condition

estimated speed and actual speed of the IM during sensorless operation. Fig. 11b is showing the waveforms of load torque and electromagnetic torque.

Case:3 Variable load and speed reversal

In this case $T_L$is varied from 0 N-m to 10 N-m at time 7sec. The input reference speed is varied from 140 rad/sec to -140 rad/sec at time 5sec.

Fig. 12a is showing the waveforms of reference speed and actual speed of the IM when speed sensor is not used. Fig. 12b is showing the waveforms of load torque and electromagnetic torque in this case.

Fig. 13a is showing the waveforms of reference speed , estimated speed and actual speed of the IM during sensorless operation. Fig. 13b is showing the waveforms of load torque and electromagnetic torque.

IV. CONCLUSION

The control schemes of indirect vector control and stator current MRAS based speed estimation have been described. These control schemes are implemented in MATLAB/Simulink platform to check the efficiency of working. The performance of the IM is analysed, with and without speed sensor under different load and speed conditions. From the results, itis observed that the independent control of speed and torque is achieved using indirect vector control with and without speed sensor. From the results of sensor less vector control, it is observed that the estimated rotor speed and measured rotor speed are approximately equal and are tending towards reference speed during all the conditions. The electromagnetic torque is also having oscillations around the load torque, which defines the stable operation of the IM. After comparing the performance of IM with and without speed sensors, it is observed that the machine control is done efficiently without using the speed sensor. This makes the sensor less vector controlled IM drives reliable and cheaper.

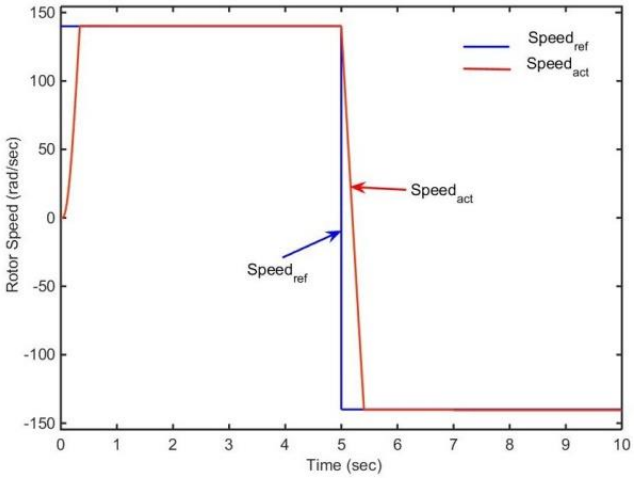

(a) Rotor mechanical speeds

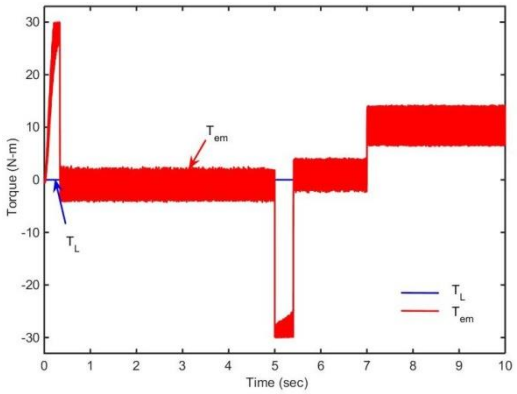

(b) Torque

Fig. 12: Speed and Torque waveforms of IM with speed sensor under variable load condition

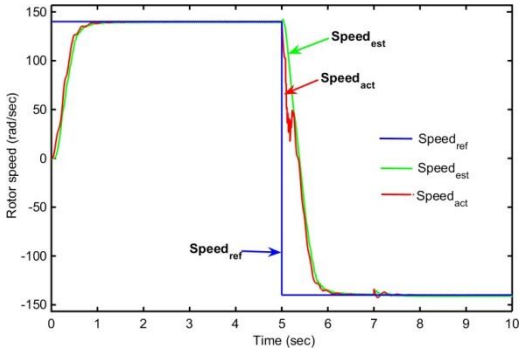

(c) Rotor mechanicalspeeds

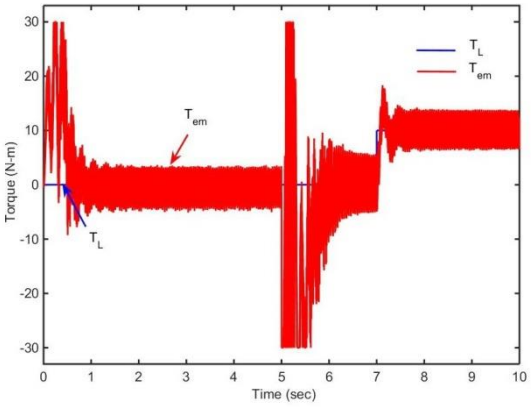

(d) Torque

Fig. 13: Speed and Torque waveforms of IM with speed sensor under variable load condition

REFERENCES

[1] R.Saidur,S.Mekhilef,M.B.Ali,A.Safari,andH.A.Mohammed,"Applications of variable speed drive (VSD) in electrical motors energy savings," Renewable and Sustainable Energy Reviews, Volume 16, Issue 1, Pages 543-550,2012.

[2] B. SrinuNaik, "Comparison of Direct and Indirect Vector Control of Induction Motor," Vol.1, Issue.1,2014.

[3] F. Blaschke, "The principle of field orientation as applied to the new transvektorclosed-Ioopcontrolsystemforrotatingfieldmachines,"1972

[4] R. J. LEE, P. PILLAY and R. G. HARLEY, " D,Q Reference Frames for the Simulation of Induction Motors, " Electric Power Systems Research, 8, 15 -26,1984/85.

[5] Sandeep Goyat, Rajesh Kr. Ahuja, "SPEED CONTROL OF INDUCTION MOTOR USING VECTOR OR FIELD ORIENTED CONTROL," InternationalJournalofAdvancesinEngineering&Technology,2012.

[6] C. Lascu, I. Boldea and F. Blaabjerg. Very-low-speed variable-structure control of sensorless induction machine drives without signal injection. IEEE Trans. On Ind. Applicat., 41(2):591598,Mar. 2005.

[7] J. Holtz. Sensorless control of induction machineswith or without signal injection. IEEE Transactions on Industrial Electronics, 53(1):7-30, Feb. 2006.

[8] F. Cupertino, A. Lattanzi, L. Salvatore and S. Stasi. Induction motor control in the low-speed range using ekf- and lkf-based algorithms. In proceeding of IEEE-ISIE, 3:12441249,1999.

[9] T. S. Kwon, M. H. Shin, and D. S. Hyun. Speed sensorless stator flux-oriented control of induction motor in the field weakening region using luenberger observer. IEEE Transactions on Power Electronics, 20(4):864869, Jul.2005.

[10] L. Kyo-Beum and F. Blaabjerg. Reduced-order extended luenberger observer based sensorless vector control driven by matrix converter with nonlinearity compensation. IEEE Transactions on Industrial Electronics, 53(1):66-75, Feb.2006.

[11] T. Raghu, J. Srinivas Rao, and S. Chandra Sekhar, "Simulation of Sensorless Speed Control of Induction Motor Using APFO Technique," International Journal of Computer and Electrical Engineering, Vol. 4, No. 4, August2012.

[12] Colin Schauder, "Adaptive Speed Identification for Vector Control of Induction Motors without Rotational Transducers," IEEE TRANSACTIONSONINDUSTRYAPPLICATIONS,VOL.28,NO.5,1992.

[13] Mohammad N. Marwali and Ali Keyhani, Senior Member, IEEE, "A Comparative Study of Rotor Flux Based MRAS and BackEMF Based MRAS Speed Estimators for Speed SensorlessVector Control of Induction Machines," IEEE Industry Applications Society Annual Meeting New Orleans, Louisiana,1997.

[14] Roberto Crdenas, Member, IEEE, Rubn Pea, Member, IEEE, Jos Proboste, Greg Asher, Senior Member, IEEE, and Jon Clare,Senior

Member,IEEE,"MRASObserverforSensorlessControlofStandaloneDoubly Fed Induction Generators," IEEE TRANSACTIONS ON ENERGY CONVERSION, VOL. 20, NO. 4, 2005.

[15] Chul-Woo Park, Woo-Hyen Kwon, "Simple and robust speedsensorless vector control of induction motor using stator current based MRAC," ElectricPowerSystemsResearch71(2004)257266.

[16] Roberto Crdenas, Senior Member, IEEE, Rubn Pea, Member, IEEE,Jon Clare, Senior Member, IEEE, Greg Asher, Fellow, IEEE, and Jos Pro- boste,"MRASObserversforSensorlessControlofDoubly-FedInduction Generators," IEEE TRANSACTIONS ON POWER ELECTRONICS, VOL. 23, NO. 3,2008.

[17] S. Maiti and C. Chakraborty. Mras-based speed estimation techniques for vector controlled double-inverter-fed slip-ring induction motor drive. In proc. of 34th Annual IEEE Conference on Industrial Electronics, pp:1275-1280, Nov,2008.

[18] S. Maiti, C. Chakraborty, and S. Sengupta. Simulation studies on mrac-based speed estimation technique for the vector controlled permanent magnet synchronous motor drive. Simulation Modelling Practiceand Theory,2008.

[19] S. Maiti, V. Verma, C. Chakraborty, and Y. Hori. An Adaptive Speed Sensorless Induction Motor Drive With Artificial Neural Network for Stability Enhancement. IEEE Transactions on Industrial Informatics, 8(4):757-766, Nov.2012.

[20] V. Verma, C. Chakraborty, and Y. Hori. Speed Sensor lessVector Controlled Induction Motor Drive Using Single Current Sensor. IEEE Transactions on Energy Conv., 28:938-950,2013.

[21] M. F. Rahman, L. Zhong, M. E. Haque, and M. A. Rahman. A direct torque controlled interior permanent magnet synchronous motor drive without a speed sensor. IEEE Trans. on Energy Conversion, 18(1):1722, Mar.2003.

A Survey on Rolling mill system with various Control techniques

B Hemakumar, A M Aminur R B, M P R Prasad

Abstract— **Different possible control techniques of rolling mill system till date has been reviewed in this paper. The control techniques explained are a) Population Adaptive Immune Algorithm (PAIA), b) Advanced Fuzzy Generalized Predictive Control (AFGPC) optimization technique, c) Hydraulic Automatic Gauge Control (AGC), d) Active Disturbance Rejection Control (ADRC), e) Impedance Controller(IC), etc. The work done by the authors on these techniques has been presented based on the variables I) Thickness, II) Strip tension, III) Roll eccentricity, IV) Loop position and V) Strip breakage. Classification of these techniques from various authors has been done. The results of various control techniques have been presented for ease of analysis in the application point of view.**

Keywords: rolling mill system, thickness, strip tension, roll eccentricity, control techniques, automatic gauge control.

I. INTRODUCTION

The technology development in the rolling mill system is changing considerably, both qualitatively and quantitatively. This may tend to the fact that with the growing technological development, the dependence on rolling mill system has been increased widely. In the present scenario rolling mill systems were facing major problems related to different aspects apart from that few problems discussed which shows large difference in the rolling system.

Population adaptive immune algorithm (PAIA) and advanced fuzzy generalized predictive control (AFGPC) optimization techniques were used to solve multi objective scheduling and advanced control of an experimental hot rolling mill [1]. An experimental work on hydraulic automatic gauge control (AGC), which control the thickness and plate position [2]. An active disturbance rejection control (ADRC) is used for better robustness and adaptability in extended state observer model [3-4]. Hamilton's principle and the Galerkin weighted residual method were used with several non- linearities. With the help of an impedance controller for strip tension and looper position is designed. The predictive accuracy is increased by improving the parameter adaptive algorithm and Automatic gauge control method were used to control and carry out the rolling process and production of ultra-thin and high strength strips [5-8]. Data analyzedin the area of non-stationary signals and detected deviations in strip movement can be improved by different time frequency based analysis methods. Control of hot roll bending under rolling pressure using WRBS (work roll bending system) in servo and proportional value.

Inter-stand tension inferential and aligning ability of the rolling mill depends on the speed of the rolling mill. Automatic strip tension control of wide strip hot rolling mill was improved with the help of hydraulic gap controller. This cross controller eliminates the impact of loop gear location on the system for specific tension control [9-18].

Investigated on severe strip breakage of thin slab rolling and casting with visual observation [19]. In this, parameter estimation and online monitoring of roll eccentricity in rolling mills. Rolling eccentricity monitoring system design based on adaptive observer optimization technique [20-22]. Strip thickness and tension controlled by model predictive controller in a cold rolling mill and some conventional controllers were used in this design. Meshless solution for rolling based on local radial basis function collection method (LRBFCM), the strip head motion control during the strip infeed in hot rolling mills. Here an optimal controller developed depends on linear programming and it is compared to standard quadratic programming. Hardware designed for wireless power supply to a signal encoder and digital data transfer between a transmitter and receiver. The response of the system commissioning at the 5000mm rolling mill [23-29]. Plate thickness is controlled based on hydraulic gap control cylinders. And compared result with an indirect method of measurement of thickness of the metal plate[30].

This paper outline as follows: The general description about rolling mill system with different controllers is explained in the following sections. The various methodologies followed for rolling mill system is explained and results compared in III section and the review of rolling mill system concluded in sectionIV.

II. ROLLING MILLSYSTEM

Metal producers balance the need for more consistent and higher quality rolled products, which the projected design is proposed by Sid-Ahmed Gaffour et.al [1]. A multi-objective optimization technique is based on Population Adaptive Immune Algorithm (PAIA). Physically-based models and Symbiotic data-driven modelling for the precise estimation of mechanical properties of alloy steel. Advanced control, including Adaptive Fuzzy Generalized Predictive Control (AFGPC) which promise the optimal performance of the mill through the rolling process. Henceforth accomplish 'right- first-time' production of these alloy steel through the anticipated final microstructure and mechanical properties. State- of-the- art mechanisms for scheduling optimization and control Steps followed by this sequence Microstructure Optimization, Rolling Schedule Optimization, Optimizing the Process Parameters. This paper projected a new optimization technique to develop an integrated model-design approach to optimize and control the hot-rolling mill. The use of 'Symbiotic' data- driven modelling and PAIA Algorithms.

Yin Yuheng et.al[2] have approached the Plate and strip hydraulic AGC (Automatic Gauge Control) mills system

[1]B. Hemakumar is with Department of Electrical Engineering, National Institute of Technology, Kurukshetra, India
[2]A M Aminur R B is with the Department of Electrical Engineering, National Institute of Technology, Kurukshetra, India
[3]M P R Prasad is with the Department of Electrical Engineering, National Institute of Technology, Kurukshetra, India
(e-mail: bhk965@gmail.com aamin.hcl@gmail.com, mprp823@gmail.com)

which comprises of electrical, mechanical, and hydraulic systems. Because of an electrohydraulic servo technology, the hydraulic AGC system's dynamic response speed has been improved very rapidly. The mill plate applied to a constant roll gap control method, thus the bite of steel, rolled and cast steel vary with the settings in the rolling course. The mill plate may meet numerous kinds of intrusions, such as the unpredictability of the strip temperature, rolling force, hardness and other parameters, which results in the alteration of operating environments. The outcomes show that the dynamic simulation results based on this model is consistent with the theory and experiment; hence, the model is a comparatively comprehensive and is satisfactory to examine several aspects which affect the final rolling accuracy in the rollingprocess.

Wang Lijun et.al [3-4] approached hydraulic automation position control (HAPC) is placed in the forward loop of the AGC system. The dynamical models of the HAPC have several uncertainties, which are results of physical characteristics, disturbances and load variations.

The straightforward knowledge of active disturbance rejection control (ADRC) method is that the total disturbances are projected and aggressively compensated in real time for an uncertain system. Owing to its disturbance rejection abilities and robustness, the ADRC method has been commonlyapplied.

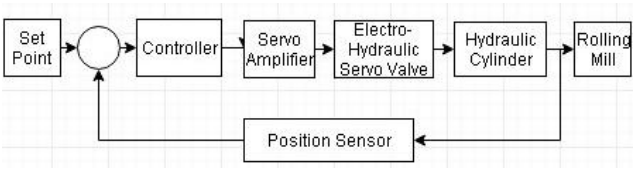

Fig. 1: The schematic diagram of HAPC system

They validated that the projected ADRC is real-world and very active in trading with the uncertainties and other peripheral disturbances. A. steinboeck et.al[5] proposed Advancedmultivariable control systems, the interactions among strip thickness, roll gap, roll speed, strip tension, dimensions, and looper angle is methodically taken into account. In view of the prevailing solutions for looper control, the purpose of the recent paper are as follows, Discover whether the bending stiff ness, the plastic deformation, and the dynamic forces of the strip are contained by a precise mathematical model of the looper. Find whether the system displays significant nonlinearities. Design an estimator for the strip tension. Design a controller that is accomplished of controlling the looper in the entire operating range, i.e., in the working position and for threading and unthreading of the strip beneath the working position[6].

Li Zhao et.al [7] approached the dynamic setting of AGC to estimate the rolling force improvement triggered by the disturbances in the rolled strip thickness resulted by gap regulation. Rendering to estimated increase in the rolling force, the thickness aberration can be removed effortlessly. In this paper, a new modeling technique called U-model is applied, which was originally planned in [8]. This U-model has less computational complexity compared to other parametric models such as, Hammerstein model, non-linear autoregressive moving average with exogenous inputs (NARMAX) model etc. This U-model doesn't facilitate modeling but provides controller design. It exploits the past input and output data for modeling and a polynomial root solving algorithm for the calculation of controllersignal.

The fundamental aim of intricate AGC is the combination of dynamic setting AGC and flow type AGC. It can recompense the varying rolling mill force with the gap regulation and dodge delay of monitor AGC. The simulation results in a better-quality.

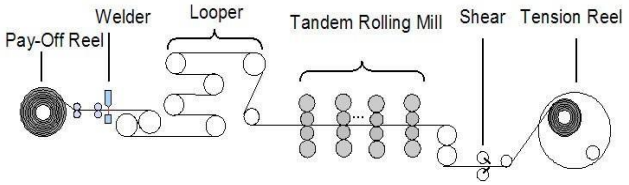

Fig. 2: Layout of a Continuous Cold Rolling Mill

AshridRother et.al [9] proposed to increase the longevity of the components, the fault finding and the identification becomes most significant in the manufacturing plants. The analysis of the data is done on the fitness of non-stationary signals. These approaches are applied to hot strip mill to notice aberrations in strip travel which affect the product excellence or causeinterruptions.

A basic introduction to the mathematical tools used for data-driven approaches is given including Short-Time Fourier Transform (STFT), Wigner–Ville Distribution (WVD), Continuous (CWT) and Discrete Wavelet Transform (DWT), and Empirical Mode Decomposition (EMD).

All approaches convert into time-frequency domain. The STFT conserves constant resolution for the entire frequencies [10], since the window is equal for the whole signal. Decent frequency resolution at low frequencies (wide windows) comes with a low time resolution at high frequencies. The main benefit of using STFT is the easy interpretation of the graphical outcome which is used in several researches regarding acoustics and vibrations, where the square of the transform outcome is plotted as a spectrogram. Hence, it is well suitable for non-stationary signals.

Maklakova E.A. et.al [13], described the type of thickness aberration which arise during hot plate rolling process. It is initiated for bending of rollers under the rolling pressure. The system results were considered as the conditions for the hot rolling plate mill. In this the width difference means the aberration on the absolute value.

Equation $\Delta_i = \boldsymbol{\delta}_i \sim \boldsymbol{\delta}_{cp}$

Where, $\delta cp = \left(\frac{1}{n}\right) * \sum_{i=1}^{n} \delta i$ is the average thickness of thesheet

$$\Delta = \left(\frac{1}{n}\right) * \sum_{i=1}^{n} \Delta i$$

Many of contemporary rolling mills are used to calculate the roller bending value through the process which are equipped with an effort of Roller Bending System (RBS) [14]. The RBS is used to control the rolling forces and it works as follows. The authentic value of the rolling force is deducted from the anticipated value. The rolling model determines the change in gain. The resultant value is

used as a supplementary signal to the force regulator. In case of rolling force aberration from the marked value, the output signal is then modified.

Shokhin v.v. et.al [15], studied continuous milling of the inter-stand tension inferential control systems are used for the rolling motor torque control. An alternate option may include torque balance which will affect the speed of the former controlled mill stand. The tension control precision depends on the determination of unhindered rolling torque. This paper finds that the features of the rolling mill depend on the rolling speed and comprises aligningability.

The above case study concludes that the alignment of the gauge is provided with the tension control system affecting the speed which proves the fact that the feature of the rolling mill along with its line up ability depends on its speed. At advanced speeds the alignment property of the roller is reduced but the inter-stand tensions suffer minor variations in the rolling operation is improved [16]. It is suggested to apply modeling methods and obtain the estimation of the regulator tension for the continuous rolling mills.

V. K. Khramshin et.al [17], trend in the development of wide-strip hot rolling (WSHR) is switching from 0.8-1.5 mm thick hot-rolled strip, whose geometry is similar to that of the cold-rolled products. Existing local systems for geometry control are designed for rolling higher thickness say 2 to 10 mm strips and do not meet the specifications because of the specific tension on roll gaugeinfluence.

The use of a cross-controller in the developed system enables the elimination of the system impact for the control of loop gear location on the system with specific tension control [18].The reconstruction of the mill facilities help in the complete commercialization of the developed system. The installed mechanical and power equipment of the stands and loop gears shall be replaced during reconstruction.

Diptak Bhattacharya et.al [19] studied about automation system recordings of roll separating forces which is experienced by the Stands during rolling of the strip under study are represented. It can be observed that the rolling force of F4 Stand was fairly stable. At the heavier concentration side of such foreign materials, rolling to lower thickness may have exposed the material on both the surfaces. Thus the material gets removed ultimately due to their low deformability, leaving behind the holes. Remnants of such foreign materials with the crack like defects are available at the corner holes in location 3 will clearly relate the origin of these holes to these foreign materials.

Presence of foreign materials in the form of secondary steelmaking slag is observed at the breakage site in the strip. Rolling Strips to low thickness when exposed the foreign materials completely they get removed subsequently because of the lack of deformability in forming the holes.

Xu Yang et.al [20] represented the parameter estimation and online monitoring of roll eccentricity in rolling mills. The strip thickness deviation and product quality degradation are observed due to Roll-eccentricity induced disturbances [21].The performance and effectiveness of the proposed eccentricity monitoring system are demonstrated through a case study of a cold rolling mill from industrial fields. The key parameters of periodic roll-eccentricity induced disturbance, although the initial parameters of roll eccentricity can be measured and extracted [22] via rolling force sensor from a preloading experiment, which is executed without a strip in a steady rolling state. It is also necessary to design and to be operated together with the conventional control loop for an automatic gauge control (AGC)system.

We have designed an online parameter estimation and monitoring system for roll eccentricity. The model and characteristic of roll eccentricity, as well as its influence on the strip exit thickness, have been introduced.

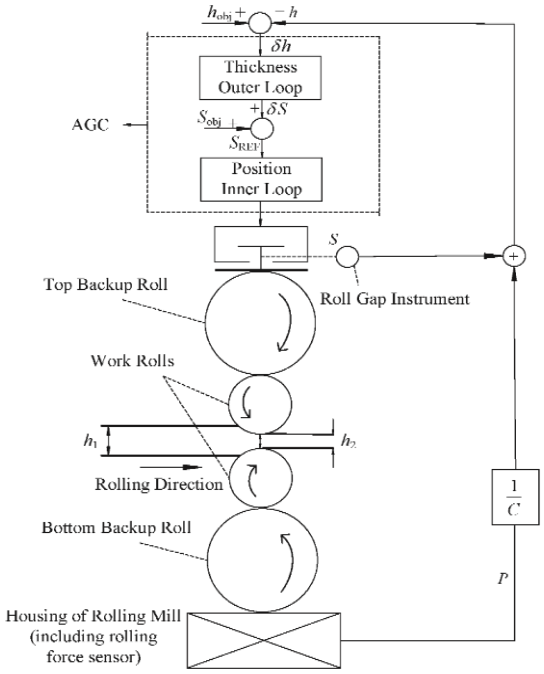

Figure 3: Structure of a mill stand with the AGC system

Tomotoshiogasahara et.al [23-27] explicit Model Predictive Control (MPC), the optimization problem in the MPC for the linear time-invariant system such as a quadratic programming problem is converted into a multi- parametric programming problem, and then the solution is obtained as a piecewise affine function of the state of the plant in offline. Hence it does not require any online optimization and can potentially reduce the implementation cost and overcome the limitation of norma lMPC.

Some of the experimental results were tabulated above which shows that speed reduces on increasing the pass number in the optimal structure and on decreasing the damping constant, we get improved performance than in the nominal system.

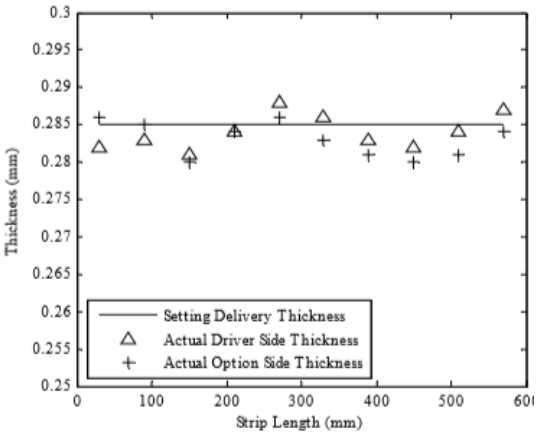

Fig. 4: Strip Thikness Data [7]

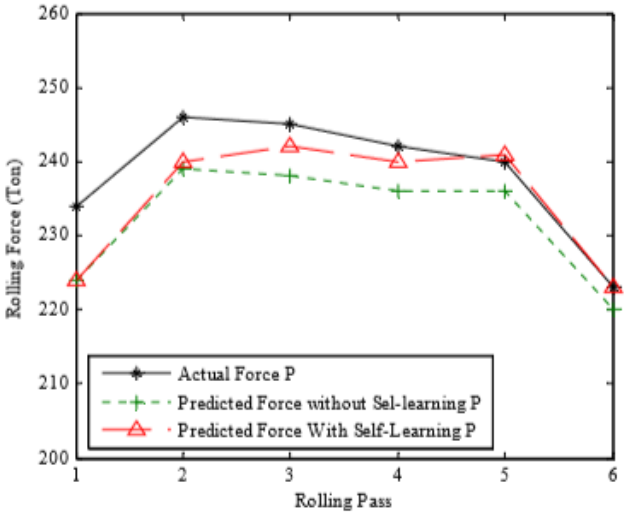

Fig. 5: Rolling force prediction [7]

Result of parameter-adaptive algorithm is presented in fig. 4 and fig. 5. Strip thickness data looks better accumulated and uniform and rolling forces are predicted with better accuracy. It can be observed that, they are resulting some good conclusions. Thus a conclusion can be made that, if we can make the system follow a particular system then we can expect a better result to come. Hence a better trial can be attempted with Model-Reference Adaptive Control method.

III. CONCLUSION

An overview on various control techniques of rolling mill system is presented and a thorough study of different features in previous research papers related to the control techniques in rolling mills have been carried out. Mainly those control techniques have been used for reduction of plate thickness, strip tension, roll eccentricity, loop position and strip breakage in them. Some of these control techniques has been discussed with their results. Among all these, model predictive controller is the best controller in the view of strip thickness and tension, which is used in practical applications. All studies give an idea that, with Model-Reference Adaptive Control (MRAC) these systems may perform better.

REFERENCES

[1] Sidahmed, Gaffour, Mahfouf, Mahdi and Panoutsos, George & Chen, Jun. "AnIntegrated System Approach for Solving Multi-Objective Scheduling Problems and Advanced Control of an Experimental Hot-Rolling Mill," *proceedings of 18thIFAC world congress*, Milano, August 2011.

[2] Yin Yuheng and Wang Yue, "Detection and analysis of dynamic characteristic of plate and strip hydraulic AGC rolling mills system," *Proceedings of 2012 International Conference on Measurement, Information and Control*, Harbin, pp. 707-711,2012.

[3] L. Wang, Q. Li, C. Tong, Y. Yin, Z. Gao and Q. Zheng, "Disturbance rejection in hydraulic automation position control system for rolling mills," *Proceedings of the 32nd Chinese Control Conference*, Xi'an, pp. 5498-5503,2013.

[4] D.L. Chern and Y. C. Wu, "An optimal variable structure control with integral compensation for electrohydraulic position servo control systems," *IEEE Trans. on Industrial Electronics*, Vol no. 5, 460–463, 1992.

[5] A. Steinboeck, G. Mühlberger, A. Kugi, "Control of Strip Tension in a Rolling Mill Based on Loopers and Impedance Control," In *IFAC Proceedings*, Vol no. 47, Pp. 10646-10651,2014.

[6] Zhong, Z. and Wang, J. "Looper-tension almost disturbance decoupling control for hot strip finishing mill based on feedback linearization," *IEEE Transactions on Industrial Electronics*, vol no. 8, pp. 3668–3679, 2011.

[7] L. Zhao and J. Wang, "The application of improved parameter-adaptive algorithm based on U-model in AGC control system of cold rolling mill," *IEEE International Conference on Information and Automation (ICIA)*, pp. 311-316,2014.

[8] Bin-hu YANG, Wei-dong YANG, Lian-gui CHEN, Lei QU, "Dynamic Optimization of Feedforward utomatic Gauge Control Based on Extended Kalman Filter, Journal of Iron and Steel Research," *International*, Vol No. 2, pp. 39–42,2008.

[9] Astrid Rother, MohieddineJelali, Dirk Söffker, "A brief review and a first application of time-frequency-based analysis methods for monitoringofstriprollingmills,"In*JournalofProcessControl*, Volume 35, 2015, Pages 65-79

[10] D. Keren, M. Werman, J. Feinberg, "A probabilistic approach to pattern matching in the continuous domain," *IEEE Trans.* Pattern Anal. Mach.Intell. 34 pp. 1873-1885,2012.

[11] C.Bisu,L.Olteanu,R.Laheurte,P.Darnis,O.Cahuc, "Experimental approach on torsordynamic analysis for milling process monitoring and diagnosis," *Procedia CIRP*, pp. 73-78,2013.

[12] K. Peng, K. Zhang, G. Li, D. Zhou, "Contribution rate plot for nonlinearqualityrelatedfaultdiagnosiswithapplicationtothehotstripmill process," *Control Eng. Pract.* Vol no. 21, 360-369,2013.

[13] E.A. Maklakova, A.S. Maklakov, V.R. Gasiyarov, S.S. Voronin, "The Work Roll Bending Control System of the Hot Plate Rolling Mill," In Procedia Engineering, Vol no. 129, Pp. 37-41, 2015.

[14] S.S. Voronin, D.U. Usatiy, "A variable compression slab technology in the vertical and horizontal rolling cages of the hot plate mills," Actual problems of modern science, technology and education. 71 (2013).

[15] V. V. Shokhin, O. V. Permyakova, "The Study of Continuous Rolling Mill Inter-stand Tension Inferential Control Systems" In Procedia Engineering, Vol no. 129, Pp. 231-238, 2015.

[16] A.A. Radionov, A.S. Karandaev, V.R. Khramshin, I.Yu. Andryushin, A.N.Gostev, "Speed and Load Modes of Rolling Hollow Billet atthe Wide-Strip Rolling Mill," Proceedings of 2014 International Conference on Mechanical Engineering, Automation and Control Systems, 2014.

[17] V.R. Khramshin, A.A. Radionov, G.P. Kornilov, K.E. Odintsov, "Improvement of Electric and Mechanical System for Automated Strip Tension Control at Continuous Wide-Strip Hot-Rolling Mill," In Procedia Engineering, Vol no. 150, Pp. 11-17, 2016.

[18] V.R. Khramshin, V.M. Salganik, V.A. Zhilina, I.M. Yachikov, "Mathematical Model of Electromechanical Systems of Wide-Strip HotRolling Mill Continuous Train," In Proceedings of 2015 International Conference on Mechanical Engineering, Automation and Control Systems, 2015.

[19] Diptak Bhattacharya, Avinash Mishra, Ganga Prasad Poddar, Siddhartha Misra, "Case study of severe strip breakage in rolling mill of Thin Slab Casting and Rolling shop of TATA Steel, Jamshedpur," In Case Studies in Engineering Failure Analysis, Vol no. 5, Pp. 15-22, 2016.

[20] X. Yang, H. Luo, M. Krueger, S. X. Ding and K. Peng, "Online Monitoring System Design for Roll Eccentricity in Rolling Mills," IEEE Transactions on Industrial Electronics, Vol no. 63, pp. 2559-2568, April 2016.

[21] S. Huang, K. K. Tan, and T. H. Lee, "Fault diagnosis and fault-tolerant control in linear drives using the Kalman filter," IEEE Trans. Ind. Electron., Vol no. 59, pp. 4285–4292, Nov. 2012.

[22] S. Yin, H. Luo, and S. X. Ding, "Real-time implementation of fault tolerant control systems with performance optimization," IEEE Trans. Ind. Electron., Vol no. 64, pp. 2402–2411, May 2014.

[23] Tomoyoshi Ogasahara, Morten Hovd, Kazuya Asano, "Explicit Model Predictive Controller Design for Thickness and Tension Control in a Cold Rolling Mill," In IFAC-Papers OnLine, Vol no. 49, Pages 126-131, 2016.

[24] Kim, K. and Won, S. "Observer-based guaranteed cost control for lateral motion of a strip in hot rolling process," IEEE International Conference on Control and Automation, pp.1479 –1484, 2013.

[25] Schausberger, F., Steinboeck, A., and Kugi, "A Mathematical modeling of the contour evolution of heavy plates in hot rolling," Applied Mathematical Modelling, Vol no. 39, pp.4534–4547, 2015.

[26] Maklakova, E.A. Gasiyarov, V.R., Maklakov, A.S., Voronin, S.S. “Simulation modeling of the rolling mill stand 5000 OJSC MMK,” 2nd International Conference on Industrial Engineering, Applications and Manufacturing, pp. 1-5, 2016.
[27] V.R. Khramshin, A.S. Evdokimov, S.A. Evdokimov, and A.S. Karandaev, “Development and Industrial Introduction of Systems for Monitoring Technical State of The Rolling Mills,” Proceedings of the 2015 IEEE NW Russia Young Researchers in Electrical and Electronic Engineering Conference (EIConRusNW), pp. 208-213, 2015.

Control of Rotary Inverted Pendulum

The rotary inverted pendulum is a nonlinear and highly unstable system which is apt forthe study of stability and self-balancing. The nonlinear modelcan be linearized about the operating region i.e. the upright position for the design of thecontroller. The controlling behavior involving in the majority of the real-life implementationssuch as height control of aero vehicles, missiles, aircraft landing, stabilization of ship against currents, altitude control of rockets and satellite, missile stabilization in upward direction, sky scrapping buildings etc. is similar to the inverted pendulum control. It has two degrees of freedom and a single actuatorwhich makes it to be in the class of less triggered system.

Designing a controller for the stabilization of pendulum is a challenging task. This design becomes more complex because of the physical limitations of applied voltage, rotation angle, and pendulum angle. Three aspects have been considered in the literature to control an inverted pendulum. The first aspect is to swing up the pendulum from original position to functioning position. Second is to stabilize the pendulum link of RIP (balancing) at the functioning location (unstable equilibrium point) and the last aspect is to track control of RIP (tracing). Different controllers of controlsystem theory can be applied to stabilize it such as state feedback control, linear quadraticregulator, sliding mode control, model reference adaptive control etc.

Two papers are included in this domain. One is ***Comparison among LQR and PID controller for stabilization of Rotary Inverted Pendulum.***Two conventional control techniques such as Two Loop Proportional, Integral and Derivative (PID) and Linear Quadratic Regulator are implemented and tested on real time hardware QUBE-SERVO setup. Second entitled ***Study of the effect of weighting matrices of LQR for control of rotary inverted pendulum*** is analysis of variation of weighting matrices of LQR for the benchmark rotary inverted pendulum. Study is mainly done for the time domain analysis and actuator dynamics.

Comparison among LQR and PID controller for stabilization of Rotary Inverted Pendulum

Ravi Kumar Gupta, Vikram Chopra

Abstract - Rotary Inverted Pendulum (RIP) is an under actuated, highly nonlinear and unstable system and is widely used for testing various control techniques. The system has two degrees of freedom, one is rotary arm position (denoted by θ) and other is the pendulum arm position (denoted by α). In this paper, the stabilization of the RIP has been achieved using conventional methods i.e. Linear Quadratic Regulator (LQR) technique and PID controller. LQR controller is the state feedback controller in which poles are placed in the desired location by using pole placement technique. Two Loop PID controller is a double feedback mechanism. In this control technique, two states theta and alpha are fed back to the PID controller and minimize the error which is the difference of reference and actual position of theta and alpha. The control schemes have implemented using MATLAB Simulink. The LQR controller has also bee implemented on QUANSER QUBE-SERVO real time hardware.

Index Terms *– Rotary Inverted Pendulum, Mathematical modelling, LQR control technique, Two Loop PID control technique, QUANSER QUBE-SERVO*

I. INTRODUCTION

Inverted pendulum is a typical benchmark problem in control industry and studied by many research scholars to established different and effective as well as robust control techniques like Pole Placement [1], PID control [2], LQR [3], Fuzzy logic control [4], neural network [5], sliding mode [6], integral sliding mode, H-infinity control [7] etc. Last few decades, most control techniques are designed and verified on the inverted pendulum. Akhtaruzzaman, Shafie [8] proposed the Two DOF PID control technique, LQR and Full State Feedback control technique for stabilizing the rotary inverted pendulum in upright position. Anvar, Hassanzadeh and Alizadeh [9] proposed the sliding mode-state feedback control scheme for stabilization of rotary inverted pendulum. Ghosh, Krishnan and Subudhi [10] proposed the two loop PID controller to stabilized the inverted pendulum arm in upright direction via Pole Placement technique. Nath, Mitra [1] proposed the controllers for swing-up and stabilization of RIP using Counter based and Pole Placement with integrator. Hassanzadeh, Mobayen [11] proposed the Binary Genetic Algorithm based input-output feedback linearization controller for stabilization of rotary inverted pendulum. Kathpal, Singla [12] proposed the different control technique like Pole Placement, Proportional Derivative (PD) and Linear Quadratic Regulator (LQR) control to stabilize the inverted pendulum in upright position and also applied above control techniques on the QUANSER QUBE-SERVO hardware. Dwivedi, P. Pandey, S. Junghare A.S. [2] proposed the fractional controller for stabilization of unstable equilibrium point of rotary inverted pendulum.

Inverted pendulums are basically divided into two categories. First, linear inverted pendulum and the other is rotary inverted pendulum. The linear inverted pendulum is further divided into four types which is depend on the direction of cart, x, x-y, x-z and x-y-z inverted pendulum. In linear inverted pendulum, the cart length is fixed, so the rotary inverted pendulum is discovered by A. Furuta [13] in 1992 which has no cart length limitation. That's why the Rotary Inverted Pendulum is also called Furuta Pendulum.

Rotary Inverted Pendulum [12] which is shown in fig.2 is a highly non-linear,dynamically unstable,underactuated and multivariable system which is widely used in many real-world applications such as maintaining equilibrium state for two legged robots, stabilization of cabin in a ship, altitude control of rockets and satellite, missile stabilization in upward direction, sky scrapping buildings etc.

Designing a controller for the stabilization of pendulum is a challenging task. This design becomes more complex because of the physical limitations of applied voltage, rotation angle, and pendulum angle. Three aspects have been considered in the literature to control an inverted pendulum. The first aspect is to swing up the pendulum from original position to functioning position. Second is to stabilize the pendulum link of RIP (balancing) at the functioning location (unstable equilibrium point) and the last aspect is to track control of RIP (tracing).

The prime objective of this paper is to implement conventional control techniques for the stabilization of pendulum arm of RIP. Basically, two conventional control techniques such as Two Loop Proportional, Integral and Derivative (PID) and Linear Quadratic Regulator are implemented and test it on real time hardware QUBE-SERVO setup. PID is the most popular classical control approach which is used in many control industries.

QUANSER provide the real time hardware setup of Rotary Inverted Pendulum called QUBE-SERVO setup. The QUBE-SERVO setup comes in types: the USB interface, Direct I/O interface and NI myRIO interface [15]. In this paper, QUBE-SERVO USB

[1]Ravi Kumar Gupta is with Department of Electrical and Instrumentation Engineering, Thapar Institute of Engineering and Technology, Patiala, India

[2]Vikram Chopra is with Department of Electrical and Instrumentation Engineering, Thapar Institute of Engineering and Technology, Patiala, India

(e-mail: vikram.chopra@thapar.edu, rgupta_me16@thapar.edu)

interface setup has been used. In USB interface setup, the power amplifier and data acquisition (DAQ) device are inbuilt. The QUANSER QUBE-SERVO setup has direct drive-18 V brushed DC motor and two encoders used for angle measurement of rotary arm and pendulum arm. One encoder is attached with DC motor and other is with pendulum. It has inbuilt PWM amplifier. The QUANSER QUBE-SERVO setup is shown in fig.1.

Fig.1: QUBE-SERVO setup

The remaining paper is organized as follows. In section II, dynamic modeling of rotary inverted pendulum is discussed. Section III describe the implementation of Two Loop PID and LQR control strategies. In Section IV, simulation and hardware results are obtained. Section V highlights the conclusions of the paper.

II. SYSTEM DYNAMICS AND MATHEMATICAL MODELLING OF RIP

A schematic representation of Rotary Inverted Pendulum is shown in Fig. 2. The equations of motion are computed using Euler-Lagrange method. The two generalized coordinates chosen in this case are θ and α, which represent the angular displacement of the rotary arm and pendulum from their reference point respectively. To derive the equations, pendulum is considered as a lumped mass at its center of mass. It consists of a rotary arm on which a pendulum is pivoted. The rotary arm is directly controlled by motor while pendulum is indirectly controlled, thus making it an under actuated system.

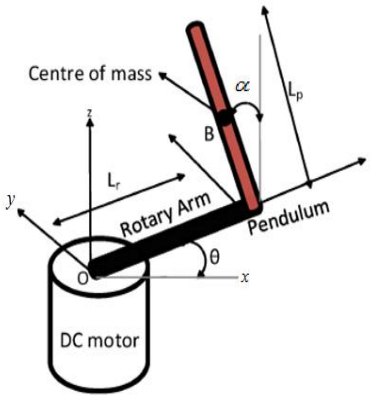

Fig.2: Schematic Diagram of Rotary Inverted Pendulum

Here, L_r represents length of rotary arm, L_p represents length of the pendulum, θ represents rotary arm angle which is taken positive in counter-clockwise direction and α represent pendulum angle from vertically upright pendulum position and is taken positive in counter clockwise direction as seen from outside of system.The servo should turn in the counter clockwise direction when the control voltage is positive i.e. $V_m>0$. The generalized coordinates of the system are θ and α. The parameters of the rotary inverted pendulum are given in Table 1.

2.1 Mathematical Modeling of Rotary Inverted Pendulum: -

In this section, dynamic modeling of RIP is performed by using analytical approach. In this approach, the Euler-Lagrange method is used to develop the equations of motion.

Total Kinetic energy (KE) is given by summation of kinetic energy of pendulum and rotary arm, which is given as:

$$KE = KE_{arm} + KE_{pend} \quad (1)$$

$$= \frac{1}{2}(m_p L_r^2 + J_r + m_p \frac{L_p^2}{4}\sin^2\alpha)\dot{\theta}^2 + \frac{1}{2}(m_p \frac{L_p^2}{4} + J_p)\dot{\alpha}^2 - \frac{1}{2} m_p L_r L_p \dot{\theta}\dot{\alpha}\cos\alpha \quad (2)$$

Table 1: Parameters of RIP System

Symbol	Description	Units	Values
m_p	Mass of pendulum	Kg	0.024
J_p	Pendulum inertia	Kgm^2	3.3×10^{-5}
L_p	Length of pendulum	m	0.129
B_p	Pendulum damping coefficient	Nms/rad	0.0005
J_r	Rotary arm inertia	Kgm^2	5.7×10^{-5}
L_r	Length of rotary arm	m	0.085
B_r	Viscous damping coefficient	Nms/rad	0.0015

In this system only, pendulum possesses potential energy. The total potential energy (PE) of the system is given as:

$$PE = PE_{arm} + PE_{pend} \quad (3)$$

$$= 0 + (-m_p g(\frac{L_p}{2} - \frac{L_p}{2}\cos\alpha)) \quad (4)$$

Due to two generalized coordinates, there are two equations of motion of the system. Therefore, Lagrange's equation of the system is given as:

$$\frac{d}{dt}\left(\frac{\partial L}{\partial \dot{\theta}}\right) - \frac{\partial L}{\partial \theta} + \frac{\partial R}{\partial \dot{\theta}} = \tau \quad (5)$$

$$\frac{d}{dt}\left(\frac{\partial L}{\partial \dot{\alpha}}\right) - \frac{\partial L}{\partial \alpha} + \frac{\partial R}{\partial \dot{\alpha}} = 0 \quad (6)$$

Where, R is the Rayleigh's dissipation function which is used to drive damping force is given as:

$$R = \frac{1}{2} B_r \dot{\theta}^2 + \frac{1}{2} B_p \dot{\alpha}^2 \quad (7)$$

Where, L = K - P and T represents torque applied by motor at rotary arm. After solving the equations and linearizing them about operating point (a = 0), the following equations of motion are obtained:

$$(m_p L_r^2 + J_r)\ddot{\theta} - \frac{1}{2} m_p L_p L_r \ddot{\alpha} + B_r \dot{\theta} = \tau \quad (8)$$

$$-\frac{1}{2} m_p L_p L_r \ddot{\theta} + (J_p + \frac{1}{4} m_p L_p^2)\ddot{\alpha} - \frac{1}{2} m_p L_p g \alpha + B_p \dot{\alpha} = 0 \quad (9)$$

Solving the acceleration term yields:

$$\ddot{\theta} = \frac{1}{J_t}(-(J_p + \frac{1}{4} m_p L_p^2) B_r \dot{\theta} - \frac{1}{2} m_p L_p L_r B_p \dot{\alpha} + \frac{1}{4} m_p^2 L_p^2 L_r g \alpha$$

$$+ (J_p + \frac{1}{4} m_p L_p^2)\tau) \quad (10)$$

$$\ddot{\alpha} = \frac{1}{J_t}(\frac{1}{2} m_p L_p L_r B_r \dot{\theta} - (J_r + m_p L_r^2) B_p \dot{\alpha}$$

$$+ \frac{1}{2} m_p L_p g (J_r + m_p L_r^2)\alpha - \frac{1}{2} m_p L_p L_r \tau) \quad (11)$$

Where,

$$J_t = J_p m_p L_r^2 + J_r J_p + \frac{1}{4} J_r m_p L_p^2 \quad (12)$$

Table 2: Parameters of Actuator

Symbol	Description	Units	Value
Rm	Terminal Resistance	Ω	8.4
Km	Motor back EMF constant	Vs/rad	0.042
Kt	Torque constant	Nm/A	0.042
Lm	Rotor inductance	mH	0.85

τ represent the torque generated by a direct-drive rotary servo system. The dynamics of the actuator is described by the following equation:

$$\tau = K_t\left(\frac{V_m - K_m \dot{\theta}}{R_m}\right) \quad (13)$$

where, the actuator parameters are described in Table 2

2.2 State-Space Representation: -

The matrix differential equation can be represented in a state-space form as:

$$\dot{x} = Ax + Bu \quad (14)$$

$$y = Cx + Du \quad (15)$$

Where, $x = \begin{bmatrix} \theta & \alpha & \dot{\theta} & \dot{\alpha} \end{bmatrix}$, is called as the state vector, u is known as the input vector and A, B, C and D are called as state-weighing coefficient matrices. The derived mathematical model of the rotary inverted pendulum system can be represented in state-state form as:

$$\begin{bmatrix} \dot{\theta} \\ \dot{\alpha} \\ \ddot{\theta} \\ \ddot{\alpha} \end{bmatrix} = \begin{bmatrix} 0 & 0 & 1 & 0 \\ 0 & 0 & 0 & 1 \\ 0 & \frac{m_p^2 g L_p^2 L_r}{4 J_t} & \frac{-B_r}{J_t}\left(m_p \frac{L_p^2}{4} + J_p\right) & -\frac{K K_t}{J R_m}\left(J_p + m_p \frac{L_p^2}{4}\right) \\ 0 & \frac{m_p L_p g (J_r + m_p L_r^2)}{2 J_t} & -\frac{B_m L_p L_r}{2 J_t} & \frac{K K_m L_p L_r}{2 J R_m} \end{bmatrix} \begin{bmatrix} \theta \\ \alpha \\ \dot{\theta} \\ \dot{\alpha} \end{bmatrix} + \begin{bmatrix} 0 \\ 0 \\ \frac{K_t}{J R_m}\left(J_p + \frac{m_p L_p^2}{4}\right) \\ \frac{K_t}{J R_m}\left(\frac{m_p L_p L_r}{2}\right) \end{bmatrix} \begin{bmatrix} V_m \end{bmatrix}$$

Incorporating the values of parameters given in Table 1 and Table 2, the state-space representation can be expressed as:

$$\begin{bmatrix} \dot{\theta} \\ \dot{\alpha} \\ \ddot{\theta} \\ \ddot{\alpha} \end{bmatrix} = \begin{bmatrix} 0 & 0 & 1 & 0 \\ 0 & 0 & 0 & 1 \\ 0 & 149.2751 & -2.0886 & 0 \\ 0 & 261.6091 & -2.0643 & 0 \end{bmatrix} \begin{bmatrix} \theta \\ \alpha \\ \dot{\theta} \\ \dot{\alpha} \end{bmatrix} + \begin{bmatrix} 0 \\ 0 \\ 49.7275 \\ 49.1493 \end{bmatrix} [V_m]$$

$$y = \begin{bmatrix} 1 & 0 & 0 & 0 \\ 0 & 1 & 0 & 0 \end{bmatrix} \begin{bmatrix} \theta \\ \alpha \end{bmatrix} + \begin{bmatrix} 0 \\ 0 \end{bmatrix} [V_m]$$

From state space equation, derive transfer function: -

$$P_1 = \frac{\theta(s)}{V_m(s)} = \frac{49.73 s^2 - 5672}{s^4 + 2.089 s^3 - 261.6 s^2 - 238.2 s} \quad (16)$$

$$P_2 = \frac{\alpha(s)}{V_m(s)} = \frac{49.15 s^2 - 5.495 \times 10^{-14} s + 7.938 \times 10^{-30}}{s^4 + 2.089 s^3 - 261.6 s^2 - 238.2 s} \quad (17)$$

III. CONVENTIONAL CONTROL TECHNIQUES

In this project, two conventional control schemes are used

a. LQR (Linear Quadratic Regulator) controller
b. Two Loop PID (Proportional Integral Derivative) controller

3.1 LQR Controller: -

The LQR is an optimal state feedback controller designed to minimize a particular quadratic performance index, which takes care of the design constraints.

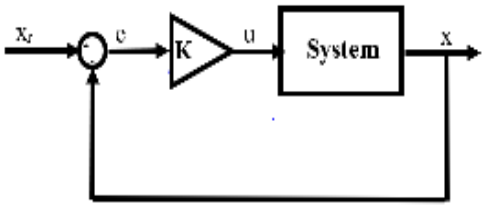

Fig.4: Block Diagram of LQR Controller

In this controller all states are fed back and multiply by the gain matrix K. So, with the help of this, poles are placed at the desired location. In this controller, pole placement algorithm is used. Pole placement algorithm is applied when the system is controllable and this is verified by controllability matrix. Controlliabity means system state move from any initial state to final state in finite time [16].

For an LTI system:

$$\dot{x} = Ax + Bu \quad (18)$$

$$y = Cx + Du \quad (19)$$

the performance index is taken as

$$J = \frac{1}{2}\int_0^\infty (x^T Q x + u^T R u)\,dt \quad (20)$$

where Q is the state-weighted matrix, which must be positive semi-definite (or positive definite), and R is the control weighted matrix, which must be positive definite. The minimization of J is obtained by solving the algebraic Riccati equation:

$$A^T P + PA - PBR^{-1}B^T P + Q = 0 \quad (21)$$

Then the optimal state feedback gain vector
K = [K1 K2 K3 K4] becomes

$$K = -R^{-1}B^T P \quad (22)$$

The A matrix being of 4th order, one may, for simplicity, choose Q = diag {q1, q2, q3, q4} where q1, q2, q3, q4 are the weights on Rotary arm position (θ), Rotary arm velocity ($\dot{\theta}$), pendulum arm position (α) and pendulum angular velocity ($\dot{\alpha}$), respectively. As the system has a single input, we choose the weight on control signal to be R = r, where r is a scalar.

3.2 Two Loop PID control scheme: -

In this scheme, θ and α have been used to give feedback to the two PID controllers. The output voltage of PID controller is defined:

$$V_d = K_d \dot{e}(t) + K_p e(t) + K_i \int e(t)\,dt \quad (23)$$

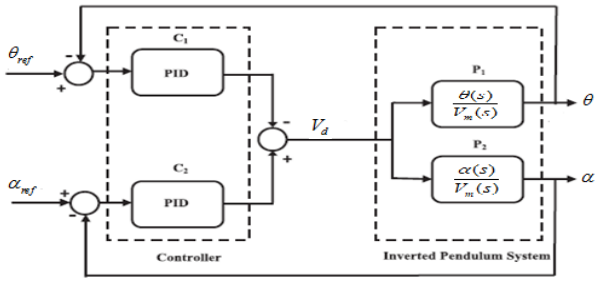

Fig.5: Block Diagram of Two Loop PID Controller

The characteristic equation of the control scheme shown in Fig.5 is written as:

$$1 - P_1 C_1 + P_2 C_2 = 0 \quad (24)$$

Where,

$$C_1(s) = K_{d1}s + K_{p1} + \frac{K_{i1}}{s} \quad (25)$$

$$C_2(s) = K_{d2}s + K_{p2} + \frac{K_{i2}}{s} \quad (26)$$

IV. SIMULATION MODEL AND RESULTS

4.1 LQR Controller Based Model: -

This model is developed in the MATLAB Simulink software. In this rotary inverted pendulum model, there is total 4 states are present. So, all states are fed back and then multiply with the appropriate gain matrix which is derived from the following MATLAB command:

K= lqr (A, B, Q, R)

Where, Q is the state weight matrix and R is the control weight matrix. In this model there is total 4 states are present then Q will be 4×4 matrix and there is only one control input is present so, R will be scalar. In this model, reference is 30-degree of amplitude for theta and constant 0 for alpha

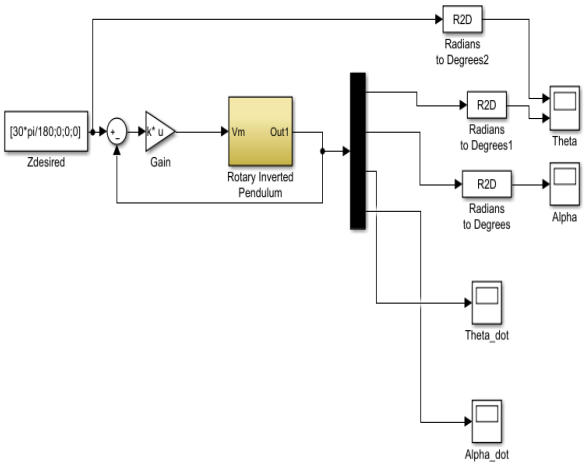

Fig.6: LQR Simulated Model

The following values of Q and R matrix are taken to find the appropriate gain matrix K:

$$Q = \begin{bmatrix} 5 & 0 & 0 & 0 \\ 0 & 1 & 0 & 0 \\ 0 & 0 & 1 & 0 \\ 0 & 0 & 0 & 20 \end{bmatrix} \quad (27)$$

$$R = [1] \quad (28)$$

Then, finally the gain matrix K is:

K= [-2.2361,53.8740, -1.7400,6.5269]

From this gain matrix K, find the eigen value

$$|sI - (A - BK)| = 0 \quad (29)$$

Eigen values represent the closed loop poles of the system, which is

$$s = -2.2042, -226.50, -3.8269 \pm 3.2805i$$

4.2 PID Controller Based Model: -

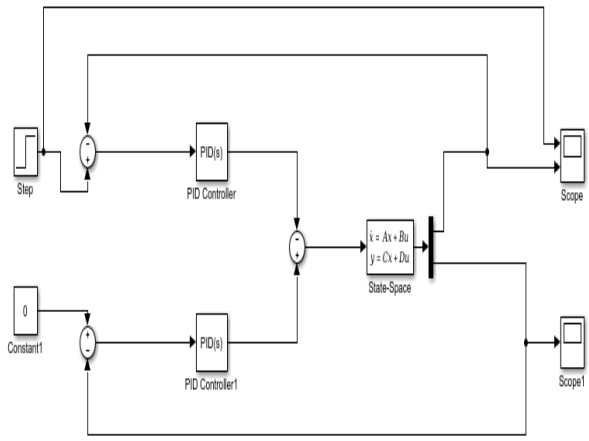

Fig.7. PID Controller Based Simulink Model

In this model, θ and α are fed back to the PID controller. At reference for theta, a signal generator is applied which provide 30-degree amplitude of square wave at 0.125 rad/sec and constant 0 is applied for alpha reference.

The parameters of PID controllers are given below:

$$k_{p1} = 28.4359, k_{d1} = 4.8624, k_{i1} = 34.5022,$$

$$k_{p2} = 154.5832, k_{d2} = 10, k_{i2} = 38.8764$$

4.3 Results: -

4.3.1 LQR Simulink Model Based Result: -

In this, 30-degree of amplitude for theta is given as a reference and 0 degree is given for alpha reference.

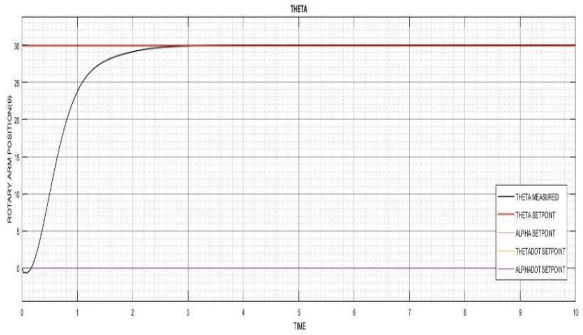

Fig.8: Theta Response of LQR Simulink Model

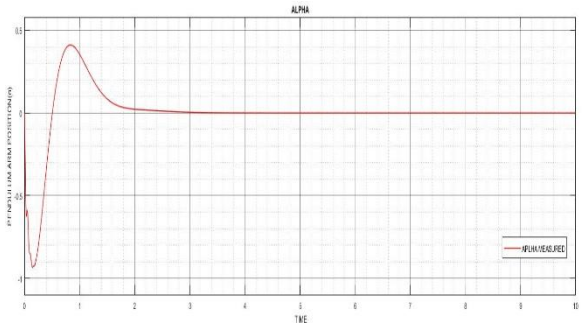

Fig. 9: Alpha Response of the LQR Simulink Model

4.3.2 Two-Loop PID Simulink Based Model Result:

In this, 30-degree of amplitude for theta is given as a reference and 0 degree is given for alpha reference.

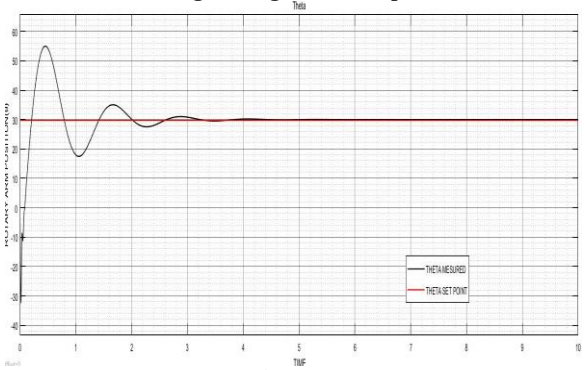

Fig.10: Theta Response of PID Controller Simulink Model

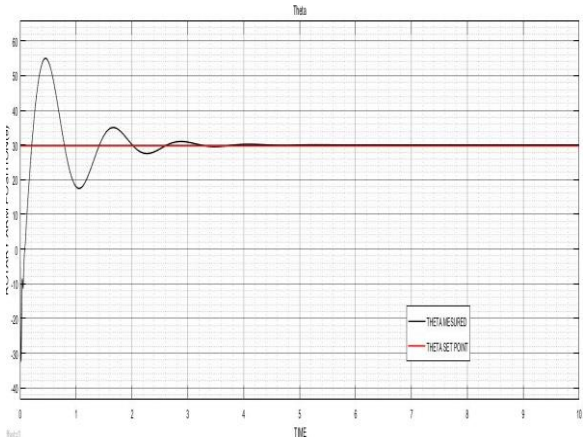

Fig.11: Alpha Response of PID Controller Simulink Model

4.3.3 LQR Hardware Based Result: -

In this, 30-degree of square wave is given for theta as a reference and 0 degree is given for alpha reference.

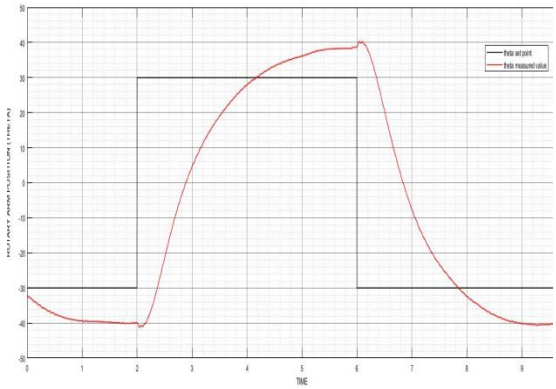

Fig.12: Theta Response of LQR hardware Model

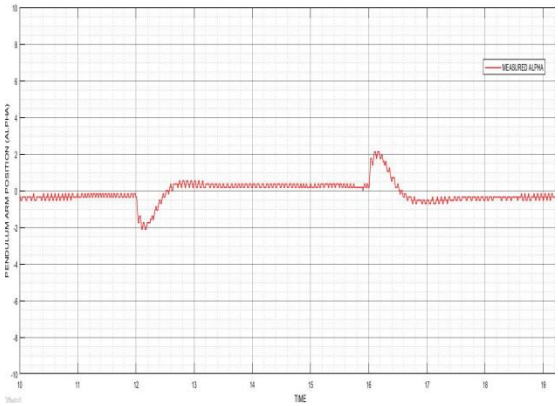

Fig. 9: Alpha Response of the LQR hardware Model

V. CONCLUSION

In this paper, prime focus on the stabilization of the pendulum arm of the Rotary Inverted Pendulum. In rotary inverted pendulum model, there is two degrees of freedom, one is the rotary arm position (θ) and other is the pendulum arm position (α). The number of closed loop transfer functions determines the degree of freedom of a control system where the transfer functions can be adjusted independently. The model was further linearized at unstable equilibrium point which is upright position and a state-space representation is obtained. The actuator dynamics are taken into account while modelling the rotary inverted pendulum. Then, two different conventional control schemes are applied to stabilize the inverted pendulum in the vertical upright position. The two conventional control schemes are LQR control scheme which is based on the Pole Placement Algorithm and the second are Two Loop PID control scheme. In this model, first LQR control scheme is applied and from where desired closed loop poles are determine. And then Two Loop Control scheme is applied to the model. The gain parameters of the PID are calculated with the help of eigen values which are derived in the LQR control scheme. The simulation response of LQR and Two Loop PID control scheme is analyzed and observe that the LQR control scheme gives the better tracking performance than the PID controller. In PID controller-based model, the simulation response is affected by overshoot and undershoot. In LQR, the theta is settled in 2.5 seconds and alpha is settled in approx. 2 seconds whereas in Two Loop PID, theta is settled in approx. 4 seconds and alpha is settled in approx. 3 seconds. So, according to this paper, the LQR is better control scheme than the Two Loop PID. The major drawback of the LQR control scheme is that it is necessary to known about all the state of the system otherwise the LQR control scheme will not work properly and sometimes it is impossible to find all the states of the system.

REFERENCES

[1] Nath, V. and Mitra, R., Swing-up and Control of Rotary Inverted Pendulum using Pole Placement with Integrator, Proceedings of 2014 RAECS UIET Panjab University Chandigarh, 06 – 08 March, 2014.

[2] Dwivedi, P., Pandey S. &Junghare, A.S., Stabilization of unstable equilibrium point of rotary inverted pendulum using fractional controller, Journal of the Franklin Institute 354 (2017) 7732–7766, 2017.

[3] Stainalaw, H. Zak.: 'Systems and Control' (Oxford University Press, NY,2003)

[4] Oltean, S.E., Swing-up and stabilization of the rotational inverted pendulum using PD and fuzzy-PD controllers, The 7th International Conference Interdisciplinarity in Engineering (INTER-ENG), 2013.

[5] Yang, C., Li, Z., Cui, R., and Xu, B., Neural network- based motion control of underactuated wheeled inverted pendulum models, IEEE transactions on neural networks and learning systems, vol. 25, no. 11, November 2014.

[6] Mathew, N.J., Rao, K.K. and Sivakumaran, N., Swing up and stabilization control of a Rotary Inverted Pendulum, 10th IFAC International Symposium on Dynamics and Control of Process Systems, The International Federation of Automatic Control, Mumbai, India, December 18-20, 2013.

[7] Rigatos, G., Siano, P., Abbaszadeh, M., and Ademi, S., Nonlinear H-infinity control for the rotary pendulum, Proceedings of the 11th International Workshop on Robot Motion and Control, Wasowo Palace, Poland, July 3-5, 2017.

[8] Akhtaruzzaman, M., Shafie A.A., Modeling and Control of a Rotary Inverted Pendulum Using Various Methods, Comparative Assessment and Result Analysis, Proceedings of the 2010 IEEE International Conference on Mechatronics and Automation, Xi'an, China, August 4-7, 2010.

[9] Anvar, S. M. M., Hassanzadeh I. and Alizadeh G., Design and Implementation of Sliding Mode-State Feedback Control for Stabilization of Rotary Inverted Pendulum, International Conference on Control, Automation and Systems. in KINTEX, Gyeonggi-do, Korea, 2010 Oct. 27-30, 2010.

[10] Ghosh, A. Krishnan, T.R and Subudhi B., Robust proportional–integral–derivative compensation of an inverted cart–pendulum

system: an experimental study, IET Control Theory Appl., Vol. 6, Iss. 8, pp. 1145–1152, 2012.
[11] Hassanzadeh I, Mobayen S., GA based input-output feedback linearization controller for rotary inverted pendulum system, Proceeding of the 5th International Symposium on Mechatronics and its Applications (ISM08), Amman, Jordan, May 27-29,2008.
[12] Kathpal, A. and Singla, A., SimMechanics Based Modeling, Simulation and Real-Time Control of Rotary Inverted Pendulum, in 11th IEEE International Conference on Intelligent Systems and Control (ISCO-2017): Coimbatore, Tamilnadu. p. 166-172, 2016.
[13] Acosta, J., Furuta's pendulum: A conservative nonlinear model for theory and practice. Mathematical Problems in Engineering, 2010.
[14] Ogata.k.: 'Modern control engineering' (Prentice Hall, 4th edition).
[15] Quanser Inc. (2014b). QUBE-Servo Balance Control Workbook (Instructor).
[16] Stefani, Shahian, Savant, Hostetter.: 'Design of feedback control system' (Oxford University Press, NY, 4th edition).

Study of the effect of weighting matrices of LQR for control of rotary inverted pendulum

Krishanu Nath, Lillie Dewan

***Abstract*—The choice of weighting matrices of the linear quadratic regulator (LQR) is one such decision which has a great effect on the dynamics of the system. Optimally choosing them by solving a defined objective can be a way to this problem. Also, algebraic approaches have been suggested for their choice as per the specified characteristics required. This paper makes a study to show the effect of LQR weighting matrices on the dynamics of the rotary inverted pendulum.**

Keywords—Linear quadratic regulator; Rotary inverted pendulum; settling time; weighting matrices

I. INTRODUCTION

The rotary inverted pendulum is a nonlinear and highly unstable system for which it is considered to a typical control problem of the modern control engineers [1]. It is relates to the class of less triggered systems which inherently have fewer actuators than the degree of freedom which makes it a standard platform for designing as well as for testing and comparison of dissimilar control techniques and also is a benchmark problem for control engineers [2]. For the control of benchmark problem there are many successful articles published. Research so far published have used pole placement based feedback control [3], PID controller [4], factional PID controller [5], etc. Robust control techniques such as sliding mode control [6],[7] and adaptive control using self-tuning regulator and model reference adaptive control [8] too has gained successful stabilization of the same. Tracking control of the rotary pendulum has also been performed using soft computing such as fuzzy logic [9] and particle swarm optimization [10].

State regulation problem is one of the important tasks of a control system engineer. The Linear Quadratic Regulator (LQR) is one of the most celebrated results of linear optimal control theory which gives an optimal response between the control input and speed of response[11] which can be used for state regulation. It has inherent robustness [12], due to a minimum phase margin of 60° and gain margin equal to infinity [13]. The only issue in real time implementation is the choice of the candidate Q and R weighting matrices; mostly they are obtained from designer experience or trial and error method which is tedious and time consuming in nature [11].Researchers have tried to optimally choose these matrices depending using various optimization techniques such as genetic algorithm [14-17], multi-objective evolutionary algorithm [18], particle swarm optimization [19], differential evolution and simulated annealing [17].

[1]Krishanu Nath is with Department of Electrical Engineering, National Institute of Technology Kurukshetra, India
[2]Lillie Dewan is with Department of Electrical Engineering, National Institute of Technology, Kurukshetra, India.
(e-mail: krishanunathee2015@gmail.com, l_dewan@nitkkr.ac.in)

This paper presents an analysis of variation of weighting matrices of LQR for the benchmark rotary inverted pendulum. Study is mainly done for the time domain analysis and actuator dynamics. The paper starts with a brief introduction in section I, section II speaks of the rotary inverted pendulum system and its model, section IIIdiscusses the LQR. In section IV simulation based analysis of the responses is discussed. Finally in section Vconclusion is drawn followed by references.

II. ROTARY INVERTED PENDULUM

A. System Description

Therotary inverted pendulum which is also known as Furuta's pendulum as it was developed by K.Futura at Tokyo Institute of Technology [20]. The setup show in in Fig. 1 comprises of four main parts which is the pendulum arm connected to a rigid link at one end and to the pendulum on the other side. The servo motor provides the necessary actuating signal or the control signal. θ is the pendulum arm angle and α is the pendulum angle.

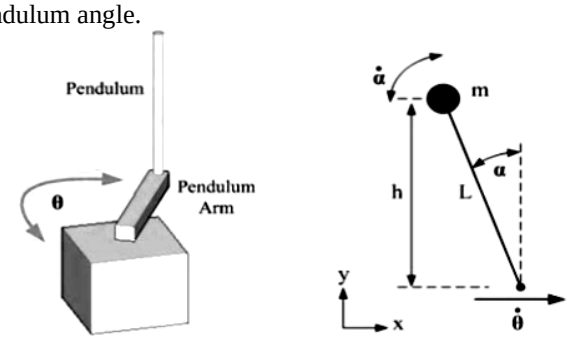

Fig. 1: Rotary inverted pendulum

B. Mathematical modelling

The assumptions considered for modeling of the system are [21]:

- Zero initial conditions are inferred when system initiates from equilibrium state.
- In order to preserve a linear model, the pendulum shows minimum deviation angle from the vertical.
- Slight disturbances can be accommodated to the linear pendulum model.

Balancing the equation of torque, the velocity segments of the center of the mass of pendulum is given by

$$v_{p\,com} = -l_p \cos\alpha(\dot{\alpha})\,\hat{x} - l_p sin\alpha(\dot{\alpha})\hat{y} \quad (7)$$

$$v_{arm} = r\dot{\theta} \quad (8)$$

The x and y part of velocity can be expressed as

$$v_x = r\dot{\theta} - l_p cos\alpha(\dot{\alpha}) \quad (9)$$

$$v_y = -l_p cos\alpha(\dot{\alpha}) \quad (10)$$

The system dynamics can be obtained from Euler-Lagrange formulation. The potential energy of the system is due to gravity can be expressed by

$$v = P.E._p = M_p g h = M_p g l_p \cos\alpha \quad (11)$$

The kinetic energy of the system arises from the arm, velocity of point mass in x-direction, velocity of point mass in y direction and rotation of pendulum about center as given in

$$T = KE_{arm} + KE_{pen} + KE_{v_x} + KE_{v_y} \quad (12)$$

$$T = \frac{1}{2}J_{eq}\dot{\theta}^2 + \frac{1}{2}J_p\dot{\alpha}^2 + \frac{1}{2}M_p r^2\dot{\theta}^2 + \frac{1}{2}M_p l_p\dot{\theta}^2 - M_p r\dot{\theta} l_p \cos\alpha(\dot{\alpha}) \quad (13)$$

The Lagrangian can be calculated by

$$L = T - V \quad (14)$$

The Euler-Lagrange equation of motion are given by

$$\frac{\partial}{\partial t}\left(\frac{\partial L}{\partial \dot{\theta}}\right) - \frac{\partial L}{\partial \theta} = \tau_{output} - B_{eq}\dot{\theta} \quad (15)$$

$$\frac{\partial}{\partial t}\left(\frac{\partial L}{\partial \dot{\alpha}}\right) - \frac{\partial L}{\partial \alpha} = -B_{eq}\dot{\alpha} \quad (16)$$

Substituting (15) (16) in (13) and linearizing about α=0 we have

$$J_{eq}\ddot{\theta} + M_p r^2\ddot{\theta} - M_p l_p r\ddot{\alpha} = \tau_{output} - B_{eq}\dot{\theta} \quad (17)$$

$$J_p\ddot{\alpha} + M_p {l_p}^2\ddot{\alpha} - M_p l_p r\ddot{\theta} - M_p g l_p \alpha = -B_{eq}\dot{\alpha} \quad (18)$$

Torque generated at arm pivot is given by

$$\tau_{output} = \frac{K_t V_m - K_t K_m \dot{\theta}}{R_m} \quad (19)$$

The state variables are defined as

$$[x_1\, x_2 x_3 x_4] = [\theta\ \alpha\ \dot{\theta}\ \dot{\alpha}] \quad (20)$$

Now, substituting (19) in (17) and changing variables as defined by (20) in (17) and (18) forms

$$\left(J_{eq} + M_p r^2\right)\dot{x}_3 - M_p l_p r\dot{x}_4 = \frac{K_t V_m - K_t K_m \dot{\theta}}{R_m} \quad (21)$$

$$\left(J_p + M_p {l_p}^2\right)\dot{x}_4 - M_p l_p r\dot{x}_3 - M_p g l_p x_2 = 0 \quad (22)$$

Converting the equation into state space can be expressed as

$$\begin{bmatrix}\dot{x}_1\\ \dot{x}_2\\ \dot{x}_3\\ \dot{x}_4\end{bmatrix} = \begin{bmatrix}0 & 0 & 1 & 0\\ 0 & 0 & 0 & 1\\ 0 & bd/e & -cg/e & 0\\ 0 & ad/e & -bf/e & 0\end{bmatrix}\begin{bmatrix}x_1\\ x_2\\ x_3\\ x_4\end{bmatrix} + \begin{bmatrix}0\\ 0\\ cK_t/R_m e\\ bK_t/R_m e\end{bmatrix} V_m \quad (23)$$

where

$$a = J_{eq} + M_p r^2;\ b = M_p l_p r;\ c = \left(J_p + M_p {l_p}^2\right)$$

$$d = M_p g l_p;\ e = ac - b^2;\ f = K_t K_m / R_m$$

TABLE VI. PARAMETERS OF ROTARY INVERTED PENDULUM [22]

Symbol	Description	Value	Unit
R_m	DC motor armature resistance	8.7	ohm
K_t	DC motor current torque constant	0.033	N.m/A
K_m	DC motor back emf constant	0.033	V/(rad/s)
B_{eq}	Equivalent viscous damping acting on DC motor shaft	0	Nms/rad
B_p	Viscous damping about pendulum pivot	0	Nms/rad
J_{eq}	Moment of inertia on DC motor shaft	0.368	g m^2
J_p	Moment of inertia of pendulum related to pivot	0.698	g m^2
r	Motor shaft to pivot of pendulum length	0.0826	m
l_p	Length of arm to center of gravity	0.153	m
M_p	Pendulum mass	0.027	kg

Putting the values of the parameters defined in Table I from the Quanser manual of a QNET rotary inverted pendulum into the state equation (23) results in

$$\begin{bmatrix}\dot{x}_1\\ \dot{x}_2\\ \dot{x}_3\\ \dot{x}_4\end{bmatrix} = \begin{bmatrix}0 & 0 & 1 & 0\\ 0 & 0 & 0 & 1\\ 0 & 22.374 & -0.274 & 0\\ 0 & 36.209 & -.0703 & 0\end{bmatrix}\begin{bmatrix}x_1\\ x_2\\ x_3\\ x_4\end{bmatrix} + \begin{bmatrix}0\\ 0\\ 8.237\\ 2.113\end{bmatrix} V_m \quad (25)$$

III. LINEAR QUADRATIC REGULATOR

To begin with the formulation of the LQR let us consider a linear time invariant system described as states space given equation

$$\dot{x(t)} = Ax(t) + Bu(t) \quad (1)$$

$$y(t) = Cx(t) + Du(t) \quad (2)$$

where

$x(t)$ is the state vector; $u(t)$ is the input vector

$y(t)$ is the output vector; A is the system matrix

B is the input matrix; C is the output matrix

D is the feed forward matrix

The classic LQR design is to obtain the optimal control input u^* by minimizing the following cost function given by

$$J(u^*) = \frac{1}{2}\int_0^\infty [x^T(t)Qx(t) + u^T(t)Ru(t)]dt \quad (3)$$

where,

$Q = Q^T$ is a positive semi definite matrix

$R = R^T$ is a positive definite matrix

For solving the cost function by forming Hamiltonian along with the state equations, the optimal feedback gain matrix K can be obtained [13] given by

$$K = -R^{-1}B^T P \quad (4)$$

Where P is the solution of the popularly known matrix Ricatti equation

$$A^T P + PA - PBR^{-1}B^T P + Q = 0 \quad (5)$$

The control is thus given by

$$u^* = Kx(t) \quad (6)$$

The Q and R matrices are suggested to be of diagonal structure which pay on as penalty on system states and its control input. These matrices have great effect on the system dynamics; and are usually chosen as trial and error basis or on the experiences of the designer. Here an effort is made to show the effect of these parameters of the weighting matrices on the dynamics of the system.

IV. SIMULATION ANALYSIS

As the state space equation that describes the system is fourth order with one input the Q and R matrices will be of the following form

$$Q = \begin{bmatrix}q_1 & 0 & 0 & 0\\ 0 & q_2 & 0 & 0\\ 0 & 0 & q_3 & 0\\ 0 & 0 & 0 & q_4\end{bmatrix} \quad R = [r_1]$$

The study of effect of the associated weights are done one by one by varying one of the parameters of the matrix and keeping other four constant at 100. The system is subjected to an initial condition of [0.1, 0.1, 0, 0] .

A. Effect on pendulum arm angle

The responses with variable values of q_1, q_2, q_3, q_4 and r_1 are shown in Fig 2-6. The pendulum angle is one of the two states whose dynamics are of interest for the stabilization of rotary

inverted pendulum. The first varied parameter is q_1 which the weight on the state itself, as it increases the undershoot and settling time decreases. The second weight q_2 seems to be of negligible importance as all the responses are similar with very little visible variation in the response. The next weight shows a tradeoff response where with increase in its value reduces the settling time but increases the undershoot of the system. Last element of Q, q_4 has similar impact on the response of the pendulum arm angleas q_2. On performing more detailed variation of q_1 the settling time droops down at higher rates till 100 and then goes on decreasing as the value goes increasing. Whereas variation of q_2 shows a dip at small values but increases the settling time with increase of its value. The weight associated with the input has a large effect on the undershoot of the system but the settling time remains to be almost constant which can be again verified from Fig 7.

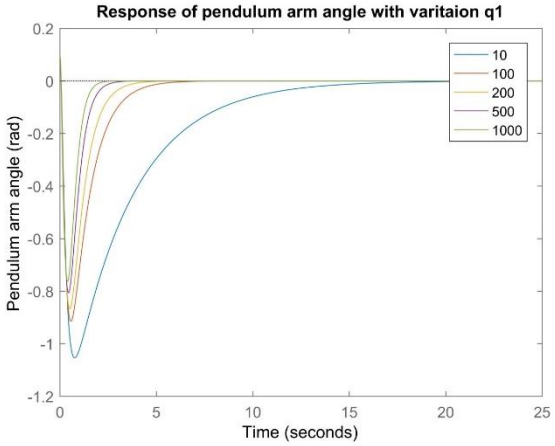

Fig. 2: Response of pendulum arm angle with variation in q_1

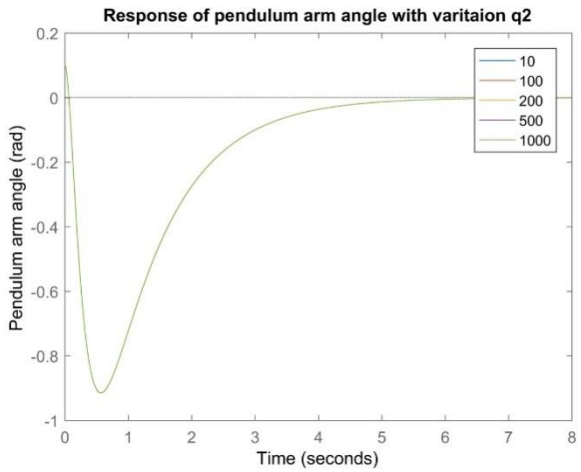

Fig. 3: Response of pendulum arm angle with variation in q_2

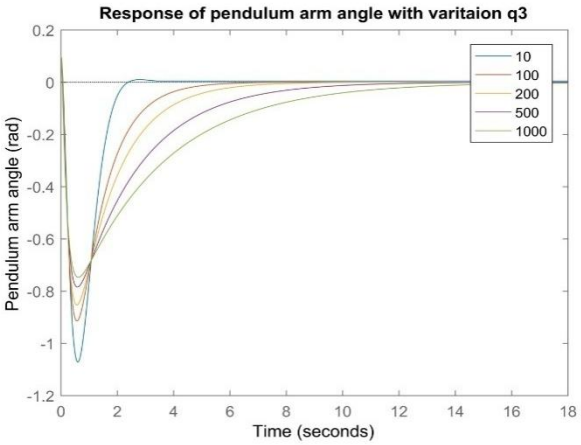

Fig. 4: Response of pendulum arm angle with variation in q_3

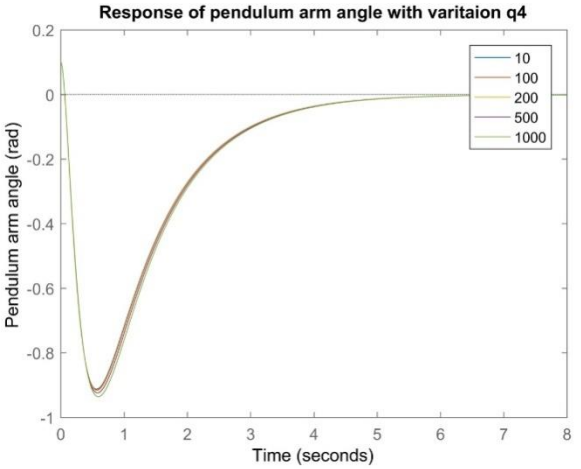

Fig. 5: Response of pendulum arm angle with variation in q_4

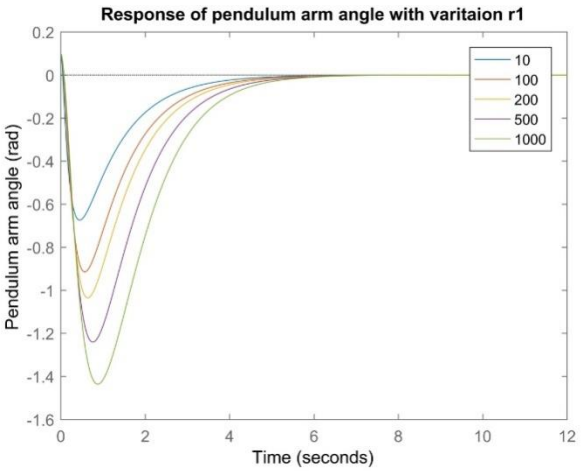

Fig. 6: Response of pendulum arm angle with variation in r_1

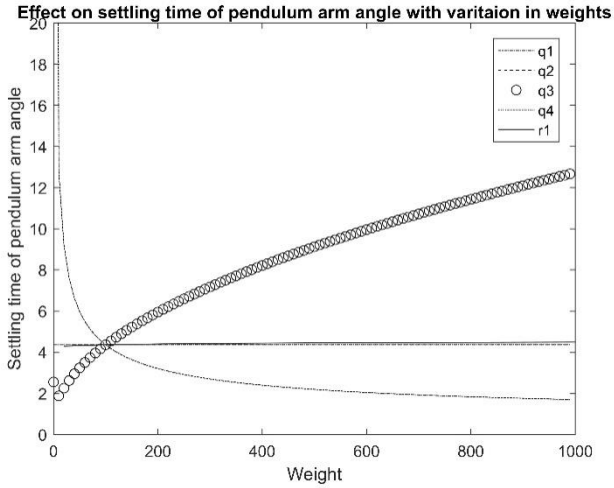

Fig. 7: Effect on settling time of pendulum arm angle with weight variation

B. Effect on pendulum angle

Figure 8-12 show the response of pendulum angle with different values of the weights of the weighting matrices. In Fig 8 increase of q_1 increases the undershoot of the system also incorporating an overshoot. A clear effect on settling time can be visible from Fig 13 where at very small values there is a rapid increase in the settling time but this reduces in the later part. As for the pendulum arm angle q_2 had very slight effect on the response same can be observed for this state. Increase of q3 is seen lowering the settling time and also undershoot present decreases considerably. The next parameter q4 too doesn't seem to affect the response by a large margin. The weight r1 yet again affects both settling time and undershoot of the response by considerable amount.

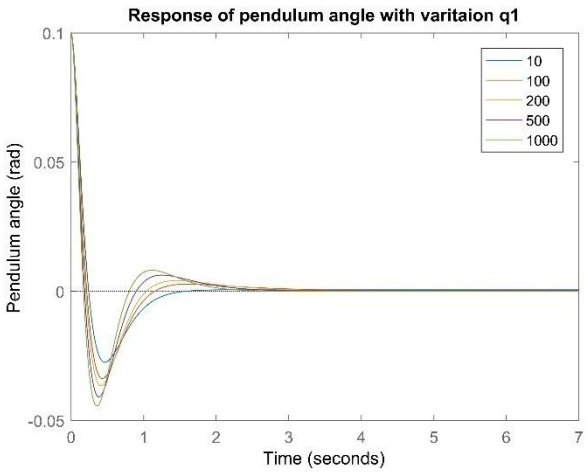

Fig. 8: Response of pendulum angle with variation in q_1

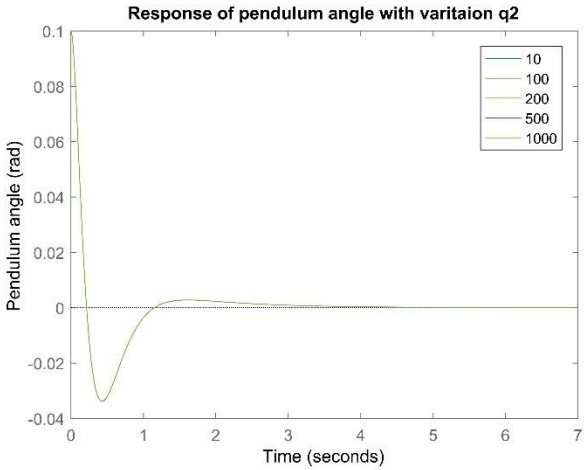

Fig. 9: Response of pendulum angle with variation in q_2

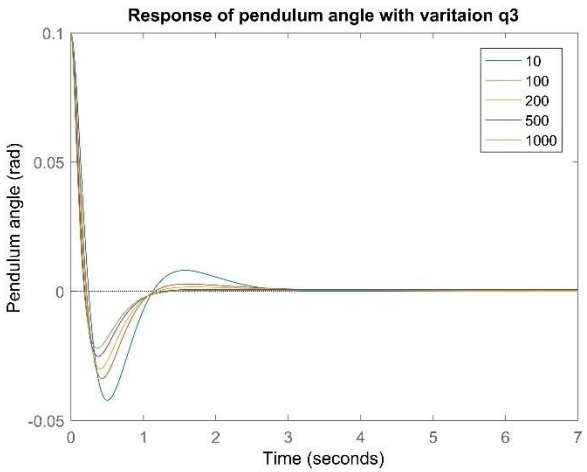

Fig. 10: Response of pendulum angle with variation in q_3

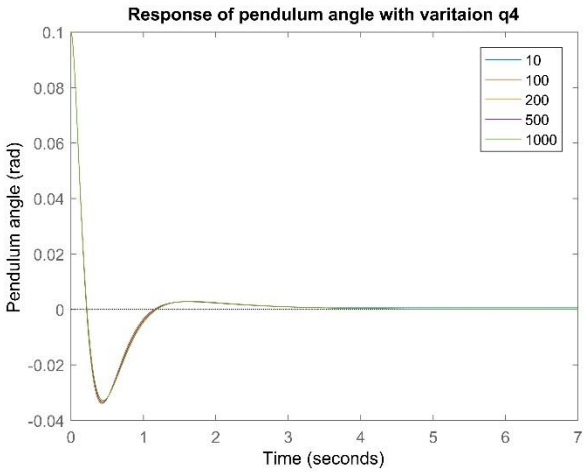

Fig. 11: Response of pendulum angle with variation in q_4

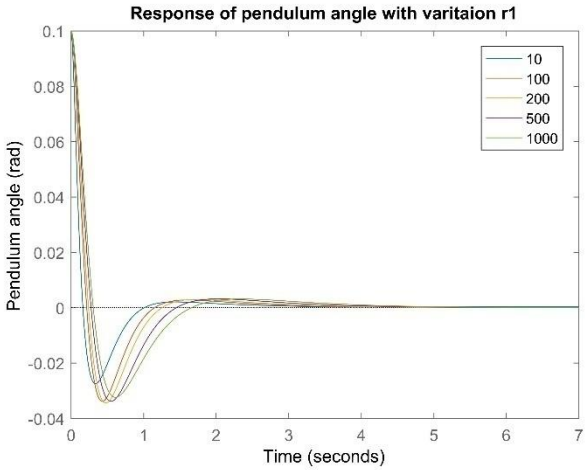

Fig. 12: Response of pendulum angle with variation in r_1

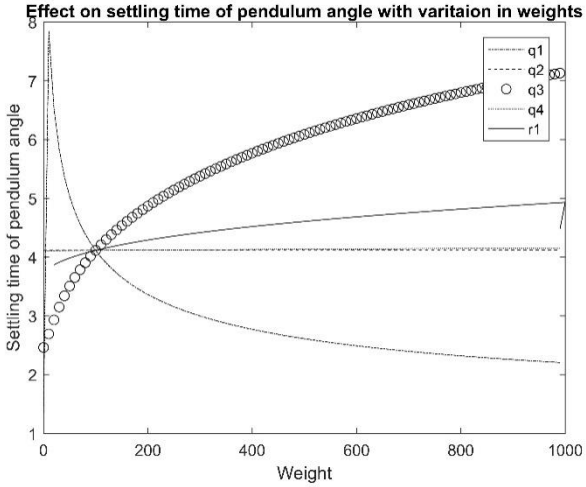

Fig. 13: Effect on settling time of pendulum angle with weight variation

C. Effect on actuator dynamics

Another constraint that arises in the implementation of any control system designed is the actuator's physical constraint to enact as per the control signal. Fig 14 shows the variation of maximum voltage to be encountered by the motor to stabilize the system. The weights associated with q_2 and q_4 have least effect on the motor voltage. The weight associated with input has drooping characteristics i.e. as it increases the maximum motor voltage decreases. Other weight whose effect is observed to be empowering the maximum voltage of the actuator is q_3 whose choice for design consideration must be made in an apt manner. The weight associated with the pendulum angle rate increases the motor voltage as it increases.

V. CONCLUSION

From the responses observed for the rotary inverted pendulum system a clear nonlinear relationship is established with the dynamics of the system and its actuator signal. Experience of the designer with hit and trial method can be one way of appropriate choice of the Q and R matrices. The other solution can be obtained by using heuristic optimization to optimally choose the values by formulating a cost function depending on the design requirements.

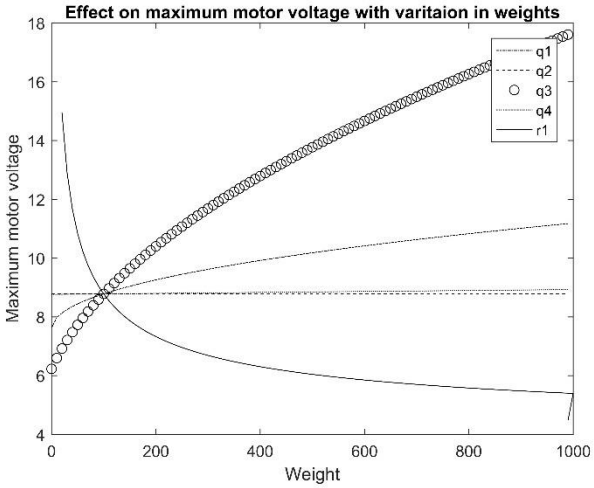

Fig. 14: Effect on maximum motor voltage with weight variation

REFERENCES

[1] A.K. Stimac, "Standup and Stabilization of the Inverted Pendulum", Department of Mechanical Engineering, Massachusetts Institute of Technology, June 1999.

[2] P. Chalupa and B. Reznicek, "Fuzzy Control of Inverted Pendulum using Real-Time Toolbox", Tomas Bata University in Zlin, Centre of Applied Cybernetics, Czech Republic.

[3] V. Nath and R. Mitra, "Swing-up and Control of Rotary Inverted Pendulumusing Pole Placement with Integrator", Proceedings of 2014 RAECS UIET Panjab University Chandigarh, 06 – 08 March, 2014.

[4] B. Prakash, B. K. Roy and R.. Biswas, "Design, Implementation and Comparisonof Different Controllers for a Rotary Inverted Pendulum", 1st IEEE International Conference on Power Electronics, Intelligent Control and Energy Systems (ICPEICES-2016).

[5] W. Liao, Z. Liu, S. Wen, S. Bi, and D.Wang, "Fractional PID based stability control for a single link rotary inverted peddulum", Proceedings of the 2015 International Conference onAdvanced Mechatronic Systems, Beijing, China, August, 22-24, 2015.

[6] A. Rajan, A.A. Kumar and C.S. Kavitha, "Robust Control Methods for Swing-Up andStabilization of a Rotary Inverted Pendulum", 2016 International Conference on Emerging Technological Trends [ICETT], Kollam, India, 21-22 Oct. 2016.

[7] P. Faradja, G. Qi and M.Tatchum, "Sliding Mode Control of a Rotary Inverted Pendulum using Higher Order DifferentialObserver", 14th International Conference on Control, Automation and Systems (ICCAS 2014), KINTEX, Gyeonggi-do, Korea, Oct. 22-25, 2014.

[8] K. Nath and L. Dewan, "Control of a rotary inverted pendulum via adaptivetechniques", International Conference onEmerging Trends in Computing and Communication Technologies (ICETCCT), 17-18 Nov. 2017.

[9] Umar Farooq, Jason Gu, Mohamed E. El-Hawary, Valentina E. Balas nad Muhammad Usman Asad, "Experimental Study of Optimal Takagi Sugeno FuzzyController for Rotary Inverted Pendulum", 2015 IEEE International Conference on Fuzzy Systems (FUZZ-IEEE), 2-5 Aug. 2015.

[10] K. Srikanth, J. S. Rao and G. V. Nagesh Kumar, "Stabilization at upright equilibrium position of RotaryInverted Pendulum using particle swarms with contrined optimization", 2015 IEEE Workshop on Computational Intelligence: Theories, Applications and Future Directions (WCI), 14-17 Dec. 2015.

[11] S. Karthick, J. Jerome, E. V. Kumar and G. Raaja, "APSO based weighting matrices selection og LQR applied to tracking control of SIMO system" 3rd International conference on advance computing, Networking and Informatics, Springer India 2016

[12] L. Wang, H.Ni, W. Zhou, P.M. Pardalos, J. Fang, M. Fei, "MBPOA-based LQR controller and its application to the double inverted pendulum system." Engineering Applications of Artificial Intelligence archive Volume 36 Issue C, November 2014 Pages 262-268J.

[13] A. Sinha, Linear Systems: Optimal and Robust Control, CRC Press

[14] Zhang Lingbo and Mao Jianqin, “An approach for selecting the weighting matrices of LQ optimal controller design based on genetic algorithms,” in 2002 IEEE Region 10 Conference on Computers, Communications, Control and Power Engineering. TENCOM ’02. Proceedings., 2002, vol. 3, pp. 1331–1334.

[15] C. Wongsathan and C. Sirima, “Application of GA to design LQR controller for an inverted pendulum system,” in 2008 IEEE International Conference on Robotics and Biomimetics, ROBIO 2008, 2008, pp. 951–954.

[16] T. Wang, Q. Wang, and Y. Hou, “Suboptimal Controller Design for Flexible Launch Vehicle based on Genetic Algorithm : Selection of the Weighting Matrices Q and R,” IEEE Int. Conf. Intell. Comput. Intell. Syst. (ICIS ’09)., pp. 720–724, 2009.

[17] K. Nath and L.Dewan, “Optimization of LQR weighting matrices for a rotary inverted pendulum using intelligent optimization techniques” in Conference on Information and Communication Technology (CICT'17), 2017.

[18] Y. Li, J. Liu, and Y. Wang, “Design approach of weighting matrices for LQR based on multi-objective evolution algorithm,” Proc. 2008 IEEE Int. Conf. Inf. Autom. ICIA 2008, no. 2, pp. 1188–1192, 2008.

[19] X. Xiong and Z. Wan, “The simulation of double inverted pendulum control based on particle swarm optimization LQR algorithm,” Proc. 2010 IEEE Int. Conf. Softw. Eng. Serv. Sci. ICSESS 2010, pp. 253–256, 2010.

[20] K. Furuta, M. Yamakita and S. Kobayashi, “Swing-up control of inverted pendulum using pseudo-state feedback”, Journal of systems and control engineering, 206(6), pp. 263-269, 1992.

[21] V. Vijayalakshmi, Z. Jenifer and A. Srinivasan, “Real time modelling and balance controller design for a rotary inverted pendulum using labview”, Ind Sci Journal Vol.1, Issue 1, Oct 2013

[22] Quanser enginnering trainer manual, 2016

Control of Robotic Manipulator

The robot technology is advancing day by day and industry is moving from the current state of automation to robotization. An important advanced robotic system is the flexible-link robotic arm. Large weight manipulator introduces limitations in terms of speed, energy consumption, and mobility. To overcome from these disadvantages researchers are focusing on fabricating flexible link manipulators. Flexible manipulators leads to lot of advantages such as lower power consumption, higher payload-to-robot weight ratio, lower manufacturing cost. Variety of controlling techniques have been employed for the design of a controller which can control the position and vibration of flexible link accurately within less time. There are several control schemes such as PID, state feedback control, self-tuning, LQR, optimal control ,model reference adaptive control and Robust control used to regulate the motion of the manipulators. Paper ***Tracking Control Of A Robotic Manipulator Using Sliding Mode Control*** are an effort inthis direction.

Tracking Control of a Robotic Manipulatorusing Sliding Mode Control

Neeraj Kumar, Jyoti Ohri

***Abstract*- This paper presents a sliding mode controller design for a 2 dof robotic manipulator. The tracking performance and effectiveness of the proposed control is demonstrated by experimental results.**

I. INTRODUCTION

This paper deals with the problem of controlling the position of a 2 dof robotic manipulator. The PID controller is very popular among industry due to its simplicity and reliability. But it has been observed that PID controller does not provide required robustness against uncertainty. Hence there is a need to explore robust controller to achieve desired performance. Under matching conditions, sliding mode control provides robustness against external disturbances and varying parameters [1-4].

In this paper, a sliding mode along with boundary layer technique is used for the same. The boundary layer technique is used to eliminate high control activity encountered in SMC (chattering). This paper is organized in the following sections. Section 2 describes the control technique, section 4 has a discussion about the manipulator dynamics and section 4 has the simulation results.

II. CONTROL METHOD

Let a nonlinear system represented by the following state-space equation

$$\dot{x} = a(x) + g(x)u + v \qquad (1)$$

where $[x_1,x_2,x_3,...,x_n]^T = [x_1, \dot{x_1}, \dots, x_1^{(n-1)}]^T$ is the state vector, v is the external disturbance and u is the control input.The tracking error is defined as $e = x - x_d$ where x_d is the desired state vector. To achieve $e \rightarrow 0$ is the control objective.

Sliding surface is designed as follows

$$n = se \qquad (2)$$

where $s = [s_1,s_2,\dots,s_n]$. The error dynamics in sliding mode become

$$s_n e^{(n-1)} + s_{n-1}e^{(n-2)} + \dots + s_1 e_1 = 0. \qquad (3)$$

$s_1, s_2, \dots s_n$ have to be positive and the polynomial $\Omega(\lambda) = s_n\lambda_{n-1} + s_{n-1}\lambda_{n-2} + \dots + s_1$ is a Hurwitz. Tracking error's decaying rate is decided by the choice of s. Thus s decides the stability of the error dynamics in SMC.

Now a control law is formulated such that n approaches zero and sustains thereafter. An appropriate control law is such that it enables the sliding surface to satisfy

$$n\dot{n} < 0 \qquad (4)$$

The control input u is assumed to be

$$u = u_0 + u_{smc} \qquad (5)$$

where u_0 deals with the nominal part in the, u_{smc}takes care of the external disturbances and plant parameter variation. Is satisfied by formulating u_0 and u_{smc}as

$$u_0 = -(sg_0(x))^{-1}(sa_0(x) - s\dot{x_d}) \qquad (6)$$

$$u_{smc} = -(sg_0(x))^{-1}ksgn(n) \qquad (7)$$

III. MODELLING

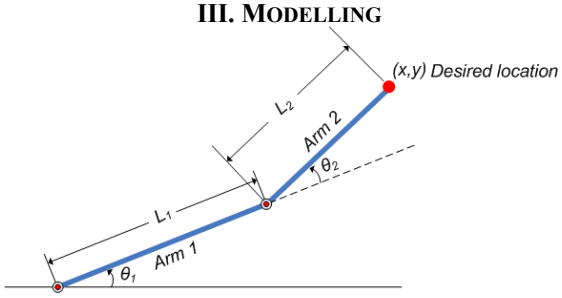

$$x_1 = L_1 cos\theta_1$$

$$y_1 = L_1 sin\theta_1$$

$$x_2 = L_1 cos\theta_1 + L_2 sin(\theta_1 + \theta_2)$$

$$y_2 = L_1 sin\theta_1 + L_2 cos(\theta_1 + \theta_2)$$

To derive the dynamic model using lagrangian dynamics, we form the lagrangian:

$$\mathcal{L} = Kinetic\ Energy - Potential\ Energy$$

Now the dynamic equations are formed using the following relation:

$$u_{\theta_{1,2}} = \frac{d}{dt}\left[\frac{\partial \mathcal{L}}{\partial \dot{\theta}_{1,2}}\right] - \frac{\partial \mathcal{L}}{\partial \theta_{1,2}}$$

After simplification, the motion of a 2 dof robotic manipulator is described by the following equations:

$$B(q)\ddot{q} + C(\dot{q},q) + g(q) = u$$

Where q = angular displacement matrix, M = mass of the link, L = length of the link, B = inertia matrix, C = centripetal and coroisal matrix, g= gravity matrix.

$$q = \begin{bmatrix}\theta_1 \\ \theta_2\end{bmatrix}$$

$\theta_1$and θ_2 are the angular deflection of link 1 and link 2 respectively. Further,

$$B(q) = \begin{bmatrix}((M_1 + M_2)L_1^2 + M_2L_2^2 + M_2L_1L_2cos\theta_2) & (M_2L_2^2 + M_2L_1L_2cos\theta_2) \\ M_2L_2^2 + M_2L_1L_2cos\theta_2 & M_2L_2^2\end{bmatrix}$$

[1]Neeraj Kumar is with Department of Electrical Engineering, National Institute of Technology Kurukshetra, India
[2]Jyoti Ohri is with Department of Electrical Engineering, National Institute of Technology, Kurukshetra, India.
(e-mail: neeraj.cancer@gmail.com, ohrijyoti@rediffmail.com)

$$C(\dot{q},q)=\begin{bmatrix}-M_2L_1L_2sin\theta_2(2\dot{\theta}_1\dot{\theta}_2+\dot{\theta}_2^2)\\ -M_2L_1L_2sin\theta_2\dot{\theta}_1\dot{\theta}_2\end{bmatrix}$$

$$g(q)=\begin{bmatrix}(M_1+M_2)gL_1sin\theta_2-M_2gL_2\sin(\theta_1+\theta_2)\\ -M_2gL_2sin(\theta_1+\theta_2)\end{bmatrix}$$

$$u=\begin{bmatrix}u_{\theta_1}\\ u_{\theta_2}\end{bmatrix}$$

This dynamic model is linearized into a simple state space model with the following state space matrices:

$$A=\begin{bmatrix}0 & 0 & 1 & 0\\ 0 & 0 & 0 & 1\\ -0.46 & -0.62 & 0 & 0\\ 0.25 & -6.62 & 0 & 0\end{bmatrix}$$

$$B=\begin{bmatrix}0 & 0\\ 0 & 0\\ 0.79 & -0.043\\ 0.043 & 0.13\end{bmatrix}$$

$$C=\begin{bmatrix}1 & 0 & 0 & 0\\ 0 & 1 & 0 & 0\end{bmatrix}$$

D=0;

A random noise is taken as the external disturbance.

IV SIMULATION RESULTS

The main objective is to make the links track a chosen trajectories. Here, the desired trajectories are [sin(t),sin(t),cos(t),cos(t)] with initial condition [0 0 1 1]. b_0 is chosen to be [10,0,1,0;0,10,0,1]. Following are the simulation results with SMC.

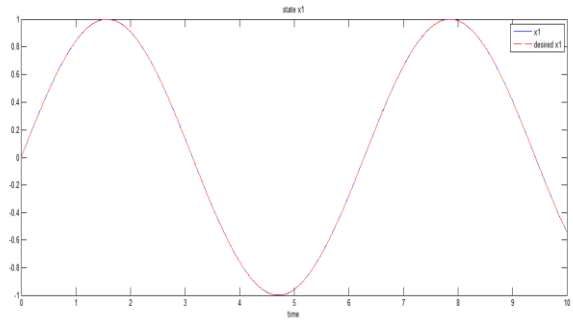

Fig. 1 tracking of x_1

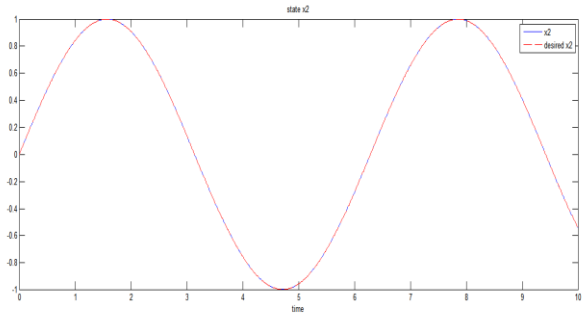

Fig.2 tracking of x_2

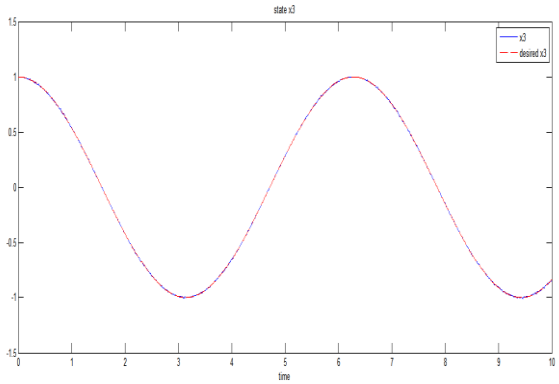

Fig. 3 tracking of x_3

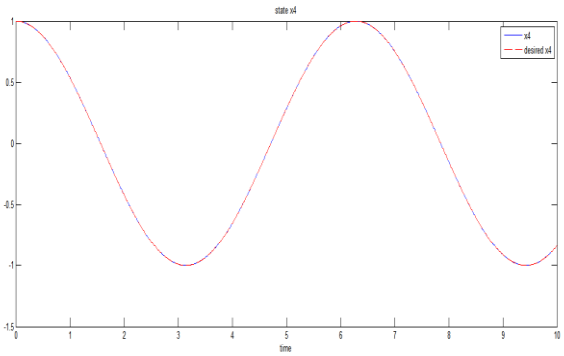

Fig. 4 tracking of x_4

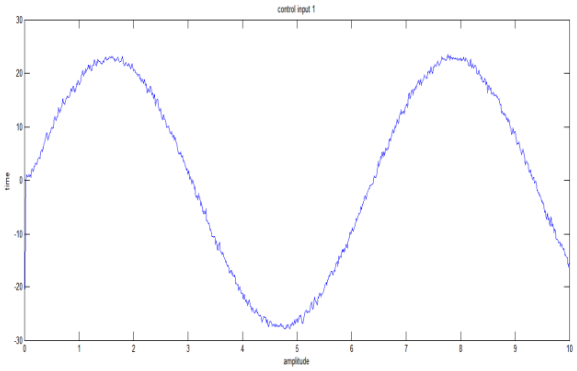

Fig.5control input for link 1

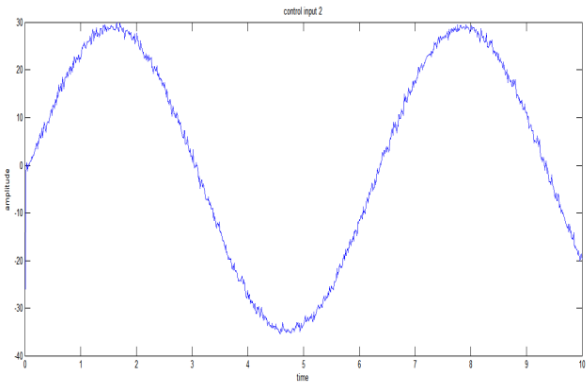

Fig. 6 control input for link 2

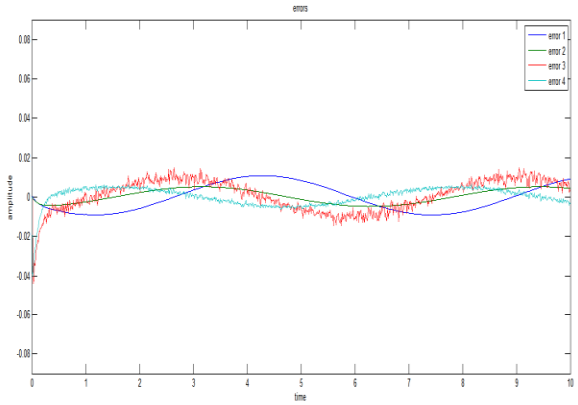

Fig. 7 errors

High frequency control activity (chattering) is quite evident from fig. 6 & 7. To minimize chattering, the discontinuous signum function (sgn(n)) is replaced by a saturation function(sat(n/a)), where a=0.001.

$$\text{Sat}(n/a) = \begin{cases} n/a, & |n/\lambda| \leq 1 \\ \text{sgn}(n/a), & |n/\lambda| > 1 \end{cases}$$

The simulation results after application of saturation function are following:

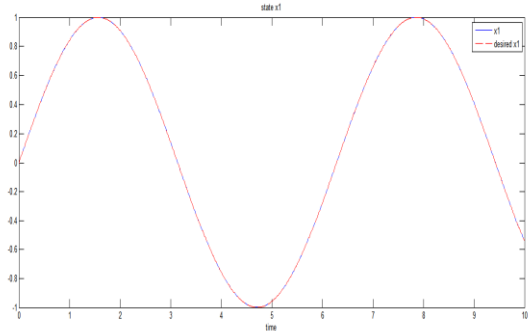

Fig. 7 tracking of x_1

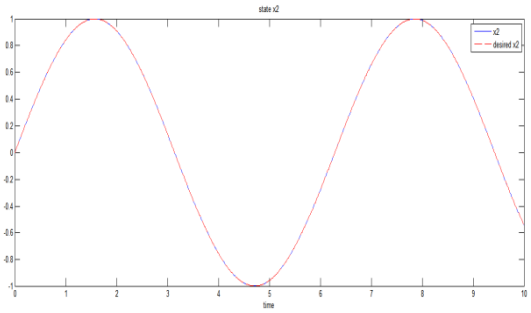

Fig.81 tracking of x_2

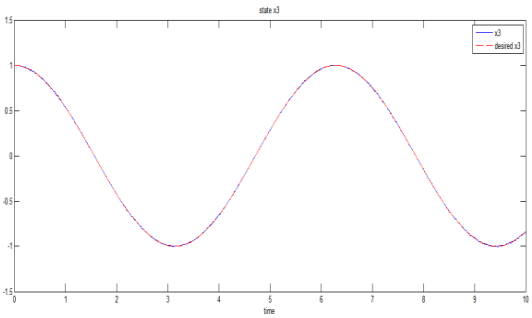

Fig. 9 tracking of x_3

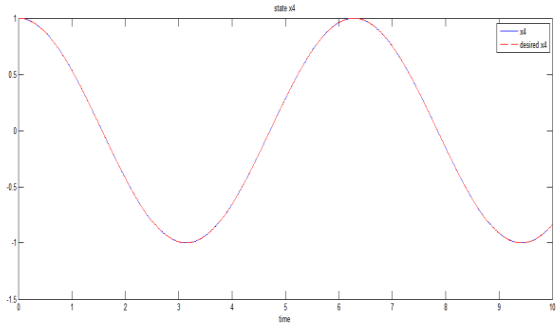

Fig. 10 tracking of x_4

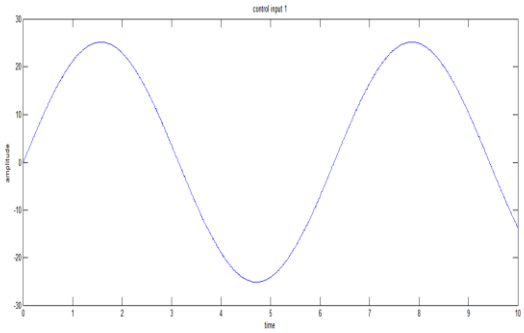

Fig. 11control input for link 1

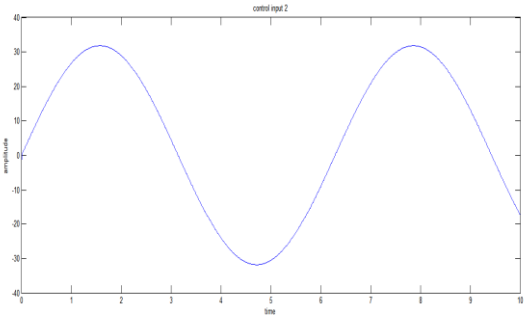

Fig.12 control input for link 2

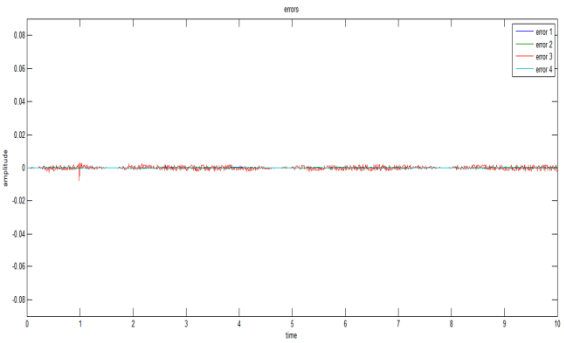

Fig. 13errors

V. CONCLUSION

Sliding mode control provides robust control of the robotic manipulator with unknown disturbances. The high frequency control activity (chattering) is minimized by replacing the signum function by saturation function. The modifications bring reduction in chattering and hence improve the tracking performance.

REFERENCES

[1] V.I. Utkin, Sliding Modes in Control and Optimization. New York, Springer- Verlag, 1992.

[2] J.Y. Huang, W Gao and J.C. Huang, "Variable structure control: A survey," *IEEE Trans. Ind. Electron.*, vol. 40, no. 1, pp. 2–22, Feb. 1993.

[3] K. D. Young, V. I. Utkin, and Ü. Özgüner, "A control engineer's guide tosliding mode control," *IEEE TransControl Syst. Technol.*, vol. 7, no. 3,pp. 328–342, May 1999.

[4] Y. J. Huang, T. C. Kuo, and H. K. Way, "Robust vertical takeoff andlanding aircraft control via integral sliding mode," *Proc. Inst. Electr.Eng.—Control Theory Appl.*, vol. 150, no. 4, pp. 383–388, Jul. 2003.

[5] J. J. Slotine and S. S. Sastry, "Tracking control of non-linear system usingsliding surfaces, with application to robot manipulators," *Int. J. Control*,vol. 38, no. 2, pp. 465–492, 1983.

[6] W. D. Chang, R. C. Hwang, and J. G. Hsieh, "Application of an autotuningneuron to sliding mode control," *IEEE Trans. Syst., Man, Cybern.C, Appl. Rev.*, vol. 32, no. 4, pp. 517–519, Nov. 2002.

[7] C. H. Chou and C. C. Cheng, "A decentralized model reference adaptivevariable structure controller for large-scale time-varying delay systems,"*IEEE Trans. Autom. Control*, vol. 48, no. 7, pp. 1213–1217, Jul. 2003.

Computer Controlled Systems

Past few decades have seen rapid developments of computer technologies. As a result, the discrete-time systems are becoming increasingly important especially after the emergence of embedded microprocessors. Compared with the traditional analog equipment, such small and flexible digital microprocessors /microcontrollers have the advantages of decreasing the energy consumption and the installation cost. As such, they are gradually forming an essential part of many diverse applicationslike in Biomedical applications Paper entitled ***Wearable Glove for Real Time Health Monitoring***.

PLC-based control systems are routinely supplied with a sequencing program, calibration menus, trending screens, data acquisition (SCADA) packages, operator-friendly alarms, and advanced safety features. Process variables are controlled and displayed from a responsive color touchscreen and can be automatically stored for seamless monitoring and reporting. In the paper,***Effective Boiler Automation using PLC and SCADA***boiler has been controlled very efficiently using the help of various sensors. SCADA is used to monitor the parameters and PLC is used to control the operation.

Control engineers are interested in using distributed control, computing, sensing and communication to design a strategy for a Multi-Agent for attaining a global control objective. Paper entitled***Review Article: Consensus and Cooperative Control for the Adaptive Distributed Observer of Discrete-Time Linear Multi-Agent System***gives a brief overview of adaptive distributed and cooperative control of multi-agent system (MAS) capabilities in control engineering applications. It has an overview of significant (important/ essential/ prime/ key/ paramount) control engineering issues which can be explored by multi-agent system and also describes essential (important/ essential/ prime/ key/ paramount) concepts of multi-agent system that are related to Control Systems.

Wearable Glove for Real Time Health Monitoring

Sakshi Vats, Amit Kumar, Bharti Sharma, Anshul Vats, Maansi Gupta

***Abstract* —Living in the technologically advanced world wearing technology is the newest trend. Monitoring a patient's health status requires constantly measuring his/her pulse rates. So here a battery powered wearable health monitoring system that constantly monitors patient heart pulses and displays it to user is proposed. The system is a wearable device which contain two sensor nodes: pulse rate sensor node and temperature sensor node. The nodes are easy installing. The system monitors the pulse rate and temperature of the patient and has a friendly user interface including a LCD (Liquid Crystal Display). Furthermore, the system would react to the critical condition of the patient by a buzzer.**

Keywords- Health Monitoring; Pulse Sensor; Temperature Sensor; Wearable Devices; Wearable Glove

I. INTRODUCTION

Sensors and wearables allow continuous physiological monitoring with reduced manual intervention and at low cost. They can be integrated into various accessories such as garments, hats, wrist bands, socks, shoes, eyeglasses and other devices such as wristwatches, headphones and smartphones.

In this paper, a wearable health monitoring glove is presented. The system includes sensor nodes: pulse rate sensor and temperature sensor.

It has the following features:

Low cost microcontroller used are cheap and all other devices are inexpensive. Low power consumption. Easy installation and friendly user interface which includes LCD. In order to ensure the wellbeing of patient , an alarm system is installed to tell the critical condition of the patient.

[1]Sakshi Vats is with Bhagwan Parshuram Institute of Technology, Delhi, India

[2]Amit Kumar is with Bhagwan Parshuram Institute of Technology, Delhi, India.

[3]Bharti Sharma is with Bhagwan Parshuram Institute of Technology, Delhi, India

[4]Anshul Vats is with Bhagwan Parshuram Institute of Technology, Delhi, India.

[5]Maansi Gupta is with Bhagwan Parshuram Institute of Technology, Delhi, India.

(e-mail: svats155@gmail.com, amitkumar524780@gmail.com, bharti34sharma@gmail.com, anshulvats96@gmail.com, maansi31@gmail.com)

The paper is organized as follows. Section II presents Literature Review. Section III presents the Proposed System, as well as its main features and components. Section IV shows the design of sensor nodes. In Section V, conclusions are presented and finally in Section VI Future Scope is presented.

II. LITERATURE REVIEW

Wearable technology may provide an integral part of the solution for providing health care to a growing world population[2.]. Smart wearable sensors are effective and reliable for preventative methods in many different facets of medicine such as, cardiopulmonary, vascular, endocrine, neurological function and rehabilitation medicine.

These sensors have also been shown to be accurate and useful for perioperative monitoring and rehabilitation medicine. People who need continuous monitoring of their health will get benefited by this glove. This can prevent high risk of injury of even death by constantly monitoring heartbeat rate and body temperature[7]. This can be advantageous mostly to the elderly people who needs continuous monitoring and who feel difficult to visit a hospital regularly. Even hospitals wants to send the patients back home as soon as possible to recover at home. During this recovery period, these patients are to monitored at home. This glove will help in remote monitoring of patients at home.

A Health Monitoring Wearable Glove which can be worn and used to display the heart rate of any individual on the display mounted on the glove. A prototype for monitoring the heartbeat rate and an accurate temperature measurement of human body is presented in this paper.The pulse on a person is sensed using a pulse sensor, which sends information to the microcontroller board & it subsequently processes the information and commands the display module to display the heart rate. The body temperature of the person is also sensed and the result is displayed on the screen simultaneously.

A Heart Beat (HB) sensor is being developed for acquainting the input signals using Light Dependent Resistance (LDR) and Light Emitting Diode (LED). Heart Beat of a person is sensed and converted into the form of electrical signals and pulses. These generated signals are amplified using the conditioning circuits. The heartbeat of a person depends on the frequency of the signal generated and this lays down the principle of

HB monitoring[4.]. This sensor is attached to the index finger of the glove and when the index finger is placed on the wrist of the patient then it displays the pulse rate of the patient on the LCD display. An accurate temperature measurement of a human body is also presented in the paper.

Temperature sensor is mounted on the wrist strap, positioned in such a way that it contact the skin, allowing it to measure the temperature of skin.Temperature sensorcan be used to measure temperature with an electrical o/p comparative to the temperature (in °C). This sensor has an output voltage that is proportional to the Celsius temperature.When the temperature sensor is placed against the body of the patient, then it detects the boy temperature of the patient. On the basis of the temperature it decides the result to be displayed on the LCD screen.If the body temperature of the person is below 97ºC then "NO FEVER DETECTED" is printed. If the body is above 97ºC then "FEVER DETECTED" is printed on the LCD screen. When the temperature is above 103ºC then "Fever DETECTED" is displayed and the buzzer gets activated. This indicates the critical stage of the patient.

III. PROPOSED SYSTEM

The general structure of the wearable health monitoring glove is shown in Fig. The system includes two sensor nodes: pulse rate sensor node and temperature senor node. Microcontroller is the central device. It receives the information coming from sensor nodes and displays out the message on the LCD(Liquid Crystal Display) and the Buzzer starts if the patient's condition is critical.

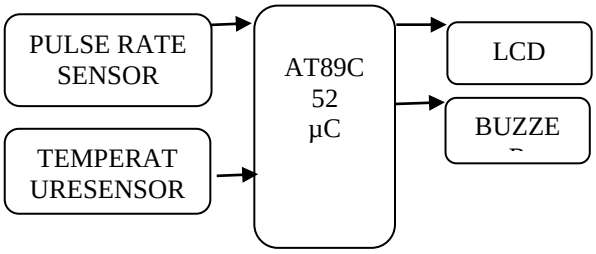

Fig. 1. Block diagram of wearable health monitoring glove

A. *Software Design of system*

The working procedure is as follows:

When the index finger is placed on the wrist of the patient then both the sensors detect the signal and sends it to microcontroller. LCD displays the information of sensor nodes.

If the temperature is above 97°C then "FEVER" is displayed on the LCD screen and the buzzer starts if the patient's condition is critical.

B. Flowchart of the System

System is initialized by putting index finger on the wrist. Pulse sensor detects the pulse of the patient and display it on the LCD.

Temperature sensor detects the body temperature of the patient and compares this temperature with the 97°C. If body temperature if below 97°C then only pulse rate along with the message " no fever" will be displayed. If the temperature is above 97°C then the pulse rate along with the message "fever" will be displayed.If the body temperature rises above the critical temperature then the buzzer is activated.

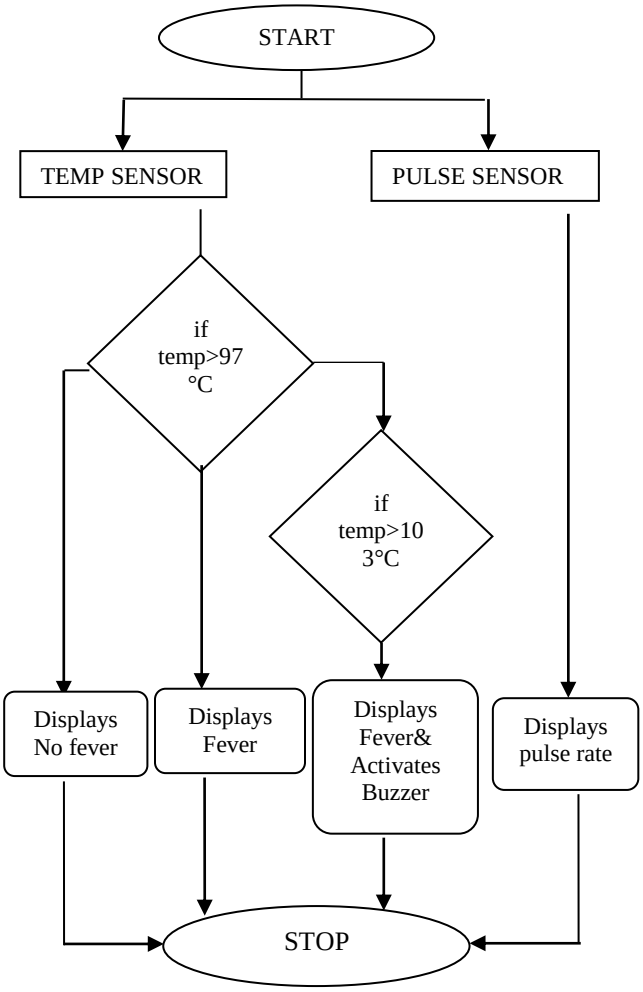

Fig. 2. Flowchart of wearable health monitoring glove

IV. SENSOR NODES

A. Pulse Sensor Node

Pulse Sensor Amped is a plug-and-play heart-rate sensor for Arduino and Arduino compatibles. Pulse Sensor Amped works with either a 3V or 5V Arduino.

A person's heart beat is the sound of the valves in his/her heart contracting or expanding as they force blood from one region to another. Heart Beat can be measured based on optical power variation as light is

scattered or absorbed during its path through the blood as the heart beat changes.

The heartbeat sensor is based on the principle of photo phlethysmography. It measures the change in volume of blood through any organ of the body which causes a change in the light intensity through that organ (a vascular region). The flow of blood volume is decided by the rate of heart pulses and since light is absorbed by blood, the signal pulses are equivalent to the heart beat pulses.

This sensor is used to find the pulse rate of the patient. This sensor is attached to the index finger of the glove and when theindex finger is placed on the wrist of the patient then it displays the pulse rate of the patient on the LCD display.

B. Temperature Sensor

Temperature sensor is a thermocouple or a resistance temperature detector (RTD) that gathers the temperature from a specific source and alters the collected information into understandable type for an apparatus or an observer.

Temperature sensor can be used to measure temperature with an electrical o/p comparative to the temperature (in °C). This sensor generates a high output voltage and may not need that the output voltage is amplified. This sensor has an output voltage that is proportional to the Celsius temperature.

When the temperature sensor is placed against the body of the patient, then it detects the boy temperature of the patient. On the basis of the temperature it decides the result to be displayed on the LCD screen. If the body temperature of the person is below 97ºC then "NO FEVER DETECTED" is printed. If the body is above 97ºC then "FEVER DETECTED" is printed on the LCD screen. When the temperature is above 103ºC then "Fever DETECTED" is displayed and the buzzer gets activated. This indicates the critical stage of the patient.

C. Sensor Function

Table I presents messages on LCD sent to user when alarms take place.

TABLE 1 Sensor Functions Of System

SENSOR	MSG DISPLAYED ON LCD
Pulse Rate Sensor	Pulse rate of the patient is displayed
Temperature Sensor	"Fever" is displayed if temp>97°C "No Fever" is displayed if the temp<97°C

V. CONCLUSION

This paper presents the design and the implementation of a wearable health monitoring system. The system has a friendly user interface and employs some methods to reduce the power consumption. The system is easy to install and use. The system is low cost, low power consumption and easily operable system. The system can lightly be expanded to other applications.

FUTURE SCOPE

Wearable electronic product has their end users in sectors such as defense, medicine, health monitoring etc.

1. Multiple parameters like Blood pressure and other controlling parameters in the future can be added to the glove.
2. This glove can be extended into a gym glove which can have features like tracking Respiration Rate, Heart Rate, Form Evaluation, Hydration, Calories Burnt etc.
3. This glove can be accommodated with the gyro sensor and contact detection sensor to enable the gesture input by physical motion and enable touch based user interface.

REFERENCES

[1.] Marius Valerian Paulet, Oana Maria Neacsu , Andrei Salceanu "Wireless monitoring system of the heart rate" DOI: 10.1109/ICEPE.2014.6969976, 04 December 2014.

[2.] Jesse Jayne Rutherford, "Wearable Technology" in IEEE Engineering in Medicine and Biology Magazine (Volume: 29, Issue: 3, May-June 2010).

[3.] Hashem etal.,"Design and Development of a Heart Rate Measuring Device using Fingertip" IEEE International Conference on Computer and Communication Engineering (ICCCE) , 2010.

[4.] Jatin Arora, Amandeep Singh, Gagandeep, Narinder Pal Singh "Heartbeat rate monitoring system by pulse technique using HB sensor" in Information Communication and Embedded Systems (ICICES), 2014 International Conference (2014).

[5.] T.S. Arulananth, B. Shilpa, "Fingertip based heart beat monitoring system using embedded systems".

Effective Boiler Automation using PLC and SCADA

Avinash kumar Dubey, R P Chauhan

***Abstract*—For some power plant, chemical industries and pharmaceutical industries boiler plays an important role which requires continuous monitoring and inspection at frequent intervals..There are possibilities for errors at measuring the various stages by human workers. So a reliable automatic system is required in order to avoid the catastrophic failure, and this can be achieved by implementing Programmable Logic Controllerand Supervisory Control And Data Acquisition system. This paper outlines the various stages of operations that convert the manual operated boiler to a fully automated boiler. As the competition increases globally, Industries have a huge demand of high quality, high accuracy and efficient automated machines. Pressure, temperature and water level are the three critical parameters of boilers which needs to be controlled very precisely. For that different pressure, temperature and level sensors/transmitters are used. There is also provision for complete shutdown of plant to avoid and catastrophic situation. For implementing above project Allen Bradley made RSLogix 500 PLC software is used and WonderwareIntouch SCADA software is used.**

***Keywords*—Boiler, Automation, PLC, SCADA, Sensors, Analog Card**

I. INTRODUCTION

A boiler or steam generator is a device used to create steam by applying heat energy to water. Boilers are made up different materials which are changing as time passes due to demand in increased strength of the pressurized vessels. Boilers are used to generate steam at very high temperature and pressure to run a steam turbine or some other equipment inside the plant. As the temperature and pressure of steam is reduced after passing the turbine section then this steam is further send for reuse where ever it is required .To produce steam at exact pressure and temperature water level in the boiler must be maintained at a certain level. To do this we need a accurate automation system which will generate steam at a desired pressure and temperature. Automation needs lots of auxiliaryequipment along with sensors, PLC and SCADA. PLC stands for Programmable logic controller which is assumed as a heart of any automation plants. SCADA is a supervisory system used to supervise a completeplant and basically consist of data accessing features and controlling process remotely.

It is usedto monitorboilertemperature pressure and level using different sensors and corresponding output is given to the PLC which controls the boiler temperature pressure and level.

II. RELATED WORK

In present situation conventional PID control is being used for boiler control. These conventional controllers in power plants are not very stable when there are fluctuations and, in particular, there is an emergency occurring. Continuous processes in power plant and power station are complex systems characterized by nonlinearity, uncertainty and load disturbances. The conventional controllers do not work accurately in a system having nonlinearity in it. So, an intelligent control using PLC& SCADA is developed to meet the nonlinearity of the system for accurate control of the boiler steam temperature and pressure level.

Embedded system based boiler automation system consist of GSM (Global System for Mobile Communication), PIC (Peripheral Interface Controller) and different sensors which is capable of monitoring the entire boiler temperature and pressure. The obtained temperature and pressure measured data are transferred through the PIC microcontroller. The microcontroller read the available data and processed.

If the temperature and pressure exceeded the maximum value then the user will be able to get information about the current temperature in any boiler by simply sending a boiler identification number [1], [3].

Fuzzy PID controller is used for temperature superheated steam of boiler based on the fuzzy control methodology. The control process is simulated through the Simulink MATLAB software. It shows that the system can demonstrate good control ability and dynamic effects even in large delay and stochastic disturbance circumstances [4]. From the literature it is evident that have several disadvantages. In the proposed system the previous papers disadvantages are overcome by using PLC & SCADA for boiler automation to monitor and control the boiler temperature, pressure and water level in thermal power plant.

III. PURPOSE OF BOILER AUTOMATION

Power plants require multiple number of boiling section. This boiling section produces the high temperature water of the steam. Steam coming out of the boiler in thermal power plant is very complex and hard to control. In past years there were many serious injuries and destruction of property due to boiler failure. It is critical for the safe operation of the boiler and the steam turbine. Critically low level of water may overheat boiler tubes and damage them as well as critically high level may interfere with separating moisture from steam and transfers moisture into the turbine, which reduces the boiler efficiency and also damages the turbine blades.

In recent years multiple efforts have been applied for the safe and efficient operation of boiler. To automate a power plant and minimize human intervention, there is a need to develop a Boiler Automation system.In order to achieve it a Programmable Logic Controller with Supervisory Control and Data Acquisition system is used to reduce the errors caused by humans and avoids the catastrophic failure.

IV. BOILER AUTOMATION

SCADA monitor various parameters of boilers like pressure, tempertaure,level any more by the help of various sensors and transmitters and sends signals to the input of the PLC. PLC pays an important role because all the instructions needed to operate the boiler are written here according to which it gives command to the output actuators and motors conneted in the plant.Communication cable plays a important role in making a proper connection betwwen PLC and SCADA system.

Figure 1 shows the block diagram of boiler Automation which consists of input module, programmable logic controller, output module, sensors and SCADA to monitor and control the entire operation of boiler. Here sensor used for measurements of various parameters are Resistance temperature detector (for measurement of temperature), RT Pressure transmitter (for pressure measurement) and Conductivity probe sensor (for level measurement).Here RTD used is of pt-100 type.

A. Boiler operation

Water plays an important role in generation of steam. When main switch is ON then feed water pump starts deliver water and addition with this coal is also fired from the bunker to the boiler.

Water is taken from the water treatment plant passed through the feed water pumps to the boiler. Two feed water pump is used so that water supply is not abrupt, if one pump fails then second pump will overcome on that. Both pumps are ON but some percentage limitation is set on both the pumps according to requirements. Heater is switched ON by using PLC. Forced fan is used to force the air into the boiler to improve the combustion efficiency and its corresponding temperature and pressure are measured by sensors.

Conversion of Water to Steam evolves in three stages.

- Heating the water from cold condition to boiling point or saturation temperature – sensible heat addition.
- Water boils at saturation temperature to produce steam

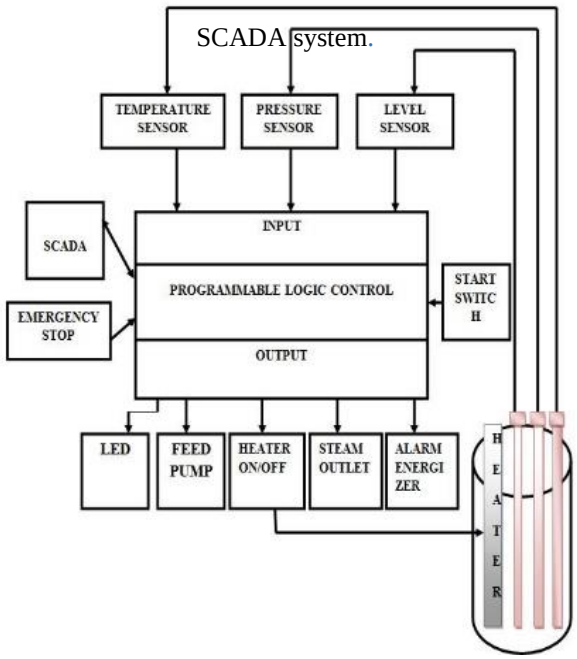

Fig. 1. Block Diagram of Boiler Automation

- Latent heat addition.

- Heating steam from saturation temperature to higher temperature called Superheating to increase the power plant output and efficiency

The first step is to get a constant supply of water at high pressure into the boiler. Since the boiler is always at a high pressure. ‘Boiler feed water pump’ pumps the water at high pressure into the boiler from the ‘feed water tank’. The pump is akin to the heart in the human body

'Feed water heaters’, using extracted steam from the turbine, adds a part of the sensible heat even before the water enters the boiler.

Most of the sensible heat is absorbed in the Economizer. These are a set of coils made from steel tubes located in the tail end of a boiler. The hot gases leaving the boiler furnace heat the water in the coils. The water temperature is slightly less than the saturation temperature. From the economizer the water is fed to the 'drum'.

The drum itself a large cylindrical vessel that functions as the storage and feeding point for water and the collection point for water and steam mixture

Boiling takes place in the 'Water Walls' which are water filled tubes that form the walls of the furnace. Water Walls get the water from the 'down comers' which are large pipes connected to the drum. The down comers and the water wall tubes form the two legs of a water column.

As the water heats up in the furnace a part of the water in the water-wall tubes becomes steam. This water steam mixture has a lower density than the water in the down comers. This density difference creates a circulation of water from the drum, through the down comers, water walls and back to the drum. Steam collects at the upper half of the drum. The steam is then sent to the next sections.

Float switch is used for level measurement are of four probes types which will show the low-low, low, high and high-high level of the tank. When water comes below the low-low value then it sends emergency alarm to the SCADA screen and try to shut down the boiler. Boiler will operate well when water level lies above low level and below high level.

If the temperature and pressure inside boiler exceeds then entire system will be in OFF state. The corresponding automated check valves are opened to avoid catastrophic failure.

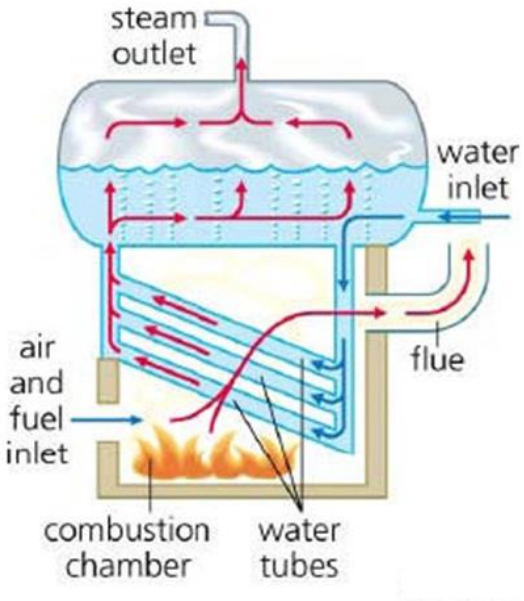

Fig 2: Water tube Boiler

B. Sensor Used

- Temperature Sensor

Resistance Temperature Detector (RTD PT 100) is used to sense the temperature variation. It works on positive temperature coefficient method where resistance increases as measured temperature increases. A PT-100 is a precision platinum resistor that exhibits 100 ohm at 0^0c. Fig.3 shows the typical RTD. To measure the resistance, it is essential to convert it to a voltage and use the voltage to drive a differential input amplifier. It is connected in wheat stone bridge. The differential input amplifier will reject the common mode noise on the leads of the RTD and provide the greatest voltage sensitivity.

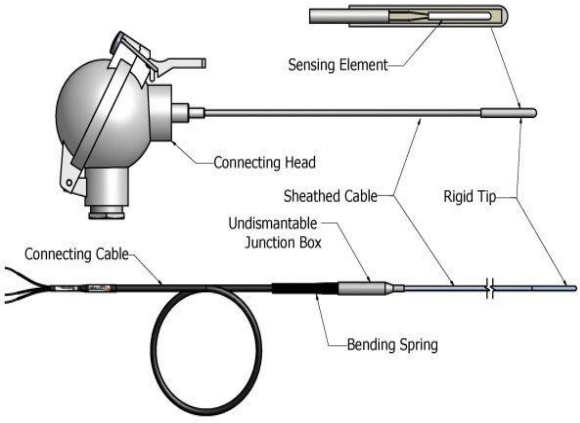

Fig 3:RTD temperature Sensor

- *Level Sensor*

  A float switch is a device used to detect the level of liquid within a tank which is illustrated in Fig.4. The switch may be used in a pump, an indicator, an alarm, or other devices. Float switches range from small to large and may be as simple as a mercury switch inside a hinged float or as complex as a series of optical or conductance sensors producing discrete outputs as the liquid reaches many different levels within the tank.

- Pressure Transmitter

  For continuous measurement of pressure inside the boiler pressure transmitter is used here which will sends signal to PLC at each instant of time. It utilize a seamless bellows as sensing element. The bellows can be either phosphor bronze or stainless steel to suit various kinds of process medium.

C. Programmable logic controller(PLC)

Programmable Logic Controller (PLC) is a digital computer used for the automation of various electromechanical processes in industries [6].A PLC is an example of a "hard" real-time system since output results must be produced in response to input conditions within a limited time, otherwise unintended operation will result.

PLCs can range from small "building brick" devices with tens of inputs and outputs (I/O), in a housing integral with the processor, to large rack-mounted modular devices with a count of thousands of I/O, and which are often networked to other PLC and SCADA systems.

Fig 4: Float Switch for level measurement

- Pressure Transmitter

  For continuous measurement of pressure inside the boiler pressure transmitter is used here which will sends signal to PLC at each instant of time. It utilize a seamless bellows as sensing element. The bellows can be either phosphor bronze or stainless steel to suit various kinds of process medium.

Fig 5: Pressure transmitter for pressure measurement

the IEC 61131/3 control systems programming standard that defines 5 languages: Ladder Diagram (LD), Structured Text (ST), Function Block Diagram (FBD), Instruction List (IL) and Sequential Flow Chart (SFC)[v].

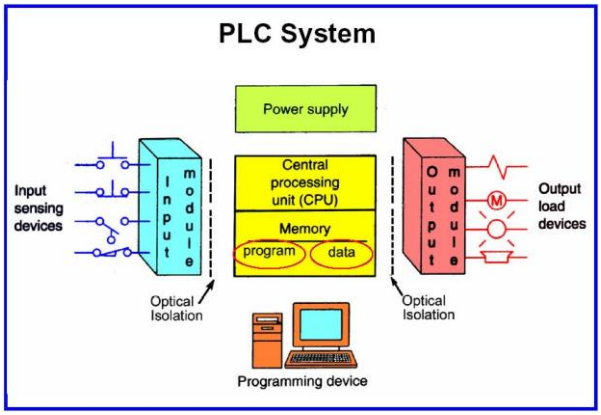

Fig 6: PLC Architecture diagram

D. Supervisory Control and Data Acquisition System(SCADA)

Supervisory control and data acquisition (SCADA) is a system of software and hardware elements that allows industrial organizations to:

- Control industrial processes locally or at remote locations
- Monitor, gather, and process real-time data
- Directly interact with devices such as sensors, valves, pumps, motors, and more through human-machine interface (HMI) software
- Record events into a log file.

SCADA systems are crucial for industrial organizations since they help to maintain efficiency, process data for smarter decisions, and communicate system issues to help mitigate downtime.

PLCs and RTUs are microcomputers that communicate with an array of objects such as factory machines, HMIs, sensors, and end devices, and then route the information from those objects to computers with SCADA software. The SCADA software processes, distributes, and displays the data, helping operators and other employees analyze the data and make important decisions.

For example, the SCADA system quickly notifies an operator that a batch of product is showing a high incidence of errors. The operator pauses the operation and views the SCADA system data via an HMI to determine the cause of the issue. The operator reviews the data and discovers that Machine 4 was malfunctioning. The SCADA system's ability to notify the operator of an issue helps him to resolve it and prevent further loss of product.

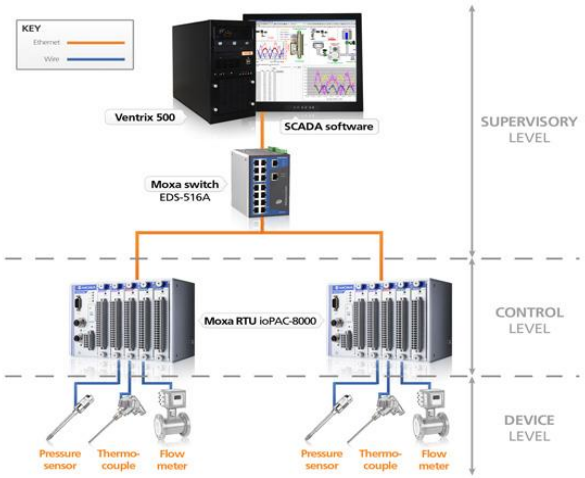

Fig 7: Hardware of SCADA Architecture

V. PLC AND SCADA SIMULATION

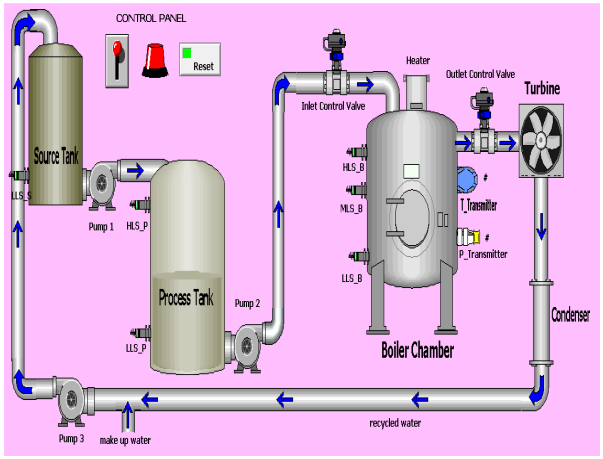

Fig 8: Intouch SCADA Window for boiler automation.

In this Simulation of Boiler Automation using PLC and SCADA are discussed. Ladder diagram of boiler Automation is generated and execution is carried out in Rslogix 500 Allen Bradley software and corresponding SCADA design is generated using IntouchWonderware and the corresponding output is viewed. PLC and SCADA interfacing is done via communication cables.

A. PLC Ladder Diagram

In this page we make use of the inputs, memories and output icons for the neat representation of the program. In the first rung we make use of a start button for starting the process and the emergency stop button as normally closed contact. In the second rung I have developed logic for manual filling of source tank. In next coming rung I have created ladder logic for pump operations.

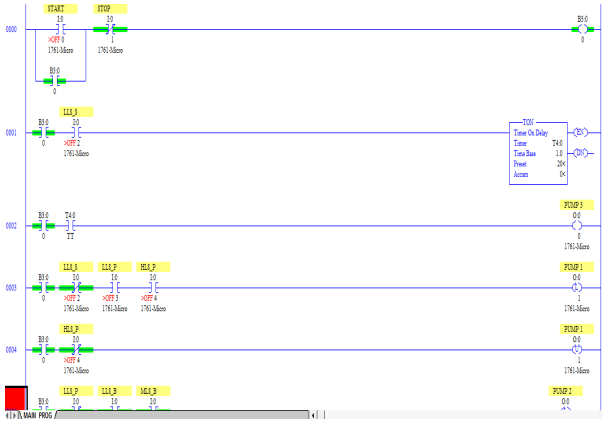

Fig 7: Hardware of SCADA Architecture

This is the next page of program for the process I have taken signal from the temperature transmitters and the pressure transmitters. Different level sensors are used for the boiler automation. This page of program is fully automated. This means that this process does not need any manual attendance, and it operated just with a single start button. Nowhere in the process, there is any activation of switch by an external force.

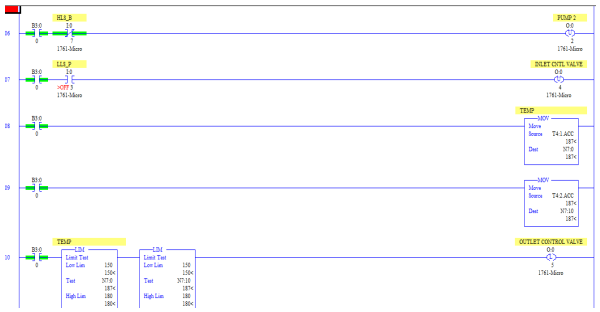

Fig 10: Sensors and transmitters data used in ladder logic

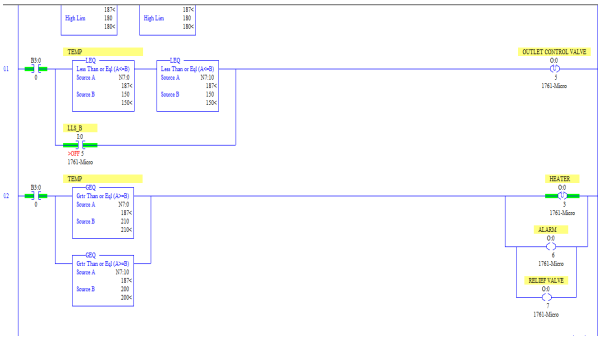

Fig 11: ladder logic for accidental plant shut down and alarm acknowledgment.

VI. CONCLUSION

In the above paper, Boiler Automation using PLC and SCADA has been designed and implemented. Boiler has been controlled very efficiently using the help of various sensors. SCADA is used to monitor the parameters and PLC is used to control the operation. If the temperature and pressure exceed predefined value then the entire setup will shut down and automatic check valves are opened to release the steam and pressure. In case of emergency alarm was energized and automatic check valves are opened to avoid catastrophic failure. Ladder diagram of Allen Bradley PLC is simulated using Rslogix 500 software and the SCADA design of boiler automation is simulated using IntouchWonderware software.

The future research is to focus on the application oriented implementation of remote monitoring of boiler Automation by SCADA and IOT .

REFERENCES

[1] T.Karuppiah, Sivasankaran V, Azha , Periasamy, Muruganand S―Embedded System Based Industrial Power Plant Boiler Automation Using GSM Technology‖ IJARCCE Vol. 2, Issue 8, August 2013.

[2] Anabik Shome, Dr. S.Denis Ashok ―Fuzzy Logic Approach for Boiler Temperature & Water Level Control‖ International Journal of Scientific & Engineering. Research, Volume 3, Issue 6, June-2012.

[3] K. Ghousiya Begum Mercy D, Kiren Vedi H, Ramathilagam V ―An Intelligent Model Based Level Control of Boiler Drum‖ IJETAE Volume 3, Issue 1, January 2013.

[4] Chuntanman, JiaLi,LanyingWang,Yantao Chi ―The fuzzy PID control system for superheated steam temperature of boiler‖ Strategic Technology (IFOST) , IEEE International Conference ,Volume 2, pp. 967-970, June-2011.

[5] Programmable Logic Controllers (PLCs) and SCADA details are available at: http://electrical-engineering-portal.com.

Review Article: Consensus and Cooperative Control for the Adaptive Distributed Observer of Discrete-Time Linear Multi-Agent System

Leela Dhar Nagar

***Abstract*—Distributed control has been a keen field of interest and has seen an increased interest in the past few years. Multi-agent System has several applications in different areas and is one of the way to implement distributed control. This paper presents a review on adaptive distributed and cooperative control of multi-agent system (MAS) capabilities in control engineering applications. It has an overview of significant (important/ essential/ prime/ key/ paramount) control engineering issues which can be explored by multi-agent system and also describes essential (important/ essential/ prime/ key/ paramount) concepts of multi-agent system that are related to Control Systems. This paper provides an overview on the basic concepts of information consensus in networks and a theoretical framework for analysis of consensus for multi-agent networked system.**

***Keywords*—Agent, Multi-Agent System, Distributed Control System, Consensus and Cooperative Control, Network Control System.**

I. INTRODUCTION

The study about the interaction and information flow between different agents in a group has played a major role for learning the coordinated movements of these agents. For a group of agent to achieve consensus on shared information in the existence of changing interaction topologies and unreliable and limited interchange of information, there is a need to design appropriate protocols and algorithms. There is a lengthy history in computer science which designs the foundation of the field of distributed computing [6]. An agent can be defined in many number of ways in the past [1,3,4, 7 and 8]. A comparative analysis of these definitions can be found in [5].

A. Agent:

An agent may be defined either a software or hardware process (or a entity), which can situate either in a virtual or in a real environment [Wooldridge, 2002]. An agent can be "a software (or hardware) entity that is situated in some environment and is able to autonomously react to changes in that environment.". As per the definition "The environment" can be either physical or Computing [5]. According to Odell (2007) among key agent attributes are autonomous, interactive, adaptive, intelligent, flexible, reactive, proactive, social, mobile and trustworthy. According to Wooldridge and Jennings [2], there are many different types of agents:

(a) Those agents that use pre specified assumption and rules to execute simple task.
(b) Those agents that execute a task at the request of user,
(c) Those agents that provide service to the user without being asked explicitly at an appropriate time.

B. Multi-Agent System:

A group of autonomous agents that operate within the networked environment has been called Multi-Agent System. Control engineers are interested in using distributed control, computing, sensing and communication to design a strategy for a Multi-Agent for attaining a global control objective [1]. A multi-agent system (MAS) may be defined as that system, which consists of two or more agents. These Agents have local goals, rather than having an overall goal [9]. In mas, the agents have the ability to connect with each other. The communication is more than mere of transferring the data between distinct software and hardware agents. It refers to the ability of negotiating and interacting in a cooperative manner. A group of different agents with their respective abilities to solve a problem by interacting among themselves is therefore it is known as a multi agent system.

C. Cooperative Control:

The purpose of cooperative control is having many autonomous agents, which work together in a well-organized way to attain collective group behaviour through local interaction. In comparison to a single complex agent, it has a major potential to improve the

Leela Dhar Nagar is with Department of Electrical Engineering, National Institute of Technology Kurukshetra, India

(e-mail: ldnagar007@gmail.com)

operational efficiency which reduces the cost price, and provides extra degrees of redundancy. The problems that are included by the normal cooperative control are coverage control, task and role assignment, distributed estimation, formation control, flocking, and consensus, among others. The dominating task for the cooperative control problem is to design suitable controllers which achieve a desired coordination objective. Distributed approach and centralized approach are mostly used in designing of the cooperative control [12, 14]. Cooperative control can achieve desirable collective behaviour through the design of individual agent control algorithms. The need of cooperative control in

i) Agents capable of performing different tasks available.
ii) There is an objective which cannot be acquired by a single agent.
iii) Collectively, the agents can achieve the objective.
iv) We can have multiple agents that are capable of performing similar individual tasks in the team. In case of an agent failure, the main objective can still be achieved [13].

D. Consensus:

Consensus is considered as the fundamental & important difficulty in the area of cooperative control of multi-agent systems, which approximately corresponds to flocking, distributed estimation, formation control, and continues. The meaning of Consensus is reaching on some common value by interaction among different agents via a communication network or sensing [12].Various consensus algorithms are

i) Rendezvous
ii) Velocity matching
iii) Flocking
iv) Formation control
v) Attitude synchronization [13].

There are two classes to categorize the existing algorithms of consensus.

i) The consensus which is having a leader
ii) Consensus which is not having a leader (i.e., leaderless consensus). The former is also called distributed tracking or leader-follower consensus.

II. LITERATURE REVIEW

Y. Su and J. Huang [10] presents that there are two groups of subsystems in the overall system. Out of which, the first group of subsystems may obtain the exogenous signal; the second subsystem is not able to do so. Which in turn results that the problem may not be solved by using decentralized approach? Problem of dynamic full information distributed control law is solved after using a distributed observer by Y. Su and J. Huang [10] under the standard assumptions. So, in this paper by improving the problem,if consider the noise or time delay in the communication links then the problem will make more sense.

In "Cooperative output regulation of multi-agent systems" (2012) Jie Huang [11] worked on the building of the above mentioned problem which can generalize the consensus problem of leader-following in the sense that the problem concurrently addresses disturbance rejection and asymptotic tracking, account for model uncertainty, and accommodate a general leader system.In this, two approaches (the internal model control and the feed forward control approach) have been also utilized for handling other cooperative control problems of multi-agent systems such as formation, rendezvous, and flocking.

Yamin Yan, Jie Huang [16] have studied the distributed observer approach which can be used for problem of the cooperative output regulation for the discrete linear time-delay multi-agent systems. When this problem of discrete linear time delay multi-agent system is compared with the same problem for linear time-delay multi-agent systems, it is seen that the problem is having two new features. Out of which the first one is that when the time delay is present, then both the systems will be having different regulator equations i.e. discrete-time linear system's regulator equations will be different from that of continuous-time linear system'sregulator equations. Second one is that by assuming the standard supposition on the communication graph's connectivity, for a continuous-time linear leader system a distributed observer will always exist. It has not been be the case for the continuous time system of the discrete counterpart of the distributed observer. [16] They had done work under the static network topology on the cooperative output regulation problem of discrete-time linear time-delay multi-agent system. They have firstly researched, an existence condition for the discrete distributed observer, and then shown that the problem can be solved by distributed dynamic output feedback control law.

He Cai, Frank L.Lewis, Guoqiang Hu and JieHuang [17] has been proposed a distributed control scheme, which uses the adaptive distributed observer, consisting of the three steps. One is an adaptive distributed observer, which can be used to evaluate both the state of the leader system and the system matrix. Then next one is an adaptive algorithm, which can be formulated for determining the solutions of the regulator equations online. Last one is that in which for finding out the solution for the cooperative output regulation problem, both adaptive measurement output feedback and the adaptive state feedback controllers has been combined, without the supposition of that each follower has knowledge about the system matrix of the leader system.On the basis of the adaptive solution of the regulator equations and the adaptive distributed observer, for solving the cooperative output regulation problem [17] have incorporated both adaptive measurement output feedback and adaptive state feedback controllers.

He Cai, Frank L.Lewis, Guoqiang Hu and JieHuang[15] have been presented the adaptive distributed observer. This, to each follower, will not only help in determination of the leader's system matrix but also help in determination of the leader's signal. They [15] worked upon the cooperative output regulation problem of linear multi-agent system by adaptive controllers. Hence, for determining the leader system dynamics, for formulating a scheme for estimating the solution of the regulator equations adaptably, and removing the supposition that each follower is having information about leader system dynamic, an adaptive distributed observer has been designed.

Q.Ma,S.Xu,F.L.Lewis, B. Zhang and Y. Zou [18] have presented general distributed observers, which have been designed to obtainthe exosystem's estimation. They have proposed distributed normal output feedback and the distributed singular output feedback controller.

For a multi-agent system, Yi Dong, Jie Chen and Jie Huang [19] have firstly proposed one self-tuning adaptive distributed observer, which has capacity of providing the estimation of the signal of the leader into different types of followers without supposing that all the followers have information about the leader's system matrix and which may avoid finding out the observer gain offline. Now after this, for solving the cooperative output regulation problem for linear heterogeneous multi-agent systems an adaptive distributed control law has been developed. This control law has two advantages, one of them is that it uses the minimum information about the network and second one is, information about the leader system, and determining the gain of observer is avoided by it.

Ruohan Yang, Hao Zhang, Huaicheng Yan and Fuwen Yang [20] have proposed a control strategy, in which the use of the minimal non-zero eigenvalue of Laplacian matrix while determining the gain matrix has been avoided, moreover, it has also been supposed that the communication topology is having one directed spanning tree only frequently. It has been demonstrated that external signals can be tracked asymptotically by the individual agents and disturbance rejection can also be achieved.

Ruohan Yang, HaoZhang , Gang Feng and Huaicheng Yan [21] have investigated two novel distributed event-triggered adaptive control strategies based on output feedback and state feedback are developed, which can avoid use of the minimal non zero eigen values of the Laplacian matrix, which also associates to global system topologies. It has been demonstrated that under the proposed control protocols, asymptotic tracking and disturbance rejection have be attained by MASs, and meanwhile, the amount of transmission data and communication cost among agents can be reduced.

According to Min Meng, Lu Liu and Gang Feng [22], a time-homogeneous Markov process governs the switching mechanism, whose states correlate with all possible communication topologies among agents. A novel distributed adaptive cooperative controller has been presented, to estimate an exogenous signal for all the agents in mean square sense the dynamic compensators are employed. The distributed control law has been dependent upon the local information about the agents, without using global information about communication topologies.

III. METHODOLOGY

Problem Statement: Consider the discrete-time linear multi-agent system:

$$x_i(t+1) = A_i x_i + B_i u_i + E_i v,\ t \in Z^+ \quad (1a)$$

$$e_i(t) = C_i x_i + D_i u_i + F_i v \quad (1b)$$

$$y_{mi}(t) = C_{mi} x_i + D_{mi} u_i + F_m v_i,\ i = 1,\dots,N \quad (1c)$$

Where $x_i \in R^{n_i}$, $u_i \in R^{m_i}$, $e_i \in R^{m_i}$, $y_{mi} \in R^{p_{mi}}$ are the state, control input, regulated output and measurement output of the i^{th} subsystem, respectively and A, B, C are constant matrices with compatible dimensions.

The design of a distributed observer for the leader system of the following form:

$$\dot{v} = Sv \quad (2)$$

where $v \in R^q$ is the state of the leader system representing the reference input to be tracked and/or the external disturbance to be rejected and $S \in R^{q\times q}$is a constant matrix. Discrete counterpart of the adaptive distributed observer in [1] for a discrete leader system of the following form:

$$v(t+1) = Sv(t). \quad (3)$$

Like in [13], let the system be composed of (3) and (1) as a multi-agent system of $(N+1)$agents with N subsystems of (1) as N followers and (3) as the leader, and a pair of graph is formed $\bar{G} = (\bar{V}, \bar{\varepsilon})$with $\bar{V} = \{0,1,\dots,N\}$being a set of N nodes or vertices and a set of edges or arcs is $\bar{\varepsilon} \subseteq \bar{V}\times\bar{V}$. Here the node $i, i = 1,\dots,N$, is associated with the i^{th} subsystem of the follower system (1) and the node 0 is associated with the leader system (3).

For $i = 0,1,\dots,N, j = 1,\dots,N, (i,j) \in \bar{\varepsilon}$iff agent$j$ can use the state or output of agent i for control. Let the neighbour set of the node i of graph $\bar{G}$is denoted by $\overline{N_k}$. Considering the control law of output feedback in the following form

$$u_i(t) = k_i\,(z_i(t))$$
$$z_i(t+1) = g_i(z_i(t), y_{mi}(t), z_j(t), y_{mj}(t), j \in \bar{N}_i)$$
$$i = 1,\dots,N \quad (4)$$

Where $y_{m0} = v, z_i \in R^{l_i}$ for some integer l_i,k_i and g_i are linear functions of their arguments. It can be seen that, for each $i = 1,\dots,N, j = 0,1,\dots,N$, u_i of (4) depends on y_{mj} only if the agent j is a neighbour of the agent i. Thus, the control law (4) is a distributed control

law. The control law (4) contains the state feedback control law as a special case when $y_{mi} = x_i, i = 1,\dots,N$.

Now defining the adaptive cooperative output regulation problem for (3) and (1) as follows:

Problem 1: A distributed control law of the form (4) is designed by the (1), (3) and graph $\bar{G}$, such that the trajectory of the closed-loop system with any initial state exists for all $t \geq 0$ and satisfies:

- Bounded trajectory(of the closed loop system)for all $t \geq 0$ is observed when v is bounded;
- the output satisfies

$$\lim_{t\to\infty} e_i(t) = 0, i = 1,\dots,N. \qquad (5)$$

The following assumptions are made for the solvability of Problem 1.

Assumption 1: The modulus of all theeigenvalues of $S$is smaller than or equal to 1.

Assumption 2: For $i = 1,\dots,N, (\mathrm{A}_i, \mathrm{B}_i)$are stabilizable.

Assumption 3: $(\mathrm{C}_{mi}, \mathrm{A}_i)$ are detectable for$i = 1,\dots,N,$.

Assumption 4: A unique solution pair (X_I, U_i) exists for the following equations for $i = 1,\dots,N,$:

$$X_i S = A_i X_i + B_i U_i + E_i \qquad (6a)$$

$$0 = C_i X_i + D_i U_i + F_i \qquad (6b)$$

Assumption 5: The graph $\bar{G}$has a spanning tree [24, 25] with the node 0 as the root.

Notation:

$\otimes$ = Kronecker product of matrices.

$||x||$ = Euclidean norm of a vector $x \in R^n$.

Z^+ = Set of nonnegative integers. It is assumed that x $Z^+ \to R^n$. $x(t), t \in Z^+$is denoted by$x$.

$\sigma(A)$ =Spectrum of A.

$\rho(A)$ = Spectral radius (the maximal magnitude of the eigenvalues of A).

1_N= a $N \times 1$ vector.

For$X_i \in R^{n_i \times p}, i = 1,\dots,m,\ col(X_1,\dots,X_M) = [X_1^T,\dots,X_M^T]^T$.

For any matrix$A \in R^{m\times n}$

$$vec(A) = [A_1 \dots . A_n]^T \qquad (7)$$

where $A_i$is the i^{th} column of A. For any column vector $X \in R^{nq}$ for some positive integers n and q

$$M_n^q(X) = [X_1 \cdots X_q] \qquad (8)$$

where, for $i = 1,\dots,q, X_i \in R^n$, and are such that $X = col(X_1,\dots,X_q)$.

Adaptive Distributed Observer: For a discrete leader system, a distributed observer was formed as (3) and proposed in [25] which have a form:

$$\eta_i(t+1) = S\eta_i(t) + \mu S \sum_{j=0}^{N} a_{ij}\left(\eta_j(t) - \eta_i(t)\right)$$

$$i = 1,\dots,N \qquad (9)$$

where $\eta_0 = v, \eta_i \in R^q, i = 1,\dots,N, \mu > 0$, and $\bar{A} = [a_{ij}]_{i,j=0}^{N}$ denote the weighted adjacency matrix of graph$\bar{G}$. Let $\eta(t) = col(\eta_1(t),\dots,\eta_N(t))$, $\hat{v}(t) = 1_N \otimes v(t)$, and$\tilde{\eta}(t) = \eta(t) - \hat{v}(t)$. Then (9) can be put in the following form:

$$\tilde{\eta}(t+1) = ((I_N \otimes S) - \mu(H \otimes S))\tilde{\eta}(t) \qquad (10)$$

where $H = [h_{ij}] \in R^{N\times N}$ with $h_{ii} = \sum_{j=0}^{N} a_{ij}$and $h_{ij} = -a_{ij}$, for any $i = j$. The eigenvalues of H are having positive real parts. If for some μ, the matrix $((I_N \otimes S) - \mu(H \otimes S))$ is Schur, then, for any $v(0)$, and $\eta_i(0), i = 1,\dots,N$, we have

$$\lim_{t\to\infty}(\eta_i(\mathrm{t}) - v(\mathrm{t})) = 0. \qquad (11)$$

Thus, the system (9) is called a distributed observer of the leader system if and only if (10) is asymptotically stable. [25, Lemma 3.1] gives a detailed discussion on the stability of (10). The eigenvalues of $S$are denoted by $\{\lambda 1,\dots,\lambda q\}$ where $0 \leq |\lambda_1| \leq \cdots \leq |\lambda q|$, and those of H by $\{a_l \pm jb_l\}$, where $b_l = 0$ when $1 \leq l \leq N_1$ with $0 \leq N_1 \leq N$ and $b_l \neq 0$ when $(N_1 + 1) \leq l \leq N_2$ where $N_1 + 2(N_2 - N_1) = N$. The matrix $((I_N \otimes S - \mu(H \otimes S))$ is Schur for all μ under Assumptions 1 and 5. Itsatisfies

$$\max_{l=1,\dots N}\left\{\frac{a_l - \sqrt{\Delta_l}}{a_l^2 + b_l^2}\right\} < \mu < \min_{l=1,\dots,N}\left\{\frac{a_l + \sqrt{\Delta_l}}{a_l^2 + b_l^2}\right\} \qquad (12)$$

Where $\Delta_l = \left(\frac{a_l^2 + b_l^2}{|\lambda_1|^2}\right) - b_l^2$. If $|\lambda_1| = 1$ for all $l = 1 \dots \dots \dots q$, then $\lambda_1 = a_l^2$ and (13) reduces to

$$0 < \mu < \min_{l=1,\dots,N}\left\{\frac{2a_l}{a_l^2 + b_l^2}\right\}. \qquad (13)$$

It may not be realistic for some applications to have every follower use the matrix S. Further proposing the adaptive distributed observer candidate as:

$$S_i(t+1) = S_i + \mu_1 \sum_{j=0}^{N} a_{ij}(S_j - S_i) \qquad (14a)$$

$$\eta_i(t+1) = S_i\eta_i + \mu_2 S_i \sum_{j=0}^{N} a_{ij}(\eta_j - \eta_i) \qquad (14b)$$

Where $S_0 = S, S_i \in R_{q\times q}, i = 1,\dots,N, \mu_1, \mu_2 > 0$. (14) Is the adaptive distributed observer for the leader system if there is some $\mu_1, \mu_2 > 0$ such that,the solution for (15) satisfies $\lim_{t\to\infty} \mathrm{S}_i(\mathrm{t}) - \mathrm{S}) = 0$, $\lim_{t\to\infty} \eta_i(\mathrm{t}) - v(\mathrm{t})) = 0$ for $i = 1,\dots,N$. It is evident from (14) that only those followers know the matrix S who are the children of the leader. Thus, more realistic observer is the adaptive distributed observer.

IV. CONCLUSION

This paper gives a small glimpse into the areas of consensus Multi-Agent System. It also provides a brief literature survey on the existing and potential applications of multi-agent system with a recent investigation into control engineering. This paper

provides an overview about the main literature review of distributed consensus of MASs under adaptive distributed observer. The second (II) section has been devoted to highlight the work done in the field of multi-agent system which deals with both adaptive observer and distributed control of MAS. Few other related work like consensus, the adaptive distributed observer etc. have also been discussed. The overview shows that the distributed consensus of MASs is still an open research topic and still further problems can be studied in the future. For future work, this overview can be extended with further details with an alternative approach followed by the references stated within it.

REFERENCES

[1] S. Russell and P. Norvig, Artificial Intelligence: A Modern Approach, Prentice-Hall, Englewood Cliffs, NJ, USA,1995.

[2] M. Wooldridge and N. R. Jennings, "Intelligent agents: theory and practice," *The Knowledge Engineering Review*, vol. 10, no.2, pp. 115–152, 1995..

[3] B. Hayes-Roth, "An architecture for adaptive intelligent systems," Artificial Intelligence, vol. 72, no. 1-2, pp. 329–365, 1995.

[4] P. Maes, "Artificial life meets entertainment: lifelike autonomous agents," Communications of the ACM, vol. 38, no.11, pp. 108–114, 1995.

[5] S. Franklin and A. Graesser, "Is it an agent or just a program?" in Proceedings of *the 3rd International Workshop Agent Theories, Architectures, and Languages*, Springer, New York, NY, USA, 1996.

[6] N. A. Lynch, *Distributed Algorithms*. San Francisco, CA: Morgan Kaufmann, 1997..

[7] L. N. Foner, "Entertaining agents: a sociological case study," in Proceedings of *the 1st International Conference on Autonomous Agents*, pp. 122–129, 1997.

[8] M. Wooldridge, "Intelligent agents," in Multi-Agent Systems, M. Wooldridge and G. Weiss, Eds., pp. 3–51, MIT Press, Cambridge, Mass, USA, 1999.

[9] [9] M. Wooldridge, An Introduction to Multi-Agent Systems, John Willey & Sons, New York, NY, USA, 2002.

[10] Y. Su and J. Huang, "Cooperative output regulation of linear multi-agent systems," *IEEE Trans. Autom. Control*, vol. 57, no. 4, pp. 1062–1066, 2012.

[11] Jie Huang, "Cooperative output regulation of multi-agent system*" in proceedings of *the 10th World Congress on Intelligent Control and Automation*, Beijing, China, July 6-8,2012.

[12] Zhongkui Li and Zhisheng Duan "Cooperative Control of Multi-Agent Systems" CRC Press Taylor & Francis Group, 6000 Broken Sound Parkway NW, Suite 300, Boca Raton, 2015.

[13] S R Sahoo "Multi-agent Coordination and Consensus" in workshop held at *Teqip School on System and Control*, IIT Kanpur, 2015.

[14] R.S. Smith and F.Y. Hadaegh. Control of deep-space formation-flying spacecraft; Relative sensing and switched information. Journal of Guidance, Control and Dynamics, 28(1):106–114, 2005.

[15] He Cai, Frank L.Lewis, Guoqiang Hu and Jie Huang, "Cooperative output regulation of linear multi-agent system by adaptive distributed observer" *2015 IEEE 54th Annual Conference on CDC*, pp. 5432-5437.

[16] Y. Yan and J. Huang, "Cooperative output regulation of discrete-time linear time-delay multi-agent systems," *IET Control Theory & Appl.*, doi:10.1049/iet-cta.2016.0106.

[17] He Cai, Frank L.Lewis, Guoqiang Hu and Jie Huang, "The adaptive distributed observer approach to the Cooperative output regulation of linear multi-agent system,"*Automania*, doi:10.1016/j.automatica.2016.09.038.

[18] Qian Ma, Shengyuan Xu, Frank L. Lewis,Baoyong Zhang, and Yun Zou, "Cooperative Output Regulation of Singular Heterogeneous Multiagent Systems," *IEEE Trans. on Cybernetics*, VOL. 46, NO. 6, pp.1471-1475,JUNE 2016.

[19] Yi Dong, Jie Chen and Jie Huang, "Cooperative Output Regulation for Networked Multi-Agent Systems based on the Self-Tuning Adaptive Distributed Observer" *2016 American Control Conference (ACC)*, pp. 1918-1923.

[20] Ruohan Yang, Hao Zhang, Huaicheng Yan, Fuwen Yang, "Cooperative control of heterogeneous multi-agent systems via distributed adaptive output regulation under switching topology" *2016 IEEE Conference on CEFC*, pp. 6770-6775.

[21] Ruohan Yang, Hao Zhang , Gang Feng and Huaicheng Yan, "Distributed Event-Triggered Adaptive Control for Cooperative Output Regulation of Heterogeneous Multi-agent Systems Under Switching Topology" *2017 IEEE Trans. on NNLS*, pp. 1-12.

[22] Min Meng, Lu Liu and Gang Feng, "Adaptive Output Regulation of Heterogeneous Multi-Agent Systems Under Markovian Switching Topologies" *2017 IEEE Trans. On Cybernetics*, pp. 1-10.

[23] Y. Su and J. Huang, "Cooperative output regulation of linear multi-agent systems," *IEEE Trans. Autom. Control*, vol. 57, no. 4, pp. 1062–1066, 2012.

[24] C. Godsil and G. Royle, *Algebraic Graph Theory*. New York: Springer Verlag, 2001.

[25] Y. Yan and J. Huang, "Cooperative output regulation of discrete-time linear time-delay multi-agent systems," *IET Control Theory & Appl.*, doi: 10.1049/iet-cta.2016.0106.

[26] J. Hu and Y. Hong, "Leader-following coordination of multi-agent systems with coupling time delays," Physica A: Statist. Mechan. and its Applic., vol. 374, no. 2, pp. 853–863, 2007.

Conclusion

This chapter focuses from modelling of system to design of controllers and their implementation to automation. Starting from some basic control strategies to advance robust controllers with different design methodologies varying from classical methods like PID controller to nature inspired methods have been summarized.

The chapter has been divided into two main sections modelling and Implementation of Controllers on a physical system. Controller implementation has been further subdivided into subsections according to application.In each of the section and subsection, some important papers deliberating that particular application have been included for quick reference.

In one of the main section Iterative method of identification of nonlinear Weiner system using the introduction of instrumental variables is takenwhich is validated using a simulation example with two different cases of noise level through Monte-Carlo simulation study.

Another main section is devoted to implementation of controllers to physical systems like variable speed motors, benchmark problem of inverted pendulum, robotic manipulator, biological system and automation. Two types of motors can be used AC and DC. Each motor has its own advantages and disadvantages and finds wide application in physical system. Papers related to both the motors have been added for ready reference with implementation of classical controllers and nature inspired controllers followed by another review paper of different controllers used in Rolling mills.

For benchmark Rotary Inverted Pendulum(RIP) if one paper is dedicated to design and implementation of classical and optimal LQR controller to RIP available in lab, other paper studies the effect of weighting matrix of LQR on the performance of RIP.

Be a biological system or thermal system simultaneous control and monitoring is required. Two papers one on biological and other a boiler are presented in this chapter which concentrate on measurement of different variables and monitor them. Very recently, the cooperation of multi-agents has been an increasingly popular topic for its potential prospects in variety realms such as military, industry, etc. Up to now,numerous results concerning the formulation, rendezvous and leader-following problems in multi-agent systems have been reported. Finally a review paper on the latest hot topic gives small glimpse into the areas of consensus Multi-Agent System.

The next third to fifth chapters will concentrate on recent headways in the field of FACTS devices, renewable energy systems and power systems respectively. A number of illustrations covering various issues involved in the whole domain of alternate energy systems and introducing efficiency in the existing power systems are included.

Chapter -3.

Recent Headways in Facts Controllers for Power System Improvement

Introduction

In power system, the reactive power in transmission line inhibits the maximum transmission and utilization of useful or active power and hence requires inductive or capacitive reactive power to be compensated. Flexible alternating current transmission system (FACTS) is an advanced techniques used for the compensation purpose and improve the network capability by diminishing the power flow limits like thermal limits, transient stability limit, voltage limit, short circuit current limit etc. FACTS devices are basically power electronic elements used along power system devices and are connected in series or parallel with the power systems according to the service requirement. As per IEEE definition, flexible alternating current transmission system (FACTS) devices are defined as "Alternating current transmission system incorporating power electronics based and another static controller to improve controllability and enhance power transfer capability".

(A) FACTS in Voltage Stability Enhancement

The transmission and distribution networks of the modern power systems are forced to operate at full capacity due to heavy power demand. This results in overloaded transmission and distribution lines and congestions. The planning and operation of modern power system are becoming more and more difficult. Conservative planning and operating methods are making power systems to become more and more insecure. For secure operation of power system, the stability of the voltage should be maintained which is very challenging. Therefore, Voltage Instability problem has become one of the few main challenges faced by the modern day power system and it has become a great concern to the power system industries.

To improve system security and increase in margins of the voltage stability, a desirable and careful plan should be made. For maximization of power transfer capabilities, compensation of FACTS Controllers (series and shunt types) is required. With respect to voltage stability, the voltage magnitudes in the buses are held close to their nominal values by compensation through FACTS Controllers and in addition, line currents and total systems losses are also reduced. In this context, sophisticated and versatile devices called FACTS Controllers are

effectively used in adjusting the bus voltage magnitude thereby contributing for the improvement in voltage stability of the power system. FACTS Controllers deal with this crucial voltage stability problem by providing voltage support properly and co-ordinate the control actions. Owing to their flexibility and fast control characteristics, FACTS Controllers can perform the active and reactive power control.

The reactive power compensator can be placed to identify the utmost critical bus for voltage stability enhancement. Lot of research work has been carried out. Several new techniques/methods have been used and several Voltage Stability Indices have been proposed. Many FACTS Controllers like STATCOM, SVC, SSSC, UPFC etc. are placed at those most critical nodes i.e. weakest buses and various techniques/methods are tested to find their effectiveness in making the power system more and more voltage stable.

(B) FACTS in Power System Stability Enhancement

Power System Stability is another important problem of the power system which is effectively addressed by FACTS Controllers. Power Systems are subjected to stability threat because they are operated under overloaded conditions due to high power demand. The reduction in the power flow on the overloaded lines, improvement of voltage profile, loadability and reduction in the transmission power losses are some of the major benefits of using FACTS Controllers. FACTS Technology is a new emerging technology which is playing a crucial role in enhancing controllability and power transfer capability of the modern power systems which are operating close to their limits. Parameters like line impedance, current, voltage, phase angle can be effectively controlled by FACTS Controllers which in turn bring in necessary and desirable results in power system indicating its performance improvement.

In, it has shown that the FACTS Controllers are useful in combating the power system stability problem. Comparison study is made on different FACTS Controllers and by comparing their performance with respect to system stability, it is found that for the improvement of power system stability, the UPFC is better when compared to the other FACTS Controllers such as SSSC, STATCOM, SVC, and TCSC.

(C) Optimal Location of Facts Controllers

FACTS Controllers give effective solution for power flow control and adaptable bus voltage in power systems, causing low system losses, and enhanced stability. These Controllers in

suitable locality assist to regulate the line flow and to retain the bus voltages in preferred level to improve power system security. To obtain optimal location and sizing of FACTS Controllers in the power system network, various conventional and heuristic optimization techniques for have been applied.

The simulation results obtained in reveal that for determination of suitable buses to optimally place and size FACTS Controllers, the power system network structural characteristics based approach saves time & computational burden and thus stands superior to the conventional power flow based approach of Genetic Algorithms.

When connected in series, it is called series controller and serves the purpose of reducing inductance of the line by acting as a controllable voltage source whereas in parallel connection, shunt controllers act as controllable current source and introduce current in phase with line voltage to reduce the capacitance of the line. The shunt capacitors also improve the power factor and the power transfer capability. Examples of FACTS devices as series compensator can be thyristor controlled series capacitor (TCSC), fixed series capacitor (FSC) static series synchronous compensators (SSSC), shunt compensator can be static variable compensator (SVC), static synchronous compensator (STATCOM), and shunt-series controller can be unified power flow controller (UPFC). TCSC and STATCOM can efficiently be integrated into the system to improve the voltage profile and stability of the system wherein, UPFC combines the properties of STATCOM and SSSC and alone provides active as well as reactive line compensation. Besides, it can be used to increase the transmission capacity, improve the security of transmission line, power flow control, and boost the stability of power system.

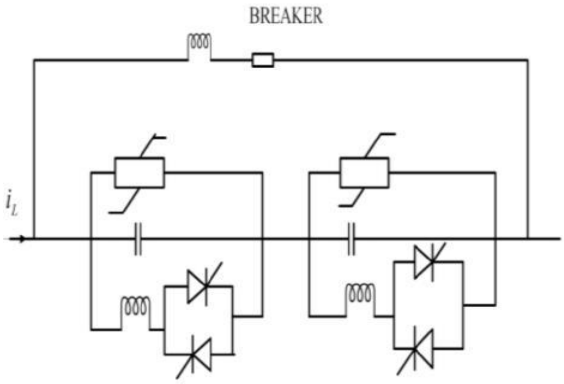

SCHEMATIC DIAGRAM OF TCSC

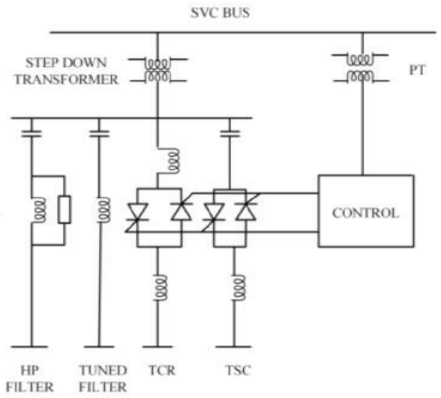

SCHEMATIC DIAGRAM OF SVC

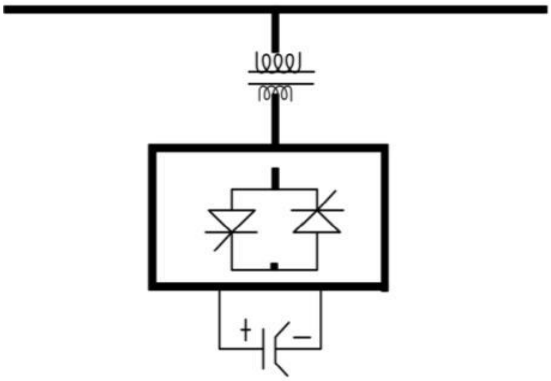

SCHEMATIC DIAGRAM OF STATCOM

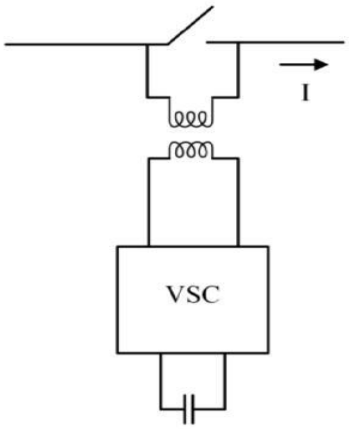

SCHEMATIC DIAGRAM OF SSSC

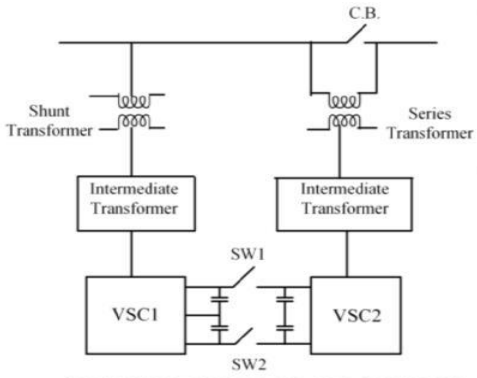

SCHEMATIC DIAGRAM OF UPFC

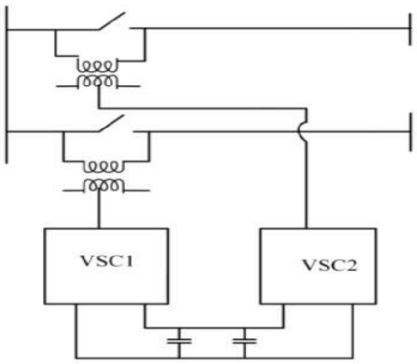

SCHEMATIC DIAGRAM OF IPFC

Power Quality Improvement with the help of FACTS Devices for Renewable energy sources in Transmission Line

Anup kumar[1], Prof. Shivam[2]

***Abstract*—normally, there are two method of generation of power one is conventional method and other method is non-conventional method. During transfer of power through transmission line, some power quality issues like Voltage sag or swell arises and due to that there is drop in voltage which produces the oscillating waves that results in low power factor. To tackle the above problem, most frequent used FACTS (flexible ac transmission systems) devices is unified power flow controller (UPFC), which increases the transmission capacity and boost the stability of power system. In this paper the effect of the UPFC in electrical power system for power flow control is presented. All the simulations for this work have been carried out using MATLAB/SIMULINK environment.**

Keywords- power flow control; FACTS controller; UPFC

I. INTRODUCTION

An electric power system, which is very complex in nature having large numbers of electrical component like generator, transformer, transmission line and different types of load which may be linear or non linear in nature. Due to large demand of power which is growing day by day requires transmission and generation control but control equipments are limited available. Now a days power systems networks are overloaded compared to the past. This requires that, power systems operation should be near to the stability limits. Therefore, it is very challenging to mount new generation unit and transmission line due to environment condition and energy requirement. Hence, it is very important need to increase the ability of power transfer through the actual transmission line instead of installing new line.

FACTs improve the actual ability of transmission line without constructing the new line. In available FACTs devices, UPFC is most flexible to develop stable systems.

UPFC can supply and absorb both active and reactive power according to the requirement of system. In this paper, mainly hydraulic turbine is used as renewable energy source in power plants 1 and 2 as presented in fig 6 (a) and 6 (b).

[1]Anup Kumar is with Department of Electrical Engineering, National Institute of Technology, Kurukshetra, India

[2]Shivam is with Department of Electrical Engineering, National Institute of Technology, Kurukshetra, India.

(e-mail: anup99saini@gmail.com, shivam55ram@gmail.com)

In general, transmission lines are under-utilized and uncontrolled [1-3]. Many factors like line impedance, receiving and sending ends voltages, and phase angle decides the power transfer [1-2]. FACTS devices can increase the maximum power carrying capacity and control power transfer capability of of an existing transmission lines [3-4]. UPFC, which provides superior flow of power and enhancing the stability of system. Many researchers includes, UPFC in their technical literature which is utilized in power system [13-14]. A stochastic based approach to determine the optimal sizing of two FACTS shames for steady state voltage and this improvement is presented in [15], because of active TCSC and UPFC two different parallel transmission lines in the power system, power sharing can be done and therefore allow the maximum transmission capability. The distributed modal control method in multi-machine power system for pole assignment utilizing UPFC is developed in [16]. A genetic algorithm is used between stabilizer and UPFC for proper co-ordination [17], which a multi-objective optimization problem is used to increase the 'ξ' of electromechanical modes, matching different numbers of PSSs with a UPFC. An application of evolutionary algorithms to optimal siting and sizing of UPFC is presented in [18], which are expressed as single and multi-objective optimization problems such as enhancement of the load ability limit.

An inclusive load flow model for the UPFC is explained in [20], which has the capability to control active and reactive powers and voltage magnitude simultaneously. The UPFC is the series-shunt combined type FACTS controller. It is used for controlling real and reactive powers and bus voltage. In this paper, the application of UPFC in power flow control in power system is investigated. Phasor model of UPFC is used.

II. UNIFIED POWER FLOW CONTROLLER

Inherently, UPFC consists of two voltage source inverters (VSI) which are connected back-to-back with the help of a dc storage capacitor which is of interconnecting nature. Each inverter is coupled with a transformer at its output. The schematic diagram of connection of the UPFC to the power system is depicted in figure 1. Usually, shunt VSC is considered as STATCOM [21] and series one as a SSSC [22]. The prime duty of UPFC is performed with the help of series converter by the injection of a series sinusoidal voltage

of controllable magnitude and phase at the system frequency with the help of a series transformer. Almost sinusoidal current of variable magnitude is injected at the point of connection through Shunt converter. SSSC is one of the FACTS devices which are based on voltage source converter (VSC). It is connected in series with transmission line. SSSC provides advanced series compensation. Some of the advantages are listed below:

- SSSC doesn't use bulky passive components such as capacitors and reactors.
- Operation capability in both inductive and capacitive mode.
- Improved technical characteristics.
- Real power exchange is possible between DC side and AC network. i.e. energy source can be connected on the DC side.

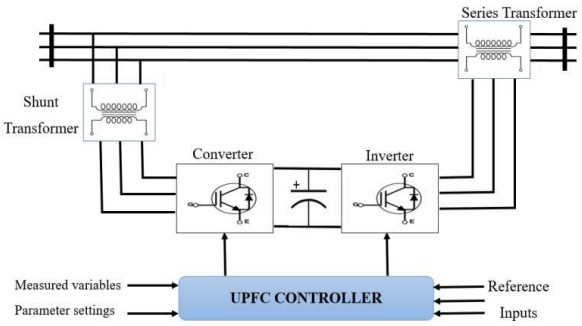

Fig.1. Connection diagram of UPFC to the power system

STATCOM is a FACTS device which is also based on VSC and it is connected in shunt with transmission line. Current flowing through converter is controlled to adjust the bus voltage, i.e. reactive power flow of the transmission line. STATCOM has many advantages over a SVC (Static Var Compensator). Some of them are listed below:

- Quick response.
- Space requirement is less because STATCOM doesn't use bulky passive components such as capacitors and reactors.
- STATCOM can be interfaced with real power sources.

III. UPFC MODEL

UPFC is made with the combination of STATCOM and SSSC. UPFC is the hybrid combination of both shunt and series type converters which are used to inject the voltage. All the three parameters which affect the power flow in the transmission line voltage, impedance, and phase angle can be controlled with the help of UPFC together of independently as per the requirement. It can also control both the real and reactive power flows in the transmission line independently [23, 24]. UPFC controller has two components: shunt and series[25]. Shunt component injects a current into the system while the series component injects a series voltage. There are three types of modeling of UPFC: electromagnetic model [26], steady-state model [27] and dynamic model [28]. The simplified model of UPFC by two voltage sources with appropriate impedances is depicted in figure 2. UPFC is pictured by two ideal voltage source U_{SE} and U_{SH} which are controllable in nature with respect to magnitude and phase angle as shown in the given model. The effective reactance of the UPFC can be seen from the transmission line side of the series transformer. The UPFC voltage sources are:

$$U_{se} = U_s(\cos\delta_s + j\sin\delta_s)$$
$$U_{sh} = U_h(\cos\delta_h + j\sin\delta_h)$$

Where, the series voltage source magnitude is denoted by Us and the series voltage source angle is indicated by **δ**s. The shunt voltage source magnitude is denoted by Uh and voltage source angle is indicated by **δ**h. The voltage magnitude of the output voltage Us provides voltage regulation is provided by the output voltage magnitude Us and the mode of power flow control is determined by phase angle **δ**s..

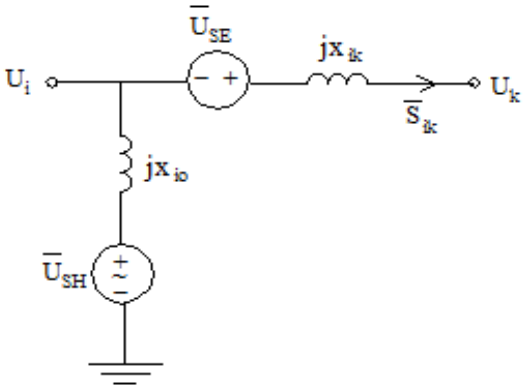

Fig. 2. UPFC model simplification (two-voltage source UPFC model)

IV. SYSTEM UNDER STUDY

The power flow of 500 KV/230 KV transmission system is controlled by UPFC. The power system through UPFC is illustrate in fig.3. It contains two power plants placed at the buses B1 and B4, five buses B1 to B5 interconnected with three transmission lines L1, L2 and L3, two loads and two transformer T1 and T2 are attached at buses B3 and B5. At the left side of transmission line L2, a UPFC is initiated between the buses B1 and B2. UPFC contains two types of converters, one is series converter which is connected between buses B1 and B2 and second one is shunt converter which is connected at bus B1. The maximum of 10% of nominal line to ground voltage (28.87 kv) is injected by the series converter in series with line L2. The plant models consist of a speed regulator, an excitation system and a power system stabilizer (PSS) [29]. The block diagrams of two power plants are shown in Figures 4 and 5. The inside the block Reg-M1 is show in Fig. 6.

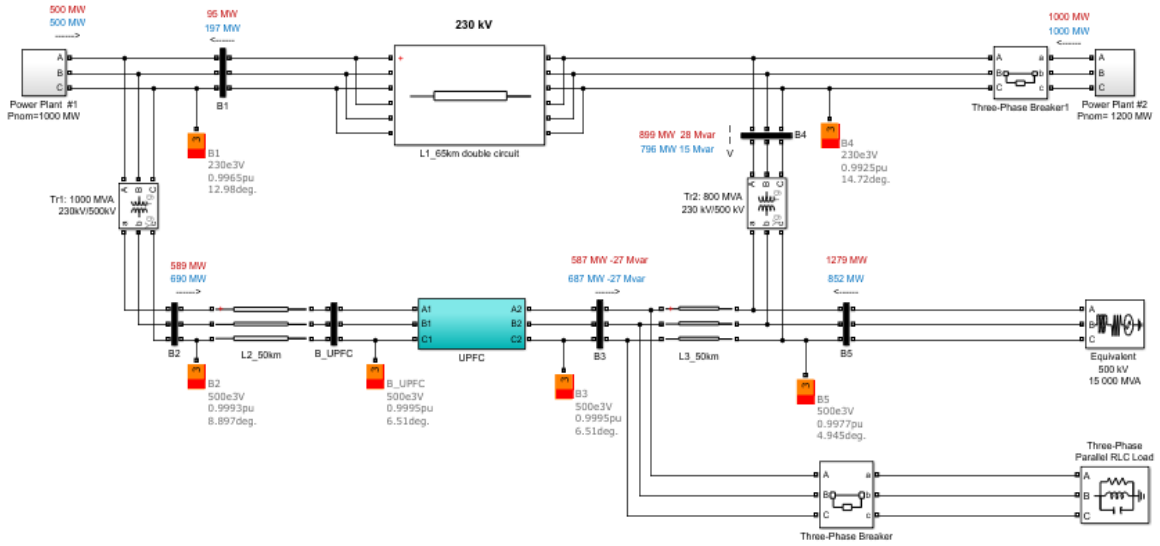

Fig.3. Block diagram of the power system with a UPFC in Matlab/Simulink

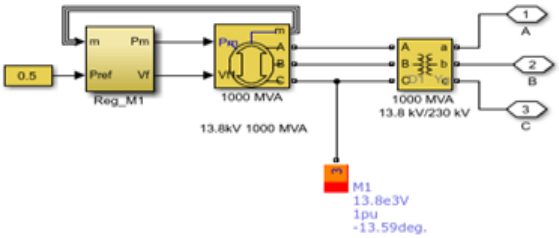

Fig. 4. Power plant 1 in Matlab/Simulink

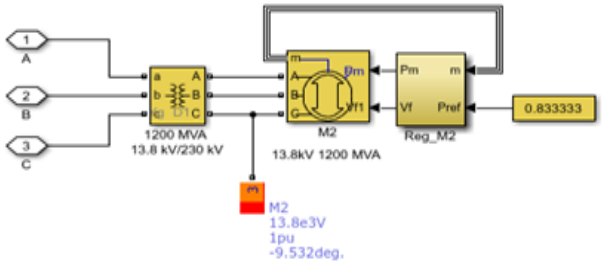

Fig. 5. Power plant 2 in Matlab/Simulink

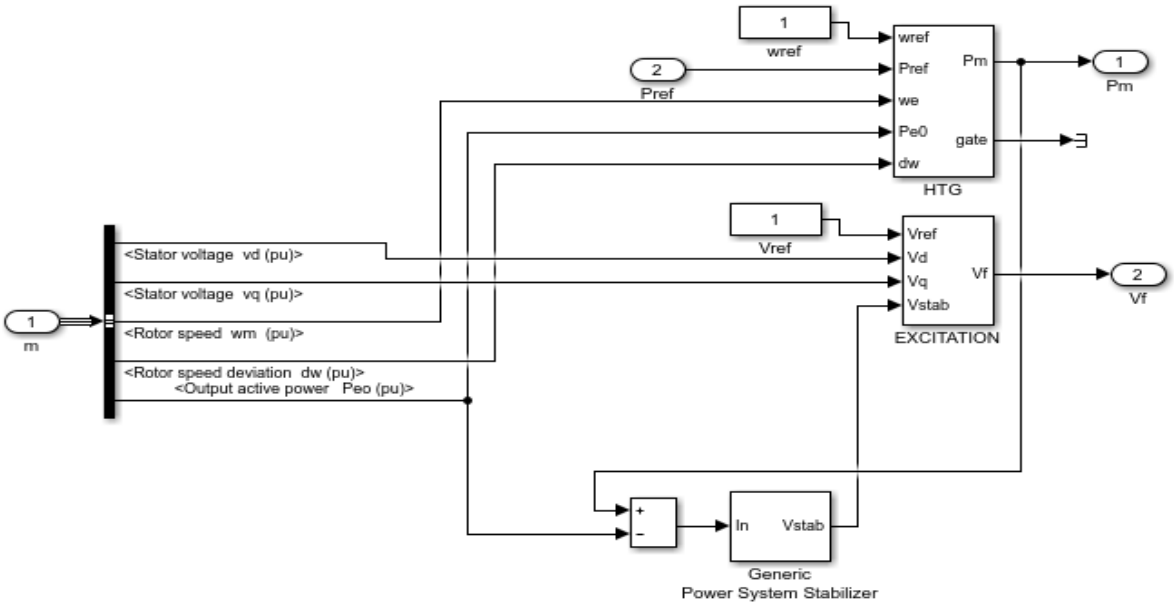

Fig. 6(a). View inside the block Reg-M1

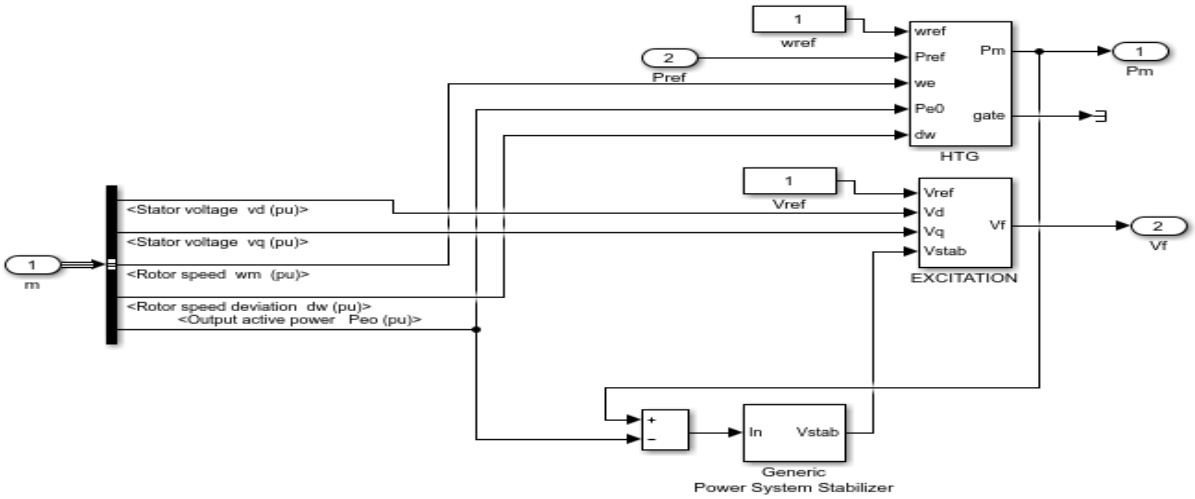

Fig.6 (b). View inside the block Reg-M2

TABLE I. SYSTEM PARAMETERS

Comments	Value
UPFC	100 MVA
Line L1	Double circuit, 230KV, 65km
Line L2	50Km,500KV
Line L3	50Km,500KV
Transformer banks T1	1000MVA, 500KV/230KV
Transformer banks T2	800MVA, 500KV/230KV
Voltage buses B1 and B4	230KV
Voltage buses B2,B3 and B5	500KV
Load at bus B3	500KV, 200MW
Load at bus B5	500KV, 1500MVA
Power plant 1	13.8KV, 1000MVA
Power plant 2	13.8KV, 1200MVA

V. SIMULATION RESULTS

The test system and UPFC data are given in table I. The voltage generated by the series inverter is controlled by two external signals. The power regulator gains are KP=0.025 and KI=1.5. Maximum rate of change for reference active power and reactive power are 1 pu/sec. At initial stage, natural power flow of 587 MW and -27 MVAR at bus B3 is achieved by closing the bypass breaker. The blue numbers on the block diagram indicate the power flow with controlling the B3 active and reactive powers respectively 687 MW and -27 MVAR. For the first five seconds the power quality route stays at the -27MVAR, 587 MW point (bypass breaker stays closed). Fig.7 and 8 illustrate the magnitude and phase of the injected series voltage. When the breaker opens, the magnitude of the injected series voltage is ramped, from 0.0094 to 0.1 pu. At t=5 sec, the angle of the injected voltage starts varying as show in Fig. 9 and measured active and reactive powers at bus B3 following the reference value are shown in Fig.10. The natural power is deviated towards the UPFC series branch without visible transient at the time when we open the bypass breaker at t=5 sec. The variations in active powers at the buses B1, B2, B3,B4 and B5 is show in Fig. 11,12,13,14 and Fig.15 respectively. At t=5 sec, the power increase at the rate of 1 pu/s. The time taken to increase the power of 687 MW is one second. With the help of injection of a series voltage of magnitude 0.089 pu and phase angle of 94 degrees, 100 MW increase of active power is achived at bus B3. As a result of it, there will be a decrease of approx 100 MW active power which was flowing through T2 and now it will be carried by an acceptable load.

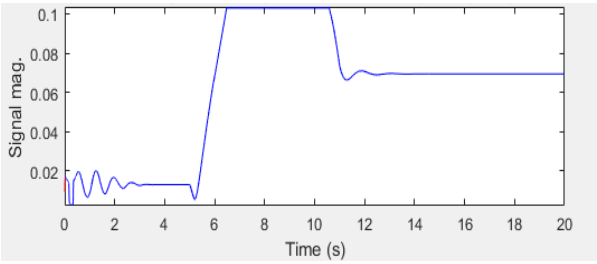

Fig. 7. Magnitude of the injected series voltage

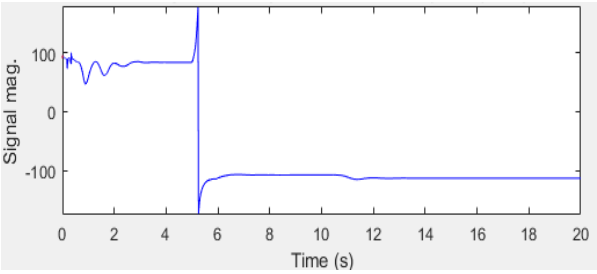

Fig. 8. Phase the injected series voltage

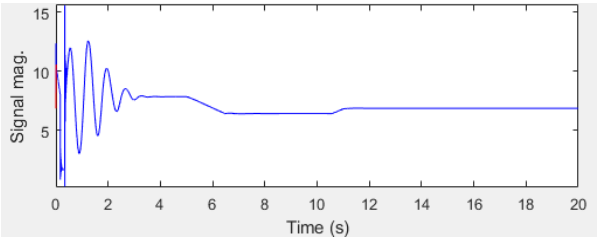

Fig. 9 Active power measured at bus B3

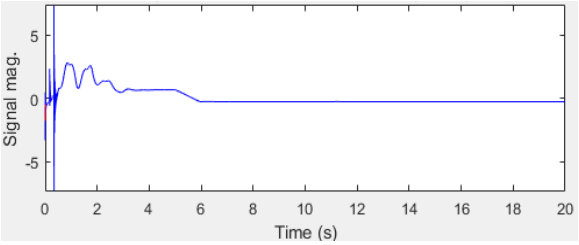

Fig .10 Reactive power measured at bus B3

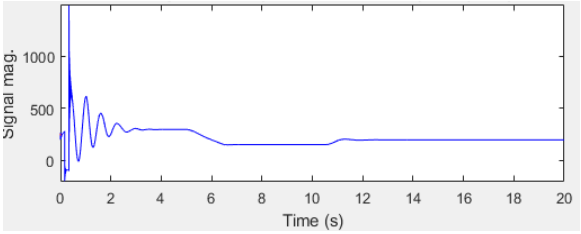

Fig. 11 Active power measured at bus B1

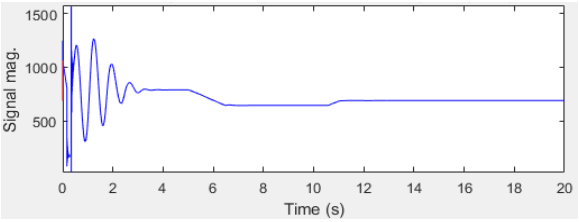

Fig. 12 Active power measured at bus B2

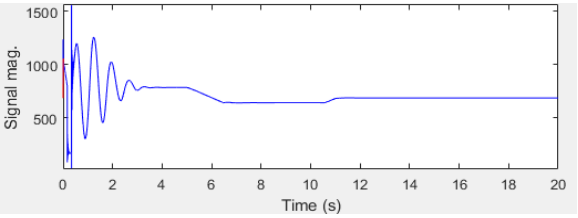

Fig. 13 Active power measured at bus B3

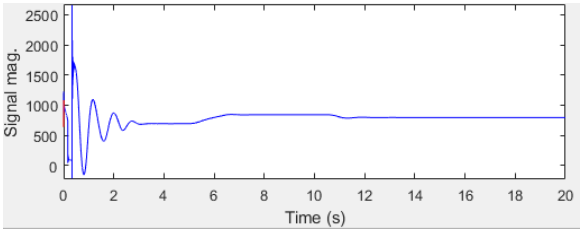

Fig. 14 Active power measured at bus B4

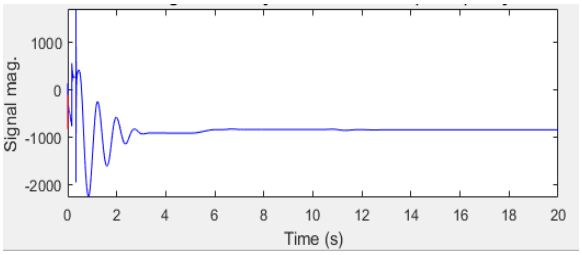

Fig. 15 Active power measured at bus B5

VI. CONCLUSION

Voltage control, reactive power compensation and power flow control are the main objectives of this paper. In order to improve the security of transmission line and power flow control, the FACTS devices are integrated in power system. Dynamic stability of power systems are enhanced using UPFC. UPFC can also improve power system dynamic performance through its supplementary control. Different simulation results are obtained with the help of MATLAB Simulink environment.

REFERENCES

[1] G. Shahgholian, A. Etesami, "The effect of thyristor controlled series compensator on power system oscillation damping control", Int. Review of Elec. Eng., Vol. 5, No. 2, pp. 1822-1830, Aug. 2011.

[2] G. Shahgholian, P. Shafaghi, S. Moalem, M. Mahdavian, "Damping power system oscillations in single-machine infinite-bus power system using a STATCOM", IEEE/ICCEE, pp.130-134, Dubai, Dec. 2009.

[3] G. Shahgholian, M. Arezoomand, H. Mahmoodian, "Analysis and simulation of the single machine infinite bus power system stabilizer and parameters variation effects", IEEE/ICIAS, pp.167-171, Kuala Lumpur,Nov. 2007.

[4] G. Shahgholian, A. Movahedi, "Coordinated control of TCSC and SVC for system stability enhancement using ANFIS method", Int. Review on Modelling and Simulations, Vol. 4, No. 5, pp. 2367-2375, Oct. 2011.

[5] F. Mogharrab-Tehrani, G. Shahgholian, H. Pourghassem, "Dynamic study and stability analyze of damping cohefision and reactance in TCSC controller connected on optimization SMIB system", IEEE/ICCSN, pp. 270-274, China, May 2011.

[6] D.B. Valle, P.B. Araujo, "The influence of GUPFC FACTS device on small signal stability of the electrical power systems", Int. J. of Elec. Pow. and Ene. Sys., Vol. 65, pp. 299–306, Feb. 2015.

[7] G. Shahgholian, A. Movahedi, "Power system stabiliser and flexible alternating current transmission systems controller coordinated design using adaptive velocity update relaxation particle swarm optimisation algorithm in multi-machine power system", IET Gen., Trans. Dist., Vol. 10, No. 8, pp. 1860-1868, May 2016.

[8] G. Shahgholian, J. Faiz, "Static synchronous compensator for improving performance of power system: A review", Int. Review of Electrical Engineering, Vol. 4, No. 2, pp. 2333-2342, Oct. 2010.

[9] G. Shahgholian, E. Haghjoo, A. Seifi, I. Hassanzadeh, "The improvement DSTATCOM to enhance the quality of power using fuzzy-neural controller", Journal of Intelligent Procedures in Elect. Technology, Vol. 2, No. 6, pp. 3-16, Summer 2011.

[10] G. Shahgholian, J. Faiz, "Coordinated control of power system stabilizer and FACTS devices for dynamic performance enhancement- State of art", IEEE/IEPS, pp. 1-6, Kyiv, Ukraine, June 2016.

[11] L.M. Castro, E. Acha, C.R. Fuerte-Esquivel, "A novel STATCOM model for dynamic power system simulations", IEEE Trans. on Pow. Sys., pp. 3145-3154, Vol. 28, No. 3, Aug. 2013.

[12] G. Shahgholian, P. Shafaghi, S. Moalem, M. Mahdavian, "Analysis and design of a linear quadratic regulator control for static synchronous compensator", IEEE/ICCEE, pp.65-69, Dubai, Dec. 2009.

[13] S.M. Abd Elazim, E.S. Ali, "Optimal SSSC design for damping power systems oscillations via gravitational search algorithm", Int. J. of Elec. Pow. and Ene. Sys., Vol. 82, pp. 161–168, Nov. 2016.

[14] J. Guo, M.L. Crow, J. Sarangapani, "An improved UPFC control for oscillation damping", IEEE Trans. on Pow. Sys., 24(1), Feb. 2009.

[15] M.T. Khosroshahi, F.M. Kazemi, M.R. Jannati-Oskuee, S. Najafi- Ravadanegh, "Coordinated and uncoordinated design of LFO damping controllers with IPFC and PSS using ICA and SFLA", J. of Central South University, Vol. 22, No. 9, pp. 3418-3426, Sep. 2015.

[16] M. Pereira, L.C. Zanetta, "A current based model for load flow studies with UPFC", IEEE Trans. on Pow. Sys., 28(2), pp. 677-682, May 2013.

[17] J. Faiz, G. Shahgholian, M. Torabiyan, "Design and simulation of UPFC for enhancement of power quality in transmission lines", IEEE/POWERCON, pp. 1-5, Hangzhou, Oct. 2010.

[18] S.O. Faried, R. Billinton, S. Aboreshaid, "Probabilistic technique for sizing FACTS devices for steady-state voltage profile enhancement", IET Gen., Trans. Dist., Vol. 3, No. 4, pp. 385-392, April 2009.

[19] M.A. Furini, A.L.S. Pereira,P.B. Araujo,"Pole placement by coordinated tuning of power system stabilizers and FACTS-POD stabilizers", Int. J. of Elec. Pow. and Ene. Sys., Vol. 33, No. 3, pp. 615–622, March 2011.

[20] L.H. Hassan, M. Moghavvemi, H.A.F. Almurib, K.M. Muttaqi, "A coordinated design of PSSs and UPFC-based stabilizer using genetic algorithm", IEEE Trans. on Ind. Appl., 50(5), pp. 2957-2966, Feb. 2014.

[21] S. Alamelu, S. Baskar, C.K. Babulal, S. Jeyadevi, "Optimal siting and sizing of UPFC using evolutionary algorithms", Int. J. of Elec. Pow. And Ene. Sys., Vol. 69, pp. 222–231, 2015.

[22] S. Shojaeian, J. Soltani, "Low frequency oscillations damping of power system including unified power flow controller based on adaptive backstepping control", Revue Roumaine Des Sciences Techniques, Vol. 58, No. 2, pp. 193–204, 2013.

[23] K.A.K. Reddy, S.P. Singh, "Congestion mitigation using UPFC", IET Gen., Trans. Dist., Vol. 10, No. 10, pp. 2433-2442, July 2016.

[24] M. Mahdavian, G. Shahgholian, N. Rasti, "Modeling and damping controller design for static synchronous compensator", IEEE/ECTICON, pp. 300-304, Pattaya, Chonburi, May 2009.

[25] H. Weihao, S. Chi, J. Fang, Z. Chen, "Comparison study of power system small signal stability improvement using SSSC and STATCOM", IEEE/IECON, pp. 1998-2003, Vienna, Nov. 2013.

[26] A. Mohanty, S. Patra, P.K. Ray, "Robust fuzzy-sliding mode based UPFC controller for transient stability analysis in autonomous winddiesel- PV hybrid system", IET Gen., Trans. Dist., 10(5), pp. 1248-1257, April 2016.

[27] A.A. Eldamaty, "Damping interarea and torsional oscillations using FACTS devices", Ph.D. Thesis, Saskatchewan, May 2005.

[28] S. Ahmad, F.M. Albatsh, S. Mekhilef, H. Mokhlis, "Fuzzy based controller for dynamic unified power flow controller to enhance power transfer capability", Energy Conversion and Management, Vol.7 9, pp. 652–665, March 2014.

[29] K.K. Sen, E.J. Stacey, "UPFC – Unified power flow controller: Theory, modeling, and applications", IEEE Trans. on Power Delivery, Vol. 13, No. 4, pp. 1453-1460, Oct. 1998.

Impact of DG and STATCOM placement on improving the reactive power loading capability and voltage stability of sub-transmission network

Ruchi Tamta[1], Mahiraj Singh Rawat[2]

Abstract- This paper presents a novel way of placing Distribution Generation (DG) and Static Compensator (STATCOM) in sub-transmission network to improve reactive loading capability and voltage stability. Optimal location for placement of DG and STATCOM is identified by using voltage stability index (VSI_2). The performance of proposed technique is evaluated using IEEE 30 bus test system. Analysis is done in load growth situation by placing DG and STATCOM separately and simultaneously in the sub-transmission network. From the results it is observed that with simultaneous placement of DG and STATCOM at weak buses of sub transmission network have high voltage stability index and reactive loading capability as compared to when these devices are placed separately.

Keywords—Distributed generation, STATCOM, Voltage stability index, Reactive loading

I. INTRODUCTION

Nowadays, voltage collapse is a vital problem in power system. As per IEEE power system engineering committee report "*Voltage stability is the capacity of a system to manage voltage so that when load admittance is raised, load power will increase and so that both power and voltage are controllable*" [1]. Since voltage stability is an essential part of power system stability therefore, cannot afford to be ignored. The problem of voltage instability arises in heavily loaded systems [2]. Voltage collapse in the power system can be avoided either by decreasing the reactive power load or by using extra source at the point of need.

Static voltage stability of the power system can be identified through various voltage stability indices (VSIs) which are used to identify the critical or weak buses or lines in a power system under certain operating condition. In this paper, voltage stability indicator VSI_2 is utilized [3]. The stability limit for VSI_2 lies between 0 and 1. If this index value is greater than 1, then the system is considered as unstable. Voltage instability was one of the main reason for several blackouts worldwide. In literature, the impact of DG and STATCOM in transmission network for improvement of voltage stability has been studied [4-5].Voltage profile can be controlled within an acceptable limit by injecting reactive power from external compensating devices such as capacitor banks, static synchronous series compensator (SSSC), STATCOM, static var compensator (SVC) etc. Among all compensating devices, STATCOM has several capabilities such as low power losses, compact size, and low cost. For improving the system stability, DG and STATCOM are placed in the critical line, which is recognized by the VSI values of all lines in the system [6-7-8].

The application of DG provides several befits such as relieving transmission and distribution congestion, system stability improvement, voltage profile improvement, pollutant emission reduction etc. The possible size of DG per module can be as little as 1 kW to as high as 250MW. Based on size DG may be classified into micro (1W TO 5KW), small (5KW to 5MW), medium (5MW to 50MW) and large (50MW to 300 MW).The power rating of medium and large DG make it feasibility to integrate such generators in sub-transmission network. Most distribution networks are weak and radial in nature with low short-circuit capacity (SCC). Therefore there is the limit in which power can be injected into the distribution network without compromising the power quality and the system stability. To overcome these challenges, there is the possibility to place DG at the sub-transmission network at higher voltage level with higher SCC compared to the distribution network.

In this paper, voltage stability index VSI_2 has been utilized for identification of weak buses in the sub transmission network. These weak buses are identified as optimal buses for placement of DG and STATCOM. In first phase DG and STATCOM are placed separately and voltage stability index VSI|_2 is evaluated under reactive load growth. In second phase DG and STATCOM are placed simultaneously and voltage stability index VSI|_2 is evaluated under reactive load growth. IEEE 30 bus test system is utilized for case study.

The paper is organized as follows: The voltage stability index VSI_2 utilized in this work for identification of weak buses/lines is explained in section II. In Section III, steady state modeling of STATCOM is explained. Case study is performed in section IV. Section V concludes the research work.

[1]Ruchi Tamta is with Department of Electrical Engineering, National Institute of Technology, Uttarakhand, India

[2]Mahiraj Singh Rawat is with Department of Electrical Engineering, National Institute of Technology, Uttarakhand, India.

(e-mail: ruchi1234.eee16@nituk.ac.in, rawat.ms85@gmail.com)

II. VOLTAGE STABILITY INDICES

Voltage instability arises due to less supply of reactive power compared to demand. This diminished supply is due to the failure of reactive power sources or high absorption of reactive power by transmission lines. To overcome this issue the reactive power demand should be fulfilled by application of reactive power compensators. In the power system the critical buses and lines are identified with the help of VSIs. Critical buses or lines are those buses or lines which are more prone to voltage collapse.

VSIs are broadly classified as bus and line voltage stability indices. A comprehensive review of all the developed VSIs has been discussed in ref. [9]. VSI contributes much in maintaining the system's stability as the prediction of weak bus or lines can be detected in earlier stage and by taking suitable remedial action, instability can be avoided. In this paper, voltage stability index VSI_2 which is a line voltage stability index is utilized for identification of the weak buses. The voltage stability index VSI_2 is formulated as follows [10].

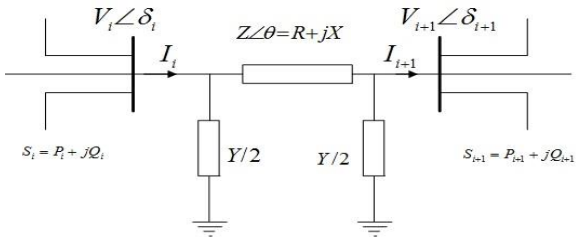

Fig.1 Two bus equivalent model of system

$$I(i) = \frac{\left|V(i)\angle\delta(i)\right| - \left|V(i+1)\angle\delta(i+1)\right|}{R(i) + jX(i)} \quad (1)$$

The complex power is given by eq. (2)

$$S(i+1) = P(i+1) + jQ(i+1 = V(i+1)I^*(i)$$

or

$$I(i) = \frac{P(i+1) - jQ(i+1)}{V^*(i+1)} = \frac{P(i+1) - jQ(i+1)}{\left|V(i+1)\right|\angle -\delta(i+1)} \quad (2)$$

From eq. (1) and (2)

$$\frac{P(i+1) - jQ(i+1)}{\left|V(i+1)\right|\angle -\delta(i+1)} = \frac{\left|V(i+1)\angle\delta(i+1)\right| - \left|V(i+1)\angle\delta(i+1)\right|}{R(i+1) + jX(i+1)} \quad (3)$$

$$\left[R(i)P(i+1) + X(i)Q(i+1)\right] + j\left[X(i)P(i+1) - R(i)Q(i+1)\right] = \left|V(i)\right|\left|V(i+1)\right|\left[\begin{matrix}\cos(\delta(i) - \delta(i+1)) \\ + j\sin(\delta(i) - \delta(i+1))\end{matrix}\right] - \left|V(i+1)\right|^2 \quad (4)$$

Voltage angle is negligibly small so $[\delta(i) - \delta(i+1)] \cong 0$ Hence $\cos(\delta(i) - \delta(i+1)) \cong 1$ and $\sin(\delta(i) - \delta(i+1)) \cong 0$ Therefore, from eq. (4)

$$V(i)V(i+1) - V^2(i+1) = [R(i)P(i+1) + X(i)Q(i+1)] + j[X(i)P(i+1) - R(i)Q(i+1)] \quad (5)$$

Equalizing the real and imaginary parts of eq. (5) we get

$$V(i)V(i+1) - V^2(i+1) = [R(i)P(i+1) + X(i)Q(i+1)] \quad (6)$$

$$0 = X(i)P(i+1) - R(i)Q(i+1) \quad (7)$$

From eq. (6)

$$\frac{R(i)}{X(i)}V^2(i+1) - \frac{R(i)}{X(i)}V(i)V(i+1) + P(i+1)\left[\frac{R^2(i)}{X(i)} - X(i)\right] + 2R(i)Q(i+1) = 0 \quad (8)$$

The eq. (8) is quadratic nature and to have real roots, the discriminate must be greater than equal to zero. Hence from eq. (8) we get:

$$\frac{R^2(i)}{X^2(i)}V^2(i) - 4\frac{R(i)}{X(i)}\left\{P(i+1)\left[\frac{R^2(i) - X^2(i)}{X(i)}\right] + 2R(i)Q(i+1)\right\} \geq 0 \quad (9)$$

or

$$\frac{4Q(i+1)[R(i) + X(i)]^2}{X(i)[V^2(i) + 8R(i)Q(i+1)]} \leq 1 \quad (10).$$

Hence VSI_2 = $\frac{4Q(i+1)[R(i) + X(i)]^2}{X(i)[V^2(i) + 8R(i)Q(i+1)]} \leq 1$ Here, V(i)is the magnitude of voltage at sending end, Q(i+1) is receiving end reactive power, and R(i) is line resistance, X(i) is line reactance. The critical value of VSI_2 is 1. The range of VSI_2 lies between 0 and 1. In order to have a stable system, the value of VSI_2 should be as minimum as possible i.e. approximately 0 whereas if in case the value of VSI_2 at any bus is increasing or moving towards 1, this signifies that the particular bus is moving towards the condition of instability. Therefore, the weak or critical buses in the system can be easily identified from the magnitude of VSI_2.

III. STATCOM MODELING

As per IEEE definition FACTS devices are defined as "*Alternating current transmission system incorporating power electronics based and another static controller to improve controllability and enhance power transfer capability*". STATCOM is a shunt-connected reactive-power compensation device that is proficient of generating and/or consuming reactive power and in which the output can be modified to control the particular parameters of an electric power system [11]. The STATCOM has better performance during low voltage situation.STATCOM can give fast and continuously changeable reactive power in response to grid voltage transients, improving the grid voltage stability.

A. Formation of STATCOM in the Newton–Raphson's load flow model

In the load flow method, the equations of real and reactive power flow for transmission line between 'i' and 'i+1' buses are given by eq. (11) and (12).

$$P_i = \sum_{i+1=1}^{N} |V_i||V_{i+1}|\left(G_{i(i+1)} \operatorname{Cos}\theta_{i(i+1)} + B_{i(i+1)} \operatorname{Sin}\theta_{i(i+1)}\right) \quad (11)$$

$$Q_i = \sum_{i+1=1}^{N} |V_i||V_{i+1}|\left(G_{i(i+1)} \operatorname{Sin}\theta_{i(i+1)} + B_{i(i+1)} \operatorname{Cos}\theta_{i(i+1)}\right) \quad (12)$$

Power flow equation in Newton Raphson method is formulated in polar coordinate as follows:

$$\begin{bmatrix} \frac{\partial P_i}{\partial \theta_i} & \frac{\partial P_i}{\partial V_i} \\ \frac{\partial Q_i}{\partial \theta_i} & \frac{\partial Q_i}{\partial V_i} \end{bmatrix} \begin{bmatrix} \Delta\theta_i \\ \Delta V_i \end{bmatrix} = -\begin{bmatrix} \Delta P_i \\ \Delta\theta_i \end{bmatrix} \quad (13)$$

Newton Raphson power flow equations describing real and reactive power interchange between point of interconnection and STATCOM are given by eq. (14) and (15).

$$P_{sh} = V_i^2 G_{sh} - V_i V_{sh}\left(G_{sh} \operatorname{Cos}(\theta_i - \theta_{sh}) + B_{sh} \operatorname{Sin}(\theta_i - \theta_{sh})\right) \quad (14)$$

$$Q_{sh} = V_i^2 G_{sh} - V_i V_{sh}\left(G_{sh} \sin(\theta_i - \theta_{sh}) - B_{sh} \cos(\theta_i - \theta_{sh})\right) \quad (15)$$

The main concern is to secure that the net active power exchange is near to zeros as much as feasible to secure highest reactive power flow. Hence, active power exchange (PE) becomes a control and presented by eq. (16).

$$\begin{aligned} PE &= P_{sh} \\ &= V_i^2 G_{sh} - V_i V_{sh}\left(G_{sh} \cos(\theta_i - \theta_{sh}) - B_{sh} \sin(\theta_i - \theta_{sh})\right) \\ &= 0 \end{aligned} \quad (16)$$

B. STATCOM control strategy

STATCOM utilized for maintaining the bus voltage, reactive power injection, impedance and current magnitude.

a) Control of reactive power injection to relevant bus presented by

$$Q_{sh} - Q_{sh}^{spec} = 0 \quad (17)$$

b) Control of load bus voltage magnitude

$$V_i - V_i^{spec} = 0 \quad (18)$$

c) Control of STATCOM inserted voltage magnitude

$$V_{sh} - V_{sh}^{spec} = 0 \quad (19)$$

d) Control of STATCOM reactive impedance

$$X_{i(i+1)} - X_{i(i+1)}^{spec} = 0 \quad (20)$$

The control functions of the STATCOM of Eq. (17-20) are combined to get the generalized control function denoted as

$$\Delta E(X) = E(X) - E(X)^{spec} \quad (21)$$

Where X= $[\theta_i, V_i, \theta_{sh}, V_{sh}]$

Here the Jacobian matrix of the STATCOM, the equations used are the net active power exchange is zero given in eq. (16) and the STATCOM reactive power presented in eq.(17). Computing the partial derivatives of these two equations into Newton's Jacobian matrix of eq.(13), we got the generalized multi STATCOM Jacobian as indicated in eq.(22).

$$[J] = \begin{bmatrix} \frac{\partial P_i}{\partial \theta_i} & \frac{\partial P_i}{\partial V_i} & \frac{\partial P_i}{\partial \theta_{sh}} & \frac{\partial P_i}{\partial V_{sh}} \\ \frac{\partial Q_i}{\partial \theta_i} & \frac{\partial Q_i}{\partial V_i} & \frac{\partial Q_p}{\partial \theta_{sh}} & \frac{\partial Q_p}{\partial V_{sh}} \\ \frac{\partial PE}{\partial \theta_i} & \frac{\partial PE}{\partial V_i} & \frac{\partial PE}{\partial \theta_{sh}} & \frac{\partial PE}{\partial V_{sh}} \\ \frac{\partial E}{\partial \theta_i} & \frac{\partial E}{\partial V_i} & \frac{\partial E}{\partial \theta_{sh}} & \frac{\partial E}{\partial V_{sh}} \end{bmatrix} \quad (22)$$

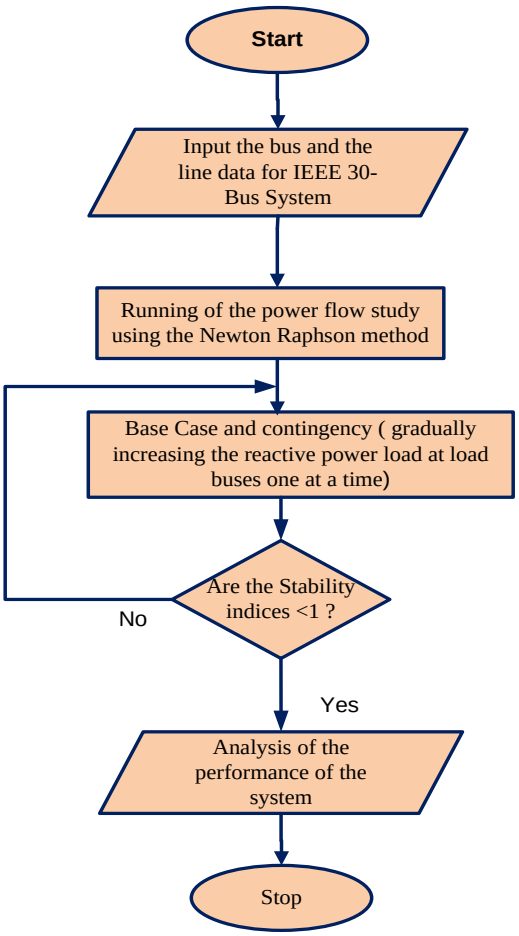

Flowchart of Proposed Methodology

IV. Result and Discussions

This section presents the simulation results of IEEE 30 bus test system. Test system have 6 generators, 20 load buses and 41 lines.

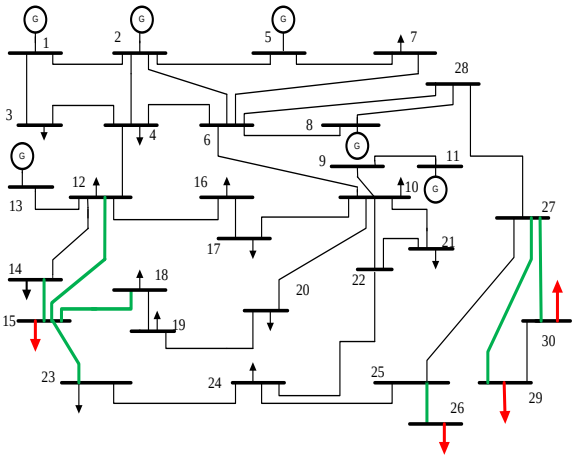

Fig. 3 IEEE 30 bus test system

A. VSI_2 calculation and identification of critical lines

Optimal locations for placement of STATCOM and DG are identified with the help ofVSI_2. The VSI_2 values are recorded by varying the load of a single bus at a time from base to maximum allowable reactive power capacity keeping the other loads constant. Line producing higher value of VSI_2 is considered as critical line of that bus. The VSI_2 of the most stressed lines of the system are given in Table I.

TABLE I VOLTAE STABILITY INDICES VSI_2

Reactive Load (pu)	Voltage (pu)	Line	VSI_2
Q15=1.22	0.859	12 – 15 14 – 15 15 - 18 15-23(Critical)	0.4731 0.3762 0.3213 0.9320
Q29=0.38	0.701	27–29 Critical)	0.9448
Q30=0.30	0.706	27–30 (Critical 29 - 30	0.9676 0.7807
Q26=0.22	0.690	25-26(Critical)	0.9798

B. Identification of best location of DG and STATCOM

VSI_2 is measured and ordered for finding optimal location to place DG and STATCOM. For the present case, utmost eight critical lines are found and the respective VSI_2 values are given in Table II. From the simulation results, it is observed that the buses 26, 29, 30 are having less reactive power capacity and lines 25-26, 27-30, 27-29, 15-23 have high values of VSI_2. Therefore these buses and lines are selected as optimal location to place DG and STATCOM.

TABLE II RANKING OF CRITICAL TRANSMISSION LINES

Sr. No.	Line (From -To)	VSI_2
1	**25 – 26**	**0.9798**
2	**27 – 30**	**0.9676**
3	**27 – 29**	**0.9448**
4	**15 – 23**	**0.9320**
5	29 – 30	0.7807
6	12 – 15	0.4731
7	14 – 15	0.3762
8	15 – 18	0.3213

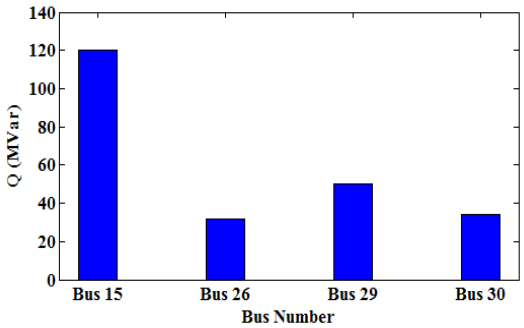

Fig. 4 Reactive power margin at load buses in IEEE 30 bus system

The loadable reactive power capacity of the buses 26, 30, 29, and 15 are shown in Fig. 4. It is observed from the Fig. 4 that bus 26 is having less loadability compared to others. Fig. 5 shows the variation of VSI_2 with respect to reactive load for the critical lines.

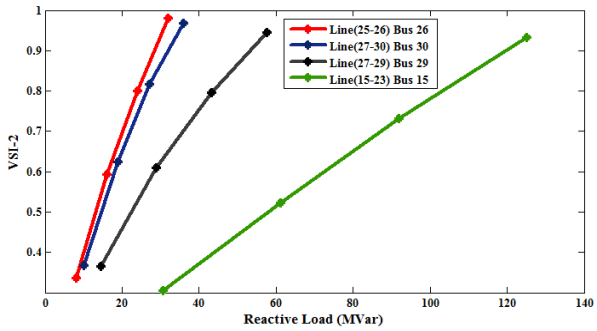

Fig. 5 VSI_2 profile computed with load varies at bus 26,30,29 and 15

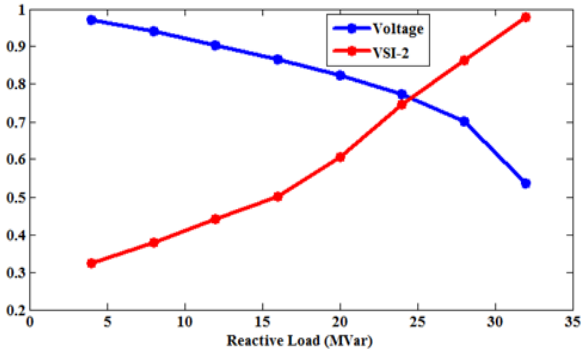

Fig. 6 VSI_2 and Bus Voltage Vs Reactive Power Demand for Bus 26

Fig. 6 is showing the variation of VSI_2 and bus voltage with respect to reactive power demand at bus 26. It is observed from Fig. 6 that as reactive power demand is increasing the VSI_2 value is approaching to 1 and bus voltage value is decreasing. From the above results it is found that the line 25-26 and bus 26 are the critical line

and bus of the system. Therefore Bus 26, 30 and 29 is the best placement of STATCOM and DG.

C. Effect of DG and STATCOM in sub-transmission network

In this case study, DG place in critical bus 29 and STATCOM place in critical bus 26 is to increase the critical reactive loading capability at load bus 30 by giving active and reactive power. Q-V curves are represented with the installation of DG and STATCOM to determine the critical loading values in each case. crucial voltage is selected as 0.9 p.u and increase in the reactive power demand is recognized at the sensitive node. Q-V curves for IEEE 30 bus system with constant power load are shown in Fig.7 and it can be seen that the crucial reactive loading capability with base case is 0.1050 p.u and after DG (14 MW) placement it reaches to 0.1220 p.u, after STATCOM (12.92 MVAr) placement it improves and reaches up to 0.1425 p.u, and after simultaneous placement of DG and STATCOM it reaches to 0.1659 p.u.

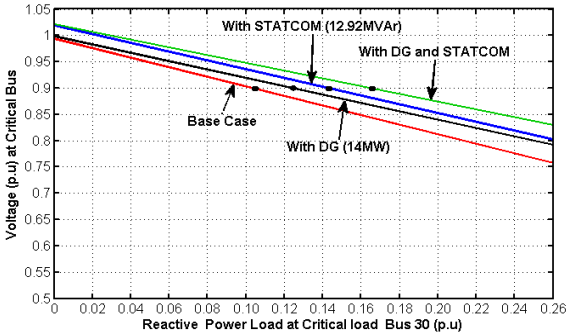

Fig.7 Q-V curves for IEEE 30 bus system

Q-V curves for IEEE 30 bus sub-transmission networkafter considering load increases is shown in Fig.8 and critical reactive loading capability with base case is 0.10 p.u and after DG (16 MW) placement it reaches to 0.12 p.u after STATCOM (14.14 MVAr) placement it improves and reaches up to 0.14 p.u and after simultaneous placement of DG and STATCOM it reaches to 0.16 p.u.

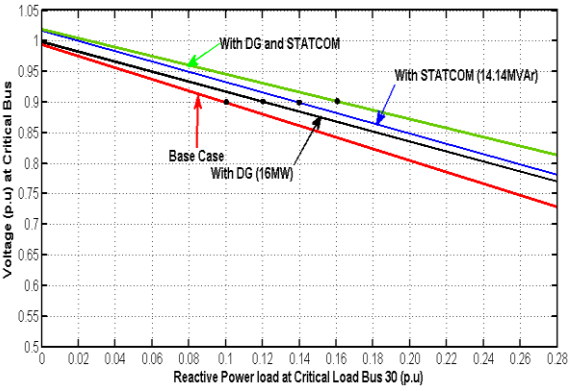

Fig. 8 Q-V curves for IEEE 30 bus system with load growth

Fig. 9 DG place in critical bus26 and STATCOM place in critical bus 30 is to increase the critical reactive loading capability at load bus 29 with base case is 0.076 p.u and after DG (16 MW) placement it reaches to 0.095 p.u after STATCOM (29.06 MVar) placement it improves and reaches up to 0.327 p.u and after simultaneous placement of DG and STATCOM it reaches to 0.367 p.u. in this case very good enhancement of reactive loading capability and voltage stability so best performance when simulaneous placement of DG and STATCOM at buses 26 and 30 respectively in IEEE 30 bus sub transmission network.

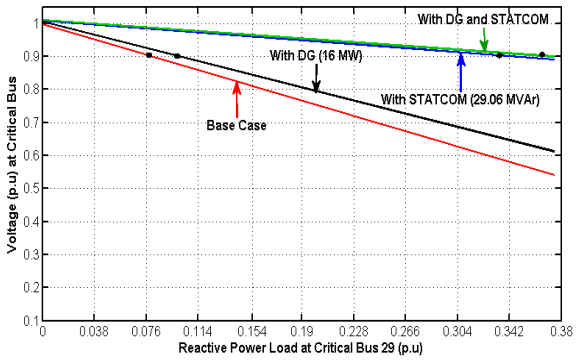

Fig.9. Q-V curves for IEEE 30 bus system with load growth

Fig. 10 and 11 shows the voltage values at all buses of IEEE 30 bus system with placing DG and STATCOM alone and also simultaneously in the sub-transmission network. It is clearly shown that simultaneous placement of DG and STATCOM gives a better voltage profile at the load bus 29 and 30 compared to others. And clearly shows Fig. 9 in best placement of DG and STATCOM at buses 26 and 30 respectively because in this time voltage profile improvement and improve the reactive loading capability.

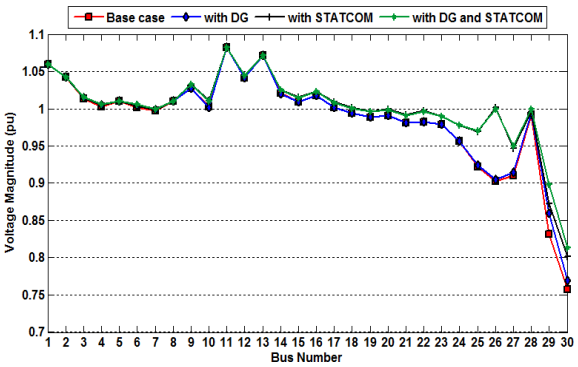

Fig.10 Voltage profile at load bus 30 with varying Load

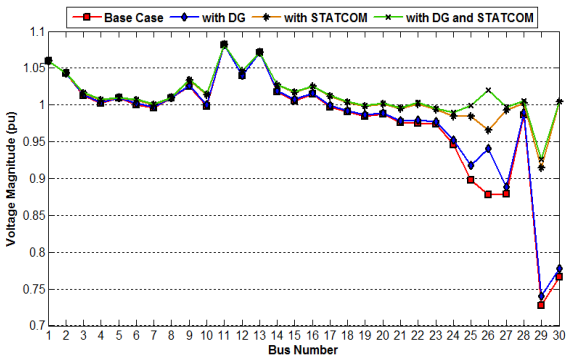

Fig.11 Voltage profile at load bus 29 with varying load

V. CONCLUSIONS

This paper explores the impact of DG and STATCOM integration on voltage stability of IEEE 30 bus test system. In order to determine the bus moving towards voltage instability, line voltage stability index VSI_2 has been utilized. From calculated values of voltage stability index VSI_2, optimal locations were selected for the placement of DG and STATCOM. Results shows that the improvement of voltage stability and critical reactive loading capability is higher in the system when simultaneous placement of DG and STATCOM is performed under load growth conditions. The critical buses 26 and 30 are found to be best location for placement of DG and STATCOM in IEEE 30 system.

REFERENCES

[1] P. Kundur, Power system stability and control, EPRI power system engineering series, McGraw-Hill, 1994.

[2] C. W. Taylor, Power system voltage stability, McGraw Hill, New York, 1994.

[3] R.Tamta, S.Painuli, M. S.Rawat, and S.Vadhera, "Comparison of line voltage stability indices for assessment of voltage instability in high voltage network" 1st International Conference on New Frontiers in Engineering Science and Technology (NFEST-2018), Jan 8-12,2018 .

[4] E. Larsen and T. Weaver, "FACTS Overview," IEEE PES Special Publication 95-TP-108, 1995.

[5] K. R. Padiyar, Power System Dynamics Stability andControl, 2nded., B S publications, 2002.

[6] A. R.Gupta, and A. Kumar, "Impact of DG and D-STATCOM placement on improving the reactive loading capability of mesh distribution system," Procedia Technology, vol.25, pp.676-683, Jan 2016.

[7] A. S.Ogunjuyigbe,T. R.Ayodele, and O. O.Akinola,"Impact of distributed generators on the power loss and voltage profile of sub-transmission network,"Journal of Electrical Systems and Information Technology, vol. 3, no. 1, pp. 94-107, May 2016.

[8] A. Gupta and P. R. Sharma, "Optimal placement of FACTS devices for voltage stability using line indicators," in: IEEE Fifth Power India Conference, pp. 1-5, Dec 2012.

[9] J. Modarresi, E. Gholipour, and A. Khodabakhshian, "A comprehensive review of the voltage stability indices,"Renew. Sustain. Energy Review, vol. 63, pp.1-12, 2016

[10] T. K. Chattopadhyay,S. Banerjee, C. K. Chanda,"Voltage stability analysis of distribution networks under critical loading conditions," in: Power and Energy Systems Conference: Towards Sustainable Energy, pp. 1-5, March 2014.

[11] D. O. Dike and S. M. Mahajan, "Voltage stability index-based reactive power compensation scheme,"Electr. Power and Energy Syst., vol. 73, pp.734-742,2015.

Optimal Placement of TCSC to Improve the Voltage Stability of Transmission Network

Ruchi Tamta[1], Mahiraj Singh Rawat[2], Vineet Kushwaha[3]

Abstract— The major cause of voltage instability in power system is due to an asymmetry between reactive power demand and supply. Due to advancement in power semiconductor technology, the utilization of FACTS devices became an efficient solution to overcome voltage instability in the system. Here, the transmission lines which are prone to voltage collapse are identified by using a line voltage stability index and considered as a weak line. Voltage stability indicator (VSI_2) is used to track the line approaching towards voltage collapse. In order to improve the voltage stability of the system, Thyristor controlled series compensation (TCSC) device is placed in series with weak transmission lines. An IEEE 30 bus test system is used for validation.

Keywords—Thyristor Controlled Series Compensation (TCSC); Voltage stability, Voltage Collapse; Reactive power; FACTS

I INTRODUCTION

NOWADAYS, voltage collapse is a vital problem in power system. As per IEEE Power System Engineering Committee "Voltage stability is the capacity of a system to manage voltage so that when load admittance is raised, load power will improve and so that both power and voltage are controllable"[1]. Since voltage stability is an essential part of power system stability therefore, cannot afford to be ignored. The problem of voltage instability arises in heavily loaded systems [2]. Voltage collapse in the power system can be avoided either by decreasing the reactive power load or by using extra source at the point of need. Static stability of the power system can be identified through various voltage stability indices(VSI).VSIs are the indices which are used to identify the critical or weak buses or lines in a power system under certain operating condition. In this paper voltage stability indicator (VSI_2) is used because this index is very fast response for the prediction of voltage collapse compare to other indices, this index is best for the power system [3]. When this index value changes from 0 to 1, the voltagestability of the system relatively decreases. If this index value is greater than 1, then the system is considered as unstable. Instability problem affects the desired operation of power system. Sometimes entire system may be collapsed.

[1]Ruchi Tamta is with Department of Electrical Engineering, National Institute of Technology, Uttarakhand, India
[2]Mahiraj Singh Rawat is with Department of Electrical Engineering, National Institute of Technology, Uttarakhand, India.
[3]Vineet Kushwaha is with Department of Electrical Engineering, National Institute of Technology, Uttarakhand, India.

(e-mail: ruchi1234.eee16@nituk.ac.in, rawat.ms85@gmail.com, vineet.eee16@nituk.ac.in)

Optimal placement of FACTS devices is an efficient method to enhance the voltage stability in the power system[4]. TCSC is an efficient FACTS device, which is employed for voltage stability improvement. It can control the transmission line impedance to increase the line transfer capacity and to manage the receiving end bus voltage. In sequence to improve the system stability, the TCSC is placed in the critical line, which is recognized by the stability index values of all lines in a system [5] [6].

Placement of TCSC device in appropriate location improves voltage stability by controlling the power flow. The suitable location to place the TCSC device is at weakest buses or lines of the system. The weakest bus in the system is determined by using a line VSI. This paper presents the Optimally place the TCSC device in implement the IEEE 30 bus test system.

The investigation paper is composed as follows: In section II presented a brief introduction of voltage stability. In section III the Voltage stability index used for the description of weak lines in a system has explained. Modelling of TCSC is performed in section IV. Proper location of TCSC and its effects on voltage stability of system has explained in Section V. Section VI concludes the research article.

II VOLTAGE STABILITY

As per the description of CIGRE Joint Task Force/IEEE, "*Voltage stability is determined as the capacity of the power system to manage acceptable voltages at all the buses under normal circumstances and after being subjected to disturbances" [*1]. Since voltage stability is an important part of power system stability, therefore, cannot afford to be neglected. The problem of voltage instability arises in heavily loaded systems.

Voltage instability arises due to less supply of reactive power compared to demand. This diminished supply is due to the failure of reactive power source or power system lines in transmitting reactive power. To overcome this issue the reactive power demand should be fulfilled by using generators or compensators.

III VOLTAGE STABILITY INDEX

In the power system the critical buses and lines are found with the help of VSIs. Critical buses or lines are those buses or lines which are more prone to voltage collapse.

VSIs are broadly classified as bus and line voltage stability indices. A comprehensive review of all the developed VSIs has been discussed in ref. [7]. VSI

contributes much in maintaining the system's stability as the prediction of weak bus or line can be detected in earlier stage and by taking suitable remedial action, instability can be avoided. In this paper, voltage stability indicator (VSI_2) which is a line voltage stability indices is utilized to calculate the weak buses for any number of buses in the system. VSI_2utilizes voltage magnitude of the busesfor the prediction of voltage collapse. For the prediction of voltage collapse, VSI_2 can be used in online as well as in offline mode with load flow study analysis for system planning. The VSI_2 is formulated as follows [8].

$$VSI\_2 = 4Qr(R + X)^2 / X\,(Vs^2 + 8RQr) \qquad (1)$$

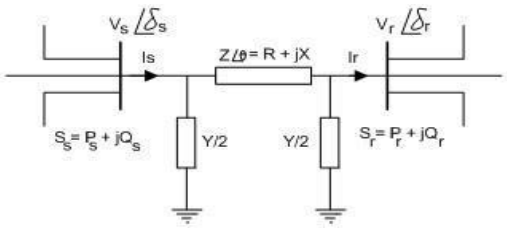

Fig. 1. Two bus equivalent model of system

Where, V_s is the magnitude of voltage at sending end,$Q_r$is reactive power at receiving end, R and Xare line resistance and reactance respectively. The critical value of VSI_2 is 1. The range of VSI_2 lies between 0 and 1. In order to have a stable system, the value of VSI_2 should be as minimum as possible i.e. approximately 0 whereas if in case the value of VSI_2 at any bus is increasing or moving towards 1, this signifies that the particular bus is moving towards the condition of voltage instability. Therefore, the weak or critical buses in the system can be easily identified from the magnitude of VSI_2.

IV. SERIES COMPENSATION USING TCSC

Maintain the bus voltages that means close to nominal values, decreasing line current and line losses so compensation suggest including reactive power for improving the power system performance. It also contributes to the voltage stability improvement. The main objective of series capacitive compensation is to decrease the overall effective series reactance of the transmission line [9]. The power supplied through a transmission line with reactance X is as given in equation 2.

$$P = (^{T/2} / X) \sin \delta \qquad (2)$$

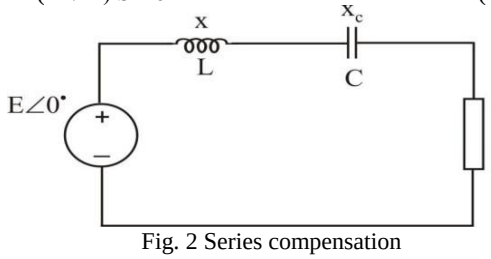

Fig. 2 Series compensation

The effective reactance X_{eff} with the series capacitive compensation is given in equation 3.

$$X_{eff} = X - X_C \qquad (3)$$

The above equation can be written as

$$X_{eff} = (1 - k)\,X \qquad (4)$$

Where $k = X_c / X$ (degree of series compensation) (5)

$$0 \le k \le 1 \qquad (6)$$

Usually, 'k" is in the range of 0.3 – 0.7. Replacing X withX_{eff} in power equation 2, it is clearly seen that the maximum deliverable power has been increased.

V. RESULTS AND DISCUSSION

This section presents the simulation results of the IEEE 30 bus test system, which is having 6 generators, 20 load buses, and 41 lines.

A. Line voltage stability indices

Here, optimal location for placement of TCSC device is found with the help ofVSI_2. The VSI_2 values are recorded by varying the load of a single bus at a time from base to maximum allowable reactive power capacity keeping the other loads constant. Line producing higher value of VSI_2 is considered as critical line of that bus. The VSI_2 of the most stressed lines of the system are given in Table I.

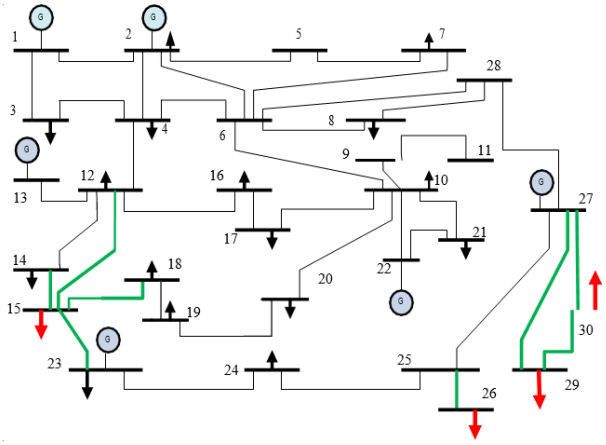

Fig. 3 IEEE 30 bus test system

TABLE I. STABILITY INDICES WITHOUT TCSC

Reactive Load (pu)	Voltage Magnitude (pu)	Line	VSI_2
Q15= 1.225	0.859	12 – 15 14 – 15 15 - 18 15 - 23 (Critical)	0.4731 0.3762 0.3213 0.9320
Q29= 0.576	0.740	27 – 29 (Critical)	0.9448
Q30= 0.513	0.706	27– 30 (Critical) 29 - 30	0.9676 0.7807
Q26= 0.3680	0.690	25 - 26 (Critical)	0.9798

A. Identification of optimal location of TCSC device

VSI_2 is measured and ordered for finding optimal location to place TCSC devices. For the present case, utmost eight critical lines are found and the respective VSI_2 values are given in Table II. From the results,

buses 26, 30, 29 in this buses having less reactive power capacity and line 25-26, 27-30, 27-29, and 15-23 the VSI_2 index value is highest. Therefore these buses and

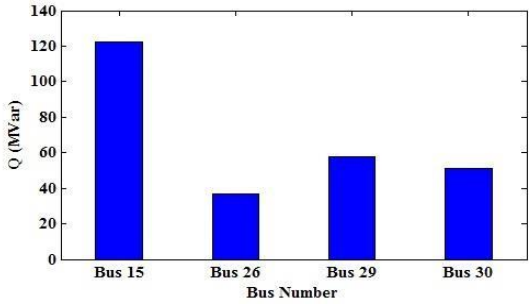

lines are selected as optimal location to place the TCSC device.

Fig. 4 Reactive power Margin for IEEE 30 Bus system

TABLE II THE HIGHEST RANKED LINES OF SYSTEM

Line (From -To)	VSI_2
25 – 26	**0.9798**
27 – 30	**0.9676**
27 – 29	**0.9448**
15 – 23	**0.9320**
29 – 30	0.7807
12 – 15	0.4731
14 – 15	0.3762
15 – 18	0.3213

The loadable reactive power capacity of the buses 26, 30, 29, and 15 are shown in Fig. 4. It is observed from the Fig. 4 that bus 26 is having less loadability compared to others. Fig. 5 shows the variation of VSI_2 with respect to reactive load for the critical lines.

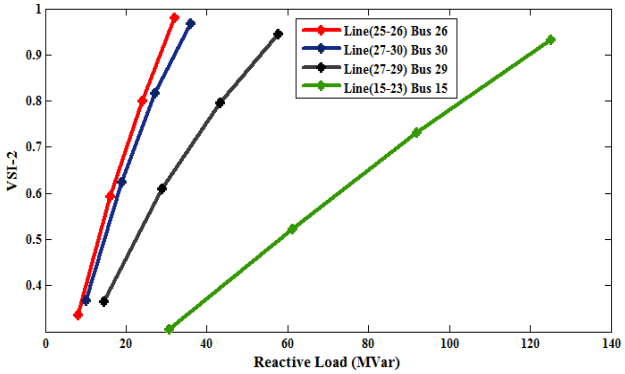

Fig. 5 VSI_2 profiles calculated with load fluctuates at bus 26, 30, 29 and 15

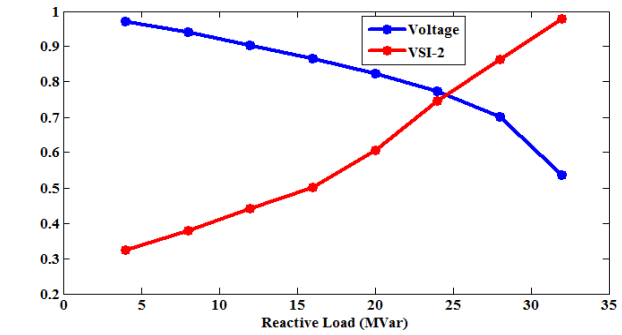

Fig. 6 VSI_2 and Voltage at Critical Bus 26 versus Reactive Power Increases

Fig. 6 is showing the variation of VSI_2 index and bus voltage with respect to reactive power demand increases at critical bus 26. It is observed from Fig. 6 that as reactive power demand is increasing the VSI_2 index value is approaching to 1 and bus voltage value is decreasing. From the above results it is found that the line 25-26 and bus 26 are the most critical line and bus of the IEEE 30 bus system. Therefore optimally place the TCSC device in line 25-26.

B. Analysis of system with TCSC Device

Line 25-26 is found as the optimal location for TCSC placement. Here, the author is analyzing the system performance by placing the TCSC in the major critical lines of system 25-26, 27-30, 27-29 and 15-23. The VSI_2 values of the eight critical lines given in Table II are recorded by placing TCSC at above mentioned places and given in TABLE III. It is observed from the results that the VSI_2 values are less when TCSC is placed in the line 25-26 compared to placement in other lines.

TABLE III STABILITY INDICES WITH TCSC

Reactive Load	Line	VSI_2 Index with			
		TCSC (25-26)	TCSC (27-30)	TCSC (27-29)	TCSC (15-23)
Q15	12 – 15 14 – 15 15 - 18 15 -23	0.0191 0.0334 0.0106 0.1045	0.0188 0.0330 0.0115 0.1047	0.0187 0.0329 0.0115 0.1045	0.3374 0.2549 0.2159 **0.9083**
Q29	27 – 29	0.0575	0.5496	**0.9051**	0.0575
Q30	27 – 30 29 - 30	0.0738 0.0238	**0.9491** 0.6015	0.5690 0.5174	0.0738 0.0238
Q26	25-26	**0.9404**	0.0936	0.0936	0.0937

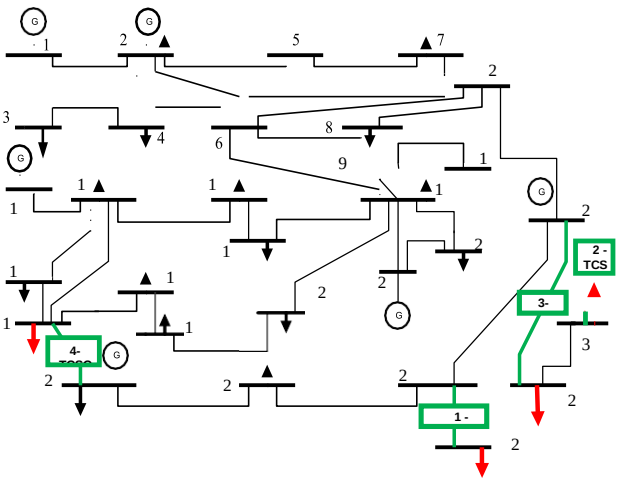

Fig. 7 IEEE-30 Bus test System with TCSC

Figs. 8 to11 give the VSI_2 Index versus reactive power demand increase at critical bus 26, 30 29 and 15 individually with and without TCSC device. Voltage profiles at certain buses with and without TCSC device are also presented in Figs. 12 to15. It can be recognized that the improvement of voltage profiles and reduces the

VSI_2 index value at these buses with TCSC injected in the system.

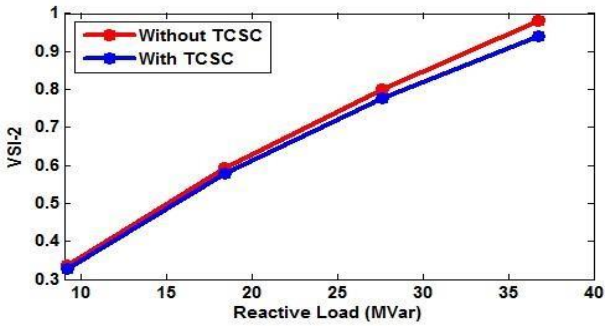

Fig. 8VSI_2 index Vs reactive power load increases at critical bus 26

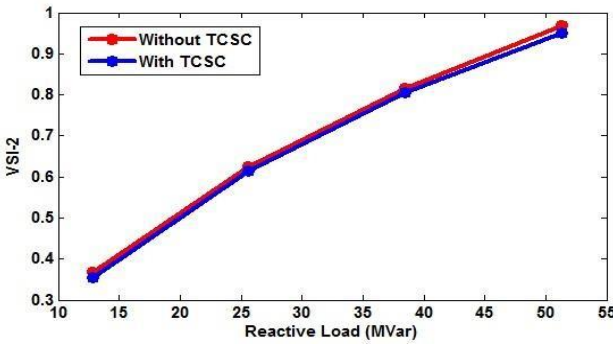

Fig .9 VSI_2 index Vs reactive power load increases at critical bus 30

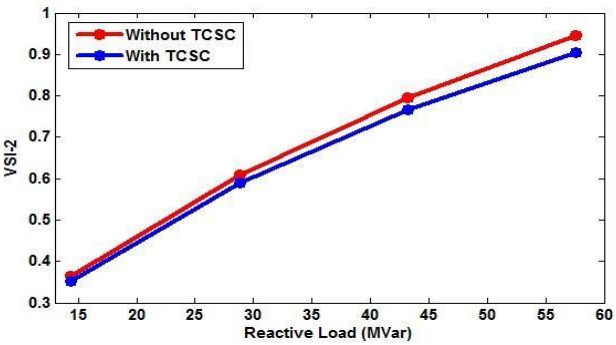

FIG .10VSI_2 INDEX VS reactive power load increases at critical bus 29

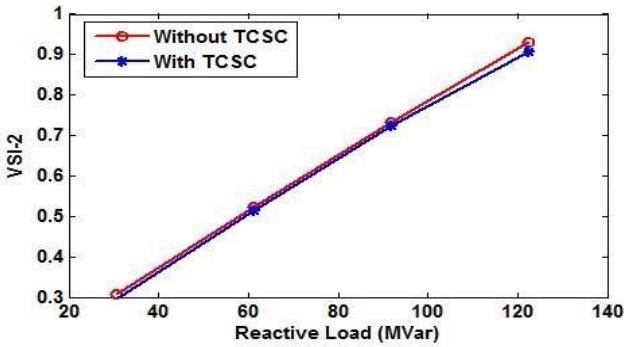

Fig. 11VSI_2 index Vs reactive power demand increases at critical bus 15

Fig .12VoltageVs reactive power load increases at bus 26

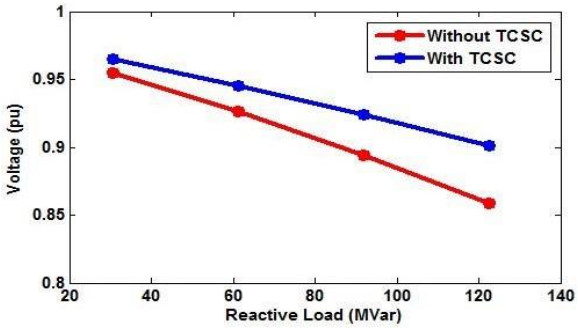

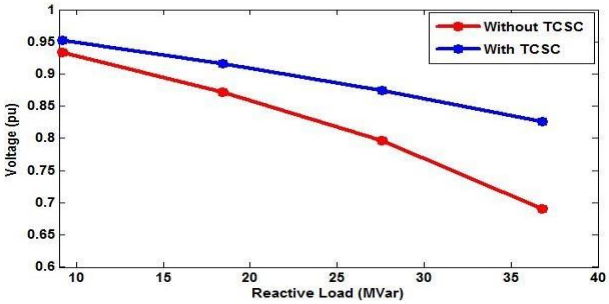

Fig.13Voltage versus reactive power load increases at bus 30

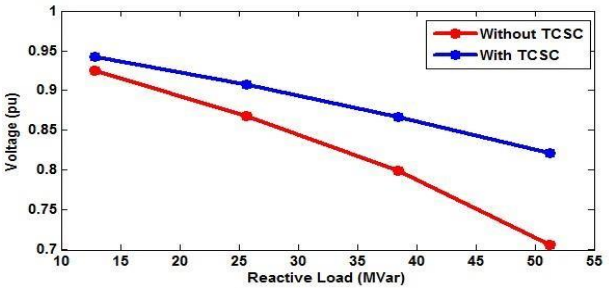

Fig .14Voltage Vs reactive power load increases at bus 29

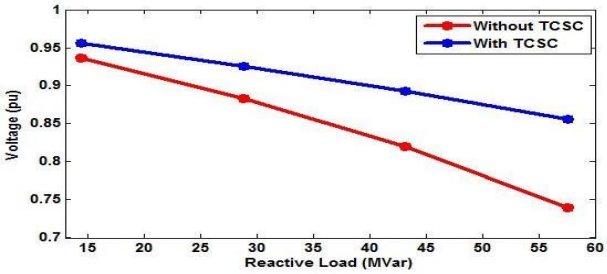

Fig.15 Voltage versus reactive power load increases at bus 15

VI. CONCLUSION

This paper explored the impact of TCSC Device on an IEEE 30-bus test system. In order to calculate the bus moving towards voltage instability i.e. approaching towards 1, a bus voltage stability index VSI_2 has been used. The simulation results showed that load bus 26 is weakest bus among bus 29, 30 and 15 for IEEE 30 bus test system. On observing the values of VSI_2, an optimal location was selected for the placement of TCSC Devices. The voltage profile of the entire system has enhance and the voltage stability indices values have decreased significantly. Also, for a 30-bus test system TCSC was sufficient to maintain the system stable.

Therefore, it is concluded that the placement of TCSC is premature enough to maintain the voltage stability of the transmission system.

REFERENCES

[1] Prabha Kundur, Power system stability and control, EPRI power system engineering series, McGraw-Hill, 1994.

[2] C.W. Taylor. Power system voltage stability,McGraw Hill, New York, 1994.

[3] Ruchi Tamta, Mahiraj Singh Rawat, "Comparison of line voltage stability indices for assessment of voltage instability in high voltage network," 1st International Conference on New Frontiers in Engineering, Science & Technology (NFEST-2018), New Delhi, 8-12 Jan 2018.

[4] K. R. Padiyar, Power System Dynamics Stability and Control, 2nd edition B S publications, 2002.

[5] M. Amroune, H.Sebaa, and T.Bouktir, "Static Voltage Stability Margin Enhancement Using SVC and TCSC"World Academy of Science, Engineering and Technology International Journal of Electrical, Computer, Energetic, Electronic and Communication Engineering, vol. 7, no. 10, 2013.

[6] A. Gupta and P. R. Sharma "Optimal Placement ofFACTS devices for voltage stability using line indicators"IEEE 5th Power India conference, pp. 1-5, 2012.

[7] J. Modarresi, E.Gholipour, and A.Khodabakhshian, "A comprehensive review of the voltage stability indices," Renew. Sustainable Energy Reviews 63 (2016) 1-12.

[8] T. K. Chattopadhyay, S. Banerjee and C. K. Chanda, "Impact of distributed generator on voltage stability analysis of distribution networks under critical loading conditions for composite loads," In: Proc. International conference on electronics, communication and instrumentation,pp.1–4, 2014.

[9] N. Hingorani and L. Gyugyi, Understanding concepts and technology of Flexible AC Transmission Systems, Wiley, 2000.

Conclusion

Power system stability is a primary concern for continuous supply of power in all sections of the society. The FACTS (Flexible AC Transmission System) Controllers can enhance the capability of power transfer in the network very effectively without increasing power generation capacity of power system. The FACTS Controllers are mostly used for control of power flow, voltage regulation, system stability improvement and damping of power system oscillations in transmission line. Use of FACTS devices in the power systems helps in improving voltage profile, transmission capacities of the transmission lines and stability of the system.

Modern power systems are operated at full or beyond its capacity. This results in high power flows in the power system network which lead to more losses and also threaten to decrease the stability and security of the system. With power demand always on the rise, there is always a need for strengthening of power transmission network. Conventional way to strengthen power transmission network is upgrading the infrastructure of the power transmission system with the addition of new transmission lines, substations, and associated equipment. But in the present power system scenario, this is not always possible. Construction of more transmission lines that too with large capability of power transfer is time consuming and need several modifications in the existing landscape. Many times it becomes controversial also. Due to environmental considerations, there are restrictions in expansion of the transmission system and there is an effect on health due to electric and magnetic fields associated with power transmission system.

A more practical and useful way is to utilize the existing transmission system network maximally with as minimum cost as possible. The application of progressive power electronics technologies enhances the utilization of the existing power system. FACTS technology provides solutions for the new technical operating challenges. It is in this context, the role of FACTS Controllers becomes significantly important. In the varying utility environment, for the flexibility and controllability in system, FACTS Controllers act as important tools in the hands of power system operators. FACTS Controllers are power-electronic based equipment and they offer cost effective solution for power transmission problems through increase in capacity of power in transmission system. By making change in the bus voltage amplitude, bus voltage angle and transmission line reactance with the help

of FACTS Controllers, the flow of power can be controlled. STATCOM, SVC, SSSC, TCSC, UPFC, etc., are some of the FACTS Controllers which are used for mitigating power system network problems.

Study of placement of distributed generation (DG) and STATCOM separately and simultaneously in the sub-transmission network results into observation that their simultaneous placement at weak buses gives high voltage stability index and increased reactive loading capability as compared to when these devices are placed separately. Optimal placement of TCSC when achieved by using voltage stability index VSI_2 further improves the voltage stability in the power system.

Chapter -4

Recent Headways in Renewable Energy: Modeling, Control and Improvised Design

The increased utilization of renewable energy sources, though overall beneficial for mankind and environment, poses issues while integrating into the existing system. Some of the challenges that may come up due to large power integration through renewable sources are maintaining power stability, lowering the harmonics in output power generated through renewable sources, storage of surplus energy during off peak load time duration and discharge the same at peak load time, improving power quality.

4.1 Wind Power Control: converter based improved design and intelligent approach

The wind turbine generator system requires a power conditioning circuit called power converter that is capable of adjusting the generator frequency and voltage to the grid. Several types of converter topologies have been developed in the last decades; each of them has some advantages and disadvantages. Mainly two converter topologies are currently used in the commercial wind turbine generator systems. Most of the proposed converters require line filters and transformers to improve the power quality and step -up the voltage level, respectively. These heavy and bulky components significantly increase the tower construction, and turbine installation and maintenance costs. Recent advances in power semiconductors and magnetic materials have led to the development of new structure of converters, which would be a possible solution to reducing the size, weight, and cost of power converters.

The renewable source based electrical power output is basically d.c. is nature while the power that we domestically consume is a.c. Also, transmission through a.c. system is highly recommendable for short and large distance transmissions as the voltages can be leveled up which makes power supply cost effective and ease to avail at different voltages by different customers is possible. The converters are the devices that convert originally produced d.c based wind power to a.c. based wind power for supply to grids and customers. Use of these converters in the wind power system plays a pivotal role in the quality of power output. The power electronic converters can introduce harmonics, lower the power factor and the overload capacity.

Advanced converters used in wind energy system serve various benefits. Diode rectifier based converter, back to back converter, matrix converter, cycloconverter, multilevel converters, z-source converter and improved z-source converter. Three phase three level diode clamped converter in a wind power system can be one of the other types of converters which prove beneficial to the system by reducing voltage ratings, showing good dynamic response and excellent harmonic spectrum. Another type of converter, modular multilevel converter (MMC) can give better waveforms, quality and compactness. MMC based HVDC system for wind farms can reduce the need of much bulky filters to eliminate harmonics but the cost and complexity of this converter based system is very high due to large numbers of switches.

The wind energy sources integrated into the grid can lack inherent inertia present in synchronous generators which may cause frequency strokes in the grid or partial grid shedding. This can be tackled by using power electronic converter with energy storage device as a virtual synchronous generator (VSG). Fast current control can strategically be achieved by using VSG to suppress voltage sag and power fluctuation in grid. This method improves the transient response and reduces the power fluctuation present in the grid.

Intelligent Wind Power Control:

Artificial intelligence, also called as machine intelligence makes a system work intelligently in a manner a human would want it to work for better performance considering all constraints and loopholes. Artificial Intelligence, due to its flexibility and versatility, has found great potential to be used in a variety of real life systems including wind or solar energy systems.

In a wind energy system, the use of particle swarm optimization (PSO) based model can figure out the parameters which affect power generation the most and also be applied to dispatch both cost and environmental pollution economically and intelligently. According to PSO technique, particles move in the search space of optimization problem and each particle updates new position based on own previous position and velocity. The swarm (population) of particles in an n-dimensional search space is simulated, where each particle has a position and a velocity. The position of a particle confirms the candidate solution to the optimization problem.PSO is an evolutionary algorithm based optimization technique. Evolutionary Algorithms are gaining popularity, as along with overcoming the

shortcomings of the traditional search methods. They work perfectly for the complex systems and provide better results.

Artificial neural technique (ANN), another AI technique, has been used to study the effect of climatic factors like pressure, humidity, temperature, precipitation etc on the wind speed. Wind speed plays a very important role for wind energy calculation. Wind with speed within a specific range only can be converted to produce useful energy. ANN uses the processing of the brain as a basis to develop algorithms that can be used to model complex patterns and prediction problems. ANNs have some key advantages that make them most suitable for certain problems and situations:

1. ANNs have the ability to learn and model non-linear and complex relationships, which is really important because in real-life, many of the relationships between inputs and outputs are non-linear as well as complex.

2. ANNs can generalize—after learning from the initial inputs and their relationships, it can infer unseen relationships on unseen data as well, thus making the model generalize and predict on unseen data.

3. Unlike many other prediction techniques, ANN does not impose any restrictions on the input variables (like how they should be distributed). Additionally, many studies have shown that ANNs can better model data with high volatility and non-constant variance, given its ability to learn hidden relationships in the data without imposing any fixed relationships in the data. This is something very useful in financial time series forecasting (e.g. stock prices) where data volatility is very high.

Interfacing Wind Energy System to the Utility Grid Using a Three Phase Three Level Diode Clamped Converter

Mohammad Shahban[1], Jayaram Nakka[2]

***Abstract*—This Paper proposes an improved control scheme to regulate the controller, a PWM generation scheme and a PWM scheme to operate the converter in integration of wind energy systems with utility grid. Wind speed is the external factor that determines the power output of wind energy system. The modeling and control of wind system using the permanent magnet synchronous generator (PMSG) connected with the grid via a three phase three level diode clamped converter. The mathematical modeling of the whole system in d-q frame and its state space equation are established to simplify the proposed control scheme. In this paper harmonics are minimized and efficiency is thus improved. Also the current is injected into the grid improved Power Quality (PQ). The performance of the proposed approach is evaluated based on the various simulations results carried out under Matlab/Simulink.**

Keywords— High Voltage & High Power Systems; Wind-Energy Conversion System; Three Level Diode Clamped Converter; grid interface; DC Voltage Regulation;, PI controller, PWM converters.

I. INTRODUCTION

Due to continuously increasing demand of energy/power, this has been a big question for all as how to fulfill the energy demand in future years? Thus to solve the problem of increasing energy demand scientist moved toward extraction of energy from sources such as Solar Energy, Wind Energy, Biomass, Tidal Energy, Geothermal Energy etc. These Sources are termed as renewable/sustainable sources of energy. Due to environmentally benign and sustainable remedies provided by these generic sources to fulfill the growing energy requirement of world, these sources are becoming popular day by day. Among several nonconventional energy resources solar and wind are the cheapest and the cleanest and abundant in nature. As demand of energy increasing day by day many power corporations focusing on solar and wind energy system, because they can be used as standalone system or grid connected system [1]. If the power generated from renewable energy source is more than to be used, than we have to transfer that extra power to the grid. Here, it becomes very much important how to feed power to grid so that less harmonics inject grid side. Converters having important role to transfer power from dc to ac side.

[1]Mohammad Shahban is with School of Renewable Energy and Efficiency, National Institute of Technology, Kurukshetra, India
[2]Jayaram Nakka is with Department of Electrical Engineering, National Institute of Technology, Kurukshetra, India.
(e-mail: shahbanqureshi1994@gmail.com, jayaram.iitr@gmail.com)

For DC-AC conversion, a three-level neutral point clamped multilevel converter [2] is being used here which is then connected to grid. Multilevel converters are of basically three types namely three-level neutral point clamped multilevel converter, cascade H-bridge multilevel converter and flying capacitors multilevel converter. It is very difficult to control the flying-capacitor multilevel converter compared to a NPC converter. Additionally, for voltage clamping purpose more number of capacitors are required and for low switching frequency, the required capacitor size should be large. There is separate dc source and non-standard transformer is required as in case of cascade H-bridge multilevel converter. The quality of output voltage and output current waveforms is improved in case of three-level NPC converter. It is having of reduced switching losses and size of output filter is also reduced in this converter. This paper introduces the modeling and simulation of wind energy conversion system. The speed of wind varies throughout the day. So efficiency of a WECS depends on the accuracy at which MPPs are tracked by MPPT algorithms. P&O is an independent MPPT control algorithm. The harmonic content present in the terminal voltage waveform of a neutral point clamped –PWM converter [3] is less than that present in the voltage waveform of a conventional converter.

In this paper, an improved PWM generation technique is adapted, and a Control scheme is implemented to achieve the improved efficiency and reduced harmonics in wind energy systems.

II. SYSTEM DESCRIPTION

A. Wind energy systems

A brief introduction about each component of wind energy system [4] is given before giving the modeling description. The main components of wind energy system are PMSG driven by fixed pitch wind turbine, a three phase diode rectifier and grid connected PWM three level NPC converter. As there is no need of any gearbox in turbine and generator, so this system is very simple and effective. Wind energy is converted into mechanical energy by wind turbine. The kinetic energy of wind turbine can be calculated by following equation

$$E = \frac{1}{2}\rho A V^2 \quad (1)$$

Where ρ is air density, V is wind velocity; A is volume of the air.

The available power available can be calculated by using the following equation

$$P = \frac{1}{2}\rho A V^3 \quad (2)$$

As the wind turbine is almost 60% efficient, so remaining power goes in losses. The actual power transferred to the turbine is given by the following equation:

$$P = \frac{1}{2} C_P \rho A V^3 \quad (3)$$

Where C_P is the power coefficient, which is the ratio of power converted in to mechanical energy to the power received by wind turbine, and calculated by following equation:

$$C_p(\lambda, \beta) = 0.5\left(\frac{116}{\lambda} - 0.4\beta - 5\right)e^{\left(\frac{21}{\lambda}\right)} \quad (4)$$

$$\frac{1}{\lambda_i} = \frac{1}{\lambda + .08\,\beta} - \frac{.035}{1 + \beta^3}$$

Where β is pitch angle λ is tip speed ratio.

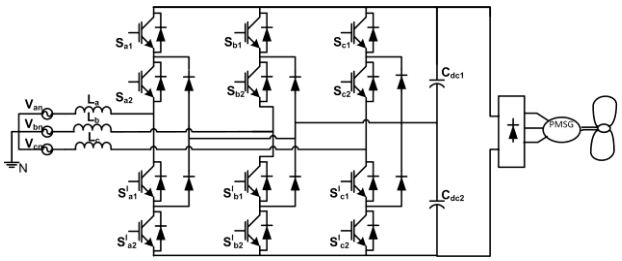

Fig.1 Circuit diagram for the system

B. Permanent magnet synchronous generator (PMSG)

Fig. 2 shows the equivalent circuit of the PMSG. In this generators the permanent magnet gives field excitation instead of the field coil. The rotor speed is equal to synchronous speed so it is called synchronous generator .The PMSG dynamic equation are expressed in d-q reference[6].

$$\frac{\partial}{\partial t} i_d = \frac{1}{L_d} v_d - \frac{R}{L_d} i_d + \frac{L_q}{L_d} p\,\omega_r i_q$$

$$\frac{\partial}{\partial t} i_q = \frac{1}{L_q} v_q - \frac{R}{L_q} i_q + \frac{L_d}{L_q} p\,\omega_r i_d - \frac{\lambda p\,\omega_e}{L_q}$$

$$V_q = \left(R + pL_q\right) i_q - \omega_r L_D i_d + \omega_r \lambda_m \quad (5)$$

$$V_d = (R + pL_q) i_q + \omega_r L_q i_q \quad (6)$$

Where R and L are the resistance inductance of the machine in per phase and V_d, V_q are the two axis voltages. Output of the PMSG rectified with the help of the three phase rectifier.

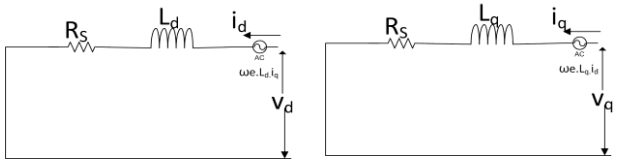

Fig.2 d axis and q axis equivelent circuits

Table-1 Parameters of PMSG

Parameter	**Values**
Pitch angle (β)	0
Wind speed (v)	12 (m/s)
Stator phase resistance	0.425Ω
Armature inductance	0.000835H
Torque constant	3.24
Voltage constant	392
Power output	6564W

C. Boost Converter

The job of a boost converter is to boost the wind power and then to transfer it [9]. The converter is switched in such a way that the global maximum power point (MPP) is determined by its operation, in accordance with the given MPPT algorithm. The input-output voltage relation of the Boost DC/DC Converter when tied-up with the PMSG is given by:

$$V_o = \frac{V}{1-D} \quad (7)$$

Where, V = input dc voltage (in volts), V_o = output dc voltage (volts)

$$(V_o > V_w)$$

$$D = \frac{T_{on}}{T_s} \qquad 0 < D < 1$$

Where T_s is the switching period, and T_s is the on-time of the power semi-conductor switch, S_{BOOST}.

D. Diode Clamped Converter

The common multilevel topologies are the Diode Clamped [10] or Neutral Point Clamped (NPC), Flaying Capacitor (FLC) and Cascaded H-Bridge (CHB) Multilevel Converters. In this paper we have used the Diode Clamped or Neutral Point Clamped (NPC) topology as shown in the fig.1. As compared to other converters the DCC is simpler and cheaper. Apart from this, These converters uses the concept of addition of multiple small voltage levels for achieving the required voltage level with the help of additional switching devices and few components like diodes or capacitors. Using this approach, the voltage stress across the switches gets equally distributed and peak inverse voltage across each switch reduced. Also, the output voltage is the addition of multiple small voltage levels, due to this concept the THD in output voltage reduces and the size of filters either reduces or filter not required. Due to the diodes connected to the neutral point N, the voltage across the switching power semiconductors is $V_{DC}/2$, and consequently the output voltage levels achievable in this topology are: $-V_{DC}/2$, 0, $V_{DC}/2$.

Table 2 shows the switching states of a three phase TLDC for phase 'a'. The switches S_{a1} & S'_{a1}, and S_{a2} & S'_{a2} are switched complementary. A PWM technique is used for the control of this converter. For implementing this PWM technique two superposed triangular carriers per phase are used. One carrier from these two carriers is connected to first complementary pair of the switches and another one is connected to the second complementary pair of switches. The switching states of S_{a1} and S'_{a1} are fixed by the positive part of the carrier while, the switching states of S_{a2} and S'_{a2} are fixed by the negative part of the carrier. For a good operation of the diode clamped converter, the DC-link capacitors must have an equal voltage. As we aren't using a DC-DC

power converter between the source and the diode clamped converter, therefore the converter control integrates the current control and the MPPT algorithm.

Table 2- Switching States for Diode Clamped Converter

Switching States	Switches On	Output Voltage	Output Current	Current Path
P	S_{a1} & S_{a2}	$V_{DC}/2$	$i_a > 0$	S_{a1} & S_{a2}
			$i_a < 0$	D_1 & D_2
O	S_{a2} & S'_{a1}	0	$i_a > 0$	D_{Z1} & S_{a2}
			$i_a < 0$	D_{Z2} & S'_{a1}
N	S'_{a1}& S'_{a1}	$-V_{DC}/2$	$i_a > 0$	D_4 & D_3
			$i_a < 0$	S'_{a2}& S'_{a1}

III. THE PROPOSED TLDC CONVERTER CONTROL SYSTEM

The main objectives of the control scheme are:

1. Generation of sinusoidal grid AC current, with low EMC, and low THD
2. Regulation of DC-link voltage for delivering the maximum power from source to the grid.
3. Mains power factor: The power generated at the generation point is to be transferred to ac mains at unity pf.

The block diagram for the control scheme of TLDC is shown in Fig 3.The control block consists of a MPPT algorithm, a DC-link capacitor voltage controller [11], a DC reference current generator, and a Current controller. The controller imposes an increment or a decrement value added to the current reference, so that the voltage of the capacitors is approximately equal. To control the DC-link voltages, is used a PI controller for each capacitor voltage regulation and a digital filter to V_{C1} *and* V_{C2}. The reference voltage is given by

$$V^*_{DC} = V_{C1} + V_{C2} \quad (8)$$

This reference voltage and the dc voltage are the inputs to the DC voltage controller, which outputs the dc current as given by the following equation

$$I_{DC} = k_p^{dc}\Delta V_{DC}(s)\,\frac{k_i^{dc}}{S}\Delta V_{DC}(s) \quad (9)$$

Where,($\Delta V_{DC} = V^*_{DC} - V_{DC}$), while k_p^{dc} and k_i^{dc} denotes the PI gains of DC voltage controller.

Converting (5) from s-domain to time-domain, we get

$$I_{DC} = k_{p1}^{dc}\Delta V_{DC}(t) + k_{i1}^{dc}\int \Delta V_{DC}(t)dt$$

Where, k_{p1}^{dc} is the proportionality constant and k_{p1}^{dc} is the integral constant used in the Voltage controller.

The total current/power made available by the wind energy system is I_W.

$$I_W = \sqrt{2}\left(\frac{P_W}{V_{grid,rms}}\right) \quad (10)$$

The reference current for the active current controller is given by:

$$I^*_d = (I_{DC} - I_W)$$

The voltage coming out from the active current controller as output in d-axis is given by:

$$V_{cond} = V_d + \omega L I_q - (I^*_d - I_d)(k_p^p + \frac{k_i^p}{S} \quad (11)$$

Also the reference current for the reactive current controller is given by:

$$I^*_q = 0$$

The voltage coming out from the reactive current controller as output in q-axis is given by:

$$V_{conq} = V_q + \omega L I_d - (I^*_q - I_q)(k_p^q + \frac{k_i^q}{S}) \quad (12)$$

Where, $\omega LI_d, \omega LI_q$ are the suckle forward compensation terms for the d, q-axis decoupling.

(k_p^p, k_i^p), (k_p^q, k_i^q) are PI gains of active current and reactive current controllers respectively.

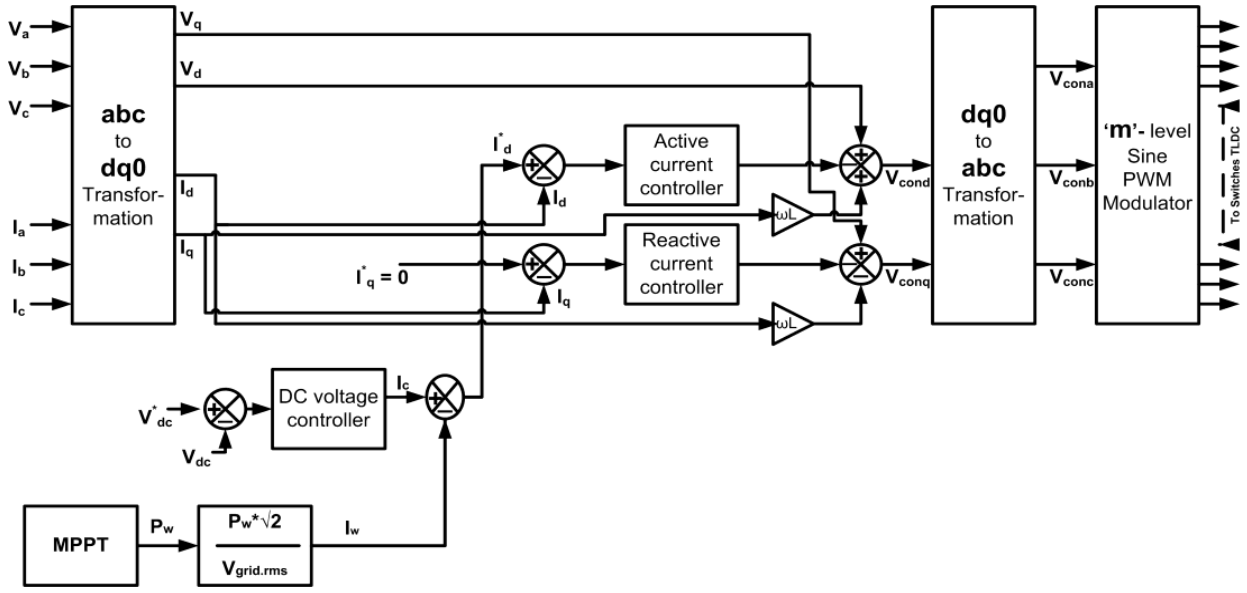

Fig. 3 Control Scheme

IV. SWITCHING STRATEGY

The PWM scheme used for generating switching signals for the switches of the TLDC converter is shown in fig.4. The modulating signals derived from the closed-loop control scheme are fed to the PWM signal generating block, which generate the switching signals for the power-semiconductor switches. In fig.4 cr_1 and cr_2 are two level shifted carriers and they are compared with modulation signal ma, comparing cr_1 with ma switching signal for S_{a1} is generated and complement of this signal used for S'_{a1}. Similarly comparing cr_2 with ma switching signal for S_{a2} is generated and complement of this signal used for S'_{a2}

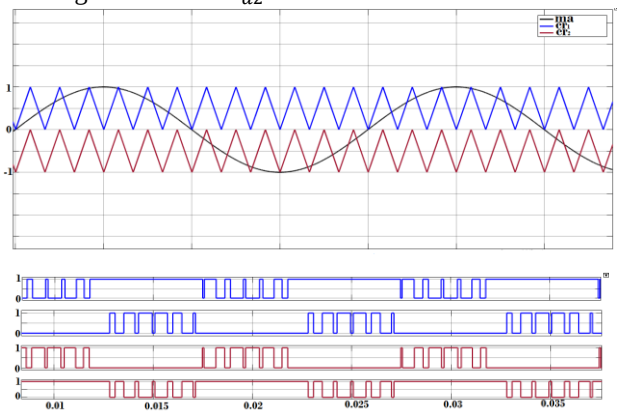

Fig.4 PWM strategy and switching signals

Table 3

Parameters	Values
DC capacitance	3300 µC
Grid Voltage (rms) (V_{grid})	240 V
Load Inductance (L_s)	0 mH
Load Resistance (R_s)	30 Ω
Reference Voltage (V^*_{DC})	400 V
Switching Frequency (f_{cr}))	2.5 kHz

V. RESULTS AND DISCUSSION

In this portion the simulation results is shown to analyze the virtue of proposed control scheme. The model is simulated and its performance is tested under steady state. Table 3 gives the details of parameters used for simulation. Fig.5 gives the characteristics of turbine used in the system [14], this figure gives the graphical relationship between the wind turbine output power and turbine speed for various wind speeds. Also, as separate maximum power point (MPP) occurs at each wind speed, thus by joining the maximum power points at each particular wind speed the maximum power line is achieved, which is described in Fig. 5. Therefore, the performance of the wind turbine at the maximum turbine speed on the maximum power curve guarantees the maximum wind energy extraction by the wind turbine below the rated wind speed. Fig.6 represents the simulated waveforms of grid voltage and current in steady state operation. It is clear from the waveforms that the fundamental components of both V and I are in phase. Also the current is sinusoidal in shape, having low harmonic distortion, and Unity Power Factor (UPF). The trace having higher magnitude is for voltage and the trace having lower magnitude is for the current. The wind dc power output is given by fig7.

At a wind speed of 12m/s, the PMSG attains its rated power of 6564W in 0.9s. Also with the increase in wind speed, the turbine speed increases and thus wind turbine output power increases and vice versa. Fig.8 represents the simulated output phase voltage waveforms. This phase voltage has three level (m). And these levels in the phase voltage trace justify the three level inverter operation, as each level is symmetrical and equal in magnitude. Similarly, the output line voltage waveform is shown in Fig.10 consisting of five (2m-1) equal and symmetrical levels. Fig.11 represents the input DC voltage which is maintained at 400 V (it is more than √2 of $V_{grid\ rms}$, which is 240V in this case). This constant value of DC voltage is maintained by voltage control in control system of converter. The load currents of phase-a, b & c are shown in fig.9. The load currents are balanced and symmetrical. The harmonic analysis of the ac side grid current is performed and the corresponding harmonic spectrum is plotted in fig. 12 with THD of 1.10%.Design of appropriate filter in the control scheme will help in reducing the THD further. Thus, the objective of the control scheme is fulfilled and its performance is tested using MATLAB Simulink.

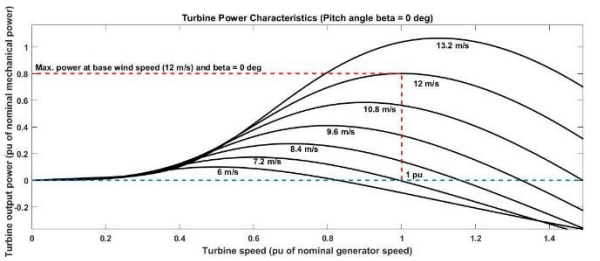

Fig.5 Turbine characteristic

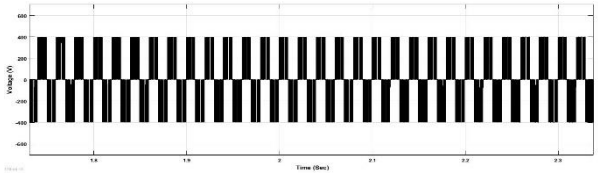

Fig.6 Grid voltage and current

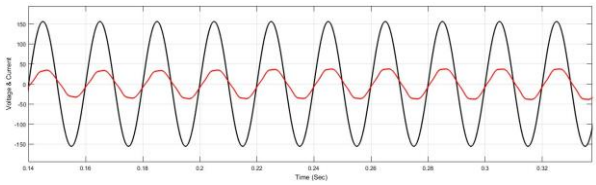

Fig.7 Wind dc power with MPPT

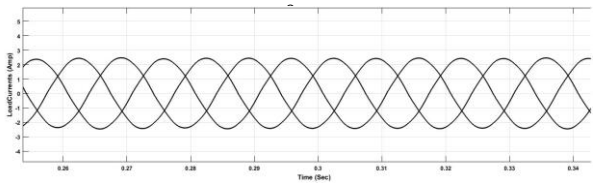

Fig.8 Three level phase voltage

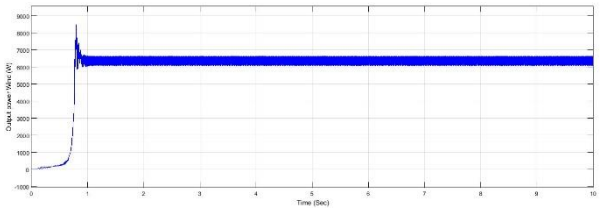

Fig.9 Three phase load Currents (i_a, i_b, i_c)

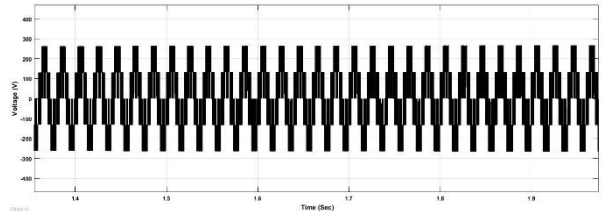

Fig.10 Five level line voltage

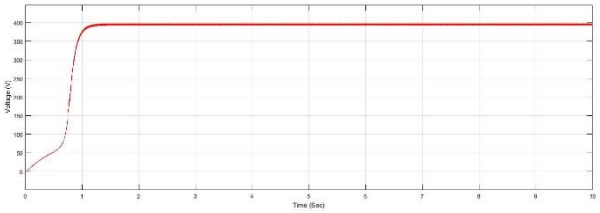

Fig.11 DC voltage

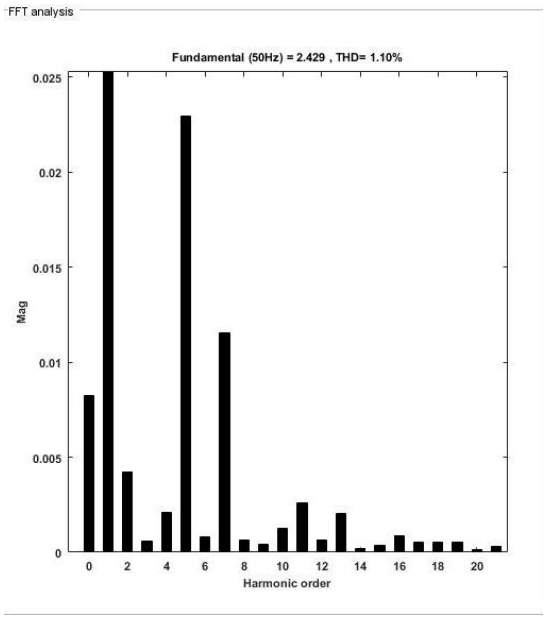

Fig. 12 Harmonic content in AC side

V. CONCLUSION

In this paper the behavior of a three phase three level diode clamped converter as an interfacing element between the sustainable energy source and the utility grid has been analyzed. These converters are a good barter solution between the cost and the performance. The DC voltage is seeding to be retained at a constant value and current injected into the grid side is closer to sinusoidal with minimum THD and in the same phase with the grid voltage. The peak inverse voltage (PIV) across the switching devices is reduced as the voltage stress across the switches get equally distributed. Reduced voltage ratings, good dynamic response and excellent harmonic spectrum are the prime benefit of these converters. The controller provides the guarantee for almost unity pf for mains, dense control of the dc-link voltage.

REFERENCES

[1] D. M. Baker, V. G. Agelidis, and C. V. Nayer, "A comparison of tri-level and bi-level current controlled grid-connected single-phase full-bridge inverters," in Proc. IEEE Int. Symp. Ind. Electron. 1997, pp. 463–46.

[2] W. Bin, High-power converters and AC drives. Piscataway: Wiley-IEEE Press, 2006

[3] A. Nabae, I. Takahashi, and H. Akagi, "A new neutral-point-clamped PWM inverter," IEEE Trans. Ind. Appl., vol. IA-17, no. 5, pp. 518–523, Sep./Oct. 1981.

[4] M Mansor, M.N. Mansori, M.F.Mmimuni, "Study and Control of a Variable Speed Wind Energy System Connected to the Grid", IJRER, Vol.1, pp.96-104,2011.

[5] S. Alepuz, J. Bordonau, and J. Peracaula, "Dynamic analysis of three level voltage-source inverters applied to power regulation," in Proc. IEEE Power Electron. Spec. Conf., 1999, pp. 721–726.

[6] "Correction to "Optimum Control Strategies in Energy Conversion of PMSG Wind Turbine System Without Mechanical Sensors"," in IEEE Transactions on Energy Conversion, vol. 19, no. 3, pp. 654-654, Sept. 2004.

[7] A. Woyte, R. Belmans, and J. Nijs, "Islanding of grid-connected ac module inverters," in Proc. IEEE Photo volt. Spec .Conf. 2000, pp.1683–1686.

[8] Q. Chongming and K. M. Smedley, "Three-phase grid-connected inverters interface for alternative energy sources with unified constant frequency integration control," in Proc. IEEE-IAS Annu. Meeting, 2001, pp. 2675–2682.

[9] S. Alepuz, J. Salaet, A. Gilabert, J. Bordonau, and J. Peracaula, "Control of three-level VSLs with a LQR-based gain-scheduling technique applied to dc-link neutral voltage and power regulation," in Proc. IEEE Conf. Ind. Electron. And Instrum, 2002, pp. 914–919.

[10] P. Panagis, F. Stergiopoulos, P. Marabeas, and S. Manias, "Comparison of State of the Art Multilevel Inverters," Power Electron. Spec. Conf. 2008. PESC 2008. IEEE, pp.4296–4301, 2008.

[11] P. C. Krause, 0. Wasynczuk and S. D. Sudhoff, Analysis of electric machinery. New York: IEEE Press, (1994).

[12] Global Wind Energy Council, Global Wind 2013 Report, available at www.gwec.net. [Accessed: May. 3, 2015].

[13] S.K.Lim, J.H.kim and K.Nam, "A DC-link voltage balancing Algorithm for 3-Level Converter Using the Zero Sequence Current," IEEE Conference.

[14] N.R. Nair, M. Ebenezer, "Operation and control of grid connected wind-pv hybrid system ", ICAGE, Dec 17-18,2014

[15] G. A. Dhomane and H.M. Suryawanshi, "Mitigation of Harmonics in Three phase AC Systems using Current Injection Technique for AC/DC Converter", Electric Power System Research,79,(2009)1374-1383.

An Improved Virtual Synchronous Generator Control for Reducing Power Fluctuation and Suppressing Voltage Sag of Grid

Amit Kumar[1], Shelly Vadhera[2]

***Abstract*— This paper highlights the improvement of power quality due to integration of renewable energy sources. Current scenario is that shifting from centralized power production to distributed generation. Due to this serious challenges may be present for operation of future power system. Renewable energy sources are integrated into the grid through power electronics converter but these converters lacks inherently inertia present in synchronous generator. This paper presents the power electronics converter with energy storage device to reduce the frequency deviation, power fluctuation and suppressing the voltage sag. The virtual synchronous generator (VSG) is able to regulate both the active and reactive power separately and by setting the virtual torque and virtual excitation to meet the power system requirements. A virtual rotating mass is implemented in the VSG in order to increase the inertia in the grid and improve the transient frequency stability. The virtual damping of the VSG can reduce the frequency and power oscillations in the grid.**

Keywords*— *virtual synchronous generator (VSG), synchronous machine (SM), synchronous reference frame (SRF) ,distributed generation (DG)

I. INTRODUCTION

The integration of power generation from sustainable energy sources and the changeover from a conventional power production model to distributed generation especially renewable generation are expected to have considerable problems to the expansion of future power system network. DG technologies include sterling engine based generators, wind turbines, fuel cells, photovoltaic, small sized turbine and micro sized turbine, and combustion engine driven generators [1]. The wind turbines are integrated to power system using power electronics converter and these power electronics converter lacks the inertia due to which it leads to frequency strokes in the grid or partial grid shedding. An amazing scheme is develop in the recent years with control of power electronic converters to behave as a synchronous generator and by intimate the virtual rotating mass, stability of the network increases. Thus VSG has large inertia value like a real synchronous machine but other issues like controlling reactive power, oscillations damping exist as such.

But with power electronic converters scheme have been proposed to solve these issues [2, 3]. To imitate the dynamic behavior of the traditional synchronous machine, control strategies of power electronics converters are designed such that it can be therefore classified in broad terms as virtual synchronous generator (VSG). Three distinct parts of a VSG, namely a power supplier, the algorithm that control power transition from energy storage and existing power system network and energy storage device that may be a battery or super-capacitor or flywheel [4].

To maintain the stability of system the traditional droop control VSG control adds the swing equation to imitate the inertia and this virtual inertia control the grid frequency [5, 6]. But, due to basic VSG control, power fluctuation and frequency oscillation may present due to sudden change in load and VSG is trying to mimic the behavior of synchronous machine [7]. In recent years, to improve the transient response various methods are proposed based on VSG control [8-11]. In [8] dynamic response of power control is taken into consideration by simply designing the various basic parameters step by step. Reference [9] discusses how the rotor inertia is important to improve the transient response and presents an enhanced droop control to achieve better dynamic response and to mimic the inertia of rotor. In [10], to damp out the oscillation in transient process, a damping parameter is used in current controller of power electronics converter to achieve steady-state. The damping parameter alone may not be able to damp out the oscillation effectively [11]. In a real SG, parameter can not be altered and value of inertia is fixed once manufactured but in VSG swing equation parameters can be changed and effectively controlled to improve the dynamic response of power and frequency. Hence alternating inertia [12] and feedforward control are proposed to improve the dynamic response and to reduce the power fluctuation present in the system.

II. C

A. Basic VSG control

The Fig.1 represents the basic VSG control strategy is used in a grid with power electronics converter where the distributed generation resources are connected to the

[1]Amit Kumar is with Department of Electrical Engineering, National Institute of Technology, Kurukshetra, India

[2]Shelly Vadhera is with Department of Electrical Engineering, National Institute of Technology, Kurukshetra, India.

(e-mail: amitmorkhi@gmail.com, shelly_vadhera@rediffmail.com)

grid through the line impedance Z_{line}. The VSG control system consists of power control part, stator electrical part and voltage/current control part, which are all implemented in synchronous reference frame (SRF). In the SRF the d-axis is oriented to the voltage reference E_{ref} which is produced by the Q-E droop control. And the swing equation produces P_{ref} as the phase angle reference of SRF which is used in the Park transformation. The stator electrical part is based on the voltage equation of SG stator which can be considered as the imitation of the stator electrical characteristics in the SG. To achieve the inertia support for power system, VSG control adds the swing equation in the active power control part. Fig.2 shows the control block diagram of the active power control part. According to Fig. 2 the swing equation can be obtained as follow

$$jw\frac{dw}{dt} = P_{ref} - P_e - D_p(w - w_s) \qquad (1)$$

$$K\frac{dw}{dt} = Q_O - Q - D_q(E - E_o) \qquad (2)$$

Where E_o and w_s are the rated voltage amplitude and frequency, P_{ref} and Q_o are output rated active power and reactive power, E and w are generated voltage amplitude and frequency reference. D_p and D_q are the active and reactive power droop coefficient. J and K are virtual inertia and excitation coefficient.

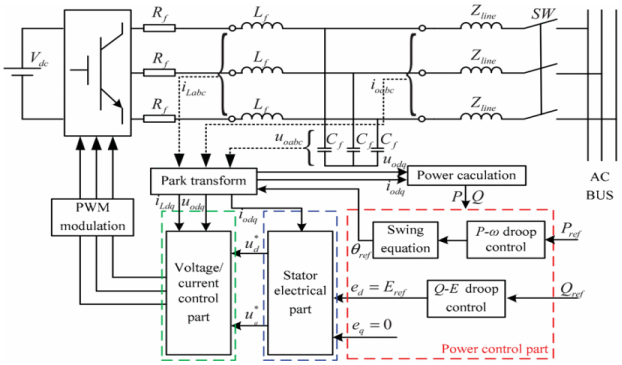

Fig.1.Interfacing of inverter based VSG control with grid

To mimic the rotational inertia in the power system, swing equation is added to control active power part. Fig.2 shows the block diagram of addition of swing equation in terms of control system blocks.

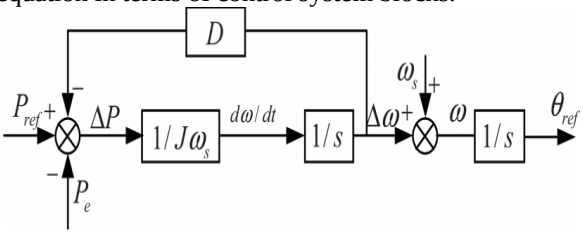

Fig. 2. Active power control structure of VSG

Overview and system configuration of virtual synchronous machine is shown in Fig.3. All the block diagram and their interconnection with other block diagram is shown in Fig.3. Virtual impedance, voltage regulator and current regulator are important block in the implementation of virtual synchronous generator.

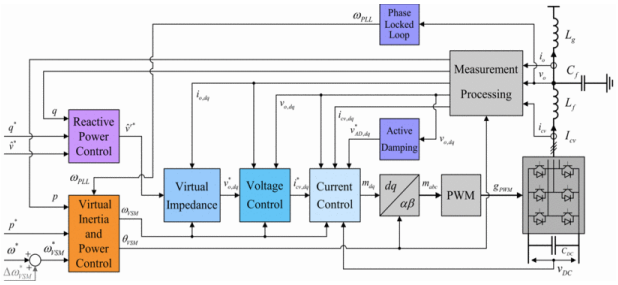

Fig.3. Overview of system configuration and control structure of virtual synchronous machine

B. *VSG with feedforward control*

The voltage-current double loop controller for the VSG of Fig.1 is shown in Fig.4. The primary aim of voltage outer loop is to produce the instruction to current reference value and to ensure that output voltage magnitude is stable. The main function of the inner current loop is to adjust the value of current to particular reference value and improve the transient response of the VSG system. Z_{ffv} *and* Z_{ffi} *are the feed*forward voltage and current control parameter respectively.

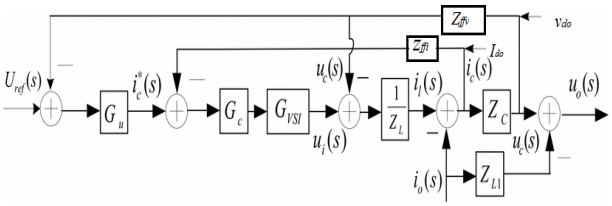

Fig.4. Block diagram of voltage and current feed forward VSG control

Where G_{VSI} is the inverter equivalent gain , K_c is the proportional coefficient of above represented current regulator G_c .K_p and K_i are the proportional and integral coefficients of the voltage regulator G_u.
Z_c,Z_Lare the impedances of capacitor C, inductor L. Capacitor voltage differential feedback exhibits rejection of disturbances in load current effectively than inductor current feedback so it is widely used in voltage feedback because an additional current sensor is not required to feedback the high-frequency capacitor current.
Transfer function without any disturbances

$$\frac{U_o(s)}{U_{ref}} = \frac{G_u G_c G_{VSI}\left(\frac{Z_c}{Z_L}\right)}{1 + G_u G_c G_{VSI}\left(\frac{Z_c}{Z_L}\right) + \left(\frac{Z_c}{Z_L}\right) + G_c G_{VSI}\left(\frac{Z_c}{Z_L}\right)} \qquad (3)$$

With feed forward control of voltage and current, disturbances should be zero. for zero disturbances Z_{ffi} and Z_{ffv} expression are calculated with basic dual loop control of VSG .

The expression for different value of Z_{ffi} and Z_{ffv} shown below:
For voltage error v_{do}=0

$$z_{ffv} = 1 + \frac{G_u G_c G_{VSI}}{Z_L} + \frac{Z_c}{Z_L} \quad (4)$$

For current error i_{do}=0

$$Z_c = 1 + \frac{G_c G_{VSI}}{Z_L} \quad (5)$$

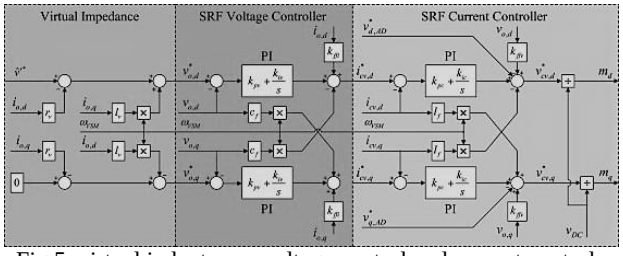

Fig.5. virtual inductance, voltage control and current control

This virtual impedance of current controller in VSG is considered as a representation of a Quasi-stationary characteristics of the synchronous impedance in a conventional synchronous machine. The term quasi-stationary is taken because it will influence both dynamic and steady state operation of VSG , and on depending upon the adjustment of virtual impedance, the dynamic characteristics a of the system is varied. The phase angle displacement between the virtual inertia position of the VSG and the grid is depending upon value of virtual impedance, so power flow can be controlled by varying virtual impedance. Voltage controller are protected from windup condition, when reference current are saturated.

C. Grid voltage sag compensation

The voltage controlled inverter able to limit current to the safe level by the coordinated control of PQ mode control with VSG. However the steady state value of current depends on the actual power flow in VSG power control loop. When there is match between the grid voltage and VSG voltage with same phase and magnitude then the feedforward control and sag compensation is used in *d-q* axis to restrain the grid voltage disturbance. The grid voltage feedforward control is added into two parts. One part is the current and voltage closed-loops and another is the VSG control swing equation to overcome effect of system excitation as shown in Fig.1. The grid voltage sag compensation added in the VSG control can improve the transient stability of the grid.

$$\frac{dp}{dp_o} = \frac{3EE_O}{w_s J z s^2 + w_s D_p Z s + 3EE_o} \quad (6)$$

Acc to Min Liu et. al paper [4] optimal control can be founded with adjustment of value of J and for better view , the step response of dp/dp_o can be shown in Fig.6.

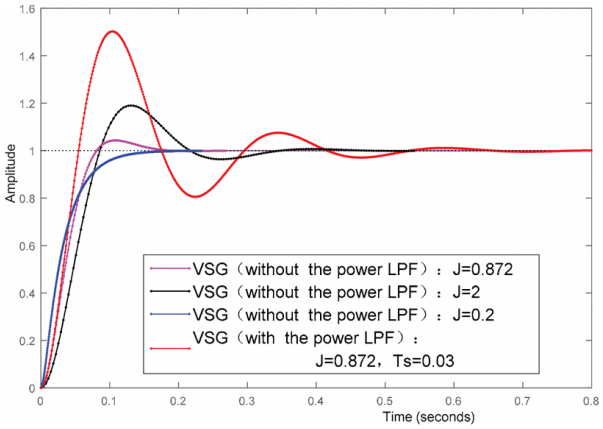

Fig.6. The step response of dp/dp_o

III. SIMULATION AND RESULTS

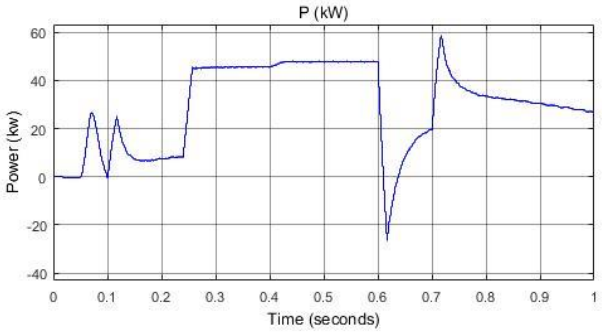

Fig.7. VSG control of power fluctuation without battery

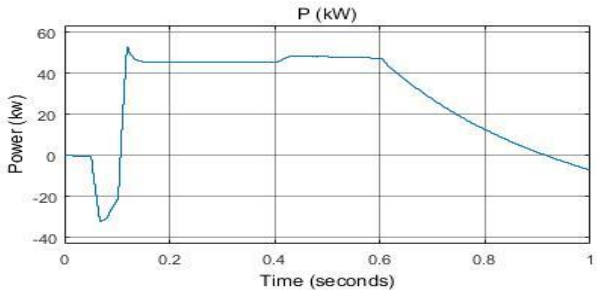

Fig.8. VSG control of power fluctuation with battery

Fig.7 and Fig.8 are shown the transient response of grid with VSG control ,better transient response is obtained when VSG control is used with energy storage.

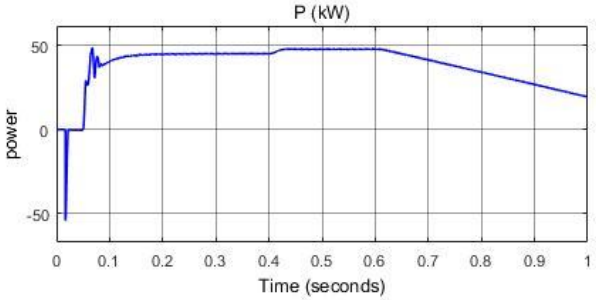

Fig.9.Power fluctuation of VSG without feedforward control

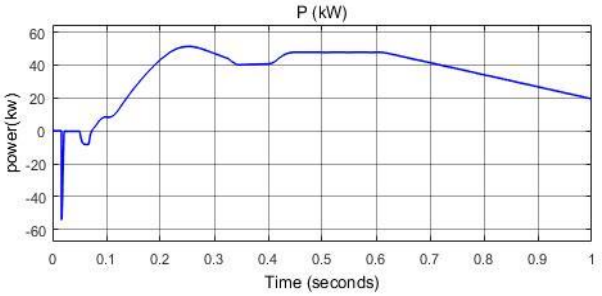

Fig.10. Power fluctuation of VSG with feedforward control

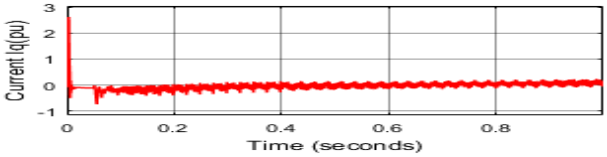

Fig.11. q-axis component of current

From the above shown Fig.9 and Fg.10, good dynamic response is obtained with feedforward control strategy. With respect to basic control strategy of VSG, transient response is better when feedforward control technique is used.Fig.11, represented the q-axis current for the feedforward control. Variation in the q-axis component of current is maximum at the time of switching.

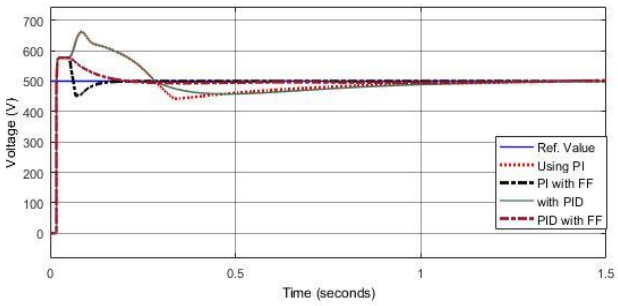

Fig.12. VSG with different controller to suppress voltage sag

From the Fig.12, voltage variation with different controller is presented. When feed forward technique is used with different controller, smooth response is obtained.

IV. CONCLUSION

This paper presents the method to improve the transient response and reduce the power fluctuation present in the grid. In this paper mathematical expression and control structure of VSG with different controller is presented to show the behavior of grid tied inverter to work as a synchronous machine. A strategy of achieving fast current control by VSG control to suppressing grid voltage sag and power fluctuation in the grid. Further feedforward control is used to suppressing the voltage within the limit and it is verified by the simulation result. The feedforward control is used to minimize the influence of load disturbance to obtain excellent dynamic response. In future work, VSG active power control structure can be used with lead lag compensator to enhance stability and reduce the power fluctuation.

REFERENCES

[1] H. P. Beck, R. Hesse, "Virtual synchronous machine", *Proc. 9th Int. Conf. Electr. Power Qual. Utilisation*, pp. 1-6, 2007.

[2] K. Visscher, S. W. H. De Haan, "Virtual synchronous machines for frequency stabilization in future grids with a significant share of decentralized generation", Proc. IET-CIRED Seminar SmartGrids Distrib., pp. 1-4, 2008.

[3] S. D'Arco and J. A. Suul, "Small-Signal analysis of an isolated power system controlled by a virtual synchronous machine," *IEEE International Power Electronics and Motion Control Conference (PEMC)*, pp. 462-469,2016.

[4] M. Liu, G. Xiao, F. Zhao, D. Yang, S. Su, X. Han, Y. Wang, and B. Ma, "An enhanced virtual synchronous generator strategy for suppressing grid voltage sag," 2017 IEEE 3rd International Future Energy Electronics Conference and ECCE Asia (IFEEC 2017 - ECCE Asia), 2017.

[5] N. Xu, Y. Wang, M. Li, W. Wang, N. Wang, and J. Li, "An Optimal Control Method of Virtual Angular Acceleration to Improve Transient Response Based on Virtual Synchronous Generator," Futur. Energy Electron. Conf. ECCE Asia (IFEEC 2017-ECCE Asia), 2017 IEEE 3rd Int., pp. 1559–1563, 2017.

[6] M. Liu, G. Xiao, F. Zhao, D. Yang, S. Su, and X. Han, "Strategy For Suppressing Grid Voltage Sag," no. 3, pp. 2064–2069, 2017.

[7] S. D'Acro, J.A. Suul, O.B. Fooso, "Automatic Tuning of Cascaded Controllers for Power Converters U sing Eigenvalue Parametric Sensitivities", IEEE Trans. Ind. Appl., vol. 51, no. 2, pp. 1743-1752, Mar./Apr 2015.

[8] Wu Heng, Ruan Xinbo, Yang Dongsheng et al., "Small-Signal Modeling and Parameters Design for Virtual Synchronous Generators", IEEE Trans on Ind. Electron., vol. 63, no. 7, pp. 4292-4303,July.2016.

[9] N. Soni, S. Doolla, M. C. Chandorkar, "Improvement of transient response in microgrids using virtual inertia", IEEE Trans. Power Del., vol. 28, no. 3, pp. 1830-1838, Jul. 2013.

[10] M. Guan, W. Pan, J. Zhang, Q. Hao, J. Cheng, X. Zheng, "Synchronous generator emulation control strategy for voltage source converter (VSC) stations", IEEE Trans. Power Syst., vol. 30, no. 6, pp. 3093-3101, Aug. 2015.

[11] Xu Ningyi, Wang Yue, Li Mingxuan et al., "Analysis and Improvement of Damping Factor Based on Virtual Synchronous Generator Control", *2016 IEEE 8th International Power Electronics and Motion Control Conference (IPEMC-ECCE Asia)*, pp. 1990-1996, July 13, 2016.

[12] Yan Du, J.M. Guerrero, Liuchen Chang, Jianhui Su, Meigin Mao, "Modeling analysis and design of a frequency-droop-based virtual synchronous generator for microgrid applications", *ECCE Asia Downunder (ECCE Asia) 2013 IEEE*, pp. 643-649, June 2013.

Performance Analysis of MMC-VSC HVDC System for Offshore Wind Farms

Abhishek Gunwant[1], Shelly Vadhera[2]

***Abstract*—These days when electrical energy became vital for living and world is becoming more and more conscious about environment, the only solution we have is the renewable energy sources. Offshore wind farms are very attractive solution in terms of meeting high load demand and also offshore wind farms offer many advantages like constant wind speed, no disturbance to the populated areas and easy availability of land etc. We use high voltage direct current technology to transmit this much of bulk electrical energy because of many advantages of HVDC transmission over HVAC transmission. Converter which converts AC to DC and DC to AC plays a very important role in this whole system. One of the most recent technology in this field is the MMC converter technology which is a type of voltage source converter but having many advancement in terms of waveform quality and compactness. This paper goes through a brief performance analysis of modular multilevel converter MMC-VSC HVDC transmission system. MATLAB simulink is used to show graphs of various parameters of our system.**

Keywords—Offshore wind farm, HVDC, VSC, LCC, MMC-VSC, SM

I. INTRODUCTION

Large amount of power can be transferred over large distances by a high voltage direct current (HVDC) connection which is far cheaper and widely used all over the world. The main concern of researchers is to transmit large power to the remote areas and islands [1].

There are numerous plus points of voltage source converter (VSC) HVDC frameworks over the traditional line commutated converter (LCC) based frameworks in large power transmission applications [2]. The features like independent control of active and reactive power [3], operation in weak AC systems [4], black start capability [5], and multi terminal connection [6] causes their tremendous use in modern power transmission systems.

LCC and VSC HVDC system has already been discussed in many literatures. There are many advantages of MMC based HVDC system out of which one main feature is the less harmonic content due to which there is no need to use bulky filters. However the main disadvantage of that system is the communication is not continuous if the AC system is weak [7-8].

This paper is organized as follows. Section II comprises of discription of MMC is given. In third section the MMC-VSC based HVDC transmission system configuration is given. Finally the performance of system under normal conditions is shown with the help of MATLAB Simulink results in Section IV followed by conclusion in Section V.

[1]Abhishek Gunwant is with School of Renewable Energy and Efficiency, National Institute of Technology, Kurukshetra, India

[2]Shelly Vadhera is with Department of Electrical Engineering, National Institute of Technology, Kurukshetra, India.

(e-mail: aa.gunwant1994@gmail.com, shelly_vadhera@rediffmail.com)

II. MMC-VSC

The Modular multilevel converter (MMC) corresponds to a promising technology with an additional advantage of being a scalable technology making high voltage and power capability possible by series connections. Similar sub modules are used to construct a MMC converter which are although similar but are independent in working. In this manner the converter behave as a controllable voltage source, with large number of discrete voltage steps. Due to this feature the mathematical and computational model of MMC is complex.

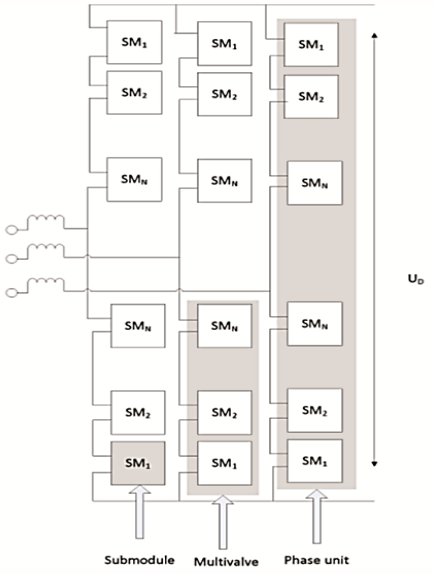

Fig. 1. Block diagram of MMC

ABB's HVDC light is the first HVDC system with the utilization of voltage source converters (VSC) in which IGBTs were used which was introduced in 1997. In old models of VSC voltage levels can be either +V or -V in a two level VSC and +V, -V and 0 in a three level VSC [9, 10]. Pulse width modulation (PWM) is utilized to estimate the preferred voltage waveform and the divergence of preferred one from the implemented waveform is the undesirable distortion which must be separated out by utilization of filters [10]. IGBTs are to be connected in series in numbers in VSCs because they have low voltage blocking capacities [9]. Complicated gate circuitry is needed to implement voltage sharing at all conditions and to perform switching so that series

connected IGBTs switched simultaneously due to which voltage across each semiconductor is bounded [11].
ABB and Siemens both in 2010 for the first time unvieled the MMC-VSC HVDC technology, Siemens HVDC plus and ABB HVDC light [9-10]. Voltage levels of MMC is controlled by submodules voltages. Submodule is basic building block of MMC, a number of submodules used to make a MMC which also decide its different voltage levels. Voltage level of each submodule can be V, 0 for half bridge or +/-V or 0 for full bridge two-level converter [11]. So this means with the help of large number of submodule this converter become a controllable voltage source with large number of distinct voltage levels. Due to large number of voltage levels the quality of waveform improved highly hence harmonic content is very low [9]. Submodule needed depend upon the votage level required, for large voltage applications also we can use this technology as this is a scalable technology [12]. The configuration is without series connection of semiconductor switches, and hence problems with simultaneous switching are irrelevant. Losses are lower than for two-level and three-level VSCs, about 1 % per converter [9]. If the switching frequency in each submodule is low and voltage across each switch is also low then the losses incurred are low [12]. However, as at different points in time submodules are switched, this increases the converter's effective switching speed, resulting in low harmonic distortion [9]

Various other feasible topologies of converter has been purposed, like other multilevel and the hybrid converters. The most important multilevel topologies are the diode-clamped multilevel converter [14], neutral point clamped converter [13], and flying capacitor multilevel converter [15], along with the MMC. We can also utilize both of the VSC and MMC technologies in hybrid HVDC system [11]. Main aim is to obtain a good output signal than with VSC jointly with utilizing lesser semiconductor switches than the MMC. Small MMCs can be utilized to be used as active filters or wave shaping circuits. Links can be made in various techniques. Only MMC topology out of all other topologies is the one which is used in commissioned projects of HVDC [21].

III. MMC BASED HVDC SYSTEM

Two technologies LCC and VSC are dominantly utilized all over the world for the HVDC connection. However there are many topologies that can be used but these two have their superior place in market. There are many advantages and disadvantages of both of them but VSC in many aspects is better than LCC.

Reactive power as well as active power can be controlled independently in case of VSCs [19], hence there is no requirement for reactive power compensation. Also the size of harmonic filter required in case of VSCs are much smaller and there is no need for the switch yards and capacitor banks. Hence a VSC station is much more compact in size than that of LCC station [9]. One of the very few disadvantages that VSC has is the higher loss of about 1.7% per converter than LCC [18], also there is no need of phase shift transformers as there is no phase shift required. Also VSC can be connected to the weak AC systems [9]. When we have d.c. grid in our system then VSC technology is more appropriate because in VSCs for power reversal only current direction have to be changed. Whereas in LCC, by reversing the direction of voltage power reversal is performed [22]. Cross-linked polyethylene (XLPE) cables are more popular with VSCs, but not capable of handling high stress but these cables are good to be used because there advantages of cost, size and weight than other cables [23]
In a three phase MMC, two multivalve are present in each phase which comprises N submodules each, and these submodules are connected in series Fig. 1 [12]. 38 submodules are required for a d.c. voltage of +/-320KV [17]. The half-bridge submodule has a capacitor with two valves (T1 and T2) as shown in Fig. 2. Freewheeling diode and IGBT which are connected in antiparallel are the components of a valve. During usual operation of MMC only a particular valve is switched on at a particularly instant of time. Charging and discharging of capacitor is depend upon the direction of current [12].

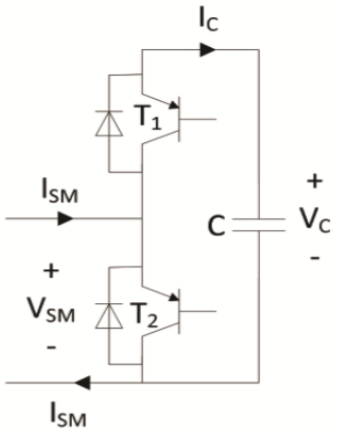

Fig. 2. Circuit of a submodule

Three possible switching states can be defined [4]:
T_1 is on and T_2 is OFF represent ON state and in that state the submodule output voltage V_{SM} equals to the capacitor voltage V_C, and depending upon the multivalve current direction capacitor charges or discharges.
• When T_1 is OFF and T_2 is ON, then this represent the OFF state and in this situation the submodule output voltage V_{SM} is 0, and the voltage across capacitor V_C is constant which means capacitor will not charges or discharges.
• When both valves are OFF then the submodule is in blocked state, and only freewheeling diodes will allow the current to flow. And if current is positive then capacitor will charge, but it cannot discharge ideally.

In each phase the blocking voltage is double of the d.c. voltage. This is described from the condition when all of the submodules of upper multivalve are bypassed, which gives d.c. voltage equal to phase voltage The lower multivalve must be capable to withstand the voltage equals to D.C. voltage. So that each switch

blocks the D.C. voltage, V_D, divided by the number of submodules in each multivalve, N, giving $V_{block} = V_D/N$ blocking voltage for each switch. Lower multivalve capacitors will also share the D.C. voltage and must be featured in the matching way as the IGBTs. Taking the same case and a negative I_{SM} with respect to Fig. 2, every IGBT in the upper valve must be capable to withstand the capacitor voltage in the same submodule [20].

IV. RESULTS

In this section various curves of different parameters of a MMC based HVDC system are analyzed. As it can be seen with the help of MMC one can get the desired smooth voltage waveform so there is no need of much bulky filters to eliminate harmonics but the cost and complexity of this converter based system is very high due to large numbers of switches. Here we will analyze a MATLAB simulink model of a MMC technology based HVDC system connected to an offshore wind farm of 1000MW capacity and with D.C. link voltage of 500KV and AC system voltage of 220KV.

It can be seen that the first and last curve is of the AC voltage and current of both side stations. Second curve is the D.C. link voltage of HVDC scheme. In third curve power flow through the HVDC system is shown. However after some time of initialization of simulation power reaches its steady state value of 1000MW.

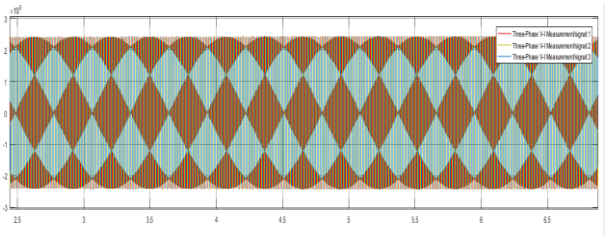

Fig. 3. Three phase voltage waveform on AC side

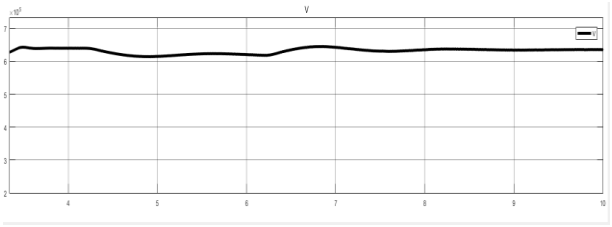

Fig. 4. D.C. voltage waveform on D.C. side

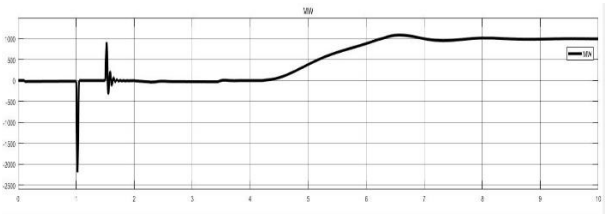

Fig. 5. Real power flow curve of the system

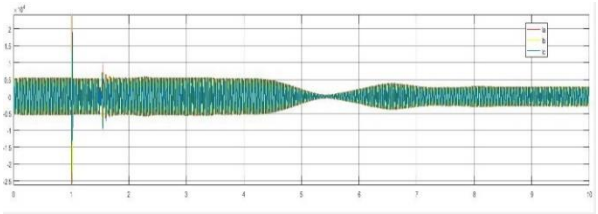

Fig. 6. AC current waveform on the AC side

V. CONCLUSION

The multi-level modular converter is an attractive topology for HVDC operation. The design and control of the MMC-VSC are generally more complex than that of the conventional VSC because of the independent sub modules circuit configuration. The paper presents the basic approach for use of this topology in HVDC transmission applications. Through simulation, it is shown that the MMC can provide an essentially sinusoidal waveform that meets accepted guidelines of harmonic content, without the need for AC filters when the number of sub modules per multi-valve are large in number. Also the simulation results reinforce the fact that the MMC HVDC system offers better operational curves and we can say that the system can be applicable to various HVDC systems where the power flow is unidirectional.

REFERENCES

[1] Li, Wanlu, Libao Shi, Liangzhong Yao, Yue Zhao, Zhou Jian, and Yixin Ni. "Comparison of HVAC and HVDC based grid integration on wind farm." In Power System Technology (POWERCON), 2014 International Conference on, pp. 2927-2932. IEEE, 2014.

[2] Bahrman, Michael P., Jan G. Johansson, and Bo A. Nilsson. "Voltage source converter transmission technologies: the right fit for the application." In Power Engineering Society General Meeting, 2003, IEEE, vol. 3, pp. 1840-1847. IEEE, 2003.

[3] Latorre, Hector F., Mehrdad Ghandhari, and Lennart Söder. "Active and reactive power control of a VSC-HVdc." Electric Power Systems Research 78, no. 10 (2008): 1756-1763.

[4] Du, Cuiqing. VSC-HVDC for industrial power systems. Chalmers University of Technology, 2007.

[5] Jiang-Hafner, Ying, Hugo Duchen, Michael Karlsson, Leif Ronstrom, and Bernt Abrahamsson. "HVDC with voltage source converters-a powerful standby black start facility." In Transmission and Distribution Conference and Exposition, 2008. T&D. IEEE/PES, pp. 1-9. IEEE, 2008.

[6] Haileselassie, Temesgen M., Marta Molinas, and Tore Undeland. "Multi-terminal VSC-HVDC system for integration of offshore wind farms and green electrification of platforms in the North Sea." In Nordic Workshop on Power and Industrial Electronics (NORPIE/2008), June 9-11, 2008, Espoo, Finland. Helsinki University of Technology, 2008.

[7] Zhang, Zheren, Zheng Xu, Yinglin Xue, and Geng Tang. "DC-side harmonic currents calculation and DC-loop resonance analysis for an LCC–MMC hybrid HVDC transmission system." IEEE Transactions on Power Delivery 30, no. 2 (2015): 642-651.

[8] Kotb, Omar, and Vijay K. Sood. "A hybrid HVDC transmission system supplying a passive load." In Electric Power and Energy Conference (EPEC), 2010 IEEE, pp. 1-5. IEEE, 2010.

[9] Jacobson, Bjorn, Patrik Karlsson, Gunnar Asplund, Lennart Harnefors, and Tomas Jonsson. "VSC-HVDC transmission with cascaded two-level converters." In Cigré session, pp. B4-B110. 2010.

[10] Friedrich, Kurt. "Modern HVDC PLUS application of VSC in modular multilevel converter topology." In Industrial Electronics (ISIE), 2010 IEEE International Symposium on, pp. 3807-3810. IEEE, 2010.

[11] Davidson, C. C., and D. R. Trainer. "Innovative concepts for hybrid multi-level converters for HVDC power transmission." (2010): 51-51.

[12] Gnanarathna, Udana N., Aniruddha M. Gole, and Rohitha P. Jayasinghe. "Efficient modeling of modular multilevel HVDC converters (MMC) on electromagnetic transient simulation programs." IEEE Transactions on Power Delivery 26, no. 1 (2011): 316-324.

[13] Nabae, Akira, Isao Takahashi, and Hirofumi Akagi. "A new neutral-point-clamped PWM inverter." IEEE Transactions on industry applications 5 (1981): 518-523.

[14] Choi, Nam S., Jung G. Cho, and Gyu H. Cho. "A general circuit topology of multilevel inverter." In Power Electronics Specialists Conference, 1991. PESC'91 Record., 22nd Annual IEEE, pp. 96-103. IEEE, 1991.
[15] Schiop, Adrian, and Petre Scortaru. "Simulink model of flying capacitor multilevel inverter." In Optimization of Electrical and Electronic Equipment, 2008. OPTIM 2008. 11th International Conference on, pp. 203-208. IEEE, 2008.
[16] Friedrich, Kurt. "Modern HVDC PLUS application of VSC in modular multilevel converter topology." In Industrial Electronics (ISIE), 2010 IEEE International Symposium on, pp. 3807-3810. IEEE, 2010.
[17] Cole, Stijn, and Ronnie Belmans. "Transmission of bulk power." IEEE Industrial Electronics Magazine 3, no. 3 (2009).
[18] Abildgaard, Elisabeth N., and Marta Molinas. "Modelling and control of the modular multilevel converter (MMC)." Energy Procedia 20 (2012): 227-236.
[19] Das, G. Tulasi Ram. "A structural & operational comparative study of converter topologies & analysis of MMC for high voltage applications." In Circuit, Power and Computing Technologies (ICCPCT), 2015 International Conference on, pp. 1-8. IEEE, 2015.

Impact of climatic condition on the wind speed of site Mumbai

K M Nisha[1] K.S Sandu[2]

Abstract— **Wind speed play a very important role for wind energy calculation. climate change is one of the key element which altering energy flow in the atmosphere, will affect the wind energy potential. here we propose a framework of evaluate the impact of climatic condition on the wind speed distribution. in this paper statistical method are used to evaluate the wind speed data of the site VABB airport situated in Mumbai district of India at 10 meter above the mean ground level, which affected by climatic condition. Present study carried out for two season winter and summer, from the analysis it has been found that most probable wind speed is 6.7m/s and 9.3 m/s respectively.**

***Keywords*— wind speed variation, temperature, pressure, seasonal wind speed.**

I. INTRODUCTION

Wind energy play a very important role in climate change mitigation, changes coupled with climate evolution will likely to be positive for wind energy industry and other expected negatively impact on wind energy potential development[1]. Basically the weather is a place represents the state of atmospheric conditions over a brief periods of a time. an analysis of a climatic condition for a particular region can help in assessing the seasons or periods during which a person may experiences painful conditions. there are various climate factor which affect the wind speed is temperature, pressure, precipitation and humidity etc. the temperature of a air in a shaded enclosure is know as ambient temperature, is represent in ºC. Temperature of given site depends on wind as well as local factor such as shading sunny condition. when wind speed is low, local factor highly affected on temperature of air but in higher wind speeds, the temperature of incoming air is less affected by local factor. temperature drops roughly 6.4 ºC for each kilometers of altitude gain under the normal working conditions. Wind speed changes according to altitude as well, increasing where temperature increasing however, it does not means linearly but according to power law wind speed function. in this paper we analyze, wind speed affected by the climatic change like temperature and pressure in Mumbai district of India and were given by the metrological department of India. Global climate model[5] and regional climate model[5] or bio climate chart is simple tool for analyzing the climate of a particular region, which is given by the MNRE[2]. In this paper, different techniques are used for analysis of climate factors. Techniques are graphic method, future data measurement and bioclimatic chart given by the MNRE. Mumbai is situated at latitude 19.12 ºN longitude 72.85ºE, Climate of Mumbai is mainly warm and humid. Even temperature is not high in summer but condition are uncomfortable due to high humidity, may is the hottest month with monthly average daily maximum temperature reaching as high as 32 ºc. here we use statistical method to calculate the wind speed variation.

[1]K M Nisha is with School of Renewable Energy and Efficiency, National Institute of Technology, Kurukshetra, India

[2]K S Sandu is with Department of Electrical Engineering, National Institute of Technology, Kurukshetra, India.

(e-mail: nisha.singh31.1992@gmail.com, kjssandhu@rediffmail.com)

II. MATHEMATICAL BACKGROUND

wind speed probability density function can be calculated as given below

$$f(v) = \frac{k}{c}(\frac{v}{c})^{k-1}\exp(-(\frac{v}{c})^{k}), \quad (1)$$

f(ν) is the probability function of observing wind speed ν, and c is the Weibull scale parameters and k is the dimension less Weibull shape parameters[3]. mostly, the scale parameters, c indicates how 'windy' a wind location under consideration is, and k is shape parameter which indicates how peaked the wind distribution is (i.e if the wind speed tend to be very close to a definite value, the distribution will have a high k value and be very peaked). if the mean, ν and the variance,σ^2 of the data are known the following approximation can be used to calculate the Weibull parameters k and c [4].

$$k = (\frac{\sigma}{\bar{v}})^{-1.086}$$

$$c = \frac{\bar{v}}{\Gamma(1 + 1/k)}$$

$$\bar{v} = \frac{1}{n}\sum_{i=1}^{n} v_i$$

where the average wind speed is v. and The variance $\sigma^2\sigma^2$, of wind velocity recordings [3].

$$\sigma^2 = \frac{1}{n-1}\sum_{i=1}^{n}(v_i - \bar{v})^2 \quad (2)$$

And the gamma function of (x) (standard formula) calculated as

$$\Gamma(x) = \int_0^{\infty} e^{-u}u^{x-1}du. \quad (3)$$

f(v) is the Weibull probability distribution of ν, the average wind power is

$$\bar{p_w} = \frac{\rho A v^{-3}\Gamma(1+3/k)}{2[\Gamma(1+1/k)]^3} \quad (4)$$

By Using that equation [4] the accessible wind energy can be calculated for any definite period of time. The energy output is calculated in watts per square meter, W/m².here ρ is the density of the wind commonly

expressed in kg/m³ and the wind area is defined by A in m².

III. DATA ANALYSIS

Ancient meteorological data of 11 year (2004-2014) comprising, such as, wind speed (in m/s), temperature(ºC), pressure (HPa) from area in and around VABB airport, Mumbai lying at geological coordinate 19.00886ºE at an altitude of 10 meters above the mean ground level has been build up for modeling and investigation purpose. each yearly sample divided into two categories, namely winter season and summer season constituting of 20 days (480 hours) each. Winter and summer data were accumulate from 28 January,00:0 hour to 16 february,23:59 hour and 28 July, 00:00 hour to 16 august, 23:59 hour, respectively, for each year at an interval of 30 minutes, building up a total of 48 observation/day/parameter. On closely inspection the data was observed that, wind speed, temperature, pressure pursue a daily trend in case of winter season and in case of summer season these parameter follow the random trends. data are shown in table I and table II.

TABLE I The data conditions at the mumbai site during the 20 days period in winter for pressure.

Year	Wind speed in m/s				Pressure (HPa)			
	Min	Max	Avg	σ^2	Min	Max	Avg	σ^2
Winter season								
2004	2.5	9	1.9	3	1006	1018	1012.2	3.9
2005	3	7.7	2	3.2	1008	1018	1013.3	4.2
2006	2	5.1	1.3	2.4	1009	1019	1013.7	3.3
2007	2.1	6.7	1.8	2.5	1010	1017	1013.2	2.3
2008	3	7.7	2	3.3	1009	1017	1012.4	2.9
2009	2.1	6.2	2.3	2.7	1008	1016	1012.2	2.5
2010	2.0	7.2	2.5	2.5	1009	1017	1012.7	2.6
2011	3.0	6.7	1.8	3.1	1006	1015	1010.9	4.1
2012	3.3	6.7	2.3	3.3	1008	1017	1012.3	2.4
2013	2.2	6.2	2.2	2.7	1007	1019	1012.0	5.3
2014	2.5	7.2	2.6	2.8	1007	1017	1011.2	3.7

TABLE II. The data conditions at the Mumbai site during the 20 days period in winter for temperature

Year	Wind speed in m/s				Temperature (ºC)			
	Min	max	Avg	σ^2	Min	max	avg	σ^2
Winter season								
2004	1.2	9	1.9	3	13	34	22.5	19.9
2005	1.5	7.7	2	3.2	15	36	26.6	12.6
2006	1.8	5.1	1.3	2.4	14	36	26.2	20.0
2007	2	6.7	1.8	2.5	18	37	25.6	10.6
2008	2.5	7.7	2	3.3	10	34	22.5	20.9
2009	2.1	6.2	2.3	2.7	16	33	25.3	12.6
2010	2.0	7.2	2.5	2.5	18	34	26.4	8.2
2011	3.0	6.7	1.8	3.1	16	35	26.2	10.5
2012	3.3	6.7	2.3	3.3	12	34	24.2	12.2
2013	2.2	6.2	2.2	2.7	15	36	25.8	11.8
2014	2.5	7.2	2.6	2.8	18	34	25.6	11.3

TABLE III The data conditions at the Mumbai site during the 20 days period in summer for temperature

year	Wind speed in m/s				Temperature (ºC)			
	Min	max	Avg	σ^2	min	max	avg	σ^2
Summer season								
2004	2.2	10.3	4.0	3.2	23.0	31.0	26.8	2.7
2005	2.5	11.3	4	2.3	24.0	31.0	27.2	1.7
2006	2.0	10.3	5.4	1.6	24.0	30.0	26.5	1.2
2007	4.0	10.8	4.4	4.0	24.0	31.0	27.6	1.9
2008	3.3	12.8	4.5	3.8	24.0	31.0	27.0	1.4
2009	1.8	9.8	5.0	1.8	26.0	31.0	28.5	.8
2010	2	8.8	3.9	2.7	25.0	31.o	27.7	1.8
2011	2	7.7	4.3	2.1	24.0	31.0	27.6	1.5
2012	1.8	9.3	4.7	1.9	25.0	31.0	28.1	.8
2013	1.3	9.3	4.8	1.5	25.0	30.0	27.2	.9
2014	2.0	9.3	4.7	1.9	25.0	31.0	27.6	1.9

TABLE IV The data conditions at the mumbai site during the 20 days period in summer for pressure

Year	Wind speed in m/s				Pressure (HPa)			
	Min	max	avg	σ^2	Min	Max	Avg	σ^2
Summer season								
2004	2.2	10.3	4.0	3.2	998.0	10009.5	1004.5	6.6
2005	2.5	11.3	4	2.3	998.0	1009.0	1004.0	5.8
2006	2.0	10.3	5.4	1.6	1000.0	1008.0	1003.8	3.2
2007	4.0	10.8	4.4	4.0	998.0	1009.0	1004.0	6.3
2008	3.3	12.8	4.5	3.8	997.0	1007.0	1002.8	5.5
2009	1.8	9.8	5.0	1.8	1002.0	1009.0	1005.9	2.2
2010	2	8.8	3.9	2.7	1000.0	1008.0	1004.3	2.8
2011	2	7.7	4.3	2.1	1000.0	1007.0	1003.3	2.4
2012	1.8	9.3	4.7	1.9	1002.0	1008.0	1004.9	2
2013	1.3	9.3	4.8	1.5	999.0	1009.0	1005.1	4.5
2014	2.0	9.3	4.7	1.9	1001.0	1009.0	1004.8	4.5

IV. METHODOLOGY

Artificial neural network based yearly auto regressive (ANNYAR) model[8] have been used to figure out the most influencing parameters affecting the wind prediction. These initialization when incorporated into any numerical weather prediction (NWR) model [8] would lead to best prediction results. data from area in and around VABB airport, Mumbai has been integrated for modelling and analysis purpose. after the prediction of wind data, analysis done with statistically technique and graph is plotted with the help of MATLAB.

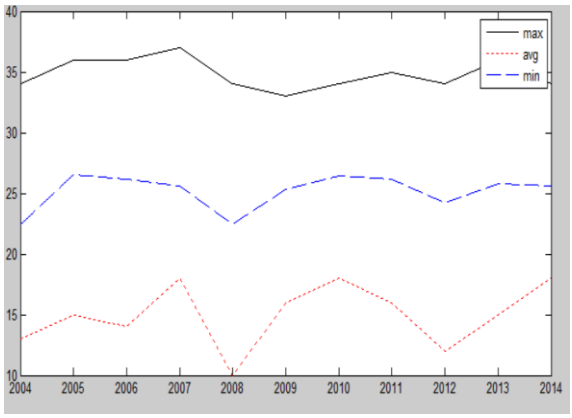

Fig 1. Temperature analysis in winter

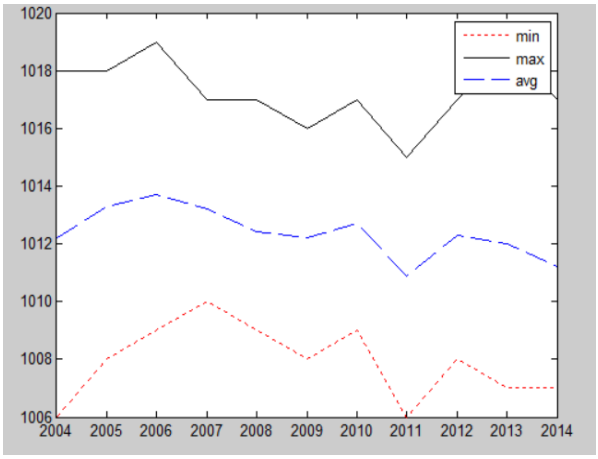

Fig 2. Pressure analysis in winter

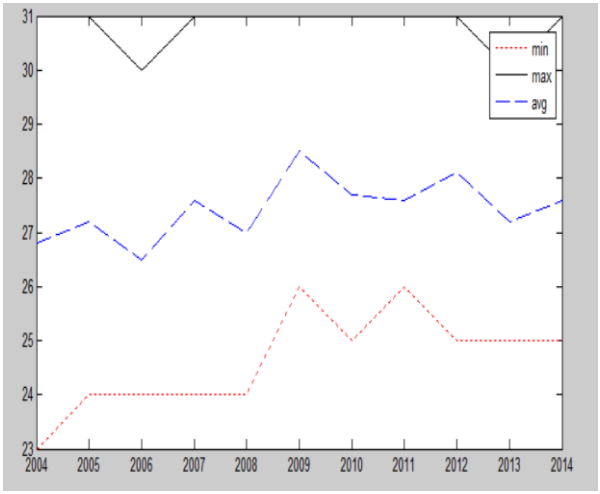

Fig 3. Temperature analysis in summer

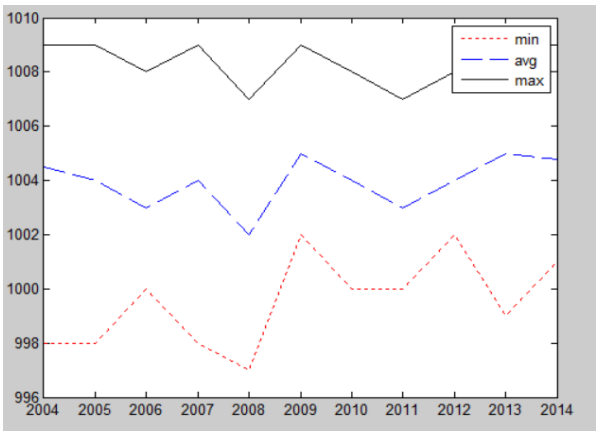

Fig 4. Pressure analysis in summer

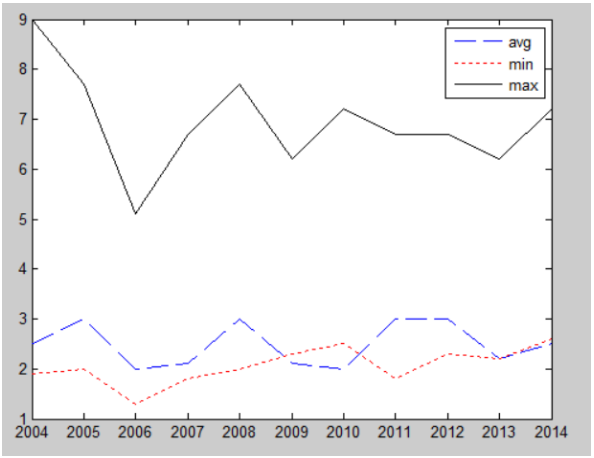

Fig 5. Wind speed in winter

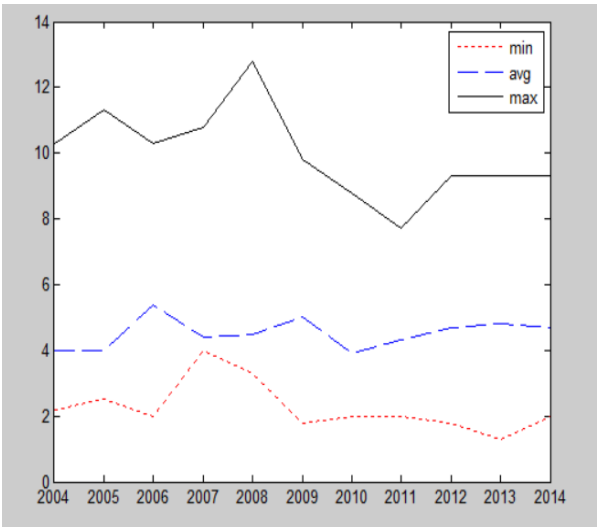

Fig 6. Wind speed in summer

V. RESULT ANALYSIS

Annual mean value of pressure based on short term observation decrease in the range of 1012 to 1019 in Mumbai. By comparing the long term data with short term data observation is concluded that large scale effect on annual pressure variation increase over 2005 to 2006.annual mean temperature values show 12 to 34 ºc increasing over 2007 to 2013 in winter and in summer decreasing from 34 to 31 and annual mean value of speed decreasing and increasing trends with respect to climatic condition.

VI. CONCLUSION

This study shows some local climatic condition pressure, humidity, temperature, and precipitation variations is cause of wind speed changes statistically. As shown in fig 1, fig 2,fig 3,fig 4,fig 5. Climate is very important factor for wind speed changes, and wind energy potential. Mumbai is having moderate wind energy potential in summer, in India.

REFERENCES

[1] Metz, et al. (Eds.), Climate change 2007: mitigation. Contribution of Working Group III to the fourth assessment report of the intergovernmental panel on climate change, Cambridge University Press, Cambridge, United Kingdom and New York, NY, USA (2007), pp. 252-32.

[2] S. Rangarajan. "Wind Energy Resource Survey for INDIA-V," 1998, pp. 159-167.

[3] S.O. Oyedepo, M.S. Adaramola and S.S. Paul. "Analysis of wind speed data andwind energy potential in three selected locations in south-east Nigeria." International Journal of Energy and Environmental Engineering, pp. 1-11, 2012.

[4] Sahin, Ahmet D., and Zekai Sen. "First-order Markov chain approach to wind speed modelling." Journal of Wind Engineering and Industrial Aerodynamics89.3 (2001): 263-269.

[5] P.L. Racsko, L. Szeidl, M. Semenov, A serial approach to local stochastic weather models, Ecol. Model. 57 (1991) 27–41.Christensen, Jens H., et al. "On the need for bias correction of regional climate change projections of temperature and precipitation." Geophysical Research Letters 35.20 (2008).

[6] Zuo H, Li D, Hu Y, Bao Y, Lu S (2005) Climate change trend and its relationships with pan evaporation in China during the last 40 years. Chin Sci Bull 50:1125–1130 (in Chinese).

[7] M.D.G. Dukes, J.P. Palutikof, Estimation of extreme wind speed with very long return periods, J. Appl. Meteor. 34 (1995) 1950–1961.

[8] H.S. Bagiorgas, M. Giouli, S. Rehman and L.M. AI-Hadhrami. "Weibull Parameters Estimation Using Four Different Methods and Most Energy-Carrying Wind Speed Analysis." International Journal of Green Energy", Vol. 8, pp. 529-554,2011.

[9] Agrawal, Alok, and Kanwarjit Singh Sandhu. "Most influential parametrical and data needs for realistic wind speed prediction", Renewable Energy, 2016.

Particle Swarm Optimization Algorithms for solving Economic Dispatch Problems Including Wind Farm for Emission Reduction

Jay Prakash Kumar Yadav[1], Pradeep Kumar[2]

***Abstract*— presently, electricity is the most popular form of energy, because of easy in its transportation at high efficiency and reasonable cost. Economic dispatch (ED) is a significant problem in power system operations and control, the objective of which is to minimize the operating cost of all the generating units in the power system network with the consideration of various system constraints. At minimum operational cost the power dispatch of thermal energy sources has been a crucial part of research since decades. This paper presents a brief overview on Economic Load Dispatch using PSO and helps to know how efficient and reliable this method is for the solution of any kind of optimization problems. In 1995, R. Eberhart, an electrical engineer along with a social psychologist J. Kennedy developed a random optimization technique to overcome some difficulties present in Genetic Algorithms (GA) which was later known as Particle Swarm Optimization. Due to problems of emission of harmful gases in the environment, the penetration of renewable energy sources, mainly wind power is increasing day by day.**

Index terms: ED Problem, wind power, optimization technique, Genetic Algorithms (GA), Particle Swarm Optimization (PSO).

I. INTRODUCTION

The economic dispatch (ED) can be defined as the problem that determines the power schedule or generation dispatch of connected generating units to the system to fulfill the requirement of the load demand at the lowest possible cost while considering the all generating units constraints. In early 1920s, the economic dispatch problem started at the time when few generators used to generate the power to satisfy the required load demand and the capacity exceeded the demand. At that time the main problem for the operator was to divide the load demand between the available power generating units. After that researchers started the study of economic load dispatch. Before 1930, some methods like "the base load method" and "the best point loading method" were developed. These methods were used in real time control to distribute the total power generation among the generating units committed to fulfill the load demand.

According to "The base load method", the most efficient generating unit used to generate the power to its maximum capacity first, after that the second most efficient generating unit was loaded. This process goes on till the demand is fulfilled. Since, the relationship between fuel cost and generated output power is quadratic, when we boost the power output of one generator, the operating cost of that generator increases immediately. Due to which, this approach does not give an economic solution. In the "best point loading method" people successively used to load the generating units to their lowest heat rate point. The operation starts with the most efficient generating unit followed by less efficient generating unit. This method is more efficient when compared with the "base load method". However, due to the quadratic cost-power relationship, this solution is also not an optimal solution.

In the beginning of 1930, "The equal incremental method" was popularly used to produce most economic results. This was described by H. Estrada in his paper "economical load allocation" in 1930 and by G.R. Hahn in his paper "Load division by the incremental method" in 1931. These two papers described the principle of "Equal incremental method" which states that the next increment in load demand should be balanced by the generating unit which has the lowest incremental cost. Steinberg also said that according to this principle, the equal incremental cost among all generating units can be achieved. Later, in 1934 Steinberg and Smith developed "The theory of incremental rates" [1-3]. In 1951, 1952 and 1953, Kron published four papers [4-7] in a series to give the idea of concise power network and loss modeling. The first two papers deliberated single area loss modeling and the latter two papers deliberated interconnected areas loss modeling.

In electric power industry, it remains always an important task to use the power generating systems efficiently. But, to use the power generating systems in an efficient manner, the availability of fuel for the production of electrical energy should be in abundant and also at optimum cost. At the same time, the power engineers and researchers always try to help the power industry to grow with the novel idea keeping in mind that during generation of the electrical power the environment should be least affected. Keeping this view in mind, in 1994[13], A. A. El-Keib published a paper on "Economic dispatch in view of the clean Air act of 1990". In 2009, Lakhwinder Singh and J.S. Dhillon presented a paper [17] on "Cardinal priority ranking based decision making for economic-emission dispatch problem". With the help of this paper Singh and Dhillon tried to pull the attention of the researchers towards the

[1]Jay Prakash Kumar Yadav is with Department of Electrical Engineering, National Institute of Technology, Kurukshetra, India
[2]Pardeep Kumar is with Department of Electrical Engineering, National Institute of Technology, Kurukshetra, India.
(e-mail: jpyadavau@gmail.com, pk@nitkkr.ac.in)

protection of the environment to dispatch the emission of the harmful gases along with the dispatch of the power generating units. This paper deals with the multi-objective optimization technique and helps to overcome the difficulties of single objective optimization technique.

PSO is a optimization technique which belongs to the class of evolutionary algorithms. Previously, the conventional PSO was used to solve only single objective problems but due to the advancement and development of new software in the field of research day by day, presently PSO is also capable to solve multi-objective problems. Inspired by the social behavior of animals and birds, in 1995, R. Eberhart and J. Kennedy developed the PSO technique which is now able to solve any kind of optimization problem. Recently, in February 2018, J.H. Lee published a paper [18] in which he has proposed the PSO technique for the study of electrical machine design.

Recently, the problems of environmental pollution have become noticeable to a great extent. Use of renewable energy resources helps to protect the environment by reducing the emission of harmful gases from fossil fuels. It also reduces the dependency of human on conventional energy sources. In modern power system operation, wind energy is utilized more than any other renewable energy resources. Worldwide, wind power installed capacity was more than 120.2 GW at the end of 2008 but this figure rises to 158.5 GW at the end of 2009, which shows a rise of 31.7% in a year. It indicates that, wind is the fastest growing renewable energy resource. On the other hand, the nature of wind is intermittent and non dispatchable, as wind speed is very much variable and restricted by site. It is crystal clear that due to the sporadic nature availability of wind energy, it degrades the system reliability. Due to the lack of well-suited techniques in the past, the utilization of wind energy has been ignored on a large scale [19, 20, 21, and 22].

With a view to know the probable advantage while using wind as a possible energy option, estimate the effect of wind energy conversion system (WECS) on system reliability. The WECS faces some problems in analyzing the generating system capabilities. Generally, modeling of WECS becomes difficult due to the nonlinear relationship between the power output of WTG and wind velocity. After the proposal of Monte Carlo approach, modeling of WECS becomes easier. Because, in this approach, an hourly random simulation is to be done, this makes the working performance of the generating system better. For hourly simulation of wind speed, an auto-regressive and moving average (ARMA) time series model is exercised, due to which, the available wind power recon with ordered characteristics[23, 24, 25, 26].

In the last few years, due to increase in cost of fossil fuels and risk of climate change Wind energy has developed rapidly. The Global Wind Energy Council anticipated that, global wind capacity will be increased from 237.7 GW at the end of 2011 to 493.3 GW at the end of 2016. The European Wind Energy Association has also predicted that the total installed wind energy capacity in Europe should reach 230 GW by 2020 and 400 GW by 2030. China became the country with largest installed wind power capacity in the world in 2011 with 62.4 GW. Wind turbines which have higher power capacity, lower cost and higher reliability are required to meet the accelerated demand to electrical power. The most likely generating systems are direct drive generators, because, the direct-drive system facilitates the drive sequence, and makes the overall efficiency and reliability better [27].

To meet the target of reducing the emission of harmful gages like carbon dioxide(CO_2), sulphur dioxide(SO_2), and oxides of nitrogen(NO_x) from the electrical power generating plants which are badly affecting our environment, the policy makers prefer to promote renewable energy sources, especially wind [28].

II. PROBLEM FORMULATION [11,17]

The multi objective optimization problem can be formulated in the following steps:

A. *Minimization of fuel cost*

$$F_i(P_{Gi}) = \sum_{i=1}^{N_g}\left(a_i {P_{Gi}}^2 + b_i P_{Gi} + c_i\right) \$/h \quad (1)$$

Where the cost coefficients of i^{th} generator are denoted by a_i , $b_i, and\ c_i$ respectively.

B. *Minimization of emission*

- Minimize NO_x emission.

$$F_i(P_{Gi}) = \sum_{i=1}^{N_g}\left(d_{1i}{P_{Gi}}^2 + e_{1i}P_{Gi} + f_{1i}\right) \text{ kg/h} \quad (2)$$

Where, the NO_x emission coefficients of i^{th} generator are denoted by $d_{1i}, e_{1i}\ and\ f_{1i}$.

- Minimize SO_x emission.

$$F_i(P_{Gi}) = \sum_{i=1}^{N_g}\left(\mathrm{d_{2i}{P_{Gi}}^2 + e_{2i}P_{Gi} + f_{2i}}\right) \text{kg/h} \quad (3)$$

Where, the SO_x emission coefficients of i^{th} generator
$are\ denoted\ by\ d_{2i}, e_{2i}\ and\ f_{2i}$.

- Minimize CO_x emission.

$$F_i(P_{Gi}) = \sum_{i=1}^{N_g}\left(\mathrm{d_{3i}{P_{Gi}}^2 + e_{3i}P_{Gi} + f_{3i}}\right) \text{ kg/h} \quad (4)$$

Where, the CO_x emission coefficients of i^{th} generator are denoted by $d_{3i}, e_{3i}\ and\ f_{3i}$.

C. *Problem Constraints*

- Equality constraint

The total real and reactive powers generated must meet the total demand and losses in the system.

$$\sum_{i=1}^{N_g} P_{Gi} = \sum_{i=1}^{N_b} P_{Di} + P_{loss} \quad (5)$$

$$\sum_{i=1}^{N_g} Q_{Gi} = \sum_{i=1}^{N_b} Q_{Di} + Q_{loss} \quad (6)$$

Where,

N_g are the numbers of generator in the system and N_b are the number of buses in the system.

The real and reactive powers of i^{th} generator are indicated by P_{Gi} and Q_{Gi} respectively.

Real and reactive power demands at i^{th} bus are denoted by P_{Di} and Q_{Di} respectively.

Real and reactive power losses in the transmission lines are denoted by P_{loss} and Q_{loss} respectively.

- Inequality constraint

To ensure stable operation, each generating unit is restricted by its lower and upper limits of real and reactive power outputs.

$$P_{Gi}^{min} \leq P_{Gi} \leq P_{Gi}^{max};\ \text{i} = 1, 2 \ldots .N_g \quad (7)$$

$$Q_{Gi}^{min} \leq Q_{Gi} \leq Q_{Gi}^{max};\ \text{i} = 1, 2 \ldots .N_g \quad (8)$$

Where, the minimum and maximum values of real power output of i^{th} unit are denoted by P_{Gi}^{min} and P_{Gi}^{max} respectively and the minimum and maximum values of reactive power output of i^{th} unit are indicated by Q_{Gi}^{min} *and* Q_{Gi}^{max} , respectively.

- Power transmission losses.

The real and reactive power transmission losses, P_{loss} and Q_{loss} are given by following equations.

$$P_{loss} = \sum_{i=1}^{N_b} \sum_{j=1}^{N_b} [A_{ij}(P_i P_j + Q_i Q_j) + B_{ij}(Q_i P_j - P_i Q_j)] \quad (9)$$

$$Q_{loss} = \sum_{i=1}^{N_b} \sum_{j=1}^{N_b} [C_{ij}(P_i P_j + Q_i Q_j) + D_{ij}(Q_i P_j - P_i Q_j)] \quad (10)$$

Where

$$P_i + jQ_i = (P_{Gi} - P_{Di}) + \text{j}\,(Q_{Gi} - Q_{Di}) \quad (11)$$

$$A_{ij} = \frac{R_{ij}}{|V_i|\,|V_j|} \cos(\delta_\text{i} - \delta_\text{j}) \quad (12)$$

$$B_{ij} = \frac{R_{ij}}{|V_i|\,|V_j|} \sin(\delta_\text{i} - \delta_\text{j}) \quad (13)$$

$$C_{ij} = \frac{X_{ij}}{|V_i|\,|V_j|} \cos(\delta_\text{i} - \delta_\text{j}) \quad (14)$$

$$D_{ij} = \frac{X_{ij}}{|V_i|\,|V_j|} \sin(\delta_\text{i} - \delta_\text{j}) \quad (15)$$

Where, loss coefficients are denoted by A_{ij}, B_{ij} , C_{ij} and D_{ij} . By performing load flow analysis, these coefficients are calculated from line data and are evaluated from line data by performing DLF analysis. Load angles at i^{th} and j^{th} buses are denoted by δ_i and δ_j respectively.

Voltage magnitude at i^{th} and j^{th} buses are indicated by V_i and V_j , respectively.

The real component of bus impedance matrix is denoted by R_{ij}.

The reactive component of impedance bus matrix is X_{ij}.

III. Principle of Multiobjective Optimization [16]

In recent days, several problems of the power industry needs the optimization of more than one objective functions at the same time. Generally, these objective functions are not of the same nature. The optimization of this type of objective functions is known as multi objective optimization which leads to a set of optimal solutions rather than one optimal solution. While considering all objective functions, due to the occurrence of set of the optimal solutions, not anyone solution can be considered to be more appropriate than other. These optimal solutions are called pareto-optimal solutions. Any two solutions x and y in multi objective optimization may have two chances: one can dominate the other or no one can dominate the other. In an optimization problem without losing universality of solution, x dominates y, if the given two conditions are fulfilled.

A. $\forall i \in \{1,2, \ldots . N_{obj}\} : f_i(x) \leq f_i(y)$

B. $\exists j \in \{1,2, \ldots . N_{obj}\} : f_j(x) < f_j(y)$

If none of the mentioned two conditions are disobeyed, then x is called non dominated solution. Within the whole search space, the non-dominated solutions are denoted as Pareto optimal and constitute a Pareto optimal set also called Pareto optimal front.

IV. Evolutionary Algorithms PSO [14, 16 &18]

A. Evolutionary algorithm (EAs)

Evolutionary Algorithms are gaining popularity, as along with overcoming the shortcomings of the traditional search methods. They work perfectly for the complex systems and provide better results. Steps of evolutionary algorithms are mentioned in the flow chart given below in fig.1.

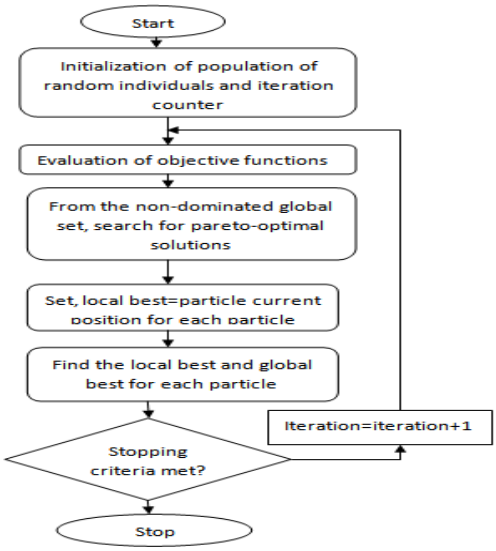

Fig.1. Flowchart of evolutionary algorithms

B. The concept of PSO

According to PSO technique, particles move in the search space of optimization problem and each particle updates new position based on own previous position and velocity. The swarm (population) of particles in an n-dimensional search space is simulated, where each particle has a position and a velocity. The position of a particle confirms the candidate solution to the optimization problem. Inspired by behavior of birds

flocking and fish schooling, each particle searches for worthier position in the search space by changing its velocity. The direction of search will be decided based on the velocity vector of an individual particle. The search will continue in the same direction if it has an explorative or an exploitive nature and each individual is treated as a volume less particle (a point) in the n-dimensional search space.

C. PSO algorithm using for EDP

STEP1: Set the initial conditions of P_{Gi}.
STEP2: Set the initial conditions of velocity V_i.
STEP3: objective function: $F_i(P_{Gi}) = \sum_{i=1}^{N_g}(\mathrm{a_i P_{Gi}}^2 + \mathrm{b_i P_{Gi}} + \mathrm{c_i})\$/\mathrm{h}$.
STEP4: Substitute the initial value of P_G in step3 and find the cost corresponding to each generator.
STEP5: Choose the best generator i.e. the least cost generator.
Step6: Initialize position of the particles as $x = [x_1, x_2, \ldots . x_i]$.
Step7: Initialize velocity of the particles as $v = [v_1, v_2, \ldots . v_i]$.
STEP8: set the time counter t=0.
STEP9: Update the time counter t=t+1.
STEP10: Update velocity:

$$v_{ij}(t+1) = w(t+1)v_{ij}(t) + r_1 c_1\left[p_{ij}(t) - x_{ij}(t)\right] + r_2 c_2\left[g_j(t) - x_{ij}(t)\right]$$

In all three added terms, the first term is called inertia term, the second term is called cognitive component and the third term is called social component.
This is the equation for updating the velocity for particle i in time step t. where, $r_1 and r_2$ are uniformly distributed random numbers in [0, 1] and $c_1 and c_2$ are positive constants. If a particle violates the velocity limits, set its velocity equal to the proper limit.

STEP11: Update position:

$$x_{ij}(t+1) = x_{ij}(t) + v_{ij}(t+1)$$

STEP12: Replace $v_{ij}(t+1)$ with $P_{Gi}(t+1)$ and $x_{ij}(t+1)$ with $F_i(P_{Gi})(t+1)$.

STEP13. Repeat the objective step by step as we go from one iteration to the next iteration.
STEP14: We calculate the cost function in each iteration till the difference in cost for time step t+1 and in time step t becomes approx. zero otherwise go to step 9.

V. MERITS AND DEMERITS OF PSO ALGORITHM

A. Merits

- PSO is a meta-heuristic algorithm which has ability to solve extensive non-convex optimization problems like optimal power flow.
- PSO algorithm does not involve selection operation or mutation calculation. The search can be carried out by repeatedly varying particle's speed.
- Simple in notion, easy in usage and computational efficiency are the main supremacy of PSO algorithm.
- By learning from group's experiences, particles fly only to good areas (where there is a possibility of finding food).
- Fast convergence speed is the distinguished quality of PSO.
- By adjusting only few parameters, PSO algorithm can be realized.
- PSO has the limberness to make the balance between the global and local reconnaissance of the search space.
- PSO may conveniently take care of non-differentiable and non-convex objective functions.

B. Demerits

- Standard PSO suffers from a considerable rise in search complexity with increase in dimension of search space.
- Tendency to a fast and premature convergence in mid optimum points

VI. MODELLING AND SIMULATION RESULTS OF WIND FARM

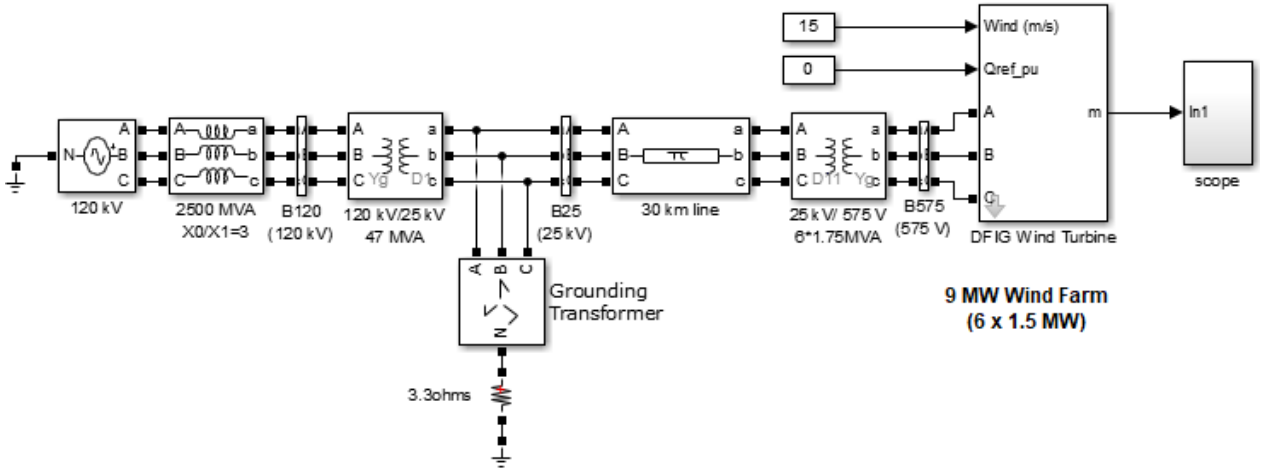

Fig. 2. Modeling of wind farm with DFIG

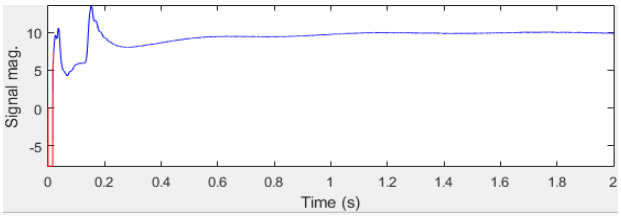

3(a) Real power Vs time graph

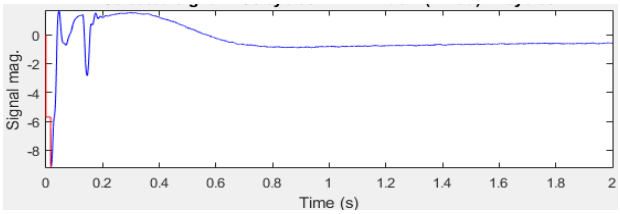

3(b) Reactive power Vs time graph

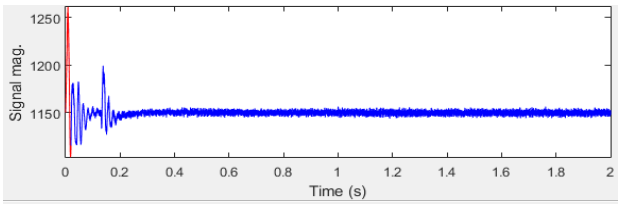

3(c) DC voltage Vs time graph

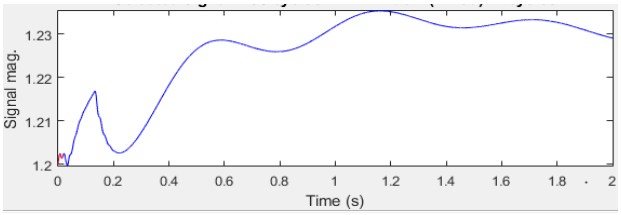

3(d) Wind speed Vs time graph

Fig.3 Simulation results of wind farm model

Modeling of wind farm and its simulation results are depicted in figure. (2) and (3). By simulating the detailed model of wind farm using DFIG, four results are obtained which are shown in figure (3). In figure 3(a), the variation of real power is obtained with increase in time. In figure 3(b), the variation of reactive power with respect to time is found. In figure 3(c), the variation of DC voltage is obtained with increasing time. In figure 3(d), the variation of wind speed with respect to time is shown.

VII. CONCLUSION

An innovative multi objective PSO technique has been reviewed in this paper and it gives a basic idea about how we can apply this technique to dispatch both cost and environmental pollution at the time when we meet the constraints given in the literature. The proposed multi objective PSO technique helps the researchers to overcome some of the difficulties of the conventional single objective PSO algorithm. A detail algorithm of how effectively multi objective PSO technique can be used to solve economic dispatch problem has been discussed. Due to the flexibility and versatility of this algorithm, it has great potential for use in a variety of real life systems. A detailed modeling of wind farm with the help of Doubly Faded Induction Generator (DFIG) and its simulation results are obtained.

REFERENCES

[1] E.C.M. Stahl, “Economic loading of generating stations,” Electrical Engineering, pp. 722-727, September 1931.

[2] M.J. Steinberg and T. H. Smith, “Incremental loading of generating stations,” Electrical Engineering, pp. 674-677, October 1933.

[3] M.J. Steinberg and T. H. Smith, “The theory of incremental rates and their practical application to load divison-part1,” Electrical Engineering, pp. 432-445, March 1934.

[4] G. Kron, “Tensorial analysis of integrated transmission systems part i. the six basic reference frames,” Transactions of the American Institute of Electrical Engineers, vol. 70, pp. 1239-1248, 1951.

[5] G. Kron, “Tensorial analysis of integrated transmission systems; part ii. Off nominal turn ratios [includes discussion],” Transactions of the American Institute of Electrical Engineers Power Apparatus and Systems, vol. 71, pp. 814-822,1952.

[6] G. Kron, “Tensorial analysis of integrated transmission systems; part iii. The "primitive" division [includes discussion],”Transactions of the American Institute of Electrical Engineers Power Apparatus and Systems, vol. 71, pp.505-512, Jan 1952.

[7] G. Kron, “Tensorial analysis of integrated transmission systems; part iv. the interconnection of transmission systems [includes discussion],” Transactions of the American Institute of Electrical Engineers Power Apparatus and Systems,vol. 72, pp. 827-839, Jan 1953.

[8] Glimn, L. Kirchmayer, R. Habermann, and R. Thomas, “Automatic digital computer applied to generation scheduling [includes discussion],” Transactions of the American Institute of Electrical Engineers Power Apparatus and Systems, Part III, vol. 73, no. 2, Jan 1954.

[9] J. E. Van Ness, “A note on incremental loss computation,” Transactions of the American Institute of Electrical Engineers Power Apparatus and Systems, Part III, vol. 81, no. 3, pp. 735-737, April 1962.

[10] J. Tudor and W. Lewis, “Transmission losses and economy loading by the use of admittance constants,” IEEE Transactions on Power Apparatus and Systems, vol. 82, no. 68, pp. 676-683, Oct 1963.

[11] W. Dommel, W.F.Tinney,” Optimal Power Flow Solutions” IEEE Transactions, Vol. PAS-87, pp. 1866-1876, March 1968.

[12] H. Happ, “Optimal power dispatch,” IEEE Transactions on Power Apparatus and Systems, vol. PAS-93, no. 3, pp. 820-830, May 1974.

[13] A. A. El-Keib “Economic Dispatch in view of the clean air act of 1990” IEEE Transactions on Power Systems, Vol. 9, No. 2, May 1994.

[14] Farag, “Economic Load Dispatch multiobjective optimization procedures using Linear Programming Techniques,” IEEE Transactions on Power Systems, Vol. 10, No. 2, May 1995.

[15] R. Eberhart and J. Kennedy, “A New Optimizer Using Particle Swarm Theory,” IEEE Transaction, pp. 39-43, 1995.

[16] M.A. Abido, “Multiobjective particle swarm optimization for environmental/economic dispatch problem”, ELSEVIER , pp. 1105-1113, 2009.

[17] Lakhwinder Singh and J.S. Dhillon, “Cardinal priority ranking based decision making for economic-emission dispatch problem,” International Journal of Engineering, Science and Technology Vol. 1, No. 1, pp. 272-282, December 2009.

[18] Jin Hwan Lee, " Particle Swarm Optimization algorithm with intelligent particle number control for Optimal design of Electric Machines," IEEE Transactions on industrial electronics , Vol. 65, NO.2, pp.1791-1798, February 2018.
[19] D. Jayaweera, G. Burt and J.R. McDonald, "Customer Security Assessment in Distribution Networks with High Penetration of Wind Power," IEEE Transactions on power systems, vol. 22, no. 3, pp. 1360-1368, August 2007.
[20] H. Bevrani and P.R. Daneshmand, "Fuzzy logic based load frequency control concerning high penetration of wind turbines," IEEE system journal, vol. 6, no. 1, pp. 173-180, March 2012.
[21] F. Yao, Z.Y. Dong, K. Meng, Z. Xu, H. Ho-Ching Iu, and K. P. Wong, "Quantum-Inspired Particle Swarm Optimization for Power System Operations Considering Wind Power Uncertainty and Carbon Tax in Australia," IEEE Transactions on industrial informatics, vol. 8, no. 4, pp. 880-888, November 2012.
[22] N. Yan, Z. Xia Xing, Wei Li, and Bo Zhang, "Economic Dispatch Application of Power System with Energy Storage Systems," IEEE Transactions on applied superconductivity, vol. 26, no. 7, October 2016.
[23] R. Billinton and R. Karki, "Capacity reserve assessment using system well-being analysis," IEEE Transactions on Power Systems, vol. 14, pp. 433–438, May 1999.
[24] P. Giorsetto and K.F Utsurogi, "Development of a new procedure for reliability modeling of wind turbine generators," IEEE Transactions on Power Apparatus and Systems, Vol. 102, No 1, pp. 134-143,January 1983.
[25] R. Billinton, H. Chen and R. Ghajar, "A sequential simulation technique for adequacy evaluation of generating systems including wind energy," IEEE Transactions on energy conversion, vol. 11, no. 4, pp. 728-734, December 1996.
[26] J. Hetzer, D.C. Yu, and K. Bhattarai, "An economic dispatch model incorporating wind power," IEEE Transactions on Energy Conversion, vol. 23, no. 2, pp. 603-611, 2008.
[27] R. Qu, Y. Liu and J. Wang, "Review of Superconducting Generator Topologies for Direct-Drive Wind Turbines," IEEE Transactions on applied superconductivity, vol. 23, no. 3, June 2013.
[28] E. Denny, and M. O'Malley, "Wind Generation, Power System Operation and Emissions Reduction," IEEE Transactions on power systems, vol. 21, no. 1, pp. 341-347, February 2006.

4.2 Solar Energy-Facilitation, Modeling and System Design

India, which ranked 6th in global solar power installed capacity production in 2017-18, has a tropical climate and has sun exposure almost all round the year in most part of the country. The solar insolation ranges between 4-7 kWh per sq. m every day. The nation gets enough solar energy to create in excess of 500,000 TWh of power, expecting approximately 10% utilization through solar PV modules.

The availability of solar radiation data from satellite has made it possible to estimate the solar resource at any location over very large geographical areas, typically on a continental scale. Combining these data with temperature and wind data from reanalysis data sets or meteorological models makes it possible to estimate the performance of PV modules taking into account many of the effects that influence their performance, and doing so at any location. A study for estimation and design of installation of rooftop solar system was done in the state of Haryana, India whereby it was found that the mean global solar radiant exposure over period of a year varies from 3.25 KWh/m²/day in the month of Jan to 7.22 KWh/m²/day in the month of May. For System sizing and specifications, statistical analysis using these data collected is immensely required which includes solar radiation data, resource availability and other factors.

It is well known that the energy conversion efficiency of photovoltaic (PV) modules depends on a number of different external influences. Among these influences are:

• The reflectivity of the module surface, and in particular the way this reflectivity depends on the angle at which the incoming light hits the module surface.

• The light conversion efficiency depends on the wavelength of the light. The module efficiency will therefore change with variations in the spectrum of the sunlight.

• The efficiency depends on the temperature of the PV module. The module temperature will in turn depend on the temperature of the surrounding air, on the light intensity and on the local wind speed.

• Even when all these influences are held constant, the efficiency will still depend on the light intensity

• Some PV module types show variations in module efficiency that is caused by long-term exposure to sunlight and/or high temperatures.

As mentioned above, the output power of photovoltaic (PV) modules and systems depends on the irradiation falling on the PV module surface. This irradiation falling on PV module surface is in turn dependent upon the orientation and tilt angle. The solar PV array output can be optimized using tilt and orientation and its estimation can be done using various models and simulation techniques .Among different modeling and simulation techniques used, MATLAB/Simulink is widely used. Simulation platforms like Simscape simulation can also be used to analyze the characteristics of PV module under controlled environmental factors viz. solar irradiance and temperature, etc.

All the effects that cause the module efficiency to deviate from the efficiency measured under Standard Test Conditions (STC), defines the rated or nominal power of a given module. In addition to these effects there are of course, other reasons why the energy production of a given PV system would vary, which range from the details of installation (inclination angle, possible shadows) to the total amount of solar radiation at the site of installation, or the probability of dust or snow deposition.

However, these are mostly not intrinsic to the module type and would tend to depend more on the details of installation than on the physical properties of the module. We could say that the effects listed above cause different modules installed in the same way and place to give different power output while these other effects would cause the same module to have different power output when mounted in a different way or place.

High initial investment and limited life span of a photovoltaic (PV) array make it hindrance for the user to extract maximum power from the PV system. The nonlinear *i–v* characteristics of the PV array and the rotation and revolution of the earth around the sun, further necessitate the application of maximum power point tracking (MPPT) to the system. In this context, grid connected PV systems have become very popular because they do not need battery back-ups to ensure MPPT. Stand alone systems can also achieve MPPT, but they would need suitable battery back-ups for this purpose.

Though, multistage systems have been reported for certain applications, grid connected PV systems usually employ two stages [Fig. 1(a)] to appropriately condition the available solar power for feeding into the grid. While the first stage is used to boost the PV array voltage and track the maximum solar power, the second stage inverts this dc power into high quality ac power. Typically, the first stage comprises of a boost or buck-boost type dc–dc converter

topology. Such two-stage configurations are time tested and work well, but have drawbacks such as higher part count, lower efficiency, lower reliability, higher cost and larger size.

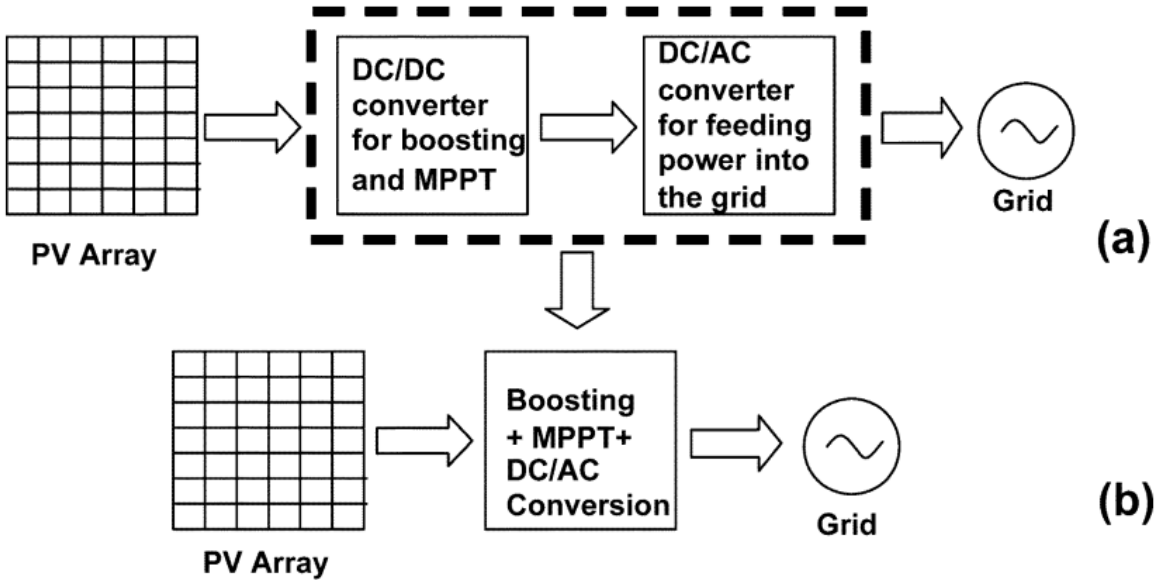

Fig. 1. Grid connected PV system topologies: (a) conventional two-stage and (b) single-stage configuration.

Facilitations and Bottlenecks of Solar Energy in India

Nivedita Naik[1], Shelly Vadhera[2]

***Abstract*— To cater the needs of 1.8 billion population of India and a growing economy, the power sector is highly pressurized to develop reliable, sustainable and clean energy. Constrained fossil reserves and environmental issues require continuous energy supply choices that utilize renewable energy sources and are economic at the same time. In India, the electricity demand is extremely high. Hence solar energy and vast unusable land areas have facilitated the purpose of clean and continuous energy supply. These elements together make India a perfect nation for the execution of power production using renewable energy sources. In this paper, ongoing schemes and targets taken up by Government of India relative to solar energy are discussed. Besides, there are a few problems which come along with the production of solar power using solar PV modules and solar thermal plants.**

Keywords—Solar energy, JNNSM,Problems.

I. INTRODUCTION

The solar energy sector has represented the biggest limit expansion to the Indian power network so far this year. Our Nation is honored with around 300 radiant days in a year and solar insolation of 4-7 kWh per Sq. m every day. If this energy is harnessed effectively, it can without much of a stretch decrease our energy deficiency situation and that to with no carbon emission. Numerous states in India have officially perceived and identified solar energy potential and other are arranged to meet their developing energy needs with perfect and everlasting solar energy.

II. SOLAR IRRADIANCE IN INDIAN SUBCONTINENT

Indian subcontinent lies in southern Asia. It has its latitude between 8.4^o and 37.68^o north and longitude between 68.7^o and 97.38^o east. The climate stays warm throughout the year as most of the regions lie in the tropics. The nation gets enough solar energy to create in excess of 500,000 TWh of power, expecting approximately 10% utilization through solar PV modules.

India has a relatively large population accounting to nearly 18% to that of world's and has the third largest economy [3]. To keep pace with the rising demand of power supply, our country mostly depends on thermal sources for power production.

[1]Nivedita Naik is with School of Renewable Energy and Efficiency, National Institute of Technology, Kurukshetra, India
[2]Shelly Vadhera is with Department of Electrical Engineering, National Institute of Technology, Kurukshetra, India.
(e-mail: niveditanaik92@gmail.com, shelly_vadhera@rediffmail.com)

TABLE I. ANNUAL REPORT OF SOLAR POTENTIAL IN DIFFERENT STATES

SI. No.	States/UTs	Solar *(MWp)*
1	Andhra Pradesh	38440
2	Arunachal Pradesh	8650
3	Assam	13760
4	Bihar	11200
5	Chhattisgarh	18270
6	Goa	880
7	Gujarat	35770
8	Haryana	4560
9	Himachal Pradesh	33840
10	Jammu & Kashmir	111050
11	Jharkhand	18180
12	Karnataka	24700
13	Kerala	6110
14	Madhya Pradesh	61660
15	Maharashtra	64320
16	Manipur	10630
17	Meghalaya	5860
18	Mizoram	9090
19	Nagaland	7290
20	Orissa	25780
21	Punjab	2810
22	Rajasthan	142310
23	Sikkim	4940
24	Tamil Nadu	17670
25	Telangana	20410
26	Tripura	2080
27	Uttar Pradesh	22830
28	Uttarakhand	16800
29	West Bengal	6260
30	Andaman & Nicobar	0
31	Chandigarh	0
32	Dadra & Nagar Haveli	0
33	Daman & Diu	0
34	Delhi	2050
35	Lakshadweep	0
36	Puducherry	0
37	Others	790
	Total	748990

To combat with the environmental issues, India is also focusing on energy production through renewable sources.

The total installed capacity in India is reported to be 330 GW as on 31.12.2017 [2].

TABLE II. CONTRIBUTION OF DIFFERENT SECTORS IN TOTAL INSTALLED CAPACITY [2]

Serial no.	Fuel	MW	% of Total
1	Total Thermal	2,18,960	66.20%
1.1	Coal	1,92,972	58.30%
1.2	Gas	25,150	7.60%
1.3	Oil	838	0.30%
2	Hydro	44,963	13.60%
3	Nuclear	6,780	2.00%
4	RES* (MNRE)	60,158	18.20%
	Total	330,861	

III. JAWAHARLAL NEHRU NATIONAL SOLAR MISSION

India aims to meet its energy demands in a mindful, practical and eco-friendly way. The National Action Plan on Climate Change (NAPCC) in June 2008 recognized the potential of solar energy in the nation and sought it as a National Mission. "Jawaharlal Nehru National Solar Mission" (JNNSM) was then approved by GOI in November 2009.

The Jawaharlal Nehru National Solar Mission (JNNSM) was established with a mission of generating 20,000 MW of grid connected and 2 GW of Off-grid capacity by 2022 and make solar power generation cost economic in the nation. The mission was to be achieved in three phases:

A. *Phase 1(2010-13)*
- Utility grid connected power: 1000-2000 MW
- Off-grid solar power: 200 MW.

B. *Phase 2(2013-17)*
- Utility grid connected power: 4000-10,000 MW
- Off-grid solar power: 1000 MW.

C. *Phase 3(2017-2022)*
- Utility grid connected power: 20000 MW
- Off-grid solar power: 2000 MW

Before declaration of JNNSM, India's solar power capacity was almost 17.8MW in mid 2010. Toward the finish of 1st phase capacity expansion of 1000 MW was accomplished through solar PV plants and solar thermal plants.

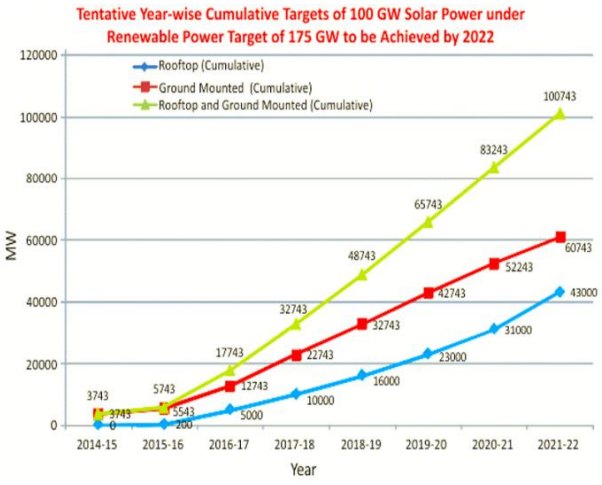

Fig 1 Tentative Year-wise cumulative targets of 100 GW solar power till 2022 [4]

TABLE III. TENTATIVE STATE-WISE DISTRIBUTION OF 175 GW OF RENEWABLE ENERGY SOURCES [6]

State/UTs	Solar Power (MW)	Wind (MW)	SHP (MW)	Biomass (MW)
Delhi	2762	-	-	-
Haryana	4142	-	25	209
Himachal Pradesh	776	-	1500	-
Jammu & Kashmir	1155		150	-
Punjab	4772	-	50	244
Rajasthan	5762	8600	-	-
Uttar Pradesh	10697	-	25	3499
Uttarakhand	900	-	700	197
Chandigarh	153	-	-	-
Northern Region	**31120**	**8600**	**2450**	**4149**
Goa	358	-	-	-
Gujarat	8020	8800	25	288
Chhattisgarh	1783	-	25	-
Madhya Pradesh	5675	6200	25	118
Maharashtra	11926	7600	50	2469
D. & N. Haveli	449	-	-	-
Daman & Diu	199	-	-	-
Western Region	**28410**	**22600**	**125**	**2875**
Andhra Pradesh	9834	8100	-	543
Telangana	-	2000	-	-
Karnataka	5697	6200	1500	1420
Kerala	1870	-	100	-
Tamil Nadu	8884	11900	75	649
Puducherry	246	-	-	-
Southern Region	**26531**	**28200**	**1675**	**2612**
Bihar	2493	-	25	244
Jharkhand	1995	-	10	-
Orissa	2377	-	-	-
West Bengal	5336	-	50	-
Sikkim	36	-	50	-
Eastern Region	**12237**	**-**	**135**	**244**
Assam	663	-	25	-
Manipur	105	-	-	-
Meghalaya	161	-	50	-
Nagaland	61	-	15	-
Tripura	105	-	-	-
Arunachal Pradesh	39	-	500	-
Mizoram	72	-	25	-
North eastern	**1205**	**-**	**615**	**-**
Region				
Andaman & Nicobar	27	-	-	-
Island				
Lakshadweep	4	-	-	-
Other	-	600	-	120
All India	**99533**	**60000**	**5000**	**10000**

The Government in year 2015 increased the target to 175 GW by the year 2022 which incorporates 100 GW from solar, 60 GW from wind, 10 GW from bio-power and 5 GW from small hydro-power. The capacity focus of 100 GW set under the National Solar Mission (JNNSM) will chiefly include 40 GW rooftop and 60 GW through large and medium scale grid.

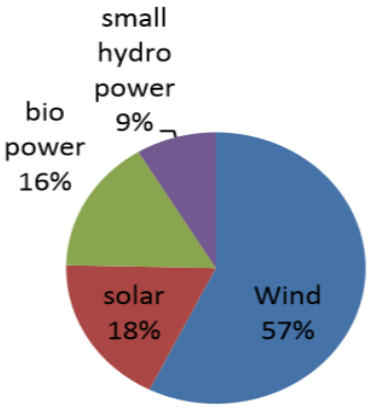

Fig 2. Graph showing sector-wise Installed Capacity of Renewable Energy in India as on 31.12.2016 in MW

IV. HIGHLIGHTS

- India now ranks 6th in global solar power installed capacity.
- By November 2017, roughly 62 GW Renewable Power installed, of which 27 GW have been introduced since May 2014 and 11.79 GW since January 2017.
- Record Low Tariffs for Solar of Rs. 2.44/unit and Wind Rs. 2.64/unit accomplished through transparent bidding and facilitation.

V. BOTTLENECKS IN SOLAR POWER PRODUCTION AND UTILIZATION

A. *Land Use*

The land is limited and per-capita land availability is low. Using land for solar energy production hinders other needs of the people. The area of land for utility-scale solar parks is approximately 1 km^2 (i.e. 250 acres) for every 40–60 MW of power being generated. An alternative for this problem is to use the water bodies like canals, lakes, solar farm ponds and the sea for large scale production of solar power. Another alternative can be to use integrated solar utilities like solar window.

B. *Manufacturing Cost*

Semi- conductor material used in solar PV cells require clean manufacturing environment and is costly to make and maintain. This increases the cost of the solar PV panels.

C. *Transportation of Power*

Big solar parks are built in desert areas which have reduced the installation cost since better economy-of-scale is made (parts, material & installation volunteers present in same location). But these large, economic land areas are found far from places where power is consumed. Advanced transmission line is required for this purpose which increases the price of installation.

D. *Maintenance Cost*

Support expenses and time is required since each portion of a solar board must be kept spotless and clear of dirt to work effectively. The efficiency drops even when a little segment is hindered by fallen debris and dust film.

E. *Storage*

The renewable sources of energy are intermittent in nature. Hence proper storage devices with high capacity are a must.

VI. CONCLUSION

Brief analysis of the present condition of schemes and targets as taken up by our nation to fulfill the reliable and sustainable energy demands is done. The capacity production till 2008 was almost 20 MW which was raised to 1000 MW by the end of 2013 and now we have a target of 175GW to be achieved by the end of 2022. Presently due to high manufacturing and maintenance cost, we are facing problems in harnessing large amount of solar power. Research and development are taking place in advancement of material used in manufacturing of PV cells so as to increase the efficiency and decrease the pricing.

REFERENCES

[1] http://terienvis.nic.in/index3.aspx?sslid=4686&subsublinkid=1476&langid=1&mid=1

[2] https://powermin.nic.in/en/content/power-sector-glance-all-india

[3] https://www.iea.org/publications/freepublications/publication/IndiaEnergyOutlook_WEO2015.pdf

[4] https://mnre.gov.in/

[5] Tariq Muneer, Muhammad Asif, Saima Munawwar, "Sustainable production of solar electricity with particular reference to the Indian economy," International Advanced Research Journal in Science, Engineering and Technology (IARJSET),vol. 2,March 2004, pp 63-65

[6] Harendra Kumar Yadav, Vijay Kumar, Vinay Kumar Yadav, "Potential of Solar Energy in India: A Review," Renewable and Sustainable Energy Reviews, 31 March 2004, pp 444-473

[7] https://mnre.gov.in/file-manager/annual-report/2016-2017/EN/pdf/1.pdf

[8] http://mnre.gov.in/file-manager/UserFiles/grid-connected-solar-power-project-installed-capacity.pdf

Estimation & Designing of Possible Solar Photovoltaic Generation Potential for N.I.T Kurukshetra

Rahul Yadav[1], J.K.Quamara[2]

***Abstract*—The rate at which conventional sources are depleting, it has become very important to look up for alternative energy sources for our daily requirements. Solar energy is a best alternative energy source as it is clean, inexhaustible, environment friendly and a potential resource among the various renewable energy sources. Photovoltaic (PV) systems produce electricity which is determined by the solar radiation, which is the main factor. This paper gives a novel method to estimate the solar photovoltaic generation potential for N.I.T Kurukshetra on the basis of Mean Global Solar Radiation data available for Kurukshetra. Further develop a system model of possible plant capacity according to availability of area The specifications and ratings of equipment's are used based on the availability of the components in India.**

Keywords*— *Solar Photovoltaic (PV) System, Insolation, Solar Radiation

I. INTRODUCTION

Solar energy has experienced an impressive technological shift. It is projected that photovoltaic (PV) systems will experience a large increase in the time to come. In order to successfully integrate latest solar technologies into the existing ones, a detailed research on solar resources is required. Therefore, electricity produced by photovoltaic (PV) systems which is usually obtained using Geographical Information System (GIS) is determined by the solar radiation. The basic step in analyzing scenarios for the future energy supply and for a rational implementation of legal and financial frameworks to support the developing industrial production of PV is the calculation of electricity generation potential by contemporary PV technology. Electricity obtained from the PV array [1- 4] is most efficient during daytime. But at night or during cloudy periods, we need storage batteries to supply electricity, thus independent power systems are used for that purpose. In grid interactive systems [5] , when the PV array cannot supply electricity, the grid acts as the battery . The energy storage devices viz. battery has been avoided in this work. This approach reduces the capital as well as the running cost. We have tried to develop a grid connected photovoltaic system.

Grid connected photovoltaic system [6-7] is well known in various parts of world, and several technologies are used. There have been efforts to develop the power electronics circuitry [8-10] involved. Several types of inverters [11-17] have been designed. But our focus is to estimate the potential of grid connected Solar photovoltaic system for N.I.T Kurukshetra and an establishment of this type of system is tried out with the existing methodologies and equipment's available**.**

[1]Rahul Yadav is with Department of Physics, National Institute of Technology, Kurukshetra, India

[2]J K Quamara is with Department of Physics, National Institute of Technology, Kurukshetra, India.

(e-mail: anirudhjkm@gmail.com)

II. METHODOLOGY

To calculate the possible solar photovoltaic generation potential, the solar radiation data over one year (Jan - Dec 2017) is taken based on the data of mean global solar radiant exposure over Kurukshetra district of Haryana and following the methods discussed in [18-19]. Then for showing the variation in different seasons, related graph is plotted. Also we assumed the efficiency of the PV module as 14.3% [20] for finding the output. In the last a grid connected photovoltaic system is designed with the available technologies for the estimated solar plant capacity on available area. The newness of this approach lies in the fact of assessing the solar photovoltaic generation potential in Kurukshetra and thereby obtain the possible plant capacity.

III. RESULT AND DISCUSSION

The mean global solar radiant exposure varies from 3.25 KWh/m²/day in the month of Jan to 7.22 KWh/m²/day in the month of May . The month wise mean global solar radiant exposure in Kurukshetra district of Haryana for year 2017 is given in table 1[21]. The Graph showing the variation for different months (Jan - Dec 2017) [21]is shown in Fig. 1. Further step involves the calculation of total load of hostel & is illustrated well in tables Then the possible plant capacity is estimated by using the value for average annual solar insolation. We have assumed in our study that the solar energy is available for about 6 hours during the normal day. After estimating the potential, the model of grid connected solar PV power plant is given further in this paper.

TABLE 1. Mean Global Solar Radiant Exposure at Kurukshetra (Monthly Average)

Jan	3.25
Feb	4.40
March	5.84
April	6.78
May	7.22
June	6.41
July	5.83

August	5.64
September	5.48
October	5.11
November	3.82
December	3.18

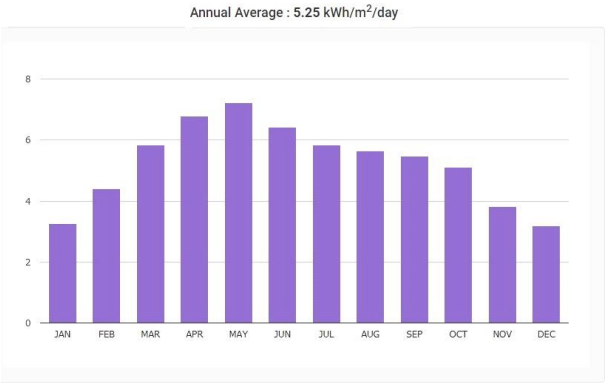

Fig 1 Variation of Mean Global Solar Radiant Exposure at Kurukshetra (in kWh/ m^2 /day)

Average annual solar insolation in Kurukshetra

$= 5.25\ kWh/m^2$

$\approx 900\ W/m^{2/day}$

IV.

OAD CALCULATION OF P G HOSTEL 6

The load of selected area is calculated as follows:

TABLE 2. Load Calculation for A block

Room	Fans (80W)	Tube Lights (35W)	6A/3Pin socket (40W)	Computers & Accessories (100W)	Exhaust Fan (50W)	CCTV Camera (30W)
R.NO. 100-154	54	54	54	40	0	0
Washrooms	0	3	0	0	3	1
Store room	3	3	3	0	0	0
Corridors	0	9	0	0	0	2
Total	57*80= 4560W	69*35= 2415W	57*40= 2280W	40*100 = 4000W	3*50= 150 W	30*3= 90W

Total load for A block = 13.495kW

Since there are 3 similar blocks so these loads will be multiplied by 3. Hence final load of all three blocks (A, B, C) is 13.495*3= 40.485kW.

TABLE 3. Load calculation for other areas

Room	Fans (80W)	Tube Lights (35W)	6A/3Pin Socket (40W)	Computers & Mess Accessories (400W)	Exhaust Fan (50W)	CCTV Camera (30 W)
Mess	12	20	5	5	8	5
Common Room	8	12	4	2	4	1
Warden and MMCA office	5	5	3	1	0	2
Temple Area	0	3	2	0	0	2
Total	25*80= 2000W	40*35= 1400W	14*40= 560W	8*400= 3200W	12*50= 600W	10*30= 300W

Total load = 8.060kW

TABLE 4. Energy Consumption

Name	Total Load (kW)	Energy Consumption per day (kWh)	Energy Consumption per Month (kWh)
Blocks (A , B , C)	40.485	242.91	7287.3
Others	8.060	40.3	1209

TABLE 5. Energy Generated at PG Hostel 6

Name of Block	Available Area (m^2)	Effective Area (m^2)	Average Peak Output (W/m^2)	Possible Plant Capacity (kW)	Energy Generated per day (kWh)	Energy Generated per month (kWh)
P G Hostel	700	490	900	40	240	7200

Effective area = 700*0.7 = 490 m^2

IV. SYSTEM SIZING

There are different methods for designing the Grid connected PV system, like with battery, without battery, with or without transformer etc. Here We have used without battery grid interconnected system. From the results obtained, we find that 40 kW solar photovoltaic power plant can be developed on 490 m2 area.

System sizing and specifications are given along with the system design. For the 40kW plant, required no. of PV modules = (40000 /180) = 222.22 ≈ 225. Now to form a solar photovoltaic power plant 225 modules are connected in series-parallel combination.25 modules are connected in series and there are 9 parallel paths of 25 modules each. Now each module produces 24 Volts. So total 25 series connected module will produce 25 × 24 = 600 V. So there are nine combinations are connected in parallel. Total output voltage from solar photovoltaic structure is = 600 Volts. This 600 Volts dc output from solar photovoltaic structure is the input of 3 phase inverter and it will convert the dc voltage into ac voltage. After the inverter a 3 phase transformer is connected, this will boost up step down the ac voltage and feeds it to the grid.

V. SYSTEM SIZING & SPECIFICATION

The system sizing and specifications for the 36KW power plant unit is shown below:

TABLE 6. Grid Specification

No. of Phases	3-φ
Voltage rating	400 Volts AC
Frequency	50 Hz.

TABLE 7.Solar Photovoltaic Power Plant Specification

Plant Capacity	40 KW
Voltage Output	600 Volts dc
Current Output	66.67A
No. of Modules	225
Area	490 m^2

PWM inverters are used here for suppressing the harmonics produced after DC to AC conversion. The

calculation for finding the output voltage of inverter is shown below:

Phase voltage - Vph = 0.4714 × Vdc = 0.4714× 600 = 282.84 Volts.

Line voltage - V_L= 0.779 × Vdc = 0.779× 600 = 467.4 Volts.

TABLE 8. Inverter Specification

KVA rating	330 KVA
Input DC voltage	600 Volts DC
Input dc current	66.67 A
Output AC voltage	282.84 Vac (phase voltage) 467.40 V ac (line voltage)
No. of Phases	3-φ
Type	PWM (for suppressing 3rd harmonics)
Efficiency	Almost 90-95%
Total harmonic distortion	< 5%

TABLE 9. Transformer specification

KVA rating	330 KVA
No of phases	3-φ
Frequency rating	50 Hz
Primary voltage rating	467.40 V
Secondary voltage rating	400 V
Primary current rating	706.03 A
Secondary current rating	825 A
Connections	Primary – delta (for suppressing3rd harmonics) Secondary – star 10 to 25 taps in secondary
Efficiency	Almost 95 %
Extra features	Air cooled

TABLE 10. Solar Panel Specification

Watt	180 Watt
Voltage	24 Volts
Current	7.5 A
Type	Polycrystalline
Efficiency	14.3%
Temperature	25 deg c
Dimensions (mm)	1593 × 790 × 50 Area of single panel = 1258470 (mm) Area of single panel = 1.259 meter²
Tilt angle(slope) of PV Module	29°52´ and 30°12´ N
Mounting	Fixed Type

Cables: For connecting the solar panels together we have used string dc Cables. The combined output of Solar system is connected to the inverter using Main dc cable. Further the output of inverter is connected to the transformer, Grid etc. is using ac cables (LT cables, HT cables).

The solar module will be equally distributed on rooftop area of three blocks (25*3 modules on each rooftop).

dc string cable required in interconnection of panels = 25 m for one row. Since there is 9 rows so total length of dc string cable = 25*9 = 225m

Average distance from junction point to the inverter is = 50m

So, total length of main dc cable = 150m.

ac cable length for connection from inverter to transformer and further to grid is roughly can be said about 300-400m

TABLE 11. Cable specification

Type of Cable	Rated Voltage	Operating Temperature(o_C)
dc string cable	600 V dc	-40 to 90
dc main cable	1800 V dc	-40 to 90
LT ac cable	1000-1500 V ac	-40 to 90
HT ac cable	11kV to 33k V ac	-40 to 90

Others: Junction Boxes, Meters, Distribution Boxes, Wiring Materials, Mounting Materials etc.

The above data is taken from reference [20] and from standard of MNRE.

VI. CONCULSION

Solar photovoltaic generation potential during the period Jan – Dec 2017 is calculated for Kurukshetra district of Haryana. It is seen that the solar radiation production is lowest in the month of December. Moreover, the expected plant capacity has been estimated from the average output available from the solar radiation readings of each month. In this paper optimization techniques have not been carried out. It can be taken up as a future extension of work because Maximum Power Point Tracking (MPPT) could have given a better result. The methodology adopted is satisfactory for determining the possible solar plant capacity for selected area. The design described is based on the solar radiation data. System design and specifications are provided based on the analysis.

ACKNOWLEDGEMENT

This work is a part of the M. Tech thesis work of Mr. Rahul Yadav conducted during the time period July2017 -May 2018 under the able guidance of Dr. JK Quamara, Prof., NIT Kurukshetra, Kurukshetra.

REFERENCES

[1] G.D.Rai, Solar Energy Utilization, 5th Edition Khanna Publication

[2] Renewable Energy Akshay Urja Vol. 3 Issue 1, Jan-Feb, 2007.

[3] S. Hasan Saeed & D.K. Sharma, Non- Conventional Energy Resources, 1st Edition
[4] Suhas P Sukhatme Solar Energy–Principles of Thermal Collection & Storage, 2nd Edition
[5] Cost and Performance Trends in Grid connected Photovoltaic Systems and Case Studies: Report IEA-PVPS T2-06:2007
[6] Mohd Shawal Jadin, Soib Taib, I Daut & eM Hadzer,'Integrated Grid-Connected PV Monitoring System', IEEE Transactions 2005.
[7] Juan Manuel Carrasco, Leopoldo Garci Franquelo, Jan T. Bialasiewicz, Eduardo Galván, Ramón C. Portillo Guisado, Ma. Ángeles Martín Prats, José Ignacio León and Narciso Moreno-Alfonso, 'Power-Electronic Systems for the Grid Integration of Renewable Energy Sources: A Survey', IEEE Transactions on Industrial Electronics Vol. 53, No. 4, August, 2006.
[8] A. Agbossou et al., 'A Comparative Study of High Power IGBT Model Behavior in Voltage Source Inverter', PESC '96, Conf. Record, June 1996, Vol. 1, pp. 56-61..
[9] H. Jin, 'Behavior-Mode Simulation of Power Electronic Circuits', IEEE Transactions on Power Electronics, May 1997, Vol. 12, No. 3, pp. 443-452.
[10] Denizar C. Martins and Kleber C. A. de Souza, 'A Single-Phase Grid-Connected PV System with Active Power Filter', International Journal of Circuits, Systems and Signal Processing, Volume 2, Issue 1, 2008.
[11] G. Ertasgin, D.M. Whaley, N. Ertugrul and W.L. Soong, 'A Current-Source Grid- Connected Converter Topology for Photovoltaic Systems', IEEE Transactions, 2008.
[12] J.S.Siva Prasad and B.G.Femandes, 'Active Commutated Thyristor CSI for Grid Connected Photovoltaic Applications', The 4th International Power Electronics &Motion Conference14th-16th August, 2004, Vol. 3, pp. 1767-1771.
[13] L. Hassaine, E. Olías1, M. Haddadi and A. Malek, 'Asymmetric SPWM used in inverter grid connected systems', Revue des Energies Renouvelables Vol. 10 No. 3, pp. 421 – 429,2007.
[14] Marco Liserre, Remus Teodorescu & Frede Blaabjerg, 'Stability of Grid-Connected PV Inverters with Large Grid Impedance Variation', 35th Annual IEEE Power Electronics Specialists Conference, 2004.
[15] S. Hiti, D. Boroyevich, 'Small-Signal Modeling of Three-Phase PWM Modulators', PESC'96, Conference Record, June 1996, Vol. 1, pp. 550-555.
[16] S. Hiti, 'Modeling and Control of Three- Phase PWM Converters', Ph.D. Dissertation, Blacksburg, VPI&SU, 1995.
[17] Sunanda Sinha, 'A Study and Estimation of Grid Quality Solar Photovoltaic Power Generation Potential in some districts of West Bengal', M. Tech Thesis, Jadavpur University, Kolkata, 2009.
[18] Souvik Ganguli, Sunanda Sinha, 'A Study and Estimation of Grid Quality Solar Photovoltaic Power Generation Potential in some districts of West Bengal', National Conference on Trends in Instrumentation & Control Engineering, Thapar University, Patiala, pp. 522-528, 2009.
[19] BP Solar Datasheet (BP 7180) for 180 Watt Photovoltaic Module-Saturn Technology.
[20] Vineet Singla, Vijay Kumar Garg 'Estimation & Design of Possible Solar Photovoltaic Generation potential for U.I.E.T K.U.K.'IJERA ISSN: 2248-9622
[21] H A R E D A , Department of renewbale energy, Govt of Haryana.

Simulation and Modelling of Photovoltaic Module using Simscape

Mittarpal[1], Asha[2]

Abstract: Incrementing energy demands, an impact of greenhouse gasses (GHG), climate changes are ineluctably foreordained challenges in front of all over world community. The one of the efficacious solution to these quandaries is the adoption and development of renewable energies. Among all the available renewable energy sources (RES), green energy-solar energy is most suitable due to its availability in excess. Deployment of solar energy can play a vital role in economic magnification and amelioration in quality of life. PV systems are interface contrivances to convert solar energy to electrical energy without involving mechanical systems and their characteristics analysis provide optimum utilization of sun energy. For the attainment of the output power of PV system, their factors analyses have been implemented utilizing a simulation environment. Matlab is a general purpose scientific computing commercial software, its diverse environment including toolboxes and blocksets are prominent as leading simulation package in simulating, analyzing and optimizing functioning of PV cell, module, and system. The present paper illustrates the utilization of simulink graphical environment and simscape to analyze the characteristics of PV module under control of environment factor viz. solar irradiance and temperature, moreover load voltage to optimize the maximum output power. Simulation models of photo voltaic cell and system have been developed utilizing simelectronics, a sub library in simscape.

Keywords: Photovoltaic (PV) Cells, module, Modeling, Simelectronics, Simscape, Simulink, Characteristics.

1. INTRODUCTION

Photovoltaic cells produce electricity directly from sunlight with the help of photovoltaic effect and its electrical characteristics such as voltage-current, power-voltage, and resistance changes when exposed to light. Photovoltaic cells also termed as PV cells or solar cells are structure blocks of photovoltaic modules, also termed as solar panels. Many PV panels are used in remote locations not connected to the electric grid.

[1]Mittarpal is with Department of Electronics and Communication, Bhagat Phool Singh Women University, Sonipat, India
[2]Asha is with Department of Electronics and Communication, Bhagat Phool Singh Women University, Sonipat India.
(e-mail: mpjangra80@gmail.com)

Paramount utilization of photovoltaic systems in an optimum manner requires a meticulous erudition of voltage current characteristic of photovoltaic modules. Eminence development in technology, incentive policy formulation by regimes, degradation in environment and ecosystem due to thermal plants, decrement in fossil fuels and elevation in price are main concern of focus for deployment of solar energy. PV cells are the constituents of solar systems. PV Solar system energy has been emerged as a consequential present and future green and renewable energy system. Solar-electric-energy system has advanced excellently and become a conspicuous resource of energy. The paramountcy deploy of solar energy is:

- Clean, green energy and liberate from sundry hazardous effects, reduce GHG.
- Reduce the conventional energy crisis and incrementing rate of environmental issues such as air pollution and ecumenical warming.
- Facilitate to all, since earth receives gargantuan amount of solar energy from sun.
- Increasing exponentially, by virtue of utilization of efficacious materials which increase in efficiency of solar cells.

The present investigation analyzes the characteristics of the PV cell, elongated to PV module. The solar cell is taken from simelectronics sub library which subsist in substratum library-simscape. On basis of semiconductor and its built up technology, conventionally PV cell engender a voltage around 0.5 to 0.8 volts which is profoundly low. The voltage and current can be incremented by connecting the cells in arrays horizontally and vertically. These modules are connected in series and parallel to compose a PV panel. When these panels are connected in series, the voltage will be integrated and the current will be same and when connected in parallel the voltage will be same and current will be integrated [6]. In Fig. 1, the coalescence of PV cell either in series or in parallel or by both combination develop a PV array and modules, moreover coalescences of PV modules in a resembling way provide an astronomically immense solar energy system.

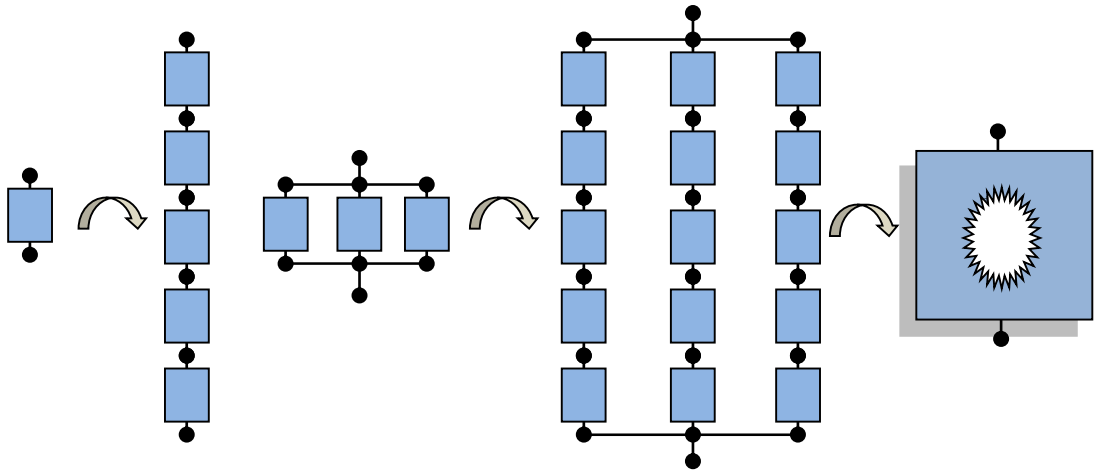

Figure 1: PV Module Cell Recipe

Basically, solar photovoltaic cell is a PN junction semiconductor diode. When cell is exposed to sunlight, it produces two types of charges i.e. electron and holes at junction. Negatively charged electrons will assemble around the N-type semiconductor and positively charged electrons around the P-type semiconductor. When load is connected the electric current will flows between the electrodes. After paying a huge cost for the installation of PV array, obviously the consumer would want to access the complete output power of the system. So PV array system should be designed in such a way that it can operate at their maximum output power level at any required temperature and solar irradiation. Initially the cost of solar PV cells was very high. Due to emerging new technology the cost is going to be decreased during last decade. The usage of photovoltaic systems in an effective manner requires a precise knowledge of the current-voltage and power-voltage characteristics curves of photovoltaic system [1]. The focus of this paper is on the understanding of characteristics of the PV module with the help of software. In present paper, simulink and simscape models are deployed to realize the characteristics of PV module. The current $I(V)$ and power $P(V)$ characteristics of the PV array have been analyzed under influence of solar irradiance and temperature.

2. MATHEMATICAL MODELING AND ELECTRICAL EQUIVALENT REPRESENTATION OF PHOTOVOLTAIC MODULE

Photovoltaic cell is also known as solar cell. The photovoltaic cell has been represented in mathematical modeling. To explore mathematical modeling of photovoltaic cell, it is necessary to conclude the equivalent circuit model in form simple elements of electrical engineering. In present chapter of this thesis the mathematical modeling and electrical equivalent of photovoltaic cell and model is explored in detail.

2.1 Ideal model of photovoltaic cell

In figure 2, electrical equivalent circuit model of photovoltaic cell is depicted. In this model the loss in the photovoltaic cell is neglected. The model consist current source and an anti-parallel diode. The current source of photovoltaic cell is generation of photo current due to solar irradiations.

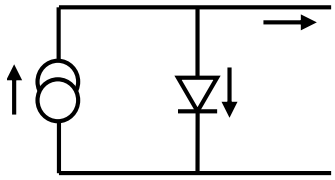

Figure 2: Ideal equivalent of photovoltaic cell

2.1.1 Mathematical Analysis of ideal model of photovoltaic cell

Photo current is also known as source current. It is produced due to exposure of solar irradiations on photovoltaic cell. This source current is branched as diode current and output current. The output current of the ideal photovoltaic cell is determined using Kirchhoff's current law.

$$I_{ph} = I_d + I_o \quad (1)$$

From eq. 1, output current is determined as below:

$$I_o = I_{ph} - I_d \quad (2)$$

Here, diode current of photovoltaic cell is depended on the reverse saturation current and saturation current.

2.2. Practical model of photovoltaic cell

In figure 3, electrical equivalent circuit model of photovoltaic cell is depicted. The model consist current source and an anti-parallel diode with shunt and series resistances.

Table 1: Key Specification of Solkar 36 W PV Module (N.P. rajan *e.l*) and MXS 60 PV Module

S. No.	Parameters	Variables	Solkar	MXS 60
1.	Rated power	Pr	37.08 W	-
2.	Maximum power	Pm	42.228 W	60 W
3.	Maximum voltage at maximum power	Vm	16.56 V	17.1 V
4.	Current at maximum power	Im	2.25 A	3.5 A
5.	Open circuit voltage	Voc	21.24 V	21.06 V
6.	Short circuit current	Isc	2.55 A	3.74 A
7.	Total number of cells in series	Ns	36	36
8.	Total number of cells in parallel	Np	1	1
9.	Ideality factor of diode	A	1.6	1.6
10.	Cell short circuit current temperature coefficient	Ki	0.00017	0.00017
11.	Reference Temperature	Tr	25^0C	25^0C
12.	Solar Irradiance	G	1 at STC	1 at STC

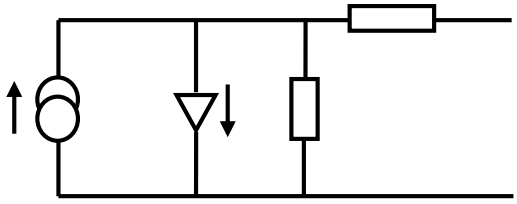

Figure 3: Ideal equivalent of photovoltaic cell

The key parameters specification of solar 36W PV module and MXS 60 PV module is represented in Table 1. The parameters of these module can be verified by using Simscape module of given model.

.

3. SIMULINK MODEL OF PV MODULE

In Fig. 3 the simulation model of the PV module is realized in simulink environment.

3.1 Simscape Model of Single PV Cell

In figure 4, the simelectronics model of solar PV cell is developed and its parameters are modulated by clicking in solar cell block according to the reference PV module.

4. RESULTS AND DISCUSSION

In figure 5, a voltage current characteristic at constant operating temperature with different level of solar insolation (light intensity) is depicted. Obviously, short circuit current and open circuit voltage increase with increase in light intensity

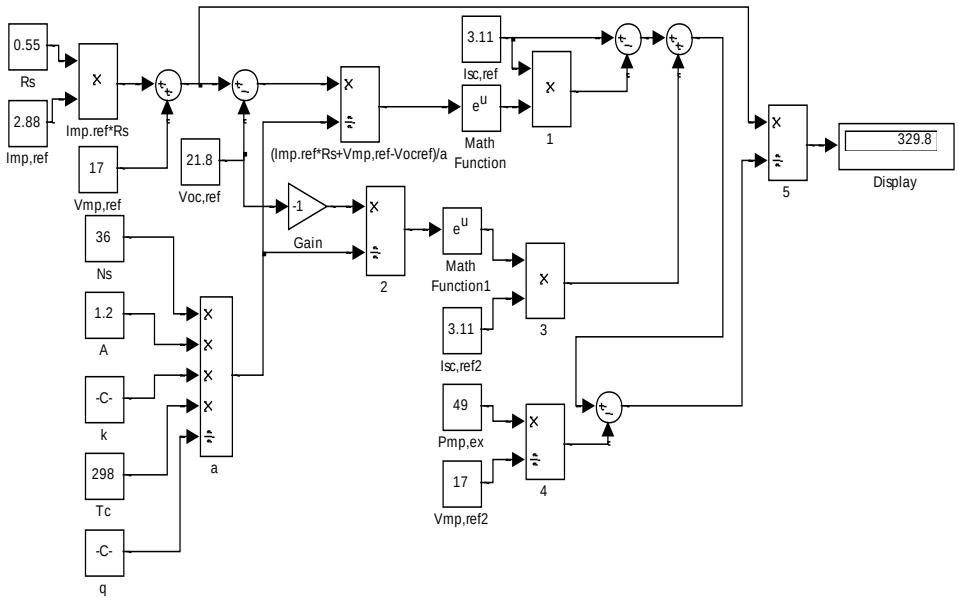

Figure 4: Simulink Model

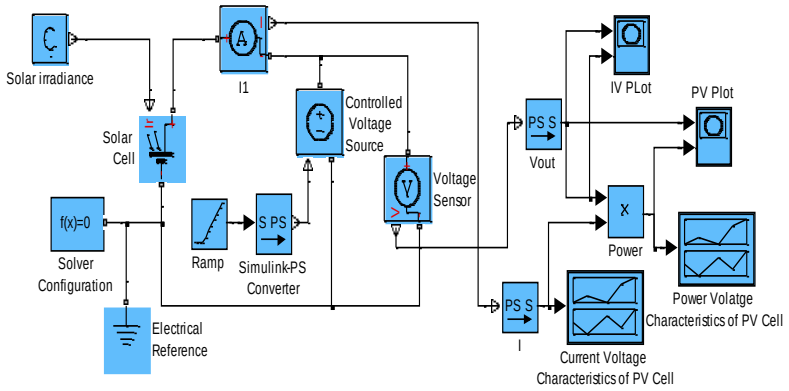

Figure 5: Simscape Model of Single PV Cell

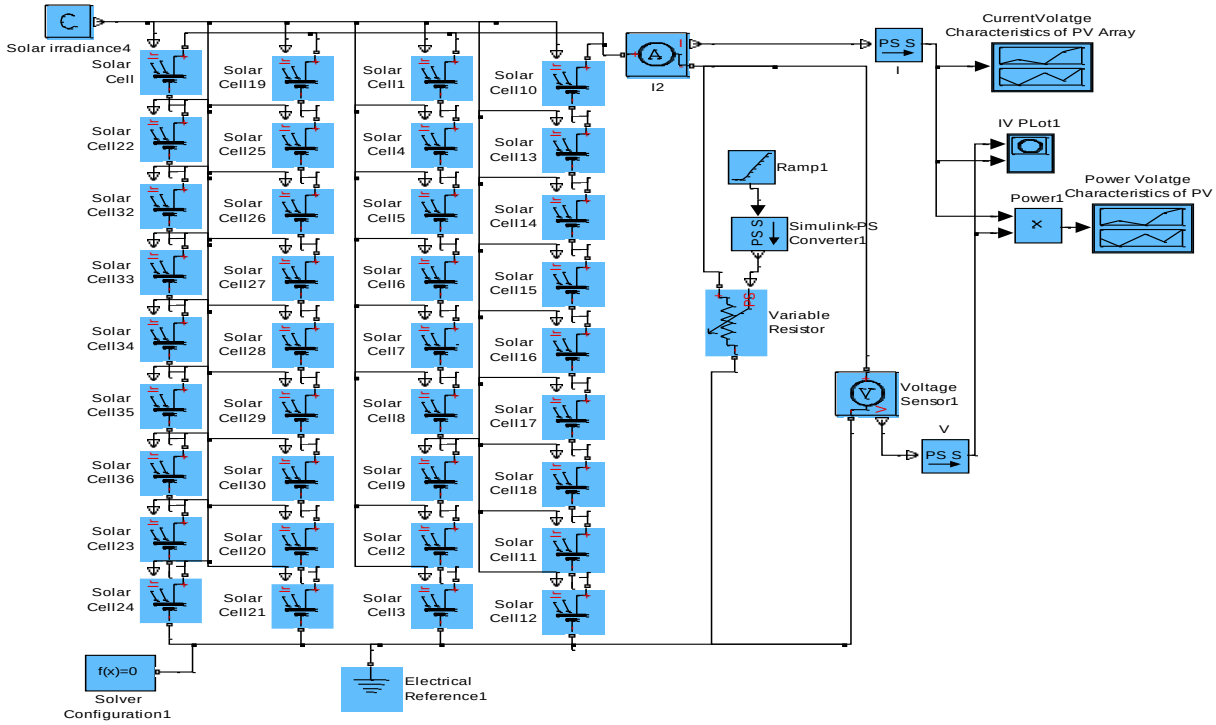

Figure 6: Simscape Model of Single PV Module

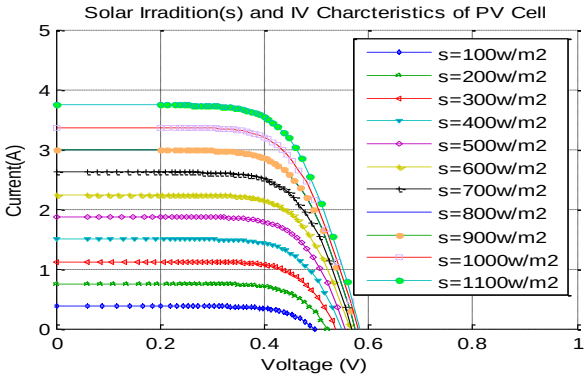

Figure 7: I-V Characteristic

In figure 7, a voltage power characteristic at constant operating temperature with different level of solar insolation (light intensity) is depicted. The maximum power is highest energy transferred to load, and increase with light luminance.

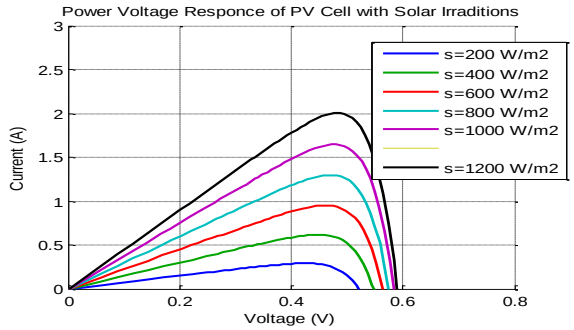

Figure 8: P-V Characteristic

In figure 8, a voltage current characteristic at constant solar insolation with different level of operating temperature is depicted. The short current is minute influenced with operating temperature but open circuit voltage decrease with increase in operating temperature.

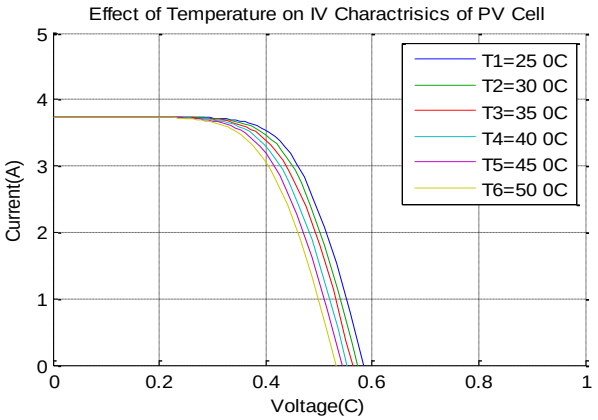

Figure 9: I-V Characteristic

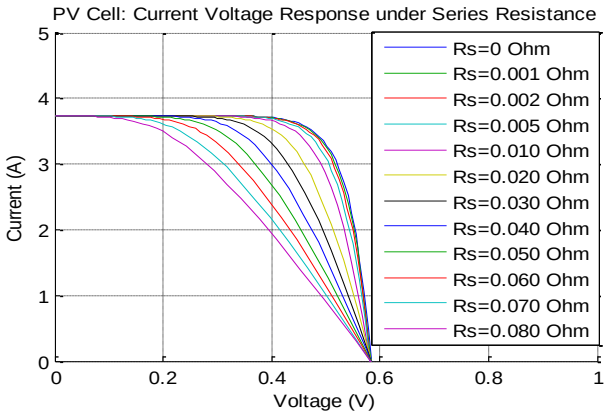

Figure 10: Current Voltage Characteristics of PV Cell in control of Series Resistance.

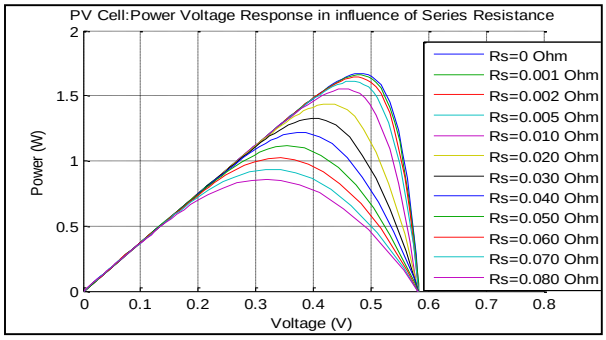

Figure 11: Current Voltage Characteristics of PV Cell in control of Series Resistance.

REFERENCES

[1] J.A. Gow, C.D. Manning "Development of a PhotovoltaicArray Model for Use in Power Electronics Simulation Studies", IEE Proceedings on Electric Power Applications,Vol. 146, No. 2, pp. 193-200, March 1999.

[2] J.A. Ramos, I. Zamora, J.J. Campayo. "Modeling ofPhotovoltaic Module", International Conference on Renewable Energies and Power Quality (ICREPQ'10)Granada, Spain, 23-25 March 2010.

[3] M.G. Villalva, J.R. Gazoli, E. Ruppert "Modeling andCircuit Based Simulation of Photovoltaic Arrays", Brazilian Journal of Power Electronics, Vol. 14, No. 1, pp. 35-45,2009.

[4] W. DeSoto, "Improvement and Validation of a Model forPhotovoltaic Array Performance", M.Sc. Thesis,Mechanical Engineering, University of Wisconsin,Madison, 2004.

[5] C. Osorio. Matlab-Simulink models, Mathworks.

[6] G. Walker, "Evaluating MPPT Converter Topologies Usinga Matlab PV Model", Journal of Electrical and Electronics Engineering, Australia, Vol. 21, No. 1, pp. 49-56, 2001.

[7] F. Gonzaez-Longatt, "Model of Photovoltaic in MatlabTM",2nd Latin American Student Congress of Electrical Engineering and Computer Science (II CIBELEC 2005),Puerto la Cruz, Venezuela, April 2006.

[8] A. Oi, "Design and Simulation of Photovoltaic WaterPumping System", Master Thesis, California PolytechnicState University, San Luis Obispo, CA, 2005.

[9] http://ecee.colorado.edu/~ecen2060/matlab.html

[10] A. Luque, S. Hegedus, "Handbook of Photovoltaic Scienceand Engineering", John Wiley & Sons Ltd., 2003.

[11] A.S. Golder, "Photovoltaic Generator Modeling for LargeScale Distribution System Studies", Master Thesis, DrexelUniversity, 2006.

[12] A. Rostami, K. Abbasian, N. Gorji, "EfficiencyOptimization in a Rainbow Quantum Dot Solar Cell", International Journal on Technical and Physical Problems of Engineering (IJTPE), Issue 7, Vol. 3, No. 2, pp. 106-109,June 2011.

[13] M. Sojoudi,R. Madatov, T. Sojoudi, "Optimization of Efficiency of Solar Cells by Accelerated Electron ray to Have an Optimal and Constant Energy", InternationalJournal on Technical and Physical Problems of Engineering (IJTPE), Issue 9, Vol. 3, No. 4, pp. 68-71, December 2011.

[14] Yuncong Jiang, Jaber A. Abu Qahouq and Mohamed Orabi, "Matlab/Pspice Hybrid Simulation Modeling of Solar PV Cell/Module", Proceedings of Twenty-Sixth Annual IEEE Applied Power Electronics Conference and Exposition (APEC 2011), pp. 1244-1250.

[15] R.K. Nema, SavitaNema, and GayatriAgnihotri, "Computer Simulation Based Study of Photovoltaic Cells/Modules and their Experimental Verification", International Journal of Recent Trends in Engineering, Vol 1, No. 3, pp. 151-156, May 2009.

[16] Sheriff M. A., Babagana B. and Maina B. T., "A Study of Silicon Solar Cells and Modules using PSPICE", World Journal of Applied Science and Technology, Vol. 3,. pp. 124-130, No.1, 2011.

[17] Yuncong Jiang, Jaber A. Abu Qahouq and I. Batarseh, "Improved Solar PV Cell Matlab Simulation Model and Comparison", Proceedings of 2010 IEEE International Symposium on Circuits and Systems (ISCAS), pp 2770 - 2773, May-June, 2010.

A Review of Modelling Techniques for Tilt angle Optimization of PV Arrays

Rohit Kumar[1], Tarlochan Kaur[2]

***Abstract*—The output power of photovoltaic (PV) modules and systems depends on the irradiation falling on the PV module surface. This irradiation falling on PV module surface is in turn dependent upon the orientation and tilt angle. But this irradiation cannot be computed directly and so various models/techniques were presented in the past for its estimation. These techniques are revisited in this paper.**

***Keywords*— Optimal tilt angle, modelling techniques, isotropic, anisotropic**

I. INTRODUCTION

Solar Energy is a form of renewable energy which is available in abundance for humans. But the technology for harvesting this energy is very new and hence very costly. However exposure to this kind of renewable energy is slowly increasing and also the costs are coming down as utilization of solar panels is increasing over time. So going by the statistics, India needs large investment in solar power in coming years. No matter what the technology is, the basic requirement for maximizing the power output of the solar PV system is to collect maximum possible irradiation at the location. Now if the solar PV panel is kept at any constant particular orientation for whole day or month, maximum possible irradiation cannot be collected as the angle between the solar panel axis and the line joining panel and sun keeps on changing. This change in solar irradiation directly impacts the output power of the solar PV system. As the irradiation decreases, the output power also decreases. And as irradiation falling on the PV surface start increasing, output power increases simultaneously. One solution to this variation in output power is to keep on changing the tilt and orientation of PV module along with change in direction of sun so that irradiation falling in the PV surface is directly perpendicular to the PV surface. Tilt angle can be defined as angle which the PV surface makes with the earth's plane at the location. This is one of the most important parameter which directly impacts the degree of optimization achieved by a particular optimization technique. This change in tilt angle can be done by using a tracker or by changing the tilt angle manually.

A tracker is a computer enhanced hardware which takes the solar radiation falling on the module as input and computes the change in tilt angle in real time. The solar radiation falling on the module is first saved into memory. Then the tracker changes the tilt angle slightly in one direction and again saves the solar irradiation amount into the memory. Now, it compares the amount of solar irradiation in both the cases and a finds the change. If the change is positive, it means that changing the tilt angle was in right direction and it can save the new tilt angle as optimized one. However, if the change is negative, it means that the solar irradiation falling on module has not increased and hence, the change in tilt angle should be reverted back and tilt angle should be increased in other direction. The main advantage of using a tracker is that it can achieve near to 100% optimization. Also no manpower is required for changing the tilt angle regularly. But using tracker also has disadvantages like increased cost, increased size of equipment, and requirement of electric power for operation which results in decreased efficiency. This is where manual control becomes advantageous as it is cheaper, requires no electricity and resulting in smaller overall equipment size compared to tracker. In manual control, the tilt angle should be changed manually. This can be done at regular intervals of time. The degree of optimization depends on how short these intervals are. Shorter the intervals, more is the degree of optimization. However, manual control also has some drawbacks like decreased optimization as tilt angle cannot be varied continuously throughout the day. It also requires constant human supervision. But usually manual control has overall more efficiency and advantages compared to use of tracker if the frequency of tilt angle variation is high. This is because continuous variation in tilt angle has a very small impact on output power as compared to when this tilt angle is varied at interval of 15 days or 1 month. This is because tracker consumes electrical power for operation and this power is much more then the improvement it provides by monitoring the tilt angle in real time. In manual control, the tilt angle at which maximum irradiation is falling needs to be computed first.

In order to determine this tilt angle, irradiation falling on the tilted surface needs to be computed. The most common approach for determining the tilt angle is using the geographical latitude where the solar panel is to be installed. Here the tilt angle is set either at the latitude or latitude +/- 15 degrees [1, 2]. However this approach is not always beneficial. So various models were presented in past literature to arrive at the amount of irradiation falling on solar panel surface. Many authors have computed the irradiation from parameters like global horizontal irradiance (GHI) and diffuse horizontal irradiance (DHI). GHI is the amount of solar radiation falling on solar panel which is horizontal to the ground surface. Direct normal irradiance (DNI) is the radiation that is falling directly onto the solar panel from the sun

[1]Rohit Kumar is with Department of Electrical Engineering, Punjab Engineering College, Chandigarh, India
[2]Tarlochan Kaur is with Department of Electrical Engineering, Punjab Engineering College, Chandigarh, India.
(e-mail: rohitkumar587@gmail.com, tarlochan.karu@gmail.com)

without any scattering. Diffuse horizontal irradiance is the irradiation which is not falling perpendicular or directly on the surface but is disbursed into the environment and then falling on the surface.

II. Prediction Models for Solar Radiation on Tilted Surface

Many models were given by various authors to calculate the radiation on tilted surface. Most of the models break up the total irradiation falling on surface into three components i.e. beam, diffuse and reflected component. These models are useful in converting the hourly measured irradiances like GHI, DHI into irradiances on tilted surface. Hourly data for GHI, DHI is available with meteorological departments of a country. The models reviewed in this paper assume either isotropic or anisotropic sky model. Isotropic models assume that sky diffuse radiation depends only on the portion of the sky dome seen by the solar panel surface. Anisotropic models take into account the anisotropy of the sky near the solar disc and for the rest of the sky it assumes isotopically distributed diffuse component. El-Sayed [3] developed a model to calculate the optimum tilt angle by taking the effect of latitude, number of glass covers, clearing index and the solar reflectivity. Some prominent models are discussed below.

A. Liu and Jordan Model

Liu and Jordan developed a relationship between irradiance on tilted surface and that on horizontal surface in 1962 [4]. They assumed isotropic diffuse sky model. The irradiance on tilted surface can be expressed as

$$I_T = I_b R_b + I_d [(1 + \cos \beta) / 2] + I_{\rho g} [(1 - \cos \beta) / 2] \quad (1)$$

Where I_T is radiation on tilted surface, I_b is beam radiation on horizontal surface, R_b is ratio of beam radiation on tilted surface to that on horizontal surface, I_d is diffuse radiation on horizontal surface, β is tilt angle, $I_{\rho g}$ is radiation from ground reflectance. The major drawback of this model was that it did not take into account the anisotropic nature of sky. So further models were developed for anisotropic diffuse sky.

B. Temps and Coulson Model

Temps and Clouson [5] in 1977 developed a model for anisotropic diffuse sky by modifying the isotropic model of Liu and Jordan. The irradiance on tilted surface can be expressed as

$$I_T = I_b R_b + I_d [(1 + \cos\beta) / 2] [1 + \sin^3 (\beta / 2)] [1 + \cos^2\theta \sin^3\theta_z] + I_{\rho g} [(1 - \cos \beta) / 2) \quad (2)$$

Where θ is the incidence angle and θ_z is the zenith angle. Zenith is the line drawn perpendicular to the earth's surface at the location of the solar PV panel and the angel is made between zenith line and the sun.

C. Klucher Model

Klucher [6] studied both the previous models i.e. Liu and Jordan model and Temps and Clouson model and observed that Temps and Clouson model was more accurate for conditions when there were no or very less cloud cover. On the other hand, Liu and Jordan model showed opposite nature i.e. it gave accurate results when the cloud cover was intense. So Klucher modified the Temps and Clouson model into the expression

$$I_T = I_b R_b + I_d [(1 + \cos\beta) / 2] [1 + F \sin^3 (\beta / 2)] [1 + F \cos^2\theta \sin^3\theta_z] + I_{\rho g} [(1 - \cos\beta) / 2] \quad (3)$$

Where $F = 1 - (I_d/I)^2$ is a function of diffuse horizontal irradiance and global horizontal irradiance. I is global horizontal irradiance.

D. Perez et al. Model

Perez et al. [7] model was governed by the following equations

$$X_c = X_h [(1 - F_1) (1 + \cos s) / 2 + F_1 (a / b) + F_2 \sin s] \quad (4)$$

Where X_c and X_h are tilted and horizontal diffuse values of irradiance respectively. s is tilt angle and F_1 and F_2 coefficients expressing the degree of circumsolar and horizon anisotropy respectively. The terms a and b are expressed as

$$a = \max (0, \cos \theta) \text{ and } b = \max (0.087, \cos Z) \quad (5)$$

Where Z is sky clearness index.

E. Klein Model

Klein [8] extended the Liu and Jordan model so that it could be used for estimating irradiance on surfaces which were not directly oriented towards the equator. He proposed the following expression

$$I_T = RI \quad (6)$$

Where R is the ratio of irradiance on tilted surface to irradiance on horizontal surface. It can be expressed as

$$R = (1 - I_d/I)R_b + I_d/I(1 + \cos s)/2 + \rho[(1 - \cos s)/2] \quad (7)$$

The coefficient R_b accounts for the change in irradiance when the solar panel is not tilted toward the equator.

III. Conclusion

In this paper, various models developed for estimating the solar irradiance on tilted surface were reviewed. As can be seen from the models discussed, solar irradiance on any surface depends on many factors like tilt, orientation, latitude, declination angle of the sun, sunrise angle, zenith angle etc. So by varying any of the above factors, the irradiance can be changed. In order to achieve maximum irradiance at a specified location, tilt angle is the most varied parameter as the orientation is usually kept towards the equator. Also the declination of sun cannot be varied. Other parameters also either do not have significant effect

on the irradiation or cannot be varied manually. So in most cases tilt angle variation is the only option to maximize the solar irradiance which in turn maximizes the power output of the solar PV array. The hourly irradiance data like GHI, DHI is usually available for any given location. This data is put into any of the above models and the corresponding irradiance on tilted surface for a particular tilt angle is found out. Then this tilt angle is varied at small steps and corresponding irradiance on the tilted surface is recorded. Now by looking at variation of irradiance on tilted surface with tilt angle, the optimum tilt angle can be found out which results in maximum irradiance. Optimum tilt angle was found using same approach in Singapore [9]. These models can be implemented using simulations on computers and then optimized tilt angle can be easily found out. This will be very helpful in improving the power output of solar panels already installed at various facilities across the world and particularly to the generation plants where trackers are used which consume large amount of energy for operation and in turn decrease the efficiency of the solar generation systems. Also, in many generation plants, solar panels are always having the same orientation and tilt angle throughout the year. This has a huge impact on the efficiency of plant in long run. These techniques will be very helpful in such cases. The simulations are usually already done for some major cities where the solar power generation plant is to be installed. But for smaller cities and towns where smaller capacity power plants are installed, usually orientation and tilt angle is constant. Here, implementing these techniques on a personal computer and determining the tilt angle locally can also be beneficial for the society. The tilt angle can be found out for any duration of time and thus can be varied according to the will of consumer.

In this way, the solar PV array output can be optimized using tilt and orientation.

REFERENCES

[1] J. Kern, L. Harris, “On the optimum tilt of a solar collector,” Solar Energy, 1975, 17, 97.

[2] lqbal, M. Optimum collector slope for residential heating in adverse climates. Solar Energy, 1979, 22, 77.

[3] EI-Sayed, M.M, “Optimum orientation of absorber plates,” Solar Energy, 1989, 42, 89.

[4] B. Liu, R. Jordan, “Daily insolation on surfaces tilted towards equator,” ASHRAE J., vol. 10, pp. 53–59, 1961.

[5] R. C. Temps, K. L. Coulson, “Solar radiation incident upon slopes of different orientations,” Solar Energy, vol.19, no. 2, pp. 179–184, 1977.

[6] T. M. Klucher, “Evaluation of models to predict insolation on tilted surfaces,” Solar Energy, vol. 23, no. 2, pp. 111–114, 1979.

[7] R. Perez, P. Ineichen, R. Seals, J. Michalsky, and R. Stewart, “Modeling daylight availability and irradiance components from direct and global irradiance,” Solar Energy, vol. 44, no. 5, pp. 271–289, 1990.

[8] S. A. Klein, “Calculation of monthly average insolation on tilted surfaces”, Solar energy, Vol. 19, pp. 325-329, 1977.

[9] Yong Sheng Khoo et al., “Optimal orientation and tilt angle for maximizing in-plane solar irradiation for PV applications in Singapore, ” IEEE Journal of Photovoltaics, Vol. 4, No. 2, March 2014.

4.3 Renewable based Hybrid Systems

As conventional fossil fuel energy sources diminish and the world's environmental concern about acid deposition and global warming increases, renewable energy sources (solar, wind, tidal, biomass and geothermal etc) are attracting more attention as alternative energy sources. The solar power or wind power production is intermittent in nature i.e. the generation units remain non-functional during the time when there is no sunlight or the wind speed is not under specific range. These systems when combined can give better results in terms of power production capacity hence it may make the system more efficient, cost effective and high reliable in terms of supply.

Hybrid System Characteristics

- Although hybrid energy systems are open, they can have the characteristics of a closed system if a subsystem with the function of "monitoring" is introduced as a feedback between output (consumer) and input (controller).
- As inputs of particular hybrid system cannot be changed. However, the load may be changed.
- With a backup system as another energy source (for example a diesel generator), the system can be designed as a partial closed-loop feedback system.
- There are various possibly to make combination of different energy sources.
- Selection of energy source for hybrid system is mainly depends upon availability at the place where it going to stabilized.
- In general in India solar energy is available almost all the places and infrastructure for power generation is rugged.
- Hence need low maintenance so it is smart to choose to have PV one of the energy sources in hybrid system.
- Wave and tidal energy available only at sea shore and need large capital investment and more maintenance, therefore not compatible for household hybrid

system but can be used in large power hybrid system. Corrosion because of seawater is a major drawback.

Wind/PV Hybrid System:

- A typical hybrid energy system consists of solar and wind energy sources.
- The power produced by the wind generators is an AC voltage but have variable amplitude and frequency that can then be transformed into DC to charge the battery.
- The controller protects the battery from overcharging or deep discharging.
- As high voltages can be used to reduce system losses, an inverter is normally in traduced to transform the low DC voltage to an AC voltage of 230V of frequency 50 Hz.

PV/Hydro Hybrid System

- In this system there is a small reservoir to store the water.
- This type of hybrid system sometimes depends upon the geographical condition where the water at some height is available.
- System capacity depends upon at the water quantity and solar radiation.
- The power supplied by falling water is the rate at which it delivers energy, and this depends on the flow rate and water head.
- The local water flow and head are limited at this project site, and a relatively simple hydro energy component is used in the project.
- Hydropower available is may be of runoff river type hence produces variable amplitude and frequency voltage.
- It can be use to charge the battery after converting it into DC.

Hybrid Controller:

- This is a controller, which maintains the energy balance during the load variation.
- It assigns the priority among the energy sources (means allow one source, which has highest priority.

- To feed the load if that source is capable and energy coming from other sources will be stored, otherwise allow multiple source to feed the load).
- It also maintains the synchronizing the voltage signal coming from the different sources.
- Suppose the instantaneous magnitude of voltage signal coming from PV sources is differ from that of coming from other source say biomass.
- Hence it causes the local circulating power flow. It can be avoid only by proper synchronizing of signal.

A renewable hybrid energy system consists of two or more renewable energy sources used together to provide increased system efficiency as well as greater balance in energy supply than relative standalone energy systems. Examples of hybrid systems can be PV-wind, PV-biogas, grid-biogas etc. These systems based on their geographical location, resource availability and proper use and maintenance can outperform each other in generating better output.

Environmental impact of the power plants during power production is a primary concern due to release of toxic elements in environment polluting the air and the water. Renewable sources based power production has witnessed lower emissions and hence regarded as clean green energy fuel. Three different hybrid combinations i.e. photovoltaic-biogas, grid-biogas and photovoltaic-wind had been compared using hybrid optimization model for electric renewable (HOMER), to calculate the amount of pollutant produced by each hybrid system whereby the PV- wind system has come out as a least pollutant emission system. HOMER software find its application in optimizing microgrid and distributed energy resource design in all sectors, and estimate the cost-effectiveness of a system

Environmental Impact of different Hybrid Systems

Mamina Patel[1], Shelly Vadhera[2]

***Abstract*— Increase in population causes increase in demand of energy. To meet the demand more power plants are established, which causes increase in pollution, greenhouse gases, global worming etc. So, environmental safety is more important and we need to concentrate on environmental impact due to power generation. To get the best combination of hybrid system for the power generation simulation is done. For the simulation purpose data has been taken from a particular location, Kurukshetra, Haryana. By using the software hybrid optimization model for electric renewable (HOMER) the data is implemented for finding the result. Then different hybrid combinations like photovoltaic-biogas, grid-biogas and photovoltaic-wind are made to calculate the amount of pollutant produced by each hybrid systems and compared on the basis of emission of pollutant**.

Keywords— Environmental impact, Hybrid, Renewable energy, HOMER.

I. INTRODUCTION

In today's world where population is increasing very rapidly, there is ever growing demand for energy. Moreover the recent climatic changes have forced the mankind to manage the tradeoff between economic development and preservation of nature. In India there are plenty of renewable energy resources which can be used to fulfill the future energy demand without harming the environment. The main cause of global warming is pollution due to power plants, cars, vehicle etc.

Ref. [1] introduces the effective levelized cost of energy (LCOE) index as the main aim of the planned design procedure for the system while reducing the energy difference between generation and demand owing to anaerobic digester generator limit and solar resource. This system targets to maximize the PV sizing to follow the forthcoming inclination of more penetration of PV.

Ref. [2] designs the modelling of photovoltaic (PV)-biomass and wind-biomass hybrid systems using hybrid optimization model for electric renewable (HOMER) application. After comparison it finds the best hybrid combination.

The focus on the economical consideration of standalone hybrid system having PV and biomass for electrification of remote area is undertaken in [3]. The data for average solar radiation and quantity of biomass required to predict the general performance of the generating system. Also the extra power is used to supply to the grid. Here the simulation is carried out using HOMER software.

Renewable energy based technology for production of electricity is suitable to remote and rural areas. So the use of standalone hybrid systems using renewable energy for production of electricity is more economical in remote areas [5].

In this paper the modelling of photovoltaic-biogas, biogas-grid and PV-wind have been done in HOMER. Also, the comparison is done on the basis of cost and environmental impact, to find out the best combination of hybrid power system for the environment among the three-system designed using HOMER.

II. SIMULATION IN HOMER

With the help of HOMER, three different systems are designed as shown in Fig. 1, Fig. 2 and Fig. 3. The first system is a configuration of solar–biogas hybrid power system, whereas the second one is a grid–biogas hybrid power system and the third one is PV-wind.

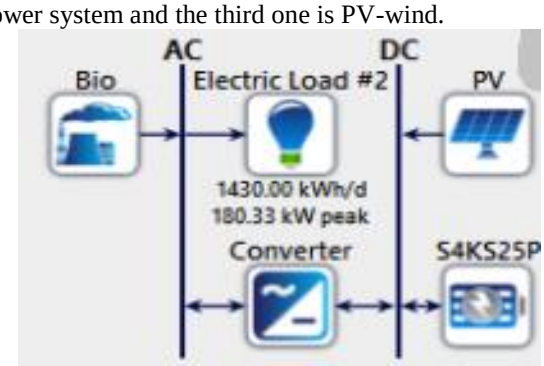

Fig. 1 PV and biogas hybrid

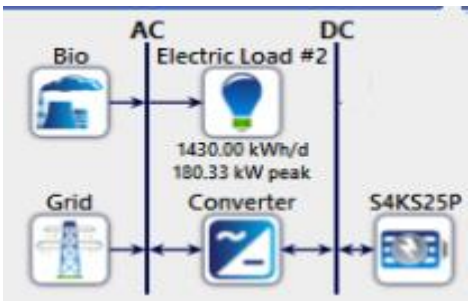

Fig.2 Biogas and grid hybrid

[1]Mamina Patel is with School of Renewable Energy and Efficiency, National Institute of Technology, Kurukshetra, India
[2]Shelly Vadhera is with Department of Electrical Engineering, National Institute of Technology, Kurukshetra, India.

(e-mail: maminapatel1993@gmail.com, shelly_vadhera@radiffmail.com)

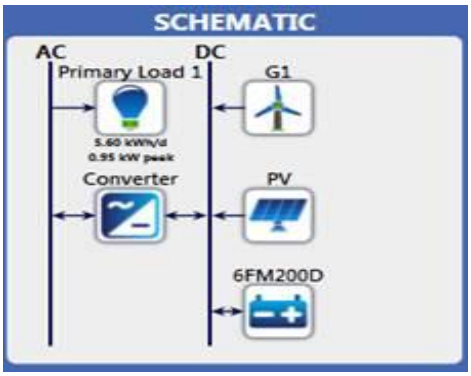

Fig.3 PV-wind hybrid

III. RESOURCES

Different resources are used for the different hybrid combinations for the simulation work.

A. Solar

A solar photovoltaic system, i.e. PV system is designed to supply power using solar energy captured by photovoltaic cells. It comprises of a group of components such as solar panel which absorbs and convert the sunrays into electrical energy, a solar inverter to convert the electric current from DC to AC, secondary wiring and additional electrical equipments to establish a working system. Solar tracking is used to enhance the overall system performance including an integrated battery solution as the prices of storage devices are declining. A solar array only includes the group of solar panels; the visible part of the PV system. Solar panels could be installed as stationary, opposite the sun or connected with some tracing mechanism. The installation ensures that no panel would cast shadow on any of the adjacent panels and those panels can be effortlessly maintained.

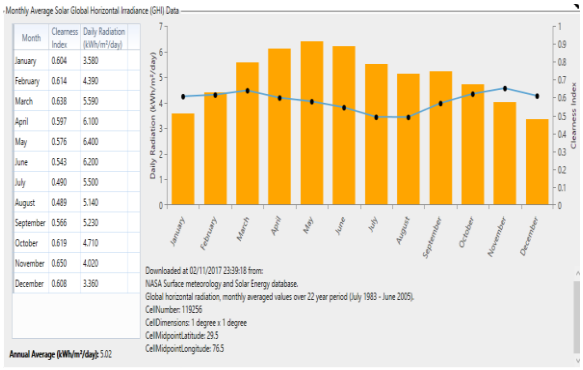

Fig.4 Solar radiation and clearness index

B. Wind

Wind power is the use of air flow through wind turbines to mechanically generators power into electric . The net effects on the environment are far less problematic than those of nonrenewable power sources. Wind power gives variable power, which is very consistent from year to year but has significant variation over shorter time scales. It is therefore used in conjunction with other electric power sources to give a reliable supply. As the proportion of wind power in a region increases, a need to upgrade the grid, and a lowered ability to supplant conventional production can occur.

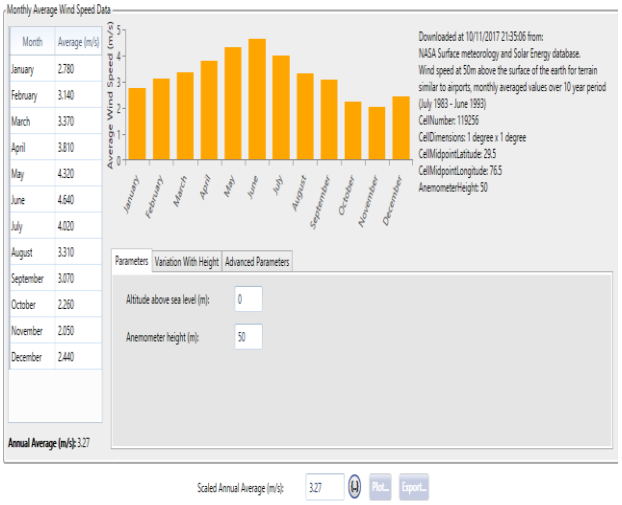

Fig. 5 Wind speed

C. Biogas

By decomposer organisms like fungi, bacteria decomposing biomass and animal waste are fragmented naturally to basic nutrients and soil humus. The process is preferred by wet, warm and dark conditions. There are two types of bacteria such as aerobic and anaerobic.

Aerobic bacteria need oxygen for their growth. The realising of some heat slowly and locally by this composite process, but for energy supply it is not a useful process. Air is to be permited for aerobic, so a loose heap of biomass is important. Emission of methane (CH_4) is very less in aerobic digestion.

In closed conditions, there is absence of oxygen from environment, and by breaking down of carbohydrate material anaerobic bacteria exist. The division of carbon may be fully oxidised CO_2 and fully reduced CH_4. In the solution nutrients such as soluble nitrogen components are available, which provide excellent fertilizer and humus. Anaerobic digestion is preferable. It is emphasized that the fundamental process of natural ecology is both aerobic and anaerobic decomposition that affect all biomass irrespective of human participation.

Fig.6 Biomass resource

D. Grid

The electricity required to meet the demand of the system is taken from grid. It supplies continuous electricity to the system. Source for the grid may be hydroelectric power plant or thermal power plant. For implementation in HOMER the cost of electricity from grid is taken as Rs.6/Unit and annually calculated the value.

E. Hybrid

Solar-biogas

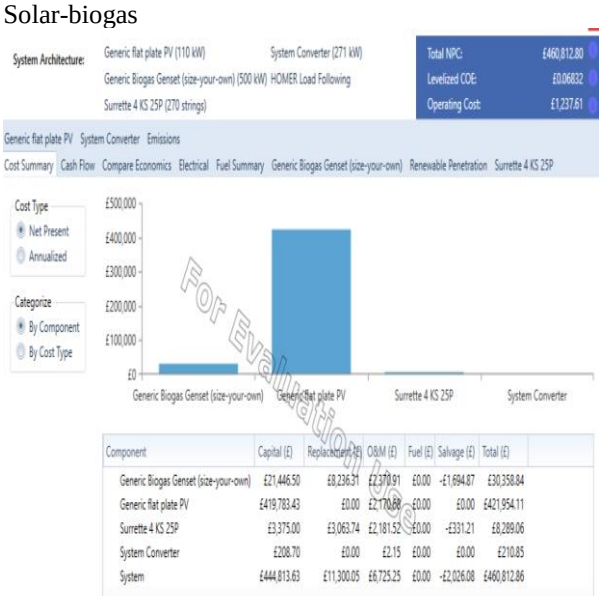

Fig.7 Solar and biogas cost analysis

Grid-biogas

Fig. 8 Grid and biogas cost analysis

Solar and wind

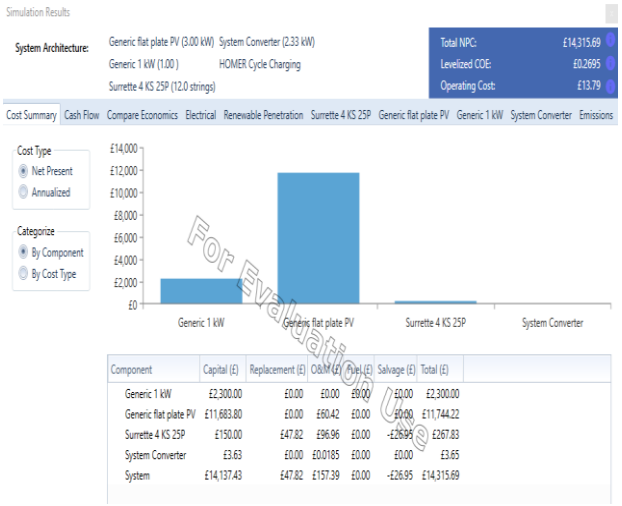

Fig. 9 Solar and wind cost analysis

IV. RESULT

As we know that the important parameter is environmental impact, so the emission analysis is done using HOMER software. Among the three hybrid system the renewable hybrid systems are have less emission of pollutant and among them PV- wind have least pollutant emission.

TABLE I Emission comparison table

Emission (kg/year)			
Pollutant	PV-biogas	Biogas-grid	PV-wind
Carbon dioxide	4	25080	2
Carbon monoxide	0	3.01	0
Unbourned hydrocarbons	0	0	0
Particulate matter	0	0	0
Sulfur dioxide	0	108	0
Nitrogen oxide	2	54.5	1

The above table represents the emission of pollutant in Kg/ year for the three hybrid systems.

V. CONCLUSION

An assessment is done between all the three hybrid system, based on environmental aspects from the reports generated by the HOMER. Finally, it is concluded that the renewable hybrid systems design are more reliable, and environmental friendly (emission of pollutant is less) as compared to biomass-grid hybrid system for electrification. Among them the PV-wind hybrid system is the best among these three systems as it contributes to less carbon footprints.

REFERENCES

[1] C. S. Lai and M. D. McCalloch, "Sizing of standalone solar PV and storage system with anaerobic digestion biogas power plants," IEEE Trans. Ind. Electron., vol. 64, no. 3, pp. 2112-2121 Mar. 2017.

[2] S. Mishra, C. K. Panigrahi and D. P. Kothari, " Design & simulation of a solar-wind-biogas hybrid system architecture using HOMER in india," International Journal of Ambient Energy, vol. 37, pp. 184-191, 2016.
[3] S. R. Pradhan, P. P. Bhuyan and S. K. Sahoo, " Design of standalone hybrid biomass & PV system of an off-grid house in a remote area," Int. journal of Engineering Research and Application, vol.3, pp. 433-437, Nov-Dec 2013.
[4] X. Li, C. P. Bowers and T. Schnier, " Classification of energy consumption in buildings with outlier detection," IEEE Trans. On Industrial Electronics, vol. 57, Nov 2010.
[5] C. S. Lai and M. D. McCalloch, "Sizing of standalone solar PV and storage system with anaerobic digestion biogas power plants," IEEE Trans. Ind. Electron, vol. 64, no. 3, pp. 2112-2121 Mar. 2017.
[6] P. Anand, S. K. Bath, and M. Rizwan, "Design of solar-biomass-biogas based hybrid system for rural electrification with environmental benefits," International Journal on Recent and Innovation Trends in Computing and Communication (IJRITCC), vol. 5, no. 6, pp. 450-456, Jun. 2017.
[7] J. D. Rozario, S. Shams, S. Rahman, A. Sharif, and E. Basher, "Cost effective solar-biogas hybrid power generation system," IEEE International Conference on Industrial Technology (ICIT), pp. 2756-2760, May 2015.
[8] S. Salehin, A. K. M. S. Islam, R. Hoque, M. Rahman, A. Hoque, and E. Manna, "Optimized model of a solar PV-biogas-diesel hybrid energy system for Adorsho Char Island, Bangladesh," 3rd International Conference on the Development in Renewable Energy Techonology (ICDRET), pp. 1-6, 2014.
[9] S. Sinha and S. S. Chandel, "Review of recent trends in optimization technique for solar photovoltaic-wind based hybrid energy system," Renewable and Sustainable Energy Review, vol. 50, pp.755-769, Oct. 2015.
[10] R. Pode, B. Diouf, and G.Pode, "Sustainable rural electrification using rice husk biomass energy: A case study of Cambodia," Energy for Sustainable Development, vol. 44, pp. 530-542, Apr. 2015.

Conclusion:

The solar power generation after its introduction in Indian power system in 2008, has gradually increased over the years. After analyzing the benefits and environmental concerns, its production is still on increase. The issues, related to the production and large integration, are being addressed with advancement in research and technology. The design parameters and system model had been simulated to reflect the effects that improve the output power. The 'direct beam' of sunlight carries about 90% of the solar energy, whereas the 'diffuse sunlight' carries the remainder. It is necessary to present the maximum surface area of the PV module to the direct beam of the sun, in order to produce the largest amount of power.

Advancement in wind power control and operation has also taken a step ahead. Virtual synchronous generator (VSG) used in wind energy systems can help to suppress voltage sag and power fluctuations, and improve the transient response in the grid. Three level three diode clamped converter provides the guarantee for almost unity power factor for mains, dense control of the dc-link voltage. Also the current injected into the grid, improves the power quality. Performance analysis of modular multilevel converter (MMC) has been done. MMC can reduce the need of much bulky filters to eliminate harmonics with an additional advantage of making high voltage and power capability possible by series connections.

Modeling of wind farm with the help of doubly fed induction generator has been done to study economic load dispatch using multi objective particle swarm optimization (PSO) technique. The proposed multi objective PSO technique helps the researchers to overcome some of the difficulties of the conventional single objective PSO algorithm. The neural network intelligence when applied to single and double diode model of solar PV-battery system delivers output power, voltage and current with less ripples and higher magnitude as compared to MPPT technology.

The exploitation of sunlight and air as a substantial Renewable Energy (RE) source is an important research and development domain over past few years. The present and future overtaking in RE mainly comprises of (i) the development of novel technology for optimum production from the available natural resources (ii) environmental awareness, and (iii) the better management and distribution system. Like other domains (food, health, accommodation,

safety, etc.), Artificial Intelligence (AI) could assist in achieving the future goals of the RE. Statistical and biologically inspired AI methods have been implemented in several studies to achieve common and future aims of the RE.

The hybrid systems have been useful to power systems in many ways. Some of them are enlisted as under:

- Hybrid systems can address limitations in terms of fuel flexibility, efficiency, reliability, emissions and / or economics.
- Incorporating heat, power, and highly efficient devices (fuel cells, advanced materials, cooling systems, etc.) can increase overall efficiency.
- Conserve energy for a hybrid system when compared with individual technologies.
- Achieving higher reliability can be accomplished with redundant technologies and/or energy storage.
- Some hybrid systems typically include both, which can simultaneously improve the quality and availability of power.
- Hybrid systems can be designed to maximize the use of renewable sources.
- Resulting in a system with lower emissions than traditional fossil-fueled technologies.
- Hybrid systems can be designed to achieve desired attributes at the lowest acceptable cost, which is the key to market acceptance

Owing to greater benefits and reduction in the carbon footprints, various ongoing schemes and targets have been mapped by Government of India related to renewable energy sources. These schemes focus on increasing the production and overcoming issues related to large production, cost effectiveness and penetration of the green energy more into the existing system. Some of the large and advanced solar power plants, onshore and off shore wind farms are under-construction while some are already commissioned in high potential areas. Policies have been framed and incentives given to the customers to induce more utilization of these sources at standalone sites like rooftop.

Chapter -5.

Recent Headways in Power System

5.1 Multilevel Inverters

Inverters are the devices used to convert low level power from d.c. to a.c. power and find application in home for emergency power back up, radio, radar and other appliances. A multilevel inverter is an advanced power electronic inverter which can take multiple low or medium level d.c. inputs and give output as a.c. voltage at different higher levels. In recent years, multilevel inverter (MLI) have become single point solution for many applications in medium and high power conversion systems thus increasing usage of power electronic devices in renewable energy systems.

The conventional inverters have limitations in handling high voltage and high power conversion. For higher output voltage capacity and reduction in harmonic distortion, these converters need to be connected in series using transformers. Also, these series connection of inverters are the contributors to problems such as bulkiness, high loss and high cost to the overall AC system. Besides that, conventional inverters have some disadvantages operating at high frequency mainly due to switching losses and constraints of the device ratings. To overcome the disadvantages of conventional inverters, multilevel inverters emerge as the new breed of converters in high and medium power applications. A multilevel converter not only achieves high power ratings, but also enables the use of renewable energy sources. Renewable energy sources such as photovoltaic, wind and fuel cells can be easily interfaced to a multilevel converter system for a high power application

FEATURES:

- The general structure of the multi-level inverter is to obtain a sinusoidal voltage from several level of voltages, obtained from various capacitor voltage sources.
- The MLI start from three-level.
- The unique structure of MLI allows them to reach high voltages with lower harmonics without the use of transformer or series-connected synchronized switching devices.

There are basically 3 topologies of Multi-Level Inverters, namely :

1. Diode Clamped MLI
2. Flying Capacitor MLI
3. Cascaded MLI

Diode Clamped Multi-level Inverter

The diode-clamped inverter is also known as the neutral-point clamped inverter (NPC) which was introduced by Nabae et al (1981). The diode-clamped inverter consists of two pairs of series switches (upper and lower) in parallel with two series capacitors where the anode of the upper diode is connected to the midpoint (neutral) of the capacitors and its cathode to the midpoint of the upper pair of switches; the cathode of the lower diode is connected to the midpoint of the capacitors and divides the main DC voltage into smaller voltages.

The advantages for the diode-clamped inverter are, (1) A large number of levels 'n' yields a small harmonic distortion. (2) All of the phases share a common dc bus. (3) Reactive power flow can be controlled. (4) High efficiency for fundamental switching frequency. (5) Relatively simple control methods.

The disadvantages are, (1) Different voltage ratings for clamping diodes are required. (2) Real power flow is difficult because of the capacitors imbalance. (3) Need high voltage rating diodes to block the reverse voltages. (4) The number of switches, capacitors, and diodes required in the circuit increases with the increase in the number of output voltage levels. Extra clamping diodes required are (n-1)(n-2) per phase.

Flying Capacitor MLI

The capacitor-clamped multilevel inverter known as flying capacitor, provides more flexibility in waveform synthesis and balancing voltage. In capacitor-clamped inverter, the diode in the diode-clamped topology is replaced by clamping capacitors or floating capacitors to clamp the voltages. Each phase-leg has an identical structure. The size of the voltage increment between two capacitors determines the size of the voltage levels in the output waveform.

The advantages of the capacitor-clamped multilevel inverter are, (1) Large 'n' allows the capacitors extra energy during long discharge transient. (2) Phase redundancies are available

for balancing the voltage levels of the capacitors. (3) Lower Total Harmonic Distortion when the number of levels ‘n’ is high. (4) Active and Reactive power flow can be controlled.
The disadvantages are, (1) Large numbers of capacitors are bulky and more expensive than the clamping diodes used in the diode-clamped multilevel inverter. (2) Complex control is required to maintain the capacitor’s voltage balance. (3) Switching utilization and Efficiency are poor for real power transmission.

Cascade Multi Level Inverter

The cascaded H-bridge inverter has drawn tremendous interest due to the greater demand of medium-voltage high-power inverters. The cascaded inverter uses series strings of single-phase full-bridge inverters to construct multilevel phase legs with separate dc sources. A single H-bridge is shown in Figure 2.5. The output of each H-bridge can have three discrete levels, results in a staircase waveform that is nearly sinusoidal even without filtering. A single H-bridge is a three-level inverter. Each single-phase full-bridge inverter generates three voltages at the output: ,0, Vdc and Vdc .
The advantages for cascaded multilevel H-bridge inverter are: (1) The series structure allows a scalable, modularized circuit layout and packaging due to the identical structure of each Hbridge. (2) No extra clamping diodes or voltage balancing capacitors are necessary. (3) Switching redundancy for inner voltage levels is possible because the phase voltage is the sum of the output of each bridge. The disadvantage for cascaded multilevel H-bridge inverter is that it needs separate DC sources.

Multilevel inverters generate sinusoidal voltages from discrete voltage levels, and Pulse Width-Modulation (PWM) strategies accomplish this task of generating sinusoids of variable voltages and frequencies. Several techniques for the implementation of PWM for multilevel inverters have been developed. Among them multi carrier PWM is popular for its simplicity and computational ease. It is classified mainly in two types- Level-shifted pulse-width modulation (LSPWM) and phase-shifted pulse-width modulation (PSPWM) scheme based on carrier signal used.

Carrier rotation schemes are employed to rotate switching patterns in cascaded H-bridge MLI to evenly distribute power losses. Many such carrier rotation schemes are available for combining the merits of equal device conduction period and even power distribution in H-bridge cell obtained from phase-shifted pulse-width modulation (PSPWM) scheme & better harmonic performance obtained from level-shifted pulse-width modulation (LSPWM) scheme. One such method of carrier rotation is obtained by combining triangular wave and staircase waveform. This type of rotation arrangement is investigated for equal power distribution through simulation on seven level cascaded modular H-bridge MLI. The results obtained lead to the observation that with carrier rotation schemes equal power distribution as PSPWM with improved THD can be achieved

Power distribution equalization in Cascaded H-Bridge Multi level Inverter by employing Carrier Rotation Schemes

Nimmi[1], Aeidapu Mahesh[2]

***Abstract*— To control the output AC voltage of a Multilevel inverter (MLI) various modulation schemes are employed. Among them Multi carrier PWM is popular for its simplicity and computational ease, and is classified mainly in two types- Level-shifted pulse-width modulation (LSPWM) and phase-shifted pulse-width modulation (PSPWM) scheme based on carrier signal used. LSPWM for Cascaded H-bridge multilevel inverter produces better harmonic performance than the phase-shifted pulse-width modulation (PSPWM) scheme, but because of the unequal device conduction time its applications are limited to low power applications. Carrier rotation schemes can be employed in PSPWM to rotate switching patterns in Cascaded H-bridge MLI to evenly distribute power losses. Many such carrier rotation schemes are presented in literature for combining the merits of equal device conduction period and even power distribution in H-bridge cell from PSPWM scheme & better harmonic performance from LSPWM scheme. Two such carrier rotation schemes are evaluated for equal power distribution among all cells of a Cascaded H- Bridge Multi level Inverter by simulating for seven level H-bridge cascaded multi-level inverter (MLI).**

Keywords—pulse width modulation, H-bridge multilevel inverter, carrier rotation scheme, equal power distribution

LIST OF ABBREVIATIONS

f_{sw} switching frequency
m_i amplitude modulation index
α Load power factor angle
T_{carr} Time period of carrier signal

I. INTRODUCTION

In recent years MLI have become single point solution for many applications in medium and high power conversion systems thus increasing usage of power electronic devices [1]-[5]. Many different MLI topologies are listed in literatures, three most famous ones are - Diode clamped, flying capacitor and cascaded H-bridge multilevel inverters. Each one has its merits and limitations.

Due to modular structure, capability of series expansion, voltage balancing ease, direct connection possibility and non requirement of pre charging of capacitors, cascaded H-bridge inverters are the first choice and hence successively commercialized for high power applications.

[1]Nimmi is with School of Renewable Energy and Efficiency, National Institute of Technology, Kurukshetra, India
[2]Aeidapu Mahesh is with Department of Electrical Engineering, National Institute of Technology, Kurukshetra, India.
(e-mail: nimmi.nits2012@gmail.com, mahesh.aeidapu@gmail.com)

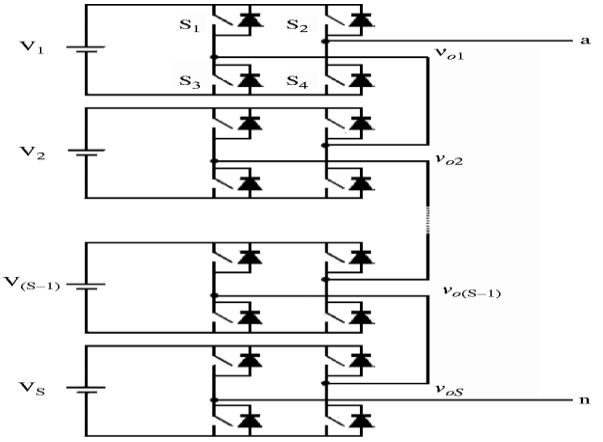

Fig. 1. Cascaded H-bridge multilevel inverter

II. MODULATION TECHNIQUES

Renewable Energy sources produce fluctuating DC power which needs to be converted to controllable AC power for integrating to grid. For controlling the output AC voltage (or power) of MLI various modulation techniques are used Sinusoidal PWM, Multi carrier PWM, Space vector modulation and Selective harmonic elimination [1], [6]-[9]. In between them multi carrier PWM is most popular due to its computational ease and simplicity [10]. Based on carrier signals, the carrier based PWM technique is classified mainly into PSPWM and LSPWM [11]-[12].

In LSPWM, the carriers are shifted vertically but in PSPWM the carriers are displaced horizontally with maintaining a specific phase shift. Due to this arrangement of carriers PSPWM has the advantage of equal power distribution between cells but LSPWM has better harmonic performance. Therefore for combining the advantages of both modulation techniques carrier rotation schemes have been proposed in literatures [13]-[17]. The present paper evaluates two such rotating strategies incorporated to LSPWM for having equal power distribution with improved harmonic. The remaining of this paper is organized as follows: In Section 3, two carrier rotation strategies are presented, section 4 covers output voltage waveforms. Calculations for power loss for the carrier rotation strategies are furnished in sections 5 followed by results and conclusion in section 6 and section 7.

III. CARRIER ROTATION STRATEGY

In multi carrier PWM scheme *(n-1)* number of carriers is required for *n* level MLI output voltage control. The carrier rotation is obtained by combining triangular wave and staircase waveform. After every time period of carrier wave (T_{carr}) carrier 1 attains position of carrier 2 and carrier 2 attains position of carrier 3 in the next T_{carr}. Remaining carriers follow this process. The time period of staircase waveform is kept as (*n-1*) times the time period of carrier wave (T_{carr}) for achieving rotation of carriers. Thus after (*n-1*) T_{carr} time the carriers attain their original positions. Fig. 2(a) depicts the carriers in PDPWM scheme for seven level cascaded H-bridge MLI, Fig. 2(b) and 2(c) depict the arrangement for carriers for the two rotation strategies.

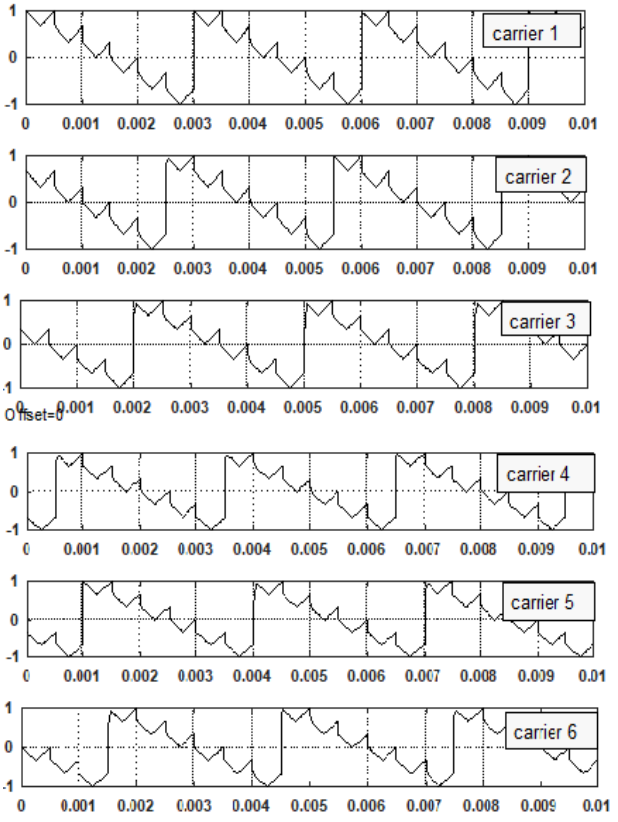

(a)

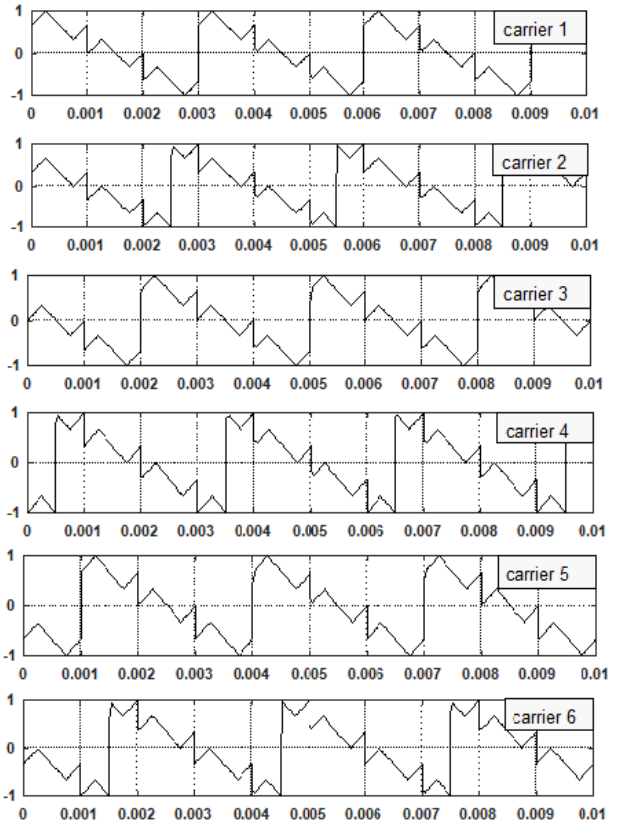

(b)

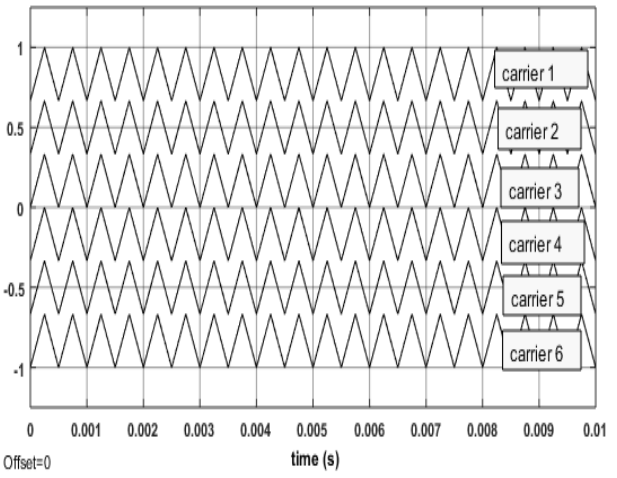

(c)

Fig. 2.Carrier rotation scheme for seven level H -bridge MLI for (a) Rotation 1 (b) Rotation 2 (c) basic PDPWM scheme

IV. OUTPUT VOLTAGE WAVEFORMS

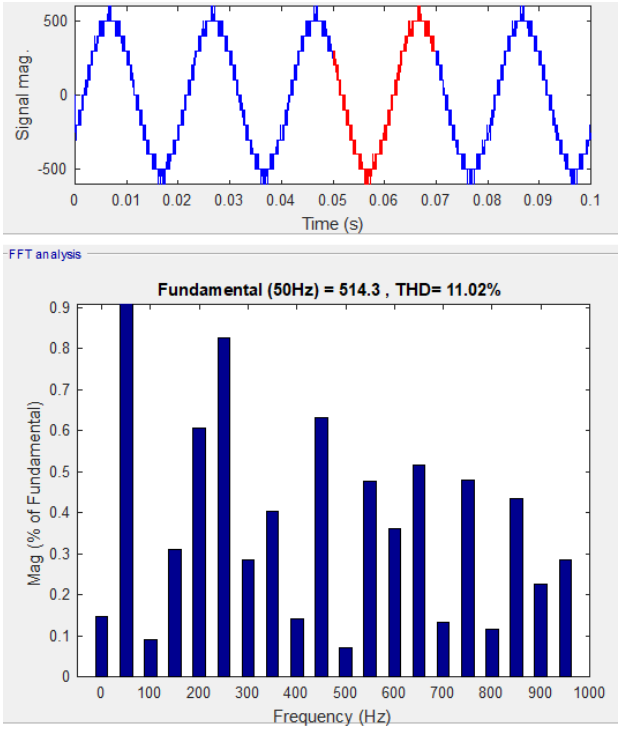

(a)

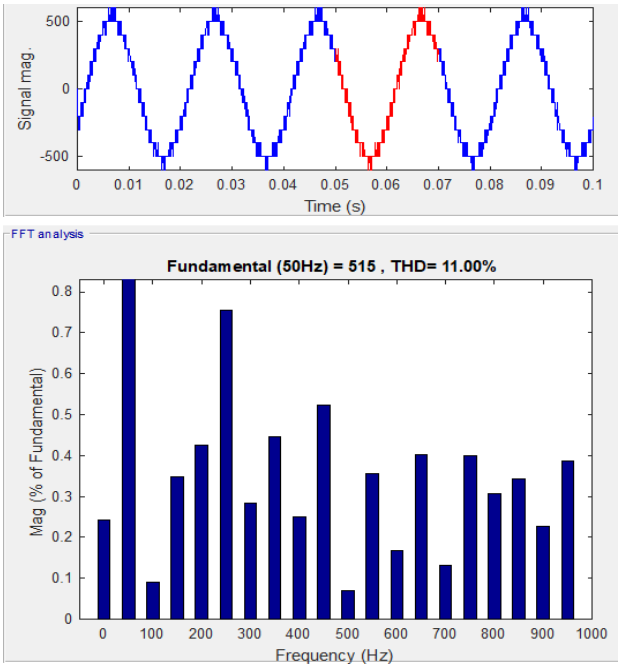

(b)

Fig. 3.Simulated waveform for Line voltage and harmonic spectrum of a basic seven level H-bridge MLI for m_a=1, m_f=40, f_m=50Hz, f_{carr}=2000Hz (a) Without rotation PD-LSPWM b) carrier rotation 1 (c) carrier rotation 2

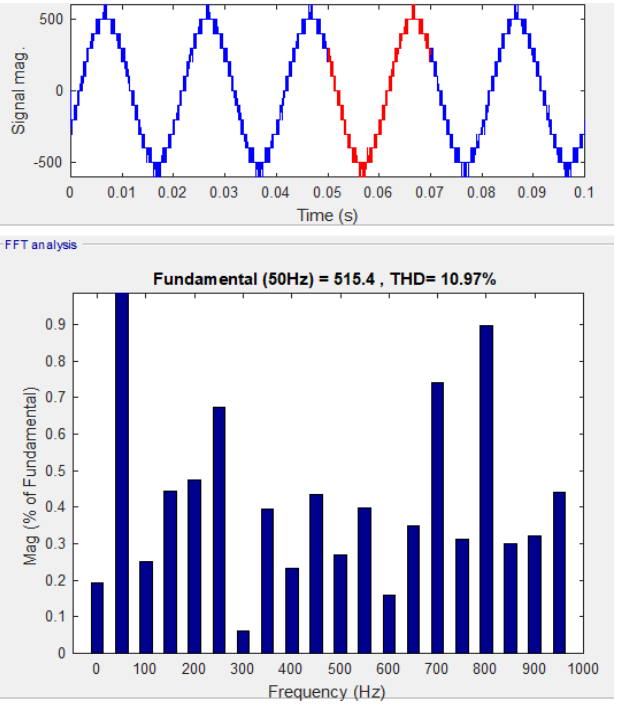

(c)

Fig. 3(a), (b) and (c) depict the output voltage and harmonic spectrum of a seven level H-bridge multilevel inverter. From Fig. 3 it can be seen that dominant harmonic is near to 40th harmonic which is the frequency modulation index. The noticed total harmonic distortions (THDs) in line voltage are 11.02%, 11.00% and 10.97% for PDPWM, arrangement-1 and arrangement-2 carrier rotation schemes, respectively.

V. POWER LOSS CALCULATIONS

The power losses can be classified into conduction and switching losses. These losses are due to on state voltage drop in the switching device. For calculating the losses the switching devices which are IGBT and diodes are modelled as series combination of voltage drop with resistance. The load current is assumed to be sinusoidal for making the calculations simple.

A. *Conduction losses*

Equations for device currents are given below

$$I_{Aavg} = I_{Lp} * \left[\frac{1}{2\pi} + \frac{m_i \cos\alpha}{8}\right] \quad (1)$$

$$I_{Arms} = I_{Lp} * \sqrt{\frac{1}{8} + \frac{m_i \cos\alpha}{3\pi}} \quad (2)$$

$$I_{Bavg} = I_{Lp} * \left[\frac{1}{2\pi} - \frac{m_i \cos\alpha}{8}\right] \quad (3)$$

$$I_{Brms} = I_{Lp} * \sqrt{\frac{1}{8} - \frac{m_i \cos\alpha}{3\pi}} \quad (4)$$

Where I_{Lp} is the peak value of load current, α denotes the load power factor angle, m_i is amplitude modulation index.

I_{Aavg} , I_{Arms} , I_{Bavg} and I_{Brms} specifies the average and rms currents of IGBT and diode respectively. Now conduction power losses (P_{con}) are calculated by below equations.

$$P_{Acon} = V_{Avd}.I_{Aavg} + I_{Arms}^2.R_A \quad (5)$$

$$P_{Bcon} = V_{Bvd}.I_{Bavg} + I_{Brms}^2.R_B \quad (6)$$

Where V_{Avd} , V_{Bvd} , R_A and R_B respectively are the onstate voltage drops and resistances of IGBT and diode which can be obtained from data-sheets. Now, the total conduction losses occurred in any individual cell comprising 4 IGBTs and 4 Diodes of of a Cascaded H-bridge MLI are givenby*:*

$$P_{Totcon} = 4(P_{Acon} + P_{Bcon}) \quad (7)$$

From the above equations, it is clear that the conduction losses are only function of loading conditions.

B. Switching losses

Switching losses in the devices occur during turning on and turning off transitions and can be calculated using the below equations.

$$P_{Asw} = \left(E_{Aon} + E_{Aoff}\right) * f_{sw} \quad (8)$$

$$P_{Bsw} = \left(E_{Bon} + E_{Boff}\right) * f_{sw} \quad (9)$$

Where E_{Aon} , E_{Aoff} , E_{Bon} , E_{Boff} are the turn on and off energy losses of IGBT and Diode respectively and can be obtained from data sheets. The above equations shows that switching losses are purely dependent on switching frequency.

$$P_{Totsw} = P_{Asw} + P_{Bsw} \quad (10)$$

Now the total power losse can be calculated as:

$$P_{Tot} = P_{Totcon} + P_{Totsw} \quad (11)$$

VI. RESULT AND DISCUSSION

Simulation models for different multi carrier PWM scheme together with carrier rotation schemes were created for seven level Cascaded H-bridge MLI. Load parameter taken as R= 55 Ω and L= 150 mH. Input DC voltage to all the three cells of MLI are given as V_{DC} = 50V each. Device parameters from datasheet are given below

IGBT	Diode
V_{Aon} = 0.85V	V_{Bon} = 0.90V
R_{Aon} = 0.0022Ω	R_{Bon} = 0.0014Ω
E_{Aon} = 3.5mJ	E_{Bon} = 2.8mJ
E_{Aoff} = 2.0 mJ	

Power losses were calculated as per equations given in section IV are presented in Table 1.

TABLE I. POWER LOSS IN WATT

Modulation Type	Power Loss		
	Cell 1	*Cell 2*	*Cell 3*
PS-PWM	24.09	24.19	23.96
PD-PWM	19.03	26.65	27.82
POD-PWM	19.26	26.46	27.22
APOD-PWM	19.72	26.88	27.8
ROTATION 1	23.82	22.91	23.59
ROTATION 2	24.36	23.12	23.27

It can be seen from Table 1 that power loss were almost equalized for rotation schemes.

VII. CONCLUSION

In employment of a multi carrier PWM technique for managing the output voltage of multilevel inverter, the two major requirements are improved harmonic performance and equal power distribution across different cells. Presented rotation arrangements are investigated for equal power distribution through simulation on seven level cascaded modular H-bridge MLI. Using calculations, power loss of all cells were computed. The results demonstrate that with carrier rotation schemes equal power distribution as PSPWM with improved THD can be achieved. It can be further applied to other modular multi level cascaded inverter topologies.

REFERENCES

[1] J. Rodriguez, J. S. Lai, and F. Z. Peng, "Multilevel inverters: Survey of topologies, controls, and applications," IEEE Trans. Ind. Electron., vol. 49, no. 4, pp. 724-738, Aug. 2002.

[2] F. Blaabjerg, Y. Yang, K. Mam, and X. Wang, "Power Electronics - the key technology for renewable energy system Integration," Proc. of 4th Intl. Conf. on renwable Energy Research and Application (ICRERA), 2015.

[3] D. G. H. B. P. McGrath and W. Y. Kong, "A decentralized controller architecture for a cascaded h-bridge multilevel converter," IEEE Transactionson Industrial Electronics, vol. 61, no. 3, pp. 1169–1178, March2014.

[4] T. Atalik, M. Deniz, E. Ko, C. . Gerek, B. Gltekin, M. Ermis, and I. adrc, "Multi-DSP and -FPGA-based fully digital control system for cascaded multilevel converters used in facts applications," IEEE Transactions on Industrial Informatics, vol. 8, no. 3, pp. 511–527, August 2012.

[5] F. Z. Peng, "A generalized multilevel inverter topology with self voltage balancing," IEEE Trans. Ind. Appl., vol. 37, pp. 611-618, Mar./Apr. 2001.

[6] F. Carnielutti, H. Pinheiro, and C. Rech, "Generalized carrier-based modulation strategy for cascaded multilevel converters operating under fault conditions," IEEE Transactions on Industrial Electronics, vol. 59, no. 2, pp. 679–689, February 2012.

[7] A. M. Massoud, S. J. Finney, and B. W. Williams, "Control techniques for multilevel voltage source inverters," in Proc. 34th Annu. Power Electron. Specialist Conf. (PESC), Jun. 2003, vol. 1, pp. 171-176.

[8] D.Far, A.Radan, and M.D.Far, "Introduction and evaluation of novel multi-level carrier-based PWM strategies using a generalized algorithm," in Proc. European Conf. on Power Electron. and Appl. (EPE), Sept. 2007, pp. 1-10.

[9] M. Sharifzadeh, H. Vahedi, A. Sheikholeslami, P. A. Labbé and K. AlHaddad,"Hybrid SHM–SHE Modulation Technique for a Four-Leg NPC Inverter With DC Capacitor Self-Voltage Balancing," in IEEE Transactions on Industrial Electronics, vol. 62, no. 8, pp. 4890-4899, Aug. 2015.

[10] Bin Wu, "High Power Converters and AC drives" Pg. no. 131-139, AJohn Wiley & Sons, Inc., Publication.

[11] G. Carrara, S. Gardella, M. Marchesoni, R. Salutari, and G. Sciutto, “A new multilevel PWM method: A theoretical analysis,” IEEE Trans. Power Electron., vol. 7, no. 3, pp. 497-505, Jul. 1992.

[12] B. P. McGrath and D. G. Holmes, “Multicarrier PWM strategies for multilevel inverters,” IEEE Trans. Ind. Electron., vol. 49, no. 4, pp. 858-867, Aug. 2002.

[13] J.Chavarria, D. Biel, F. Guinjoan, C. Meza and J. J. Negroni, “Energy-balance control of PV cascaded multilevel grid-connected inverters under level-shifted and phase-shifted PWMs,” IEEE Trans. Ind. Electron., vol. 60, no. 1, pp. 98-111, 2013.

[14] Mariusz Malinowski, K. Gopakumar, Jose Rodriguez, and Marcelo A. Prez, “A survey on cascaded multilevel inverters,” IEEE Trans. Ind. Electron., vol. 57, no. 7, pp. 2197-2206, Jul. 2010.

[15] S. Dharmavarapu, P. Agarwal, and B. Das. "Performance evaluation of carrier rotation strategy in levelshifted pulse-width modulation technique", IET Power Electronics, 2013.

[16] Sarkar, Indrajit, and B. G. Fernandes, "Modifiedhybrid multi-carrier PWM technique for cascaded H-Bridge multilevel inverter," Proc. Of
40th Anl. Conf. of the IEEE Industrial Electronics Society(IECON), 2014.

[17] M. Angulo, P. Lezana, S. Kouro, J. Rodriguez and B. Wu, “Level-shifted PWM for cascaded multilevel inverters with even power distribution,”in Proc. IEEE Power Electron. Spec. Conf.(PESC), Jun. 2007, pp. 2373-2378.

5.2 Gas Insulated Substation

It is very much required to establish an electrical substation at load center. Since, establishing a substation at load center is quite economical and profitable in many aspects. As it reduces length of feeders and due to short length feeders, the quality of voltage regulation improves. But the main obstruction of establishing a substation at load center is space. Generally main load center of any place is situated at very congested place where, sufficient land for establishing conventional electrical substation is very hardly available. This problem can be solved by using gas insulated switchgear technology. In this type of switchgear, all the necessary components of switchgear can be assembled in very limited space. GIS is a kind of metal enclosed switchgear. That means, all the equipments of the electrical switchgear are enclosed by gas tight metal enclosure and SF6 gas is used as insulation between live parts of the equipments and earthed metal enclosure. This type of switchgear, means, and gas insulated switchgear is available from 12 KV systems to 800 KV system. For establishing electrical substation in very limited place this type of SF6 insulated electrical switchgear plays the major role.

In gas insulated substation (GIS), different grid components including electrical bus bars, electrical isolators or disconnectors, circuit breakers, current transformers. voltage transformers, earth switches, surge arrestors or lightning arresters are insulated with sulphur hexafluoride (SF6) gas and installed inside grounded metal enclosures. SF6 gas is a colorless, odorless, non-toxic and non-inflammable gas. This gas has high dielectric strength and electronegativity, denser than air, provides excellent insulation and better reliability than air insulation. The high electronegativity property enables the molecules of this gas to absorb free electrons in the arc path making it highly suitable for arc quenching. The SF6 gas used as medium in circuit breakers is highly preferable and accurate among other conventional mediums used.

The Switching operations in a GIS substations lead to very fast electromagnetic transients which can affect the performance of the secondary equipment. Estimation of magnitudes of these fields is essential to decide the quality of shielding to be provided to the control equipment mounted directly on the switchgear or on the bus bar enclosure. The accurate computer

simulations provide deeper imminent in transient phenomena which are important for insulation coordination, protection techniques and best possible substation design.

The development of GIS started in 1960's and got accepted all over the world. In India, approximately 40 GIS have been installed at voltage class of 800kv, 420kv, 245kv or below. GIS is preferred in those locations where land is not available in abundance or is congested enough to locate a high voltage substation e.g. near cities. This system decreases the occurrence of faults and outages due to its high reliability as compared to the conventional substations. But the problem with this system is its high cost and high maintenance requirement while installation i.e. utmost care has to be taken to maintain the SF6 gas pressure constant and keep the environment dust-free to let no dust or foreign particle enter the compartments where live components are present as these conditions may lead to faults and flashovers. However, less maintenance is required after the system has been commissioned because all the live parts are isolated from atmosphere dust and abrasion in an insulated environment. A fault occurring inside the system is difficult to be located due to the closed structure. Hence a great care is taken while designing the system and installing the parts of the system.

In gas insulated medium voltage switchgear, vacuum technology is used as interrupting purpose and SF6 gas is used as insulation material. Although for both interruption and insulation, SF6 gas is used in many medium voltage GIS system. But for such equipments rated SF6 gas pressures are different for interruption and insulation. SF6 gas pressure for insulating purpose is generally kept below 2.5 bar whereas SF6 gas pressure for interrupting purpose is ranged from 5 bar to 7 bar. As vacuum technology is not available for high voltage, so for GIS or gas insulated switchgear system above 72.5 KV, only SF6 is used both as interruption medium and insulation.

There are different types of gas insulated metal enclosed switchgears available depending upon their constructional feature.

Isolated Phase GIS

In this configuration, each phase of the bay is assembled separately. That is, for each phase, one pole of circuit breaker, a single pole of electrical isolator, one phase assembly of current transformer are assembled together. This type of GIS requires larger bay width as compared to other gas insulated switchgear system.

Integrated 3 Phase GIS

In this configuration all three phase of circuit breaker, 3 phases of disconnectors and three phase current transformer are encapsulated in an individual metal enclosure. The arrangement forms a three phase module for the element. The size of this type of module is one third of the isolated phase GIS.

Hybrid GIS System

It is a suitable combination of isolated phase and three phase common elements. Here three phase common bus bar system simplifies the connection from the bus bar. The isolated phase equipment prevents phase to phase faults. This is an optimum design considering, both facts in mind, i.e. space requirement and maintenance facility.

Compact GIS

In this GIS or gas insulated switchgear system than one functional element are encapsulate in a single metal enclosure. For example, in some design, a three phase circuit breaker, current transformer, earth switches, even other feeder elements are covered together in a single metal capsule.

Highly Integrated System

This design was introduced in the year of 2000, where, total substation equipments are encapsulated together in single enclosure housing. This single unit gas insulated substation has gained user appreciation as it is a complete solution for an outdoor substation, in a single unit. As such, only equipment (HIS) is substitute of a total outdoor switch yard.

Construction and Design Features of Gas Insulated System (GIS)

Hemant Kumar

Abstract - Energy demands are increasing day by day and so is the burden on conventional & other non-conventional sources of energy. Power Sector and associated energy demands in India are growing at an accelerated pace. In a bid to further enhance the transmission capacity, India has moved towards ULTRA HIGH VOLTAGE (UHV) transmission level and has adopted 1200kV (UHV) AC system to transfer power over a large geographical area. One of today's major challenges in power transmission is to bring high voltage levels right into the urban area, which in turn requires switchgear that has small footprint, utmost reliability, very low noise and electromagnetic emissions. Usage of Gas Insulated System (GIS) serves as the most convenient option having high reliability, availability, high degree of safety, compact design, long service life etc.

I. INTRODUCTION

Gas insulated substations (GIS) have become a major component of power networks and have been used with considerable success over the past 40 years. GIS are exposed to different over-voltages compared to conventional substations (i.e., lightning, switching and temporary over-voltages). In conventional substations the protection of transformers against over-voltages is the most important concern [1]. In GIS, the entire gas insulated assembly (including enclosures, circuit breakers, disconnect and grounding switches) must be protected against severe over-voltages because the gas insulated system is partially non-self-restoring. Introduction of gas-insulated switchgear technology during the seventies allowed the end-users, in a first step, to take advantage of the compactness and the insensitivity to the environmental conditions of SF6 Gas Insulated Switchgear (GIS). Further reasons based on geographically difficult areas, pollution and/or environmental issues, visual appearance of a substation, but also crime, terrorism and material damage are forcing hidden solutions. Underground, indoor GIS substations have proven their superior reliability in the Middle East and Europe, and thus represent the proper answer to the world electrical delivery challenges [2]. World utilities are today also looking for upgrade, refurbishment and extension of infrastructure with new solutions, predictably higher reliability and long-term availability [3].

Hemant Kumar is with Department of Electrical and Instrumentation Engineering, Thapar Institute of Engineering & Technology, Patiala (Punjab), India

(e-mail: hkumar_me17@thapar.edu)

II. PLANNING AND INSTALLATION OF GIS

A deliberate and complete installation plan, including the future addition of similar equipment, is essential so that all aspects of construction can be reviewed. The preassembled sections of the equipment and the manufacturer's instructions dictate the assembly sequence and, in most instances, follow a series of steps categorized as follows:

- Preconstruction meeting between user, equipment installer, and manufacturer
- Site preparation including grading, installation of drainage, foundations, and ground grid, access roads, and auxiliary power
- Staging of construction equipment required during the installation
- Final alignment and leveling of foundation supports
- Receiving, unloading, and storing GIS equipment
- On-site assembly and lay-down area

- Grounding of GIS equipment to ground grid
- Local control cabinet installation
- Connection of control wires
- Evacuation and filling with insulating SF6 gas
- Leak testing
- Mechanical or operational testing
- Dielectric testing of primary circuits with conditioning steps
- Cleanup in accordance with applicable regulations
- Testing between GIS equipment and balance of plant for system integration
- Energization

The overall installation process for GIS may encompass many months, during which time other activities associated with the project should continue. Coordination of activities among the project's responsible parties is a necessity, especially with regard to the interface with the HV power transformer and HV cable connections. Time spent in these coordination processes will help to ensure the minimum number of disruptions during the installation process. Disruptions will nevertheless occur and a certain degree of flexibility on the part of all parties is essential. A typical sequence for the installation of new GIS could be as follows:

- The anchoring/support system is installed and leveled to accommodate civil works tolerances.
- Complete bays and single- or three-phase bay components are installed on their respective supports.

- Inter-bay connecting elements are installed and bus-coupled.
- GIS equipment is grounded to a ground grid.
- Installation of local control cabinets and interconnecting cables.
- Commencement of SF6 gas vacuum-filling process.
- Gas insulated buses, including SF6 gas-to-air bushings to outgoing power transformers or line positions, are installed.
- Interface components are installed (e.g., GIS to HV cable or power transformers), but bus links remain uncoupled.
- Site commissioning tests are completed, including local control cabinets.
- GIS is subjected to the high voltage withstand tests.
- Ancillary GIS devices (e.g., voltage transformers and surge arresters) are installed and bus links to high voltage cables and/or transformers are coupled.
- Means of dust control during installation should be taken into account.

In general, GIS is essentially immune to many of the degradation mechanisms that affect air insulated equipment. The following is a partial list of some of the major degradation mechanisms -:

- Frequent operation above thermal limits
- Frequent high electrical stresses due to surges
- Particles in the high voltage encapsulation from production and/or installation
- Excessive moisture in the SF6 gas
- Impurities in the SF6 gas
- Contaminants entering flanges and affecting O-rings
- Mechanical wear/aging
- Poor assembly techniques
- Poor management of decomposition products due to switching or interruption of currents

III. DESIGN OF 400/220 KV GIS SYSTEM

PART I – BUS SWITCHING SCHEME

PART II – SINGLE LINE DIAGRAM AND GENERAL ARRANGEMENT

PART III – SUBSTATION LAYOUT

PART IV – SELECTION OF TECHNICAL PARAMETERS OF MAJOR SUB - STATION EQUIPMENTS

PART I –

The various types of well-known schemes are given below:

a. Single/Sectional Bus –

- Simplest and cheapest bus bar scheme
- Maintenance and extensions of bus bars are not possible without shutdown of the substation
- Operation of bus bar is easy

b. Main and Transfer Bus

- Similar to the single bus scheme except the sectionalizing breaker or isolator
- By keeping the sectionaliser open one section can be in service and the other can be taken for maintenance or extension

c. Sectionalized Main and Transfer Bus

- Individual CB can be taken out for maintenance on-load at a time
- The transfer bus coupler acts as the breaker for the circuit under bypass

d. Double Main with bypass Isolator

- This bus arrangement provides the facilities of a double bus arrangement & a main and transfer bus arrangement
- The bus to which the transfer bus isolator is connected can be used as a transfer bus also
- During the time a circuit is under bypass, the bus coupler will act as the breaker for the bypassed circuit

e. Double Main and Transfer Bus

- In this bus scheme, in addition to the main buses there will be a separate transfer bus also
- Since separate transfer bus is available there will be no need of transferring the load from one bus to other bus unlike in a double main cum transfer bus arrangement

f. Ring Bus

- This arrangement is very popular
- Extension of mesh station is almost impossible
- No bus bar protection required

g. One and Half Breaker

- In this layout, two circuits have three breakers; the middle breaker ties the two circuits and hence is called the tie breaker.
- The combination of three breakers is called a diameter.
- One great advantage of this scheme is that even both the buses are out of service, power can be transferred from feeder to another

h. Double Bus and Double Breaker

- This arrangement is very expensive one and hence followed in very important circuit only
- In this arrangement breaker maintenance for each circuit is possible

PART II –

- Bay Allocation:- The identification of various feeders in any substation is done keeping following points in view
- Minimum Line Crossings
- Compactness and Flexibility of S/S expansion
- Sub Station Layout:- For 400/200 KV substation low level or rigid bus bar layout is been used due to following advantages
- Each feeder of D/C lines/Auto transformers can be directly connected to separate buses
- Less structures and associated Civil Works
- Better aesthetic appearances of substation
- ROAD AND RAIL TRACKS:- Road and rail track layout is an important aspect from operation and maintenance point of view

- The road and rail layout is judiciously chosen keeping in view higher cost of rail track, rolling/shifting of heavy equipment's in substation without causing shutdown of heavy equipment's.
- For 400/220 KV S/S, Roads have been provided near main and tie equipment’s and along the inside boundary of substation.
- LOCATION OF CONTROL ROOM AND OTHER AUXILIARY BUILDINGS:-The location of control room and other auxiliary buildings play a major role for economic design of S/S
- Easy access to control room with minimum routing through S/S area
- Clear view of substation, control room is referred to be in center considering future bays requirements also.

PART III –

- There can be several combinations in which the equipment's, bus-bars, structures *etc*. can be arranged to achieve a particular switching scheme.
- The first objective of sub-station scheme is to translate the selected scheme into a layout so as to physically achieve the feeder switching requirements, maintaining safety clearances and clearances required for ease in erection and maintenance.
- For 400/220 KV sub-station, Breaker and Half scheme for 400 KV s/s and Double main with transfer bus scheme for 220 KV s/s have been considered.

Factors Influencing the Choice:-

- Reliability
- Electrical and safety clearance
- Ease of construction and extension
- Ease of operation and maintenance
- Safety of operating personnel
- Safety of equipment and installation
- Economy

PART IV –

- AUTO TRANSFORMER: - For interconnection between two systems at very high voltage for bulk power transfer, use of auto transformers are recommended as a single transportable limit.
- Keeping in view of the transport, manufacturing & testing limitation in Indian condition 315 MVA, 3-phase capacity has been standardized as the largest unit
- For 400/220 KV substation 315 MVA, 3-phase capacity has been used
- 420 KV SHUNT REACTORS & NEUTRAL GROUNDING REACTOR:-Shunt reactors are meant for shunt connection in a system to compensate capacitive current and switching operation
- As 400 KV lines are practically compensated type, reactors of capacities ranging from 50 to 100 MVAR shall be required
- Shunt reactors shall have ONAN cooling so that failure of cooling system does not necessitate tripping of line or shunt reactor
- CIRCUIT BREAKER:- SF6 type of Circuit breakers are of state of art design and are reasonably maintenance free
- SF6 circuit breakers are capable of breaking a number of full short circuit currents before needing to replace/repair their main/arcing contacts
- SF6 circuit breakers complying to latest IEC 56/ IS 2516 standard are specified
- ISOLATORS:- Isolator of Double break type conforming to IEC 129/IS 9921 standard are most commonly used and have a reasonably good reliability level
- Isolators are provided with earth switches where required as per layout requirements for ease maintenance of adjoining equipment

REFERENCES

[1] S. Okabe, J. Takami, "Occurrence probability of lightning failure rates at substations in consideration of lightning stroke current waveforms," *IEEE Trans. Dielectrics and Insulation*, Vol. 18, No. 1, pp. 221-231, Jan. 2011

[2] G.F. Montillet, E. Mikes et al. "Underground transmission and distribution GIS solutions" IEEE/PES T&D Exposition and Conference, Dallas USA, 2003.

[3] E. Mikes, Ch. Tschannen, et al. "GIS substation extensions and upgrades" CEPSI Paper T1-068, 2000, Manila, Philippines.

5.3 SPV based Water Pumping System

SPV water pumping system based on solar photovoltaic, has drawn a major attention in agricultural, domestic and industrial sectors in last few years. A solar photovoltaic (SPV) water pumping system consists of a PV array, a DC/AC surface mounted/ submersible/ floating motor pump set, electronics, if any, interconnect cables and an "On-Off" switch. PV Array is mounted on a suitable structure with a provision of tracking. Electronics could include Maximum Power Point Tracker (MPPT), Inverter and Controls/Protections. Storage batteries will not constitute a part of the SPV Water Pumping System. The SPV water pumping system should be operated with a PV array capacity in the range of 200 Watts peak to 5000 Watts peak, measured under Standard Test Conditions (STC).

Sufficient number of modules in series and parallel could be used to obtain the required PV array power output. The power output of individual PV modules used in the PV array, under STC, should be a minimum of 74 Watts peak, with adequate provision for measurement tolerances. Use of PV modules with higher power output is preferred. Components and parts used in the SPV water pumping system including the PV modules, pumps, metallic structures, cables, junction box, switch, etc. should conform to the BIS/ IEC/ international specifications, wherever such specifications are available and applicable.

The Solar PV Water Pumping System should provide a minimum of 85 liters of water per watt peak of PV array used per day under average daily solar radiation conditions of 5.5 KWh/sq.m. on a horizontal surface, from a total head of 10 metres (Suction head up to a maximum of 7 metres). Use of a tracking system to enhance the availability of solar radiation to lift desired quantity of water is desirable. It should be specified whether the minimum water output is achieved directly or through tracking of PV Array. The actual duration of pumping of water on a particular day and the quantity of water pumped could vary depending on the location, season, etc.

The MPPT is a charge controller that compensates for the changing Voltage Current characteristic of a solar cell. MPPT technique may include different algorithms and switch between them based on the operating conditions of the array. Few of these algorithms are perturb and observe (P&O), incremental conductance, Current sweep, Constant voltage,

Temperature Method. In perturb and observe technique the controller adjusts the array voltage and measures power; adjustments are made till power keeps changing. This is most common technique, although this may result into oscillations of power output. In the incremental conductance method, the controller estimates incremental changes in PV array current and voltage to predict the impact of a voltage change. This technique requires more computation in the controller, however can track changing conditions more rapidly than the perturb and observe method (P&O).

A comparative study of solar photovoltaic (SPV) water pumping system is done between different maximum power point tracking (MPPT) techniques i.e. incremental conductance MPPT controller and perturb and observation (P&O) algorithm of MPPT techniques using Induction motor drive (IMD) as a model controlled by Direct torque and flux control with space vector modulation (DTFC-SVM). DTFC-SVM is a type of vector control which is used for better efficiency and accuracy in solar water pumping system with induction motor drives. The advantages of using this technique are fast control and high dynamic response. It is observed that INC MPPT technique is better than P&O algorithm based MPPT controller method as it is more stable and fast with better transient behavior.

Induction motors have been most popular in India in irrigation however they are used with electric circuits to convert d.c. power generated by solar panels to a.c. which leads to power losses, increased complexity and cost, and reduced efficiency of the system. The permanent magnet brushless d.c. (PMBLDC) motor comprises permanent magnet as rotor and polyphase armature winding as stator. Productivity is an essential offering of BLDC motors. Since the rotor is the sole conveyor of the magnets, it requires no power, i.e., no connections, no commutator, and no brushes. Instead of these, the engine utilizes control hardware. To identify the location of rotor at certain times, BLDC motors utilize, alongside controllers, rotating encoders or a Hall sensor. The brushes are absent hence the commutation is done using electronic drive by electrically feeding stator winding. PMBLDC motor advantages include high efficiency, high power density, maintenance free, brushless, longer life, noiseless and excellent dynamic performance compared to the conventionally used dc motors and induction motors. The cost of this type of motor was initially very high however it declined with

advancement in materials and design. The contribution of PMBLDC can be strengthened by careful design of PMBLDC motor for solar water pumps which is the best alternative to induction motors

Design and Analysis of BLDC Motor For Water Pumping System

Ankita Bharti[1], Sanjay Marwaha[2]

***Abstract*—This work deals with the utilization of solar photovoltaic (SPV) energy in the Brushless DC (BLDC) motor drives water pump. Solar energy is required to the next generation for sustainable growth. The solar powered pumping system is being used extensively but it can be used in rural areas to great advantage which faces energy crisis. Induction Motors have been most popular in India for irrigation however they are used with electric circuits to convert DC power generated by solar panels to AC which leads to power losses, increased complexity, cost and reduced efficiency of the system. The Permanent Magnet Brushless DC (PMBLDC) motors is one of the best alternatives which can solve problems of low operating power factor, low operating efficiency and cost. This paper focuses on design, simulation and development of highly durable, reduced weight, low cost, 1.2kW PMBLDC motor suitable for solar water pumping applications. The Electromagnetic analysis has been done with the help of Finite Element Method (FEM) using Maxwell-15 software.**

Keywords— Energy efficient motor; Ansoft Maxwell; FEM; PMBLDC Motor; Solar Water Pump.

I. INTRODUCTION

The water pumping system has become the most attractive application of solar photovoltaic energy, particularly in the remote areas where power transmission is either impossible or uneconomical. Needs for Electricity has grown exponentially over the years all over the world. India has also seen the same pattern in rise in demand of energy to fuel its growing economy. Conventional energy resources being limited are becoming scarce day by day, this calls for finding solutions through Renewable Energy resources like Solar, Wind, Tidal, etc to make growth more suitable [1]. Induction motors (IM) are usually preferred over DC motors, due to their low maintenance and ruggedness [2]. However, they are relatively inefficient compared to permanent magnet brushless DC motors, particularly in the submersible pumps [3]. This results in the increased power rating of the motor, and thus the initial cost of PV array. PMBLDC motors offer high efficiency, which reduce the cost of the PV arrays.

Till now, focus is on Induction Motor based PV water pumping system. There is scarce literature available on BLDC Motor based PV water pumps. It offers various advantages over induction motor water pumps as given below:

[1]Anikita Bharti is with Department of Electrical and Instrumentation Engineering, Sant Longowal Institute of Engineering and Technology Sangrur (Punjab), India

[1]Sanjay Marwaha is with Department of Electrical and Instrumentation Engineering, Sant Longowal Institute of Engineering and Technology Sangrur (Punjab), India

(e-mail: anki02912@gmail.com, marwaha_sanjay@yahoo.co.in)

- Higher power conversion efficiency compared to Induction Motor.
- Reduced cost of PV array and overall system cost.
- Reduction of power rating of DC-AC inverter owing to the higher power factor of BLDC motor.
- Reduction of sensing requirements unlike induction motor drive which requires sensing phase currents for speed control.

II. COMPARISION

A. Comparision of Conventional Motor

The popularity of BLDC Motors is increasing rapidly nowadays. Due to several advantages, BLDC motors are widely used in several applications namely air conditioners, defense industry, electrical appliances, robots, submarine application and etc.

TABLE I COMPARISION OF MOTORS

S. No.	Features	DC Motor	AC Motor	BLDC Motor
1.	Speed/Torque characteristics	Moderately Flat	Non-Linear	Flat
2.	Output Power/Frame size	Moderate or low	Moderate	Higher
3.	Speed range	Lower	Moderate	Higher
4.	Efficiency	Moderate	Moderate	Higher

The advantages of BLDC motor include high efficiency, high power density, maintenance free, brushless, longer life, very less noise and excellent dynamic performance.

In this paper, optimization of BLDC Motor is carried out for submersible pump-set application.

B. Comparision of Energy Resources

The Solar PV are increasingly replacing conventional resources like using motors with Diesel and Gasoline as their primary source of fuel due to added advantages like unattended operation, lower maintenance cost, longer life and above all lower emission and much more environmental friendly then their conventional counterparts. Diesel-electric or fuel-cell based technologies are unreliable, that requires frequent maintenance and pollute the environment [4].

III. FINITE ELEMENT METHOD

It is a powerful and versatile technique for handling problems involving complex geometries and homogeneous media. The basic principle of this method is to divide continuous domain into the number of sub domains which is usually called an element. Finite Element Method (FEM) is a numerical approach to boundary value problems in the mathematical physics. The greatest advantage is flexibility as compared to other traditional methods.

The inherent capability of this method is to simplify the complex boundaries which further reduces and simplifies the programming.

A. Configuration of Water Pumping System

Brushless motors consist of two main parts namely stator and the rotor. The stator carries the windings and the rotor carries the magnets. BLDC Motors can have inside rotors called "Inrunner" or outside rotors called "Outrunner". In either case the stationary stator windings are allowing direct winding access without brushes or slip rings. The stator which carries the winding does not rotate and the rotor which carries the magnet does. Then, the windings are placed in the slots in a laminated steel structure called the core. The purpose of the steel is to allow more number of magnetic flux through the winding which is not possible with a ferrous core. The section between the two slots is called a tooth. In order to size and design a system correctly, the designer must know:

- How much water you need?
- Whether your water source is a stream, pond, etc.?
- Water needed in gallon per minute (gpm)?
- Depth of Well?
- How far the water needs to be pumped?
- How much volume is available in storage tanks?

B. Design Equation of BLDC Motor

- Permanent Magnet Brushless DC motor is essentially a DC motor. The torque is depend on the size of machine and the basic equation of the torque is as follow [5]:

$$T = D^2 \times L \quad (1)$$

The Power rating of the motor can be derived from the following equation:

$$\text{Output Power} = \frac{2\times\pi\times N\times T}{60{,}000}\ \text{KW} \quad (2)$$

- EMF Generated by the motor is given as:

$$\text{EMF} = \frac{2\times\pi\times N\times K}{60} \quad (3)$$

where N is the speed of the Motor.

- Number of conductors calculated is given by

$$\text{Number of conductors} = \frac{60\times E\times A}{\phi\times N} \quad (4)$$

Where E is the EMF, A is the number of parallel paths and P is the number of Poles in the motors.

- Electric loading calculation is given below:

$$\text{Electric Loading (ac)} = \frac{Z\times I}{2\times\pi\times D} \quad (5)$$

Where (ac) Electric loading is the combinations of the Number of conductors Z, I represent current & stator outer diameter D.

IV. DESIGNING OF MOTOR USING RMXPRT (MAXWELL-15)

The concerned software uses FEM to solve differential equations. It is an electromagnetic field simulation software that help to design innovative electrical and electronic products faster and more cost effectively. In today's world of high performance advanced electrification system, the effect of electromagnetic fields on circuit and system cannot be ignored. This software can uniquely simulate electromagnetic performance across components, circuit & system design and can evaluate temperature, vibration and other critical mechanical effects.

A. Stator Design -

The Stator is a static part of motor. Its dimension should be optimized for efficient design.

TABLE II SPECIFICATION OF BLDC MOTOR

S. No.	Parameter	value
1.	Rated Power	1.2KW
2.	Rated Voltage	72V
3.	Rated Speed	2880 rpm
4.	Frictional Loss	10W
5.	Winding Loss	20W

- The rating of power, voltage and speed are shown in table which has been used to simulate the BLDC Motor on this software.

TABLE III DESIGN PARAMETERS OF STATOR

S.NO.	Parameter	Value
1.	Outer Diameter(mm)	270
2.	Inner Diameter(mm)	180
3.	Core Length(mm)	47
4.	Rotor Position	Outer

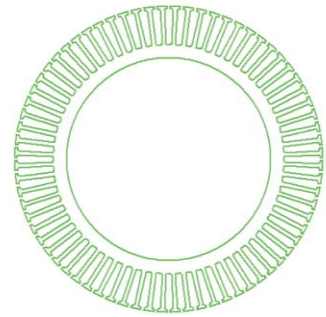

Fig. 1. Stator Geometry

Fig1 shows the stator geometry of the BLDC Motor which is initial step required for designing.

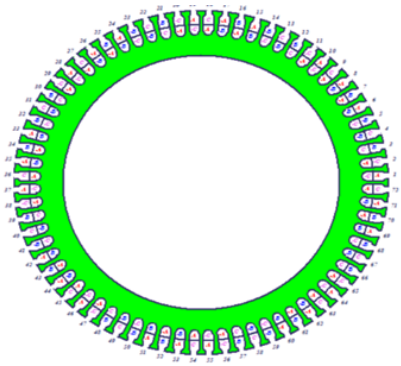

Fig.2. Stator Winding

Fig.2 shows the cross-sectional view of stator winding and geometry.

The aim of the design is to minimize the armature copper losses while keeping the slot fill factor in practical limits.

B) Slot Design- The technical data that has been used for selection of slot, (slot type 4) is shown in fig.3 [6].

C) Slot Parameters –The Shape and dimensions of concerned is given below:

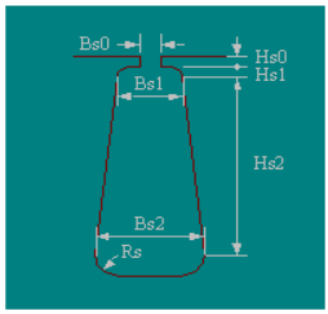

Fig.3. Slot Dimension

TABLE IV SLOT PARAMETERS

S.NO.	Parameters	Value
1.	Hs0	2.5mm
2.	Hs1	1mm
3.	Hs2	30mm
4.	Bs0	3mm
5.	Bs1	8mm
6.	Bs2	5.3mm
7.	Rs	0.5mm

B) ROTOR DESIGN -

It is the moving component of the electromagnetic system in the electric motor. The general data for the machine rotor is tabulated below:

TABLE V DESIGN PARAMETERS OF ROTOR

S.NO.	Parameter	Value
1.	Inner Diameter (mm)	290
2.	Outer Diameter (mm)	272
3.	Length of Core (mm)	47
4.	Type of Steel	Steel_1010
5.	Embrace	0.7
6.	Thickness of Magnet(mm)	4
7.	Magnet Type	NdFe35

- Due to outer geometry of the BLDC machine only pole type 1 has been considered for analysis.

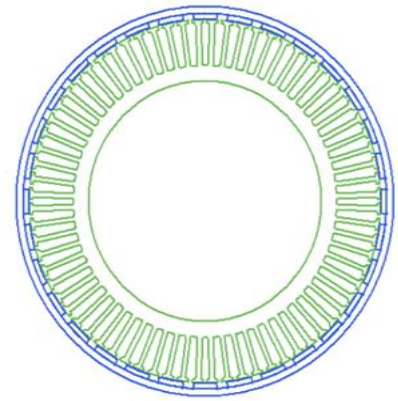

Fig.4. Cross-section view of BLDC Motor

V. SOLUTION DATA

Now according to Design Sheet some important curves have been derive when we performed simulation of model on RMxprt.

TABLE V. DESIGN SHEET OF BLDC MOTOR

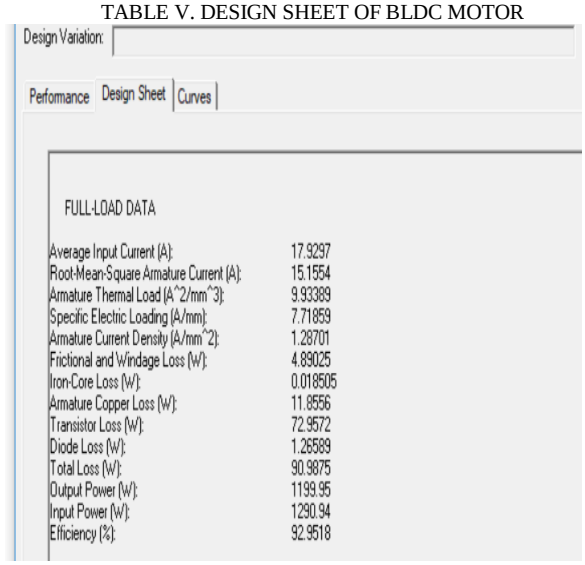

- Design sheet shows the power output and the required power input of the BLDC Motor and the result shows the efficiency of the motor. RMxprt provides an entire range of data types and variables. Some important output parameters and plots are shown below:

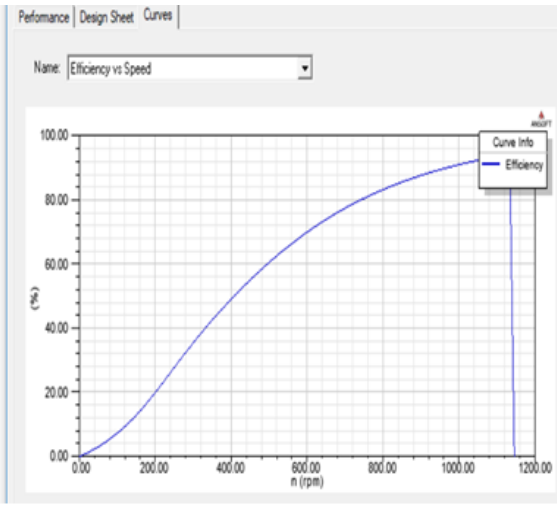

Fig.5.Efficiency Vs Speed Curve

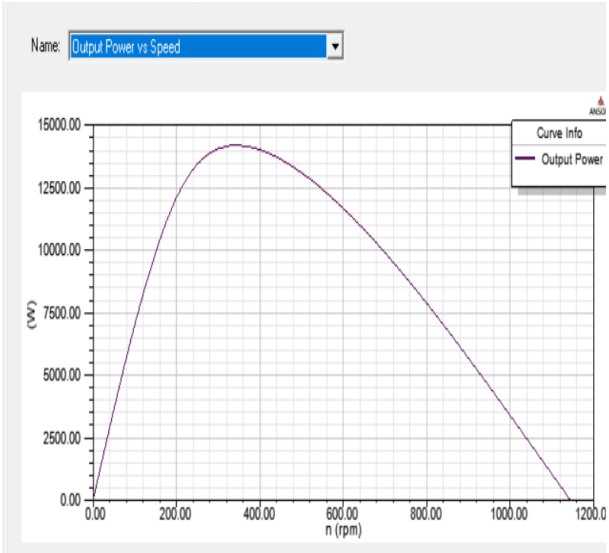

Fig.6. Power Vs Speed

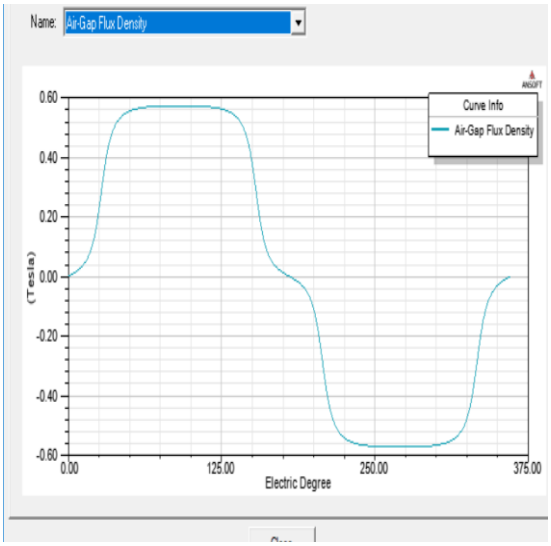

Fig.7. Air gap flux density Vs Electric degree

VI. MAXWELL 2D SIMULATION

Motor Design created on RMxprt has been exported in Maxwell 2D. This software generates mesh using Finite Element Analysis (FEA). Electromagnetic analysis is done with the help of MAXWELL 2D.

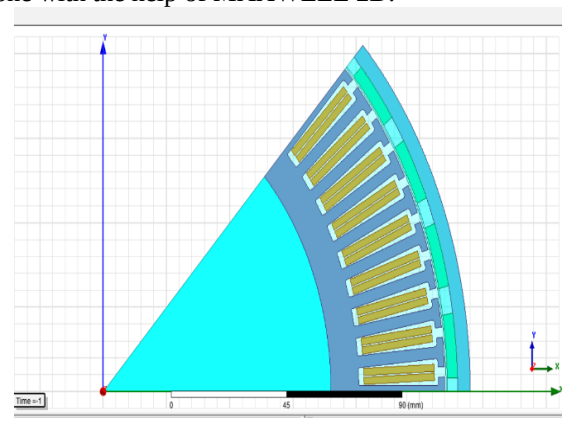

Fig.8. Motor design in 2D

VII. CONCLUSIONS

The cost effective and performance effective design of water pumps used in agriculture sector contribute to energy efficient measure taken against the global energy crisis. The utilization of solar energy for water pumping system application is also one of the effective measures. The contribution was strengthened by careful design of PMBLDC motor which is the best alternative to Induction Motor. A PMBLDC Motor for solar water pumping application has been designed and simulated. The obtained results are in good agreement with the available reported results in the literature.

REFERENCES

[1] C.S. Solanki, Solar Photovaoltaic, 2nd ed. New Delhi, India Prentice Hall of India, 2011.

[2] J.L Davies and M.Malengret, "Application Of Induction Motor For Solar Water Pumping System," in proc. 3rd AFRICON Conf. Ezulwini Valley, Sept 1992, pp. 209-212.

[3] T. Brinner, R.McCoy and T.Kopecky, Induction Vs. Permanent Magnet Motors For Electric Submersible Pumps Fields And Laboratory Comaprisions," IEEE Trans. Ind. Appl., vol.50, Issue:1, pp. 174-181,Jan 2014.

[4] M. Mahmoud, Experience results and techno-economic feasibility of using photovoltaic generators instead of Diesel motors for water pumping from rural desert wells in Jordan," IEEE Proceedings C-Genration, Transmission and Distribution, Vol.137, no.6, pp.391-394, Nov 1990.

[5] R. A.K. "Sawhney, A Course in Electrical Machine Design," Dhanpat Rai and Sons, New Delhi, 1984.

[6] B.Kavitha and S.Karthikeyan, B.Ishwarya, "Design of Solar PV water pumping system using BLDC drive using sensorless method", Vol3, March 2014.

[7] M.Fazil and K.Rajagopal, "Development of External rotor single -phase PM BLDC motor based drive for ceiling fan," in Proc. Drives Energy Syst .Int. Conf., NewDelhi, Dem. 2010.

Comparison of Solar Water Pumping System with Different MPPT techniques

Jaipal[1], Tejavathu Ramesh[2], Ramakrishna Pothuraju[3]

***Abstract*- This paper presents a comparative study of solar photovoltaic (SPV) water pumping system with two different maximum power point tracking techniques (MPPT). The whole model has two cascaded sections. The first section includes PV array with DC-DC converter in which output is controlled by MPPT controller. In the second section the output of the boost converter if fed to DC-AC converter which is input to induction motor drive (IMD) which controls the centrifugal water pump. Direct torque and flux control with space vector modulation (DTFC-SVM) is implemented as the control strategy for the second section. The system is developed in the MATLAB/Simulink and the results are compared and studied significantly.**

Keywords- Solar PV array, MPPT, P&O Algorithm, INC Algorithm, DC-DC Boost converter, DTFC-SVM, Induction motor

I. INTRODUCTION

With growth of population, the consumption has been increasing rapidly. The consumption in every manner as in food, shelter, security and energy etc. but it is quite difficult to balance the production and the consumption as consumption rate is much higher than the production rate.. Renewable energy is one of the best options evolved, particularly solar energy. Stand-alone solar power systems are becoming popular, especially in rural and remote regions. SPV water pumping system has drawn a major attention in agricultural, domestic and industrial sectors in last few years. For reliable and rugged operation, the best choice is to use induction motor drive (IMD).

The conversion efficiency of solar PV module is low around 16-20%. [1] The non-linear I-V curve of PV array illustrates a unique point which is known as Maximum Power Point (MPP), where the maximum output power is produced by the PV array. Maximum Power Point Tracking (MPPT) techniques must be implemented so that the operating point of PV array is sustained at its MPP. There are several types of MPPT algorithms available in literature [2]-[6]. Among various MPPT techniques, incremental conductance (INC) and perturb and observation (P&O) algorithms are discussed in this paper.

[1]Jaipal is with School of Renewable Energy and Efficiency, National Institute of Technology, Kurukshetra, India
[2]Tejavathu Ramesh is with Department of Electrical Engineering, National Institute of Technology, Kurukshetra, India.
[3]Ramakrishna Pothuraju is with Department of Electrical Engineering, National Institute of Technology, Kurukshetra, India.

(e-mail: singhjaipal27@gmail.com, tramesh.ee@gmail.com, 232ramakrishna@gmail.com)

The speed of IMD can be controlled by scalar as well as vector control. DTFC-SVM is a type of vector control which is used for better efficiency and more accuracy. DTFC-SVM method controls torque and flux efficiently. The advantages of using this technique are fast control and high dynamic response. Electromagnetic torque and stator flux are assessed with stator voltage and currents. This prediction only depends on stator resistance of the motor.

II. DESIGN OF PROPOSED SYSTEM

The outline of solar water pumping is shown in fig.1. The first unit comprises of PV array followed by boost converter. MPPT algorithm controls the duty cycle of the boost converter. The second unit consist of a VSI and induction motor tangled to a pump. A closed lood DTFC-SVM technique is used to speed control of IMD.

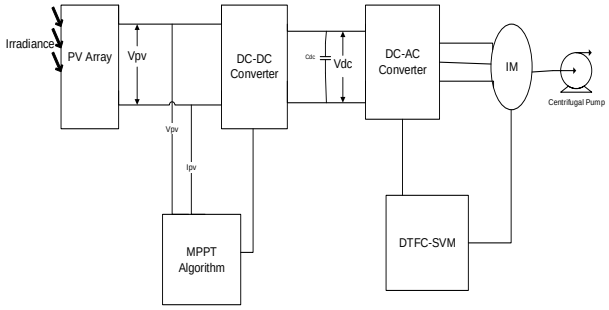

Fig-1: Solar Water Pumping System

A. PV Array

The Conversion of solar insolation into electricity is known as photovoltaic effect [7]. PV cells are typically found linked to each other and mounted on a frame called a module. Multiple modules can be wired together to form an array, which can be scaled up or down to produce the amount of power needed.The PV array chosen should be carefully selected such that ot satisfies the motor ratings to be used for pumping application with losses neglected. The modelling of basic PV cell can be repesented by the following figure-2.

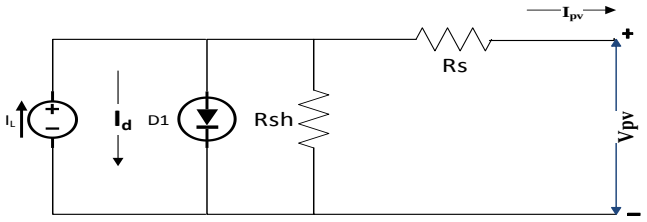

Fig.-2 : Equivalent circuit of PV cell

The photovoltaic cell can be mathematically modelled as:

$$I_{pv} = N_p I_{ph} - N_p I_o \left[\exp\left(\frac{q(V_{ph} + I_{pv} R_s)}{N_s kTA} \right) - 1 \right] - \frac{V_{ph} + I_{pv} R_s}{R_{sh}} \quad (1)$$

Where,

I_{pv} =Phovoltaic current(Amp)
I_{ph} = photo current(Amp)
I_0 = Diode saturation current(Amp)
q = Electric charge(coulomb)
R_s = Series resistance of PV cell(ohms)
N_s = Number of solar cells connected in series
N_p = Number of solar cells connected in parallel
K = Boltzmann's constant
A = Diode Ideality factor
T = Ambient Temperature(K)
R_{sh} = Shunt resistance of PVcell(ohms)

The above equation used for photovoltaic cell is for single diode model. To get higher voltage PV cells are connected in series and in parallel for higher current. The above mathematical equation describes the I-V characterstics of a PV cell. The I-V and P-V characteristics of solar array is shown below in fig. 3.

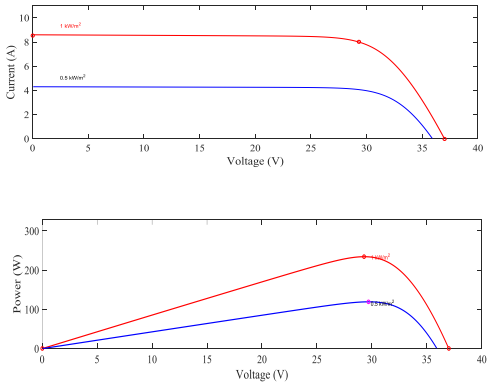

Figure 3: I-V and P-V characteristics of Solar Array

a) Variation of Irradiance

The P-V and I-V curves of a solar cell varies with as per solar irradiation.Irradiation is the measure of energy density of sun rays. As the environmental circumstances changes during daytime which tends to bring the change in solar irradiationand this variation can be traced by certain control methods. As per the load operation of solar cell can be attuned. For the same voltage value, input to solar cell will be increase if the solar irradiance is high inturn increases the power magnitude. The open circuit voltage and the short circuit current upsurges with the increment in solar irradiance resultin in the variation of maximum power point. More power is produced when more sunlight is incident on solar cell as it increases the electron mobility.

b) Variation of Temperature

The variation in temperature adversely effects the output of the solar cell. It has a negative impression on the power generation capability. Rise in temperature is convoyed by a decline in the open circuit voltage value reduces as the the temerature is increased because the band gap of the substantial increases with temperature increase and therefore extra energy is required to cross the potential barrier. Therefore, varying temerature negatively effects the efficiency of the solar PV cell as shown in Fig.4

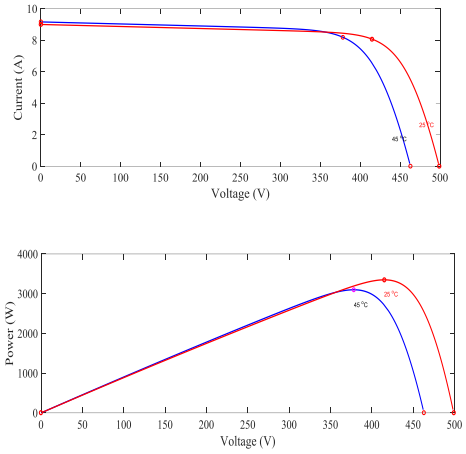

Figure:4 waveforms showing effect of temperature

The power output of solar PV array is given as:

$$P_m = (n_p \times I_m) \times (n_s \times V_m) = 3.7kW \quad (2)$$

Where,

P_m is the maximum power that can be extracted from the array (in kW). The induction motor used in system is of 3.7kW, so the number of strings ov PV panel should be such that it should meet the capacity of motor. n_p is the number of strings connected in parallel and n_s is the number of series connected modules per string. V_m and I_m are voltage and current of the solar PV array at maximum power point(MPP). So, the 15 strings are connected in series and 1 in parallel as to match the power of IMD

V_{oc} =37x15=555 V

The current of the panel is,$I_m = n_p \times I_m$=8.2

B. DC-DC Boost Converter

Boost converter is used in the first phase with the solar PV panel in the solar powered water pumping system. The design of boost converter is initiated by assuming the value of duty cycle[1].

The boost inductor L_m at duty cycle, k = 0.045. is given as,

$$L_m = \frac{V_m \times D}{\Delta I_l \times fs} = \frac{435 \times 0.045}{0.2 \times 7.6 \times 5000} = 2.5mH \quad (3)$$

Where, ΔI_l is the ripple current and f_s is the switching frequency. So, the 3mH inductor is selected for the boost converter.

C. DC Link Capacitor of VSI

This capacitor is necessarily between the cascading of boost converter and VSI as it helps in maintaing the required voltage level during trasients like fall of solar insolation and load increment[1].

$$\frac{1}{2} C_{dc} [V_{dc}^2 - V_{dc}'^2] = 3\beta V_{ph} I_{ph} t \quad (4)$$

$$\frac{1}{2}C_{dc}[460^2 - 435^2] = 3 \times 1.2 \times 153 \times 8.2 \times 0.005$$
$$= 2018.5\mu F$$

Where,

C_{dc} = DC link capacitor
V_{dc} = reference dc voltage of VSI
V'_{dc}= minimum required DC voltage
β = overloading factor
V_{ph} = phase voltage of VSI
I_{ph} = phase current of VSI
t = time required in which dc link voltage attains its minimum value.

III. PERTURBATION AND OBSERVATION ALGORTIHM FOR MPPT

The most popular and widely accepted MPPT algorithm is P&O algorithm. The algorithm conducts by perturbing (increasing or decreasing) the PV array voltage periodically and then the comparison between PV output power and PV output of the previous perturbation cycle. However, the P&O algorithm has a slow response under rapidly changing environmental conditions. This algorithm decides the duty ratio of the boost converter on the basis of change in voltage, current, and power[8]–[10].

The power of the previous step and the new step is compared so that an increment or decrement is made in the voltage or current. Operating on the left of the MPP, it is noticeable that incrementing (decrementing) the voltage allows to increase (decrease) the power and decrease (increase) the power when on the right of the MPP. So, accordingly duty ratio is adjusted. The perturbation is kept the same to reach the MPP when there is an increase in power and vice-versa. P&O has a good behavior when the irradiance does not change quickly with time. However, the power oscillates around the MPP in steady state operation and it fails with variations of temperature and irradiance. The logic can be explained as the power output of the solar cell

$$P = V_{pv} * I_{pv} \quad (5)$$

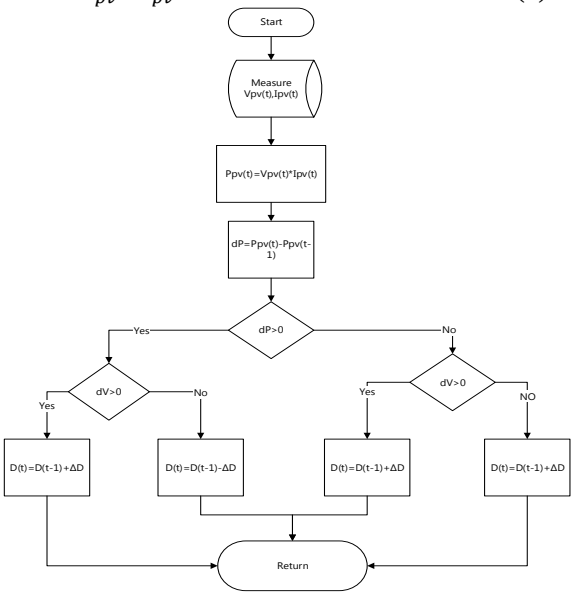

Figure 5: Flow chart of P&O algorithm

For maximum power, $\frac{dP}{dV} = 0$

So,

$$\frac{dP}{dV_{pv}} = \frac{d(V_{pv} * I_{pv})}{dV} = 0 \quad (6)$$

$$I_{pv} + V_{pv}\frac{dI_{pv}}{dV_{pv}} = 0 \quad (7)$$

$$\frac{dI_{pv}}{dV_{pv}} = -\frac{I_{pv}}{V_{pv}} \quad (8)$$

$\frac{dP}{dV} = -\frac{I_{pv}}{V_{pv}}$, at MPP (9)

$\frac{dP}{dV} > -\frac{I_{pv}}{V_{pv}}$, left of MPP (10)

$\frac{dP}{dV} < -\frac{I_{pv}}{V_{pv}}$, right of MPP (11)

IV. INCREMENTAL CONDUCTANCE MPPT TECHNIQUE

The flaws of P&O method for the tracking of peak power beneath rapidly fluctuating atmospheric conditions can be resolved by INC technique. The INC can identifies the MPPT has achieved the MPP and stop upsetting the operating point. On the violation of this condition, the path of the agitation of MPPT operating point can be found using the relationship between dI/dV and –I/V. When dP/dV is negative when the MPPT is to the right of the MPP and positive when it is to the left of the MPP. Using this algorithm has the advantages over P&O that it identifies when the MPPT has reached the maximum power point, where P&O oscillates around the maximum power point. IC has higher accuracy than P&O and can track rapid variations in irradiation conditions [9][10].

The basic equations of this method are as follows

$\frac{dI}{dV} = -\frac{I_{pv}}{V_{pv}}$, at MPP (9)

$\frac{dI}{dV} > -\frac{I_{pv}}{V_{pv}}$, left of MPP (10)

$\frac{dI}{dV} < -\frac{I_{pv}}{V_{pv}}$, right of MPP (11)

This technique has the postulation of the ratio of change in output conductance is equal to the negative output Conductance Instantaneous conductance. We have,

$$P = V_{pv} * I_{pv}$$

On application of chain rule the derivative of products comes out to be

$$\frac{dP}{dV_{pv}} = \frac{d(V_{pv} * I_{pv})}{dV}$$

At MPP, as $\frac{dP}{dV_{pv}} = 0$

The MPPT regulates the PWM control signal of the dc – to – dc boost converter until the condition: $\frac{dI_{pv}}{dV_{pv}} + \frac{I_{pv}}{V_{pv}} = 0$ is satisfied. The Flow chart of incremental conductance MPPT is shown below.[8]

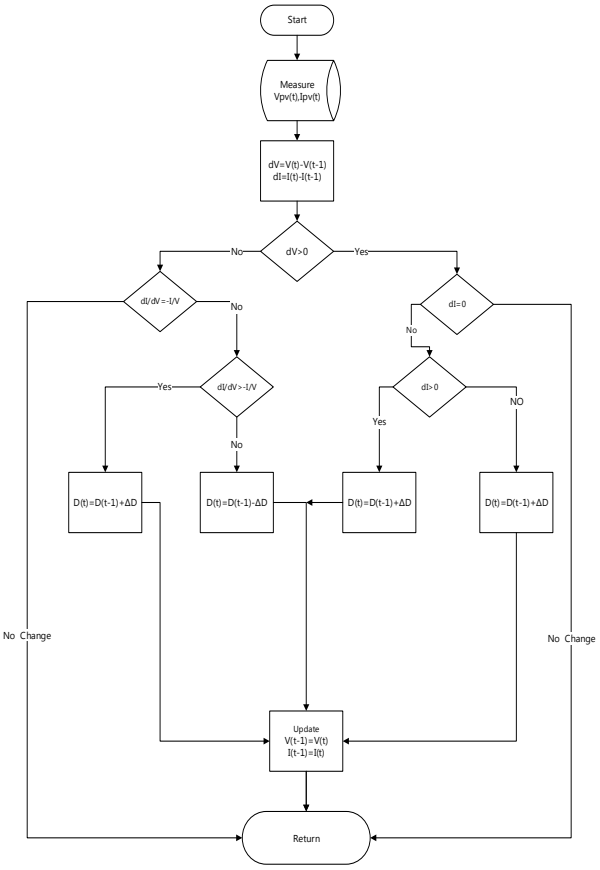

Figure 6 Flow chart of INC algorithm

V. DTFC-SVM Technique for IMD

Different practices adopted for speed control of induction motor drive such as scalar control, field-oriented control (FOC) and direct torque and flux control (DTFC). DTFC technique is operated through direct control of flux linkages and electromagnetic torque by selecting appropriate inverter switching. While operating at low speeds, the performance of DTFC is not up to the mark because of hysteresis controllers (torque and flux ripples with variable switching frequency). These flaws can be overcome by DTFC-SVM technique. SVM is basically adjusting stator flux position by inserting zero voltage vector to control generated torque. This technique gives quick dynamic response.

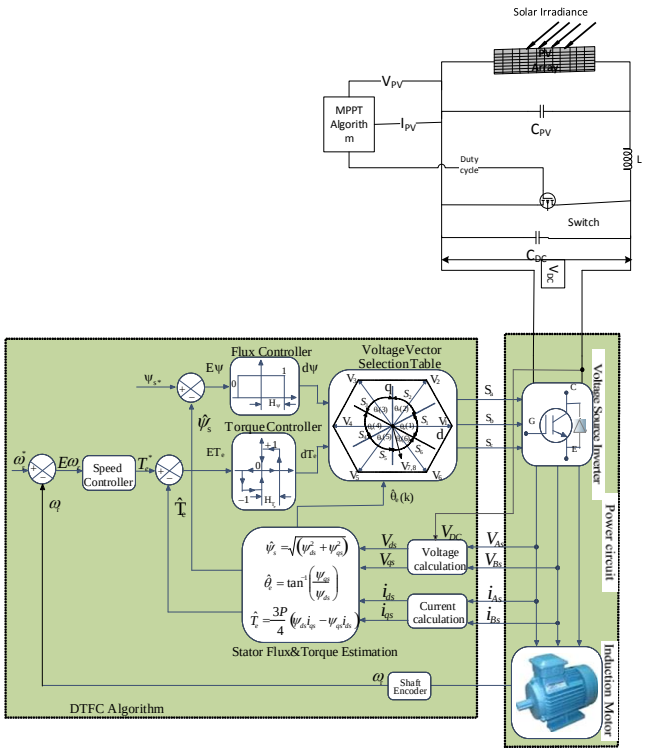

Figure 7: The schematic model of DTFC-SVM scheme with closed-loop torque and flux control operating in stator flux oriented coordinates

TABLE-I Switching States of the two level VSI

Space vector		Switching state conditions	Vector definition
Zero vector	$\vec{V}_0$	0 0 0	$\vec{V}_0 = 0$
	$\vec{V}_7$	1 1 1	$\vec{V}_0 = 0$
Active vector	$\vec{V}_1$	1 0 0	$\vec{V_1} = \frac{2}{3} V_{dc}.e^{-j0}$
	$\vec{V}_2$	1 1 0	$\vec{V_2} = \frac{2}{3} V_{dc}.e^{-j\frac{\pi}{3}}$
	$\vec{V}_3$	0 1 0	$\vec{V_2} = \frac{2}{3} V_{dc}.e^{-j\frac{2\pi}{3}}$
	$\vec{V}_4$	0 1 1	$\vec{V_2} = \frac{2}{3} V_{dc}.e^{-j\frac{3\pi}{3}}$
	$\vec{V}_5$	0 0 1	$\vec{V_2} = \frac{2}{3} V_{dc}.e^{-j\frac{4\pi}{3}}$
	$\vec{V}_6$	1 0 1	$\vec{V_2} = \frac{2}{3} V_{dc}.e^{-j\frac{5\pi}{3}}$

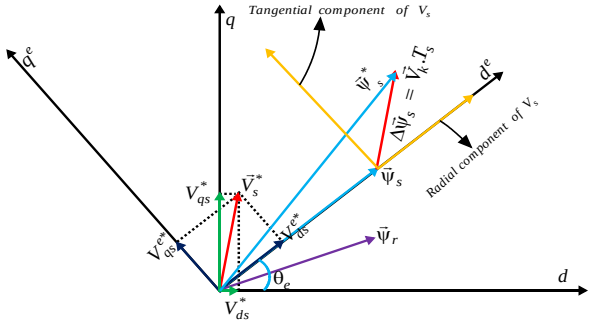

Fig. 8. Vector diagram of DTFC-SVM with closed-loop torque and flux control operating in stator flux-oriented coordinates.

Among different DTFC-SVM schemes, closed loop torque and flux control operating in polar coordinates is used in this paper. It is considered to be the best and optimal method. The calculated reference stator voltage is fed to the SVPWM.

VI. SPACE VECTOR MODULATION FOR TWO LEVEL VSI

SVM technique is considered as the best technique among all the PWM techniques for VSI. The SVM for two level VSI is shown in figure. Eight switching patterns can be made on the basis of switching state. Zero inverter output voltage is produced by two null states (V_0 and V_7). V_1 to V_6 are active states and have the magnitude of $0.667V_{dc}$ and are equally displaced by phase displacement of 60^0 in the vector plane. The area covered by two adjacent vectors is called sector. There are six sectors as tips of the vectors form a hexagon. Zero switching state vectors (having magnitude zero) are at origin in d-q plane. The DTFC-SVM technique evaluates reference voltage vector($\vec{V}_{ref}$) and this voltage vector is applied to motor in the next sampling period. Gate pulses are produced by this SVM techniques are fed to the two level VSI. The magnitude of the reference voltage vector can be changed by using zero vectors and the direction and position can be changed by using active vectors.

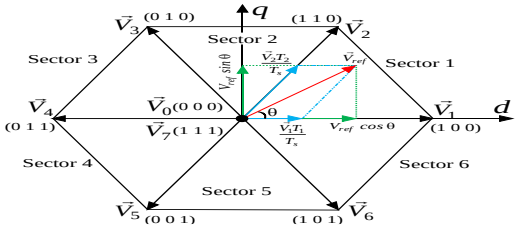

Fig. 9. Space vector representation for two-level VSI

A. Dwell Time Calculations

For the recognition of the gate pulses dwell time is calculated on the assumption that to consider the reference voltage vector as constant sampling period (T_s) should be small enough. In a particular sampling period (T_s) assume that the reference voltage vector is settled in sector 1.

From Figure 8 it is clear that the reference voltage vector (V_{ref}) can be synthesized by $\vec{V}_1, \vec{V}_2$ and $\vec{V}_0$. The volt-second balancing equation can be written as:

$$\vec{V}_{ref} \cdot T_s = \vec{V}_1 \cdot T_1 + \vec{V}_2 T_2 + \vec{V}_0 \cdot T_0 \qquad (12)$$

$$T_s = T_1 + T_2 + T_0 \qquad (13)$$

Where T_1, T_2 and T_0 are the dwell times for the vectors $\vec{V}_1, \vec{V}_2$ and $\vec{V}_0$ respectively, and the space vectors $\vec{V}_{ref}, \vec{V}_1, \vec{V}_2$ and $\vec{V}_0$ can be expressed as:

$$\vec{V}_{ref} = V_{ref}(\cos\theta + j\sin\theta),\ \vec{V}_1 = \frac{2}{3}V_{dc},$$

$$\vec{V}_2 = \frac{2}{3}V_{dc}\left(\cos\frac{\pi}{3} + j\sin\frac{\pi}{3}\right) \text{ and } \vec{V}_0 = 0 \qquad (14)$$

By substituting equation (14) in (12) and separating the real and imaginary parts, we get:

$$V_{ref}\cos\theta \cdot T_s = \frac{2}{3}V_{dc} \cdot T_1 + \frac{1}{3}V_{dc} \cdot T_2 \qquad (15)$$

$$V_{ref}\sin\theta \cdot T_s = \frac{1}{\sqrt{3}}V_{dc} \cdot T_2 \qquad (16)$$

By solving equations (13), (15) and (16), the dwell times in sector-1 can be written as:

$$T_2 = \sqrt{3}\frac{V_{ref}}{V_{dc}} \cdot T_s \cdot \sin\left(\frac{\pi}{3} - \theta\right), \quad \forall\ \theta \in \left[0, \frac{\pi}{3}\right) \qquad (17)$$

$$T_2 = \sqrt{3}\frac{V_{ref}}{V_{dc}} \cdot T_s \cdot \sin\theta, \quad \forall\ \theta \in \left[0, \frac{\pi}{3}\right) \qquad (18)$$

$$T_0 = T_s - T_1 - T_2 \qquad (19)$$

Even though, the above dwell times are calculated when the reference voltage vector is in sector 1, they can also be used when V_{ref} is in other sectors by making a small modification in the angular displacement (θ). The modified angular displacement (θ') can be written as:

$$\theta' = \theta - (k-1)\frac{\pi}{3}, \quad \forall\ \theta' \in \left[0, \frac{\pi}{3}\right) \qquad (20)$$

Where *k* is the sector number (i.e. *k=1, 2… 6*)

VII. DESIGN OF THE PUMP

There are many types of water pumps available in the market. In this paper centrifugal pump is used , as it is best suited for irrigation purposes. The relationship between the torque and speed of the motor is given as

$$T \propto \omega^2 \qquad (21)$$

$$T = K_p\omega^2 \qquad (22)$$

Where K_p is the propotionality constant.

The output power is defined as,

$$P = \omega T \qquad (23)$$

So,

$$P = K_p\omega^3 \qquad (24)$$

And K_p can be estimated as

$$K_p = \frac{P}{\omega^3} \qquad (25)$$

$$K_p = \frac{3700}{\left(2 * \pi * \frac{1500}{60}\right)^3} = 9.54 \times 10^{-4} kW/(r/s)^3$$

Selecting the pump for solar water pumping application is basically depends on factors like water requirement, water height and water quality[11].

VIII. SIMULATION RESULTS AND DISCUSSION

The solar powered based water pump using IMD is simulated in the Matlab and the results are discussed. The dc link voltage variation with time is shown in below fig.10. The results are obtained at standard environmental conditions i.e. at $1000W/m^2$, 25^0C . The steady state in case of P&O technique (blue) is achieved at 0.76secs whereas in INC method (black) steady state is achieved at 0.75secs.

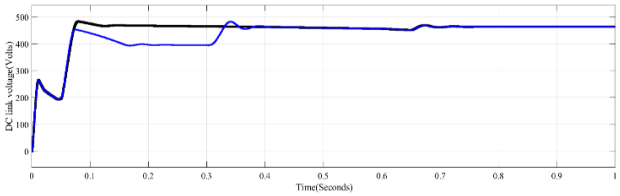

Fig. 10. DC link voltage (output voltage of the boost converter)

The DTFC-SVM of an IM drive is mathematically modelled in the MATLAB/SIMULINK environment using PI controller. The performance of motor with these two MPPT technique is quite similar, characterstics differs slightly which can be seen the results shown in fig11.The Simulink model is then used to verify the performance of the DTFC-SVM of an IMD under various working situations, such as, under no-load torque, load torque, abrupt changes in speed and low speed, respectively.

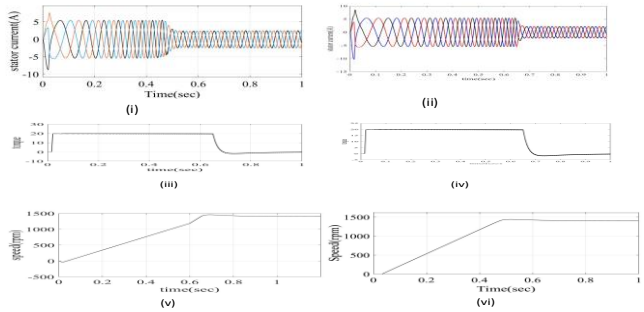

Fig. 11. output waveform of IMD with P&O method(i, iii, v) and INC algorithm(ii, iv, vi)

IX. CONCLUSION

In this paper a solar water pumping system using IMD with DTFC-SVM technique is demonstrated. A comparitive analysis between P&O and INC MPPT method is presented.From the simulation results it can be concluded that INC MPPT technique is better than P&O method as it is more stable and fast. In INC the operating point does not oscillate around maximum power point, it just reaches there and stablizies. And transient behaviour of INC algorithm is much better than P&O technique. As per view of irrigation system , the SPV array has been operated under standard enviromental conditions. Water flow rate and stator current of motor is controlled by the speed PI controller.

Appendix A

The parameters of solar PV module are: open circuit voltage (V_{OC})=37V, short circuit current(I_{SC})=8.54A, Voltage at MPP (V_m) =29V,current at MPP (I_m)=8.2A. ratins and specifications of IM are: power rating 3.7 kW, stator resistance (R_s)=5.51 Ω, rotor resistance (R_r)=4.5 Ω, stator leakage inductance (L_s)=0.3065 H, rotor leakage inductance (L_r)=0.3065 H, mutual inductance (L_m)=0.2919 H, moment of inertia (J)=0.089 Kg-m^2, number of poles (P)=4, rated speed=1440 rpm and sampling time (T_s)=200μs

REFERENCES

[1] U. Sharma, S. Kumar, and B. Singh, "Solar array fed water pumping system using induction motor drive," 1st IEEE Int. Conf. Power Electron. Intell. Control Energy Syst. ICPEICES 2016, 2017.

[2] M. A. G. De Brito, L. P. Sampaio, L. G. Jr, G. A. Melo, and C. A. Canesin, "Comparative Analysis of MPPT Techniques for PV Applications," pp. 99–104, 2011.

[3] D. P. Hohm, "Comparative Study of Maximum Power Point Tracking Algorithms Using an Experimental, Programmable, Maximum Power Point Tracking Test Bed," 2000.

[4] S. Member, "A Comparative study of different MPPT techniques using different dc-dc converters in a standalone PV system," pp. 1690–1695, 2016.

[5] Z. Ben Mahmoud, M. Ramouda, and A. Khedher, "A Comparative Study of Four Widely-Adopted MPPT Techniques for PV Power Systems," no. 1, pp. 16–18, 2016.

[6] A. Kchaou, "Comparative Study of Different MPPT techniques for a Stand-alone PV System," 2016.

[7] G. J. K. J. J. L. P. W. Lehn, "Modelling and control of photovoltaic panels utilising the incremental conductance method for maximum power point tracking," no. December 2011, 2012.

[8] C. S. Chin, P. Neelakantan, H. P. Yoong, and K. T. K. Teo, "Optimisation of Fuzzy Based Maximum Power Point Tracking in Pv System for Rapidly Changing Solar Irradiance," no. June, 2011.

[9] P. Upadhyay, B. Das Vairagi, V. Kumar, and R. R. Joshi, "Fuzzy Logic Based Maximum Power Point Tracking System for Solar Energy Conversion System," vol. 3, no. 7, pp. 1436–1441, 2014.

[10] A. K. Gautam, S. P. Singh, J. P. Pandey, R. P. Payasi, and A. Verma, "Fuzzy Logic Based MPPT Technique for Photo-Voltaic Energy Conversion System," pp. 275–281, 2016.

[11] K. Meah, S. Ula, and S. Barrett, "Solar photovoltaic water pumping-opportunities and challenges," Renew. Sustain. Energy Rev., vol. 12, no. 4, pp. 1162–1175, 2008.

5.4 Electrical Vehicle-Charging Infrastructure

Vehicles accompanying internal combustion engine utilizes conventional energy thus releases toxic and unfavorable pollutants. Electric vehicle (EV) is one of the possible and practical solutions to lower down the emission rate of such pollutants. However, the rate of penetration of electric vehicles leads to various barriers since they will consume power from the grid in order to charge their batteries. As a result of which with the increase in penetration rate of electric vehicles, the power system parameters such as losses, voltage regulation, harmonic distortion, power quality and efficiency gets influenced. To curb these problems, a relationship between the distribution system parameters like losses, load factor and load variance can be derived. On the basis of this, objective functions are formulated for minimizing distribution system losses which improves the voltage profile of the grid.

At present, management of EV charging can be categorized under two categories: synchronized charging and unsynchronized charging. Unsynchronized charging, also known as uncoordinated charging is a random charging phenomenon where the EV owners don't have required information for scheduling the charging cycle of their EVs. On the other hand, synchronized charging is a smart charging approach in which the charging cycle of EVs is distributed uniformly during desired period. Synchronized charging also has the advantage of rectifying the problem of getting peak in losses during the charging zones. The objective here is to cut down the peak in losses during peak hours and shift that peak to off-peak hours in order to level the load of EVs in the distribution system.

Charging infrastructures for electric vehicle including different charging mode can be a.c and d.c charging architectures and ultrafast charging architectures. A.C. architecture would be suitable to realize a smart charging scenario presenting different strategies of V2G energy management. D.C. architecture helps to reduce the losses which are due the conversion of energy in d.c./a.c. converter. In ultrafast charging infrastructure, charging time is very short approximately around 5 minutes and with the use of energy storage buffer there will be less effect on power grid.

Chargers provide a DC charging voltage from an AC source whether from a common socket outlet or more recently from a purpose built DC charging station. Most important are the

methods of controlling the charge and protecting the battery from over-voltage, over-current and over-temperature. These charger functions are integrated with and unique to the battery.

Chargers for electric bikes are usually low cost, separate units. To save weight they are not usually mounted on the bike and charging takes place at home. Their power handling capacity is only sufficient for charging the relatively low power bike batteries and entirely unsuitable for passenger car applications.

Chargers for passenger cars are normally mounted inside the car. This is because the vehicle may be used a long way from home, further than the range possible from a single battery charge. For this reason they have to carry the charger with them on board the vehicle. Charging can be carried out at home from a standard domestic electricity socket outlet but the available power is very low and charging takes a long time, possibly ten hours or more depending on the size of the battery. Since charging is usually carried out overnight this is not necessarily a problem, but it could be if the car is away from its home base. Such low power charging is normally used in an emergency and most cars are fitted with a higher power charging option which can be used in commercial locations or with a higher power domestic installation. In many countries this higher power facility is implemented by means of a three phase electricity supply.

Commercial electric vehicles need bigger batteries which need higher power charging stations to achieve reasonable charging times but they also have extra options. Many of them follow prescribed delivery routes within a limited range from base and return to base in the evening. In these cases off board charging is possible saving weight and space on the vehicle. Such applications can also be adapted to battery swap options. Each vehicle may have two batteries with one being charged while the other is in use. When used in long distance shuttle applications this can double the effective range of the vehicle. The vehicle depletes the battery during each journey and picks up a fully charged battery at the terminus leaving the discharged battery to be recharged ready for the next trip. This shuttle option however needs three batteries per vehicle.

Early HEVs used Nickel Metal Hydride batteries, but they are mostly being superseded by a range of variants of Lithium ion batteries which is the technology of choice for most new EV

applications since they can store more energy and deliver higher power. For this reason most EV chargers are designed to work exclusively with Lithium ion batteries.

Charging Stations: Charging stations merely deliver the energy to the vehicle, usually in the form of a high voltage AC or DC supply. They don't normally have the functions of the charger which must transform the electrical energy into a form which can be applied directly to the battery.

From the wide range of potential consumers noted above, it can be seen that the EV community needs several power supply options. Broadly speaking, three different power levels have been defined but within these levels a very wide range of options are available to accommodate the different existing power grid standards of the national electricity generating utilities.

Level 1 refers to Single Phase Alternating Current (AC) using grounded receptacles as used in domestic applications. The EV may incorporate a standard domestic power cord to connect the vehicle to a domestic socket outlet or a Level 1 charging station.

Level 2 delivers power from either Single or Three Phase Alternating Current (AC) sources. Individuals can install a level 2 charging station at home, while businesses and local government can also provide level 2 charging for a fee or free if they wish.

Level 3 refers to Direct Current DC charging, or “fast charging.” To achieve very short charging times, Level 3 chargers supply very high currents of up to 400 Amps at voltages up up to 600Volts DC delivering a maximum power of 240kW.

Minimization of Losses considering Electric Vehicles

Shefali Painuli[1], Mahiraj Singh Rawat[2], Durga Rao Rayudu[3]

***Abstract*—Vehicles accompanying internal combustion engine utilizes conventional energy thus releases toxic and unfavorable pollutants. Electric vehicle is one of the possible and practical solution to lower down the emission rate of such pollutants. However, the rate of penetration of electric vehicles leads to various barriers since they will consume power from the grid in order to charge their batteries. As a result of which with the increase in penetration rate of electric vehicles, the power system parameters such as losses, voltage regulation, harmonic distortion, power quality and efficiency is influenced. In this paper, relationship between the factors affecting losses is addressed and on the basis of that distribution system losses is minimized. The implementation of the addressed relationship is done on an IEEE 15 bus radial distribution system. The paper also focused on the area of synchronized charging and unsynchronized charging.**

Keywords—Load Factor, Load Variance, Losses, Synchronized Charging, Unsynchronized Charging.

I. INTRODUCTION

Transportation is considered as one of the basic need of humans and also, considered as the leading consumer of fossil fuels. Consumption of fossil fuels by vehicles with internal combustion engines have exploited several environmental constraints due to the release of harmful pollutants. Several attempts have been taken for developing and constructing coherent infrastructures for creating technologies which will be free of pollution with least dependency on carbon based fuels. One of the practical and possible solution to this is electric vehicles (EVs).

The success of EVs adoption in daily life highly relies on energy storage which should be capable of supplying surplus energy to charge their batteries. In fact, the growing number of EVs is directly proportional to the requested electrical energy. With the increase of EVs inclusion in market, the electrical energy demand also increases. Hence, it can be concluded that EVs are soon going to behave as an additional load in power system which cannot afford to be neglected. Therefore, studies on power system should be done considering the impact of EVs on distribution system with all the possible parameters influencing the characteristics of the system in order to rectify unfavorable characteristics. Studies in [1]-[7] presents various charging algorithms for attenuating the unfavorable effect of EVs in distribution system. These unfavorable effect includes power losses, harmonic distortion, voltage and frequency deviation.

At present, management of EV charging can be categorized under two categories: synchronized charging and unsynchronized charging. Unsynchronized charging, also known as uncoordinated charging is a random charging phenomenon where the EV owners doesn't have required information for scheduling the charging cycle of their EVs. In unsynchronized charging the charging of EVs is done randomly after arriving home from office or workplaces during the peak hours in evening time. On the other hand, synchronized charging is a smart charging approach in which the charging cycle of EVs is distributed uniformly during desired period. This charging approach is a key solution, of increasing peak by adjusting the charging cycle over off peak hours. The application of synchronized or coordinated charging and unsynchronized or uncoordinated charging is described in [8]-[13].

In order to adopt and utilize synchronized charging, its implementation should be performed and analyzed during planning stage. In this paper, relationship between distribution system parameters like load factor, load variance and losses is examined considering grid to vehicle technology. For evaluating the effectiveness of the expressed relationships, its utilization is done in the area of synchronized charging on an IEEE 15 bus radial distribution system in Matlab environment. Results proved that the formulated relationship between the above mentioned distribution parameters for synchronized charging is independent of the system topology and minimizes system losses thereby improves voltage regulation.

The paper is arranged as: Section I gives a brief introduction about the trends in EVs. Section II explores the parameters influencing the distribution system losses. Section III provides objection function for minimizing losses in the system. Section IV gives information about the test system along with the assumptions considered in the paper. Section V provides the results of the theoretical concept explained in above mentioned sections. Section VI concludes the whole paper.

II. MINIMIZATION OF LOSSES

In this section relationship between load factor, load variance and losses is examined. The main objective of the paper is to minimize system losses, which in effect will improve the voltage profile. The mathematical modelling is shown below.

[1]Shefali Painuli is with Department of Electrical Engineering, National Institute of Technology, Uttarakhand, India
[2]Mahiraj Singh Rawat is with Department of Electrical Engineering, National Institute of Technology, Uttarakhand, India.
[3]Durga Rao Rayudu is with Department of Electrical Engineering, National Institute of Technology, Uttarakhand, India.

(e-mail: shefalipainuli28@gmail.com, rawat.ms85@gmail.com, venu.rayudu@gmail.com)

A. Losses

Losses in the system can be directly calculated using the following equation,

$$\sum_{t=1}^{T(total)} \sum_{l=1}^{L(total)} [I(l,t)]^2 * R(l) \quad (1)$$

B. Load Factor

Load Factor (L.F) is defined as the ratio between the average demand and maximum demand [14]. From the utilities point of view, the system should be designed in such a way that it can hold the maximum demand therefore, optimal L.F should be unity.

Proof: Let us consider that voltage is constant or near to constant then current at time't' can be expressed as,

$$I(t) = k_1 D(t) \quad ; k_1 \text{ is a constant and } k_1 \geq 0 \quad (2)$$

Similarly, current at average and maximum load can be written respectively as,

$$I(avrg) = k_1 D(avrg) \quad (3)$$

$$I(\max) = k_1 D(\max) \quad (4)$$

Total energy losses in the system over a time interval 'T' can be expressed as,

$$Losses(total) = L * losses(\max) * T(total) \quad (5)$$

where, L is loss factor, losses(max) is maximum losses and T(total) is the total time. Loss factor was first derived by Woodrow and Buller formula in [15], [16].

Now, losses(max) in (5) can be expressed as a function of I(max),

$$Losses(\max) = k_2 [I(\max)]^2 \quad ; k_2 \text{ is a constant and } k_2 \geq 0 \quad (6)$$

Thus, (5) can be written as,

$$Losses(total) = L * k_2 [I(\max)]^2 * T(total) \quad (7)$$

Since L, k_2 and T(total) are constant therefore Losses(total) depends on I(max) i.e

$$Losses(total) \alpha\ I(\max) \quad (8)$$

and L.F can be expressed as,

$$L.F = \frac{\sum_{t=1}^{T(total)} D(t) / T(total)}{D(\max)} \quad (9)$$

On substituting the value of D (t) and D (max) from (2) and (4) respectively in (6), L.F can be written as,

$$L.F = \frac{\sum_{t=1}^{T(total)} \left\lceil \frac{I(t)}{k_1} / T(total) \right\rceil}{\frac{I(\max)}{k_1}} = \frac{\sum_{t=1}^{T(total)} [I(t) / T(total)]}{I(\max)}$$

$$L.F = \frac{I(avrg)}{I(\max)} \quad (10)$$

From (6) and (10) the following relationship can be concluded,

$$Losses(total) \alpha\ I(\max) \quad \text{Or} \quad I(\max) \alpha\ Losses(total)$$

$$L.F\ \alpha\ \frac{1}{I(\max)} \quad \text{Or} \quad I(\max) \alpha\ \frac{1}{L.F}$$

Thus,

$$Losses \alpha\ \frac{1}{L.F} \quad \text{Or} \quad L.F\ \alpha\ \frac{1}{Losses}$$

As shown above losses are directly proportional to I(max) and on the other hand load factor is indirectly proportional to I(max). From here, it can be concluded that there is an inverse relationship between load factor and losses. So, losses in the system can be decreased by increasing the load factor.

C. Load Variance

Proof: Total losses in the system is given by,

$$Losses(total) = \mu(I^2) * R \quad (11)$$

where, R is a constant and

$$\mu(I^2) = \frac{1}{T(total)} \sum_{t=1}^{T(total)} [I(t)]^2 \quad (12)$$

Now,

$$\mu(I) = \frac{1}{T} \sum_{t=1}^{T(total)} I(t) = I(avrg) \quad (13)$$

Since I(avrg) is constant therefore μ(I) will be also constant.

Now, L.V as seen by the substation is given by,

$$[\sigma(I)]^2 = \frac{1}{T(total)} \sum_{t=1}^{T(total)} [I(t) - \mu(I)]^2 \quad (14)$$

$$= \frac{1}{T(total)} \sum_{t=1}^{T(total)} [(I(t)]^2 + \frac{1}{T(total)} \sum_{t=1}^{T(total)} [\mu(I)]^2 - \frac{2\mu(I)}{T(total)} \sum_{t=1}^{T(total)} I(t)$$

From (12) and (13) the above equation can be written as,

$$[\sigma(I)]^2 = \mu(I^2) + \frac{1}{T(total)} \sum_{t=1}^{T(total)} [\mu(I)]^2 - 2\mu(I) * \mu(I)$$

Since $\frac{1}{T(total)} \sum_{t=1}^{T(total)} [\mu(I)]^2 = [\mu(I)]^2$ thus,

$$[\sigma(I)]^2 = \mu(I^2) + [\mu(I)]^2 - 2[\mu(I)]^2$$

$$[\sigma(I)]^2 = \mu(I^2) - [\mu(I)]^2$$

$$\mu(I^2) = [\sigma(I)]^2 + [\mu(I)]^2 \quad (15)$$

Since $[\mu(I)]^2$ is constant thus from (15), it can be concluded that $\mu(I^2)$ is directly proportional to $[\sigma(I)]^2$ and from (11), it can be observed that total losses are directly proportional to $\mu(I^2)$. Mathematically,

$$[\sigma(I)]^2 \alpha \ \mu(I^2)$$

$$Losses(total) \ \alpha \ \ \mu(I^2)$$

Thus,

$$Losses(total) \alpha \ [\sigma(I)]^2$$

So, on minimizing L.V total losses of the system can be minimized.

III. Objective Functions

The main idea behind this paper is to minimize and reduce distribution system losses incorporating the effect of EVs in the system. Since, reduction of losses results in a better voltage profile therefore here, the focus area is losses reduction which is formulated on the basis of the above derived relationships and expressions. The formulation of objective functions is as follows:

(1) Maximization of L.F

$$\max\left[\frac{\mu(D)}{\max\left(\sum_{n=1}^{nodes} EV(n,t)\right)}\right] \quad (16)$$

(2) Minimization of L.V

$$\min\left[\sum_{t=1}^{T(total)}\left(\frac{1}{T(total)}\left(\sum_{n=1}^{nodes} EV(n,t) - \mu(D)\right)\right)\right] \quad (17)$$

(3) Minimization of line losses

$$\min\left[\sum_{t=1}^{T(total)}\sum_{l=1}^{L(total)} [I(l,t)]^2 * R(l)\right] \quad (18)$$

where,

$\mu(D)$ is the distribution system average load during T(total) given by,

$$\mu(D) = \frac{\sum_{t=1}^{24} EV(n,t)}{24} \quad (19)$$

EV(n,t) is the EV load at node 'n' and at time 't'

L(total) is the total number of lines

I(l,t) is the current at line 'l' and at time 't'

R(l) is the resistance of line 'l'

IV. Case Study

A. Study Test System & Assumptions

IEEE 15 bus radial distribution system as shown in Fig.1 is used in this paper. The branch and line data of the test system can be found in [17]. EVs are modelled, which draws constant real power from the grid [18]. These EVs are placed randomly at bus no. 2, 5, 10 and 15 at different penetration levels of 10%, 20%, 50% and 100%. It is assumed that the total power drawn at 100% penetration is 700kW on the basis of which other mentioned percentage of penetration levels are also calculated. Further forward-backward sweep method is used for all power flows.

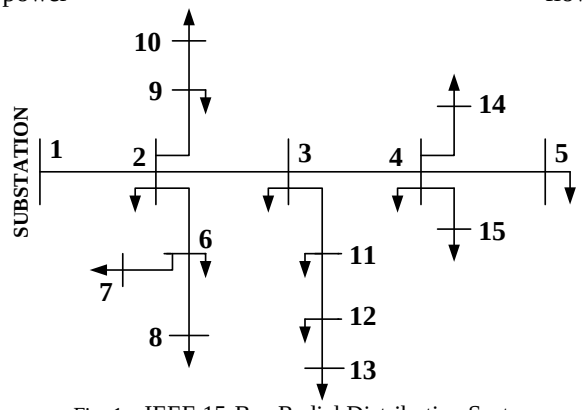

Fig. 1. IEEE 15-Bus Radial Distribution System

B. Daily Household Load Profile

Fig. 2 shows the daily household load profile of a single house [10].

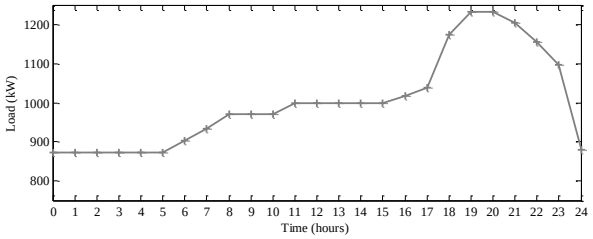

Fig. 2. Daily Load Profile of a Single House

The daily load profile of a house is divided into four zones:

(1) Zone-A: Load profile from 0 to 5 hour comes under the category of Part-A profile. Here, the load demand is low and constant.

(2) Zone-B: Load profile from 5 to 18 hour is Part-B profile. Under this category, the load demand is of increasing order.

(3) Zone-C: Load profile from 18 to 24 hour is Part-C profile. This is the peak residential profile where there is peak load demand during peak hours.

V. Results & Discussions

In order to investigate the behavior of various parameters, different penetration levels are studied. Taking the reference of Fig. 1 as base case of 0% penetration, daily household load profile for different levels of penetration are shown in Fig. 3.

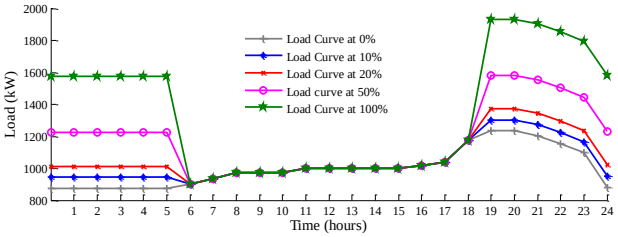

Fig. 3. Single Household Load Profile at Different EV Penetration Levels

Fig. 4 shows load factor at different penetration level of EVs for a day. The calculation of load factor is done using the objective function mentioned in (16).

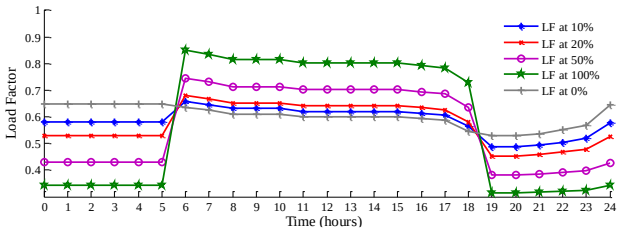

Fig. 4. Load Factor at Different EV Penetration Levels

Fig 5. presents a plot for losses at different penetration levels for a complete day calculated using (18). It can be observed from the plot that during zone-A and zone-C the distribution system losses increases with the increase in penetration percentage since the EVs start to charge from zone-C till zone-A as it is a household profile. Whereas in zone-B all the penetration level follows the same graph of losses because during this period EV owners leave their home for work stations. It can also be concluded from the graph that during the charging zones i.e. zone-A and zone-C, losses are indirectly proportional to load factor which satisfies the relationship derived in section II. Among both the charging zones, zone-C is having peak in losses therefore the duration of time in zone-C will be termed as peak hours.

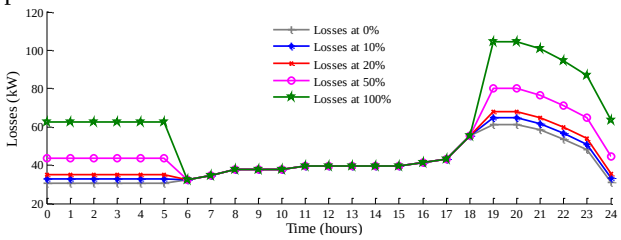

Fig. 5. Losses at Different EV Penetration Levels

In Fig. 6, plot for variance at different EV penetration levels is shown which is calculated using (17). Here during the charging zones, with the increase in penetration percentage the variance also increases. This again closely satisfies the derived relationship between variance and losses since from Fig. 5, the losses are in increasing order for increasing penetration level during the charging zones whereas variance are also following the same scenario.

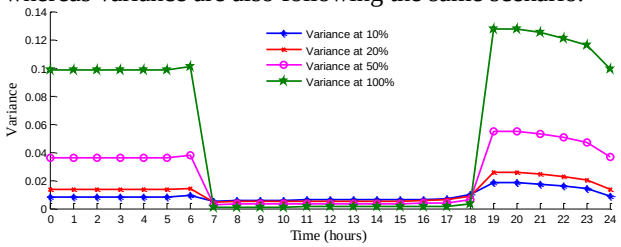

Fig. 6. Load Variance at Different EV Penetration Levels

Plots for load factor, losses and load variance in Fig. 4, 5 and 6 respectively satisfies the relationship derived in section II as shown below in the figure.

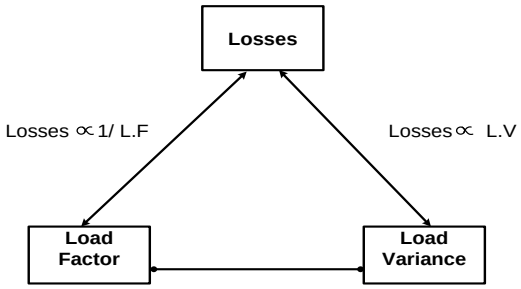

Fig. 7. Load Factor at Different EV Penetration Levels

Now, in order to rectify the problem of getting peak in losses during the charging zones, synchronized charging is adopted. The objective here is to cut down the peak in losses during peak hours and shift that peak to off-peak hours in order to level the load of EVs in the distribution system. For that purpose, load factor during peak hours in zone-C is leveled by shifting the peak or charging cycle during zone-A as shown in Fig. 8. Since Load factor is the ratio of average current and maximum current therefore for leveling load factor, maximum current is reduced and average is increased.

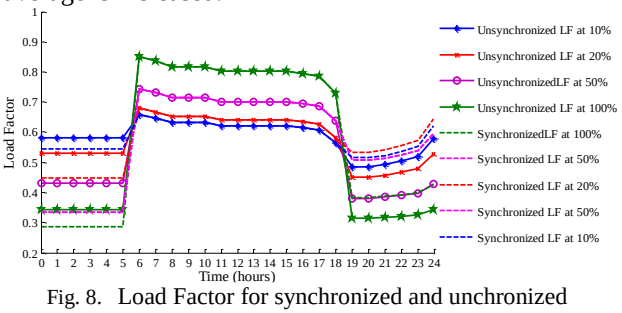

Fig. 8. Load Factor for synchronized and unchronized charging at Different EV Penetration Levels

Because of shifting of charging cycle to zone-A from zone-C under the concept of synchronized charging, there remains a balance between the losses in the charging zones. Due to the shifting of load factor as shown in Fig. 8 there is shifting in the losses as well which is shown in fig. 9. As shown in the figure in case of synchronized charging for all the penetration levels, there is a leveled curve for losses during both the charging zones. Similarly, load variance can also be adopted for synchronized charging to reduce distribution system losses.

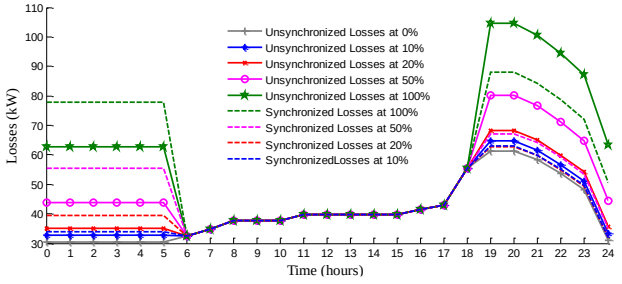

Fig. 9. Losses for synchronized and unchronized charging at Different EV Penetration Levels.

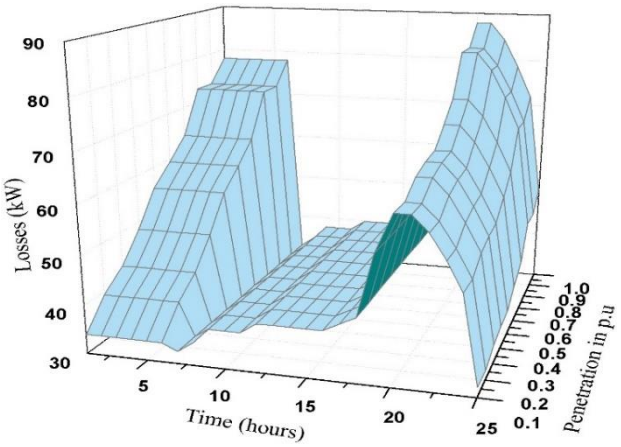

Fig. 10. Losses for synchronized charging at Different EV Penetration Levels.

For better visuality of losses leveling, a three dimensional plot for losses with synchronized charging is shown in Fig. 10.

VI. CONCLUSION

In this paper, relationship between distribution system parameters like losses, load factor and load variance is explored. The dependency of load factor and load variance on losses is derived. On the basis of which objective functions are formulated for minimizing distribution system losses. The concept of synchronized and unsynchronized charging is also presesnted. A better point view of results is presented in the paper in the context of synchronized and unsynchronized charging at various penetration level of EVs.

REFERENCES

[1] H. Farzin, M. Moeini-Aghtaie and M. Fotuhi-Firuzabad, "An investigation of reliability impacts of V2G-capable vehicles in municipal parking decks," in Proc. 23rd International Conference on Electricity Distribution (CIRED), Lyon, France, 2015.

[2] H. Farzin, M. Moeini-Aghtaie and M. Fotuhi-Firuzabad, "Reliability Studies of Distribution Systems Integrated With Electric Vehicles Under Battery-Exchange Mode," IEEE Trans. Power Del., vol. 31, no. 6, pp. 2473-2482, Dec. 2016.

[3] M. Moeini-Aghtaie, H. Farzin, M. Fotuhi-Firuzabad and R. Amrollahi, "Generalized Analytical Approach to Assess Reliability of Renewable-Based Energy Hubs," IEEE Trans. Power Syst., vol. 32, no. 1, pp. 368-377, Jan. 2017.

[4] J. Lopes, F. Soares, and P. Almeida," Integration of electric vehicles in the electric power system," Proc. of the IEEE, vol. 99, no. 1, pp.168 183, 2011.

[5] E. Sortomme, M. M. Hindi, S. D. James MacPherson and S. S. Venkata, "Coordinated charging of plug-in hybrid electric vehicles to minimize distribution system losses," IEEE Trans. Smart Grid, vol. 2,no.1, pp. 198-205, March 2011.

[6] C. Ahn, C.-T. Li, and H. Peng "Optimal decentralized charging control algorithm for electrified vehicles connected to smart grid," J. Power Sources, vol. 196, no. 2, pp. 10369-10379, 2011.

[7] M. C. Caramanis and J. M. Foster, "Coupling of day ahead and realtime power markets for energy and reserves incorporating local distribution network costs and congestion," 48th Annual Allerton Conf. on Communication, Control, and Computing pp. 42-49, 2010

[8] K. P. Schneider, C. E. Gerkensmeyer, M. C. W. Kintner-Meyer, andR. Fletcher, "Impact assessment of plug-in hybrid vehicles on pacific northwest distribution systems," in Proc. Power Energy Soc. Gen.Meet., Jul. 2008, pp. 1–6.

[9] K. Clement, E. Haesen, and J. Driesen, "Coordinated charging of multiple plug-in hybrid electric vehicles in residential distribution grids," in Proc. Power Syst. Conf. Expo., 2009, pp. 1–7.

[10] K. Clement-Nyns, E. Haesen, and J. Driesen, "The impact of charging plug-in hybrid electric vehicles on a residential distribution grid," IEEE Trans. Power Syst., vol. 25, no. 1, pp. 371–380, 2010.

[11] S. Han, S. Han, and K. Sezaki, "Development of an optimal vehicle-to-grid aggregator for frequency regulation," IEEE Trans. Smart Grid, vol. 1, no. 1, pp. 65–72, 2010.

[12] A. Y. Saber and G. K. Venayagamoorthy, "Plug-in vehicles and renewable energy sources for cost and emission reductions," IEEE Trans. Ind. Electron., to be published.

[13] A. Hajimiragha, C. A. Cañizares,M.W. Fowler, and A. Elkamel, "Optimal transition to plug-in hybrid electric vehicles in Ontario, Canada, considering the electricity-grid limitations," IEEE Trans. Ind. Electron., vol. 57, no. 2, pp. 690–701, Feb. 2010.

[14] William H. kersting, Distribution System Modeling and Analysis. CRC Press, Boca Raton London New York Washington, D.C, 2002..

[15] M. W. Gustafson and J. S. Baylor, "The equivalent hours loss factor revisited," IEEE Trans. Power Syst., vol. 3, no. 4, pp. 1502–1508, 1988.

[16] D. Das, D. P. Kothari, and a. Kalam, "Simple and efficient method for load flow solution of radial distribution networks," Int. J. Electr. Power Energy Syst., vol. 17, no. 5, pp. 335–346, 1995.

[17] H. Farzin and M. Fotuhi-firuzabad, "Charging / Discharging Management of Electric Vehicles : Technical Viewpoint," Smart Grids Conf., pp. 20–21, 2016.

Charging Infrastructures of Electric Vehicle: Overview of Power Quality management, Issues and Technologies

Antariksha Verma[1], Shelly Vadhera[2]

***Abstract*- This paper reflects an overview of power quality management, issues and technologies related to charging and discharging of electric vehicle. Analysis is done on the basis that electric vehicle charging station is integrated to the smart grid which is further connected to the main grid with distributed power plants, different electric storage devices and different renewable sources. In the analysis it is also included that both stationary and on-board application needs different types of storage systems. Power quality issues in electric vehicle are due to the many factors: presence of harmonics, discontinuity of supply respect to disturbance on the grid, max time of power failure in faults situation, brownouts. Power quality issue disturbs distribution system at all voltage level (low, medium, high) but in particular those in LV and MV. The development of power electronics worked in both ways. On one hand it introduced disturbing loads, undesired harmonic component in current and voltage of distribution system; on the other hand, has led to the development of devices like FACTS to improve power quality.**

Power conditioning system (PCSs) known as active filters, are power electronic devices work on low voltage (LV) and medium voltage (MV) power transmission networks that improve the power quality (power factor correction, peak shaving, short interruption or voltage sag). These types of devices having primary function of peak shaving are coupled perfectly with electric vehicle with quick charging stations (EVQCCs) because considerable power is absorbed by these devices from the 3 phase network working on 400V, 50Hz. This paper presents charging infrastructures for electric vehicle including different charging mode, AC and DC charging architectures and ultrafast charging architectures.

Keywords- Electric vehicle, Power conditioning system(PCSc), Distribution system, Energy storage, Recharging station, RESs.

I. INTRODUCTION

Nowadays, green house gases are big issue to the environment, to decrease these gases and pollution in the environment Electric Vehicle turns out into a better substitute of fossil fuel depended vehicle. In order to sustain in the automobile market it is necessary to give features of travel ranges and charging times of electric vehicle comparison to traditional fossil fuel based vehicles. Due to these reasons electric vehicles need battery which have high value of charging rates and energy storage capacity. Batteries having lithium compounds are more suitable for these requirement. These batteries have charging time less than 10 minutes [1]. Due to high power and energy density, electric vehicle can show high performance in terms of driving range and acceleration [2].

Electric vehicle charging station is directly connected to the distribution grid which is further connected to the power grid. Any disturbance in charging station directly effect the power quality. Power quality means

- Voltage and current quality, that is the quality of waveform (frequency, amplitude, harmonics variations).
- A continuous power supply without any interruption.

Active filters or custom power systems are designed for the specific application and specific requirement of the power quality and targeted at load sensitive to the disturbances in the power networks (noisy load, voltage dip or sag), and in any case where economic evaluations of cost/benefits ratio can justify the adoption, in the consideration of the high costs of these custom equipment[3]. In dependence of their control logic and power conFiguration, common functions of custom power system are as follows: active power factor correction, reduction of the impact of the harmonics due to noisy load in network, voltage regulation of long line, peak shaving. These custom power system are known as STATCOM, SVS ,STS etc.

Basically there are two modes of charging the battery of electric vehicle: slow charge and quick charge. In slow charge mode, battery is mounted inside the vehicle having small power (2-3 kW). Recharging time in slow charging mode is approximately 8 hours. These batteries can be charged all night and can be used in the day time for travelling. In fast charging special equipments are needed which is connected to public grid installed at appropriate place in towns and cities. In this mode recharging time period is 15-30 minutes, depending on the size of electric vehicle battery pack (50-200 kW) [4]. Longer distance travelling requires frequent electric service charging stations along the way. These electric service charging station should be able to provide significant amount of power when it is required instantly like oil based fuel vehicles [4]. The existing electric infrastructure may not be able to provide sufficient amount of power quickly and there might be affect on power grid due to large number of charging or discharging of electric vehicle. Strategies should be adopted that can minimize the affect on power

[1]Antariksha Verma is with Department of Electrical Engineering, National Institute of Technology, Kurukshetra, India

[2]Shelly Vadhera is with Department of Electrical Engineering, National Institute of Technology, Kurukshetra, India.

(e-mail: antrikshvv@gmail.com, shelly_vadhera@radiffmail.com)

grid and distribution grid. These strategies consist of how much amount of electric vehicle should be charged in days and night. A proper integration of renewable energy sources with the charging station can give the edge in power quality improvement [5].

The evaluation strategies should consider the habit of the EVs owner and energy price. On this regard the EVs aggregation agent acts as an important role between electricity market, DSO, transmission system operator and electric vehicle owner [6]. The role of EV aggregation agent can be justified by the fact that each electric vehicle owner can not handle energy trades between electric vehicle and power grid, due to their low electric power capacity. An aggragation agent make smart charging of vehicles simpler and easier. Different charging scenarios which is probable from the view of electric vehicle owner discussed further [7].

TABLE 1
Different charging scenarios

Dumb charging	Energy cost is same along the days; owner are free to charge vehicle at any time
Multiple tariff	Energy cost changes along the day; owner are free to charge vehicle at any time
Smart charging	It is based on two hierarchical control structures; first one managed by the aggregation agent and the other managed by DSO
V2G	The DSO and the aggregation agent control the discharging of electric vehicle towards the grid and also electric vehicle smart charging

II. TOPOLOGY OF ELECTRIC VEHICLE CHARGING STATION WITH STORAGE DEVICES (SMES)

In Fig. 1 electric vehicle charging station topology is shown. PV system and energy storage devices are also being connected to the DC bus through DC/DC converter. In this topology the advantage is DC/AC converter are not being used that will reduce the losses as well as cost.

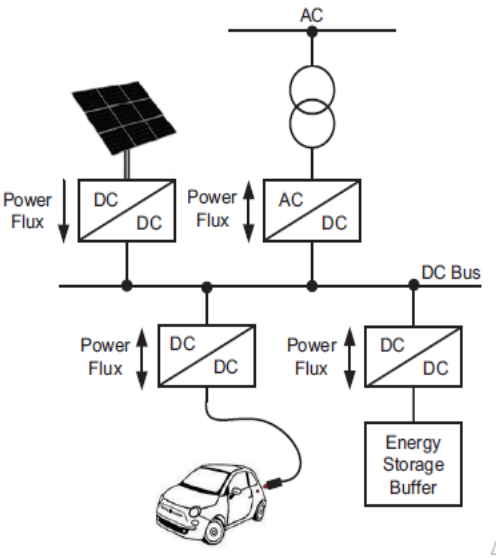

Fig.1. EV charging with DC bus and PV system

At the place of energy storage buffer, SMES can be used. There are other option like super capacitor, fly wheel devices that can be placed at energy storage buffer. SMES is superconducting magnetic energy storage device, in which superconducting magnet works at cryogenic temperature at 20 K.

SMES is used to maintain the transient energy balance of electric vehicle charging station [8]. Energy management strategy of electric vehicle charging station with SMES is shown in the workflow which is shown in the Fig. 2.

$$P_{grid} + P_{PV} = P_{EV} + P_{SMES} \quad (0.1)$$

In transient condition SMES only supply power which is shown in the equation (0.1). In steady condition SMES do not supply power and energy balance is shown by equation (0.2). Here Isc is super conducting magnet current and Iset is known as reference current.

$$P_{grid} + P_{PV} = P_{EV} \quad \text{Steady} \quad (0.2)$$

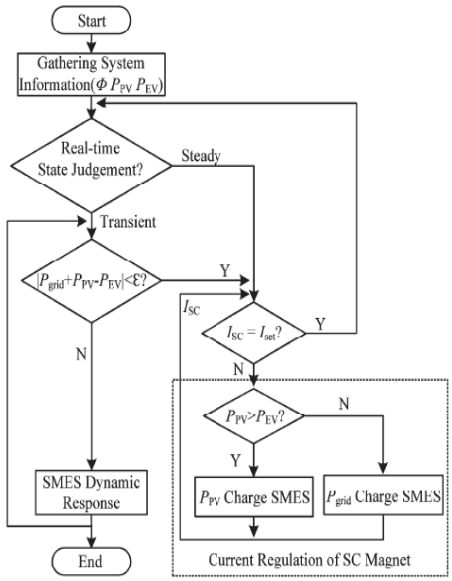

Fig.2. Workflow of EV charging station with DC bus and energy storage devices

III. CHARGING INFRASTRUCTURE OF ELECTRIC VEHICLE

Electric vehicle charging system mainly contains electronic parts. These can be off board or on board to provide the energy for the electric vehicle energy storage system. On board charger reduces the charging power due to their weight, cost and space constraints. These chargers basically take large time to charge the battery pack. On the other hand off board chargers have quality to charge fast. These chargers are not as much of exaggerated by weight and size limitations.

A. Charging Modes

Different recharging modes are classified according to the international standard IEC 61851-1 [9].

Mode 1

In this mode electric vehicle is connected to the AC line 250 V or 3 phase AC line 480 V 50 Hz, using domestic plug and socket system not greater than 15 A with

protective earth conductors. This mode is known as most economical charging mode because this is used at home and office and there is not any need of extra infrastructures. This mode is slowest mode and battery of EV is refilled during the night. This mode is economical because in the night there will be less load on the grid.

Mode 2

In this charging mode electric vehicle is connected to the AC supply same as mode 1 by using standard wall sockets and plugs not exceeding 31 A with protective earth conductors.

Mode 3

In this mode electric vehicle is connected to the AC supply through the EVSE not greater than 62 A, which is known as electric vehicle supply equipment. This mode is known as semi fast and charging can be done within few hours during driving and everyday work.

Mode 4

In this mode CHAdeMO consortium is implemented by using off board chargers in which control pilot function is extended to the equipment permanently connected to AC network [10].

Fig.3. CHAdeMO [10]

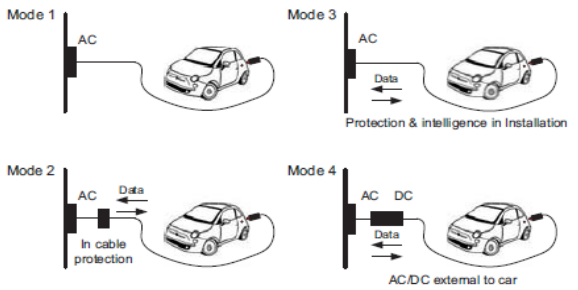

Fig.4. IEC 61851-1 charging modes

Charging time of mode 4 is 15 to 25 minutes. Charging time in this case is limited to allowable current 120 A and voltage 500 V of CHAdeMO standard connector [10].

TABLE 2 IEC 61851-1 charging modes

Charging mode	Max current per phase	Charging time(max)	Vehicle battery charger (Board)
4	390DC	25 minutes	Off
3	62 A	2 hours	On
2	31 A	3 hours	On
1	15 A	7 hours	On

There are three types of socket-outlets presently [10].

1. IEC 62196-2 (Type 1)- 1 phase vehicle coupler - reflecting the SAE J1772/2009 automotive plug specifications - Yazaki.
2. IEC 62196-2 (Type 2)- 1 and 3phase vehicle coupler - reflecting the VDE-AR-E 2623-2-2 plug specifications - Mennekes.
3. IEC 62196-2 (Type 3)- 1 and 3 phase vehicle coupler with shutters - reflecting the EV Plug Alliance proposal- SCAME.

TABLE 3 Electrical ratings of different EVs charge methods in EUROPE

Charge method	Connection	Power (kW)	Max current (A)	Location
Normal Power	1 phase AC	6	15	Domestic
Medium power	1 or 3 phase AC	6-21	31	Semi Public
High Power	3 phase AC	>21	>31	Public
High power	DC connection	>21	>3200	Public

TABLE 4 Actual mode and type of plugs for EVs charger in EUROPE

	Private domestic socket	Private dedicated E-Mobility socket	Semi Public AC	Public AC	Public DC
Power connection	1 phase AC	Up to 21 kW	Up to 21 kW	Up to 21 kW	50 kW Chade Mo
Plug (Infrastructure side)	Domestic	IEC 60309-25 Type 2/ Type 3	Type 2/ Type 3	Type 2/ Type 3	Yazaki Chade Mo
Charging mode	Mode 2	Mode 2 Mode 3	Mode 2 Mode 3	Mode 2 Mode 3	Mode 4

In table 4 actual mode and types of plugs for electric vehicle charging is shown. On the basis of private domestic socket, semi-public AC, public AC and public DC power connection, plug (infrastructure side) charging mode is shown. For public DC power connection will be 50 kW ChadeMo and Yazaki ChadeMo plug can be used.

B. AC and DC Charging Architecture

There are two types of charging architectures AC or DC [11]. AC charging architecture is based on AC bus and all the energy shared between RES, energy storage buffer and electric power grid would be through AC bus. These AC bus consists of DC/AC converter and because of these converter losses will be there in the network. AC architecture is shown in the Fig.5. This architecture would be suitable to realize a smart charging scenario presenting different strategies of V2G energy management, obtained with a proper EV aggregation agent.

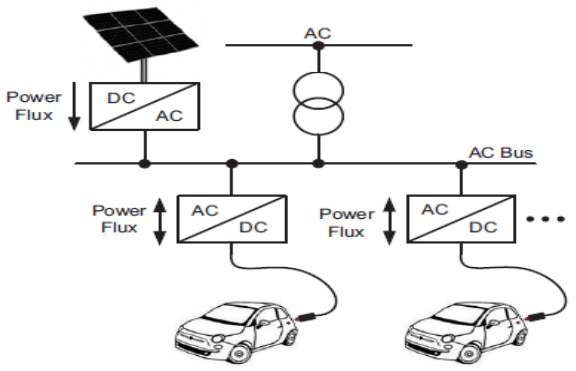

Fig.5. EV Charging Architecture with AC Bus

In Fig.6 DC architecture is shown. In this DC architecture only DC/DC converter is connected between PV system and DC bus. This architecture helps to reduce the losses which are due the conversion of energy in DC/AC converter [6].

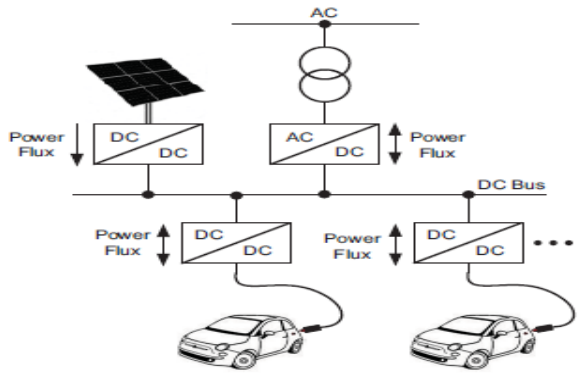

Fig.6. EV Charging Architecture with DC Bus

C. *Ultra-fast charging Architecture*

Ultra-fast charging is shown in the Fig.1. charging time in this architecture is less than 5 minutes and this is the main objective of this architecture reducing the charging time. In Fig.6 charging condition became critical when more and more number of electric vehicle are being charged. To simplify the charging process a energy storage system is added to the architecture shown in Fig.6 which works as power buffer interposed between grid and Electric Vehicle [6].

IV. POWER QUALITY ISSUES AND TECHNOLOGIES IN ELECTRIC VEHICLE CHARGING STATION

Power conditioning system (PCS) is connected to the same bus where CHAdeMO quick charger (max power 50 kW) is connected. The test site configuration is shown in the Fig.7. In this paper main focus is on the results related to peak shaving mode because this will help to manage new scenarios both for users and DSOs.

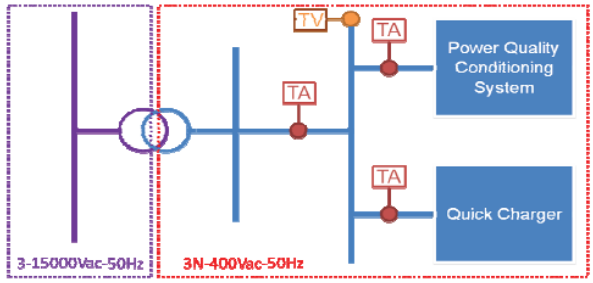

Fig.7. Test site connection scheme

Example of system behaviour is shown in the Fig.8. In this Fig we can see as system reaches towards the end of charging of ultra-capacitors, the jump of power equal to the provision that had at that time is seen by the network and reason behind is the low energy that the system under test presents, being designed to make services in power not in energy [3].

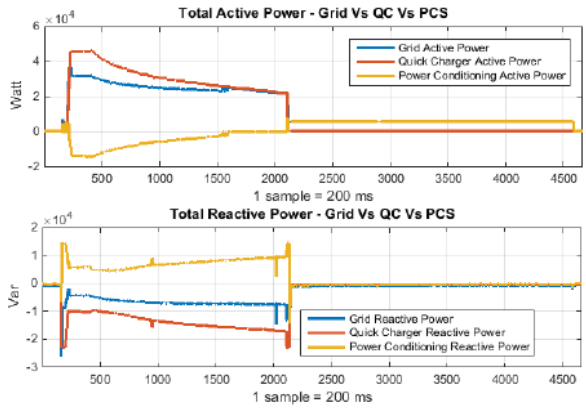

Fig.8. Total active and reactive power graph

Basically this system is prepared for small energy need. Even with the cell discharged, system allows to adjust the reactive power (second graph in Fig.8). This all reflects as advantage on the power factor seen by the grid (Fig.9) [11].

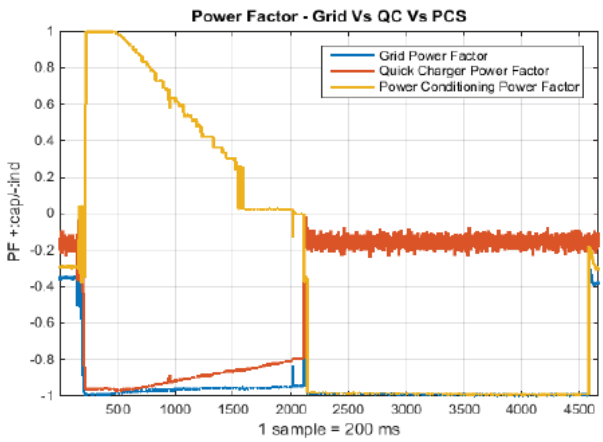

Fig.9. Power factor graph

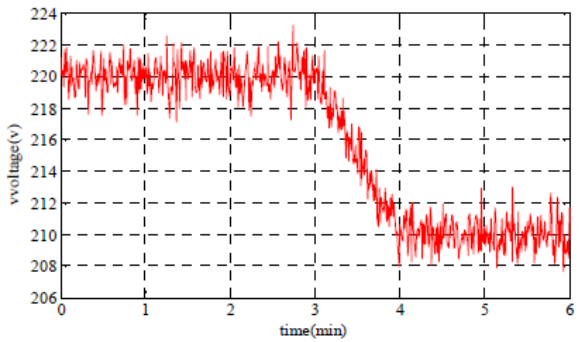

Fig.10. Charging station voltage without SMES

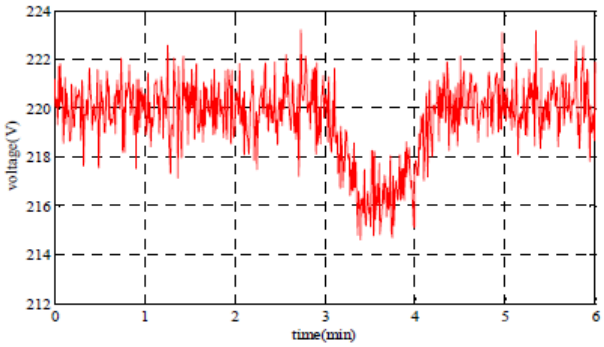

Fig.11. Charging station voltage with SMES

In Fig.11 effect of using SMES is shown. Which shows voltage transient and stability is improving when SMES is being as energy storage buffer in the Fig.1. This is the main advantage of using SMES in place of flywheel energy storage device [8].

V. CONCLUSION

In this paper overview of charging station infrastructures of electric vehicle is discussed with technologies and issues. AC and DC charging station infrastructure are being compared. Advantage of using ultra-fast charging architecture is also discussed. In ultra-fast charging infrastructure, due to using energy storage buffer there will be less effect on power grid. Advantages of using SMES as energy storage devices are also being discussed. Active and reactive power of the system having electric vehicle and PCS with advantage on power factor seen from the grid are also discussed. Lithium compound batteries are seen as promising technology because of their high charging capacity.

REFERENCES

[1] M. Etezadi-Amoli; K. Choma; J. Stefani, “Rapid-Charge Electric-Vehicle Station,” IEEE Transactions On Power Delivery, vol. 25(3), July 2010.

[2] S. Dhameja,” Electric Vehicle Battery Systems,” Newnes, Boston, 2002.

[3] Ultracapacitors for Electric Vehicles Quick Charging Stations," 2015 International Conference on Electrical Systems for Aircraft, Railway, Ship Propulsion and Road Vehicles (ESARS), Aachen, pp. 1-6, 2015.

[4] D. Aggeler; F. Canales; H. Zelaya; A. Coccia; N. Butcher; O. Apeldoorn, “Ultra-Fast DC-Charge Infrastructures for EV-Mobility and Future Smart Grids. Innovative,” Smart Grid Technologies Conference Europe (ISGT Europe) IEEE PES, pp. 1-8, Oct 2010.

[5] J. A. P Lopes, F. J. Soares, P. M. R. Almeida, “Integration of Electric Vehicles in the Electric Power System,” Proceedings of the IEEE, vol. 99 (1), pp. 168-183, Jan. 2001.

[6] O. Veneri, L. Ferraro, C. Capasso and D. Iannuzzi, "Charging infrastructures for EV: Overview of technologies and issues," 2012 Electrical Systems for Aircraft, Railway and Ship Propulsion, Bologna, pp. 1-6, 2012.

[7] J. A. P. Lopes; F. J. Soares, P. M. R. Almeida, “Identifying Management Procedures to deal with connection of Electric Vehicles in the grid,” PowerTech, IEEE Bucharest, pp. 1-8, 2009.

[8] Y. Liu, Y. Tang, J. Shi, X. Shi, J. Deng and K. Gong, "Application of Small-Sized SMES in an EV Charging Station With DC Bus and PV System," in IEEE Transactions on Applied Superconductivity, vol. 25, no. 3, pp. 1-6, June 2015.

[9] Electric vehicle Conductive Charging System - Part 1: General Requirements - IEC 61851-1, 2001.

[10] M. C. Falvo, D. Sbordone, I. S. Bayram and M. Devetsikiotis, "EV charging stations and modes: International standards," 2014 International Symposium on Power Electronics, Electrical Drives, Automation and Motion, Ischia, pp. 1134-1139, 2014.

[11] B. Sanzhong, Y. Du; S. Lukic, “Optimum design of an EV/PHEV charging station with DC bus and storage system,” Energy Conversion Congress and Exposition IEEE ECCE, Atlanta, GA, USA, pp.1178-1184, Sept. 2010.

Conclusion:

With rigorous research in the field, solutions are being developed to nullify power system problems and improve the system continuously. To make the appliances cost effective for local consumers and lowering the power losses are the primary concerns of developing improved versions. The applications like solar water pumps and electric vehicles can efficiently replace the conventional machines. To enhance the performance of SPV water pumping systems, it is desirable to use a tracking system. Manual, passive and auto tracking are permitted. Different MPPT techniques have been compared and discussed to find the output giving best results.

In recent years the problems of "range anxiety" associated with electric vehicles (EVs) have been alleviated by the introduction of hybrids (HEVs) and plug in hybrids (PHEVs) and the development of higher energy density batteries capable of storing more energy in the same space. With the increasing popularity of electric vehicles, "range anxiety" is now being replaced by "charging anxiety". The low energy cost is one of the attractions of owning an EV. The development of chargers, the design and roll out of a network of public and private charging stations with associated user authentication and billing systems, public safety and planning issues, the negotiation of international standards and beefing up the electricity grid to carry the increased load have aided the development of electric vehicles. Different charging methods and charging infrastructures have been discussed.

Gas insulated systems have been in use since 40 years ago. Gas-insulated high voltage switchgear is a compact metal encapsulated switchgear consisting of high-voltage components such as circuit-breakers and disconnectors, which can be safely operated in confined spaces. GIS is used where space is limited, for example, extensions, in city buildings, on roofs, on offshore platforms, industrial plants and hydro power plants. This type of switchgear is designed and constructed in such a way, that, normal operation, maintenance, inspection can be carried out very easily and safely. All the components can easily be replaced. Another essential feature of metal enclosed switchgear is that, it should have proper interlocking arrangement between different components to ensure most safe operation. To ensure safe and proper sequence of operation, the provisions to be provided are: • The circuit breaker cannot be removed or drawn out from its compartment unless it is in OFF condition. • Not only that, it should be impossible to isolate the circuit breaker from

bus bar unless it is in OFF condition. The operation of the CB is impossible unless it is in service position, isolated position, earthed position, and removed from the compartment. • It is impossible to switch ON the circuit breaker in its service position unless auxiliary circuit is connected with it.

Multilevel inverters continue to receive more and more attention because of their high voltage operation capability, low switching losses, high efficiency and low output of Electro Magnetic Interference (EMI). A multilevel inverter has several advantages over a conventional two-level inverter that uses high switching frequency pulse width modulation (PWM). The most attractive features of a multilevel inverter are as follows: 1) They can generate output voltages with extremely low distortion and lower dv/dt. 2) They draw input current with very low distortion. 3) They generate smaller common-mode (CM) voltage. 4) They can operate with a lower switching frequency. It finds some of its applications in the following:

- Static VAR compensators.
- Back to Back High Voltage intertie
- Adjustable Speed Drives
- Only reactive power flows between the converter and the system in VAR compensation.

Bidirectional real power flows in ASDs.

Chapter 6

Recent Headways in communication engineering paradigm

The advancements in communication technology have raised communication research to significant level in communication world. We spend two- third of our working hours in communication. Communication is nothing but "elucidation transportation" from the sender to receiver. The key idea of communication is assertiveness. Significant advancements have been made in the era of wireless communication since last three decades.

In order to reinforce and augment telecommunication system, telecommunication engineering focuses on electrical and computer engineering. This chapter deals with various paradigm advancements in communication engineering fields like IoT, Fog Computing and optical wireless communication.

Optical wireless communication (OWC) technology has also emerged as potential complementary technology to the radio frequency wireless communications in various fields. Optical communication employs Orthogonal Frequency-Division Multiplexing (OFDM) scheme for better communication. The Orthogonal Frequency-Division Multiplexing (OFDM) modulation is now extensively employed in various communication standards. To cater the need of higher data rates, communication systems try to operate over broad bandwidth. Thus, for transmitting over frequency selective channels, multicarrier schemes are clear convenience.

In communication engineering, Internet of Things (IoT) is a new paradigm that has acquired more popularity in neoteric years. The term IoT was coined by Kevin Ashton in 1999. The expansion of scaling down and astuteness as well as unification of communication capabilities into an extraordinary plethora of devices have been the essential leverage of the new and innovative popular paradigm referred to as internet of things. IoT has mobilized two revolutions i.e. Fog Computing and Internet of Vehicle.

Significance of IoT (Internet of Things) in IoV (Internet of Vehicle):

The idea of IoT is to affix all devices to the internet. With the intensity and size of IoT components, the IoT applications have been enhanced utilizing diverse strategies, systems, and models inferred from gadget driven-installed structures. It has permitted communication with and among smart items, thus leading to the foresight of "anytime, anywhere, any media, anything"

communication and has aggrandized the experience of connectivity in the form of vehicular communication, sensor networking and smart metering.

One of the revolutions mobilized by IoT is Internet of Vehicle (IoV). IoV is unfolded from Vehicular Ad hoc Networks (VANETs) to achieve the vision of `from smart phone to smart car'. Safety, pollution and casualties are prime issues related to on-road traffic. These are the main factors for design and advancement in IoV. Another key driver for the expansion of IoV is the current advancements and higher market penetration rate of IoT. The Internet of Vehicle paradigm empowers the trading of information amid the vehicle and its encompassing through diverse communication mediums. As a repercussion of the incorporation of the Internet of Things (IoT) innovation with Intelligent Transportation Systems (ITS), IoV will devise an incorporated system to reinforce diverse operations, (like smart traffic organization, dynamic information services, and smart motor vehicle control among others). IoV coordinates two intelligent perceptions: vehicle's networking and astuteness. Moreover, it centers around the incorporation of objects such as man, motor vehicles, things, networks and atmosphere to devise a smart network grounded on computing and communication intelligence that reinforce amenities (like management service based on pollution levels, road conditions, congestion traffic level, or vehicular safety assistance) for substantial urban communities or even an entire nation. IoV is ubiquitous network of wireless access technology recognized vehicles comprising internet and other diverse networks. The heterogeneous network design of IoV comprises of 5 types of vehicular communication and these are: Vehicle-to-Vehicle (V2V), Vehicle-to-Roadside unit (V2R), Vehicle-to-Infrastructure (V2I) of mobile networks, Vehicle-to-Personal devices (V2P) and Vehicle-to-Sensors (V2S).

One of the types i.e. V2R is being modelled in this section for proper communication at high speed and far distance. This paper seeks to discern how design optimization parameters i.e. speed, propagation environment and RSU-OBU distance greatly influences the performance of the IoV (sensor based) environment. This paper discusses general framework to address effect on parameters in high speed IoT environment leading to Internet of Vehicle (IoV) framework which is a typical scenario where Road Side Unit (RSU) and Onboard Unit (OBU) is allowed to communicate under different propagation environment. IoV prototype is designed on NETSIM Simulator to analyze the effect of speed of OBU in terms of throughput and energy consumption during communication. A different pitfall of the RPL protocol and path loss models is also investigated. Simulation results manifests that design optimization parameters i.e. speed, propagation environment and RSU-OBU distance greatly influences the performance of the IoV (sensor based) environment. The simulation result shows that there is an 11.1 % increase in total

energy consumption when speed increases from 1m/s to 20 m/s. Further the performance degrades by 3.26% for COST 231 HATA model, when RSU-OBU distance is switched from 5m to 10 m. The propound model will be augmented for successful communication with hyper-velocity (100 - 300 m/s) devices.

Effect of mobility on Energy consumption and throughput of a V2I prototype for Green Internet of Vehicle under Hostility

Divya Punia[1], Rajender Kumar[2]

***Abstract*—Internet of Things (IoT) is a prevailing innovative technology edifice on the ubiquitous connectivity of things and people. It renders unification of various sensors and objects that can disseminate directly with one another without human intervention. This paper discusses general framework to address effect on parameters in high speed IoT environment leading to Internet of Vehicle (IoV) framework which is a typical scenario where Road Side Unit (RSU) and Onboard Unit (OBU) is allowed to communicate under different propagation environment. IoV prototype is designed on NETSIM Simulator to analyze the effect of speed of OBU in terms of throughput and energy consumption during communication. A different pitfall of the RPL protocol and path loss models is also investigated. Simulation results manifests that design optimization parameters i.e. speed, propagation environment and RSU-OBU distance greatly influences the performance of the IoV (sensor based) environment. The simulation result shows that there is an 11.1 % increase in total energy consumption when speed increases from 1m/s to 20 m/s. Further the performance degrades by 3.26% for COST 231 HATA model, when RSU-OBU distance is switched from 5m to 10 m. The propound model will be augmented for successful communication with hyper-velocity (100 - 300 m/s) devices.**

Keywords— IoV, IoT, mobility, RSU

I. INTRODUCTION

Internet of Things (IoT) is a paradigm that has acquired more popularity in neoteric years. The expansion of scaling down and astuteness as well as unification of communication capabilities into an extraordinary plethora of devices have been the essential leverage of the new and innovative popular paradigm referred to as internet of things [2]. In IoT, gadgets that surround us in our day by day existence are adhering to a network. It is reckoned as free access of ubiquitous internet. The "things" in IoT comprise physical devices like sensor nodes that monitor and congregate all type of data on machines and human social life [20]. For flawless transfer of data among devices, an appropriate layered architecture of IoT is required. Epitome architecture of IoT ecosystem is not available. For reference purpose a layered architecture is depicted in this paper.

[1]Divya Punia is with Department of Electronics and Communication Engineering, National Institute of Technology, Kurukshetra, India
[2]Rajender Kumaris with Department of Electronics and Communication Engineering, National Institute of Technology, Kurukshetra, India.
(e-mail: dpunia92@gmail.com, rkumar.kkr@gmail.com)

The idea of IoT is to affix all devices to internet. It has permitted communication with and among smart items, thus leading to the foresight of ''anytime, anywhere, any media, anything" communications and has aggrandize the experience of connectivity in the form of vehicular communication [1], sensor networking, smart metering [12]. One of the revolutions mobilized by IoT is Internet of Vehicle (IoV). IoV is unfolded from Vehicular Ad hoc Networks (VANETs) to achieve the vision of `from smart phone to smart car' [21]. Safety, pollution and casualties are prime issues related to on-road traffic. These are the main factors for design and advancement in IoV. Another key driver for the expansion of IoV is the current advancements and higher market penetration rate of IoT.

IoV is ubiquitous network of wireless access technology accredited vehicles comprising internet and other heterogeneous networks. The heterogeneous network architecture of IoV comprise of five types of vehicular communications and these are: Vehicle-to-Vehicle (V2V), Vehicle-to-Roadside unit (V2R), Vehicle-to-Infrastructure (V2I) of mobile networks, Vehicle-to-Personal devices (V2P) and Vehicle-to-Sensors (V2S) as shown in Fig. 1.

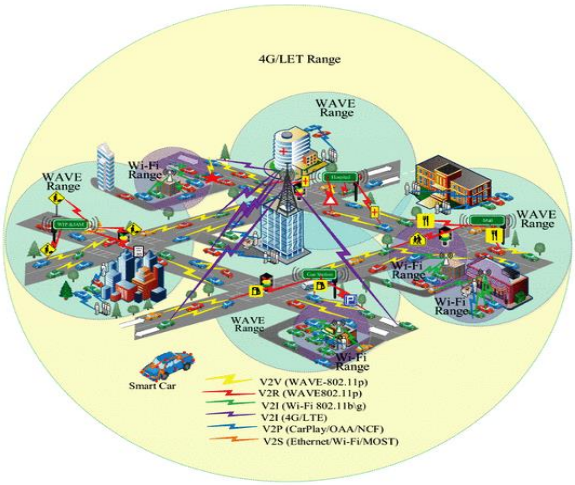

Fig. 1. IoV intelligence in heterogeneous vehicular network.

In this paper, one of the types i.e. V2R is being modelled for proper communication at high speed and far distance. The breakdown of paper is as follows: Section 2 depicts the critique of IoT perception and the research related to RPL protocol and IoV. Section 3 provides proposed reckoned model for IoV ecosystem and describes effect of sensor mobility and bit error rate

on IoV environment. Subsequently, in Section 4 the primary results of performance investigation based on sensor mobility in IoV framework is provided. Lastly, Section 5 manifests the performance of RPL routing protocol with path loss model in terms of throughput, bit error rate and total energy consumed.

II. LITERATURE SURVEY

The term IoT was coined by Kevin Ashton in 1999 [11]. Internet of things has been discerned as one of the emanate technologies in IT as illustrated in Gartner's IT Hype Cycle. A Hype Cycle [8] is an approach to delineate the emergence, adoption, maturity, and impact on applications of specific technologies. For market acquisition by IoT, it has been predicted that IoT will take 5–10 years.

The proliferation of internet has drawn consciousness towards IoT [11]. IoT is a domain where physical things are reliably integrated to compose an information network with the concrete end goal of giving advanced and perspicacious accommodations to users [5]. With the intensity and size of IoT components, the IoT applications have been enhanced utilizing diverse strategies, systems, and models inferred from gadget driven-installed structures [17]. Ubiquitously, there is no assent on anatomy of IoT. Various taxonomy of IoT has been proposed by different researchers. One of them is three and five layer [10-11] architectures. Three layered architecture came into neoteric research in this era. This architecture comprise of 3 layers. But this architecture was not sufficient for research purpose because it only gives conceptualization about IoT. Thus there are more taxonomy as proposed in literature. One of them is five layer architecture, [12] which additionally comprise of business and processing layer as shown in Fig. 2. In this paper, we deal with network layer and try to establish scenario enabling RPL protocol.

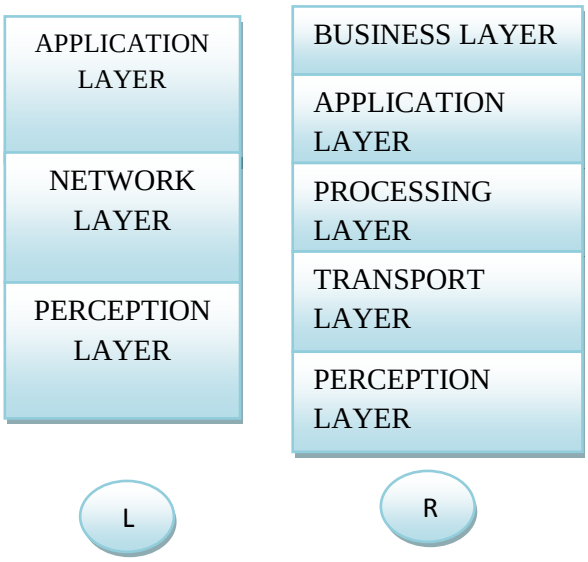

Fig. 2. Taxonomy of IoT L: Three layer, R: Five layer.

IoT caters connectivity of objects from anytime, anywhere to anything. It is ubiquitous and provides platform for every device to communicate with each other via internet as shown in Fig. 3.

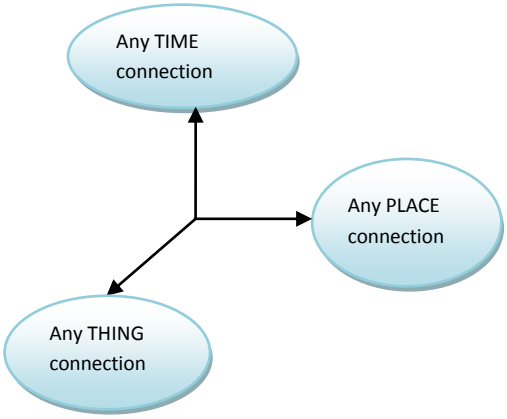

Fig. 3. A neoteric dimension.

RPL is a customary routing [1] scaffold for low-power and lossy networks (LLNs). It is a distance-vector and a source routing etiquette which is intended to maneuver on top of several link layer mechanisms together with IEEE 802.15.4 PHY and MAC layerS [7]. RPL primarily target collection-based networks, where nodes sporadically sense and give data to a collection spot. Many design fundamentals of internet of vehicle environment are flexible with RPL as we will confer in detail. This doesn't mean that one can apply RPL precisely to a vehicular environment. The main idea of this paper is to present a simulation analysis of RPL and RPL tweaking for vehicle hopping to infrastructure under various routing metrics. The commuting dynamics of the network in real time must be attune by proficient routing protocol. Discrete features of RPL complements it's wield for such kind of applications. The contemporary [6] advancement of the internet is 'Internet of Vehicles', which usually comprise of objects having sensors and networking intelligence in order to accumulate, delineate records and acknowledge control instructions via internet [18-19]. IoV wield mobility facet and fundamentals of conventional social networks, in order to build neoteric approach of message swap via recognition of dynamic social anatomy[19]. For ``smart transport," Internet of Vehicles (IoV) is developing as a new theme of research and development from vehicular ad hoc networks (VANETs). Researchers have anticipated a novel design on social network service termed as Drive and Share which provides intelligence to vehicles wielding anticipated design [9]. VSNs are termed as decentralized opportunistic dissemination networks created amongst vehicles [20]. The idea of mobility of networks was being anticipated on the basis of conventional networks to swap messages with social networks. Design of virtual marketplace is also estimated on the basis of VSNs [18]. Analyzing real-time data and handling imperfect information represent the main challenges of smart cities [4]. In our research, we sited mobile node in IoT environment and allocate essential facts to ascertain effect of mobile sensor node and pathloss model on throughput and delay parameters. This paper seeks to discern how design

optimization parameters i.e. speed, propagation environment and RSU-OBU distance greatly influences the performance of the IoV (sensor based) environment.

III. PROPOSED IOV PROTOTYPE

Proactive routing protocols preserve paths like subsequent forward hopping in the environment despite of the communication requests. Control packets are persistently transmitted and flooded amongst motes to maintain the routes and the link states connecting any pair of nodes even if few paths are never utilized. Unlike nodes in other proactive routing protocols, RPL is reactive protocol in which nodes only require the rank and ETX (expected transmission count) intelligence to build downward paths. Reactive routing protocols construct routes upon request. RPL preserves the route in the environment at minimum overhead. In our construction, there is road-side static sensor node and one OBU node acting as vehicle, which will try to connect to a route using RPL protocol.

In order to interpret the effect of sensor node mobility w.r.t static node in IoV environment, a basic prototype is designed as shown in Fig. 4. The propound IoV model comprehends two nodes, one is static i.e. sensor B and other is moving sensor A. Mobile node effect is analyzed at different speeds at a distance of 20m and 40m from static node. Two sensor nodes are linked to Low PAN gateway, which auxiliary connects the nodes to wired link E via router D. The terrain condition is 1000 m × 1000 m flat area. All the nodes communicate via RPL routing protocol. Two application layer connections are constructed subsequently between node 1 to node 2 and node 2 to node 5. Wired link connections are between gateway and router and wired node and gateway. Mobile node A moves at 1-20m/s speed w.r.t node B.

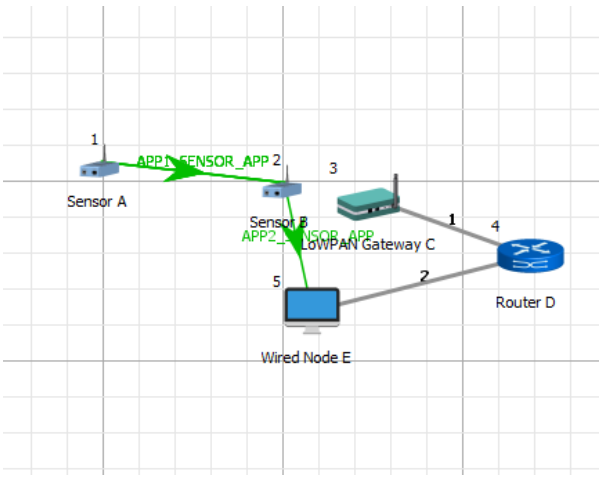

Fig. 4. Scenario A in NETSIM Simulator.

Pathloss is the diminution in power density of an electromagnetic wave as it propagates through space [14]. The general formula [14] wielded for pathloss calculation is given equation 1, where overall gain is function of transmitter and receiver antenna gain. Pathloss calculation formula is as follows:

$$RX_{Power} = TX_{Power} + Gain_{TX} + Gain_{RX} - PL_{1Meter} - 10Log\ D^{n} \quad (1)$$

where:

n = pathloss exponent, it's value is 2

D = distance between transmitter and receiver (metre)

PL_{1Meter} = path loss at reference distance (1m)

Analysis is made on the basis of 2 types of pathloss models namely, friss free space model and COST-231 HATA Urban model. Path loss is extremely ineludible in analyzing networks performance and capacity as regards proficient and reliable coverage regions in the intensification of communication. Friss free space is wielded to model LOS path loss incurred in the channel. It follows the inverse square law of distance which tells that the received power decays by a factor of square of the distance from the transmitter. The pathloss exponent taken for this model is 2. Then HATA model is radio propagation model which speculate the path loss of cellular dissemination in exterior environments, applicable for frequencies from 150 to 1500 MHz, while COST-231 HATA extends the urban Hata model to traverse 1500 to 2000 MHz range of frequencies. A comparative evaluation of three different pathloss models is done at different speeds of sensor node A. Also, bit error rate is formalized in environment. General framework characteristics of the network are shown in Table I as follows:

TABLE I. GENERAL SCENARIO PROPERTIES

Scenario Properties	**Specification**
Number of Nodes	2
Terrain size	1000m*1000m
Path loss Model	Friis free path loss model, COST-231 HATA Urban model
Routing Protocol	RPL
Gateway	LowPAN
Power transmitted by Sensor A and B	1dBm
Simulation Time	100 sec
Mobility of Node A	1m/s, 5m/s, 10m/s, 15m/s, 20m/s
BIT Error Rate	10^-5
Simulator	NETSIM version 10.2

IV. PERFORMANCE PERUSAL AND RESULTS

Effect of mobility of sensor node and path loss models in IoV network is scrutinized in this section. The execution of anticipated model is accomplished wielding NETSIM simulator standard version 10.2 on 64 bit build simulation scale. In our edifice, there is a road-side static sensor node and one On-Board unit node acting as vehicle, which will try to connect to a route using RPL routing protocol.

Two scenarios are reinforced in NETSIM. In the first scenario, distance between mobile node A and sensor node B is 5m as shown in Fig. 4 and node A (X,Y) coordinates at starting point is (100, 495) while static node B coordinates are set to (200,500) throughout the simulation. Performance of network is evaluated on varying speeds of 1 to 20m/s. Moreover, in second scenario the gap between node A and B is 10m and node A (X,Y) coordinates at beginning point is (100, 490) while static node B coordinates are set to (200,500) throughout the simulation. Also, bit error rate for both the environment is set to 0.00001. The bit error rate (BER) is defined as the number of error bits divided by the total number of transferred bits during a time interval. Impact of mobility of sensor node 1 is estimated on different metrics of anticipated simulation model.

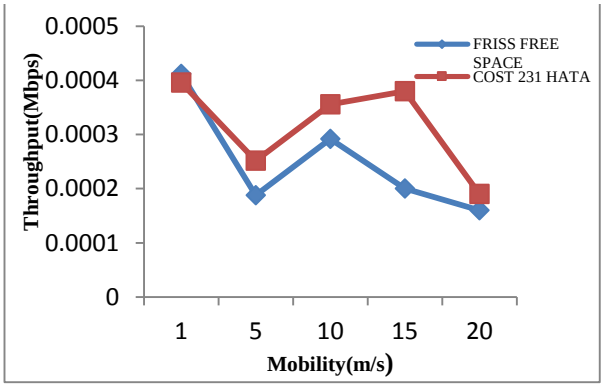

Fig. 5. Variation of mobility and throughput at 5m distance between nodes.

In scenario A, transmitter power is set to 1dBm, and static node is at 5m distance from mobile node and the effect of friss free space path loss model and COST-231 HATA model, mentioned in section 3, is evaluated via simulations. Time for simulation is kept 100 second. It is observed that, throughput decreases with the mobility of node and throughput (Mbps) is evaluated [14] as: total bytes transmitted in the link * 8 divided by simulation time (Micro sec), as shown in Fig. 5 and effect of decreasing bit error rate leads to lower throughput value.

When node A moves from 1m/s to 20m/s at a distance of 5m from node B, then throughput is decreased by 61.16% in friss free space path loss model while it decreases by 52.02% in COST 231 HATA model, overall decrease in throughput is obtained for both the models, but for COST 231 HATA model better throughput is maintained which is 9.14% more than that of friss free space model. At 1m/s speed, maximum throughput value is obtained. Corollary to increase in mobility, total energy consumption (mJ) also increases for high speed node as shown in Fig. 6, excessive energy is consumed in COST 231 HATA model than friss free space path loss model.

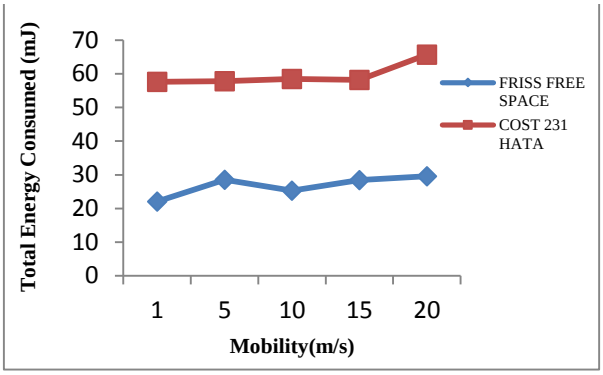

Fig. 6. Energy consumption (mJ) variation with mobility (m/s) at 5m.

For scenario B, static node is placed at distance of 10m from mobile node and the consequence of friss free space path loss model and COST-231 HATA model, mentioned in section 3, is evaluated. It is analyzed from outcome that throughput is decreased by 64.64% in friss free space path loss model while it decreases by 58.76% in COST 231 HATA model, overall decrease in throughput is obtained for both the models, but COST231 HATA model outperforms friss free space model, as throughput values obtained were 5.88% better at high speed.

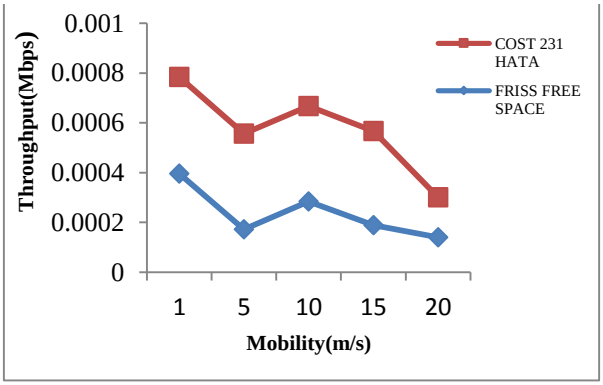

Fig. 7. Variation of mobility and throughput at 10m distance between nodes.

Total energy consumption (mJ) for scenario B is depicted in Fig. 8, which illustrates that as speed of mobile node increases, energy consumed also increases, which must be lower for higher speed value, which is there in friss free space pathloss model. Highest value of energy consumption is 64.21mJ for COST 231 model while for friss free model value is 39.876mJ, which is nearly half of the value of COST 231 model. Finally, we analyzed that as diatance and speed of the node increases, energy consumption also increases. There is nearly 11.1% increase in total energy consumption in both the models.

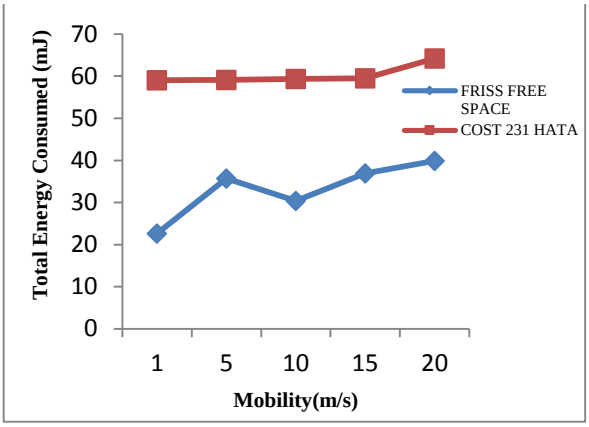

Fig. 8. Energy consumption (mJ) variation with mobility (m/s) at 10m.

V. CONCLUSION

In Green technology regime, the energy consumption model plays a vital role. Therefore, the performance analysis for proposed framework is done in terms of total energy consumption and throughput. The paper suggests that there is a need to carefully explore various mobility models under hostile propagation environment in order to optimize the performance of IoV topologies in terms of throughput and energy consumption (conflicting scenarios). When RSU is at 5m distance from OBU and the speed of OBU is increased from 1m/s to 20 m/s then this scenario results in 9.14% less decrease in throughput in COST 231 HATA model w.r.t friss free space model, subsequently at 10m distance, COST231 HATA model outperforms friss free space model, as throughput values obtained were 5.88% more than friss free value. Further the distance between RSU-OBU (5m/ 10m) is the third objective to jointly optimize the overall performance. There is an 11.1% increase in total energy consumption in both the models, but COST 231 HATA model consumes more amount of energy. Thus, increase in throughput is there in COST 231 HATA model while total energy consumption is less in friss free space path loss model. The performance degrades by 3.26% for COST231 HATA model, when RSU-OBU distance is switched from 5m to 10 m. Investigation concludes that sub-optimal solutions can be obtained for high velocity environment (10-40 m/s) provided that scenario is addressed through Joint Optimization Problem.

FUTURE SCOPE OF THE WORK

The framework may be extended to hypervelocity environment (>> 50 m/s) for avionics and defense applications. A joint analytical model may be designed to obtain a Joint optimized solution. The results also suggest retrospection of routing protocols, mobility and various propagation models to foster green technology.

REFERENCES

[1] A.G. Gawande, A.B. Ahmad Shaheen, " Comparison and analysis study between AODV and DSR routing protocols in VANET with IEEE 802.11b," J. Ubiquitous Syst. Pervasive Network, pp. 7-12, 2016.

[2] A.J.Jara, S.Varakliotis, A.F.Gmez, P.T.Kirstein, " Extending the Internet of Things to the future internet through IPv6 support," J. Mob. Inf. Syst., vol. 10, pp. 3-17, 2014.

[3] A.J.Jara, L.Ladid, A. Skarmeta, "The internet of everything through IPv6: An analysis of challenges, solutions and opportunities," J.Wireless Mobile Networks, vol. 4, pp. 97-118, 2013.

[4] B. Hatem, "Quality and the efficiency of data in Smart-Cities," Future Gener. Comput. Syst., pp. 409–416, 2017.

[5] Botta, De Donato, W. Persico, V.Pescape, "Integration of cloud computing and internet og thimgs: a survey," Future Generation Comput. Syst., pp. 684-700, 2016.

[6] C.-M. Huang, M.-S. Chiang, D.-T. Dao, H.-M. Pai, S. Xu, H. Zhou, "Vehicle-to-infrastructure (V2I) offloading from cellular network to 802.11p Wi-Fi network based on the software-defined network (SDN) architecture," Veh. Commun., pp. 288–300, 2017.

[7] Ed Winter et al.., "RPL:IPv6 Routing Protocol for Low-Power and Lossy Networks," Internet Engineering Task Force (IETF), 2012.

[8] Gartner , "Gartner's hype cycle report 2011," U.S.A, 2012.

[9] I. Lequerica, M.G. Longaron, P.M. Ruiz, "Drive and share: Efficient provisioning of social networks in vehicular scenarios, "IEEE Commun. Magazine, vol. 48, pp. 90–97,2010.

[10] A. McEwen, H. Cassimally, Designing the Internet of Things, Wiley, pp. 336, 2013.

[11] K. Ashton, That ''Internet of Things'' thing, RFiD Journal, June 2009.

[12] L. Atzori, A. Iera, G. Morabito, ''The internet of things: a survey," Computer Networks, vol. 54, pp. 2787–2805, June 2010.

[13] M. Wu, T.-J. Lu, F.-Y. Ling, J. Sun, and H.-Y. Du, "Research on the architecture of internet of things," in Proceedings of the 3rd International Conference on Advanced Computer Theory and Engineering, Chengdu, China, August 2010.

[14] NETSIM User Manual, Tetcos, Bangalore, IN, 2015.

[15] O.Saidand M. Masud, "Towards internet of things: survey and future vision," International Journal of Computer Networks, vol. 5, pp. 1–17, 2013.

[16] Pethuru Raj, Anupama C. Raman, The Internet of Things Enabling Technologies, Platforms, and Use Cases, Taylor & Francis, 2017.

[17] R.Khan, S. U. Khan, R. Zaheer, and S. Khan, "Future internet: the internet of things architecture, possible applications and key challenges," in Proceedings of the 10th International Conference on Frontiers of Information Technology (FIT '12), December2012, pp. 257–260.

[18] U. Lee, M. Lee, J.S. Park, M. Gerla, FleaNet, "A virtual market place on vehicular networks," IEEE Trans. Veh. Technol., vol. 59, pp. 344–355, 2010.

[19] V. Vegni, M. Loscri, "A survey on vehicular Social networks," IEEE Commun. Surv. Tutor., pp. 2397–2419, 2015.

[20] Yan et al., "A survey on trust management for Internet of Things," J. Netw. Comput. Appl. vol. 42, pp. 120–134, 2014.

[21] Y. Fangchun, W. Shangguang, L. Jinglin, L. Zhihan and S. Qibo, "Am overview of Internet of Vehicles," China Communication, vol. 11, pp. 1-15, 2014.

[22] W. Fawaz, R. Atallah, C. Assi, M. Khabbaz, " Unmanned aerial vehicles as store-carry-forward nodes for vehicular networks," IEEE Access, pp. 23710–23718, 2017.

Evolution of Fog Computing from IoT

Internet of Things (IoT) is a prevailing innovative technology that edifice on the ubiquitous connectivity of things and people. Serious endeavor is being put by artificers to provide solutions enabling wide IoT employment. Therefore, enormous amount of information generated, huge network, surveillance and privacy issues, QoS parameters requirement and heterogeneity in universal network, makes its execution an exigent task. The IoT opens new doors for real-time, latency-sensitive applications like battlefield surveillance, e-healthcare etc. These applications demand huge storage space and fast processing capability. Cloud Computing came into the picture to handle these demands but because of it being remotely located, it adds latency to the services. So, the need was to bring these services from cloud that is located far –away from users to near-by location, in the proximity of users. This led to the development of Fog Computing, and the term Fog was first coined by Cisco.

Fog Computing is an IT paradigm which brings the cloud services from far away regions i.e., core towards the users i.e., edges. It can be defined as the extension of the cloud computing for the real-time, latency-sensitive applications which consists of a combination of heterogeneous, decentralized devices communicating and cooperating among them to perform data storage and various data computation tasks. Fog Computing has a variety of applications not only in real-time services but in storage, computation and routing also. The requirement is to make these applications more secured so that the users can enjoy the services without any hesitation. It consists of various security and Privacy threats which need to be handled for the success of Fog Computing.

Fog computing, a new networking paradigm, has decreased management intricacy in present day scenario. Moreover, Fog computing, a ubiquitous network has provided efficient solution to security issues. Moreover it reduces the expenditure (i.e. high delay and bandwidth requirement) of big data analytics transportation from the network edge to the core network. Characteristic features of Fog Computing are described below:

- **Location Awareness**: The location of the Fog nodes can be tracked easily to provide real-time services to the user devices. Based on the knowledge of location of Fog nodes, devices region can also be identified easily.

- **Geographic Distribution**: The Fog nodes are geographically distributed may be on the roof of the building, on smart phones, on top of the vehicle and at the point of interest so

that it is able to provide services to IoT devices i.e., collect high data stream from IoT devices for processing.

- **Low Latency**: Fog nodes being deployed nearer to the user devices and possessing the necessary capability of storing and computing data are able to provide services with much less delay as compared to that made by the Cloud.

- **Large Scale IoT Application support**: Large scale IoT application including large number of sensors, thus a large number of data for computation and processing to be handled in real-time, which is a cumbersome task for cloud computing but can be easily handled by Fog nodes which are ubiquitous and has the expertise to manage huge number of IoT Devices.

- **Decentralization**: Fog Computing is a decentralized network. No central server is present to provide services and resources. Fog nodes arrange it automatically to provide real-time services to the IoT devices.

One such paper, critically reviewing the fog computing-based solutions to conquer the security issues is highlighted in the following section. Fog computing provides various Fog assisted IoT real-time applications, which due to security and privacy threats has not been utilized fully. Some security solutions about Fog computing is provided in the paper provided in this section. Fog Computing is not a replacement of Cloud Computing, but it complements it. Both the technology when used together forms a new breed of technology, that serves various IoT devices applications which may deal with computing, or storing temporary data, or acting as an interface between two layers, or serving real-time applications. This new technology in spite of making our life autonomous is surrounded by some security and privacy threats which need to be resolved to enjoy Fog Computing. Some of the techniques to resolve the challenges have been discussed but this is an open research issue and needs more inputs.

Fog Computing Security: A Major Issue

Charul Thareja[1], Niraj Pratap Singh[2]

Abstract **—Internet of Things as the name suggests is an interconnection of daily usage things. With the inception of IoT, each and every item in this world would have an IP address. It would transform our way of interaction, making our life more autonomous. The essential requirement for the upcoming of this technology includes real-time response, low latency, fast processing and computation capabilities. These features being difficult to be handled by Cloud Data Centers, mainly because they are remotely located, away from users leading to poor QoS. It leads to development of a new technology called Fog Computing, which is an extension of Cloud Computing, extending the services provided by the cloud towards the edge users. This technology comes with some security and privacy threats discussed in this paper which need to be resolved so that people use Fog-based IoT applications without any hesitation. The different solutions proposed for various challenges faced by fog nodes are also discussed in this paper.**

Keywords—IoT; Fog Computing; Security; applications; challenges

I. INTRODUCTION

With the upcoming of 5G, there comes in era of Internet of Things (IoT), which is the interconnection of billions of devices that can interact and share resources with the help of embedded software, sensors and other electronic equipment[1]. The IoT opens new doors for real-time, latency-sensitive applications like battlefield surveillance, e-healthcare etc. These applications demand huge storage space and fast processing capability. Cloud Computing came into the picture to handle these demands but because of it being remotely located, it adds latency to the services. So, the need was to bring these services from cloud that are located far – away from users to near-by location, in the proximity of users. This led to the development of Fog Computing, and the term Fog was first coined by Cisco.

Fog Computing has a variety of applications not only in real-time services but in storage, computation and routing also. The requirement is to make these applications more secured so that the users can enjoy the services without any hesitation. It consists of various security and Privacy threats which needs to be handled for the success of Fog Computing.

The promising techniques to resolve the security issues have been discussed in section VI.

[1]Charul Thareja is with Department of Electronics and Communication Engineering, National Institute of Technology, Kurukshetra, India
[2]Niraj Pratap Singh with Department of Electronics and Communication Engineering, National Institute of Technology, Kurukshetra, India.
(e-mail: tharejacharul19@gmail.com, npsingh@nitkkr.ac.in)

Section II shows the contribution of various researchers in securing Fog Computing. The brief overview of Fog Computing along with its features and architecture are discussed in section III. Various IoT applications have been discussed in section IV and its threats are discussed in section V.

II. RELATED WORKS

A brief overview of fog security and privacy issues is discussed in [2] and [3]. However, this survey has not covered the research challenges in security and privacy issues for fog computing. Stojmenovic et al. [4], [5], also discussed the security and privacy issues. Security and privacy preservation are discussed in fog-based vehicularnetworks by J.Ni et al. [6]. In[7], Alrawais A. et al. discussed various security and privacy issues and proposed a certificate revocation scheme for authentication. While the aforementioned contributions [2], [3], [7] have laid a solid foundation for the understanding of security and privacy issues in fog computing, this article differs from previous surveys in many aspects. For example, the work in [6] considers only vehicular based crowd sensing,[2] discussed a brief overview of privacy and security. The above-mentioned study partially considered the security and privacy issues. An up-to-date summarization in these privacy and security aspects in fog computing is missing. The following summarizes our key contributions.

1) The security and privacy challenges of fog computing and their existing solutions and mechanisms.

2) The overall insights on the security and privacy issues that the state-of-the-art solutions cannot address due to its unique features.

III. BRIEF OVERVIEW

This section consists of the definition of Fog computing, its features along with its architecture.

Definition of Fog Computing

Fog Computing is an IT paradigm which bring the cloud services from far away regions i.e., core towards the users i.e., edges. It can be defined as the extension of the cloud computing for the real-time, latency-sensitive applications which consists of a combination of heterogeneous, decentralized devices communicating and cooperating among them to perform data storage and various data computation tasks[8].

Features of Fog Computing

Many of the features of fog computing are similar to that of the cloud computing but some are different. Both have been described briefly. The similar feature include:

- **Mobility Support**[9]: Mobility is the ability to move. Through Fog Computing, IoT devices acquire

this ability without being disconnected from the Fog nodes. Fog Services are ubiquitous in nature. Hence, Mobility support offered by Cloud Data Centers is limited as compared to the support provided by Fog Nodes.

- **Heterogeneity**[10]: The data is collected from internet-connected devices, that can be either mobile IoT devices including wearable devices (fitness tracker, smart cameras, etc.) and mobile smart devices (vehicles, smart watches, etc.) or fixed IoT devices including sensors and RFID tags deployed on specific areas of product. Collected data is then transferred to the fog nodes (basically routers, gateways, and switches) which are deployed in diverse environment like on the roof of buildings, in smart phones, in traffic lights and so on, making the whole architecture heterogeneous. Same heterogeneity is seen in Cloud Computing but with the difference that data instead of being collected by Fog nodes is collected by Cloud Data Centers which are remotely located.
- **Online analytics and Interplay with Cloud**[11]: Fog nodes acts as an intermediate between the IoT devices from which the data is being collected and the Clouds where the data is to be sent for storage. This feature of fog computing can be explained with the help of an example of smart e-healthcare center. The data from the sensors deployed on the patient's body is being collected continuously by Fog nodes, which is being analyzed in real-time to detect emergent event. If everything seems to be normal then the data is sent to the Cloud for storage. Otherwise some necessary steps are taken to help patient like ringing alarms and sending alertmessages to the doctor. Until the doctor arrives, sensors on the patient's body take active actions to give them intensive care. It can be said Fog layer is an interface between the device layer and the Cloud layer. Similar analysis is performed by the Cloud Data Centers but with some delay and with only two layers (Device Layer and Cloud Layer).

Some of the distinguishing features from the cloud computing are enlisted below:

- **Location Awareness**[12]: The location of the Fog nodes can be tracked easily to provide real-time services to the user devices. Based on the knowledge of location of Fog nodes, devices region can also be identified easily.
- **Geographic Distribution**[12]: The Fog nodes are geographically distributed may be on the roof of the building, on smart phones, on top of the vehicle and at the point of interest so that it is able to provide services to IoT devices i.e., collect high data stream from IoT devices for processing.
- **Low Latency**[11]: Fog nodes being deployed nearer to the user devices and possessing the necessary capability of storing and computing data are able to provide services with much less delay as compared to that made by the Cloud.
- **Large Scale IoT Application support**[10]: Large scale IoT application including large number of sensors, thus a large number of data for computation and processing to be handled in real-time, which is a cumbersome task for cloud computing but can be easily handled by Fog nodes which are ubiquitous and has the expertise to manage huge number of IoT Devices.
- **Decentralization**[10]: Fog Computing is a decentralized network. No central server is present to provide services and resources. Fog nodes arrange itself automatically to provide real-time services to the IoT devices.

- *Architecture*

The Fog Computing architecture is illustrated in Figure 1. It is a three tier architecture.

Tier 1:- The bottom tier known as the device layer consists of the different smart devices including mobile IoT devices i.e., the devices carried by their users like fitness trackers, bracelets and smart devices like smart phones, vehicles, smart watches, etc. and the fixed IoT devices including RFID and sensor nodes which are attached on the items to perform some specified task. These heterogeneous devices transmits data to the upper tier.

Tier 2:- The second tier known as the fog computing layer consists of intelligent devices like routers, gateways, etc. that possess the ability of data storage, computation, routing and packet forwarding.

Tier 3:- The uppermost layer is known as the cloud computing layer, which consists of data centers and big servers. The data which requires large historical data for processing are sent to the Cloud layer.

Different smart devices also known as the terminal nodes, join together to form Virtual Clusters (VCs). Different VCs together form an EVPN (Edge Virtual Private Network). The data from the VCs is sent to the Fog Instances (FIs) via edge gateways for computing, storage, etc. The Fog layer is divided into two parts, one is Fog abstraction layer, which manages the fog resources, enables virtualization and provides user's privacy. Another part is Fog orchestration layer, consisting of a software agent called Foglet, which checks the state of the device. Within the fog instances, data is processed and analyzed, whether it requires real-time service, temporary storage or permanent storage. For permanent storage or long-term storage, data is sent to the data center's or cloud layer but for short-term evaluation, data is processed in fog layer only. Thus, the fog computing architecture allows the efficient utilization of Cloud Layer[13].

IV. APPLICATIONS

Fog nodes plays four important roles namely Real time service for Fog, Transient Storage for Fog, Data disseminationfor Fog and Decentralized computation for Fog. Based on these roles, some of the important applications have been discussed below.

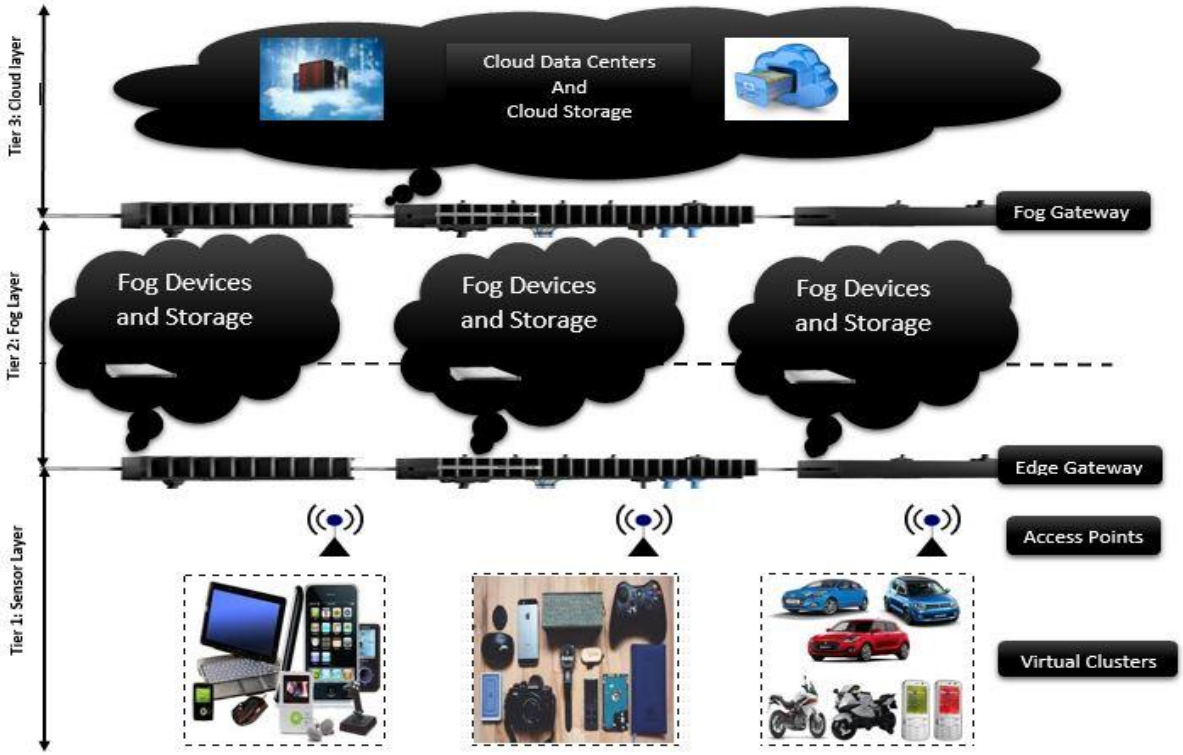

Fig 1: Fog Computing Architecture

- *Real-Time Services for Fog*

Cloud data centers are far away from the user devices and hence are not able to provide real time services. For fast computation and analysis results, Fog nodes play an important role being closer to user devices. These Fog nodes acts like a private cloud for the IoT Devices.

Some applications of fog nodes which offer real-time control and fast decision making capability are Smart Traffic Light, decentralized vehicular navigation, home energy management, e-healthcare services, etc.

*1) Smart Traffic Light:*At the Carrefour, the flashy lights of the ambulance and the police cars are detected by the traffic light sensors which then takes necessary steps to let these emergency vehicles go first. These fog nodes on traffic light can also sense the pedestrians and bicycles and provide them time accordingly to cross roads. Not only this but it can detect the vehicles speed that is approaching towards them and send them warning messages to avoid collisions. Thus, reducing the number of accidents.

2) Healthcare and Activity Tracking: The scenario can be understood in three layers: in first layer, all the sensors are included which are deployed on the body of the patient for collecting data from each of the room. In second layer, Fog node i.e., Private cloud of hospital is present to deliver fast responses after analyzing the data provided by sensors like sending messages to doctor or starting alarms during emergency situation and giving necessary instructions to the sensors to take preventive actions until the doctor arrives. Third layer consists of a cloud, which is just for storing all the details of the patient. If there is a need to check history of patients or if some necessary details about patient has to be stored which can be referred in future, then this layer comes in use.

- *Transient Storage for Fog*

When the data is to be stored temporarily i.e., for about 1-2 hours, or if the data is to be accessed frequently then instead of storing it in Clouds (because storage space and bandwidth would be wasted) it can be stored in Fog nodes and when the necessary updates has been done on the data then it can be either discarded or sent to the Clouds for permanent storage. When some files which need to be accessed continuously for real-time application are stored in cloud, then delay is added to the response.

This role of fog node is useful in various applications including content caching, shopping cart management, software and credential updating, etc. Some of them are discussed below.

3) Content Caching[10]*:* The data which is accessed by the user for the first time comes from the Cloud and gets stored into the Fog node. Second time when some other user wants to use the same information then there is no need to go to the Tier 3 again as the data has already been cached from Cloud to the Fog node. Hence, second user gets faster response as compared to the first one. Its working is same as that of the cache memory in computers. This application can be used in

interstate buses by employing a fog node on the top of the bus providing free Wi-Fi as a social service and then all the passengers can access the data using that fog node and may be most of the passengers wants to use the same websites then the delay in accessing them gets reduced.

4) Shopping Cart Management[10]*:*Traditionally while e-shopping, the data of e-cart needs to get updated in the Cloud, which used to add delay to the services of the customer. But with the advent of Fog Computing, the cart information gets cached into the fog nodes and after the necessary updates has been done by the customer and when the customer logs out his/ her account, then the data is sent back to the cloud for storage. This procedure reduces the amount of delay in services and even increases customer's satisfaction.

- *Data Dissemination for Fog*

Being the middle tier in the fog computing architecture, fog nodes acts like an interface between the IoT devices and the cloud data centers. The fog nodes either collects data from IoT devices and send it to Cloud or collect data from Cloud data centers and send it to IoT devices. Fog nodes acts as a router, helps in packet forwarding , can work as a data aggregator, and can also perform simple processing, so that the proper audiences can be selected to whom the information is need to be sent.

The applications including Data Dissemination for Fog includes energy consumption collection, local content distribution and fog-based malware defense. Some of them are discussed below:

5) Local Content Distribution[10] *:*Local fog nodes provide the useful information to the users passing by e.g. users are given updates about the traffic, hotels, restaurants, gas stations, while they are travelling.

- This application can also be used in parking navigation service[14], by suggesting the drivers the right place to park, with the help of various sensors and cameras being deployed in the parking lot.

6) Fog-based Malware Defense[10]: If malware defense hardware and software are installed in each of the devices, then it would waste a lot of storage space and would require timely processing (more battery backup). So to avoid it, if the malware defense system is installed on the fog nodes, then it would act as shared resource for all the IoT Devices, to detect the infected files on compromised devices, and then clean them.

- *Decentralized Computation for Fog*

Fog nodes provide decentralized computation services, which aids both the ends i.e., user devices and cloud centers from heavy computations.

The applications supporting the above feature are computation offloading, aided computation, big data analytics. Some of them are discussed below.

Computation Offloading[15] *:*Though Clouds possess huge computational capability, but it consumes a lot of energy and adds latency in providing services to the devices. Fog computing brings these computational services towards the user devices. The IoT devices can fully exploit the computing resources of the Fog nodes even for simple processing and it also reduces the computation burden on clouds.

Big Data Analytics[16] : As the number of IoT devices are increasing, the amount of data collected by these devices is also increasing. Performing data analytics of huge data at the cloud is not right method for latency-sensitive applications like finding a killer, it needs the investigation of almost each of the video cameras installed in parks, malls, street lights, etc. When this analytics is performed on the cloud, it would add latency to the process, so for local data analytics, which involves a large amount of data can be performed at the Fog, and then the final result can be updated to the cloud.

V. THREATS OF FOG COMPUTING

The threats which have restricted the growth of Cloud Computing and Fog Computing are Security and Privacy Threat. These are discussed below.

- *Security Threat*

Fog computing is more secured than Cloud Computing because of two main reasons. First is, the data is transferred locally between the data sources and the fog nodes, and the dependency on internet connection is reduced. Since the data is being stored, analyzed and transferred locally, so it becomes difficult for hackers to access user's data. Second is, the information exchange between the cloud and the smart devices does not take place in real-time which does not let the tracker to find critical information of the user.

Fog computing being more secured than cloud computing cannot be said to be fully secured as the users data reaches to the employees employed at Fog nodes, they may misuse their data and this even leads to privacy leakage. Some of the security threats are:

1) *Forgery and Spam:*Some attackers may make their fake profiles and may even add fake information about them on it, to mislead other users. This also causes wastage of storage, bandwidth and energy. Spam refers to the redundant or unwanted information, which unnecessarily, wastes the storage resources.
2) *Tampering:*Some attackers try to interfere with the data sent by the user. They can either alter the data or drop the data, the purpose is that the real data should not reach the destination. Being wireless communication, it becomes difficult to detect whether this drop occurred due to transmission failure or by some intruder.
3) *Jamming:*Some attackers generate a huge amount of redundant or fake messages, so that no other user can utilize the computation and routing services of Fog. The purpose is to jam the communication channels. It can also be said as Denial-of-Service, when some legitimate user is not able to use the services of fog because it is being flooded with

fraudulent data. It is common in fog because of its limited resources.

4) *Eavesdropping:* Some attackers continuously listens the communication channel, to get the important details. This type of attack is common when data encryption techniques are not used.
5) *Collusion:*Two or more parties can combine together to fraud a legal user. The two parties combined can be IoT devices, Fog and IoT device or Cloud and Fog, etc. This is going to double the attack capability.
6) *Man-in-the-Middle*:There may be an attacker sitting in between the two parties, listening to their conversations, who is secretly modifying the data being exchanged between them and the two parties does not even get to know it.
7) *Impersonation:*There can be a situation in which an illegal user can act as a legitimate user to utilize the services provided by the Fog nodes or it may happen a fake Fog is providing services to the legal users and maliciously utilizing the information provided by them.

- *Privacy Threat*

It is also an important issue as the user's data is being processed, shared and collected and no user wants his/ her data to be leaked. There are 4 kinds of privacy threats which includes identity, data, location and usage privacy.

1) Identity Privacy: User's identity includes his/her name, address , Aadhar card number, and some more personal details which are easily disclosed during checking the authenticity of a person while they are availing for the services of the Fog.

*2) Data Privacy:*When users utilize the Fog services, some of the information about user like its occupation, health status, preferences, are exposed to some third party which maintains the user's data at the fog node.

3) Usage Privacy:Usage pattern tells when the users utilize the Fog node services, which gives the information about the living pattern of the user including, when they sleep, when they wake, at what time they go to office and many more details, which are really dangerous if it gets into wrong hands.

*4) Location Privacy:*Location privacy is something which every user has to sacrifice in order to enjoy different online applications. If a user utilizes some fog node services, his/her location can easily be accessed by finding the fog node to which it is connected and an attacker can even detect the trajectory of a user.

VI. FOG SECURITY

The threats mentioned above leads to the unwillingness of users to utilize Fog based IoT applications. So, this generates need to secure Fog Computing. In this section, the security and privacy challenges have been further discussed and the measure which should be taken to avoid these challenges are also discussed. It is divided into four parts similar to the applications studied above.

A. Challenges and Solutions on Real-Time Services

Fog computing provides various Fog assisted IoT real-time applications, which due to security and privacy threats has not been utilized fully. Some of the challenges faced in these applications with the solutions to them are enlisted in the Table II.

TABLE II: SECURITY CHALLENGES AND SOLUTIONS IN REAL-TIME SERVICES APPLICATION OF FOG COMPUTING[10]

Role	**Security Challenges**	**Security Solutions**
Real-time Services	Identity Authentication	Identity Authentication Cooperative Authentication Anonymous Authentication
	Access Control	Role-based Access Control Policy Attribute-based Access Control Policy Device and Key Management
	Light Weight Protocols Design	Light Weight Cryptographic Schemes Light Weight Elliptic Curve Cryptosystem
	Intrusion Detection	Host-based Intrusion Detection System Network-based Intrusion Detection System Distributed Intrusion Detection System
	Resilience to Sybil Attack	Mobile Sybil Defense Cryptography-based Sybil Defense
	Trust Management	Evidence-based Trust Model Reputation Management Monitoring-based Trust Model

B. Challenges And Solutions On Transient Storage

Transient storage capability provided by fog allow users to maintain their data provisionally. The users will be using these services only if they are sure that their data is safe, there would be no privacy leakage. The challenges faced in transient storage and the solutions which can be used to provide security are enlisted in Table III.

		Encryption

TABLE III: SECURITY CHALLENGES AND SOLUTIONS IN TRANSIENT STORAGE ROLE OF FOG COMPUTING[10]

Role	Security Challenges	Security Solutions
Transient Storage	Sensitive Data Identification and Protection	Symmetric Encryption Asymmetric Encryption
	Data Integrity Protection	Provable Data Possession
	Secure Data Sharing	Proxy Re-encryption Attribute-based Encryption Key-Aggregate

C. Challenges And Solutions On Data Dissemination

Fog nodes acts as an intermediate between the IoT devices and the Clouds. So, it requires the information which is being passed between the two ends should be accurate. The challenges which are faced and the measures which can be taken for efficient data transmission are listed in Table IV.

TABLE IV: SECURITY CHALLENGES AND SOLUTIONS IN FOG COMPUTING FOR DATA DISSEMINATION[10]

Role	Security Challenges	Security Solutions
Data Dissemination	Privacy-preserving Data Aggregation	Homomorphic Encryption One-way Trapdoor Permutation Key Distribution and Key Agreement Homomorphic Signature
	Secure Data Search	Symmetric Searchable Encryption Asymmetric Searchable Encryption
	Secure Content Distribution	Secure Service Discovery Broadcast Encryption Key Management Mechanism Anonymous Broadcast Encryption
	Privacy-preserving Packet Forwarding	Privacy-preserving Packet Forwarding

D. Challenges and Solutions on Decentralized Computation

Fog nodes instead of storage capabilities, also possess computational capabilities. These computations can be hacked by an attacker, he/she may be controlling them and misguiding user. Not only this but there are some more problems which can be faced by user and various solutions to resolve these challenges are listed in Table V.

TABLE V: SECURITY CHALLENGES AND SOLUTIONS IN FOG COMPUTING USED FOR DECENTRALIZED COMPUTATION[10]

Role	Security Challenges	Security Solutions
Decentralized Computation	Verifiable Computation	Privately Verifiable Computation Publicly Verifiable Computation
	Secure Aided Computation	Server-aided Exponentiation Server-aided Verification Server-aided Encryption Server-aided Function Evaluation Server-aided Key Exchange
	Secure Big Data Analysis	Fully Homomorphic Encryption Differential Privacy

VII. CONCLUSION

Fog Computing is not a replacement of Cloud Computing, but it complements it. Both the technology when used together forms a new breed of technology, that serves various IoT devices applications which may deal with computing, or storing temporary data, or acting as an interface between two layers, or serving real-time applications. This new technology in spite of making our life autonomous, is surrounded by some security and privacy threats which need to be resolved to enjoy Fog Computing. Some of the techniques to

resolve the challenges have been discussed but this is an open research issue and needs more inputs.

REFERENCES

[1] J. Gubbi, R. Buyya, S. Marusic, and M. Palaniswami, "Internet of Things (IoT): A vision, architectural elements, and future directions," Futur. Gener. Comput. Syst., vol. 29, no. 7, pp. 1645–1660, 2013.

[2] S. Yi, C. Li, and Q. Li, "A Survey of Fog Computing: Concepts, Applications and Issues," Proc. 2015 Work. Mob. Big Data - Mobidata '15, 2015.

[3] S. Yi, Z. Qin, and Q. Li, "Security and privacy issues of fog computing: A survey," Lect. Notes Comput. Sci. (including Subser. Lect. Notes Artif. Intell. Lect. Notes Bioinformatics), vol. 9204, pp. 685–695, 2015.

[4] I. Stojmenovic and S. Wen, "The Fog Computing Paradigm: Scenarios and Security Issues," Proc. 2014 Fed. Conf. Comput. Sci. Inf. Syst., vol. 2, pp. 1–8, 2014.

[5] I. Stojmenovic, "Fog computing: A cloud to the ground support for smart things and machine-to-machine networks," in 2014 Australasian Telecommunication Networks and Applications Conference, ATNAC 2014, 2015, pp. 117–122.

[6] J. Ni, A. Zhang, X. Lin, and X. S. Shen, "Security, Privacy, and Fairness in Fog-Based Vehicular Crowdsensing," IEEE Commun. Mag., vol. 55, no. 6, pp. 146–152, 2017.

[7] A. Alrawais, A. Alhothaily, C. Hu, and X. Cheng, "Fog {Computing} for the {Internet} of {Things}: {Security} and {Privacy} {Issues}," IEEE Internet Comput., vol. 21, no. 2, pp. 34–42, 2017.

[8] L. M. Vaquero and L. Rodero-Merino, "Finding your Way in the Fog: Towards a Comprehensive Definition of Fog Computing," ACM SIGCOMM Comput. Commun. Rev., vol. 44, no. 5, pp. 27–32, 2014.

[9] A. Munir, P. Kansakar, and S. U. Khan, "IFCIoT: Integrated Fog Cloud IoT: A novel architectural paradigm for the future Internet of Things," IEEE Consum. Electron. Mag., vol. 6, no. 3, pp. 74–82, 2017.

[10] J. Ni, K. Zhang, X. Lin, and X. Shen, "Securing Fog Computing for Internet of Things Applications: Challenges and Solutions," IEEE Commun. Surv. Tutorials, vol. 20, pp. 601–628, 2017.

[11] F. Bonomi, R. Milito, J. Zhu, and S. Addepalli, "Fog computing and its role in the internet of things," Proc. first Ed. MCC Work. Mob. cloud Comput. - MCC '12, pp. 13-16, 2012.

[12] J. Shropshire, "Extending the Cloud with Fog : Security Challenges & Opportunities," Am. Conf. Inf. Syst., pp. 1–10, 2014.

[13] S. Sarkar, S. Chatterjee, and S. Misra, "Assessment of the Suitability of Fog Computing in the Context of Internet of Things," IEEE Trans. Cloud Comput., vol. 6, pp. 46–59, 2015.

[14] R. Lu, X. Lin, H. Zhu, and X. Shen, "An intelligent secure and privacy-preserving parking scheme through vehicular communications," IEEE Trans. Veh. Technol., vol. 59, no. 6, pp. 2772–2785, 2010.

[15] C. Wang, C. Liang, F. R. Yu, Q. Chen, and L. Tang, "Computation Offloading and Resource Allocation in Wireless Cellular Networks with Mobile Edge Computing," IEEE Trans. Wirel. Commun., vol. 16, no. 8, pp. 4924–4938, 2017.

[16] W. Shi, J. Cao, Q. Zhang, Y. Li, and L. Xu, "Edge Computing: Vision and Challenges," IEEE Internet Things J., vol. 3, no. 5, pp. 637–646, 2016.

New trends in Fiber Optic Communication

Nowadays, telecommunication communities are deploying optical fiber to broadcast various signals like internet, telephone signals and cable signals. The phenomenon of transmitting information in the form of pulses of light from sender to receiver is known as Optical Fiber Communication. The light pulse thus pattern as electromagnetic wave which is further modulated to carry information. Fiber optic cable provides immunity to interference, enormous bandwidth and safe communication over long distance i.e. why it is preferred over electric cabling.

"Telecom windows" determine the wavelength operating region of optical fiber communication. Conventionally, first window of 800–900 nm was utilized. However, this window suffered from very high losses i.e. why it is appropriate only for short range communication. The wavelength employed by second window is approximately 1.3 μm. Therefore, silica fiber losses are minimum, resulting in minimization of dispersive broadening. This telecom window was initially utilized for long distance transmission but due to low dispersion, optical non linearity also increases. The most popular is third telecom window that employ the wavelength range of 1.5 μm. This window yields minimum losses and high performance as erbium doped fiber amplifiers are utilized in it. Further division of second and third telecom window wavelength bands is as follows:

Types of Band	Explanation	Range of wavelength
O band	Original	1260–1360 nm
E band	Extended	1360–1460 nm
S band	Short wavelengths	1460–1530 nm
C band	Conventional ("erbium window")	1530–1565 nm
L band	Long wavelengths	1565–1625 nm
U band	Ultra long wavelengths	1625–1675 nm

Optical fiber communication is envisioned as data communication future. The expansion of communication technology has lead to expansion of fiber optic communication. Some of the envisioned headways in fiber optics communication are described below:

1. Optical Networks carrying Multi–Terabit:

For multi-terabit transmission, Dense Wave Division Multiplexing (DWDM) technique is employed. The increasing entailment of enormous bandwidth is driving force for development of multi-terabit optical networks. Nowadays, 4 terabit networks of 40 Gb/sec information rate multiplexed with 100 DWDM channels prevails. Artificers are searching for 100 Gb/sec information transmission rate.

2. Optical fibers made up of Polymers:

Due to cheap processing of optical signals and flexibility for plug interconnection, Polymer optical fibers are preferred over glass optical fibers. Research and Development groups are trying to incorporate polymer optical fibers in aircrafts because of its immense benefits.

3. Expansion in Optical Submarine Systems Network Configuration:

In optical submarine communication systems, expansion of technology to configure mesh network is envisioned as flexibility advancement of network configuration.

There are many more applications of optical fiber communication but in this section, the design and optimization of optical band passes and notch filter using the multilayer thin-film structures is discussed. Optical equipment consists of optical surfaces that are used to control the amount light passing through the instruments. The performance of all the optical devices depends the way optical surfaces reflect, transmit or scatter light. These work on the principle of either constructive or destructive interferences. Band pass and notch filters are one of the optical filters that selectively reject or pass the band of wavelength. The entire notch filters works on the principle of destructive interference. The demands of the optical coating industries have resulted in a dramatic increase in the use of thin film filters. Band pass and notch filter are those optical filters that selectively reject and pass a band of wavelength. All the notch and pass band filters works on the principle of destructive interference. In the present work, we have done design of optical band pass and notch filter using the multilayer thin-film structures and optimized for incidence angles and BK47 glass are used for substrates. The ion assistive E-beam deposition technology is the mostly used in coating production. Alternate layers of two materials are the simplest way to design the filters with using the different thicknesses at high temperature was coated. It reduces the defects but also, it increases the adhesion strength along with proper chemical stoichiometry. The design principal is based on the thin film interference and characteristic matrix theory. The author chooses alternative layers of materials like (SiO_2) / (Al_2O_3) and (SiO_2) / (TiO_2) having refractive indices 1.46, 1.63 and 2.1 respectively. Each layer

has one-quarter wave thickness of a predetermined wavelength of 550 nm for angle of incidence. The design was simulated using the filmstar^{TM} software. The transmittance obtained from multilayer stack was approximately 95 % at 550 nm wavelength with a reasonably appropriate bandwidth for selective filtering.

Design and optimization of optical band pass and notch filter using the dielectric multilayer Thin-film structures

Sanjay Kumar[1], Vemuri SRS Praveen Kumar[2], Mukesh Kumar[3], Neelam Kumari[4], Vinod Karar[5], Ashavani Kumar[6], Amit L Sharma[7]

***Abstract*—Notch filters or pass band filters are important type of thin film filter technology that have resulted in a dramatic increase in the performance. So, they have high demand in commonplace within the electro optics industry. This work discusses about the design and optimization of optical band passes and notch filter using the multilayer thin-film structures. The band pass and notch filter are optical filters that selectively reject and pass a wavelength band and reflect both shorter and longer wavelengths. Such filters have various scientific and technological applications, including protection from laser radiation, laser-based fluorescence instrumentation, Raman spectroscopy, and other applications. In this paper comparison of single and multi-cavity notch filters were designed using the dielectric oxides such as Silicon dioxide (SiO_2), Aluminum oxide (Al_2O_3), Titanium oxide (TiO_2) with a peak transmittance of ~ 95%. All these designs were designed at fundamental wavelength of 550nm for normal incidence. The reflectance and transmission calculations were done using the filmstar^{TM} software.**

Keywords*— *Thin films, Homogeneous coatings, Design, Optimization, notch filters

I. INTRODUCTION

Optical equipment consists of optical surfaces that are used to control the amount light passing through the instruments. The performance of all the optical devices depends the way optical surfaces reflect, transmit or scatter light. These works on the principle of either constructive or destructive interference.

[1]Sanjay Kumar is with Department of Physics, National Institute of Technology, Kurukshetra, India
[2]Vemuri SRS Praveen Kumar with Optical Devices and System Division, CSIR-CSIO, Chandigarh, India.
[3]Mukesh Kumar with Optical Devices and System Division, CSIR-CSIO, Chandigarh, India.
[4]Neelam Kumari with Optical Devices and System Division, CSIR-CSIO, Chandigarh, India.
[5]Vinod Karar with Optical Devices and System Division, CSIR-CSIO, Chandigarh, India.
[6]Ashavani Kumar with Department of Physics, National Institute of Technology, Kurukshetra, India.
[7]Amit L Sharma with Optical Devices and System Division, CSIR-CSIO, Chandigarh, India.

(e-mail: sanjaykkr25@gmail.com, vsrsrangasai@gmail.com, mukeshcet@gmail.com, neelamk7@gmail.com, vkarar@rediffmail.com, ashavani@yahoo.com, amitsharma_csio@yahoo.co.in)

Band pass and notch filters are one of the optical filters that selectively reject or pass the band of wavelength. All the notch filters works on the principle of destructive interference. The demands of the optical coating industries have resulted in a dramatic increase in the use of thin film filters. Band pass and notch filter are those optical filters that selectively reject and pass a band of wavelength. All the notch and pass band filters works on the principle of destructive interference [1] [2].

In an another way notch filter are reflect a narrow band from a wide specified spectral range and transmit on both short wavelength and long wavelength sides of this band[10]. The selective bands are determined by two cut off wavelengths .The optical filter consists of number of thin-films of transparent optical materials deposited on a substrate. Even, if filter consists of single layer coating, the interface between the material and substrate is small reflection coefficient due to a small difference in refractive index and if the multilayer coating is on the substrate, then the reflections from many interfaces can constructively interfere to result in a very high overall reflectivity of the device. The quarter-wave designs have restricted applications owing to the non-availability of suitable materials for the required design and the limited spectral range of applicability. Multilayer optical thin film coatings have been extensively used for high reflectivity modulation in various optical systems like display systems, optical instrumentation, avionics, military, defence sector, optoelectronic components and many more.

In the present work, we have done design of optical band pass and notch filter using the multilayer thin-film structures and optimized for incidence angles and BK47 glass are used for substrates. The ion assistive E-beam deposition technology is the mostly used in coating production. Alternate layers of two materials are the simplest way to design the filters with using the different thicknesses at high temperature was coated. it reduces the defects but also, it increases the adhesion strength along with proper chemical stoichiometry. The design principal is based on the thin film interference and characteristic matrix theory. We choose the Alternative layers of materials are (SiO_2) / (Al_2O_3) and (SiO_2) / (TiO_2) having refractive indices 1.46, 1.63 and 2.1 respectively . Each layer has one-quarter wave thickness of a predetermined

wavelength of 550 nm for angle of incidence. The design was simulated using the filmstar™ software. The transmittance obtained from multilayer stack was approximately 95 % at 550 nm wavelength with a reasonably appropriate bandwidth for selective filtering[10].

A. Characteristic Matrix theory for single layer and multilayers

The mathematical matrix model was used to evaluate the transmission and reflection profile. The multilayer optical coating usually consists of a stack of several layers of non-absorbing dielectric materials with different refractive indices. Characteristic matrix is the product of the individual layers.

Optical performance also includes the variation in properties with angle of incidence for the modes of polarization. Based on that, the refraction indices S-polarization and P-polarization are two modes of wave [4].

Which are demonstrated as following :

N_P= n/cosθ p-polarization of the effective refractive index.

N_S= n* cosθ s-polarization of the effective refractive index

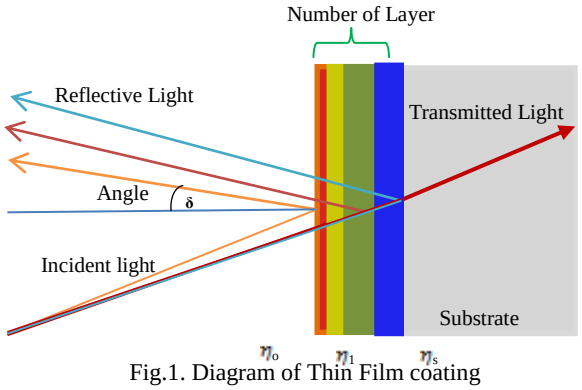

Fig.1. Diagram of Thin Film coating

Where symbols denote-

η_0 - Refractive index of air

η_1- Refractive index of layer 1

η_s- Refractive index of Substrate

The multilayer reflective index for this design is:

Air/HL/glass

HL- arrangement of layer according to high and low refractive indices.

B. Equations

The equations are an exception to the prescribed specifications of this template.

For the assorted thickness and incidence angle, we have to calculate the values of transmittance and reflectance. We know the value of wavelength as λ (center wavelength) as 550 nm, refractive index of material to be coated also thickness of the thin film coating in nm.

Now, we would use the formula,

$$\delta = \frac{2\pi\eta d}{\lambda}$$

Now, we have to calculate the parameters X, Y for single layer coating.

$$\begin{bmatrix} X \\ Y \end{bmatrix} = \begin{bmatrix} \cos\delta & i\sin\delta/\eta \\ i\eta\sin\delta & \cos\delta \end{bmatrix} \begin{bmatrix} 1 \\ \eta(sub) \end{bmatrix}$$

This is the expression for calculations the single layer coatings for multilayer coating expression given below.

$$\begin{bmatrix} X \\ Y \end{bmatrix} = \begin{bmatrix} \cos\delta 2 & \frac{i\sin\delta 2}{\eta 2} \\ i\eta 2\sin\delta 2 & \cos\delta 2 \end{bmatrix} \begin{bmatrix} \cos\delta 1 & \frac{i\sin\delta 1}{\eta 1} \\ i\eta 1\sin\delta 1 & \cos\delta 1 \end{bmatrix} \begin{bmatrix} 1 \\ \eta(sub) \end{bmatrix}$$

Transmission and absorbance values are also can be calculated by the given formula is:

$$T = \frac{4n_o Re(n^m)}{(n_o X+Y)(n_o X+Y)*}$$

$$A = \frac{4n_o Re(XY-n^m)}{(n_o X+Y)(n_o X+Y)*}$$

II. DESIGN FOR BANDPASS AND NOTCH FILTER

Band pass filters feature is transmitted all the incident light in one spectral range **of a** high transmission on either side rejects all the other radiation of very high reflection and another way notch filter are reflect a narrow band from a wide specified spectral range and transmit on both short wavelength and long wavelength sides of this band. The designing the optical filters mostly using alternating layers of and low (L) index and high (H) index dielectric materials with any multiple of quarter wave optical thicknesses[4].

The multilayer reflective index stack for this design is:

Sub/ $(HL)^n$ H 2L H $(LH)^n$/ Air

Mirror Space Mirror

H- Quarter wave thickness of high index layer
L- Quarter wave thickness of low index layer

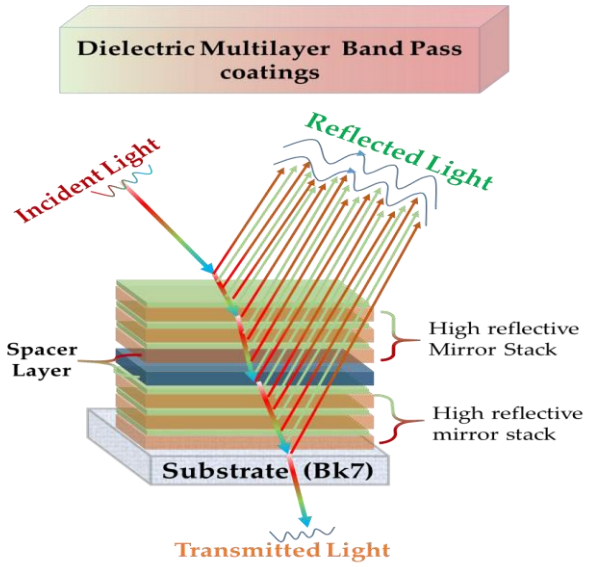

Fig.2. Diagram of arrangement of single cavity layers

The multilayer stacks structure of single cavity filter it's characterized by a spacer layer. The filter has two mirror first and second inner mirrors. both the mirror are separated by an inner spacer.The spacer layer can be any even number of quarter waves and the value of n can be any positive integer. The optical thicknesses of the spacers are substantially identical, and are sized to align the resonant frequency of the filter. In the filter using solid spacer(s) is disclosed where in a plurality of spacers are formed from a single wafer of material. In the increasing the value of n, the rejection band increases and thus the high transmission band becomes narrower. In order to obtain the multiple cavities the expressed as fellow [4]

$$\text{Sub/ } (HL)^n \text{ H 2L H } (LH)^n \text{ L } (HL)^n \text{ H 2L H } (LH)^n \text{ / Air}$$

⇩

Coupling layer

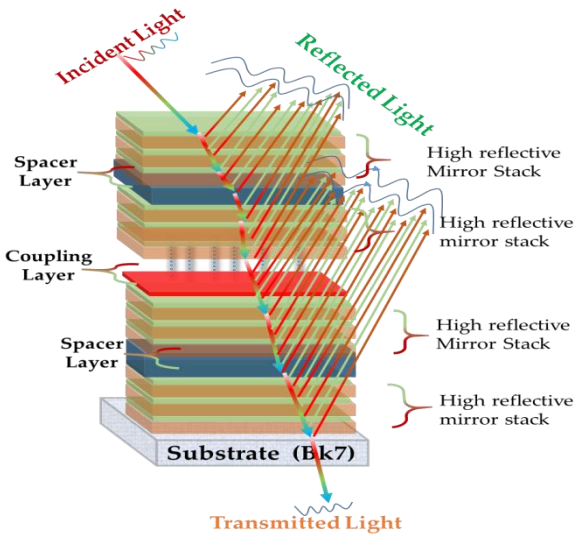

Fig.3. Diagram of arrangement of the multi cavity layer

In multilayer structures coating in metallic sheets or any material can be used as *coupling* elements. In this paper, both low and high refractive index materials are used as a coupling element.

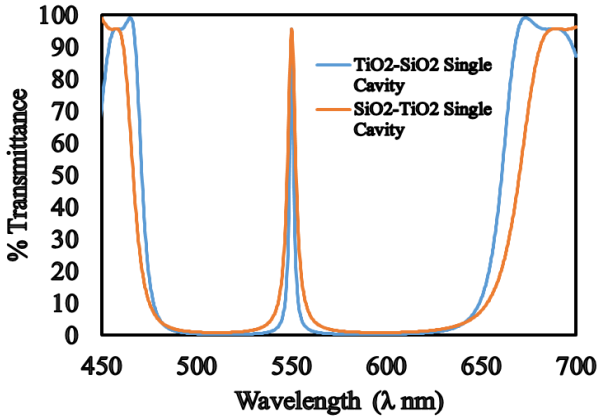

ig.4. Diagram of compare single cavity layers of TiO_2/SiO_2 and SiO_2/TiO_2

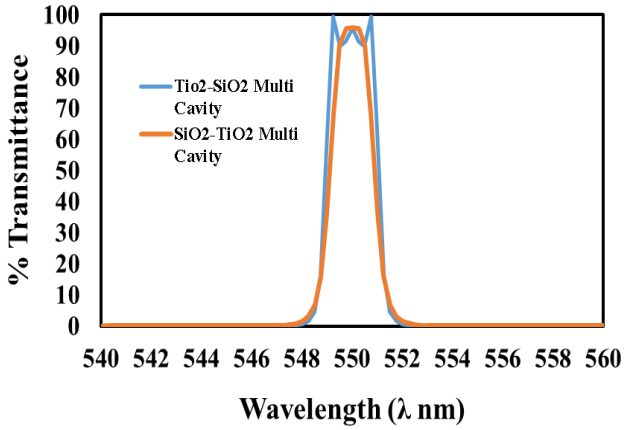

Fig.5. *Diagram of compare multi cavity layers of TiO_2/SiO_2 and SiO_2/TiO_2*

"Fig.4," shows a theoretical comparison of single cavity layers of TiO_2/SiO_2 and SiO_2/TiO_2. in the single cavity graph their one peak transmission and similarly in "Fig. 5," show the comparison between the multi cavity layers of TiO_2/SiO_2 and SiO_2/TiO_2 bandpass filter with the same basic layer structure with (HL….) and (LH…) as above with n = 5 at reference wavelength of 550 nm .

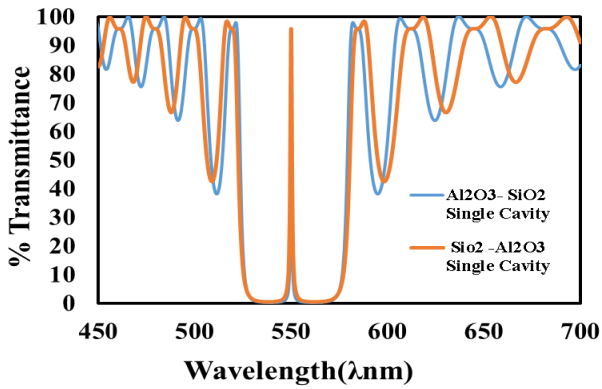

Fig.6. Diagram of compare single cavity layers of Al_2O_3/SiO_2 and $Si0_2/ Al_2O_3$

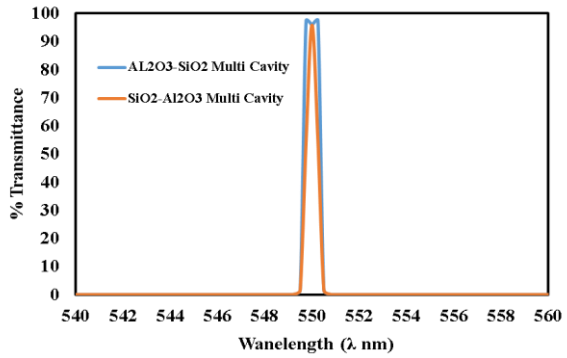

Fig.7. Diagram of compare multi cavity layers of Al_2O_3/SiO_2 and SiO_2/Al_2O_3 /Al_2O_3

"Fig. 6," shows a theoretical comparison of multi cavity layers of Al_2O_3/SiO_2 and SiO_2/Al_2O_3 also "Fig.7," comparison between the multi cavity layers of $Al2O_2/SiO_2$ and SiO_2/Al_2O_3 bandpass filter with the same basic layer structure with (HL….) and (LH…) as above with n = 20 at reference wavelength of 550 nm .

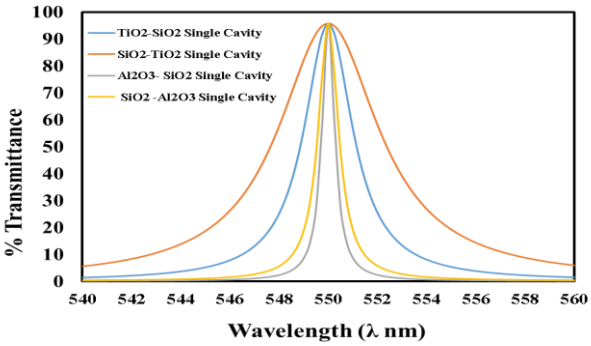

Fig.8. Diagram of compare single cavity layers of TiO_2/SiO_2, $SiO2/TiO_2$, Al_2O_3/SiO_2 and SiO_2/Al_2O_3

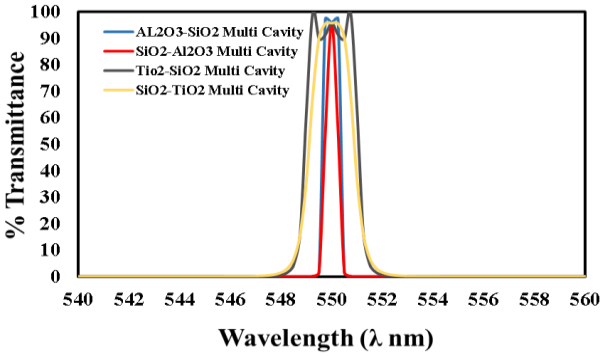

Fig.9. Diagram of compare Multi cavity layers of TiO_2/SiO_2, $SiO2/TiO_2$, Al_2O_3/SiO_2 and SiO_2/Al_2O_3

"Fig.8," shows the comparison between the single cavity layers of TiO_2/SiO_2, SiO_2/TiO_2, Al_2O_3/SiO_2 and SiO_2/Al_2O_3. "Fig. 9," shows the comparison between the multi cavity layers of TiO_2/SiO_2, SiO_2/TiO_2, Al_2O_3/SiO_2 and SiO_2/Al_2O_3.

After comparing the all result of single cavity layer and multi cavity layer the bandwidth of the filter are increase and decrease same manner. In the design countinously change the number of the layers, this effect is come on the top of the cavity structure. Due to this ripple effect are come on the top of the band pass filter. This ripples are remove by the design of multi cavity layers $SiO2/TiO_2$, and SiO_2/Al_2O_3. In the design SiO_2 is low reflective index and number of layers is also different.

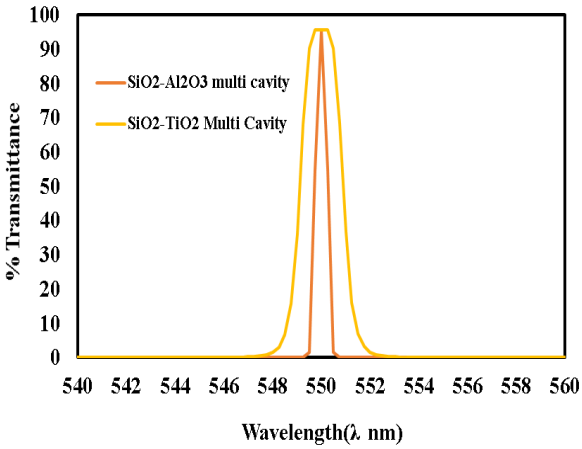

Fig.10. Diagram of compare multi cavity layers of $SiO2/TiO_2$, and SiO_2/Al_2O_3

We can be seen multiple symmetric cavities add ripple to the top of the pass band region. This effect is come only by the addition of several non-quarter wave layers on the top of the cavity structure. "Fig. 7," in design of multi cavity layers helps to match the optical stack into air and reducing the ripple. In this SiO_2 is low reflective index and Al_2O_3 and TiO_2 is high refractive index. in the NBPF used for the utilizes an AR coating and is designed with multi cavities consisting of quarter wave layers referenced at 550 nm.

III. RESULTS

The designs of both bandpass filters and notch filter were explored and optimization using the filmstar™ software. The BK7 substrates are used to as a substrate with anti-reflective coating and high reflective coating. In the design compression between the (SiO_2) / (Al_2O_3) and (SiO_2) / (TiO_2) for single cavity and multi cavity with in peak transmissions is 95%. Based on the results of this study shows the increase in the number of layers of material the bandwidth of spectra is decrease and also the reduce ripple but the peak transmission is almost 95%.

ACKNOWLEDGMENT

Authors are thankful to The Director, CSIR-CSIO, and Chandigarh for his support. SK also acknowledge financial grant from GATE awarded by MHRD, Government of India.

REFERENCES

[1] H. A. Macleod, “Thin Film Optical Filters”, 3rd ed., Institute of Physics, London, 2001.

[2] Kumar, Vemuri SRS Praveen, et al. "Design and optimization of high reflectance graded index optical filter with quintic apodization." International Conference on Optics and Photonics 2015. Vol. 9654. International Society for Optics and Photonics, 2015.

[3] J. A. Dobrowolski, A. V. Tikhonravov, M. K. Trubetskov, B. T. Sullivan, and P. G. Verly, “Optimal single-bandnormal-incidence antireflection coatings,” Appl. Opt. 35, 644–658 (1996

[4] George, Jason. "deposition of Visible narrow Bandpass Filters using spectoR dual Ion Beam deposition system."

[5] U. Schulz, U. Schallenberg, and N. Kaiser, “Symmetrical periods in antireflective coatings for plastic optics,” Appl.Opt. 42, 1346–1351 (2003

[6] N. Kumari, M. Kumar, P.K. Rao, A.L. Sharma, V. Karar, Design and development of multilayer antireflection coatings for avionics displays devices, National Conference on Emerging Trends in Aircraft Design and Manufacturing, ATHAL Press and Media, India, (2014), 71-73

[7] M. Kumar, N. Kumari, P.K. Rao, A.L. Sharma, V. Karar, Performance comparison of Silica-Titania and Silica-Alumina multilyer reflective filters for avionics displays

[8] K. Narasimha Rao, M.A. Murthy, S. Mohan, Optical properties of electron beam evaporated TiO2 films, ThinSolid Films, 176 (1989) 181.

[9] Leyson G.P.1 and Gong H.2, Design of Narrow Bandpass Filters using Thin Films

[10] Jinlong Zhang,1,2 Yujiang Xie,1,2 Xinbin Cheng, 1,2 Hongfei Jiao,1,2 and ZhanshanWang1,2 “Thin-film thickness-modulated designs for optical minus” (Doc. ID 192043); published 8 August 2013

Conclusion:

This chapter investigates recent headways in communication systems especially focusing Internet of Things, Fog computing and fiber optics. The expansion of scaling down and astuteness as well as unification of communication capabilities into an extraordinary plethora of devices have been the essential leverage of the new and innovative popular paradigm referred to as headways of communication system. Recent headways, ongoing trends and issues have been reviewed to accustom readers about advancements in communication engineering.

This specific chapter describes three domains i.e. Internet of Things, Fog computing and fiber optics and elucidate each domain in subsections with research papers. And in each of the subsection, some important papers deliberating that particular application have been included for quick reference. For example, first section illustrates the application of IoT in IoV. IoV is ubiquitous network of wireless access technology recognized vehicles comprising internet and other diverse networks. One of the types i.e. V2R is being modelled in this section for proper communication at high speed and far distance. This paper seeks to discern how design optimization parameters i.e. speed, propagation environment and RSU-OBU distance greatly influences the performance of the IoV (sensor based) environment. IoV prototype is designed on NETSIM Simulator to analyze the effect of speed of OBU in terms of throughput and energy consumption during communication. The simulation result shows that there is an 11.1 % increase in total energy consumption when speed increases from 1m/s to 20 m/s. Further the performance degrades by 3.26% for COST 231 HATA model, when RSU-OBU distance is switched from 5m to 10 m. The propound model will be augmented for successful communication with hyper-velocity (100 - 300 m/s) devices.

Next subsection deals with techniques to conquer security issues in Fog computing. Fog computing provides various Fog assisted IoT real-time applications, which due to security and privacy threats has not been utilized fully. Some security solutions about Fog computing is provided in the paper provided in this section. Fog Computing is not a replacement of Cloud Computing, but it complements it. Both the technology when used together forms a new breed of technology, that serves various IoT devices applications

which may deal with computing, or storing temporary data, or acting as an interface between two layers, or serving real-time applications.

The last section describes the headways of optical fiber communication and includes one paper related to the design and optimization of optical band passes and notch filter using the multilayer thin-film structures. The performance of all the optical devices depends the way optical surfaces reflect, transmit or scatter light. These work on the principle of either constructive or destructive interferences. Band pass and notch filters are one of the optical filters that selectively reject or pass the band of wavelength. The entire notch filters works on the principle of destructive interference. The demands of the optical coating industries have resulted in a dramatic increase in the use of thin film filters. Band pass and notch filter are those optical filters that selectively reject and pass a band of wavelength. All the notch and pass band filters works on the principle of destructive interference. The paper presents design and optimization of optical band pass and notch filter using the multilayer thin-film structures and optimized for incidence angles and BK47 glass are used for substrates. The ion assistive E-beam deposition technology is the mostly used in coating production. Alternate layers of two materials are the simplest way to design the filters with using the different thicknesses at high temperature was coated. It reduces the defects but also, it increases the adhesion strength along with proper chemical stoichiometry. The design principal is based on the thin film interference and characteristic matrix theory. The author chooses alternative layers of materials like (SiO2) / (Al2O3) and (SiO2) / (TiO2) having refractive indices 1.46, 1.63 and 2.1 respectively. Each layer has one-quarter wave thickness of a predetermined wavelength of 550 nm for angle of incidence. The design was simulated using the filmstar TM software. The transmittance obtained from multilayer stack was approximately 95 % at 550 nm wavelength with a reasonably appropriate bandwidth for selective filtering.

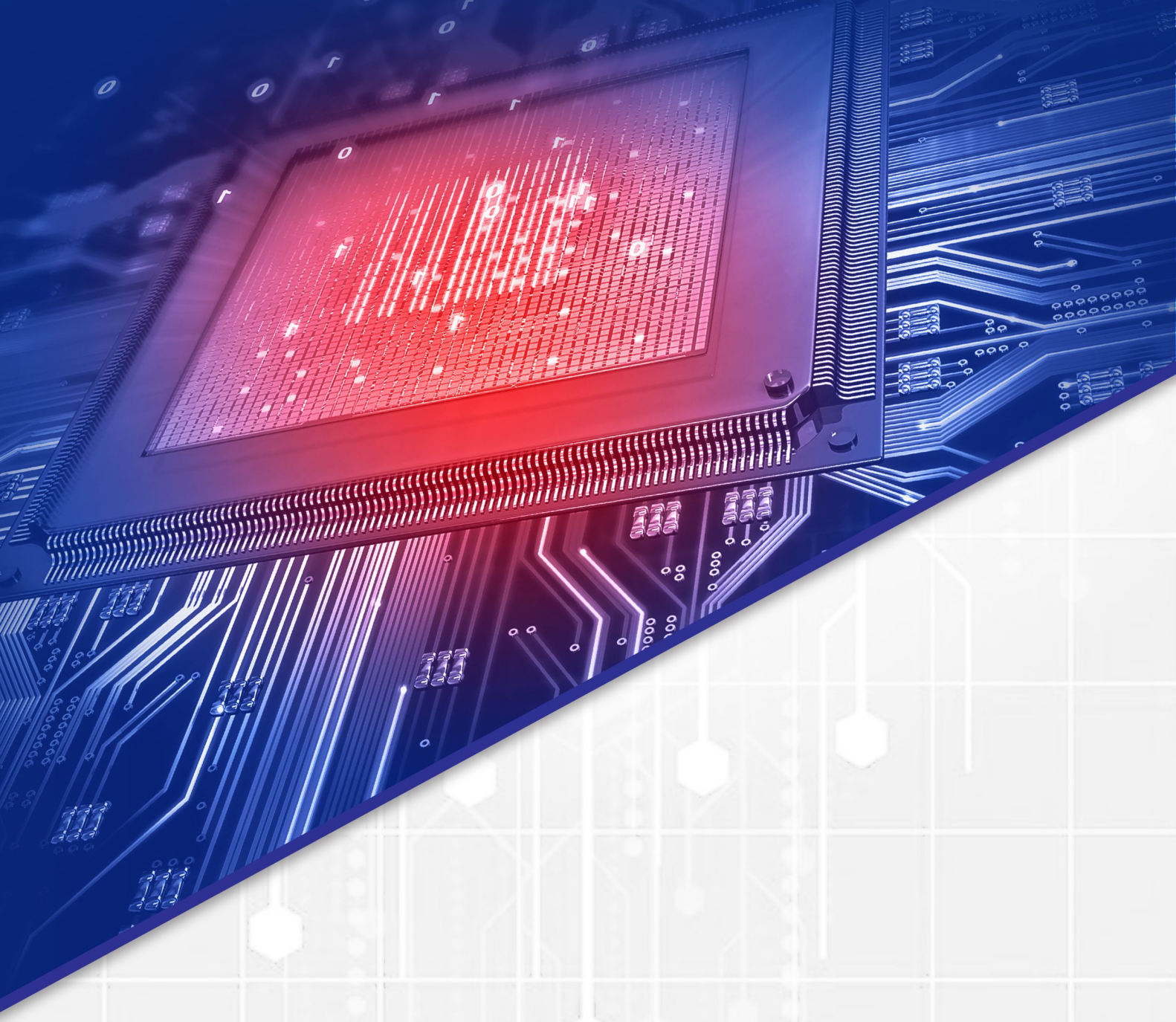

Cover Designed By : Jugaad Sobti

Elixir PUBLICATIONS

A unit of
Athal Services Pvt. Ltd.

ISBN 978-81-933897-2-0